PROCEEDINGS OF THE NINETEENTH WORKSHOP ON GENERAL RELATIVITY AND GRAVITATION IN JAPAN

TACHIKAWA MEMORIAL HALL, RIKKYO UNIVERSITY

TOKYO, JAPAN

THE 30TH OF NOVEMBER TO THE 4TH OF DECEMBER 2009

Edited by

Motoyuki Saijo, Umpei Miyamoto, Tomohiro Harada, Misao Sasaki, Tetsuya Shiromizu, Shinji Mukohyama

Organising Committee

Hideki Asada (Hirosaki University)
Takeshi Chiba (Nihon University)
Tomohiro Harada (Rikkyo University)
Akio Hosoya (Tokyo Institute of Technology)
Kunihito Ioka (High Energy Accelerator Research Organization)
Hideki Ishihara (Osaka City University)
Hideo Kodama (High Energy Accelerator Research Organization)
Yasufumi Kojima (Hiroshima University)
Kei-ichi Maeda (Waseda University)
Umpei Miyamoto (Rikkyo University)
Shinji Mukohyama (Institute for the Physics and Mathematics of the Universe)
Takashi Nakamura (Kyoto University)
Ken'ichi Nakao (Osaka City University)
Yasusada Nambu (Nagoya University)
Ken-ichi Oohara (Niigata University)
Motoyuki Saijo (Rikkyo University)
Misao Sasaki (Yukawa Institute for Theoretical Physics)
Noriaki Shibazaki (Rikkyo University)
Masaru Shibata (Yukawa Institute for Theoretical Physics)
Tetsuya Shiromizu (Kyoto University)
Jiro Soda (Kyoto University)
Naoshi Sugiyama (Nagoya University)
Takahiro Tanaka (Yukawa Institute for Theoretical Physics)
Shoichi Yamada (Waseda University)
Jun'ichi Yokoyama (Research Center for the Early Universe)

List of Participants

	Full name	Institution
1	Masaru Adachi	Hirosaki University
2	Alikram Aliev	Feza Gursey Institute, Turkey
3	Fumitoshi Amemiya	Keio University
4	Hideyoshi Arakida	Waseda University
5	Frederico Arroja	Yukawa Institute for Theoretical Physics
6	Hideki Asada	Hirosaki University
7	Luca Baiotti	Yukawa Institute for Theoretical Physics
8	Kazuharu Bamba	National Tsing Hua University, Taiwan
9	Cosimo Bambi	Institute for the Physics and Mathematics of the Universe
10	Swastik Bhattacharya	Tata Institute of Fundamental Research, India
11	Martin Bojowald	The Pennsylvania State University, USA
12	Li-Ming Cao	Kinki University
13	Takeshi Chiba	Nihon University
14	Takeshi Chikamatsu	Miyagi Gakuin Women's University
15	Alan Coley	Dalhousie University, Canada
16	Alan Cornell	University of the Witwatersrand, South Africa
17	Ben Craps	Vrije Universiteit Brussel, Belgium
18	Antonio De Felice	Tokyo University of Science
19	Youri Doeleman	Yukawa Institute of Theoretical Physics
20	Jason Doukas	Yukawa Institute for Theoretical Physics
21	Damien Easson	Institute for the Physics and Mathematics of the Universe
22	Antonino Flachi	Yukawa Institute for Theoretical Physics
23	Akihiko Fujii	The University of Tokyo
24	Ryuichi Fujita	Raman Research Institute, India
25	Hitoshi Fujiwara	Tokyo University of Science
26	Takao Fukui	Dokkyo University
27	Hajime Goto	Graduate University for Advanced Studies
28	Bogeun Gwak	Sogang University, Korea
29	Jakob Hansen	Korea Institute for Science and Technology Information
30	Tomohiro Harada	Rikkyo University
31	Hirotsugu Hayash	High Energy Accelerator Research Organization
32	Kenta Hioki	Waseda University
33	Takashi Hiramatsu	Institute for Cosmic Ray Research
34	Yuta Hiranuma	Niigata University
35	Akio Hosoya	Tokyo Institute of Technology
36	Kenta Hotokezaka	Kyoto University
37	Tsuyoshi Houri	Osaka City University
38	Qing-Guo Huang	Korea Institute for Advanced Study
39	Scott Hughes	Massachusetts Institute of Technology, USA
40	Daisuke Ida	Gakushuinn University
41	Takahisa Igata	Osaka City University
42	Hideo Iguchi	Nihon University
43	Kouhei Inayoshi	Kyoto University
44	Kunihito Ioka	High Energy Accelerator Research Organization
45	Akihiro Ishibashi	High Energy Accelerator Research Organization
46	Hideki Ishihara	Osaka City University
47	Soichiro Isoyama	Yukawa Institute for Theoretical Physics
48	Noriki Iwanaga	Research Center of Computational Mechanics, Inc.
49	Keisuke Izumi	Institute for the Physics and Mathematics of the Universe
50	Kohei Kamada	Reserch Center for the Early Universe
51	Syo Kamata	Rikkyo University

	Full name	Institution
52	Nahomi Kan	Yamaguchi Junior College
53	Masumi Kasai	Hirosaki University
54	Kazumi Kashiyama	Kyoto University
55	Masashi Kimura	Osaka City University
56	Shunichiro Kinosshita	Yukawa Institute for Theoretical Physics
57	Shunji Kitamoto	Rikkyo University
58	Kenta Kiuchi	Waseda University
59	Koichiro Kobayashi	Yamaguchi University
60	Shinpei Kobayashi	Gunma National College of Technology
61	Taichi Kobayashi	Nagoya University
62	Takeshi Kobayashi	Institute for Cosmic Ray Research
63	Tsutomu Kobayashi	Waseda University
64	Makoto Kobayashi	
65	Hideo Kodama	High Energy Accelerator Research Organization
66	Shinji Koide	Kumamoto University
67	Tatsuhiko Koike	Keio University
68	Yasufumi Kojima	Hiroshima University
69	Shigeru Konno	Tokai University
70	Yusuke Korai	Yukawa Institute for Theoretical Physics
71	Hiroshi Kozaki	Ishikawa National College of Technology
72	Yasunari Kurita	Kanagawa Institute of Technology
73	Tsunehide Kuroki	Rikkyo University
74	Koutarou Kyutoku	Yukawa Institute for Theoretical Physics
75	Chia-Min Lin	National Tsing Hua University, Taiwan
76	Kei-ichi Maeda	Waseda University
77	Satoshi Maeda	Kyoto University
78	Tomohiro Matsuda	Saitama Institute of Technology
79	Mitsuhiro Matsumoto	Graduate University for Advanced Studies
80	Mami Matsumoto	Waseda University
81	Akihiro Matsuzaki	Rikkyo University
82	Masato Minamitsuji	Sogang University, Korea
83	Takashi Mishima	Nihon University
84	Takaho Miura	Hirosaki University
85	Umpei Miyamoto	Rikkyo University
86	Akihito Miyazaki	Nagasaki University
87	Makoto Miyoshi	National Astronomical Observatory of Japan
88	Ryosuke Mizuno	Kyoto University
89	Yoshiyuki Morisawa	Osaka University of Economics and Law
90	Masaaki Morita	Nagaoka University of Technology
91	Hayato Motohashi	Reserch Center for the Early Universe
92	Shinji Mukohyama	Institute for the Physics and Mathematics of the Universe
93	Jiro Murata	Rikkyo University
94	Keiju Murata	Kyoto University
95	Hiroki Nagaoka	Rikkyo University
96	Ryo Nagata	High Energy Accelerator Research Organization
97	Kouji Nakamura	National Astronomical Observatory of Japan
98	Ken-ichi Nakao	Osaka City University
99	Kazunori Nakayama	Institute for Cosmic Ray Research
100	Yasusada Nambu	Nagoya University
101	Toshiya Namikawa	The University of Tokyo
102	Yuji Naramoto	Yamaguchi University
103	Tatsuya Narikawa	Hiroshima University
104	Atsushi Naruko	Yukawa Institute for Theoretical Physics

	Full name	Institution
105	Wade Naylor	Ritsumeikan University
106	Hiroya Nemoto	Rikkyo University
107	Kazufumi Ninomiya	Rikkyo University
108	Ryusuke Nishikawa	Osaka City University
109	Atsushi Nishizawa	National Astronomical Observatory of Japan
110	Masato Nozawa	Waseda University
111	Junko Ohashi	Tokyo University of Science
112	Seiju Ohashi	Tokyo Institute of Technology
113	Shinya Ohkubo	Rikkyo University
114	Yuji Ohsumi	Nagoya University
115	Nobuyoshi Ohta	Kinki University
116	Daisuke Ohtsuki	Rikkyo University
117	Hirotada Okawa	Yukawa Institute for Theoretical Physics
118	Satoshi Okuda	Rikkyo University
119	Ken-ichi Oohara	Niigata University
120	Seong Chan Park	Institute for the Physics and Mathematics of the Universe
121	Ethugal Pedige Berni Ann Thushari	Kyushu University
122	Soebur Razzaque	U.S. Naval Research Laboratory
123	Antonio Enea Romano	Yukawa Institute for Theoretical Physics
124	Norichika Sago	Yukawa Institute for Theoretical Physics
125	Hiromi Saida	Daido University
126	Amano Saijo	Hirosaki University
127	Motoyuki Saijo	Rikkyo University
128	Keiki Saito	Graduate University for Advanced Studies
129	Makoto Saito	Niigata University
130	Masakazu Sano	Hokkaido University
131	Yukinori Sasagawa	Waseda University
132	Misao Sasaki	Yukawa Institute for Theoretical Physics
133	Masaki Satoh	Kyoto University
134	Toyokazu Sekiguchi	Institute for Cosmic Ray Research
135	Yuichiro Sekiguchi	National Astronomical Observatory of Japan
136	Yuniti Sendouda	Yukawa Institute for Theoretical Physics
137	Naoki Seto	Kyoto University
138	Osamu Seto	Hokkai-Gakuen University
139	Masaru Shibata	Yukawa Institute for Theoretical Physics
140	Noriaki Shibazaki	Rikkyo University
141	Masaru Shiino	Tokyo Institute of Technology
142	Atsushi Shimabukuro	Rikkyo University
143	Masahiro Shimano	Rikkyo University
144	Akie Shimizu	High Energy Accelerator Research Organization
145	Hisaaki Shinkai	Osaka Institute of Technology
146	Kiyoshi Shiraishi	Yamaguchi University
147	Maresuke Shiraishi	Nagoya University
148	Tetsuya Shiromizu	Kyoto University
149	Jiro Soda	Kyoto University
150	Alexei Starobinsky	Landau Institute for Theoretical Physics, Russia
151	Kazuyuki Sugimura	Yukawa Institute for Theoretical Physics
152	Takayuki Suzuki	Yamaguchi University
153	Hiromi Suzuki	
154	Masaaki Takahashi	Aichi University of Education
155	Ryuichi Takahashi	Hirosaki University
156	Tomohiro Takahashi	Kyoto University

	Full name	Institution
157	Yousuke Takamori	Osaka City University
158	Takashi Tamaki	Nihon University
159	Kentaro Tanabe	Yukawa Institute for Theoretical Physics
160	Norihiro Tanahashi	Kyoto University
161	Takahiro Tanaka	Yukawa Institute for Theoretical Physics
162	Tomo Tanaka	Waseda University
163	Sugure Tanzawa	Yukawa Institute for Theoretical Physics
164	Shinya Tomizawa	High Energy Accelerator Research Organization
165	Takashi Torii	Osaka Institute of Technology
166	Takuya Tsuchiya	Waseda University
167	Shinji Tsujikawa	Tokyo University of Science
168	Naoki Tsukamoto	Rikkyo University
169	Tetsuya Turuta	
170	Yuko Urakawa	Waseda University
171	Tomoaki Wakabayashi	Rikkyo University
172	Ryo Wakebe	Waseda University
173	Masaaki Watanabe	Kyoto University
174	Kent Yagi	Kyoto University
175	Shigeaki Yahikozawa	Rikkyo University
176	Kohji Yajima	Rikkyo University
177	Yuta Yamada	Osaka Institute of Technology
178	Motohisa Yamada	Waseda University
179	Masahide Yamaguchi	Aoyama Gakuin University
180	Daisuke Yamauchi	Yukawa Institute for Theoretical Physics
181	Norio Yamazako	Waseda University
182	Jun'ichi Yokoyama	Reserch Center for the Early Universe
183	Shuichiro Yokoyama	Nagoya University
184	Chul-Moon Yoo	Asia-Pacific Center for Theoretical Physics, Korea
185	Ying-Li Zhang	Shanghai Normal University, China

Programme of the Workshop

Oral Presentations (Multi-Purpose Hall, Second Floor of Tachikawa Memorial Hall)

Nov. 30, Mon.
10:55 Opening remark

Chair: J. Yokoyama
11:00-12:00 (Invited talk: 60min)
Alexei Starobinsky (LITP and RESCEU, University of Tokyo)
"Cosmology of f(R) gravity"
12:00-12:40 (20min × 2)
Hayato Motohashi (RESCEU, University of Tokyo)
"Evolution of density fluctuation in f(R) gravity"
Kazuharu Bamba (National Tsing Hua University)
"Equilibrium description of thermodynamics in modified gravitational theories"

12:40-14:00 Lunch

Chair: S. Mukohyama
14:00-15:00 (Invited talk: 60min)
Alan Coley (Dalhousie University)
"Averaging in cosmology"
15:00-16:00 (20min × 3)
Shinpei Kobayashi (Gunma National College of Technology)
"Emergence of Spacetimes and Noncommutativity"
Antonio De Felice (Tokyo University of Science)
"Cosmological perturbations of a perfect fluid and non-commutative geometry"
Kentaro Tanabe (Yukawa Institute for Theoretical Physics)
"Asymptotic flatness at null infinity in five dimensions"

16:00-16:20 Coffee and posters

Chair: H. Kodama
16:20-18:00 (20min × 5)
Tsutomu Kobayashi (Waseda University)
"Large scale evolution of the curvature perturbation in Horava-Lifshitz cosmology"
Keisuke Izumi (IPMU)
"No Static Star Solution in Horava Gravity"
Takayuki Suzuki (Yamaguchi University)
"Constrain on Brans-Dicke Cosmology from view point of Cosmic age"
Masakazu Sano (Hokkaido University)
"Wrapped brane gas as a candidate for Dark Matter"
Takeshi Kobayashi (ICRR, University of Tokyo)
"Curvatons in Warped Throats"

Dec. 1, Tue.
Chair: K. Maeda
9:00-10:00 (Invited talk: 60min)
Ben Craps (Vrije Universiteit Brussel)
"Cosmological Singularity Problem"
10:00-10:40 (20min × 2)
Seong Chan Park (IPMU)
"Randall-Sundrum Black holes at colliders"

Hirotada Okawa (Yukawa Institute for Theoretical Physics)
"High-velocity collision of two black holes"

10:40-11:00 Coffee and posters

Chair: A. Hosoya
11:00-12:40 (20min × 5)
Keiju Murata (Kyoto University)
"Instability of Myers-Perry Black Holes"
Masashi Kimura (Osaka City University)
"Dynamical black rings with a positive cosmological constant"
Shinya Tomizawa (KEK)
"A uniqueness theorem for charged rotating black holes in five-dimensional minimal supergravity"
Alikram Aliev (TUBITAK, Feza Gursey Institute)
"Uniqueness of Rotating Charged Black Holes in Five-Dimensional Minimal Gauged Supergravity"
Akihiro Ishibashi (KEK)
"All Near-Horizon Geometries of Extremal Vacuum Black Holes"

12:40-14:00 Lunch

Chair: T. Harada
14:00-15:00 (Invited talk: 60min)
Martin Bojowald (The Pennsylvania State University)
"Quantum gravity's effects on space-time"
15:00-16:00 (20min × 3)
Tomo Tanaka (Waseda University)
"Robustness of singularity avoidance in loop quantum cosmology"
Fumitoshi Amemiya (Keio University)
"Gauge-invariant construction of quantum cosmology"
Kazumi Kashiyama (Kyoto University)
"Quantum Back Reaction to asymptotically AdS Black Holes"

16:00-16:20 Coffee and posters

Chair: M. Sasaki
16:20-17:20 (Invited talk: 60min)
Qing-Guo Huang (Korea Institute for Advanced Study)
"A story of the primordial non-Gaussianity"
17:20-18:00 (20min × 2)
Masato Nozawa (Waseda University)
"Dynamical black holes from intersecting M-branes"
Tsuyoshi Houri (Osaka City University)
"Geodesic Integrability of Charged Rotating Black Holes"

Dec. 2, Wed.
Chair: J. Soda
9:00-10:00 (Invited talk: 60min)
Tsunehide Kuroki (Rikkyo University)
"Boundary condition for D-brane from Wilson loop at the AdS boundary"
10:00-10:40 (20min × 2)
Toyokazu Sekiguchi (ICRR, University of Tokyo)
"Constraining single-field slow-roll inflation models with Bayesian model selection"

Frederico Arroja (Yukawa Institute for Theoretical Physics)
"On the full trispectrum in multi-field DBI inflation"

10:40-11:00 Coffee and posters

Chair: Y. Kojima
11:00-12:40 (20min × 5)
Yuko Urakawa (Waseda University)
"Adiabatic regularization of primordial perturbations generated during inflation"
Antonio Enea Romano (Yukawa Institute for Theoretical Physsics)
"Inhomogeneities , cosmic acceleration and dark energy."
Yuji Ohsumi (Nagoya University)
"Entanglement between two points separated by the sound horizon scale in the inflationary universe"
Shinji Koide (Kumamoto University)
"Generalized GRMHD equations of plasmas in the black hole magnetospheres"
Masaaki Takahashi (Aichi University of Education)
"Black Hole Aurora powered by a Rotating Black Hole"

12:40-14:00 Lunch

Chair: M. Saijo
14:00-15:00 (Invited talk: 60min)
Scott Hughes (Massachusetts Institute of Technology)
"Probing strong field gravity and testing black holes with gravitational waves"
15:00-15:40 (20min × 2)
Ryuichi Fujita (Raman Research Institute)
"Post-Newtonian gravitational wave polarisations and spherical harmonic components for a particle in circular orbit around a Schwarzschild black hole"
Luca Baiotti (Yukawa Institute for Theoretical Physics)
"Binary neutron star mergers"

15:40-16:00 Coffee and posters

Chair: H. Asada
16:00-17:00 (20min × 3)
Koutarou Kyutoku (Yukawa Institute for Theoretical Physics)
"Black hole-neutron star binaries in numerical relativity"
Atsushi Nishizawa (National Astronomical Observatory of Japan)
"Searching for nontensorial polarizations of stochastic gravitational waves with laser interferometers"
Kent Yagi (Kyoto University)
"Constraining alternative theories of gravity with space-borne gravitational wave interferometers"

17:00-18:00 Poster session

18:30-20:30 Conference Dinner

Dec. 3, Thu.
Chair: Y. Sekiguchi
9:00-9:40 (Invited talk: 40min)
Shunji Kitamoto (Rikkyo University)
"X-Ray Observation of Black Hole Candidates"
9:40-10:40 (20min × 3)
Makoto Miyoshi (National Astronomical Observatory of Japan)
"An Earliest Black Hole Imager at Andes"

Cosimo Bambi (IPMU)
"Numerical simulations of the accretion process in Kerr spacetimes with arbitrary value of the Kerr parameter"
Taichi Kobayashi (Nagoya University)
"Backscatter radiation by black hole superradiance of electromagnetic waves emitted from disk surface"

10:40-11:00 Coffee and posters

Chair: Y. Nambu
11:00-12:40 (20min × 5)
Hiromi Saida (Daido University)
"Relativistic Dissipative Accretion Flow onto Black Hole"
Chul-Moon Yoo (Asia-Pacific Center for Theoretical Physics)
"Testing the Copernican Principle with the kSZ Effect"
Masato Minamitsuji (Sogang University)
"Cosmic acceleration and higher-dimensional gravity"
Daisuke Yamauchi (Yukawa Institute for Theoretical Physics)
"Skewness in CMB temperature fluctuations from bended cosmic (super-)strings"
Atsushi Naruko (Yukawa Institute for Theoretical Physics)
"Non-Gaussianity in the CMB temperature fluctuations from Cosmic Strings"

12:40-14:00 Lunch

Chair: K. Ioka
14:00-15:00 (Invited talk: 60min)
Soebur Razzaque (U.S. Naval Research Lab.)
"High Energy Astrophysics and Gamma Ray Bursts in the Fermi Era"
15:00-16:00 (20min × 3)
Kenta Kiuchi (Waseda University)
"Taylor instability in neutron star"
Yousuke Takamori (Osaka City University)
"On the Meissner-like effect of an extreme black hole"
Kohei Kamada (RESCEU, University of Tokyo)
"Gravitational waves and Q-ball formation"

16:00-16:20 Coffee and posters

Chair: K. Oohara
16:20-18:00 (20min × 5)
Maresuke Shiraishi (Nagoya University)
"Constraints on neutrino masses from WMAP5 and BBN in the lepton asymmetric universe"
Masaki Satoh (Kyoto University)
"Background evolution of vector inflation"
Tomohiro Matsuda (Saitama Institute of Technology)
"Inflation, modulation and baryogenesis with warm directions"
Masaaki Watanabe (Kyoto University)
"Inflationary universe with anisotropic hair"

Dec. 4, Fri.
Chair: K. Nakao
9:00-10:00
Posters and free discussion

10:00-10:40 (20min × 2)
Tomohiro Harada (Rikkyo University)
"Einstein-Rosen waves and the self-similarity hypothesis in cylindrical symmetry"
Jakob Hansen (Korea Institute for Science and Technology Information)
"Interior of a charged black hole with an exotic scalar matter"

10:40-11:00 Coffee

Chair: T. Shiromizu
11:00-12:40 (20min × 5)
Swastik Bhattacharya (Tata Institute of Fundamental Research)
"Collapse of a massless scalar field"
Masahiro Shimano (Rikkyo University)
"Outer trapped surface in higher dimentional Vaidya spacetimes"
Tomohiro Takahashi (Kyoto University)
"Instability of Small Lovelock Black Holes in Even-dimensions"
Kazunori Nakayama (ICRR, University of Tokyo)
"Dark matter annihilation effects on the CMB anisotropy"
Osamu Seto (Hokkai-Gakuen University)
"Higgs portal heavy neutrino dark matter"

12:40-14:00 Lunch

Chair: T. Chiba
14:00-15:40 (20min × 5)
Keiki Saito (Graduate University for Advanced Studies)
"Analytic formulae for CMB anisotropy in LTB cosmology"
Alan Cornell (National Institute for Theoretical Physics; University of the Witwatersrand)
"Asymptotic iteration method for spheroidal harmonics of higher-dimensional Kerr-(A)dS black holes"
Jason Doukas (Yukawa Institute for Theoretical Physics)
"Graviton emission from simply rotating Kerr-de Sitter black holes: Transverse traceless tensor graviton modes."
Ryusuke Nishikawa (Osaka City University)
"Stability of charged squashed Kaluza-Klein black holes"
Yukinori Sasagawa (Waseda University)
"Asymptotically Linear Dilaton Black Hole Solution in Dilatonic Higher Curvature Gravity Theory"

Poster Presentations (Ground and Second Floors, Tachikawa Memorial Hall)

Poster Place 1 (Poster Numbers P1-P12, Second Floor, Tachikawa Memorial Hall)

P1. Wade Naylor (Ritsumeikan University)
"Towards detection of motion-induced radiation"
P3. Junko Ohashi (Tokyo University of Science)
"Assisted dark energy"
P4. Umpei Miyamoto (Rikkyo University)
"Minimal surfaces in flat and curved spacetimes of arbitrary dimensionality"
P5. Takashi Tamaki (Nihon University)
"Stability of gravitating Q-balls via a catastrophe theory"
P6. Hajime Goto (Graduate University for Advanced Studies)
"Gravitational lensing effects in the LTB model"
P7. Kouji Nakamura (National Astronomical Observatory of Japan)
"Consistency of equations for the single scalar field case in second-order gauge-invariant cosmological perturbation theory"
P9. Takuya Tsuchiya (Waseda University)
"To keep the constraint values without depending on background metric"
P10. Hideki Asada (Hirosaki University)
"Inverse problem for gravitational waves by three-body system in Lagrange's orbit"
P11. Satoshi Maeda (Kyoto University)
"Quantitative evaluation of the amplitude of the primordial magnetic field generated at the pre-recombination era"
P12.Takahisa Igata (Osaka City University)
"Toroidal Spiral Strings in Higher-dimensional Spacetime"

Poster Place 2 (Poster Numbers P13-P39, Ground Floor, Tachikawa Memorial Hall)

P13. Hitoshi Fujiwara (Tokyo University of Science)
"Constraints on viable potentials for chameleon scalar fields."
P14. Ethugal Pedige Berni Ann Thushari (Kyushu University)
"Magnitude redshift relation in the Brans Dicke model constrains from Big Bang Nucleosynthesis"
P15. Li-Ming Cao (Kinki University)
"Thermodynamics of Black Holes in Horava-Lifshitz gravity"
P16. Tatsuya Narikawa (Hiroshima University)
"Characterising linear growth rate in f(R) gravity"
P17. Amano Saijo (Hirosaki University)
"Perturbative approach to the quadrupole gravitational lens"
P18. Seiju Ohashi (Tokyo Institute of Technology)
"Riemannian Penrose inequality and a virtual gravitational collapse"
P19. Yuta Yamada (Osaka Institute of Technology)
"Black Objects and Hoop Conjecture in Five-dimensional Space-time"
P20. Shunichiro Kinoshita (Yukawa Institute for Theoretical Physics)
"Stability of warped Freund-Rubin solutions"
P21. Norihiro Tanahashi (Kyoto University)
"Toward numerical relativity in RS-II model"
P22. Takashi Mishima (Nihon University)
"Physical and Mathematical Behavior of Black Diring Solutions"
P23. Antonino Flachi (Yukawa Institute for Theoretical Physics)
"Thick Black Branes"
P25. Ryo Wakebe (Waseda University)
"Supersymmetric Intersecting Branes in time-dependent Backgrounds"

P26. Nahomi Kan (Yamaguchi Junior College)
"Boson Stars under Deconstruction"
P27. Motoyuki Saijo (Rikkyo University)
"Formation of Rapidly Rotating Dynamic Black Holes"
P28. Yuichiro Sekiguchi (National Astronomical Observatory of Japan)
"Rotating PopIII core collapse in Full general relativity"
P29. Bogeun Gwak (Sogang University, Korea)
"The Geodesics of Extra-ordinary solution"
P30. Norichika Sago (Yukawa Institute for Theoretical Physics)
"Gravitational self-force effect on the periastron shift in Schwarzschild spacetime"
P31. Takaho Miura (Hirosaki University)
"A possible explanation of the secular increase of the astronomical unit"
P32. Kenta Hioki (Waseda University)
"Measurement of the Kerr spin parameter by observation of a compact object's shadow"
P33. Hideyoshi Arakida (Waseda University)
"Cosmological Influence on Gravitationally Bound Local System: Case of Lemaitre–Tolman–Bondi Spacetime
P34. Yasufumi Kojima (Hiroshima University)
"Black Hole Magnetosphere for Two-fluid Flows"
P35. Ryuichi Takahashi (Hirosaki University)
"Simulations of Baryon Acoustic Oscillations: Likelihood Analysis of the Matter Power Spectrum"
P36. Masaru Adachi (Hirosaki University)
"Re-analysis of the supernova data to test the accelerating expansion of the universe"
P37. Shuichiro Yokoyama (Nagoya University)
"Density Fluctuations in Thermal Inflation and Non-Gaussianity"
P38. Chia-Min Lin (National Tsing Hua University, Taiwan)
"Supernatural Hilltop Inflation"
P39. Kazufumi Ninomiya (Rikkyo University)
"Short Range Gravity Experiment in NEWTON experiment"

Table of Contents

Invited Presentation

Contributed Presentation

Preface

The nineteenth workshop on General Relativity and Gravitation (JGRG19) has been held at the Tachikawa Memorial Hall of Rikkyo University between the 30th of November and the 4th of December 2009.

The aim of this workshop is to cover the wide-spread topics in general relativity and its surrounding fields, including astrophysics and cosmology, and trigger new visions with participants of the workshop. We have invited 9 speakers to overview the following topics: quantum gravity (Martin Bojowald), averaging in cosmology (Alan Coley), cosmological singularity (Ben Craps), primodial non-gaussianity (Qing-Guo Huang), gravitational waves (Scott Hughes), X-ray astronomy (Shunji Kitamoto), string theory (Tsunehide Kuroki), high energy astrophysics (Soebur Razzaque) and f(R) cosmology (Alexei Starobinsky). We have also had 61 oral presentations together with 37 poster presentations for contributing the success of this workshop. We believe that the workshop has been a great success with a plenty of stimulating discussions.

We cannot help thanking for those who have supported our workshop. Our secretaries, Ms. Kiyoe Yokota (Kyoto University) and Ms. Kumiko Inagawa (Rikkyo University), have taken care of plenty of administrative stuffs including reimbursement issues. Ms. Kimiko Saito and Ms. Kumi Araya from Research Initiative Center has taken care of the administrative issues of Rikkyo University Special Fund for Research 2009. Ms. Asako Endo from the Financial division has taken care of the reimbursement issues. Mr. Isamu Nemoto and Mr. Satoshi Ishiguro have taken care of the cgi server and the wireless network service. Our graduate students have taken care of many issues for organising the workshop.

Finally, we acknowledge that our workshop is supported by the Rikkyo University Special Fund for Research 2009 and by the JSPS Grant-in-Aid for Creative Scientific Research No. 19GS0219.

Tokyo, 14th of February, 2010

Motoyuki Saijo
Umpei Miyamoto
Tomohiro Harada

Quantum gravity effects on space-time

Martin Bojowald[1]

Institute for Gravitation and the Cosmos, The Pennsylvania State University, 104 Davey Lab, University Park, PA 16802, USA

Abstract

General relativity promotes space-time to a physical, dynamical object subject to equations of motion. Quantum gravity, accordingly, must provide a quantum framework for space-time, applicable on the smallest distance scales. Just like generic states in quantum mechanics, quantum space-time structures may be highly counterintuitive. But if low-energy effects can be extracted, they shed considerable light on the implications to be expected for a dynamical quantum space-time. Loop quantum gravity has provided several such effects, but even in the symmetry-reduced setting of loop quantum cosmology no complete picture on effective space-time geometries describing especially the regime near the big bang has been obtained. The overall situation regarding space-time structures and cosmology is reviewed here, with an emphasis on the role of dynamical states, effective equations, and general covariance.

1 Introduction

In modern cosmology, according to the common scenarios, one is using the universe and its own expansion as a microscope aimed at the smallest distance scales of space and time. In order to understand the resulting phenomena to be expected, the nature of the correct microscopic degrees of freedom, out of which space-time and its dynamics is to emerge, must be understood. There are no direct observations to guide us, and so we are required to make use of further input, of principles that are strong enough to support a large theoretical edifice.

A well-known example for the theoretical derivation of new microscopic degrees of freedom from an underlying principle is the electroweak theory. One of its motivations was a well-defined description of β-decay, a reaction of four particles (seen at least via the energy carried away in the case of the neutrino). As a pointlike interaction between the four particles involved, the perturbative quantum field theoretical description does not lead to well-defined decay rates. A new principle, renormalizability, is used to look for a more suitable theoretical framework. Its implementation requires the inclusion of new quantum degrees of freedom, the exchange bosons of the electroweak theory. Based on the principle of renormalizability, they were predicted theoretically well before direct observations by particle accelerators became possible.

In quantum gravity, we are currently in a situation similar to that before the direct detection of the exchange bosons. We do not have direct evidence for the microscopic degrees of freedom of quantum gravity, but we do know several problems of the classical theory, chiefly the singularity problem of general relativity. Again, extra input for a theoretical description is needed in the form of principles. One may decide to use those already tried and true, such as renormalizability in this case leading to string theory (as per current understanding). In this way, a quantization of gravitational (and other, unified) excitations on space-time becomes possible. There are, however, difficulties in the description of strong gravitational fields, as we find them at the big bang or in black holes. The interaction of matter with the space-time structure is relevant in those regimes, and so we must consider the quantum nature of full space-time. While this is not impossible in string theory, the theory's setup makes the analysis of such questions rather indirect.

An alternative principle offers itself, based on what we know about regimes of strong gravitational fields: the principle of background independence. It states the requirement of quantizing the full metric $g_{\mu\nu}$ known as the representative of space-time geometry as it must emerge at large distances or low energies; it is not enough to just quantize perturbations $h_{\mu\nu}$ on a given (e.g. Minkowskian) background

[1]Email address: bojowald@gravity.psu.edu

where $g_{\mu\nu} = \eta_{\mu\nu} + h_{\mu\nu}$. If only $h_{\mu\nu}$ is quantized and $\eta_{\mu\nu}$ kept as a classical metric background, the theory does not describe the complete space-time geometry in a quantized way. There will be physical quantum degrees of freedom for $h_{\mu\nu}$, but a classical, rigid background $\eta_{\mu\nu}$ remains in the theory. It may be possible to find observables insensitive to which $\eta_{\mu\nu}$ is used, but this would be difficult to achieve and to demonstrate. Moreover, regimes of strong gravitational fields, especially near classical singularities, do not allow a perturvative treatment with a small $h_{\mu\nu}$: The metric becomes degenerate, and so at least some of the crucial components of $h_{\mu\nu}$ are as large as those of $\eta_{\mu\nu}$. Here, a background independent quantization of the full $g_{\mu\nu}$ becomes most useful, a treatment realized in loop quantum gravity.

2 Background independence

Quantum field theory on a background Minkowski space-time may be formulated by operators $a_{\mathbf{k}}$ and $a^\dagger_{\mathbf{k}}$ that describe the annihilation and creation of particles of momentum $\mathbf{k}$. Using $a^\dagger_{\mathbf{k}}$ introduces a new particle and increases the total energy, while products of operators in a Hamiltonian amount to interactions. One problem to be faced in quantum gravity is that particles can only be created on a given space-time, whose metric is used in the very definition of $a_{\mathbf{k}}$ and $a^\dagger_{\mathbf{k}}$. A possible solution is to define operators for space-time itself. Such operators would increase distances, areas and volumes; not energy.

Loop quantum gravity [1–3] provides a specific realization of this solution, at least for spatial geometry. Creation operators turn out to be holonomies [4] $h_I = \mathcal{P}\exp(\int_{e_I} \mathrm{d}t\dot{e}^a_I A^j_a \tau_j)$ along spatial curves e_I, evaluated for a connection $A^j_a = \Gamma^j_a + \gamma K^j_a$ called the Ashtekar–Barbero connection [5, 6]. The structure group of the theory is SO(3), referred to by the index j and geometrically corresponding to local spatial rotations. (The matrices $\tau_j = -\frac{1}{2}i\sigma_j$ are generators of su(2), proportional to the Pauli matrices σ_j.) In the definition of the connection, we use the spatial spin connection Γ^i_a and extrinsic curvature K^i_a, with the Barbero–Immirzi parameter $\gamma > 0$ [6, 7], whose value parameterizes a family of canonical transformations. Classically, the connection is canonically conjugate to a densitized vector field E^a_i, the densitized triad related to the spatial metric q_{ab} by $E^a_i E^b_j = \det q q^{ab}$: $\{A^i_a(x), E^b_j(y)\} = 8\pi\gamma G\delta^b_a\delta^i_j\delta(x,y)$. This field determines the (torsion-free) spin connection

$$\Gamma^i_a = -\epsilon^{ijk} e^b_j(\partial_{[a}e^k_{b]} + \tfrac{1}{2}e^c_k e^l_a \partial_{[c}e^l_{b]})\,. \tag{1}$$

Only the extrinsic curvature part of A^i_a is independent of the triad.

To start setting up the connection representation for a quantum formulation, we define a basic state $|0\rangle$ by $\langle A^i_a|0\rangle = 1$, fully independent of the connection. A basis of states is obtained by using holonomies as creation operators, which in the simplified U(1)-example (where $h_e = \exp(i\int_e \mathrm{d}t\dot{e}^a A_a)$) can be written as

$$|e_1, n_1; \ldots; e_I, n_I\rangle = \hat{h}^{n_1}_{e_1}\cdots\hat{h}^{n_I}_{e_I}|0\rangle\,.$$

Similar, though more tedious formulas apply for the SU(2)-case of quantum gravity, whose states can be expanded in terms of spin networks [8]. A general state is labeled by a graph g with integers n_e as quantum numbers on its edges e:

$$\psi_{g,n}(A_a) = \prod_{e\in g} h_e(A_a)^{n_e} = \prod_{e\in g}\exp(in_e\int_e \mathrm{d}t\dot{e}^a A_a)\,.$$

Holonomies h_I create quantum-gravity states by excitations of two types. (i) one can use operators several times for the same curve, or (ii) use different curves. In this way, an irregular lattice, or spin network, arises which intuitively can be seen as the microscopic structure of space. For a macroscopic geometry, a dense mesh, or strong excitations of the quantum gravity state, are necessary; in order to model near-continuum geometries for which general relativity may approximately apply, one has to consider "many-particle" states.

In order to extract geometrical notions from the visualization of states, operators representing the densitized triad must be introduced. From the densitized triad, the spatial metric and then usual geometrical quantities result [9–11]. As we had to integrate the connection along curves to obtain holonomies, the densitized triad must be integrated 2-dimensionally in order to obtain well-defined operators: the fluxes $\int_S \mathrm{d}^2y E^a N_a$ integrated over spatial surfaces S with the metric-independent co-normal N_a (again

written here for the U(1)-simplification). Obtained from momenta conjugate to the connection, fluxes are quantized to derivative operators. Their specific action shows that they measure the excitation level of a state along edges intersecting the surface:

$$\int_S \mathrm{d}^2y N_a \hat{E}^a \psi_{g,n} = 8\pi\gamma G \int_S \mathrm{d}^2y N_a \frac{\hbar}{i}\frac{\delta\psi_{g,n}}{\delta A_a(y)} = 8\pi\gamma\ell_{\mathrm{P}}^2 \sum_{e\in g} n_e \mathrm{Int}(S,e)\psi_{g,n}$$

with the intersection number $\mathrm{Int}(S,e)$ and the Planck length $\ell_{\mathrm{P}} = \sqrt{G\hbar}$. This is an eigenvalue equation with discrete eigenvalues read off as $8\pi\gamma\ell_{\mathrm{P}}^2 \sum_{e\in g} n_e \mathrm{Int}(S,e)$, and so spatial geometry, represented by the fluxes, is discrete in this framework. The graphs obtained from elementary excitations represent the atomic nature of space, and geometry results from intersections.

In order to see how discrete spatial structures of this kind evolve, dynamics must be introduced. For gravity, this is determined by the Hamiltonian constraint, the phase space functional

$$C_{\mathrm{grav}}[N] = \frac{1}{16\pi\gamma G}\int_\Sigma \mathrm{d}^3x N \left(\epsilon_{ijk}F^i_{ab}\frac{E^a_jE^b_k}{\sqrt{|\det E|}} - 2(1+\gamma^{-2})(A^i_a-\Gamma^i_a)(A^j_b-\Gamma^j_b)\frac{E^{[a}_iE^{b]}_j}{\sqrt{|\det E|}}\right)$$

in Ashtekar variables. In addition to the fields already introduced, we use the curvature F^i_{ab} of A^i_a and the lapse function N. As a constraint, $C_{\mathrm{grav}}[N]$ must vanish for all choices of N.

There are several apparent obstacles in turning this expression into an operator, using the basic holonomies and fluxes. First, an inverse determinant of the densitized triad is required but seems problematic at the operator level, where fluxes, with discrete spectra containing zero, lack densely-defined inverse operators. Nevertheless, as shown by [12], the quantity needed can be obtained from a relation such as

$$\left\{A^i_a, \int\sqrt{|\det E|}\mathrm{d}^3x\right\} = 2\pi\gamma G\epsilon^{ijk}\epsilon_{abc}\frac{E^b_jE^c_k}{\sqrt{|\det E|}} \tag{2}$$

whose left-hand side is free of inverses. The volume operator, made from fluxes, can be used for $\int\sqrt{|\det E|}\mathrm{d}^3x$, A^i_a can be expressed in terms of holonomies, and the Poisson bracket is finally turned into a commutator divided by $i\hbar$.

Similarly, the curvature components F^i_{ab} of the Ashtekar connection can be expressed in terms of holonomies using identities such as $s^a_1s^b_2F^i_{ab}\tau_i = \Delta^{-1}(h_\lambda - 1) + O(\Delta)$, where λ is a square loop of small coordinate area Δ, with tangent vectors s^a_I at one of its corners. Finally, extrinsic curvature components $K^i_a = \gamma^{-1}(A^i_a - \Gamma^i_a)$, the most complex expressions in the Hamiltonian constraint owing to the spin connection (1) as a functional of the densitized triad, can be obtained from what has already been constructed:

$$K^i_a = \gamma^{-1}(A^i_a-\Gamma^i_a) \propto \left\{A^i_a, \left\{\int \mathrm{d}^3x F^i_{ab}\frac{\epsilon^{ijk}E^a_jE^b_k}{\sqrt{|\det E|}}, \int\sqrt{|\det E|}\mathrm{d}^3x\right\}\right\}.$$

In this way, a well-defined class of Hamiltonian constraint operators arises, parameterized by certain ambiguities as they arise in the choices to be made. Examples for ambiguities are the exact rewriting of the inverse determinant, or routings and representations for the holonomies used. In spite of ambiguities, several characteristic properties can be extracted and evaluated phenomenologically. In particular, there are three main sources of quantum corrections:

- Inverse volume corrections arise from quantizing the inverse triad determinant in an indirect manner. Comparing eigenvalues of the resulting operators quantizing the left hand side of (2) with the expressions expected from simply inserting flux eigenvalues into the right hand side of (2) shows strong deviations for small flux scales; see Fig. 1

- Higher order corrections result from the use of holonomies, contributing higher powers of the connection components.

- As in any interacting quantum field theory, quantum back-reaction results from the influence of quantum variables such as fluctuations, correlations or higher moments of a state on the expectation values. These variables provide extra degrees of freedom, which can sometimes be interpreted in the sense of higher derivative terms.

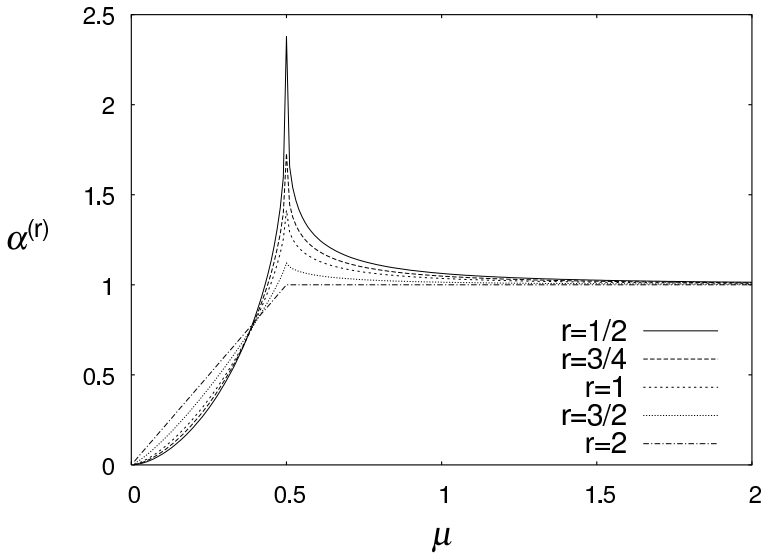

Figure 1: Inverse triad correction function, depending on an ambiguity parameter r. All curves approach the classical expectation one from above for large flux values μ. (See [13, 14] for explicit derivations of correction functions.)

A simplified form of the Hamiltonian, as it arises from the general constructions of [12, 15], is

$$\hat{C}_{\rm grav}[N] = \frac{i}{16\pi\gamma G\hbar} \sum_{v,IJK} N(v) \sum_{\sigma_I\in\{\pm 1\}} \sigma_1\sigma_2\sigma_3\epsilon^{IJK} {\rm tr}(h_{v,I}h_{v+I,J}h^{-1}_{v+J,I}h^{-1}_{v,J}h_{v,K}[h^{-1}_{v,K},\hat{V}]) \qquad (3)$$

of interacting form: excitations of geometry take place dynamically by the factors of holonomy operators included in the expression. All this depends on the spatial geometry through the volume operator $\hat{V}$. The discreteness contained in the resulting dynamics is significant at high densities (such as the big bang), or if many small corrections add up in a large universe (for dark energy, perhaps).

3 Loop quantum cosmology

In full generality, it is difficult to analyze the dynamics of quantum gravity, but several results are known in model systems (based on symmetry reduction or perturbative inhomogeneities). One can easily imagine simplifications from the considerable reduction of the number of degrees of freedom, but also from another effect: level-splitting, well-known from energy spectra of atoms and molecules. Also in quantum geometry, levels split when symmetries are relaxed, making spectra of symmetric situations much simpler than non-symmetric ones. In particular, the volume spectrum, which despite significant numerical progress [16, 17] is rather difficult to compute in the full case, splits when symmetry is relaxed from homogeneity to spherical symmetry as shown in Fig. 2. The most highly symmetric systems should then the easiest to analyze, also concerning the dynamics. This is the realm of quantum cosmology.

Loop quantum cosmology [19] provides a quantization of symmetry reduced models by the techniques of loop quantum gravity. Many of its ingredients, in particular its states and basic operators, can be induced from the full holonomy-flux algebra [20–24] or by other means [25, 26]; in this sense loop quantum cosmology is a sector of (kinematical) loop quantum gravity. Just the dynamics, which is problematic and not yet in a settled stage even in the full theory, is too complicated to be reduced directly from a full Hamiltonian constraint such as (3). In formulating the dynamics, based on the basic operators, additional assumptions and extra input are sometimes required and cannot yet be derived from the full theory. This may introduce an amount of ambiguity larger than that already realized in the full theory.

Hamiltonian isotropic cosmology in Ashtekar variables (here written only for spatially flat models), has the basic phase space variables $A^i_a = c\delta^i_a$ with $c = \gamma\dot{a}$, $E^a_i = p\delta^a_i$ with $|p| = a^2$. (For a triad

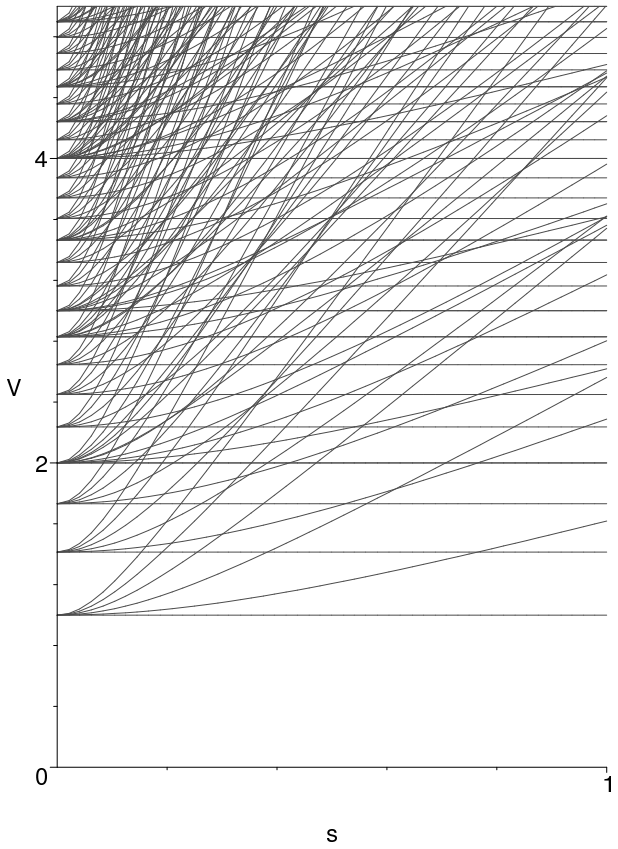

Figure 2: Level splitting of volume eigenvalues as a symmetry parameter s is tuned from zero (homogeneity) to one (spherical symmetry); see [18] for details.

with the option of two different orientations, p can take both signs; see [27] for details of the classical reduction.) The coefficients c of an isotropic connection and p of an isotropic triad are canonically conjugate: $\{c,p\} = 8\pi\gamma G/3$. Inserting these reductions into the full Hamiltonian constaint provides

$$C := -\frac{c^2\sqrt{|p|}}{\gamma^2} + \frac{8\pi G}{3} H_{\rm matter} = 0$$

as the isotropic constraint equation, equivalent to the Friedmann equation. (For homogeneous cosmology, the lapse function N must be spatially constant, thus providing a single constraint function.) The gauge-flow in time, $\dot{p} = \{p, C\}$ and $\dot{c} = \{c, C\}$, generated by the constraint amounts to the Raychaudhuri equation.

In loop quantum cosmology, just as in Wheeler–DeWitt quantum cosmology [28, 29], the constraint is quantized to an operator annihilating physical states: $\hat{C}|\psi\rangle = 0$. In contrast to the Wheeler–DeWitt representation, however, the use of $\exp(i\delta c)$ for c — matrix elements of holonomies as required for a background-independent representation — makes us regularize the constraint before it can be quantized. For instance, with an ambiguity parameter δ (which can and often should be allowed to be a phase-space function; see Sec. 5) we may write

$$-\frac{\sin^2(\delta c)\sqrt{|p|}}{\gamma^2\delta^2} + \frac{8\pi G}{3} H_{\rm matter} = 0 \tag{4}$$

as an expression that agrees very well with the classical one for small curvature ($\delta c \ll 1$) and at the same time is quantizable in terms of holonomies. Effects of such a modification easily trickle down to low-curvature equations [30, 31].

Replacing connection components by matrix elements of holonomies constitutes a regularization[2] motivated from quantum geometry via background independence; it is not in itself a quantum effect even if, as sometimes done in improvised versions, δ is related to $\hbar$ or $\ell_{\rm P}$ by further ad-hoc arguments. Indeed, in a systematic derivation of effective equations describing loop quantum cosmology, (4) is recognized simply as the pure tree-level contribution where all quantum corrections vanish [36, 37]; see also [38, 39] for discussions of the regularization. Although care must always be exercised, using just the regularization allows one to explore the potential consequences of quantum gravity. The regularization is, of course, easy to implement in exactly homogeneous models, and it is far from being unique. The real issues to be faced arise when one tries to extend the regularization to inhomogeneous situations, at least of perturbative nature, in which extremely tight constraints due to covariance arise. Consistent implementations may strongly reduce the ambiguities — and possibly eliminate effects seen in simple homogeneous models. Such issues related to inhomogeneity will be discussed in more detail in Sec. 6.

An immediate implication of using holonomies is that the constraint equation is not differential, but a difference equation for a wave function of the universe [27, 40]. Writing $\hat{C}|\psi\rangle = 0$ for a state $|\psi\rangle = \sum_\mu \psi_\mu(\phi)|\mu\rangle$ expanded in triad eigenstates $|\mu\rangle$ (with an extra collective label ϕ for matter fields) requires the coefficients $\psi_\mu(\phi)$ to satisfy

$$C_+(\mu)\psi_{\mu+\delta}(\phi) - C_0(\mu)\psi_\mu(\phi) + C_-(\mu)\psi_{\mu-\delta}(\phi) = \hat{H}_\phi(\mu)\psi_\mu(\phi)\,. \tag{5}$$

All coefficients of this equation can be derived, but are not fixed uniquely owing to the non-uniqueness of the Hamiltonian constraint operator. Nonetheless, several qualitative properties, insensitive to ambiguities, have been found. The left-hand side quantizes the gravitational contribution to the constraint and shows the discreteness, while the right-hand side shows what role is played by the matter Hamiltonian $\hat{H}_\phi$. If we view the size variable μ as an "internal time," evolution proceeds discretely.

Loop quantum cosmology is non-singular [41]: any wave function evolves uniquely across the classical singularity (situated at $\mu = 0$). Quantum hyperbolicity [42] of this form has been realized not only in isotropic models, but also in anisotropic ones [43, 44] and even in some inhomogeneous situations such as spherical symmetry [45]. Physically, one may explain this phenomenon by a limited storage for energy provided in a discrete space-time: Quantum waves must now be supported on a discrete lattice, providing a natural cut-off for wave-lengths. Dynamically, a repulsive force arises once energy densities become too large, counter-acting the classical attraction and preventing singularities.

In simple models in which also the matter content is severely restricted by being close to a free, massless scalar — resulting in an exactly solvable, harmonic model as shown below —, numerical [46] and exact solutions [36] indeed show that the expectation value of the scale factor bounces, reaching a non-zero minimum value. This geometrical picture is, however, not available in strong quantum regimes in which several of the quantum variables matter: a state changes considerably as the big bang is approached or traversed, a dynamical behavior which can no longer be formulated just in terms of the classical variables of geometry (solely the scale factor in isotropic cosmology). To handle such situations, effective equations are useful.

4 Effective equations

To illustrate the derivation of effective equations in canonical quantum systems we start with a simple example from quantum mechanics: the harmonic oscillator. Its dynamics is defined by the closed, linear algebra

$$[\hat{q},\hat{p}] = i\hbar \quad , \quad [\hat{q},\hat{H}] = i\hbar\frac{\hat{p}}{m} \quad , \quad [\hat{p},\hat{H}] = -i\hbar m\omega^2\hat{q}$$

of basic operators and the Hamiltonian $\hat{H}$. Any quantum system with such a closed and linear algebra has dynamical solutions whose wave functions may spread, but do so without disturbing the mean position.

[2] Some models — including cosmological ones with specific matter contents [32], parameterized free particle field theories [33, 34] and certain dilaton gravity models [35] — can be quantized by loop quantization techniques without requiring any regularization of their Hamiltonians or constraints. If such quantizations could be performed in general, they would be strongly preferred. Generic models, however, suggest that regularization, and thus a role of quantum geometry effects for the quantum space-time dynamics, cannot be avoided completely.

Indeed, a closed set of equations results for expectation values of $\hat{q}$ and $\hat{p}$ via $\mathrm{d}\langle\hat{O}\rangle/\mathrm{d}t = \langle[\hat{O},\hat{H}]\rangle/i\hbar$. To solve these equations, we need not know how fluctuations, correlations or higher moments of the state behave; there is no quantum back-reaction. Similarly, there is a closed set of equations just for the fluctuations and correlations, without coupling to moments of higher than second order.

A similarly solvable system exists in loop quantum cosmology [36, 47], with the conditions of an isotropic, spatially flat space and matter given by a free, massless scalar ϕ. Using the loop-quantized Hamiltonian (in a particular factor ordering and ignoring inverse volume corrections at this stage) again produces a closed algebra of basic variables, provided we choose them as the volume V (or, more generally, $|p|^{1-x}$ to absorb any p-dependence of δ provided it is a power-law $\delta(p) = \delta_0|p|^x$) and the holonomy-related quantity $J = V\exp(i\delta_0 P)$ with the Hubble parameter P (or $|p|^x c$) conjugate to V. This time, using the Hamiltonian $p_\phi \propto h := \mathrm{Im}J$ with respect to evolution in ϕ as internal time, as it follows from the regularized Hamiltonian (4) with $H_{\mathrm{matter}} = p_\phi^2/2a^3$, the algebra is $\mathrm{sl}(2,\mathbb{R})$:

$$[\hat{V},\hat{J}] = -\delta_0\hbar\hat{J} \quad , \quad [\hat{V},\hat{h}] = \tfrac{1}{2}i\delta_0\hbar(\hat{J}+\hat{J}^\dagger) \quad , \quad [\hat{J},\hat{h}] = i\delta_0\hbar\hat{V}\,.$$

(The Hamiltonian constraint for a free, massless scalar field can be written as $p_\phi^2 - VC_{\mathrm{grav}} = 0$, and easily be deparameterized. One is taking a square root in the process to solve for p_ϕ, but this does not spoil the linearity of the dynamics of states just required to be semiclasical once [47]. Alternatively, direct treatments of effective constraints, avoiding deparameterization, are available [48–50].)

Equations of motion

$$\frac{\mathrm{d}\langle\hat{O}\rangle}{\mathrm{d}\phi} = \frac{\langle[\hat{O},\hat{h}]\rangle}{i\hbar}$$

generated with respect to ϕ now provide the behavior of physical observables: There is no absolute time in this fully constrained system; instead, change is measured by relational observables, such as $\langle\hat{V}\rangle(\phi)$ between the degrees of freedom. (For a complete reduction to physical quantities, reality conditions must be imposed to ensure the correct adjointness properties for a quantization of the real P appearing in the complex J. Appropriate conditions turn out to be easily formulated, relating expectation values to fluctuations and correlations [47].) Also here, there is no quantum back-reaction in the solvable model. Fluctuations do not back-react on the expectation values, which results in simple, cosh-like solutions for the volume; see Fig. 3. Clearly, the volume never becomes zero, and the singularity, of these specific models, is replaced by a bounce. While the expectation value follows its trajectory undisturbed, states in general do spread. In particular, squeezed states (with non-vanishing correlations) describe oscillating fluctuations between different universe phases, expansion and collapse. As it turns out, fluctuations can change by an order of magnitude even in dynamical coherent states — the most strongly controlled type of states —, and this change is very sensitive to initial values. This cosmic forgetfulness makes it difficult to estimate specific quantities in the pre-bounce phase for realistic models [51, 52].

Generic models are more complicated since they are subject to quantum back-reaction. To illustrate this, we consider a model with a cosmological constant, but ignore the quantum geometry corrections of loop quantum cosmology for the sake of simplicity. The Hamiltonian for ϕ-evolution, as treated for a negative cosmological constant in [53], then is $p_\phi \propto V\sqrt{P^2-\Lambda} =: h(V,P)$. (The same system was analyzed numerically in [54].) Now, expectation values couple to fluctuations and other moments:

$$\begin{aligned}
\frac{\mathrm{d}\langle\hat{V}\rangle}{\mathrm{d}\phi} &= \frac{3}{2}\frac{\langle\hat{V}\rangle\langle\hat{P}\rangle}{\sqrt{\langle\hat{P}\rangle^2-\Lambda}} + \frac{9}{4}\Lambda\frac{\langle\hat{V}\rangle\langle\hat{P}\rangle}{(\langle\hat{P}\rangle^2-\Lambda)^{5/2}}(\Delta P)^2 - \frac{3}{2}\Lambda\frac{C_{VP}}{(\langle\hat{P}\rangle^2-\Lambda)^{3/2}} + \cdots\\
\frac{\mathrm{d}\langle\hat{P}\rangle}{\mathrm{d}\phi} &= -\frac{3}{2}\sqrt{\langle\hat{P}\rangle^2-\Lambda} + \frac{3}{4}\Lambda\frac{(\Delta P)^2}{(\langle\hat{P}\rangle^2-\Lambda)^{3/2}} + \cdots
\end{aligned}$$

with the $\hat{P}$-fluctuation ΔP and the covariance $C_{VP} = \frac{1}{2}\langle\hat{V}\hat{P}+\hat{P}\hat{V}\rangle - \langle\hat{V}\rangle\langle\hat{P}\rangle$. Fluctuations are dynamical,

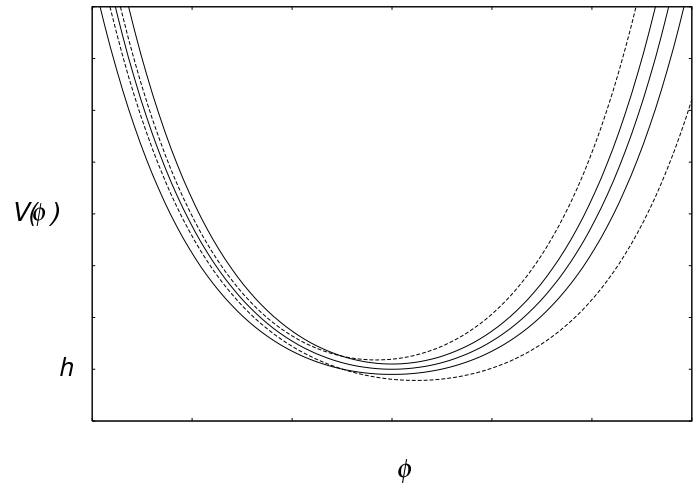

Figure 3: Bouncing solutions of the exactly solvable model of loop quantum cosmology, showing the expectation value of the physical observable $\langle\hat{V}\rangle(\phi)$, as well as the spread $\Delta V(\phi)$of a physical wave function. The label "h" indicates the size of the (conserved) ϕ-Hamiltonian, which determines the volume at the bounce.

too:

$$\begin{aligned}
\frac{\mathrm{d}(\Delta P)^2}{\mathrm{d}\phi} &= -3\frac{\langle\hat{P}\rangle}{\sqrt{\langle\hat{P}\rangle^2-\Lambda}}(\Delta P)^2+\cdots\\
\frac{\mathrm{d}C_{VP}}{\mathrm{d}\phi} &= -\frac{3}{2}\Lambda\frac{\langle\hat{V}\rangle}{(\langle\hat{P}\rangle^2-\Lambda)^{3/2}}(\Delta P)^2+\cdots\\
\frac{\mathrm{d}(\Delta V)^2}{\mathrm{d}\phi} &= -3\Lambda\frac{\langle\hat{V}\rangle}{(\langle\hat{P}\rangle^2-\Lambda)^{3/2}}C_{VP}+3\frac{\langle\hat{P}\rangle}{\sqrt{\langle\hat{P}\rangle^2-\Lambda}}(\Delta V)^2+\cdots.
\end{aligned}$$

(In all these equations, dots indicate that higher order moments have been ignored here.)

Analyzing coupled equations like this is the canonical procedure for effective equations. (For anharmonic oscillators in quantum mechanics, employing a semiclassical as well as an adiabatic approximation, the usual low-energy effective action is reproduced [55, 56].) Often, higher moments can be ignored in certain regimes, starting with a semiclassical state whose moments of order n are suppressed by a factor of $\hbar^{n/2}$. But long evolution, as is prevalent in cosmology, can drastically change a state even if it starts out semiclassically to a high degree. Moments may then grow, and higher ones will become important. Severe quantum back-reaction effects can be expected, especially in the infamously strong quantum regime around the big bang. But also other regimes exist where large moments are perhaps more surprising. One example is that of the large-volume regime of models with a positive cosmological constant. As can be seen from the preceding equations, several of the coefficients then have denominators that can come close to zero when the curvature scale squared approaches the cosmological constant. For a small, perhaps realistic, cosmological constant, this regime is approached at large volume, where moments can grow large despite the classical appearance of the phase.

The back-reaction equations of loop quantum cosmology are much more lengthy [57], but can be summarized in a quantum Friedmann equation including the effects from holonomy corrections and quantum back-reaction [58, 59]. With a scalar mass or a self-interacting potential, the equation

$$\left(\frac{\dot{a}}{a}\right)^2=\frac{8\pi G}{3}\left(\rho\left(1-\frac{\rho_Q}{\rho_{\mathrm{crit}}}\right)\pm\frac{1}{2}\sqrt{1-\frac{\rho_Q}{\rho_{\mathrm{crit}}}}\eta(\rho-P)+\frac{(\rho-P)^2}{(\rho+P)^2}\eta^2\right) \tag{6}$$

describes the evolution of the scale factor's expectation value. Compared to the classical equation,

pressure P enters, as well as η which parameterizes quantum correlations. Moreover,

$$\rho_Q := \rho + \epsilon_0\rho_{\rm crit} + (\rho - P)\sum_{k=0}^{\infty}\epsilon_{k+1}(\rho - P)^k/(\rho + P)^k$$

is an expression for a quantum corrected energy density with fluctuation parameters ϵ_k, and $\rho_{\rm crit} = 3/8\pi G(a\delta)^2$ is a critical density with scale $a\delta$ as determined by the δ used in the regularization (4) by holonomies. The critical density is constant only if $\delta \propto a^{-1}$ (a special case introduced in [60]). The behavior following from this equation is simple if $\rho = p$ (the free, massless scalar case) or if $\rho + p$ is large (large p_ϕ, or kinetic domination). Then, solutions with $\dot{a} = 0$ exist near $\rho = \rho_{\rm crit}$, producing a bounce.

For regimes not of kinetic domination, the behavior of many moments, contained in η and ρ_Q, must be known for a precise picture, requiring a long analysis still to be completed. Only such an analysis can show what effective geometrical picture corresponds to the general singularity avoidence by the difference equation of loop quantum cosmology. In particular, it has *not* been shown that loop quantum cosmology generically replaces the big bang singularity by a bounce.

Currently, all existing indications for bounces — numerical as in [61, 62] or analytic as in [58] — exist only for kinetic-dominated regimes of a scalar matter source. The situation is slightly more general for demonstrating an upper bound of energy density, but such a statement is weaker than showing the existence of bouncing solutions. (Bounces can easily be produced quite generally even in potential-dominated regimes using the tree-level approximation of loop quantum cosmology. However, the tree-level approximation itself does not appear reliable in potential-dominated regimes.)

5 Lattice refinement

Loop quantum cosmology aims to model the dynamical behavior of loop quantum gravity in a tractable manner. Since no procedure is known for a complete reduction of the Hamiltonian constraint to isotropy or homogeneity, several choices are to be made in specifying the Hamiltonian constraint of loop quantum cosmology, giving rise to the difference equation (5). One such freedom concerns the parameter δ in (4), which may be a phase-space function as alluded to above.

This function carries important information about the reduction [21, 63]. It appears as a coefficient of the connection component in holonomies as used for the dynamics. If we look at the schematic full constraint of (3), it is clear that holonomies in that operator refer to edges in one of the graph states, as it evolves according to the dynamics of loop quantum gravity. Reducing such a holonomy to isotropic variables leads to an expression of the form $\exp(i\delta c)$, exactly as used in the reduced constraint. In the reduced model, δ appears as a parameter which can only be chosen by hand to have a specific value; no argument has been found to fix it. In the full context, on the other hand, δ is clearly related to the coordinate length of the edge used, and thus refers to the underlying inhomogeneous state. (Although δ is coordinate dependent, the combination $\delta c = \gamma\delta\dot{a}$ appearing in holonomies is not.) In the reduction to homogeneity, that information in the state is lost; one can only bring it back by making certain phenomenological choices for δ.

The underlying inhomogeneous state is dynamical: new edges may be created or old ones removed. Edge lengths change, and so does δ. One way to model this in an isotropic description is to allow δ to depend on the scale factor a, implying that the underlying inhomogeneous state changes as the universe expands or contracts. By analyzing the resulting models, phenomenological restrictions for the behavior of δ can be found [64–66]. What is so far indicated is that a power-law form of $\delta = \delta_0|p|^x$ works best for x near $-1/2$.

Lattice refinement has been formulated in a parameterized way for anisotropic models, also at the level of underlying difference equations. Compared to isotropic models, the difference equations then generically become non-equidistant, complicating an analysis. A complete formulation of the dynamics (avoiding ad-hoc assumptions), especially for the Schwarzschild interior but also providing Misner-type variables for Bianchi models, has been provided in [67]. Numerical tools to evaluate non-equidistant difference equations have been introduced in [68, 69].

6 Cosmology

With matter interactions and inhomogeneities, a complicated form of back-reaction results that can be handled only by a systematic perturbation theory around the solvable model. The solvable model of loop quantum cosmology then plays the same role as free quantum field theories do for the Feynman expansion. An analysis of this form can show possible indirect effects of the atomic space-time where individual corrections which are small even at high energies might add up coherently. If this magnification effect is strong enough, one might come close to observability. Two prime examples exist: cosmology, which is a high energy density regime with long evolution times for corrections to add up; and high energy particles from distant sources.

But before one analyzes complete equations — those containing all possible quantum corrections for possible physical consequences — there is an interesting geometrical set of problems related to general covariance. Compared to homogeneous models, where modifications such as those in (4) can consistently be implemented at will, general covariance in inhomogeneous situations is a strong consistency requirement. For instance, the contracted Bianchi identity $\nabla_\mu G^\mu_\nu = 0$ implies $\partial_0 G^0_\mu = -\partial_a G^a_\mu - \Gamma^\nu_{\nu\kappa} G^\kappa_\mu + \Gamma^\kappa_{\mu\nu} G^\nu_\kappa$. The right-hand side is at most of second order in time derivatives, and so G^0_μ must be of first order. The corresponding components of Einstein's equation provide constraints for initial values rather than evolution equations: the Hamiltonian constraint

$$C[N] = \int \mathrm{d}^3x N(x)\sqrt{\det q}(G^0_0 - 8\pi G T^0_0) = 0 \tag{7}$$

(with the spatial metric tensor q_{ab} used in the integration measure) and the diffeomorphism constraint

$$D[N^a] = \int \mathrm{d}^3x N^a(x)\sqrt{\det q}(G^0_a - 8\pi G T^0_a) = 0 \tag{8}$$

where q_{ab} is again the spatial metric. The constraints must be preserved under the second order equations that follow from the spatial components G^a_b.

This kind of conservation law leads to symmetries: The constraints satisfy a closed algebra

$$\begin{aligned} \{D[N^a], D[M^a]\} &= D[\mathcal{L}_{M^a} N^a] \\ \{C[N], D[M^a]\} &= C[\mathcal{L}_{M^a} N] \\ \{C[N], C[M]\} &= D[q^{ab}(N\partial_b M - M\partial_b N)] \end{aligned}$$

as the generators of gauge transformations. Importantly, this algebra is first class: Poisson brackets of the constraints vanish when the constraints are imposed. On the solution space, constraints are invariant under the flow they generate, and thus provide gauge-invariant equations. In the case of gravity, the combination $C[N] + D[N^a]$ generates infinitesimal space-time diffeomorphism along $\xi^\mu = (N, N^a)$, as can be checked by a direct calculation and comparison with Lie derivatives. General covariance can be expressed fully in terms of this algebra, as emphasized by Dirac [70]:

> "It would be permissible to look upon the Hamiltonian form as the fundamental one, and there would then be no fundamental four-dimensional symmetry in the theory.
>
> The usual requirement of four-dimensional symmetry in physical laws would then get replaced by the requirement that the functions have weakly vanishing [Poisson brackets]."

Such a viewpoint is convenient especially in canonical quantum gravity. It is not guaranteed that quantization preserves the usual space-time or differential-geometric notions, and that it leads to the same relationship between symmetries and Lie derivatives. In contrast to differential geometry, an algebra of constraints, which will become a commutator algebra of the corresponding operators, can directly be carried over to the quantum theory. In this way, the realization of symmetries, and correspondingly of space-time structures, can be tested at the quantum level. Quantum corrections usually change the constraints as gauge generators and may thus lead to changes in the space-time structures. Also the algebra of constraints may be corrected, but for a consistent formulation, corrections must respect the first-class nature of the algebra. If the first-class nature is respected, symmetries may be deformed but are not lost; the quantum system is then called anomaly-free.

"Effective" constraints, including some of the corrections from quantum geometry (in this case inverse volume corrections), can be made anomaly-free [71]:

$$\begin{aligned}\{D[N^a], D[M^a]\} &= D[\mathcal{L}_{M^a} N^a]\\ \{C_{(\alpha)}[N], D[M^a]\} &= C_{(\alpha)}[\mathcal{L}_{M^a} N]\\ \{C_{(\alpha)}[N], C_{(\alpha)}[M]\} &= D[\alpha^2 q^{ab}(N\partial_b M - M\partial_b N)]\end{aligned}$$

where α is the correction function from inverse volume operators. This algebra is indeed first class, but deformed. To interpret the corrections, we first note that in an effective action they cannot be purely of higher curvature type, for such corrections would still produce the classical algebra [72]. We are thus dealing with a more general type of effective action (such as one on a non-commutative space-time). Similar deformations have been constructed for holonomy corrections, although not for the complete case of cosmological perturbations. The first example was found for spherically symmetric models [73] (see also [74, 75]), with a similar form produced for $2+1$-dimensional gravity [76]. (Although the deformations in those two cases are quite similar, there is a difference in that the $2+1$-example requires a non-vanishing cosmological constant for the deformation to appear. This circumstance may just be a consequence of the special form of $2+1$-dimensional gravity in the formulation used, where the theory without a cosmological constant has vanishing on-shell curvature and is topological.) Constructing consistent deformations corresponding to quantum geometry corrections is the non-trivial part of an analysis making simple modifications such as (4) relevant.

Practically, one consequence of the deformation is that the potential size of quantum corrections is larger than often expected, that is larger than $\ell_{\rm P}\mathcal{H}$ as higher curvature terms would produce it in cosmological situations. The main physical mechanism is non-conservation of power on large scales, modifying an approximate conservation which classically follows very generally from the conservation of stress-energy, or the Bianchi identity; see e.g. [77–79]. The Bianchi identity, however, takes a different form for the corrected constraint algebra, and so quantum corrections affect large-scale modes, removing the constant one [80, 81]. Local corrections for the slope of increase or decrease of super-Hubble power, for scalar and tensor modes, are small, but realized during long evolution times. They may add up to sizeable effects.

Explicitly, the resulting cosmological perturbation equations (for all scales on a background Friedmann–Robertson–Walker space-time with conformal Hubble rate $\mathcal{H}$ and the background scalar $\bar{\varphi}$) are [81]

$$\partial_c\left(\dot{\Psi} + \mathcal{H}(1+f)\Phi\right) = 4\pi G\frac{\bar{\alpha}}{\bar{\nu}}\dot{\bar{\varphi}}\partial_c\delta\varphi \tag{9}$$

from the diffeomorphism constraint,

$$\Delta(\bar{\alpha}^2\Psi) - 3\mathcal{H}(1+f)\left(\dot{\Psi} + \mathcal{H}\Phi(1+f)\right) = 4\pi G\frac{\bar{\alpha}}{\bar{\nu}}(1+f_3)\left(\dot{\bar{\varphi}}\delta\dot{\varphi} - \dot{\bar{\varphi}}^2(1+f_1)\Phi + \bar{\nu}a^2V_{,\varphi}(\bar{\varphi})\delta\varphi\right) \tag{10}$$

from the Hamiltonian constraint, and

$$\begin{aligned}&\ddot{\Psi} + \mathcal{H}\left(2\dot{\Psi}\left(1 - \frac{a}{2\bar{\alpha}}\frac{\mathrm{d}\bar{\alpha}}{\mathrm{d}a}\right) + \dot{\Phi}(1+f)\right) + \left(2\dot{\mathcal{H}} + \mathcal{H}^2\left(1 + \frac{a}{2}\frac{\mathrm{d}f}{\mathrm{d}a} - \frac{a}{2\bar{\alpha}}\frac{\mathrm{d}\bar{\alpha}}{\mathrm{d}a}\right)\right)\Phi(1+f)\\ =\ & 4\pi G\frac{\bar{\alpha}}{\bar{\nu}}\left(\dot{\bar{\varphi}}\delta\dot{\varphi} - a^2\bar{\nu}V_{,\varphi}(\bar{\varphi})\delta\varphi\right)\end{aligned} \tag{11}$$

as the evolution equation. These equations are accompanied by $\Phi = (1+h)\Psi$, which follows from off-diagonal components of the corrected Einstein equation, and a corrected Klein–Gordon equation for $\delta\varphi$. In addition to the gauge-invariant metric perturbations Φ and Ψ and the scalar perturbation $\delta\varphi$ as well as the primary correction function $\bar{\alpha}$ from inverse volume (and $\bar{\nu}$ for the matter term), several other corrections, f, f_1, f_3, h arise, but are related to the primary correction.

The consistency issue now becomes a very practical problem: There are five equations for three free functions, Φ, Ψ and $\delta\varphi$. Classically the system is consistent and not overdetermined thanks to general covariance. But will this closure of the equations be preserved in the presence of quantum corrections from discrete geometry? As indicated by the possibility of a first-class (but deformed) algebra of constraints,

consistency can be realized. There are no anomalies (checked to linear order in perturbations in [71]) if the quantum correction functions satisfy equations such as

$$-h - f + \frac{a}{\bar{\alpha}}\frac{\partial\bar{\alpha}}{\partial a} = 0 \quad , \quad 3f - 2a\frac{\partial f}{\partial a} - \frac{a}{\bar{\alpha}}\frac{\partial\bar{\alpha}}{\partial a} = 0$$
$$\frac{1}{6}\frac{\partial\bar{\alpha}}{\partial a}\frac{\delta E^c_j}{a^3} + \frac{\partial\alpha^{(2)}}{\partial(\delta E^a_i)}(\delta^a_j\delta^c_i - \delta^c_j\delta^a_i) = 0\,.$$

The last of these equation relates higher perturbative orders of α to the background value $\bar{\alpha}$ achieved for isotropic geometries. If these equations are satisfied, which is possible even in non-classical cases of $\alpha \neq 1$, the whole set of cosmological perturbation equations is consistent. Moreover, all coefficients for quantum corrections are fixed in terms of $\bar{\alpha}$, and this function can be derived in isotropic models (up to ambiguities). Inverse volume corrections, resulting from discrete features of spatial quantum geometry, provide a consistent deformation: The underlying discreteness (for this type of corrections) does not destroy general covariance.

General covariance is a statement about the quantum constraint algebra, and thus can be ensured only by considering perturbation theory without fixing the space-time gauge. After consistent equations have been derived, one may certainly pick a gauge (such as the longitudinal one) if that simplifies calculations. But fixing the gauge before deriving perturbation equations and observables does not verify covariance and can easily lead to spurious effects. Explicit examples can be seen by comparing [82] with [81], the first one with gauge-fixing, the second one without. As turns out, the relationship between the metric perturbations Φ and Ψ is affected by the treatment, as is the precise form of non-conserved power on large scales. Only without gauge-fixing is it possible to ensure consistency; only those results are reliable. When computing the effects of an underlying discrete space-time structure on inflationary structure formation, or on the propagation of modes through a potential bounce, that kind of consistency is especially important. For evolution through a bounce, no consistent form for scalar modes has been found yet; existing treatments all use gauge-fixing [83–85].

One of the implications for cosmological scenarios is that quantum geometry corrections (inverse volume or holonomy) often imply super-inflation at high densities [86]. There may not be many e-foldings in terms of $\log(a_{\rm f}/a_{\rm i})$, referring only to the final and initial values of the scale factor (see Fig. 4), but $\log\left((a\mathcal{H})_{\rm f}/(a\mathcal{H})_{\rm i}\right)$ can be large due to the growth of $\mathcal{H}$ during super-inflation [87]. Viable scenarios thus exist, but the degree of fine-tuning has not yet been fully estimated. Regarding details, several analyses have been performed depending on the scalar potential and quantization ambiguities. Unfortunately, perturbation results are currently on a rather weak basis in strong quantum (or high density) regimes since anomaly-free effective equations are difficult to control. For instance, no consistent evolution of scalar modes through the bounce yet exists. Nevertheless, in weaker regimes some parameters, such as the power-law of a scalar potential, can already be constrained (in [88], using WMAP5 data). At the current stage, primordial gravitational waves [89] are under better analytical control since they are not subject to gauge transformation or overdeterminedness. Some implications for the tensor power spectrum have been evaluated in [64, 90–95].

7 Outlook

Consistent deformations exist in model systems of canonical quantum gravity: discreteness can be realized without spoiling covariance. These results of anomaly freedom show that discrete structures are able to preserve covariance; when realized, they make simple modifications as they are possible in homogeneous models highly non-trivial. So far, this demonstration has been achieved only in relatively tame regimes, but not yet close to the classical big bang singularity, or even through bounce phases.

Examples have been constructed for cosmological perturbations and for black holes. This is mainly based on canonical effective equations, whose tools, analytical as well as numerical ones, are currently being developed. In some cases, these equations already provide a link to cosmological, astrophysical and particle observations. One general result seems to be that the quantum space-time structure is certainly important in high-energy regimes, but, thanks to magnification effects, not necessarily just at the Planck scale. This allows one to set bounds on parameters of quantum space-time, an extensive investigation that is still ongoing.

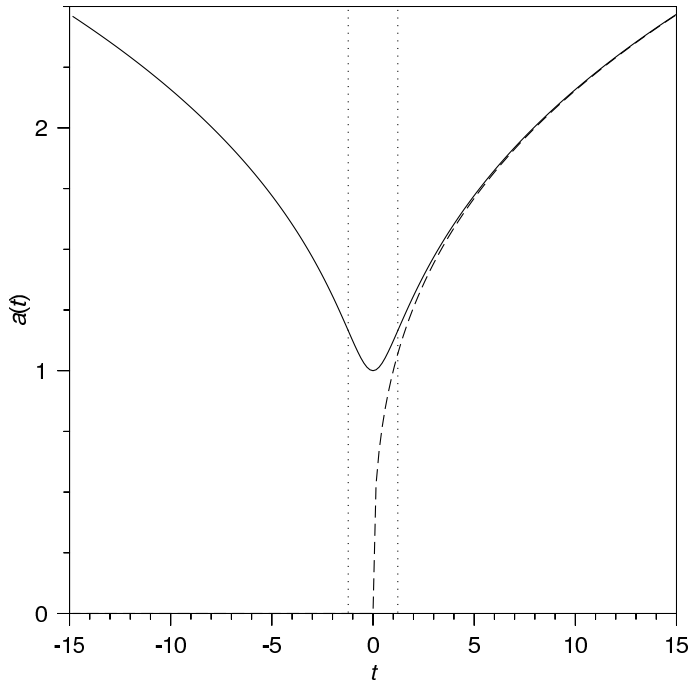

Figure 4: A bouncing scale factor, with super-inflation between the dotted lines (and the singular classical solution as the dashed line). In this phase, the scale factor varies only by a few percent, but $a\mathcal{H}$ changes more. The effective solution corresponds to the solvable model as plotted in Fig. 3, transformed to proper time. Similar solutions have been found in [96] directly in proper time.

Acknowledgements

Work reported here was supported by NSF grant PHY0748336 and a grant from the Foundational Questions Institute (FQXi).

References

[1] A. Ashtekar and J. Lewandowski, Class. Quantum Grav. **21**, R53 (2004), gr-qc/0404018.

[2] C. Rovelli, *Quantum Gravity* (Cambridge University Press, Cambridge, UK, 2004).

[3] T. Thiemann, *Introduction to Modern Canonical Quantum General Relativity* (Cambridge University Press, Cambridge, UK, 2007).

[4] C. Rovelli and L. Smolin, Nucl. Phys. B **331**, 80 (1990).

[5] A. Ashtekar, Phys. Rev. D **36**, 1587 (1987).

[6] J. F. Barbero G., Phys. Rev. D **51**, 5507 (1995), gr-qc/9410014.

[7] G. Immirzi, Class. Quantum Grav. **14**, L177 (1997).

[8] C. Rovelli and L. Smolin, Phys. Rev. D **52**, 5743 (1995).

[9] A. Ashtekar and J. Lewandowski, Class. Quantum Grav. **14**, A55 (1997), gr-qc/9602046.

[10] A. Ashtekar and J. Lewandowski, Adv. Theor. Math. Phys. **1**, 388 (1998), gr-qc/9711031.

[11] C. Rovelli and L. Smolin, Nucl. Phys. B **442**, 593 (1995), gr-qc/9411005, erratum: Nucl. Phys. B **456**, 753 (1995).

[12] T. Thiemann, Class. Quantum Grav. **15**, 839 (1998), gr-qc/9606089.

[13] M. Bojowald, Class. Quantum Grav. **19**, 5113 (2002), gr-qc/0206053.

[14] M. Bojowald, H. Hernández, M. Kagan, and A. Skirzewski, Phys. Rev. D **75**, 064022 (2007), gr-qc/0611112.

[15] C. Rovelli and L. Smolin, Phys. Rev. Lett. **72**, 446 (1994), gr-qc/9308002.

[16] J. Brunnemann and D. Rideout, Class. Quant. Grav. **25**, 065001 (2008), arXiv:0706.0469.

[17] J. Brunnemann and D. Rideout, Class. Quant. Grav. **25**, 065002 (2008), arXiv:0706.0382.

[18] M. Bojowald and R. Swiderski, Class. Quantum Grav. **21**, 4881 (2004), gr-qc/0407018.

[19] M. Bojowald, Living Rev. Relativity **11**, 4 (2008), gr-qc/0601085, `http://www.livingreviews.org/lrr-2008-4`.

[20] M. Bojowald, Class. Quantum Grav. **21**, 3733 (2004), gr-qc/0407017.

[21] M. Bojowald, Gen. Rel. Grav. **38**, 1771 (2006), gr-qc/0609034.

[22] M. Bojowald and H. A. Kastrup, Class. Quantum Grav. **17**, 3009 (2000), hep-th/9907042.

[23] T. Koslowski, (2006), gr-qc/0612138.

[24] T. Koslowski, (2007), arXiv:0711.1098.

[25] J. Engle, Class. Quant. Grav. **23**, 2861 (2006), gr-qc/0511107.

[26] J. Engle, Class. Quantum Grav. **24**, 5777 (2007), gr-qc/0701132.

[27] M. Bojowald, Class. Quantum Grav. **19**, 2717 (2002), gr-qc/0202077.

[28] B. S. DeWitt, Phys. Rev. **160**, 1113 (1967), .

[29] D. L. Wiltshire, in *Cosmology: The Physics of the Universe*, edited by B. Robson, N. Visvanathan, and W. S. Woolcock (World Scientific, Singapore, 1996), pp. 473–531.

[30] G. Date and G. M. Hossain, Class. Quantum Grav. **21**, 4941 (2004), gr-qc/0407073.

[31] K. Banerjee and G. Date, Class. Quant. Grav. **22**, 2017 (2005), gr-qc/0501102.

[32] M. Varadarajan, Class. Quantum Grav. **26**, 085006 (2009), arXiv:0812.0272.

[33] A. Laddha and M. Varadarajan, Phys. Rev. D **78**, 044008 (2008), arXiv:0805.0208.

[34] A. Laddha and M. Varadarajan, arXiv:1001.3505.

[35] A. Laddha, Class. Quant. Grav. **24**, 4969 (2007), arXiv:gr-qc/0606069.

[36] M. Bojowald, Phys. Rev. D **75**, 081301(R) (2007), gr-qc/0608100.

[37] M. Bojowald, Class. Quantum Grav. **26**, 075020 (2009), arXiv:0811.4129.

[38] J. Haro and E. Elizalde, arXiv:0901.2861.

[39] R. Helling, arXiv:0912.3011.

[40] M. Bojowald, Class. Quantum Grav. **18**, 1071 (2001), gr-qc/0008053.

[41] M. Bojowald, Phys. Rev. Lett. **86**, 5227 (2001), gr-qc/0102069.

[42] M. Bojowald, AIP Conf. Proc. **910**, 294 (2007).

[43] M. Bojowald, Class. Quantum Grav. **20**, 2595 (2003), gr-qc/0303073.

[44] M. Bojowald, G. Date, and K. Vandersloot, Class. Quantum Grav. **21**, 1253 (2004), gr-qc/0311004.

[45] M. Bojowald, Phys. Rev. Lett. **95**, 061301 (2005), gr-qc/0506128.

[46] A. Ashtekar, T. Pawlowski, and P. Singh, Phys. Rev. D **73**, 124038 (2006), gr-qc/0604013.

[47] M. Bojowald, Phys. Rev. D **75**, 123512 (2007), gr-qc/0703144.

[48] M. Bojowald, B. Sandhöfer, A. Skirzewski, and A. Tsobanjan, Rev. Math. Phys. **21**, 111 (2009), arXiv:0804.3365.

[49] M. Bojowald and A. Tsobanjan, Phys. Rev. D **80**, 125008 (2009), arXiv:0906.1772.

[50] M. Bojowald and A. Tsobanjan, arXiv:0911.4950.

[51] M. Bojowald, Nature Physics **3**, 523 (2007).

[52] M. Bojowald, Proc. Roy. Soc. A **464**, 2135 (2008), arXiv:0710.4919.

[53] M. Bojowald and R. Tavakol, Phys. Rev. D **78**, 023515 (2008), arXiv:0803.4484.

[54] E. Bentivegna and T. Pawlowski, Phys. Rev. D **77**, 124025 (2008), arXiv:0803.4446.

[55] M. Bojowald and A. Skirzewski, Rev. Math. Phys. **18**, 713 (2006), math-ph/0511043.

[56] M. Bojowald and A. Skirzewski, Int. J. Geom. Meth. Mod. Phys. **4**, 25 (2007), hep-th/0606232.

[57] M. Bojowald, H. Hernández, and A. Skirzewski, Phys. Rev. D **76**, 063511 (2007), arXiv:0706.1057.

[58] M. Bojowald, Phys. Rev. Lett. **100**, 221301 (2008), arXiv:0805.1192.

[59] M. Bojowald, Gen. Rel. Grav. **40**, 2659 (2008), arXiv:0801.4001.

[60] A. Ashtekar, T. Pawlowski, and P. Singh, Phys. Rev. D **74**, 084003 (2006), gr-qc/0607039.

[61] A. Ashtekar, T. Pawlowski, and P. Singh, Phys. Rev. Lett. **96**, 141301 (2006), gr-qc/0602086.

[62] D. Brizuela, G. A. Mena Marugán, and T. Pawlowski, arXiv:0902.0697.

[63] M. Bojowald, Gen. Rel. Grav. **40**, 639 (2008), arXiv:0705.4398.

[64] J. Grain, T. Cailleteau, A. Barrau, and A. Gorecki, (2009), arXiv:0910.2892.

[65] W. Nelson and M. Sakellariadou, Phys. Rev. D **76**, 044015 (2007), arXiv:0706.0179.

[66] W. Nelson and M. Sakellariadou, Phys. Rev. D **76**, 104003 (2007), arXiv:0707.0588.

[67] M. Bojowald, D. Cartin, and G. Khanna, Phys. Rev. D **76**, 064018 (2007), arXiv:0704.1137.

[68] S. Sabharwal and G. Khanna, Class. Quantum Grav. **25**, 085009 (2008), arXiv:0711.2086.

[69] W. Nelson and M. Sakellariadou, Phys. Rev. D **78**, 024030 (2008), arXiv:0803.4483.

[70] P. A. M. Dirac, Proc. Roy. Soc. A **246**, 333 (1958).

[71] M. Bojowald, G. Hossain, M. Kagan, and S. Shankaranarayanan, Phys. Rev. D **78**, 063547 (2008), arXiv:0806.3929.

[72] N. Deruelle, M. Sasaki, Y. Sendouda, and D. Yamauchi, (2009), arXiv:0908.0679.

[73] J. D. Reyes, Ph.D. thesis, The Pennsylvania State University, 2009.

[74] M. Bojowald, T. Harada, and R. Tibrewala, Phys. Rev. D **78**, 064057 (2008), arXiv:0806.2593.

[75] M. Bojowald, J. D. Reyes, and R. Tibrewala, Phys. Rev. D **80**, 084002 (2009), arXiv:0906.4767.

[76] A. Perez and D. Pranzetti, arXiv:1001.3292.

[77] D. S. Salopek and J. R. Bond, Phys. Rev. D **42**, 3936 (1990).

[78] D. Wands, K. A. Malik, D. H. Lyth, and A. R. Liddle, Phys. Rev. D **62**, 043527 (2000), astro-ph/0003278.

[79] E. Bertschinger, Astrophys. J. **648**, 797 (2006), astro-ph/0604485.

[80] M. Bojowald *et al.*, Phys. Rev. Lett. **98**, 031301 (2007), astro-ph/0611685.

[81] M. Bojowald, G. Hossain, M. Kagan, and S. Shankaranarayanan, Phys. Rev. D **79**, 043505 (2009), arXiv:0811.1572.

[82] M. Bojowald *et al.*, Phys. Rev. D **74**, 123512 (2006), gr-qc/0609057.

[83] M. Artymowski, Z. Lalak, and L. Szulc, JCAP **0901**, 004 (2009), arXiv:0807.0160.

[84] J. Mielczarek, (2009), arXiv:0908.4329.

[85] J.-P. Wu and Y. Ling, arXiv:1001.1227.

[86] M. Bojowald, Phys. Rev. Lett. **89**, 261301 (2002), gr-qc/0206054.

[87] E. J. Copeland, D. J. Mulryne, N. J. Nunes, and M. Shaeri, Phys. Rev. D **77**, 023510 (2008), arXiv:0708.1261.

[88] M. Shimano and T. Harada, Phys. Rev. D **80**, 063538 (2009), arXiv:0909.0334.

[89] M. Bojowald and G. Hossain, Phys. Rev. D **77**, 023508 (2008), arXiv:0709.2365.

[90] A. Barrau and J. Grain, arXiv:0805.0356.

[91] A. Barrau and J. Grain, Phys. Rev. Lett. **102**, 081301 (2009), arXiv:0902.0145.

[92] J. Grain, A. Barrau, and A. Gorecki, Phys. Rev. D **79**, 084015 (2009), arXiv:0902.3605.

[93] J. Mielczarek, JCAP **0811**, 011 (2008), arXiv:0807.0712.

[94] J. Mielczarek and M. Szydłowski, arXiv:0710.2742.

[95] J. Mielczarek and M. Szydłowski, Phys. Lett. B **657**, 20 (2007), arXiv:0705.4449.

[96] J. Mielczarek, T. Stachowiak, and M. Szydłowski, arXiv:0801.0502.

Averaging in cosmological models

A.A. Coley[1]

Department of Mathematics and Statistics,
Dalhousie University, Halifax, NS B3H 3J5, Canada

Abstract

The averaging problem in cosmology is of considerable importance for the correct interpretation of cosmological data. We review cosmological observations and discuss some of the issues regarding averaging. We present a precise definition of a cosmological model and a rigorous mathematical definition of averaging, based entirely in terms of scalar invariants.

1 Introduction

Cosmological observations [1], based on the assumption of a spatially homogeneous and isotropic Friedmann-Lemaître-Robertson-Walker (FLRW) model plus small perturbations, are usually interpreted as implying that there exists dark energy, the spatial geometry is flat, and that there is currently an accelerated expansion, giving rise to the so-called standard ΛCDM-concordance model. Although the concordance model is quite remarkable, it does not convincingly fit all data (see below). Unfortunately, if the underlying cosmological model is not a perturbation of an exact flat FLRW solution, the conventional data analysis and their interpretation is not necessarily valid.

For example, the standard analysis of type Ia supernovae (SNIa) and cosmic microwave background (CMB) data in FLRW models cannot be applied directly when inhomogeneities or backreaction effects are present. However, supernovae data can be explained without dark energy in inhomogeneous models, where the full effects of general relativity (GR) come into play. In one approach exact inhomogeneous cosmological models can be utilised. Indeed, it has been shown that the Lemaître-Tolman-Bondi (LTB) solution can be used to fit the observed data without the need of dark energy, although it may be necessary to place the observer at a preferred location [2].

A second approach, and the one of interest here, is backreactions through averaging. The averaging problem in cosmology is of considerable importance for the correct interpretation of cosmological data. The correct governing equations on cosmological scales are obtained by averaging the Einstein field equations (EFE) of GR (plus a theory of photon propagation; i.e., information on what trajectories actual particles follow). By assuming spatial homogeneity and isotropy on the largest scales, the inhomogeneities affect the dynamics though correction (backreaction) terms, which can lead to behaviour qualitatively and quantitatively different from the FLRW models; in particular, the expansion rate may be significantly affected.

2 Cosmological observations

From the evidence of the CMB radiation, the universe was very smooth at the time of last scattering. By the Copernican principle, the assumption of global isotropy and spatial homogeneity is then justified at the epoch of last scattering. Thus, the paradigm for our current standard model of the universe assumes the underlying geometry is FLRW, with additional Newtonian perturbations, and in matching the cosmological observables that derive from such a geometry we have been led to the conclusion over the past decade that the present–day universe is dominated by a cosmological constant, Λ, or other fluid–like "dark energy", which violates the strong energy condition. In the case of the ΛCDM paradigm, dark energy only becomes appreciable at late epochs. Dark energy is widely described as the biggest problem in cosmology today.

[1]Email address: aac@mathstat.dal.ca

There are several problems regarding the ΛCDM model. First, it is difficult to understand the large value for Λ and why the contributions of ordinary matter and the repulsive component are roughly equal today, at around 10 billion years (the coincidence problem). Second, the universe is not perfectly homogeneous and isotropic (or even perturbatively near homogeneity and isotropy). There are non-linear structures in the real universe which are not described by perturbations around a smooth background, with a distribution that is statistically homogeneous and isotropic above a scale of about 100 Mpc (or, more precisely, 100 h^{-1} Mpc, but we shall omit the factor h^{-1} for simplicity here) [3]. Linear perturbations are only valid when both the curvature and the density contrasts remain small, which is certainly not the case in the non-linear regime of structure formation when the SNIe observations are made.

Indeed, the largest structures so far detected are limited only by the size of the surveys that found them [4]. At the present epoch the distribution of matter is far from homogeneous on scales less than 150–300 Mpc. The actual universe has a sponge–like structure, dominated by huge voids surrounded by bubble walls, and threaded by filaments, within which clusters of galaxies are located. Locally there two enormous voids, both 35 to 70 Mpc across, associated with the so-called velocity anomaly [5], a large filament known as the Sloan great wall about 400 Mpc long [6] and the Shapely supercluster with a core diameter of 40 Mpc at a distance of ~ 200 Mpc [7]. In addition, there has been detection of anomolously large local bulk flows [8] and evidence for a significant anisotropy in the local Hubble expansion at distances of ~ 100 Mpc [9]. Recent surveys suggest [10] that some 40–50% of the present volume of the universe is in voids of a characteristic scale 30 Mpc. If smaller minivoids and larger supervoids are included, then our observed universe is presently void–dominated by volume; thus within regions as small as 100 Mpc density contrasts ~ -1 are observed leading to substantial gradients in the (local Ricci) spatial curvature [11]. Therefore, spatial homogeneity is valid only on scales larger than at least 100 Mpc [3], in contradiction with the predictions of the ΛCDM model in which the scale beyond which the distribution should become uniform is about 10 Mpc [4].

The present distribution of matter is clearly very complex, and since we cannot solve the EFE for this distribution of matter analytically, there is an important question as to how we operationally match the average geometry of this distribution to the simple FLRW models. The mere fact that the universe is presently inhomogeneous means that the assumptions implicit in the FLRW approximation can no longer be justified at the present epoch in the almost exact sense that they were justified at the epoch of last scattering. The situation is further complicated by the fact that most data analysis based on the standard model (FLRW + perturbations; ΛCDM) is model- and prior- dependent [18].

Consequently, spatial homogeneity only applies at the present day in an averaged sense. Given the observed inhomogeneities and that the nonlinear growth of structure appears to be roughly correlated to the epoch when cosmic acceleration is inferred to begin, it has been suggested that the FLRW geometries are inadequate as a description of the universe at late times and the introduction of a smooth dark energy is a mistaken interpretation of the observations. A universe which is homogeneous and isotropic only statistically does not generally expand like an exactly homogeneous and isotropic universe, even on average. It is possible that there are large effects on the observed expansion rate (and hence on other observables) due to the backreaction of inhomogeneities in the universe. Anything that affects the observed expansion history of the universe alters the determination of the parameters of dark energy; in the extreme it may remove the need for dark energy. Indeed, it has been suggested in that inhomogeneities related to structure formation could be responsible for accelerated expansion [15].

The effects of averaging can be signicant. Using perturbation theory, effects of order $\sim 10^{-4}$ are often quoted. However, these affects occur by averaging over the Hubble volumes and not over regions of $\sim 100 - 200$ Mpc. At best this is (only) a self-consistency analysis. In addition, there are highly non-Gaussian inhomogeneities in the late universe, and the coherence of structures causes small deviations in observations to sum to a large deviation, and there can be significant effects on observations from the backreaction of inhomogeneities [12].

In [14] the hierarchy of the critical scales for large scale inhomogeneities (backreaction effects) were calculated, at which 10% effects show up from averaging at different orders over a local domain in space-time. The dominant contribution comes from the averaged spatial curvature, observable up to scales of ~ 200 Mpc. The averaged spatial curvature typically leads to 10% (1%) effects up to ~ 80 (240) Mpc. The cosmic variance of the local Hubble rate is 10% (5%) for spherical regions of radius 40 (60) Mpc. Below ~ 40 Mpc, the cosmic variance of the Hubble rate is larger than 10%. At lower scales the kinematical

backreaction, due to second order perturbations caused by local inhomogeneities and anisotropies, are important. The crude estimates are comparable to the actual density variance determined from large scale structure surveys [3, 4, 11]. In addition, it has been found that a matter model with discrete masses (rather than an idealised continuous fluid) leads to corrections for cosmological parameters $\sim 10-20\%$ [13]. Indeed, it has been argued that the effects of averaging can theoretically be as large as $\sim 40\%$ when the equivalence principle of GR is properly applied [11].

There are also a number of other potential problems with the standard model. Apart from WMAP date ($z \sim 1100$), the standard model is based on local observations ($z < 2$), and consequently it has been argued that the data does not convincingly imply acceleration [14]. It is noteworthy that the quality of fit of the ΛCDM model has decreased with the introduction of each new SNIa data set, which may hint at inadequacy of the ΛCDM description [15]. Indeed, the standard model does not fit all data; there is tension between different SNIa data sets [16] and tension between different data sets, especially between SNIa data and CMB data [16, 17], but also with nucleosynthesis and other large scale structure data [11].

2.0.1 Discussion: spatial curvature

Clearly, backreaction (averaging) effects are real, but their relative importance still need to be determined. Within perturbation theory, the value of the normalized spatial curvature, Ω_k, is expected to be small. However, different authors have argued that Ω_k can be as large as $5-10\%$ [11, 13, 15]. In particular, CMB data does not necessarily imply flatness [15]; the position of the CMB peaks is consistent with significant spatial curvature provided that the expansion history is sufficiently close to the spatially flat ΛCDM model. Indeed, conclusions drawn about spatial curvature from the CMB are model- and prior-dependent; in a clumpy universe, the usual expression is inapplicable due to the non-trivial evolution of the spatial curvature as well as the fact that clumping contributes to the expansion rate, and there is no simple argument for obtaining the position of the CMB peaks. In addition, if the spatial curvature (parameter k) is allowed to be a function of position, then considerable spatial curvature (locally) is permissable (consistent with CMB observations) [13, 15], since curvature can affect different observations at different scales in different ways (e.g., large scale structure, $z < 2$, and CMB, $z \sim 1100$).

Observational data perhaps suggests a normalized spatial curvature $|\Omega_k| \approx 0.01-0.02$ (i.e., of about a percent). Combining these observations with large scale structure observations then puts stringent limits on the curvature parameter in the context of adiabatic ΛCDM models; however, these data analyses are very model- and prior-dependent, and care is needed in the proper interpretation of the data. There is a heuristic argument that $\Omega_k \sim 10^{-3}-10^{-2}$ ($\Omega_k \sim 1\%$) [20], which is consistent with CMB observations [1] and agrees with estimates for intrinsic curvature fluctuations using realistically modelled clusters and voids in a Swiss-cheese model. In particular, the MG equations (see below) were explicitly solved in a FLRW background geometry and it was found that the correlation tensor (backreaction) is of the form of a spatial curvature [19]. Thus, the averaged EFE for a flat spatially homogeneous, isotropic macroscopic space-time geometry has the form of the EFE of GR for a non-flat spatially homogeneous, isotropic space-time geometry.

It must be appreciated that such a value for Ω_k, at the 1% level, is relatively large and may have a significant dynamical effect on the evolution of the universe and the interpretation of cosmological observations. Indeed, in such a scenario the current contribution from the spatial curvature is comparable to the energy density in luminous matter. In addition, such a value cannot be naturally explained by inflation. From standard analysis, depending on the initial conditions and the details of a specific model of inflation, $|\Omega - 1|$ would be extremely small. Therefore, any value for Ω_k at the 1 % level can only be naturally explained in terms of an averaging effect. In addition, such an effect would compromise any efforts to use data to constrain dark energy models (within the standard paradigm) with a variable equation of state [21].

3 The averaging problem in cosmology

3.1 General Approaches

The Universe is not isotropic or spatially homogeneous on local scales. The gravitational FE on large scales are obtained by averaging the EFE of GR. It is necessary to use an exact covariant approach which gives a prescription for the correlation functions that emerge in an averaging of the full tensorial EFE.

There are a number of approaches to the averaging problem. In the approach of Buchert a 3+1 cosmological space-time splitting is employed (i.e., this procedure is not generally covariant) and only scalar quantities are averaged (and thus the governing equations are not closed) [22]. The perturbative approach (backreaction about an FLRW background [12]) involves averaging the perturbed EFE. However, a perturbation analysis cannot provide any information about an averaged geometry; thus perturbation theory cannot be conclusive and provide a complete solution.

To date the macroscopic gravity (MG) approach is the only approach to the averaging problem in GR which gives a prescription for the correlation functions which emerge in an averaging of the nonlinear FE (without which the averaging of the EFE simply amount to definitions of the new averaged terms) [23]. The MG space-time averaging approach is a fully covariant, gauge independent and exact method, in which the averaged EFE are written in the form of the EFE for the macroscopic metric tensor when the correlation terms are moved to the right-hand side of the averaged EFE to serve as the geometric modification to the averaged (macroscopic) matter energy-momentum tensor. For the cosmological problem additional assumptions are required: with reasonable cosmological assumptions, the correlation tensor in Zalaletdinov's scheme takes the form of a spatial curvature [19], and Buchert's scheme can be realized as a consistent limit [24].

There are other approaches to averaging. The formal mathematical issues of averaging tensors on a differential manifold has recently been revisted. We note that integrating scalars on spacetime regions is always well-defined and it may be possible to avoid several of the technical problems of averaging by adopting an approach based on scalar curvature invariants.

4 Cosmological models

A cosmological model is a *mixed* model, in that the matter is already assumed to be averaged but the geometry is not (necessarily). Therefore, we need a consistent model for the matter, represented on the characteristic averaging scale, and its appropriate (averaged) physical properties. It is known that the separation between the gravitational field and the matter is not scale invariant and the notion of a perfect fluid is not scale invariant; averaging (in the presence of a gravitational field) modifies the equation of state of the matter. In addition, since averaging does not conserve geodesics, we need further assumptions in order to be able to compare the models with observational data.

A precise definition of a cosmological model is necessary; i.e., a framework in which to do averaging. The definition we shall adopt is given by the following conditions C1 – C5 [25]: **C1. Spacetime Geometry:** The spacetime geometry $(\mathbf{M}, \mathbf{g})$ is defined by a smooth Lorentzian metric $\mathbf{g}$ (characterizing the macroscopic gravitational field) defined on a smooth differentiable manifold $\mathbf{M}$. The macroscopic metric geometry is obtained by an appropriate spacetime averaging of the microgeometry; thus part of the definition of a cosmological model consists of specifying *the averaging scheme* (which must be consistent with the physical assumptions of the model encapsulated in the conditions C3 and C4 below) and *the cosmological scale* over which averaging or the smoothing occurs (i.e., we must specify the averaging scale ℓ or averaging region).

C2. Timelike Congruence: There exists a timelike congruence $(\mathbf{u})$ (in principle locally), representing a family of fundamental observers. Mathematically this means that the spacetime is $\mathcal{I}$*-non-degenerate* and hence the spacetime is uniquely characterized by its scalar curvature invariants [26]. In addition to the formal parts C1 and C2 of the definition of a cosmological model $(\mathbf{M}, \mathbf{g}, \ell, \mathbf{u})$, we must also specify the physical relationship (interaction) between the macroscopic geometry and the matter fields, including how the matter responds to the macroscopic geometry.

C3. Macroscopic FE: There exists an appropriate set of macroscopic FE relating the averaged matter and appropriately averaged (or macroscopic) geometry. This is based on an underlying microscopic

theory of gravity (such as, for example, GR), and an appropriate formalism to average the geometry and find corrections (correlations) due to averaging the Einstein tensor in the resulting FE:

$$\tilde{G}^a_{\ b} + C^a_{\ b} = T^a_{\ b}, \tag{1}$$

where $\tilde{G}^a_{\ b} \equiv \tilde{R}^a_{\ b} - \frac{1}{2}\delta^a_{\ b}\tilde{R}$ and $\tilde{R}^a_{\ b}$ is the Ricci tensor of the averaged macrogeometry, $C^a_{\ b}$ is the correlation tensor, and $T^a_{\ b}$ is the energy momentum tensor (already assumed averaged).

C4. Equations of motion: We also need to know the trajectories along which the cosmological matter moves (and also the light trajectories, which determine observational relations). In principle, the average motion of a photon need not be a null geodesic in the averaged geometry [20]. **C5. Observations:** Finally, we need to be able to relate averaged quantities with physical observables, which ultimately must be consistent with cosmological data.

In the standard FLRW model there are a number of simplifications and assumptions. The past approaches to averaging have been ideally suited to the FLRW models (with small, vanishing in the limit, perturbations). In these models, the macrometric $\mathbf{g}$ is the FLRW metric (C1) and $\mathbf{u}$ also has a geometric meaning (C2). In the usual point of view there are no correlations due to averaging (i.e., $C^a_{\ b} = 0$) or, more precisely, they are negligible (C3). In this case it follows from the contracted Bianchi identities that energy-momentum is conserved: $T^c_{\ b;c} = 0$, which relates the matter to the averaged geometry. All other effects are assumed negligible (C4). However, there is no formal argument that such assumptions arise from a rigorous averaging scheme of some appropriate (physically motivated) microgeometry. In addition, there are some important effects in the standard model which are not necessarily small perturbations.

Since there are no scales explicitly specified in the model, in a sense the model is incomplete. Indeed, the model does not even have the ability to determine whether there is a scale above which the geometry is exactly FLRW or whether at all scales the geometry is only approximately FLRW (with a given perturbation scale). Furthermore, regarding C5, we can ask whether the model agrees with observations? If it does not, then even if the model agrees in some approximate sense with most observations, there is no structure within which to discuss the potential small discrepancies with observed data, which is a deficiency of the model. If the model does, then it would be remarkable, although there is still the need for a physical explanation for the dark energy. Finally, if observations indicate that $\Omega_k \approx 1 - 2\%$, then there is no physical mechanism within the model (particularly if there is an inflationary period) to produce an intrinsic curvature parameter k of this magnitude, whereas an effective curvature parameter $\hat{k}$ of about a percent arises naturally from averaging.

5 An approach to averaging using scalars

For any given spacetime $(\mathbf{M}, \mathbf{g})$ we define the set of all scalar polynomial curvature invariants

$$\mathcal{I} \equiv \{R, R1, R2, R3, R^2, R^\mu_{\ \nu}R^\nu_{\ \mu}, \dots, C^2, \dots\} \tag{2}$$

(where the Ri are eigenvalues of the Ricci tensor, and $C^2 \equiv C^{\mu\nu\alpha\beta}C_{\mu\nu\alpha\beta}$). Consider a spacetime $(\mathbf{M}, \mathbf{g})$ with a set of invariants $\mathcal{I}$. Then, if there does not exist a continuous metric deformation of g having the same set of invariants as g, the set of invariants will be called *non-degenerate*, and the spacetime metric, g, *$\mathcal{I}$-non-degenerate*. This implies that for a metric which is $\mathcal{I}$-non-degenerate the invariants characterize the spacetime uniquely, at least locally. It was proven [26] that a 4D spacetime is either $\mathcal{I}$-non-degenerate or the metric is a degenerate Kundt metric. This is a striking result because it tells us that the only metrics not locally determined by their scalar invariants must be of Kundt form.

Hence, in general, since we know how to average scalar quantities, we can average all of the scalar curvature invariants that then represents an averaged spacetime (with that set of averaged scalar invariants). In particular, we note that cosmological models (as defined above) belong to the set of spacetimes completely characterized by their scalar invariants, suggesting that we can average a cosmological model using scalar invariants. Therefore, we have a microgeometry completely characterized by its set of scalar curvature invariants $\mathcal{I}$. We then average these microgeometry scalar curvature invariants to obtain a new set of macrogeometry scalar curvature invariants $\tilde{\mathcal{I}}$, which now completely characterizes the macrogeometry [25].

5.1 Averaging the geometry

In the general mathematical context we want to describe the averaged geometry (represented by the Riemann tensor and its covariant derivatives) and interpret the results. Let us consider, $\mathcal{I}$, defined by (2), which is an ordered set of functions on $\mathbf{M}$. Let us we write $\tilde{\mathcal{I}} \equiv \{\tilde{R}, \dots, \widetilde{R^{\mu}{}_{\nu} R^{\nu}{}_{\mu}}, \dots\}$, which is also an ordered set of functions. The question is then: does the ordered set of functions $\tilde{\mathcal{I}}$ correspond to the associated scalar curvature invariants for some metric $\tilde{g}$ (which could then serve to *define* the macrometric $\tilde{g}$).

It is certainly plausible that (some appropriately defined subset of) the ordered set of functions $\tilde{\mathcal{I}}$ correspond to the associated scalar curvature invariants for some macrometric $\tilde{g}$ for the class of $\mathcal{I}$-non-degenerate geometries that constitute the class of cosmological models defined. Since the geometries are $\mathcal{I}$-non-degenerate and in 4D the properties of the geometry can be represented in terms of scalars, and since relations between different terms (functions) in the set $\mathcal{I}$ (e.g., R and R^2 are functionally dependent) and the corresponding terms in the set $\tilde{\mathcal{I}}$ (e.g., $\tilde{R}$ and $\tilde{R}^2$) are functionally related in exactly the same way and syzygies (e.g., describing the algebraic type) are maintained under averaging, it follows that in general the set $\tilde{\mathcal{I}}$ gives rise to a macrometric $\tilde{g}$ (which will have similar algebraic properties to the micrometric g).

5.1.1 Proposal: Scalar Averaging Procedure

Let us consider the ordered set of functions $\mathcal{I}$ in the form of (2). First, let us omit any scalars from this set that are not algebraically independent (e.g., $\{R^2, R^{\mu}{}_{\nu} R^{\nu}{}_{\mu} \dots\}$) to obtain an (appropriate 'independent') subset $\mathcal{I}_A$. Second, for a particular spacetime, we omit any scalars from $\mathcal{I}_A$ that can be obtained from syzygies defining that particular spacetime (e.g., defining the algebraic type of the spacetime, such as the Segre type or the Petrov type). For example, for a Ricci tensor corresponding to the algebraic form of a perfect fluid we could omit $\{R2, R3\}$ (relative to $\{R, R1\}$). We consequently obtain the subset $\mathcal{I}_{SA}$: e.g., $\mathcal{I}_{SA} \equiv \{R, R1, \dots, C^2, \dots\}$. For the spacetimes under consideration the microgeometry is then completely characterized by the (sub)set of scalar curvature invariants $\mathcal{I}_{SA}$.

We now construct the new ordered set of functions $\tilde{\mathcal{I}}_{SA}$ by averaging the various scalar invariants of $\mathcal{I}_{SA}$: $\tilde{\mathcal{I}}_{SA} \equiv \{\tilde{R}, \widetilde{R1}, \dots, \widetilde{C^2}, \dots\}$, where all of the original scalar invariants omitted from the original set $\mathcal{I}$ are replaced by a new set of functions obeying exactly the same algebraic properties (or syzygies) as $\mathcal{I}_{SA}$. Therefore, it is assumed that $\tilde{\mathcal{I}}_{SA}$ comes equiped with these syzygies, so that we could construct the corresponding set $\tilde{\mathcal{I}}$ consisting of the members of $\tilde{\mathcal{I}}_{SA}$ and all of the corresponding syzygies. Consequently, the set $\mathcal{I}_{SA}$ is an ordered set of functions (scalar curvature invariants) on $\mathbf{M}$ which uniquely determines the macrogeometry with exactly the same algebraic properties as the original microgeometry.

5.1.2 Cosmological models

In the case of a cosmological model, from C3 we have an effective set of FE and we only need to consider the macrogeometric Ricci tensor $\tilde{R}^{a}{}_{b}$ (the correlation tensor is obtained from the averaging procedure). The microgeometric Ricci tensor $R^{a}{}_{b}$ is completely characterized by a set of scalar curvature invariants $\mathcal{I}_R$. Averaging these scalar curvature invariants we obtain the set $\tilde{\mathcal{I}}_{\tilde{R}}$, which completely characterizes the macrogeometric Ricci tensor $\tilde{R}^{a}{}_{b}$. Since constructing the Ricci tensor from a set of scalar curvature invariants $\mathcal{I}_R$ is relatively simple compared to the corresponding problem for the Riemann tensor, and since the reduced set of scalar curvature invariants $\mathcal{I}_R$ is considerably smaller than $\mathcal{I}$, we have reduced the complexity of the problem in this new averaging approach. Indeed, for a Ricci tensor of the algebraic form of a perfect fluid, there are effectively (only) two independent zeroth order scalar invariants, the Ricci scalar and a single Ricci eigenvalue (corresponding to the effective energy density, ρ, and pressure, p, of the perfect fluid). Therefore, in the context of the scalar averaging procedure, we have the set $\{\tilde{R}, \widetilde{R1}\}$.

It is necessary to determine whether the correlations due to averaging alter the geometry or affect the effective energy-momentum tensor. This is partly a question of interpretation, which must be done within the context of the underlying cosmological model. In particular, in the cosmological application

it may be appropriate to reinterpret the averaging correlations as corrections to the matter fields (and hence the effective equation of state) through the EFE.

In [26] the specific example of a static spherically symmetric perfect fluid spacetime was considered. This is a simple and appropriate model for illustration since it can include an arbitrary function of one variable, there is a non-vanishing pressure, the averaging region does not change with time and there are no gravitational waves. The average correlations can be interpreted as contributing a small constant curvature term, arising from the averaging of local inhomogeneities in the micro-Ricci tensor to the smooth macro-Ricci tensor (consistent with the results of [19]).

Acknowledgements. This work was supported by NSERC of Canada.

References

[1] C. L. Bennett *et al*, Ap. J. Suppl. **148**, 1 (2003); D. N. Spergel *et al*, Ap. J. Suppl. **148**, 175 (2003) & arXiv:0603.4490; P. Astier *et al*, Astron. Astrophys. **447**, 31 (2006); T.M. Davis *et al*, Ap. J. **666**, 716 (2007); J. Dunkley *et al*, Ap. J. Suppl. **180**, 306 (2009); A. G. Reiss *et al*, Ap. J. **699**, 539 (2009).

[2] M. N. Celerier, New Adv. Phys **1**, 29 (2007); M. N. Celerier, K. Bolejko and A. Krasinski: arXiv:0906.0905; M. N. Celerier arXiv:0911.2597.

[3] D.W. Hogg *et al*, Ap. J. **624**, 54 (2005); M. Joyce *et al*, Astron. Astrophys. **443**, 11 (2005).

[4] F. S. Labini: arXiv0912.1191; F. S. Labini *et al*: arXiv:0903.0950.

[5] L. Rizzi *et al*, Mon. Not. Roy. Astron. Soc. **380**, 1255 (2007).

[6] J.R. Gott *et al*, Ap. J. **624**, 463 (2005).

[7] R.B. Tully *et al*, Ap. J. **388**, 9 (1992).

[8] A. Kashlinsky *et al*, arXiv:0809.3733.

[9] M. L. McClure and C. C. Dyer, New. Astron. **12**, 533 (2007).

[10] F. Hoyle and M.S. Vogeley, Ap. J. **607**, 751 (2004).

[11] D.L. Wiltshire, New J. Phys. **9**, 377 (2007); Phys. Rev. Letts. **99**, 251101 (2007); Int. J. Mod. Phys. **D 17**, 641 (2008); Phys. Rev. **D 78**, 084032 (2008).

[12] V. Marra *et al*, Phys. Rev. **D 76**, 123004 (2007) & **D 77**, 023033 (2008); E. W. Kolb, V. Marra and S. Matarrese, Gen. Rel. Grav. [arXiv:0901.4566].

[13] T. Clifton and P. G. Ferreira, JCAP, **0910** 26 (2009) & arXiv:0907.4169.

[14] N. Li and D.J. Schwarz, Phys. Rev. **D 76**, 083011 (2007) & **D 78**, 083531 (2008).

[15] S. Räsänen, JCAP **0611** 003 (2006) & **0804** 026 (2008) & **0902** 011 (2009) & arXiv:0912.3370.

[16] M. Hicken *et al*, Ap. J. **700**, 1097 (2009).

[17] W. J. Percival *et al*, Mon. Not. Roy. Astron. Soc. **381**, 1053 (2007).

[18] C. Shapiro and M. S. Turner, Ap. J. **649**, 563 (2006).

[19] A. A. Coley *et al*, Phys. Rev. Letts. **595**, 115102 (2005) [gr-qc/0504115]; A. A. Coley and N. Pelavas, Phys. Rev. D **75**, 043506 (2006) & **74**, 087301 (2006); R.J. van den Hoogen, J. Math. Phys. **50**, 082503 (2009).

[20] A. Coley, arXiv:0812.4566 & arXiv:0704.1734.

[21] A. Shafieloo, V. Sahni and A.A. Starobinsky: arXiv:0903.5141.

[22] T. Buchert. Gen. Rel. Grav., **32** 105 (2000) & **33** 1381 (2001); G.F.R. Ellis and T. Buchert, Phy. Lett. **A 347**, 38 (2005).

[23] R.M. Zalaletdinov, *Gen. Rel. Grav.* **24**, 1015 (1992) & **25**, 673 (1993).

[24] A. Paranjape and T.P. Singh, Phys Rev. **D 76**, 044006 (2007); A. Paranjape, Phys Rev. **D 78**, 063522 (2008).

[25] A. Coley, Gen. Rel. Grav. arXiv:0908.4281.

[26] A. Coley, S. Hervik and N. Pelavas, Class. Quantum Grav. **26**, 025013 (2009) [arXiv:0904.4877]; A. Coley, Class. Quant. Grav. **25**, 033001 (2008) [arXiv:0710.1598].

The cosmological singularity problem

Ben Craps[1]

Theoretische Natuurkunde, Vrije Universiteit Brussel, and
International Solvay Institutes
Pleinlaan 2, B-1050 Brussels, Belgium

Abstract

Despite impressive phenomenological successes, cosmological models are incomplete without an understanding of what happened at the big bang singularity. Depending on the model, one would like to understand how appropriate initial conditions were selected at the big bang singularity, or how a pre-existing contracting universe underwent a big crunch/big bang transition, if such transitions are possible at all. In this talk, after an introduction to these questions, an attempt is described to study cosmological singularities using the AdS/CFT correspondence. A specific model in which asymptotically AdS initial data evolve into a big crunch singularity is discussed and a dual field theory description is provided.

1 Introduction: inflation, open questions, and an alternative

The last two decades have witnessed enormous progress in our understanding of the composition and evolution of the universe. One of the remaining challenges is to understand how the very early universe reached a nearly homogeneous, nearly flat state with a specific spectrum of density perturbations consistent with present observations.

The most popular explanation is that the very early universe underwent a period of inflation [1]. If one assumes that inflation started and lasted long enough, it is able to explain the flatness and homogeneity of the universe. It also solves the monopole problem. The greatest success of inflation is that "simple" (single-field, slow-roll) inflationary models predict nearly scale-invariant, nearly Gaussian adiabatic density perturbations [2]. These are the seeds of large scale structure and are visible as temperature anisotropies in the cosmic microwave background (CMB).

It is important, though, to ask what predictions inflation makes for upcoming observations. Two of the holy grails of observational cosmology in the coming years are the possible observation of non-gaussianities in the CMB, and of CMB polarization due to primordial gravitational waves (tensor modes). The "simplest" inflationary models (single-field, slow-roll, two-derivative) predict that non-gaussianities are too small to be observed. However, other models allow for observable levels of non-gaussianity. Simple field theory models of inflation predict a level of tensor modes that might be observable (though it is not guaranteed). Many other models predict a non-detectable level of tensor modes. So we see that the future predictions of inflation are strongly model-dependent. It would therefore be desirable to understand which specific models (if any) are preferred from a particle physics point of view.

In this context, an important feature of inflationary models is that they need ultraviolet (UV) completions. This can be seen in several ways. First, the slow-roll conditions of simple inflationary models can be destroyed by $(1/M_P^2)$-suppressed quantum gravity corrections to the inflaton potential, where M_P is the Planck mass. Sufficient control over the UV of the theory is needed to compute such terms. Second, in models with observable primordial gravity waves, the inflaton ϕ moves over distances in field space much larger than M_P [3]. Terms involving arbitrarily high powers of ϕ/M_P are thus important, and their coefficients depend on the UV of the theory. Third, in single field, slow-roll inflation, only higher derivative models can give rise to observable levels of non-gaussianity. But in the presence of some higher derivative terms, one needs to know the UV theory to argue why other higher derivative terms are not present. We conclude that a satisfactory theory of inflation requires a theory beyond general relativity.

In recent years, important progress has been made on constructing inflaton actions in string theory. This is technically not straightforward because it is necessary to stabilize all moduli and to compute

[1]Email address: Ben.Craps@vub.ac.be

all relevant Planckian corrections. See [4] for a recent review. But even if such effective field theory models with suitable inflaton potentials are found, one may wonder how the universe emerged in a state that allowed inflation to start. In other words, how was a suitably fine-tuned initial state selected? In particular, in general relativity, inflationary solutions are past geodesically incomplete [5]. The question should then be asked whether singularity resolution in a more fundamental theory puts constraints on which solutions of the effective theory are allowed.

As we have discussed, even though inflation has had important phenomenological successes, important theoretical questions with phenomenological implications are yet to be answered. This state of affairs has motivated the construction of several alternative models, one of which is the cyclic universe [6]. Inflation (ultra-rapid expansion) is the only known mechanism to dynamically generate the required nearly scale-invariant spectrum of density perturbation in an expanding universe. In a contracting universe, however, the ekpyrotic mechanism (ultra-slow contraction) generates a spectrum of perturbations very similar to that of inflation [7]. In general relativity, the transition from a contracting to an expanding (spatially flat) universe requires going through a singularity [8]. At present, it is unclear whether such a transition is possible and whether perturbations would go through essentially unchanged. The answer will have to come from a theory beyond general relativity.

We have seen that for the inflationary universe, and even more for alternative models, it is important to try and understand the big bang singularity. The work described in this talk is motivated by several fundamental questions. Can we describe the big bang itself? How do space and time emerge from the big bang? Is it consistent to have a contracting universe before the big bang? Does the universe have a natural initial state, and if so, does it lead to inflation?

In section 2, we will first briefly review the concept of emergent space-time as well as the holographic principle. In section 3, we will discuss the AdS/CFT correspondence and "AdS cosmologies". In section 4, we will give a slightly more detailed account of specific (AdS_4/ABJM) models with cosmological singularities. Section 5 contains our conclusions and an outlook.

2 Emergent space-time and the holographic principle

We first briefly review the concept of emergent space-time – a more elaborate review can be found in [9]. To perform a measurement with desired resolution Δx, one needs light with wavelength $\lambda < \Delta x$. During the measurement, the energy $E = hc/\lambda$ of a photon gets concentrated in region with dimension Δx. This energy is within its own Schwarzschild radius if Δx is smaller than the Planck length $\ell_P = (hG/c^3)^{1/2} \approx 10^{-35}\, m$. If one attempts to probe space with a resolution smaller than ℓ_P, one creates a black hole with size larger than ℓ_P. As a consequence, the concept "space" loses its meaning below the Planck length.

An emergent concept in physics is absent in the fundamental description of a theory, but appears in a macroscopic description. Examples include the classical path of a particle, which has no fundamental meaning in quantum mechanics, but emerges as a good approximation for macroscopic objects, and the description of water as a continuous fluid, which is only valid on scales greater than the mean free path of the water molecules.

Since space loses its meaning near the Planck scale, a natural idea is that space may be an emergent concept. This idea raises many questions, though. If space only plays a role in a "macroscopic" description of reality, then what is the fundamental, underlying theory? In other words, what are the "molecules" in the analogy with water? How exactly does space emerge on "macroscopic" scales? In particular, how does space originate in cosmology? And if space is emergent, then how about time?

A framework in which the emergence of space has been realized is the holographic principle. In optics, holography means that 3d information is completely encoded on a 2d photographic plate and can be reconstructed starting from the 2d image. In quantum gravity, the holographic principle [10] says, roughly speaking, that gravitational physics in a space-time is exactly equivalent to a non-gravitational theory on the boundary of this space-time.

The motivation for the holographic principle goes back to studies of black hole entropy. Since the number of bits of information in a black hole is proportional to the area of the horizon rather than the volume inside the horizon [11], maybe the carriers of the information live on the horizon rather than in the interior.

3 The AdS/CFT correspondence and AdS cosmologies

In the second half of the 90s, the holographic principle has been realized rather precisely in the context of string theory. String theory is a proposed framework for force unification, in which elementary particles are described as small oscillating strings. The theory automatically contains gravity and it is consistent with the rules of quantum mechanics, making it a model of quantum gravity. Important features of the theory are that, in the simplest models, space-time has more than four dimensions, and that, in addition to strings, the theory contains extended objects known as branes.

We will mention two string theory realizations of the holographic principle and then focus on one of them. One realization is matrix theory [12], a quantum mechanical theory of large matrices. At large distances, the model is well-approximated by gravity in a space-time (the analogue of water as a continuous fluid). On the other hand, at small distances, the description in terms of space-time no longer applies – the notion of space is replaced by non-commuting matrices (the analogue of the molecular structure). The second realization, which will be the focus of the remainder of this talk, is the AdS/CFT correspondence, which relates string theory in asymptotically anti-de Sitter (AdS) space-times to conformal field theories on the conformal boundary of AdS [13].

The four-dimensional AdS_4 space (in global coordinates) has a time coordinate t, a radial coordinate r and angular coordinates θ and ϕ. The conformal boundary consists of the time direction (labeled by t) multiplied by the two-sphere (labeled by θ, ϕ). One can therefore wonder how the radial position r in AdS is encoded in the dual field theory. It turns out that the radial position r of an object in AdS corresponds to the energy of the corresponding object in the field theory. The radial direction is emergent.

The hope is now that a dual field theory description will enable us to describe gravitational physics in regimes where gravity breaks down, such as near black hole or cosmological singularities – the latter will be the focus of the remainder of this talk. Our starting point is the existence of supergravity solutions in which smooth, asymptotically AdS initial data evolve to a big crunch singularity, by which we mean a spacelike singularity that reaches the boundary in finite global time [14]. Such solutions are called "AdS cosmologies". The question is whether a dual gauge theory can be used to study the singularity in quantum gravity.

To be a little bit more specific, to define (super-)gravity in AdS, one has to specify boundary conditions at spatial infinity (since light signals can reach the boundary in finite time). With the usual, supersymmetric boundary conditions, AdS is perfectly stable and a big crunch is not generated from smooth, asymptotically AdS initial data. This changes, however, when certain modified, non-supersymmetric boundary conditions are imposed [14]. The modified boundary conditions in the bulk are reflected in the dual field theory by the presence of a potential unbounded from below. This potential is so steep that it causes an operator to reach infinity in finite time. Therefore, the goal becomes to learn something about cosmological singularities (in the bulk) by studying unbounded potentials (in the boundary theory).

In quantum mechanics (as opposed to quantum field theory), steep potentials unbounded from below are well-understood. A priori, the danger is that wavepackets disappear at infinity in finite time, causing a violation of unitarity. This problem can be cured by considering a self-adjoint extension of the Hamiltonian [15]. This amounts to restricting the space of allowed wavefunctions so that the Hamiltonian becomes self-adjoint and time evolution therefore unitary. The simplest choices of self-adjoint extensions can be visualized as putting a "brick wall" boundary condition at infinity, such that a "mirror" wavepacket appears when the original wavepacket disappears, thereby conserving probability. There also exist consistent self-adjoint extensions, though, where a wavepacket disappears at one boundary at infinity and reappears at another boundary, again preserving total probability. While well-understood in quantum mechanics, the extension of the method of self-adjoint extensions to quantum field theory is highly non-trivial – a first attempt appeared in [16] and an update will appear elsewhere [17].

4 Cosmological singularities in AdS_4/ABJM

Eleven-dimensional supergravity on $S^7/\mathbb{Z}_k$ allows a consistent truncation to four-dimensional gravity coupled to a single scalar field φ. The potential has a maximum for vanishing scalar field that corresponds to the AdS_4 vacuum solution. Small fluctuations around the the AdS solution have a mass in the range $m_{BF}^2 < m^2 < m_{BF}^2 + 1$. Since the Breitenlohner-Freedman bound [18] is satisfied, the

maximally supersymmetric solution, with the standard boundary conditions, is both perturbatively and non-perturbatively stable. In global coordinates, asymptotically AdS_4 metrics satisfy

$$ds^2 \sim -(1+r^2)dt^2 + \frac{dr^2}{1+r^2} + r^2 d\Omega_2^2 \quad (r \to \infty)\,. \tag{1}$$

In any asymptotically AdS solution, the scalar field behavior at large radial coordinate is

$$\varphi(t,r,\Omega) \sim \frac{\alpha(t,\Omega)}{r} + \frac{\beta(t,\Omega)}{r^2} \quad (r \to \infty)\,. \tag{2}$$

The standard, supersymmetric boundary conditions correspond to $\beta = 0$. There exists however a whole one-parameter family of AdS invariant boundary conditions,

$$\beta = -h\alpha^2\,, \tag{3}$$

where h is an arbitrary constant [19]. For $h \neq 0$, smooth asymptotically AdS initial data can evolve into a big crunch singularity [14].

M-theory in asymptotically $AdS_4 \times S^7/\mathbb{Z}_k$ space-times with $\beta = 0$ boundary conditions is dual to the three-dimensional superconformal field theory that describes the low energy dynamics of coincident M2-branes. In [20], Aharony, Bergman, Jafferis and Maldacena (ABJM) proposed a specific three-dimensional $\mathcal{N} = 6$ superconformal $U(N) \times U(N)$ Chern-Simons-matter theory with levels k and $-k$ as the world-volume theory of N coincident M2-branes on a $\mathbb{C}^4/\mathbb{Z}_k$ singularity. Here, $\mathbb{Z}_k$ is generated by $y^A \to \exp(2\pi i/k)\, y^A$. Besides the two $U(N)$ gauge fields A and $\hat{A}$, the theory contains scalar fields Y^A, $A = 1, \ldots, 4$, transforming in the fundamental representation of the $SU(4)_R$ R-symmetry group and in the bifundamental $(N, \bar{N})$ of the gauge group, as well as fermions. The scalars come with a sextic single trace potential (which can be thought of as the analogue of the commutator squared potential of $\mathcal{N} = 4$ super-Yang-Mills theory). The ABJM theory has a 't Hooft limit $N \to \infty$ with N/k fixed; in this limit, one actually finds a weakly coupled type IIA string theory. The operator dual to the bulk scalar φ is the dimension one chiral primary operator [21]

$$\mathcal{O} \sim Tr\left(Y^1 Y_1^\dagger - Y^2 Y_2^\dagger\right). \tag{4}$$

The boundary condition (3) corresponds to adding a classically marginal triple trace deformation to the boundary action

$$S = S_{ABJM} + \text{conf. coupl.} + \frac{h}{N^4}\int d^3x \left[Tr\left(Y^1 Y_1^\dagger - Y^2 Y_2^\dagger\right)\right]^3 . \tag{5}$$

The second term is the conformal coupling of the scalars due to the curvature of S^2. Two things to note about this deformation of the ABJM theory are that it is conformal in the planar limit, and that it reduces to the $O(2N^2) \times O(2N^2)$ vector model in the weak coupling limit $N \to \infty,\ N/k \to 0$ [21].

Recently, a brane interpretation of the instability of (5) has been provided in [22]. Consider spherical M2-branes in $AdS_4 \times S^7$, extended along the time direction and a two-sphere inside AdS_4 and localized at a point in S^7. Such branes could either nucleate out of empty $AdS_4 \times S^7$ or be present in an initial state. Now compute the effective potential for the radius R of such branes, or rather, for the canonically normalized field $\phi \equiv \sqrt{R}$. With the standard supersymmetric boundary conditions, cancellations related to supersymmetry leave behind a quadratic potential for ϕ, which precisely corresponds to the conformal coupling terms in (5). If a spherical brane nucleates, this potential causes it to shrink again and disappear. With the modified boundary conditions (3), however, an unbounded term sextic in $\phi \equiv \sqrt{R}$ is added to the potential, in agreement with the triple trace term in (5). The presence of this term implies that a sufficiently large spherical M2-brane will be pulled to infinite radius in finite time. M2-branes are domain walls in AdS_4: the 4-form flux inside a spherical brane is one unit smaller than outside. In a process in which spherical branes nucleate and grow, the 4-form flux N_{eff} at a fixed radial position r decreases with time. As a consequence, the effective 't Hooft coupling N_{eff}/k decreases as a function of time. Since small 't Hooft coupling corresponds to large curvature in the bulk, the result in a gravity approximation

will be a curvature singularity, namely the big crunch singularity visible in the supergravity solutions describing AdS cosmologies.[2]

To understand the dual description of our AdS cosmology, we need to study the dynamics of the field theory defined by (5). For now, we will do so in the weakly coupled 't Hooft limit $N \to \infty$, $N/k \to 0$, in which the model reduces to the $O(2N^2) \times O(2N^2)$ vector model. Let us therefore first review the well-studied $O(N)$ vector model, defined by the action

$$S = \int d^3x \left(-\frac{1}{2} \partial_\mu \vec{\phi} \cdot \partial^\mu \vec{\phi} - \frac{\lambda}{6N^2} \left(\vec{\phi} \cdot \vec{\phi} \right)^3 \right). \tag{6}$$

Its perturbative beta function is given by [23]

$$\beta_{\rm pert}(\lambda) = \frac{3}{2\pi^2 N} \left(\lambda^2 - \frac{\lambda^3}{192} \right) + \text{ higher order in } \frac{1}{N}. \tag{7}$$

For negative values of the coupling ($\lambda < 0$), there is a UV fixed point at $\lambda = 0$, so that the model is asymptotically free (though of course it has a potential unbounded from below) [24]. For positive coupling ($\lambda > 0$), the model exhibits a perturbative fixed point at $\lambda^* = 192$ [23]. There is, however, a non-perturbative instability at leading order in the $1/N$ expansion whenever $\lambda > \lambda_c \equiv 16\pi^2$ [25]; the perturbative fixed point lies in the unstable regime. Working with Poincaré invariant states, one can show that the effective potential approaches minus infinity as the renormalized value of $\langle \phi^2 \rangle$ goes to minus infinity. (If one introduces a cutoff, the effective potential is bounded from below, but all masses are of the order of the cutoff, so that there is no interesting continuum limit.) Recently, time-dependent states have been considered in this model. It has been found that states with

$$\langle \phi^2 \rangle_{\rm ren} = -\frac{CN}{t} \tag{8}$$

exist at least up to some time $t = 0$ [26].

We can summarize the analysis of the $O(N)$ vector model as follows. There is a classical instability for $\lambda < 0$, in which case $\phi \sim 1/\sqrt{|t|}$. There is a quantum instability for $\lambda > \lambda_c$, in which case $\langle \phi^2 \rangle_{\rm ren} \sim 1/|t|$. The perturbative fixed point lies in the quantum unstable regime.

Now let us consider the $O(N) \times O(N)$ vector model [27] (where in the application we have in mind, N will be replaced by $2N^2$):

$$\begin{aligned} S \;=\; & \int d^3x \left[-\frac{1}{2} \partial_\mu \vec{\phi}_1 \cdot \partial^\mu \vec{\phi}_1 - \frac{1}{2} \partial_\mu \vec{\phi}_2 \cdot \partial^\mu \vec{\phi}_2 - \frac{\lambda_{111}}{6N^2} \left(\vec{\phi}_1 \cdot \vec{\phi}_1 \right)^3 - \frac{\lambda_{222}}{6N^2} \left(\vec{\phi}_2 \cdot \vec{\phi}_2 \right)^3 \right. \\ & \left. - \frac{\lambda_{112}}{6N^2} \left(\vec{\phi}_1 \cdot \vec{\phi}_1 \right)^2 \left(\vec{\phi}_2 \cdot \vec{\phi}_2 \right) - \frac{\lambda_{122}}{6N^2} \left(\vec{\phi}_1 \cdot \vec{\phi}_1 \right) \left(\vec{\phi}_2 \cdot \vec{\phi}_2 \right)^2 \right]. \end{aligned} \tag{9}$$

As a special case, we recover the potential corresponding to the last term in (5),

$$V = \frac{\lambda}{6N^2} \left(\vec{\phi}_1 \cdot \vec{\phi}_1 - \vec{\phi}_2 \cdot \vec{\phi}_2 \right)^3, \tag{10}$$

where by convention we choose $\lambda < 0$ (the other choice would correspond to interchanging the roles of $\vec{\phi}_1$ and $\vec{\phi}_2$). The results of the analysis in [21] are as follows. If one starts with the potential (10) and follows the four independent sextic couplings under perturbative renormalization group flow towards the UV, one approaches a UV fixed point with $\lambda_{222} = \lambda^*$, $\lambda_{112} = \lambda_{122} = \lambda_{111} = 0$ – the approach of the fixed point has also been computed. However, as in the $O(N)$ vector model, a quantum instability will kick in before λ_{222} reaches λ^*.

Taking into account this quantum instability, the dynamics is as follows. Start with a small negative value of λ, so that $\vec{\phi}_1$ is classically unstable. As $\vec{\phi}_1$ rolls to large values, a lot of energy becomes available, so one needs to run the couplings towards the UV. At some time, the coupling λ_{222} becomes larger than λ_c, so that $\vec{\phi}_2$ becomes quantum unstable. The coupled system of $\vec{\phi}_1$ and $\vec{\phi}_2$ needs to be studied – this is work in progress [17]. Once the approach of the singularity ($t = 0$) is understood, it will be interesting to study if and how time evolution can be extended beyond $t = 0$.

[2] I would like to thank Y. Nakayama for a related discussion.

5 Conclusions and outlook

In this talk, we have argued that cosmological models are incomplete without an understanding of the cosmological singularity. Then we have seen that the holographic principle maps difficult questions in gravity to (hopefully simpler) questions in quantum field theory. In particular, the AdS/CFT correspondence relates gravitational theories allowing big crunch singularities to field theories with potentials unbounded from below. Therefore, it is interesting to study the dynamics of field theories with unbounded potentials. We have seen preliminary results in a concrete model, namely a deformation of ABJM theory.

What can we hope these models will lead to? In principle, one would like to carry out the following program. Start with a state in the bulk theory (with modified boundary conditions) corresponding to a large, asymptotically AdS space-time with some profile for the scalar field. Translate this state, using the AdS/CFT correspondence, to a state in the dual field theory on the boundary (with a steep unbounded potential). In the dual field theory, evolve the state through the singularity using a self-adjoint extension (if a consistent and natural self-adjoint extension exists). Finally, translate the evolved state back to a state in the bulk theory, and ask whether it has a geometric interpretation. If the boundary theory described only homogeneous modes, experience with self-adjoint extensions in quantum mechanics would suggest that the final state would roughly resemble the initial state, which would suggest a cosmological bounce. Inhomogeneous modes can drastically change this picture, though: particle creation can be potentially attractive for cosmology, but one needs to make sure that backreaction is sufficiently small for the computations to be reliable. In fact, self-adjoint extensions of "brick wall" type tend to lead to too much particle creation. Preliminary results suggest that other boundary conditions may be better behaved [17].

Acknowledgements

I am grateful to the organizers of JGRG19, in particular Kei-ichi Maeda, for their kind invitation to this stimulating workshop. I would also like to thank Alice Bernamonti, Thomas Hertog and Neil Turok for collaboration on the results presented in this talk. This research is supported in part by the Belgian Federal Science Policy Office through the Interuniversity Attraction Pole IAP VI/11 and by FWO-Vlaanderen through projects G.0428.06 and G011410N.

References

[1] A. H. Guth, Phys. Rev. D **23** (1981) 347; A. D. Linde, Phys. Lett. B **108** (1982) 389; A. J. Albrecht and P. J. Steinhardt, Phys. Rev. Lett. **48** (1982) 1220.

[2] A. H. Guth and S. Y. Pi, Phys. Rev. Lett. **49** (1982) 1110; J. M. Bardeen, P. J. Steinhardt and M. S. Turner, Phys. Rev. D **28** (1983) 679; S. W. Hawking, Phys. Lett. B **115** (1982) 295; A. A. Starobinsky, Phys. Lett. B **117** (1982) 175.

[3] D. H. Lyth, Phys. Rev. Lett. **78** (1997) 1861 [arXiv:hep-ph/9606387].

[4] D. Baumann and L. McAllister, Ann. Rev. Nucl. Part. Sci. **59** (2009) 67 [arXiv:0901.0265 [hep-th]].

[5] A. Borde, A. H. Guth and A. Vilenkin, Phys. Rev. Lett. **90**, 151301 (2003) [arXiv:gr-qc/0110012].

[6] P. J. Steinhardt and N. Turok, arXiv:hep-th/0111030.

[7] J. Khoury, B. A. Ovrut, P. J. Steinhardt and N. Turok, Phys. Rev. D **66** (2002) 046005 [arXiv:hep-th/0109050].

[8] J. Khoury, B. A. Ovrut, N. Seiberg, P. J. Steinhardt and N. Turok, Phys. Rev. D **65** (2002) 086007 [arXiv:hep-th/0108187].

[9] N. Seiberg, arXiv:hep-th/0601234.

[10] G. 't Hooft, arXiv:gr-qc/9310026; L. Susskind, J. Math. Phys. **36**, 6377 (1995) [arXiv:hep-th/9409089].

[11] J. D. Bekenstein, Phys. Rev. D **7** (1973) 2333; S. W. Hawking, Commun. Math. Phys. **43** (1975) 199 [Erratum-ibid. **46** (1976) 206].

[12] T. Banks, W. Fischler, S. H. Shenker and L. Susskind, Phys. Rev. D **55**, 5112 (1997) [arXiv:hep-th/9610043].

[13] J. M. Maldacena, Adv. Theor. Math. Phys. **2**, 231 (1998) [Int. J. Theor. Phys. **38**, 1113 (1999)] [arXiv:hep-th/9711200]; S. S. Gubser, I. R. Klebanov and A. M. Polyakov, Phys. Lett. B **428**, 105 (1998) [arXiv:hep-th/9802109]. E. Witten, Adv. Theor. Math. Phys. **2**, 253 (1998) arXiv:hep-th/9802150].

[14] T. Hertog and G. T. Horowitz, JHEP **0407**, 073 (2004) [arXiv:hep-th/0406134].

[15] M. Reed and B. Simon, "Methods Of Modern Mathematical Physics. 2. Fourier Analysis, Selfadjointness," *New York 1975, 361p*; M. Carreau, E. Fahri, S. Gutmann, P. F. Mende, Ann. Phys. **204** (1990) 186.

[16] B. Craps, T. Hertog and N. Turok, arXiv:0712.4180 [hep-th].

[17] B. Craps, T. Hertog, N. Turok, in progress.

[18] P. Breitenlohner and D. Z. Freedman, Annals Phys. **144** (1982) 249.

[19] T. Hertog and K. Maeda, JHEP **0407** (2004) 051 [arXiv:hep-th/0404261].

[20] O. Aharony, O. Bergman, D. L. Jafferis and J. Maldacena, JHEP **0810**, 091 (2008) [arXiv:0806.1218 [hep-th]].

[21] B. Craps, T. Hertog and N. Turok, Phys. Rev. D **80**, 086007 (2009) [arXiv:0905.0709 [hep-th]].

[22] A. Bernamonti and B. Craps, JHEP **0908**, 112 (2009) [arXiv:0907.0889 [hep-th]].

[23] R. D. Pisarski, Phys. Rev. Lett. **48** (1982) 574.

[24] S. R. Coleman and D. J. Gross, Phys. Rev. Lett. **31**, 851 (1973).

[25] W. A. Bardeen, M. Moshe and M. Bander, Phys. Rev. Lett. **52**, 1188 (1984).

[26] V. Asnin, E. Rabinovici and M. Smolkin, JHEP **0908**, 001 (2009) [arXiv:0905.3526 [hep-th]]; B. Craps, T. Hertog, N. Turok, in progress.

[27] E. Rabinovici, B. Saering and W. A. Bardeen, Phys. Rev. D **36** (1987) 562.

A story of the primordial non-Gaussianity

Qing-Guo Huang[1]

School of Physics, Korea Institute for Advanced Study, 207-43, Cheongryangri-Dong, Dongdaemun-Gu, Seoul 130-722, Korea

Abstract

We will discuss how to get a large local form primordial non-Gausianity, including bispectrum and trispectrum, from inflation model. In particular, we will focus on the curvaton model and the curvature perturbation generated at the end of multi-field inflation due to a nontrivial condition for multi-field inflation to end.

1 Introduction

One of the elegant ideas in modern cosmology is represented by the inflationary paradigm [1]. It is widely believed that there was an early epoch in the history of the Universe – before the epoch of primordial nucleosynthesis – when the Universe expansion was accelerated. Such an accelerated expansion in the early Universe can easily address several puzzles, such as flatness problem, horizon problem and so on, in the hot big bang model. On the other hand, inflation also provides a natural explanation about the production of the first density perturbations in the early Universe which seeds the formation of the large scale structure (LSS) in the distribution of galaxies and the temperature anisotropies in the cosmic microwave background radiation (CMBR) [2]. In fact inflation has become the dominant paradigm to understand the initial conditions for the anisotropies in CMBR and formation of LSS.

The primordial cosmological perturbations are so tiny that the generation and evolution of fluctuations during inflation has been investigated at the linear level. In this level, the fluctuations are described by a free field theory and the distribution of the primordial fluctuations is just Gaussian. However the mechanism how the primordial cosmological perturbations are generated is not yet well established. In order to distinguish different mechanisms, we need to consider the interaction of the curvature perturbation ζ. Once the interaction is taken into account, the Fourier components of curvature perturbation are not uncorrelated and the distribution of curvature perturbation is not Gaussian any more [3]. At the leading order, we take into account the irreducible three and four-point correlation function of ζ, namely

$$\langle\zeta_{\mathbf{k}_1}\zeta_{\mathbf{k}_2}\zeta_{\mathbf{k}_3}\rangle_c = (2\pi)^7\delta^{(3)}(\sum_{i=1}^{3}\mathbf{k}_i)B_\zeta(k_1,k,k_3), \tag{1}$$

$$\langle\zeta_{\mathbf{k}_1}\zeta_{\mathbf{k}_2}\zeta_{\mathbf{k}_3}\zeta_{\mathbf{k}_4}\rangle_c = (2\pi)^9\delta^{(3)}(\sum_{i=1}^{4}\mathbf{k}_i)T_\zeta(k_1,k,k_3,k_4), \tag{2}$$

where $\zeta_{\mathbf{k}}$ is the Fourier mode of ζ in momentum space, and both B_ζ and T_ζ encode how much the distribution of primordial curvature perturbation deviates from exact Gaussian distribution. In general, $B_\zeta(k_1,k_2,k_3)$ and $T_\zeta(k_1,k_2,k_3,k_4)$ are the complicated functions of k_i. Here we only plan to discuss a well established non-Gaussianity which has a local shape. For the local shape non-Gaussianity, the curvature perturbation ζ can be expanded to the non-linear orders at the same spatial point,

$$\zeta(\mathbf{x}) = \zeta_g(\mathbf{x}) + \frac{3}{5}f_{NL}^{loc.}\left(\zeta_g^2(\mathbf{x}) - \langle\zeta_g^2\rangle\right) + \frac{9}{25}g_{NL}^{loc.}\left(\zeta_g^3(\mathbf{x}) - 3\langle\zeta_g^2\rangle\zeta_g\right), \tag{3}$$

where ζ_g is the Gaussian part of curvature perturbation. In this special case, the sizes of B_ζ and T_ζ are

[1]Email address: huangqg@kias.re.kr

characterized by three parameters:

$$B_\zeta(k_1,k_2,k_3) = \frac{3}{10}f_{NL}^{loc.}P_\zeta^2\cdot\frac{\sum_{i=1}^3 k_i^3}{\prod_{i=1}^3 k_i^3}, \tag{4}$$

$$T_\zeta(k_1,k_2,k_3,k_4) = \frac{27}{100}g_{NL}^{loc.}P_\zeta^3\cdot\frac{\sum_{i=1}^4 k_i^3}{\prod_{i=1}^4 k_i^3} \tag{5}$$

$$+ \frac{1}{16}\tau_{NL}^{loc.}P_\zeta^3\cdot\left(\frac{1}{k_{12}^3k_2^3k_3^3}+23\text{ perms.}\right), \tag{6}$$

where $k_{ij}=|\mathbf{k}_i+\mathbf{k}_j|$ and P_ζ is the dimensionless power spectrum which is defined by

$$\langle\zeta_{\mathbf{k}}\zeta_{\mathbf{k}'}\rangle = (2\pi)^3\delta^{(3)}(\mathbf{k}+\mathbf{k}')\frac{2\pi^2}{k^3}P_\zeta(k). \tag{7}$$

If $f_{NL}^{loc.}\neq 0$, B_ζ blows up in the limit of $k_1\simeq k_2\gg k_3$. If $g_{NL}\neq 0$, the term with $g_{NL}^{loc.}$ blows up when one or two of k_i goes to zero. If the curvature perturbation is generated by single scalar field, $\tau_{NL}^{loc.}$ is not an independent parameter which is related to $f_{NL}^{loc.}$ by

$$\tau_{NL}^{loc.} = (\frac{6}{5}f_{NL}^{loc.})^2. \tag{8}$$

As long as $\tau_{NL}^{loc.}$ does not vanish, the term with $\tau_{NL}^{loc.}$ blows up in the limit of $k_{ij}\to 0$, even when $k_1=k_2=k_3=k_4\neq 0$. Because the local shape bispectrum and trispectrum do blow up for these special configurations in the momenta space, it is much more sensitive to the cosmological observations than that with non-local shape.

The present constraints on the non-Gaussianity parameters from experiments are still loose. For example, WMAP 5yr data [4] implies

$$-9 < f_{NL}^{loc.} < 111 \tag{9}$$

at 2σ level. The latest limit on f_{NL}^{local} is

$$f_{NL}^{loc.} = 38\pm 21 \tag{10}$$

at 1σ level in [5]. Even though the Gaussian distribution is still consistent with data within 2σ level, the allowed negative part of $f_{NL}^{loc.}$ has been cut from the WMAP 3yr data significantly. The present limit on $g_{NL}^{loc.}$ is

$$-3.5\times 10^5 < g_{NL}^{loc.} < 8.2\times 10^5 \tag{11}$$

from the compilation of LSS data [6], and

$$-5.6\times 10^5 < g_{NL}^{loc.} < 6.4\times 10^5 \tag{12}$$

from WMAP 5yr data [7] at 95% CL. In the future the uncertainties of $f_{NL}^{loc.}$, $\tau_{NL}^{loc.}$ and $g_{NL}^{loc.}$ will be reduced to $\Delta f_{NL}^{loc.}=5$, $\Delta\tau_{NL}^{loc.}\simeq 560$ and $\Delta g_{NL}^{loc.}\simeq 2.6\times 10^4$ by Planck at 95% CL. Any detection of non-Gaussianity will have a profound implication for the physics in the early universe.

It is well-known that the single field inflation predicts $f_{NL}^{loc.}\sim\mathcal{O}(\epsilon,\eta)$ [8, 9]. Detection of local shape non-Gaussianity will rule out all of the single-field inflation models. From the viewpoint of fundamental physics, multiplicity of the scalar fields is expected for going beyond standard model. Some of these scalar fields might be heavy compared to the Hubble scale of inflation H_*. But we can still expect that there are many light scalar fields. It is unnatural to assume that all of these light scalar fields stay at their local minimums from the beginning. They roll down their potentials along a one-dimensional trajectory in the field space. Each of them has the amplitude of quantum fluctuation $H_*/2\pi$. We can always decompose these light scalar fields into two kinds: one ϕ is along the tangent direction to the trajectory, the others $\phi_{s,i}$ are transverse to the trajectory. The quantum fluctuations of these fields $\delta\phi$ and $\delta\phi_{s,i}$ are called adiabatic fluctuation and entropic fluctuations respectively. The perturbation along the adiabatic direction affects the value of the energy density and cause the density perturbation during inflation. However the perturbations along the entropic directions only perturber the field values, but

not the energy density, and don't lead to the density perturbation during inflation. However it is possible that the entropic perturbations can be converted into adiabatic perturbation on the superhorizon scale at/after the end of inflation and generate a large local shape non-Gaussianity. Here we only consider a simplest multi-field case where the trajectory of inflaton in the field space is a straight line and we will focus on two typical models: curvaton model [10–16] and the curvature generated at the end of multi-field inflation due to a non-trivial condition for inflation to end [17–23].

2 Curvaton model

As we know, there might be many light scalar fields in supersymmetric theory or string theory. These light scalar fields which are subdominant during inflation can be taken as the candidates of curvaton. The energy density in the epoch of inflation is dominated by the potential of inflaton. In the usual inflation model the fluctuations of inflaton make the main contribution to the total curvature perturbations. The energy density and the perturbations caused by these light scalar fields can be ignored during inflation. However it is possible that the fluctuations of curvatons become relevant and generates a large local type non-Gaussianity if its energy density is a significant fraction of the total energy at the time when curvaton decays into radiation. In the simplest version of curvaton model the perturbations from the inflaton field are assumed to be negligible.

In general the curvaton field does not have only a mass term in its potential. Instead of the simplest curvaton potential $\frac{1}{2}m^2\sigma^2$, we adopt a form for the potential which allows a range of possibilities

$$V(\sigma) = \frac{1}{2}m^2\sigma^2 + \sum_{n\geq 4}\lambda_n\frac{\sigma^n}{M^{n-4}}. \tag{13}$$

The terms with $n > 4$ are non-renormalizable and suppressed by a UV scale M. If all of the interaction terms are negligible, we have, roughly speaking,

$$\zeta \sim \frac{\delta\rho}{\rho} \sim \Omega_{\sigma,D}\frac{\delta\rho_\sigma}{\rho_\sigma} \sim 2\Omega_{\sigma,D}\frac{\delta\sigma}{\sigma} + \Omega_{\sigma,D}(\frac{\delta\sigma}{\sigma})^2 \sim \zeta_g + \frac{1}{\Omega_{\sigma,D}}\zeta_g^2, \tag{14}$$

where

$$\Omega_{\sigma,D} = \frac{\rho_{\sigma,D}}{\rho}, \quad \zeta_g \sim \Omega_{\sigma,D}\frac{\delta\sigma}{\sigma}, \tag{15}$$

and $\Omega_{\sigma,D}$ is the curvaton density parameter at the time of its decay. Comparing to (3), we obtain

$$f_{NL}^{loc.} \sim \frac{1}{\Omega_{\sigma,D}}, \quad g_{NL}^{loc.} \sim 0. \tag{16}$$

If $\Omega_{\sigma,D} \ll 1$, $f_{NL}^{loc.} \gg 1$, but $g_{NL}^{loc.}$ is expected to be small if the curvaton self-interaction term is negligibly small. However, if the interaction term becomes dominant during inflation, we can expand $\delta\rho_\sigma/\rho_\sigma$ to higher non-linear orders, namely

$$\frac{\delta\rho_\sigma}{\rho_\sigma} \sim n\frac{\delta\sigma}{\sigma} + \frac{1}{2}n(n-1)(\frac{\delta\sigma}{\sigma})^2 + \frac{1}{6}n(n-1)(n-2)(\frac{\delta\sigma}{\sigma})^3 + \dots, \tag{17}$$

and then

$$f_{NL}^{loc.} \sim \frac{1}{\Omega_{\sigma,D}}, \quad g_{NL}^{loc.} \sim \left(\frac{1}{\Omega_{\sigma,D}}\right)^2. \tag{18}$$

In this case, $g_{NL}^{loc.}$ can be roughly the same order as $(f_{NL}^{loc.})^2$. We will discuss these two cases more carefully in the next two subsections.

2.1 Mass term dominant

The amplitude of the quantum fluctuation of curvaton field in a quasi-de Sitter space is given by

$$\delta\sigma = \frac{H_*}{2\pi}, \tag{19}$$

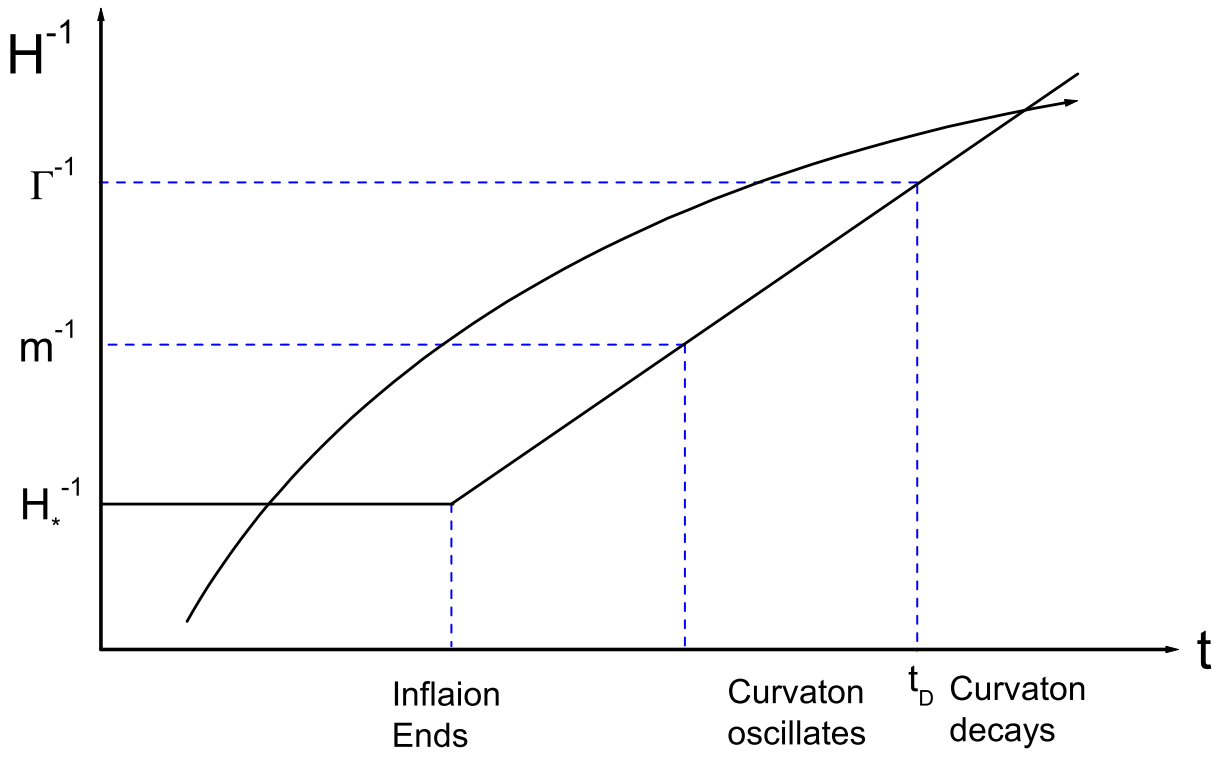

Figure 1: Evolution of the perturbation mode and the Hubble radius.

where $*$ denotes the epoch of horizon exits $k_* = a_* H_*$ during inflation. The quantum fluctuation of curvaton field is frozen at horizon exit to a classical perturbation with a flat spectrum. Since the curvaton energy density is subdominant in this epoch, its fluctuations are initially taken as isocurvature/entropy fluctuations. After the end of inflation the inflaton energy density is converted into radiations and then the Hubble parameter decreases as a^{-2}. The curvaton field will remain approximately constant σ_* until $H \sim m$. At this epoch the curvaton starts to oscillate harmonically about $\sigma = 0$. During the stage of oscillating the curvaton energy density goes like $\rho_\sigma \propto a^{-3}$ which increases with respect to the energy density of radiation $\rho_R \propto a^{-4}$. When the Hubble parameter goes to the same order of the curvaton decay rate Γ, the curvaton energy is converted into radiations. Finally, before primordial nucleosynthesis, the curvaton field is supposed to completely decay into thermalized radiation, thus the perturbations in the curvaton field are converted into curvature perturbations and become the final adiabatic perturbations which seed the matter and radiation density fluctuations observed in the Universe. We illustrate the evolution of one curvaton perturbation mode and Hubble radius in Fig. 1.

In the literatures the vacuum expectation value (VEV) of curvaton field σ_* is taken as a free parameter. However this treatment seems too naive. The curvaton mass is much smaller than the Hubble parameter during inflation, which means the Compton wavelength is large compared to the curvature radius of the de Sitter space H^{-1}. So the gravitational effects may play a crucial role on the behavior of the light scalar field in such a scenario. In [24] the authors explicitly showed that the quantum fluctuation of the light scalar field σ with mass m in de Sitter space gives it a non-zero expectation value of the square of a light scalar field

$$\langle \sigma^2 \rangle = \frac{3H_*^4}{8\pi^2 m^2}, \tag{20}$$

where the Hubble parameter H_* is assumed to be a constant. In [14] we estimated the value of curvaton as $\sigma_* \sim H^2/m$ and we found that $f_{NL}^{loc.}$ in this curvaton model is bounded from above by the tensor-scalar ratio, namely

$$f_{NL}^{loc.} < 10^3 r^{\frac{1}{4}}. \tag{21}$$

If a subdominant interaction term is taken into account, the non-linear evolution of curvaton field after inflation, but before it starts to oscillate, on large scales should be taken into account. Now the amplitude of the primordial scalar power spectrum and the non-Gaussianity parameters are modified to be, [13],

$$P_\zeta = \frac{1}{9\pi^2} f_D^2 q^2 \frac{H_*^2}{\sigma_*^2}, \tag{22}$$

$$f_{NL}^{loc.} = \frac{5}{4f_D}(1+h_2) - \frac{5}{3} - \frac{5f_D}{6}, \tag{23}$$

$$g_{NL}^{loc.} = \frac{25}{54}\left[\frac{9}{4f_D^2}(h_3+3h_2) - \frac{9}{f_D}(1+h_2) + \frac{1}{2}(1-9h_2) + 10f_D + 3f_D^2\right], \tag{24}$$

where

$$q = \frac{\sigma_* \sigma_o'}{\sigma_o}, \quad f_D = \frac{3\Omega_{\sigma,D}}{4-\Omega_{\sigma,D}}, \tag{25}$$

$$h_2 = \frac{\bar{\sigma}_o \sigma_o''}{\sigma_o'^2}, \quad h_3 = \frac{\bar{\sigma}_o^2 \sigma_o'''}{\sigma_o'^3} \tag{26}$$

where $\Omega_{\sigma,D}$ is still the fraction of curvaton energy density in the energy budget at the time of curvaton decay, σ_o is the curvaton VEV when curvaton starts to oscillate, and the prime denotes the derivative with respect to σ_*. If the curvaton potential is purely quadratic, $h_2 = h_3 = 0$ and then

$$g_{NL}^{loc.} + \frac{10}{3} f_{NL}^{loc.} \simeq 0. \tag{27}$$

We see that $g_{NL}^{loc.}$ is not exactly zero, but has the same order of magnitude as $f_{NL}^{loc.}$. Any deviation from the above relation implies that the curvaton potential does not take the purely quadratic form.

The curvaton dynamics after inflation was discussed in [25–27] and $f_{NL}^{loc.}$ can be small even when $f_D \ll 1$, but $g_{NL}^{loc.}$ should be large [25–27]. For example, assume the curvaton potential is given by

$$V(\sigma) = \frac{1}{2}m^2\sigma^2 + \lambda m^4 \left(\frac{\sigma}{m}\right)^n, \tag{28}$$

where $n \geq 2$. If $n < 2$, the correction term becomes dominant around $\sigma = 0$. The correction in the equation of motion is small if $|s| \ll 1/n$, where

$$s = \lambda \left(\frac{\sigma_*}{m}\right)^{n-2}. \tag{29}$$

The general result is given in [26]. Now $f_{NL}^{loc.}$ and $g_{NL}^{loc.}$ take the form

$$f_{NL}^{loc.} \simeq \frac{5}{4f_D}, \tag{30}$$

$$g_{NL}^{loc.} \simeq -\frac{25}{24} v(n) \frac{s}{f_D^2} - \frac{25}{6f_D}, \tag{31}$$

where

$$v(n) = -n^2(n-1)(n-2)2^{\frac{n-1}{4}}\Gamma(5/4)^{n-1}\pi \times \left[J_{\frac{1}{4}}(\frac{1}{2})\int_0^{\frac{1}{2}} J_{\frac{1}{4}}^{n-1}(x) Y_{\frac{1}{4}}(x) x^{\frac{6-n}{4}} dx - Y_{\frac{1}{4}}(\frac{1}{2})\int_0^{\frac{1}{2}} J_{\frac{1}{4}}^{n}(x) x^{\frac{6-n}{4}} dx\right], \tag{32}$$

which shows up in Fig. 2.

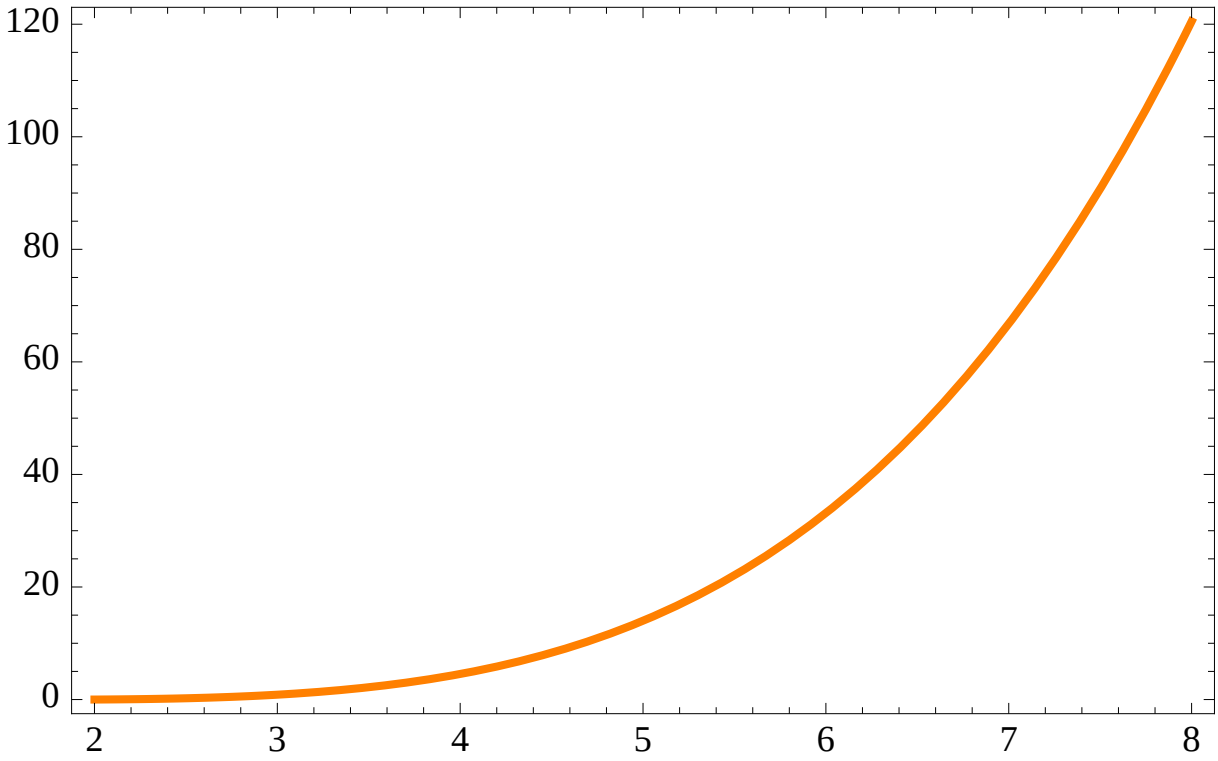

Figure 2: Plot of $v(n)$ as a function of n.

2.2 Interaction term dominant

The self-interaction term can be dominant if the curvaton mass is small enough and/or the curvaton VEV during inflation is large enough. If so, the higher order non-Gaussianity parameters are also expected to be larger. In this subsection, we focus on the cases in which the self-interaction term dominates the curvaton potential in the inflation epoch. The value of curvaton when it starts to oscillate is roughly the same as σ_*. So we also assume that the curvaton energy density is dominated by the self-interaction term when it starts to oscillate. As demonstrated in [28], the energy density of an oscillating scalar field in an expanding universe with potential $V \sim \sigma^n$ scales as

$$\rho_\sigma \sim a^{-6n/(n+2)}. \tag{33}$$

If $n < 4$, the energy density of curvaton increases with respect to radiation, but decreases with respect to radiation if $n > 4$. On the other hand, the amplitude of the curvaton oscillations also decreases, and it is possible that the self-interaction term becomes subdominant before it decays. But it is also possible that this transition does not happen before curvaton decays. We calculated the primordial curvature perturbation for these two cases respectively in [16].

• **Curvaton potential is dominated by the interaction term before it decays.** The amplitude of the primordial power spectrum and the non-linear parameters are respectively given by

$$P_\zeta = \left(\frac{n+2}{12\pi}\right)^2 f_D^2 q^2 \frac{H_*^2}{\sigma_*^2}, \tag{34}$$

and

$$f_{NL}^{loc.} = \frac{5}{6}\left[\frac{6(n-1+h_2)}{(n+2)f_D} - \frac{8(n-1)}{n+2} - \frac{2(4-n)}{n+2}f_D\right], \tag{35}$$

$$\begin{aligned} g_{NL}^{loc.} &= \frac{25}{54}\left[\frac{36}{(n+2)^2 f_D^2}[(n-1)(n-2)+h_3+3(n-1)h_2]\right. \\ &- \frac{144}{(n+2)^2 f_D}(n-1)(n-1+h_2) + \frac{4}{(n+2)^2}[44n^2-121n+68-9(4-n)h_2] \\ &- \left.\frac{80}{(n+2)^2}(n-1)(n-4)f_D + \frac{12}{(n+2)^2}(4-n)^2 f_D^2\right]. \end{aligned} \tag{36}$$

• **The mass term becomes dominant before curvaton decays.** The amplitude of the primordial power spectrum and the non-linearity parameters are

$$P_\zeta = \left(\frac{n+2}{12\pi}\right)^2 f_D^2 q^2 \frac{H_*^2}{\sigma_*^2}, \tag{37}$$

$$f_{NL}^{loc.} = \frac{5}{6}\left[\frac{3(n+2h_2)}{(n+2)f_D} - 2 - f_D\right], \tag{38}$$

$$\begin{aligned} g_{NL}^{loc.} &= \frac{25}{54}\left[\frac{9}{(n+2)^2 f_D^2}[n(n-2)+4h_3+6nh_2]\right. \\ &- \left.\frac{18}{(n+2)f_D}(n+2h_2) + \frac{2}{n+2}(5-2n-9h_2) + 10f_D + 3f_D^2\right]. \end{aligned} \tag{39}$$

To summarize, if the curvaton potential is dominated by the interaction term during inflation, a large $g_{NL}^{loc.}$ is obtained and $g_{NL}^{loc.} \sim \mathcal{O}\left((f_{NL}^{loc.})^2\right)$ which is consistent with our previous estimation. The value of $g_{NL}^{loc.}$ encodes the information of the self-interaction of curvaton field.

2.3 Mixed curvaton model

The spectral index is an important quantity to characterize the primordial power spectrum. In simplest version of curvaton model, the total curvature perturbation is generated by curvaton field and the scale dependence of the primordial power spectrum is the same as that of $\delta\sigma$. So the spectral index of the primordial power spectrum in the curvaton model takes the form

$$n_s^{cv} = 1 + \frac{2\tilde{m}_*^2}{3H_*^2} - 2\epsilon, \tag{40}$$

where $\tilde{m}_*$ is the effective mass of curvaton at $\sigma = \sigma_*$ and $\epsilon = -\frac{\dot{H}_*}{H_*^2}$ is a slow-roll parameter. This result is valid for all of the previous scenarios. Since we have $\tilde{m}_* \ll H_*$ in the curvaton model, a small value of ϵ and a closely scale-invariant power spectrum are expected. However WMAP 5yr data prefers a red-tilted power spectrum. In [15], we suggested a mixed scenario in which the curvature perturbation generated by inflaton also makes a significant contribution to the primordial power spectrum in order to naturally obtain a red-tilted power spectrum in curvaton model. The curvature perturbation generated by curvaton and inflaton are denoted by P_ζ^{cv} and P_ζ^{inf} respectively and then $P_\zeta^{tot} = P_\zeta^{cv} + P_\zeta^{inf}$. Introducing a new paremater

$$\beta = P_\zeta^{cv}/P_\zeta^{tot} \in [0,1], \tag{41}$$

the spectral index of the total primordial power spectrum becomes

$$n_s = \beta n_s^{cv} + (1-\beta) n_s^{inf}, \tag{42}$$

where $n_s^{inf} = 1 - 6\epsilon + 2\eta$ is the spectral index of the power spectrum generated by inflaton. Considering the perturbation of inflaton cannot generate a large local shape non-Gaussianity and $P_\zeta^{cv} = \beta P_\zeta^{tot}$, the observed non-Gaussianity parameters become

$$f_{NL}^{loc.} \simeq \beta^2 f_{NL}^{cv}, \quad \tau_{NL}^{loc.} \simeq \beta^3 \tau_{NL}^{cv}, \quad g_{NL}^{loc.} \simeq \beta^3 g_{NL}^{cv}. \tag{43}$$

Since $\tau_{NL}^{cv} = (\frac{6}{5} f_{NL}^{cv})^2$, we have

$$\tau_{NL}^{loc.} = \frac{36}{25\beta}(f_{NL}^{loc.})^2, \tag{44}$$

which is enhanced by a factor $1/\beta$ in the mixed curvaton model. In the case where curvaton potential is dominated by its self-interaction term, g_{NL}^{cv} is proportional to $(f_{NL}^{cv})^2$, i.e. $g_{NL}^{cv} = c(f_{NL}^{cv})^2$ where the coefficient c is different in different case, and hence

$$g_{NL}^{loc.} = \frac{c}{\beta}(f_{NL}^{loc.})^2, \tag{45}$$

which is also enhanced. If $\epsilon \simeq 0$, $n_s \simeq 1 + 2(1-\beta)\eta$ and a red tilted primordial power spectrum is obtained if $\beta < 1$ and $\eta < 0$.

3 A geometric description of non-Gaussianity generated at the end of multi-feld inflation

In this section we mainly focus on the curvature perturbation generated at the end of multi-field inflation and adopt the unit of $M_p = 1$. For simplicity, the trajectory of inflaton is assumed to be a straight line in the field space and then the entropy perturbations do not contribute to the curvature perturbation during inflation. As long as the background inflaton path is not orthogonal to the hyper-surface for inflation to end, the entropy perturbation can make a contribution to the curvature perturbation at the end of inflation and generate a large non-Gaussiantiy. Since the curvature perturbation is produced by the entropy perturbations on the super-horizon scale, the bispectrum and trispectrum have a local shape.

We consider the inflation model with n inflaton fields. The dynamics of inflaton fields for slow-roll inflation along a straight line in the field space is described by

$$\frac{d\phi_i}{dN} \simeq \alpha_i, \tag{46}$$

where $dN = -Hdt$ constant and α_i for $i = 1, 2, ..., n$. The unit vector along the adiabatic direction is

$$\mathbf{e}_\sigma = -(\alpha_1, \alpha_2, ..., \alpha_n)/\alpha, \tag{47}$$

where

$$\alpha = \left(\sum_{i=1}^{n} \alpha_i^2\right)^{\frac{1}{2}}. \tag{48}$$

The inflaton field vector in the field space is denoted by

$$\Phi = (\phi_1, \phi_2, ..., \phi_n), \tag{49}$$

and its quantum fluctuation is

$$\delta\Phi = (\delta\phi_1, \delta\phi_2, ..., \delta\phi_n). \tag{50}$$

The equation of motion can be written by

$$\frac{d\Phi}{dN} = -\alpha \mathbf{e}_\sigma. \tag{51}$$

Assume that the values of inflaton fields at the end of inflation are given by

$$\Phi_f = (\phi_{1,f}, \phi_{2,f}, ..., \phi_{n,f}), \tag{52}$$

which satisfies the equation

$$F(\Phi_f) = F(\phi_{1,f}, \phi_{2,f}, ..., \phi_{n,f}) = 0. \tag{53}$$

The solution of the above equation is described by a $(n-1)$-dimensional hyper-surface S in the n-dimensional field space. This hyper-surface S associated with the field configuration at the end of inflation in the field space has a normal vector at Φ_f as

$$\bar{\mathbf{e}}_n = (\frac{\partial F}{\partial \phi_{1,f}}, \frac{\partial F}{\partial \phi_{2,f}}, ..., \frac{\partial F}{\partial \phi_{n,f}}), \tag{54}$$

which can be normalized to be

$$\mathbf{e}_n = \frac{\bar{\mathbf{e}}_n}{||\bar{\mathbf{e}}_n||}, \tag{55}$$

where

$$||\bar{\mathbf{e}}_n|| = \left(\sum_{i=1}^{n} (\frac{\partial F}{\partial \phi_{i,f}})^2\right)^{\frac{1}{2}}. \tag{56}$$

There are $(n-1)$ independent vectors along the entropy directions which are orthogonal to the adiabatic direction. In particular, one of them is very important, namely $\mathbf{e}_s$ who stays on the plane P determined by $\mathbf{e}_n$ and $\mathbf{e}_\sigma$. Assume $\mathbf{e}_\sigma$ is not orthogonal to the hyper-surface S; otherwise, the entropy perturbations do not contribute to the curvature perturbation and this n-field inflation model is reduced to the single-field case. Now the vector along this special entropy direction can be given by

$$\bar{\mathbf{e}}_s = \mathbf{e}_n - \langle \mathbf{e}_n, \mathbf{e}_\sigma \rangle \mathbf{e}_\sigma \tag{57}$$

which can be normalized to be a unit vector

$$\mathbf{e}_s = \frac{\bar{\mathbf{e}}_s}{||\bar{\mathbf{e}}_s||}, \tag{58}$$

with

$$||\bar{\mathbf{e}}_s|| = \sqrt{1 - \langle \mathbf{e}_\sigma, \mathbf{e}_n \rangle^2}. \tag{59}$$

Similarly, the unit tangent vector of S on the plane P can be expressed by

$$\mathbf{e}_t = \frac{\bar{\mathbf{e}}_t}{||\bar{\mathbf{e}}_t||}, \tag{60}$$

where

$$\bar{\mathbf{e}}_t = \mathbf{e}_\sigma - \langle \mathbf{e}_n, \mathbf{e}_\sigma \rangle \mathbf{e}_n, \tag{61}$$

and

$$||\bar{\mathbf{e}}_t|| = \sqrt{1 - \langle \mathbf{e}_\sigma, \mathbf{e}_n \rangle^2}. \tag{62}$$

Here the vectors $\mathbf{e}_t$ and $\mathbf{e}_s$ are constructed by $\mathbf{e}_\sigma$ and $\mathbf{e}_n$, and then we obtain two simple relations, namely

$$\langle \mathbf{e}_t, \mathbf{e}_s \rangle = -\langle \mathbf{e}_n, \mathbf{e}_\sigma \rangle, \tag{63}$$

and

$$\langle \mathbf{e}_n, \mathbf{e}_\sigma \rangle \langle \mathbf{e}_t, \mathbf{e}_s \rangle - \langle \mathbf{e}_t, \mathbf{e}_\sigma \rangle \langle \mathbf{e}_n, \mathbf{e}_s \rangle = -1. \tag{64}$$

These vectors are illustrated in Fig. 3. The curve C is the intersection curve between the hyper-surface S and the plane P.

There are still $(n-2)$ independent entropy directions orthogonal to the plane P. The unit vectors along these $(n-2)$ entropy directions are denoted by $\mathbf{e}_{s,A}$ for $A = 1, 2, .., n-2$. Since $\mathbf{e}_{s,A}$ is orthogonal to $\mathbf{e}_\sigma$ and $\mathbf{e}_s$ which are the two independent vectors living on the plane P, $\mathbf{e}_{s,A}$ must be orthogonal to the plane P and then $\mathbf{e}_{s,A}$ for $A = 1, 2, ..., n-2$ are also the unit tangent vectors of S at the point Φ_f, namely

$$\mathbf{e}_{t,A} = \mathbf{e}_{s,A}. \tag{65}$$

Denote ℓ as the arc-length parameter along the tangent direction $\mathbf{e}_t$ and ℓ_A as the arc-length parameter along the tangent direction $\mathbf{e}_{t,A}$ for $A = 1, 2, ..., n-2$. Therefore

$$\mathbf{e}_t = \frac{\partial \Phi_f}{\partial \ell}, \quad \mathbf{e}_{t,A} = \frac{\partial \Phi_f}{\partial \ell_A}. \tag{66}$$

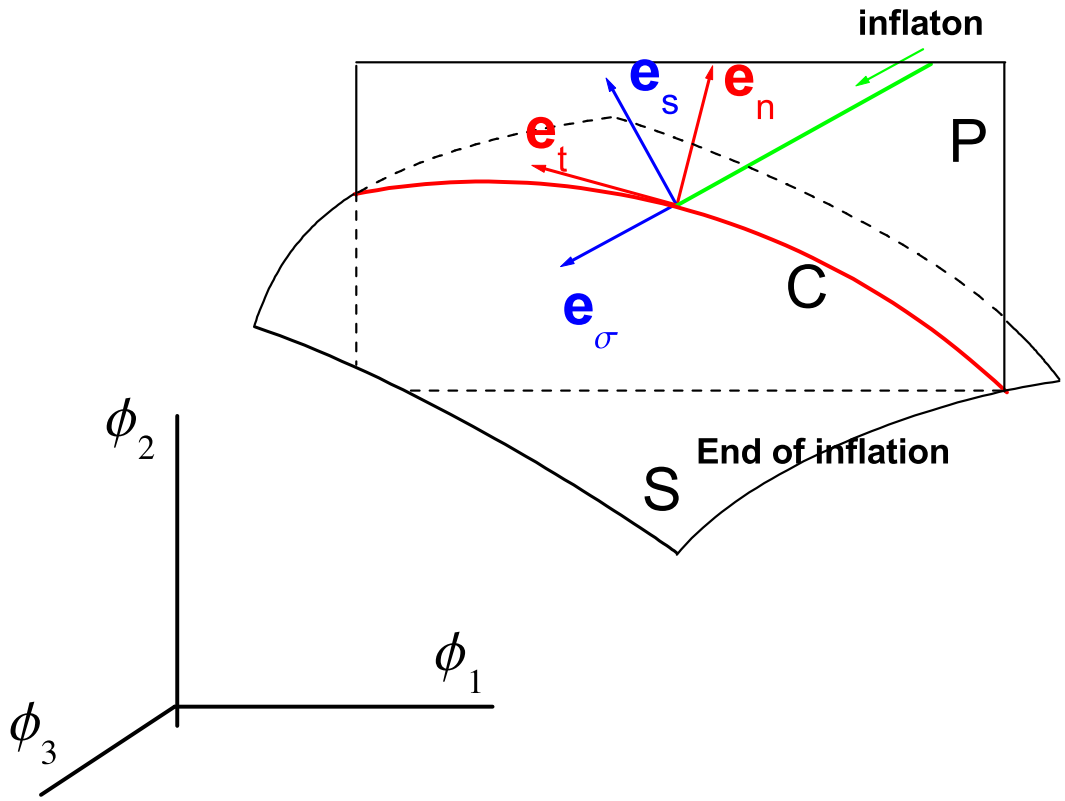

Figure 3: The green line is the trajectory of inflaton fields during inflation and the hyper-surface corresponds to the field configuration at the end of inflation.

Using the δN formalism [29–33], we found the sizes of both bispectrum and trispectrum are determined by how curved this hyper-surface is. See [21] in detail. The amplitude of the primordial curvature perturbation is

$$P_\zeta = \frac{1}{\alpha^2 \langle \mathbf{e}_n, \mathbf{e}_\sigma \rangle^2} (\frac{H_*}{2\pi})^2. \tag{67}$$

Here we need to stress that only the fluctuations along the adiabatic direction $\mathbf{e}_\sigma$ and the special entropy direction $\mathbf{e}_s$ make contribution to the total power spectrum. The amplitude of the gravitational wave fluctuations is related to the inflation scale by

$$P_T = 8(\frac{H_*}{2\pi})^2, \tag{68}$$

and then the tensor-scalar ratio takes the form

$$r = P_T / P_\zeta = 8\alpha^2 \langle \mathbf{e}_n, \mathbf{e}_\sigma \rangle^2. \tag{69}$$

The spectral index of the scalar power spectrum is

$$n_s = 1 + \frac{d \ln P_\zeta}{d \ln k} = 1 - \frac{d \ln P_\zeta}{dN} = 1 - \alpha^2. \tag{70}$$

A red-tilted primordial power spectrum is predicted. Since $\langle \mathbf{e}_n, \mathbf{e}_\sigma \rangle^2 \leq 1$,

$$r \leq 8(1 - n_s). \tag{71}$$

The tensor-scalar ratio in this model is bounded from above by the deviation from the exact scalar invariance. Similarly, the spectral index of the tensor perturbation is given by

$$n_T = -\alpha^2 = -\frac{r}{8\langle \mathbf{e}_n, \mathbf{e}_\sigma \rangle^2}, \tag{72}$$

which is bounded from above by the tensor-scalar ratio,

$$n_T \leq -\frac{r}{8}. \tag{73}$$

In single-field inflation model, the consistency relation is $n_T = -r/8$ which saturates the upper bound in the above inequality. In the multi-field case, the spectrum of the tensor perturbation can be more red-tilted. We also calculate the non-Gaussianity parameters in [21],

$$f_{NL}^{loc.} = \frac{5}{6} \cdot \alpha\kappa \frac{\langle \mathbf{e}_t, \mathbf{e}_\sigma \rangle^2}{\langle \mathbf{e}_n, \mathbf{e}_\sigma \rangle}, \tag{74}$$

$$\tau_{NL}^{loc.} = \alpha^2 \left(\kappa^2 + \kappa_s^2 \langle \mathbf{e}_n, \mathbf{e}_\sigma \rangle^2 \right) \frac{\langle \mathbf{e}_t, \mathbf{e}_\sigma \rangle^2}{\langle \mathbf{e}_n, \mathbf{e}_\sigma \rangle^2}, \tag{75}$$

$$g_{NL}^{loc.} = -\frac{25}{54} \cdot \alpha^2\kappa^2 \left(\tau - 3\frac{\langle \mathbf{e}_n, \mathbf{e}_s \rangle}{\langle \mathbf{e}_n, \mathbf{e}_\sigma \rangle} \right) \frac{\langle \mathbf{e}_t, \mathbf{e}_\sigma \rangle^3}{\langle \mathbf{e}_n, \mathbf{e}_\sigma \rangle}, \tag{76}$$

where

$$\kappa = \langle \frac{\partial \mathbf{e}_t}{\partial \ell}, \mathbf{e}_n \rangle, \tag{77}$$

$$\kappa_s^2 = \sum_{A=1}^{n-2} \kappa_A^2, \quad \kappa_A = \langle \frac{\partial \mathbf{e}_t}{\partial \ell_A}, \mathbf{e}_n \rangle = \langle \frac{\partial \mathbf{e}_{t,A}}{\partial \ell}, \mathbf{e}_n \rangle, \tag{78}$$

$$\tau = \frac{d\kappa^{-1}}{d\ell}. \tag{79}$$

Here both $f_{NL}^{loc.}$ and $g_{NL}^{loc.}$ are determined by the geometry of the curve C. But $\tau_{NL}^{loc.}$ encodes much richer information of the geometry of the hyper-surface S. The term with κ_s^2 is contributed by the quantum fluctuations along the entropy directions transverse to the plane P which do not contribute to the power spectrum at the leading order. If the curve C is a straight line, $\kappa = 0$ and hence all of the non-Gaussianity parameters are equal to zero. Here we need to point out that κ is not definitely positive and $f_{NL}^{loc.}$ can be positive or negative. The sign of $f_{NL}^{loc.}$ depends on whether the curve C is convex (+) or concave (−). See Fig. 4.

4 Summary

To summarize, curvaton model and the mechanism for generating curvature perturbation at the end of multi-field inflation can produce a fairly large local shape non-Gaussianity.

In curvaton model, $g_{NL}^{loc.}$ implies the self-interaction of the curvaton field. When the self-interaction term dominates the curvaton potential during inflation, the order of magnitude of the second-order non-Gaussianity parameters $\tau_{NL}^{loc.}$ and $g_{NL}^{loc.}$ is roughly $\mathcal{O}((f_{NL}^{loc.})^2)$. A red-tilted primordial power spectrum can be naturally achieved in the mixed curvaton model where the fluctuation of inflaton also makes a significant contribution to it. In the mixed scenario, it is also possible to detect the non-local shape non-Gaussianity generated by inflaton field ϕ. Another interesting observation in the mixed scenario is that the second order non-Gaussianity parameters $\tau_{NL}^{loc.}$ and/or $g_{NL}^{loc.}$ are enhanced for fixed $f_{NL}^{loc.}$.

In the single-field slow-roll inflation model, usually the inflation is assumed to end when the slow-roll condition is violated. However the inflation terminated by a water-fall field is more generic in the multi-field inflation model. In particular, it is quite natural that a tachyonic field appears towards the end

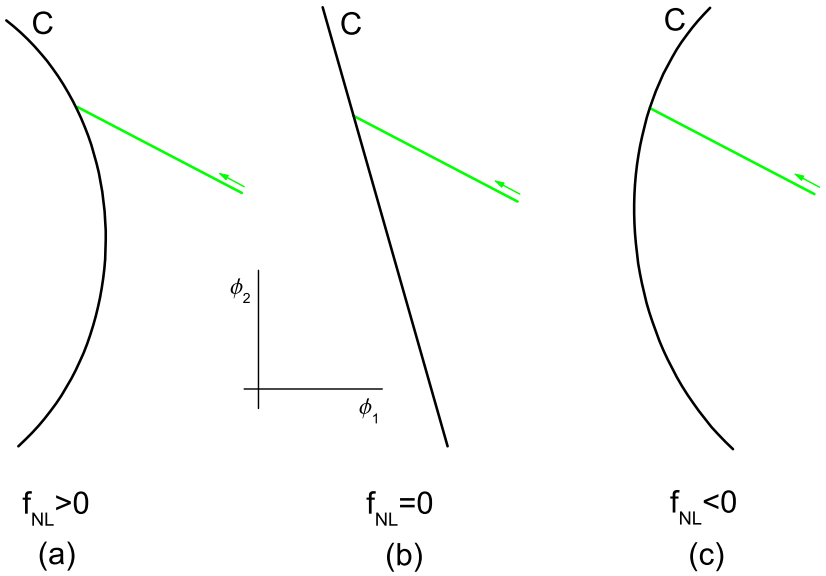

Figure 4: The green straight line is the trajectory of inflaton fields during inflation and the curve C corresponds the field configuration at the end of inflation. C is a straight line in (b).

of inflationary epoch in many scenarios inspired by string theory. The quantum fluctuations along the entropy directions can contribute to the total curvature perturbation as long as the trajectory of inflaton is not orthogonal to the hyper-surface of the end of inflation. The size of the non-Gaussianity is related to how curved this hyper-surface is. The three independent non-Gaussianity parameters are controlled by three geometric quantities associated with the hyper-surface of the end of inflation, i.e. κ, κ_s and τ. In principle, there is no constraint on these three non-Gaussianity parameters in this model.

References

[1] A. H. Guth, Phys. Rev. D **23**, 347 (1981).

[2] A. H. Guth and S. Y. Pi, Phys. Rev. Lett. **49**, 1110 (1982).

[3] N. Bartolo, E. Komatsu, S. Matarrese and A. Riotto, Phys. Rept. **402**, 103 (2004) [arXiv:astro-ph/0406398].

[4] E. Komatsu *et al.* [WMAP Collaboration], Astrophys. J. Suppl. **180**, 330 (2009) [arXiv:0803.0547 [astro-ph]].

[5] K. M. Smith, L. Senatore and M. Zaldarriaga, JCAP **0909**, 006 (2009) [arXiv:0901.2572 [astro-ph]].

[6] V. Desjacques and U. Seljak, arXiv:0907.2257 [astro-ph.CO].

[7] P. Vielva and J. L. Sanz, arXiv:0910.3196 [astro-ph.CO].

[8] J. M. Maldacena, JHEP **0305**, 013 (2003) [arXiv:astro-ph/0210603].

[9] X. Chen, M. x. Huang, S. Kachru and G. Shiu, JCAP **0701**, 002 (2007) [arXiv:hep-th/0605045].

[10] K. Enqvist and M. S. Sloth, Nucl. Phys. B **626**, 395 (2002) [arXiv:hep-ph/0109214].

[11] D. H. Lyth and D. Wands, Phys. Lett. B **524**, 5 (2002) [arXiv:hep-ph/0110002].

[12] T. Moroi and T. Takahashi, Phys. Lett. B **522**, 215 (2001) [Erratum-ibid. B **539**, 303 (2002)] [arXiv:hep-ph/0110096].

[13] M. Sasaki, J. Valiviita and D. Wands, Phys. Rev. D **74**, 103003 (2006) [arXiv:astro-ph/0607627].

[14] Q. G. Huang, Phys. Lett. B **669**, 260 (2008) [arXiv:0801.0467 [hep-th]].

[15] Q. G. Huang, JCAP **0809**, 017 (2008) [arXiv:0807.1567 [hep-th]].

[16] Q. G. Huang, JCAP **0811**, 005 (2008) [arXiv:0808.1793 [hep-th]].

[17] D. H. Lyth, JCAP **0511**, 006 (2005) [arXiv:astro-ph/0510443].

[18] M. Sasaki, Prog. Theor. Phys. **120**, 159 (2008) [arXiv:0805.0974 [astro-ph]].

[19] A. Naruko and M. Sasaki, Prog. Theor. Phys. **121**, 193 (2009) [arXiv:0807.0180 [astro-ph]].

[20] Q. G. Huang, JCAP **0905**, 005 (2009) [arXiv:0903.1542 [hep-th]].

[21] Q. G. Huang, JCAP **0906**, 035 (2009) [arXiv:0904.2649 [hep-th]].

[22] S. Renaux-Petel, JCAP **0910**, 012 (2009) [arXiv:0907.2476 [hep-th]].

[23] J. Kumar, L. Leblond and A. Rajaraman, arXiv:0909.2040 [astro-ph.CO].

[24] T. S. Bunch and P. C. W. Davies, "Quantum Field Theory In De Sitter Space: Renormalization By Point Splitting," Proc. Roy. Soc. Lond. A **360** (1978) 117.

[25] K. Enqvist and T. Takahashi, JCAP **0809**, 012 (2008) [arXiv:0807.3069 [astro-ph]].

[26] Q. G. Huang and Y. Wang, JCAP **0809** (2008) 025 [arXiv:0808.1168 [hep-th]].

[27] P. Chingangbam and Q. G. Huang, JCAP **0904**, 031 (2009) [arXiv:0902.2619 [astro-ph.CO]].

[28] M. S. Turner, Phys. Rev. D **28**, 1243 (1983).

[29] A. A. Starobinsky, "Multicomponent de Sitter (Inflationary) Stages and the Generation of Perturbations," JETP Lett. **42** (1985) 152.

[30] M. Sasaki and E. D. Stewart, Prog. Theor. Phys. **95**, 71 (1996) [arXiv:astro-ph/9507001].

[31] M. Sasaki and T. Tanaka, Prog. Theor. Phys. **99**, 763 (1998) [arXiv:gr-qc/9801017].

[32] D. H. Lyth, K. A. Malik and M. Sasaki, JCAP **0505**, 004 (2005) [arXiv:astro-ph/0411220].

[33] C. T. Byrnes, M. Sasaki and D. Wands, Phys. Rev. D **74**, 123519 (2006) [arXiv:astro-ph/0611075].

Probing strong-field gravity and black holes with gravitational waves

S. A. Hughes[1]

Department of Physics and MIT Kavli Institute, Massachusetts Institute of Technology, 77 Massachusetts Avenue, Cambridge, MA, 02139 United States

Abstract

Gravitational wave observations will be excellent tools for making precise measurements of processes that occur in very strong-field regions of spacetime. Extreme mass ratio systems, formed by the capture of a stellar mass body compact by a massive black hole, will be targets for planned space-based interferometers such as LISA and DECIGO. These systems will be especially powerful tools for testing the spacetime nature of black hole candidates. In this writeup of the talk I gave at JGRG19, I describe how the properties of black holes are imprinted on their waveforms, and how measurements can be used to study these properties and thereby learn about the astrophysics of black holes and about strong-field gravity.

Detectors for measuring gravitational waves (GWs) have recently completed their first multiyear data runs. As this article is written, some of these detectors are being run at "enhanced" sensitivity. It is expected that a final upgrade to "advanced" sensitivity will be needed in order for GWs from astrophysical sources to be measured regularly. Once that state is reached, we can turn this process around, using the GWs that we measure to learn about their sources, using GWs for observational astronomy. The purpose of this article (and the talk on which it is based) is to give a brief review of the state of this field, focusing in particular on how the characteristics of black holes and strong-field gravity are imprinted on a system's GWs.

1 Gravitational waves: Physics and astrophysics

We begin with a brief description of how GWs arise in general realtivity (GR). Our purpose is to introduce the main concepts which describe this phenomenon; later, we will revisit this calculation, showing how to go to higher order in order to describe realistic astrophysical sources. We conclude this section with a quick summary of the astrophysics of binary GW sources.

1.1 Leading waveform

We begin by considering "weak" gravity, so that spacetime is nearly that of special relativity,

$$g_{\alpha\beta} = \eta_{\alpha\beta} + h_{\alpha\beta} \ . \tag{1}$$

Take the correction to flat spacetime to be small, so that we can linearize in $h_{\alpha\beta}$ when we build our curvature tensors. The Einstein tensor in particular becomes

$$G_{\alpha\beta} = \frac{1}{2}\left(\partial_\alpha\partial^\mu h_{\mu\beta} + \partial_\beta\partial^\mu h_{\mu\alpha} - \partial_\alpha\partial_\beta h - \Box h_{\alpha\beta} + \eta_{\alpha\beta}\Box h - \eta_{\alpha\beta}\partial^\mu\partial^\nu h_{\mu\nu}\right) \ , \tag{2}$$

where $h \equiv \eta^{\alpha\beta}h_{\alpha\beta}$ is the trace of $h_{\alpha\beta}$, and $\Box \equiv \eta^{\alpha\beta}\partial_\alpha\partial_\beta$ is the flat spacetime wave operator.

Equation (2) is rather messy. To clean it up, we first introduce the *trace-reversed* metric perturbation $\bar{h}_{\alpha\beta} \equiv h_{\alpha\beta} - (1/2)\eta_{\alpha\beta}h$. With this definition, Eq. (5) becomes

$$G_{\alpha\beta} = \frac{1}{2}\left(\partial_\alpha\partial^\mu \bar{h}_{\mu\beta} + \partial_\beta\partial^\mu \bar{h}_{\mu\alpha} - \Box\bar{h}_{\alpha\beta} - \eta_{\alpha\beta}\partial^\mu\partial^\nu \bar{h}_{\mu\nu}\right) \ . \tag{3}$$

[1]Email address: sahughes@mit.edu

Next, we take advantage of the *gauge-freedom* of linearized gravity. In electrodynamics, we may adjust the potential by the gradient of a scalar, $A_\mu \to A_\mu - \partial_\mu \Lambda$. This leaves the field tensor $F_{\mu\nu} = \partial_\mu A_\nu - \partial_\nu A_\mu$ unchanged. In linearized GR, a similar operation follows by adjusting coordinates: If one changes coordinates $x^\alpha \to x^\alpha + \xi^\alpha$ (requiring $\partial_\mu \xi^\alpha \ll 1$), then

$$h_{\mu\nu} \to h_{\mu\nu} - \partial_\mu \xi_\nu - \partial_\nu \xi_\mu \ . \tag{4}$$

One can easily show that changing gauge leaves all curvature tensors unchanged.

We take advantage of our gauge freedom to choose ξ^α so that $\partial^\mu \bar{h}_{\mu\nu} = 0$. This is called "Lorenz gauge" in analogy with the electrodynamic Lorenz gauge condition $\partial^\mu A_\mu = 0$. This simplifies our Einstein tensor considerably, yielding

$$G_{\alpha\beta} = -\frac{1}{2} \Box \bar{h}_{\alpha\beta} \ . \tag{5}$$

The Einstein equation for linearized gravity thus takes the simple form

$$\Box \bar{h}_{\alpha\beta} = -\frac{16\pi G}{c^4} T_{\alpha\beta} \ . \tag{6}$$

Using a radiative Green's function [e.g., [1], Sec. 12.11], we find the solution

$$\bar{h}_{\alpha\beta}(\mathbf{x}, t) = \frac{4G}{c^4} \int \frac{T_{\alpha\beta}(\mathbf{x}', t - |\mathbf{x} - \mathbf{x}'|/c)}{|\mathbf{x} - \mathbf{x}'|} d^3 x' \ . \tag{7}$$

Here, $\mathbf{x}$ is a spatial "field point," where $\bar{h}_{\alpha\beta}$ is evaluated, and $\mathbf{x}'$ is a "source point," the spatial coordinate we integrate over the source's extent. Notice that the solution at t depends on what happens to the source at *retarded time* $t - |\mathbf{x} - \mathbf{x}'|/c$. Information must causally propagate from $\mathbf{x}'$ to $\mathbf{x}$.

Equation (7) is an exact solution to the linearized field equation. It gives the unfortunate impression that every component of the metric perturbation is radiative. Just as one can choose a gauge such that an isolated point charge has an oscillatory potential, the Lorenz gauge makes *all* components of the metric appear radiative, even if they are static[2]. Fortunately, it is not difficult to see that only a subset of the metric represents the radiative degrees of freedom in *all* gauges. We will only quote the result here; interested readers can find the full calculation in Ref. [3], Sec. 2.2: *Given a solution $h_{\alpha\beta}$ to the linearized Einstein field equations, only the* **spatial**, **transverse**, *and* **traceless** *components $h_{ij}^{\rm TT}$ describe the spacetime's gravitational radiation in a gauge-invariant manner.* Traceless means

$$\delta_{ij} h_{ij}^{\rm TT} = 0 \ ; \tag{8}$$

"transverse" means

$$\partial_i h_{ij}^{\rm TT} = 0 \ . \tag{9}$$

Expanding $h_{ij}^{\rm TT}$ in Fourier modes, we see that Eq. (9) requires $h_{ij}^{\rm TT}$ to be orthogonal (in space) to each mode's wave vector $\mathbf{k}$.

Conditions (8) and (9) make it simple to construct $h_{ij}^{\rm TT}$ given some h_{ij}. Let n_i denote components of the unit vector along the propagation direction. The tensor

$$P_{ij} = \delta_{ij} - n_i n_j \tag{10}$$

projects spatial components orthogonal to $\mathbf{n}$. It is then simple to verify that

$$h_{ij}^{\rm TT} = h_{kl} \left(P_{ki} P_{lj} - \frac{1}{2} P_{kl} P_{ij} \right) \tag{11}$$

represents the "TT" metric perturbation. We can now manipulate the solution (7) into

$$h_{ij}^{\rm TT} = \frac{2}{D} \frac{G}{c^4} \frac{d^2 I_{kl}}{dt^2} \left(P_{ik} P_{jl} - \frac{1}{2} P_{kl} P_{ij} \right) \ , \tag{12}$$

[2] In the electromagnetic case, it is unambiguous which *field* components are radiative and which are static. Similarly, one can always tell which *curvature* components are radiative and which are static. Eddington [2] appears to have been the first to use the curvature tensor to categorize gravitational degrees of freedom in this way.

where D is distance to the source, and where

$$I_{ij} = \int x^{i'} x^{j'} T_{tt}(\mathbf{x}', t)\, d^3x' \tag{13}$$

is the source's *quadrupole moment*. It is straightforward to show that the trace $I \equiv I_{ii}$ does not contribute to Eq. (12), so it is common to use the "reduced" quadrupole moment,

$$\mathcal{I}_{ij} = I_{ij} - \frac{1}{3}\delta_{ij} I \ . \tag{14}$$

The waveform then takes the form in which it is usually presented,

$$h_{ij}^{\rm TT} = \frac{2}{R}\frac{G}{c^4}\frac{d^2\mathcal{I}_{kl}}{dt^2}\left(P_{ik}P_{jl} - \frac{1}{2}P_{kl}P_{ij}\right) \ , \tag{15}$$

the *quadrupole formula* for GW emission.

GWs also carry energy from their source. Isaacson [4] first carefully analyzed this in a tensorial manner, showing that GWs produce a stress-energy tensor given by

$$T_{\mu\nu}^{\rm GW} = \frac{c^4}{32\pi G}\langle \hat{\nabla}_\mu h_{\alpha\beta} \hat{\nabla}_\nu h^{\alpha\beta}\rangle \ , \tag{16}$$

where $\hat{\nabla}_\mu$ denotes a covariant derivative in the background spacetime. (This assumes the waveform is in a gauge such that it is transverse and traceless; more general expressions exist.) Notice that the energy content is quadratic in the wave amplitude; computing it correctly requires taking our perturbative analysis to second order. We defer the details of this derivation to Ref. [4].

Now consider a binary system with Newtonian orbital dynamics, radiating GWs according to Eq. (15) and evolving by energy and angular momentum carried off in accordance with Eq. (16). Begin with the binary's members in circular orbit of separation R. This binary has orbital energy

$$E^{\rm orb} = \frac{1}{2}m_1 v_1^2 + \frac{1}{2}m_2 v_2^2 - \frac{G m_1 m_2}{R} = -\frac{G\mu M}{2R} \ , \tag{17}$$

(where $M = m_1 + m_2$ and $\mu = m_1 m_2/M$) and orbital frequency

$$\Omega_{\rm orb} = \sqrt{\frac{GM}{R^3}} \ . \tag{18}$$

Far from the source, Eq. (16) tells us the flux of energy carried by GWs:

$$\frac{dE^{\rm GW}}{dAdt} = \frac{c^4}{32\pi G}\langle \partial_t h_{ij}^{\rm TT} \partial_k h_{ij}^{\rm TT}\rangle n^k \ . \tag{19}$$

Plugging in Eq. (15) and integrating over the sphere, we find

$$\frac{dE}{dt}^{\rm GW} = \int dA\, \frac{dE}{dAdt} = \frac{G}{5c^5}\left\langle \frac{d^3\mathcal{I}_{ij}}{dt^3}\frac{d^3\mathcal{I}_{ij}}{dt^3}\right\rangle \ . \tag{20}$$

For the Newtonian binary,

$$\mathcal{I}_{ij} = \mu\left(x_i x_j - \frac{1}{3}R^2\delta_{ij}\right) \ ; \tag{21}$$

we choose coordinates such that the components of the separation vector are $x_1 = R\cos\Omega_{\rm orb}t$, $x_2 = R\sin\Omega_{\rm orb}t$, $x_3 = 0$. Inserting into Eq. (20), we find

$$\frac{dE}{dt}^{\rm GW} = \frac{32}{5}\frac{G}{c^5}\mu^2 R^4 \Omega^6 \ . \tag{22}$$

We now assert that the binary evolves quasi-statically — any radiation carried off by GWs is accounted for by the evolution of its orbital energy, $dE^{\rm orb}/dt + dE^{\rm GW}/dt = 0$. Allow the orbital radius to slowly change in time, so that $dE^{\rm orb}/dt = (dE^{\rm orb}/dR)(dR/dt)$. Combining this rule with Eq. (22), we find

$$R(t) = \left[\frac{256G^3\mu M^2(t_c - t)}{5c^5}\right]^{1/4} . \tag{23}$$

This in turn tells us that the orbital frequency changes according to

$$\Omega_{\rm orb}(t) = \left[\frac{5c^5}{256(G\mathcal{M})^{5/3}(t_c - t)}\right]^{3/8} . \tag{24}$$

We have introduced the *chirp mass* $\mathcal{M} \equiv \mu^{3/5}M^{2/5}$, so called because it sets the rate at which the binary sweeps upward in frequency, or "chirps." We have also introduced the coalescence time t_c, which formally describes when the separation goes to zero (or when frequency goes to infinity). Corrections for eccentricity can be computed by separately accounting for the evolution of the binary's energy and angular momentum; see Ref. [5], Exercise 16.10 for details.

We conclude this section by writing the gravitational waveform predicted for quadrupole emission from the Newtonian, circular binary. Evaluating Eq. (15), we find that h_{ij} has two polarizations. These are labeled "plus" and "cross," from the lines of force associated with their tidal stretch and squeeze:

$$\begin{aligned} h_+ &= -\frac{2G\mathcal{M}}{c^2 D}\left(\frac{\pi G\mathcal{M} f}{c^3}\right)^{2/3}(1+\cos^2\iota)\cos 2\Phi_N(t) , \\ h_\times &= -\frac{4G\mathcal{M}}{c^2 D}\left(\frac{\pi G\mathcal{M} f}{c^3}\right)^{2/3}\cos\iota \sin 2\Phi_N(t) , \end{aligned} \tag{25}$$

where the phase

$$\Phi_N(t) = \int \Omega_{\rm orb}\, dt = \Phi_c - \left[\frac{c^3(t_c - t)}{5G\mathcal{M}}\right]^{5/8} , \tag{26}$$

and where $f = (1/\pi)d\Phi_N/dt$ is the GW frequency. The system's inclination ι is just the projection of its orbital angular momentum, $\mathbf{L}$, to the wave's direction of propagation $\mathbf{n}$: $\cos\iota = \hat{\mathbf{L}}\cdot\mathbf{n}$ (where $\hat{\mathbf{L}} = \mathbf{L}/|\mathbf{L}|$). Note that h_+ and $h_\times$ depend on, and thus encode, the chirp mass, distance, the position on the sky (via the direction vector $\mathbf{n}$), and the orientation of the binary's orbital plane (via $\hat{\mathbf{L}}$). In later discussion, we will amend Eq. (25) and (26) to include higher order contributions to the binary's waves and evolution.

1.2 Astrophysical binary sources

The binary example considered in the previous section is particularly germane since compact binary systems are among the most important astrophysical sources of GWs. Indeed, our best data on GWs and GW sources comes from observations of *binary pulsar* systems, pairs of neutron stars at least one of which is a pulsar. The pulsar member of the pair acts as an outstanding clock, allowing the properties of the binary to be mapped with great precision.

Some binary neutron stars are in such strong field orbits that the evolution of the binary's orbital period due to GW emission can be discerned over long observational baselines. The prototypical example is the first such system discovered, PSR 1913+16. Over 30 years of study have found extraordinary agreement between prediction and observation for the evolution of this system's orbit [6]. Additional inspiraling systems have been discovered; in all cases for which we have enough data to discern period evolution, the data agree with theory to within measurement precision [7–11]. At least one additional recently discovered system is likely to show a measurable inspiral in the next few years [12].

Turn from binary neutron stars to compact binaries more generally. Such systems are organized most naturally by their masses. At the low end we have *stellar-mass* binaries, including binary pulsars. The data on these binaries are quite solid, since we can tie models for their birth and evolution to observations. At least some fraction of short gamma-ray bursts are likely to be associated with the mergers of neutron

star-neutron star (NS-NS) or black hole-neutron star (BH-NS) systems [13, 14]; as such, gamma-ray telescopes may already be telling us about compact binary merger many times per year [15].

There is also evidence that nature produces *supermassive* binaries, in which the members are black holes with $M \sim 10^6 - 10^8\,M_\odot$ such as are found at the centers of galaxies. Theoretical arguments combining hierarchical galaxy growth scenarios with the hypothesis that most galaxies host black holes generically predict the formation of such binaries. We have now identified many systems with properties indicating that they may host such binaries. The evidence includes active galaxies with double cores [16–18]; systems with doubly-peaked emission lines [19, 20]; helical radio jets [21–23]; and periodic or semi-periodic systems, such as the blazar OJ287 [24]. As surveys go deeper and resolution improves, we may expect the catalog of candidate supermassive black hole binaries to expand.

Now consider theoretical models. Assuming that our galaxy is typical and that the inferred density of NS-NS systems in the Milky Way carries over to similar galaxies (correcting for factors such as typical stellar age and the proportion of stars that form neutron stars), we can estimate the rate at which binary systems merge in the universe. References [25] and [26] first made such estimates, finding a "middle-of-the-road" rate that about 3 binaries per year merge to a distance of 200 Mpc. More recent calculations based on later surveys and observations of NS-NS systems have amended this number somewhat; the total number expected to be measured by advanced detectors is around several tens per year. See, for example, [27] for a detailed discussion of methodology.

Another technique uses population synthesis. These calculations combine data on the observed distribution of stellar binaries with models for how stars evolve. This allows us to estimate the rate of formation and merger for systems which we cannot at present observe, such as stellar mass black hole-black hole (BH-BH) binaries, or for which we have only circumstantial evidence, such as neutron star-black hole (NS-BH) binaries (which presumably form some fraction of short gamma ray bursts). A disadvantage is that the models of stellar evolution in binaries have many uncertainties. There are multiple branch points in binary evolution, such as whether the binary remains bound following each supernova, and whether the binary survives common envelope evolution. As a consequence, the population synthesis predictions can be quite diverse. Though different groups generally agree well with the rates for NS-NS systems (by design), their predictions for NS-BH and BH-BH systems differ by quite a bit. New data are needed to clear the theoretical cobwebs.

Binaries can also form dynamically in dense environments, such as globular clusters. The most massive bodies will tend to sink to a cluster's core through mass segregation [28]; as such, the core will become populated with the heaviest bodies, either stars which will evolve into compact objects, or the compact objects themselves. As those objects interact with one another, they will tend to form massive binaries; calculations show that the production of BH-BH binaries is particularly favored. It is thus likely that globular clusters will act as "engines" for the production of massive compact binaries [29–31].

The hierarchical growth scenario for galaxies, coupled with the hypothesis that most galactic bulges host large black holes, generically predicts the formation of supermassive binaries, especially at high redshifts when mergers were common. The first careful discussion of this was by Begelman, Blandford, and Rees [21]. The coevolution of black holes and galaxies in hierarchical scenarios has now become a very active focus of research (e.g., Refs. [32–34]). Galaxy mergers appear to be a natural mechanism to bring "fuel" to one or both black holes, igniting quasar activity; the formation of a binary may thus be associated with the duty cycle of quasars [35–37]. Such scenarios typically find that most black hole mergers come at fairly high redshift ($z \gtrsim 3$ or so), and that the bulk of a given black hole's mass is due to gas it has accreted over its growth.

A subset of binaries in the supermassive range are of particular interest to the relativity theorist. These binaries form by the capture of a "small" ($1 - 100\,M_\odot$) compact object onto an orbit around a black hole in a galactic center. Such binaries form dynamically through stellar interactions [38, 39]; the formation rate predicted by most models is typically $\sim 10^{-7}$ extreme mass ratio binaries per galaxy per year [39]. If the inspiraling object is a white dwarf or star, it could tidally disrupt as it comes close to the massive black hole, producing an x-ray or gamma-ray flare [40, 41]. If the inspiraling object is a neutron star or black hole, it will be swallowed whole by the large black hole. As such, it will almost certainly be electromagnetically quiet; however, its GW signature will be loud, and is a particularly interesting target.

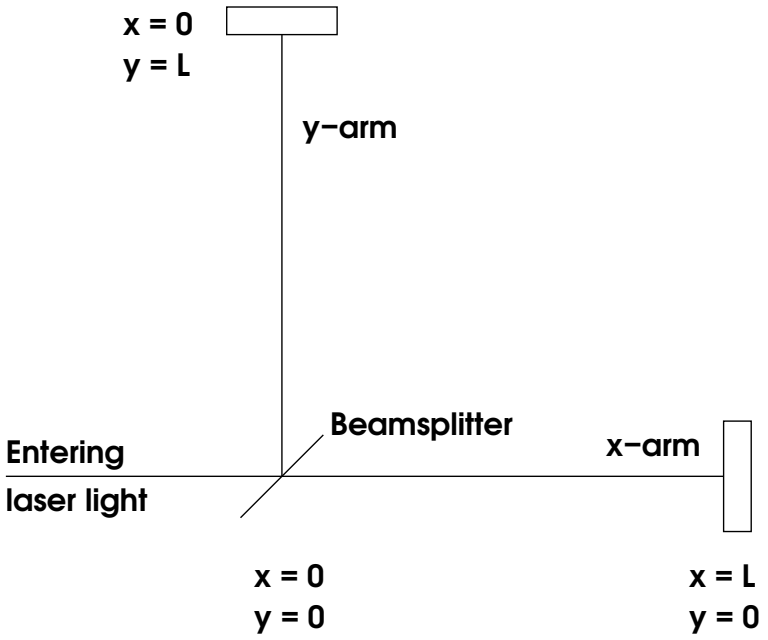

Figure 1: Schematic of an interferometer that could be used to detect GWs. Though real interferometers are vastly more complicated, this interferometer topology contains enough detail to illustrate the principle by which such measurements are made.

2 Measuring gravitational waves: Principles and experiments

Before moving to a discussion of how black hole characteristics and strong-field physics are imprinted on GWs, let us briefly summarize the key principles by which a GW interferometer operators. Begin with the simple limit in which we treat the spacetime in which our detector lives as flat plus a simple GW propagating down our coordinate system's z-axis:

$$ds^2 = -c^2dt^2 + (1+h)dx^2 + (1-h)dy^2 + dz^2 \ , \tag{27}$$

where $h = h(t-z)$. We neglect the influence of the earth (clearly important for terrestrial experiments) and the solar system (which dominates the spacetime of space-based detectors). Corrections describing these influences can be added; we neglect them as they vary on much longer timescales than the GWs.

Figure 1 sketches an interferometer that can measure a GW. Begin by examining the geodesics describing the masses at the ends of the arms, and the beam splitter at the center. Take these objects to be initially at rest, so that $(dx^\mu/d\tau)_{\rm before} \doteq (c,0,0,0)$. The GW shifts this velocity by an amount of order the wave strain: $(dx^\mu/d\tau)_{\rm after} = (dx^\mu/d\tau)_{\rm before} + \mathcal{O}(h)$. Now examine the geodesic equation:

$$\frac{d^2x^j}{d\tau^2} + \Gamma^j{}_{\alpha\beta}\frac{dx^\alpha}{d\tau}\frac{dx^\beta}{d\tau} = 0 \ . \tag{28}$$

All components of the connection are $\mathcal{O}(h)$. Combining this with our argument for how the GW affects the various velocities, we have

$$\frac{d^2x^j}{d\tau^2} + \Gamma^j{}_{00}\frac{dx^0}{d\tau}\frac{dx^0}{d\tau} + \mathcal{O}(h^2) = 0 \ . \tag{29}$$

It is simple to show that the connection coefficient $\Gamma^j{}_{00} = 0$, as the relevant metric components are all constant. We conclude that

$$\frac{d^2x^j}{d\tau^2} = 0 \ . \tag{30}$$

In other words, *the test masses are unaccelerated to leading order in the GW amplitude h.*

This seems to say that the GW has no impact! However, the geodesic equation describes motion *with respect to specified coordinates*. Our coordinates are effectively "comoving" with the interferometer's components. Using the fact that our mirrors are at constant position in these coordinates, it is simple to see that the *proper* length of the arms does change. For instance, the x-arm has a proper length

$$D_x = \int_0^L \sqrt{g_{xx}}\, dx = \int_0^L \sqrt{1+h}\, dx \simeq \int_0^L \left(1+\frac{h}{2}\right) dx = L\left(1+\frac{h}{2}\right) . \tag{31}$$

Likewise, the y-arm has a proper length $D_y = L(1-h/2)$.

This means that the armlengths as measured by a ruler will vary with h. One might worry that, in practice, the ruler will vary with the wave, cancelling the measurement. This does not happen because rulers are not made of freely-falling particles: Its elements are *bound* to one another, and act against the GW. The ruler feels some effect due to the GW, but it is far smaller than the variation in D_x and D_y.

The ruler used by the most sensitive current and planned detectors is based on laser interferometry. We will not describe the details of how a GW is imprinted on the output observable of an interferometer such as that sketch in Fig. 1; for our purposes, it is enough to note that in essence one uses the (highly stable) frequency of the laser as a clock, and times the light travel in the two arms. We recommend the nicely pedagogical article by Faraoni [42] for a clear discussion, as well as a relatively recent analysis by Finn [43] for more detailed discussion.

From basic principles, we now give a brief summary of current and planned detectors. Our goal is not an in-depth discussion, so we refer readers interested in these details to excellent reviews by [44] (which covers in detail the characteristics of the various detectors) and [45] (which covers the interferometry used for space-based detectors). When thinking about GW detectors, a key characteristic is that the frequency of peak sensitivity scales inversely with armlength. The ground-based detectors currently in operation are sensitive to waves oscillating at 10s – 1000s of Hertz. Planned space-based detectors will have sensitivities at much lower frequencies, ranging from 10^{-4} – 0.1 Hz (corresponding to waves with periods of tens of seconds to hours).

The ground-based detectors in operation are LIGO (*Laser Interferometer Gravitational-wave Observatory*), with antennae in Hanford, Washington and Livingston, Louisiana; Virgo near Pisa, Italy; and GEO near Hanover, Germany. The LIGO interferometers have 4-kilometer arms, and a peak sensitivity near 100 Hz. Virgo has 3-kilometer arms, and sensitivity comparable to the LIGO detectors. GEO has 600-meter arms; as such, its peak sensitivity is at higher frequencies than LIGO and Virgo. Using advanced interferometry techniques, it achieves sensitivity competitive with the kilometer-scale instruments. All of these instruments will be upgraded over the course of the next few years, installing more powerful lasers, and reducing the impact of local ground vibrations. The senstivity of LIGO should be improved by roughly a factor of ten, and the bandwidth increased as well. See [46] for detailed discussion.

There are plans to build additional kilometer-scale instruments. The detector AIGO (*Australian International Gravitational Observatory*) is planned as a detector very similar to LIGO and Virgo, but in Western Australia [47]. This location, far from the other major GW observatories, has great potential to improve the ability of the worldwide GW detector network to determine the characteristics of GW events [48]. The Japanese GW community, building on their experience with the 300-meter TAMA interferometer, hopes to build a 3-kilometer *underground* instrument. Dubbed LCGT (*Large-scale Cryogenic Gravitational-wave Telescope*), the underground location takes advantage of the fact that local ground motions tend to decay fairly rapidly as we move away from the earth's surface. They plan to use cryogenic cooling to reduce noise from thermal vibrations.

In space, the major project is LISA (*Laser Interferometer Space Antenna*), a 5-million kilometer interferometer under development as a joint NASA-ESA mission. LISA will consist of three spacecraft placed in orbits so that their relative positions form an equilateral triangle lagging the earth by 20°, inclined to the ecliptic by 60°; see Fig. 2. The spacecraft are free and do not maintain this constellation precisely; however, their armlength variations occur on a timescale far longer than the periods of their target waves. The review by [45] discusses in great detail how one does interferometry on such a baseline with time-changing armlengths. LISA targets waves with periods of hours to several seconds, a rich band for signals involving massive black holes. The LISA *Pathfinder*, a testbed for some of the mission's components, is scheduled for launch in the very near future [49].

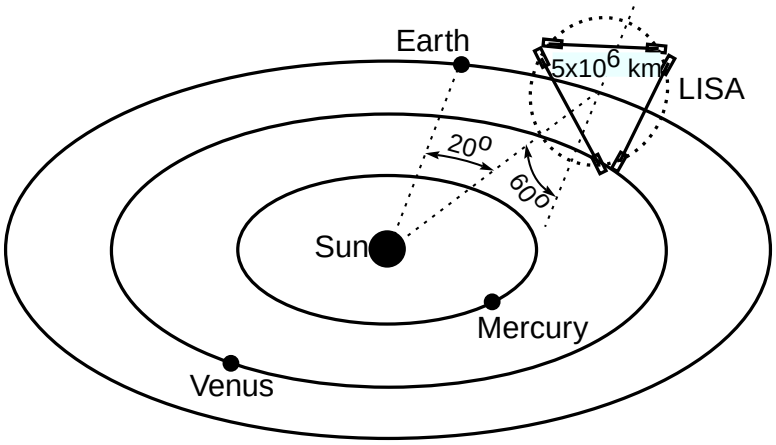

Figure 2: Schematic of the LISA constellation in orbit about the sun. Each arm of the triangle is 5×10^6 km; the centroid of the constellation lags the Earth by 20°, and its plane is inclined to the ecliptic by 60°. Note that the spacecraft orbit freely; there is no formation flying in the LISA configuration. Instead, each spacecraft is in a slightly eccentric, slightly inclined orbit; their individual motions preserve the near-equilateral triangle pattern with high accuracy for a timescale of decades.

Somewhat smaller than LISA, The Japanese GW community has proposed DECIGO (*DECI-hertz Gravitational-wave Observatory*), a space antenna to target a band at roughly 0.1 Hz. This straddles the peak sensitivities of LISA and terrestrial detectors, and may thus act as a bridge for signals that evolve from one band to the other. See Ref. [50] for further discussion.

3 Comparable mass binary waves

We now at last begin to examine how the characteristics of black holes and strong-field gravity are imprinted on the GWs these systems generate. We first must go somewhat beyond the leading-order waveform discussed in Sec. 1.1. After developing the necessary formal tools, we discuss how the interesting characteristics appear in the waves.

3.1 Going beyond leading order

In the analytic treatment of comparable mass binary waves, one begins by considering the *post-Newtonian*, or pN, expansion. This expansion in turn begins by considering the binary in so-called harmonic or deDonder coordinates. In these coordinates, one defines

$$h^{\mu\nu} \equiv \sqrt{-g}g^{\mu\nu} - \eta^{\mu\nu} \ , \tag{32}$$

where g is the determinant of $g_{\mu\nu}$. This looks similar to the flat spacetime perturbation defined in Sec. 1.1; however, we do not assume that h is small. We next impose the gauge condition

$$\partial_\alpha h^{\alpha\beta} = 0 \ . \tag{33}$$

With these definitions, the *exact* Einstein field equations are

$$\Box h^{\alpha\beta} = \frac{16\pi G}{c^4}\tau^{\alpha\beta} \ , \tag{34}$$

where $\Box = \eta^{\alpha\beta}\partial_\alpha\partial_\beta$ is the *flat* spacetime wave operator. The form of Eq. (34) means that the radiative Green's function we used to derive Eq. (7) can be applied here, yielding

$$h^{\alpha\beta} = -\frac{4G}{c^4}\int \frac{\tau_{\alpha\beta}(\mathbf{x}', t - |\mathbf{x} - \mathbf{x}'|/c)}{|\mathbf{x} - \mathbf{x}'|} d^3x' \ . \tag{35}$$

Equation (35) is exact. Note, however, that we never defined the source $\tau^{\alpha\beta}$. It is given by

$$\tau^{\alpha\beta} = (-g)T^{\alpha\beta} + \frac{c^4\Lambda^{\alpha\beta}}{16\pi G} \; ; \tag{36}$$

$T^{\alpha\beta}$ is the usual stress energy tensor, $\Lambda^{\alpha\beta}$ encodes the nonlinear structure of the Einstein field equations:

$$\Lambda^{\alpha\beta} \equiv 16\pi(-g)t_{\rm LL}^{\alpha\beta} + \partial_\nu h^{\alpha\mu}\partial_\mu h^{\beta\nu} - \partial_\mu\partial_\nu h^{\alpha\beta}h^{\mu\nu} \tag{37}$$

$$= N^{\alpha\beta}[h,h] + M^{\alpha\beta}[h,h,h] + L^{\alpha\beta}[h,h,h,h] + \mathcal{O}(h^5) \; . \tag{38}$$

On the first line, $t_{\rm LL}^{\alpha\beta}$ is the Landau-Lifshitz pseudotensor, a quantity which (in certain gauges) allows us to describe how GWs carry energy through spacetime ([51], Sec. 96). On the second line, the term $N^{\alpha\beta}[h,h]$ means a collection of terms quadratic in h and its derivatives, $M^{\alpha\beta}[h,h,h]$ is a cubic term, etc. Our solution $h^{\alpha\beta}$ appears on both the left- and right-hand sides of Eq. (35). Such a structure can be handled very well *iteratively*. We write

$$h^{\alpha\beta} = \sum_{n=1}^{\infty} G^n h_n^{\alpha\beta} \; . \tag{39}$$

The $n = 1$ term is essentially the linearized solution from Sec. 1.1. To go higher, let $\Lambda_n^{\alpha\beta}$ denote the contribution of $\Lambda^{\alpha\beta}$ to the solution $h_n^{\alpha\beta}$. We find

$$\Lambda_2^{\alpha\beta} = N^{\alpha\beta}[h_1,h_1] \; , \tag{40}$$

$$\Lambda_3^{\alpha\beta} = M^{\alpha\beta}[h_1,h_1,h_1] + N^{\alpha\beta}[h_2,h_1] + N^{\alpha\beta}[h_1,h_2] \; , \tag{41}$$

etc.; higher contributions to Λ^{ab} can be found by expanding its definition and gathering terms. By solving the equations which result from this procedure, we can build the spacetime metric and describe the motion of the members of a binary and the radiation that they emit.

We defer details of this construction to the literature (Blanchet's review, Ref. [52], is particularly useful for this purpose), and turn to a study of the interesting features of the pN binary waveform. Take the members of the binary to have masses m_1 and m_2, let their separation be r, and let $\hat{\mathbf{r}}$ point to body 1 from body 2. In the harmonic gauge used for pN theory, the acceleration of body 1 is given by

$$\mathbf{a} = \mathbf{a}_0 + \mathbf{a}_2 + \mathbf{a}_4 + \mathbf{a}_5 + \mathbf{a}_6 + \mathbf{a}_7 \ldots \; . \tag{42}$$

The zeroth term,

$$\mathbf{a}_0 = -\frac{Gm_2}{r^2}\hat{\mathbf{r}}, \tag{43}$$

is the usual Newtonian gravitational acceleration. Each $\mathbf{a}_n$ is a correction of order $(v/c)^n$. The first is

$$\mathbf{a}_2 = \left[\frac{5G^2m_1m_2}{r^3} + \frac{4G^2m_2^2}{r^3} + \frac{Gm_2}{r^2}\left(\frac{3}{2}(\hat{\mathbf{r}}\cdot\mathbf{v_2})^2 - v_1^2 + 4\mathbf{v_1}\cdot\mathbf{v_2} - 2v_2^2\right)\right]\frac{\hat{\mathbf{r}}}{c^2} \; . \tag{44}$$

For the acceleration of body 2 due to body 1, exchange labels 1 and 2 and replace $\hat{\mathbf{r}}$ with $-\hat{\mathbf{r}}$. So far, the pN acceleration has been computed to order $(v/c)^7$. As we go to high order, the expressions for $\mathbf{a}_n$ become quite lengthy. An excellent summary is given in Ref. [52], Eq. (131) and surrounding text.

PN theory also introduces a distinctly non-Newtonian element to binary dynamics: its members' spins *precess* in the binary's curved spacetime. If the spins are $\mathbf{S}_1$ and $\mathbf{S}_2$, one finds [53]

$$\frac{d\mathbf{S}_1}{dt} = \frac{G}{c^2r^3}\left[\left(2+\frac{3}{2}\frac{m_2}{m_1}\right)\mu\sqrt{Mr}\hat{\mathbf{L}}\right]\times\mathbf{S}_1 + \frac{G}{c^2r^3}\left[\frac{1}{2}\mathbf{S}_2 - \frac{3}{2}(\mathbf{S}_2\cdot\hat{\mathbf{L}})\hat{\mathbf{L}}\right]\times\mathbf{S}_1 \; , \tag{45}$$

$$\frac{d\mathbf{S}_2}{dt} = \frac{G}{c^2r^3}\left[\left(2+\frac{3}{2}\frac{m_1}{m_2}\right)\mu\sqrt{Mr}\hat{\mathbf{L}}\right]\times\mathbf{S}_2 + \frac{G}{c^2r^3}\left[\frac{1}{2}\mathbf{S}_1 - \frac{3}{2}(\mathbf{S}_1\cdot\hat{\mathbf{L}})\hat{\mathbf{L}}\right]\times\mathbf{S}_2 \; . \tag{46}$$

We now discuss the ways in which aspects of pN binary dynamics color a system's waves.

3.1.1 Gravitational-wave amplitudes.

Although a binary's *dominant* waves come from variations in its mass quadrupole moment, higher moments also generate GWs. In the pN framework, these moments contribute to the amplitude of a binary's waves beyond the quadrupole form, Eq. (25). Write the gravitational waveform from a source as

$$h_{+,\times} = \frac{2G\mathcal{M}}{c^2 D}\left(\frac{\pi G\mathcal{M}f}{c^3}\right)^{2/3}\left[H^0_{+,\times} + v^{1/2}H^{1/2}_{+,\times} + vH^1_{+,\times} + \ldots\right] , \tag{47}$$

where $v \equiv (\pi GMf/c^3)^{1/3}$ is roughly the orbital speed of the binary's members (normalized to c). The $H^0_{+,\times}$ terms reproduce the waveform presented in Eq. (25). The higher-order terms $H^{1/2}_{+,\times}$ and $H^1_{+,\times}$ can be found in [52], his Eqs. (237) through (241). A key point to note is that these higher-order terms introduce new dependences on the binary's orbital inclination and its masses. As such, measurement of these terms provides additional constraints on the system's characteristics.

3.1.2 Orbital phase.

The motion of a binary's members about each other determines the orbital phase. Specializing to circular orbits, we can determine the orbital frequency from the acceleration of the its members; integrating up this frequency, we define the phase $\Phi(t)$. The first few terms of this phase are given by [54]

$$\begin{aligned}\Phi \;=\; & \Phi_c - \left[\frac{c^3(t_c-t)}{5G\mathcal{M}}\right]^{5/8}\left[1 + \left(\frac{3715}{8064}+\frac{55}{96}\frac{\mu}{M}\right)\Theta^{-1/4} - \frac{3}{16}\left[4\pi - \beta(t)\right]\Theta^{-3/8}\right. \\ & \left. + \left(\frac{9275495}{14450688}+\frac{284875}{258048}\frac{\mu}{M}+\frac{1855}{2048}\frac{\mu^2}{M^2}+\frac{15}{64}\sigma(t)\right)\Theta^{-1/2}\right] ,\end{aligned} \tag{48}$$

where

$$\Theta = \frac{c^3\eta}{5GM}(t_c - t) . \tag{49}$$

The leading term is just the Newtonian quadrupole phase, Eq. (26). Each power of Θ connects to a higher order in the expansion. Equation (48) is taken to "second post-Newtonian" order, meaning that corrections of $(v/c)^4$ are included. Corrections to order $(v/c)^6$ are summarized in [52]. In addition to the chirp mass $\mathcal{M}$, the reduced mass μ enters Φ when higher order terms are included. Including higher pN effects in our wave model makes it possible to determine both chirp mass and reduced mass, fully constraining the binary's masses.

Equation (48) also depends on two parameters, β and σ, which come from the binary's spins and orbit orientation. The "spin-orbit" parameter β is

$$\beta = \frac{1}{2}\sum_{i=1}^{2}\left[113\left(\frac{m_i}{M}\right)^2 + 75\eta\right]\frac{\hat{\mathbf{L}}\cdot\mathbf{S}_i}{m_i^2} ; \tag{50}$$

the "spin-spin" parameter σ is

$$\sigma = \frac{\eta}{48m_1^2m_2^2}\left[721(\hat{\mathbf{L}}\cdot\mathbf{S}_1)(\hat{\mathbf{L}}\cdot\mathbf{S}_2) - 247\mathbf{S}_1\cdot\mathbf{S}_2\right] \tag{51}$$

[54]. These parameters encode valuable information, especially when spin precession is taken into account.

3.1.3 Spin precession.

Although the spin vectors $\mathbf{S}_1$ and $\mathbf{S}_2$ wiggle around according to Eqs. (45) and (46), the system must preserve a notion of *global* angular momentum. Neglecting for a moment the secular evolution of the binary's orbit due to GW emission, pN encodes the notion that the total angular momentum

$$\mathbf{J} = \mathbf{L} + \mathbf{S}_1 + \mathbf{S}_2 \tag{52}$$

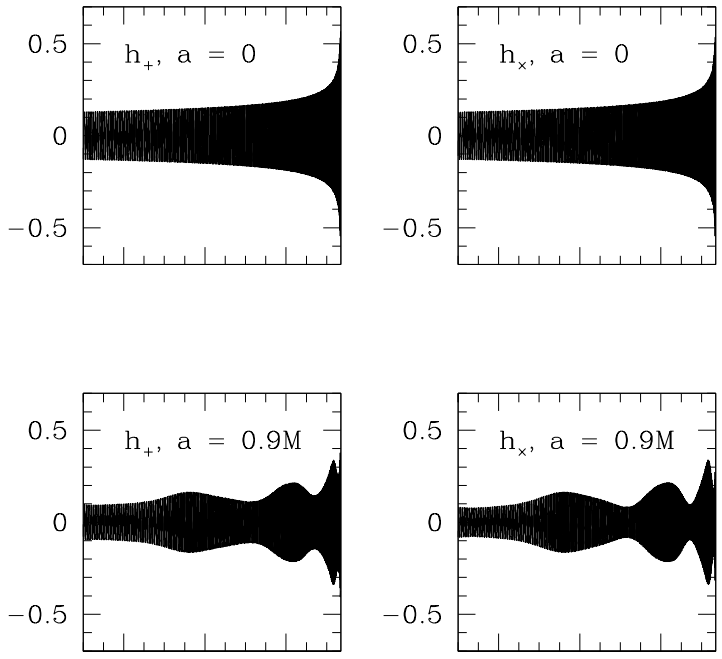

Figure 3: Illustration of precession's impact on a binary's waves. The top panels show h_+ and $h_\times$ for a binary that contains nonspinning black holes; the lower panels show the waveforms for a binary with rapid rapidly rotating ($a = 0.9M$) holes. The strong amplitude modulation is readily apparent in this figure. Less obvious, but also included, is the frequency modulation that enters through the spin-dependent orbital phase parameters β and σ [cf. Eq. (48)].

must be conserved. This means $\mathbf{L}$ must oscillate to compensate for the spins' dynamics, and guarantees that, when spin precession is accounted for in our evolutionary models, the phase parameters β and σ become time varying. Likewise, the inclination angle ι varies with time. Precession thus leads to phase and amplitude modulation of a source's GWs. Figure 3 illustrates precession's impact, showing the late inspiral waves for binaries that are identical aside from spin.

Careful analysis shows that accounting for these effects in our wave model makes it possible to measure the spins of a binary's members, in many cases with excellent precision [55]. By measuring both masses and spins, instruments such as LISA for example become tools for tracking the cosmic evolution of black hole masses and spins, opening a window onto the growth of these objects from early cosmological epochs.

4 Extreme mass ratio binary waves

We conclude by examining waves from extreme mass ratio binaries — stellar mass (roughly $1-100\,M_\odot$) compact bodies spiraling into a much more massive (roughly $10^5-10^7\,M_\odot$) black holes. Such systems are very well modeled using black hole perturbation theory, so we begin with a quick review of this subject.

4.1 Brief overview of black hole perturbation theory

Black hole perturbation theory can be developed much like the weak gravity limit described in Sec. 1.1, replacing the flat spacetime metric $\eta_{\alpha\beta}$ with the spacetime of a black hole:

$$g_{\mu\nu} = g^{\rm BH}_{\mu\nu} + h_{\mu\nu}\ . \tag{53}$$

For astrophysical scenarios, one uses the Schwarzschild (non-rotating black hole) or Kerr (rotating) solutions for $g^{\rm BH}_{\mu\nu}$. It is straightforward (though somewhat tedious) to then develop the Einstein tensor for

this spacetime, keeping terms only to first order in the perturbation h.

This approach works very well when the background is non-rotating,

$$ds^2 = g^{\rm BH}_{\mu\nu} dx^\mu dx^\nu = -\left(1 - \frac{2\hat{M}}{r}\right) dt^2 + \frac{dr^2}{\left(1 - 2\hat{M}/r\right)} + r^2 d\Omega^2 \,, \tag{54}$$

where $d\Omega^2 = d\theta^2 + \sin^2\theta d\phi^2$ and $\hat{M} = GM/c^2$. Our discussion for this special case is adapted from [56]. Because the background is spherically symmetric, we decompose the perturbation into spherical harmonics. For example, under rotations in θ and ϕ, h_{00} should transform as a scalar. We thus put

$$h_{00} = \sum_{lm} a_{lm}(t,r) Y_{lm}(\theta,\phi) \,. \tag{55}$$

The components h_{0i} transform like components of a 3-vector, and can be expanded in vector harmonics; h_{ij} can be expanded in tensor harmonics. One can decompose further with parity: Even harmonics acquire a factor $(-1)^l$ when $(\theta,\phi) \to (\pi-\theta, \phi+\pi)$; odd harmonics acquire a factor $(-1)^{l+1}$.

By imposing these decompositions, choosing a particular gauge, and requiring that the spacetime satisfy the vacuum Einstein equation $G_{\mu\nu} = 0$, we find an equation that governs the perturbations. Somewhat remarkably, the t and r dependence for all components of $h_{\mu\nu}$ for given spherical harmonic indices (l,m) can be constructed from a function $Q(t,r)$ governed by the simple equation

$$\frac{\partial^2 Q}{\partial t^2} - \frac{\partial^2 Q}{\partial r_*^2} - V(r) Q = 0 \,, \tag{56}$$

where $r_* = r + 2\hat{M}\ln(r/2\hat{M} - 1)$. The potential $V(r)$ depends on whether we consider even or odd parity:

$$V_{\rm even}(r) = \left(1 - \frac{2\hat{M}}{r}\right)\left[\frac{2q(q+1)r^3 + 6q^2\hat{M}r^2 + 18q\hat{M}^2 r + 18\hat{M}^3}{r^3\left(qr + 3\hat{M}\right)^2}\right] \,, \tag{57}$$

where $q = (l-1)(l+2)/2$; and

$$V_{\rm odd}(r) = \left(1 - \frac{2\hat{M}}{r}\right)\left[\frac{l(l+1)}{r^2} - \frac{6\hat{M}}{r^3}\right] \,. \tag{58}$$

For even parity, Eq. (56) is the *Zerilli equation* [57]; for odd, it is the *Regge-Wheeler equation* [58]. See [56] for further discussion, including how gauge is chosen and how to construct $h_{\mu\nu}$ from Q. When the spacetime perturbation is due to a body orbiting the black hole, these equations acquire a source term. One can find the waves from an orbiting body by using the source-free equation to build a Green's function, and then integrating over the source.

How does this procedure fare for rotating holes? The background spacetime,

$$ds^2 = -\left(1 - \frac{2\hat{M}r}{\rho^2}\right) dt^2 - \frac{4a\hat{M}r\sin^2\theta}{\rho^2} dt d\phi + \frac{\rho^2}{\Delta} dr^2 + \rho^2 d\theta^2 + \left(r^2 + a^2 + \frac{2\hat{M}ra^2\sin^2\theta}{\rho^2}\right) d\phi^2 \,, \tag{59}$$

where

$$a = \frac{|\vec{S}|}{cM} \,, \qquad \rho^2 = r^2 + a^2\cos^2\theta \,, \qquad \Delta = r^2 - 2\hat{M}r + a^2 \,, \tag{60}$$

is now nonspherical, and the decomposition into spherical harmonics is not useful. One could in principle simply expand $G_{\mu\nu} = 0$ to first order in $h_{\mu\nu}$ and obtain a partial differential equation in t, r, and θ. (The metric is axially symmetric, so we can easily separate the ϕ dependence.)

Rather than expanding the metric, Teukolsky [59] examined perturbations of curvature:

$$R_{\alpha\mu\beta\nu} = R^{\rm BH}_{\alpha\mu\beta\nu} + \delta R_{\alpha\mu\beta\nu} \,. \tag{61}$$

The curvature tensor is invariant to first-order gauge transformations, an attractive feature. This tensor obeys a nonlinear wave equation which can be derived from the Bianchi identity; see [60] for discussion. By expanding this wave equation to linear order in $\delta R_{\alpha\mu\beta\nu}$, Teukolsky showed that perturbations to Kerr black holes are governed by the equation

$$\left[\frac{(r^2+a^2)^2}{\Delta}-a^2\sin^2\theta\right]\partial_t^2\Psi-4\left[r+ia\cos\theta-\frac{\hat{M}(r^2-a^2)}{\Delta}\right]\partial_t\Psi+\frac{4i\hat{M}amr}{\Delta}\partial_t\Psi-\Delta^2\partial_r\left(\Delta^{-1}\partial_r\Psi\right)$$
$$-\frac{1}{\sin\theta}\partial_\theta\left(\sin\theta\partial_\theta\Psi\right)-\left[\frac{a^2}{\Delta}-\frac{1}{\sin^2\theta}\right]m^2\Psi+4im\left[\frac{a(r-\hat{M})}{\Delta}+\frac{i\cos\theta}{\sin^2\theta}\right]\Psi-\left(4\cot^2\theta+2\right)\Psi=\mathcal{T}\,. \tag{62}$$

The field Ψ is a complex quantity built from a combination of components of $\delta R_{\alpha\mu\beta\nu}$. It describes a spacetime's radiation; see [59] for details. (We have assumed $\Psi\propto e^{im\phi}$.) Likewise, $\mathcal{T}$ describes a source function built from the stress-energy tensor describing a small body orbiting the black hole.

Somewhat amazingly, Eq. (62) separates: putting

$$\Psi=\int d\omega\sum_{lm}R_{lm\omega}(r)S_{lm\omega}(\theta)e^{im\phi-i\omega t} \tag{63}$$

and applying a similar decomposition to the source $\mathcal{T}$, we find that $S_{lm\omega}(\theta)$ is a "spin-weighted spheroidal harmonic" (a basis for tensor functions in a non-spherical background), and that $R_{lm\omega}(r)$ is governed by a simple ordinary differential equation. Ψ characterizes Kerr perturbations in much the same way that Q [cf. Eq. (56)] characterizes them for Schwarzschild. Although the perturbation equations are often solved numerically, analytic solutions are known [61], and can dramatically improve one's scheme for solving for black hole perturbations; see Refs. [62, 63].

How do we describe the motion of a small body about a black hole? The most rigorous approach is to enforce $\nabla^\mu T_{\mu\nu}=0$, where $T_{\mu\nu}$ describes the small body in the spacetime of the large black hole. Neglecting the small body's perturbation to the spacetime, we find the geodesic equation $u^\mu\nabla_\mu u^\nu=0$, where u^μ is the small body's 4-velocity. Geodesic black hole orbits have been studied extensively; see, for example, Ref. [64], Chapter 33. They are characterized (up to initial conditions) by three conserved constants: energy E, axial angular momentum L_z, and "Carter's constant" Q. If the black hole does not rotate, Carter's constant is related to the orbit's total angular momentum: $Q(a=0)=\mathbf{L}\cdot\mathbf{L}-L_z^2$. When the black hole rotates rapidly, Q is not so easy to interpret; the idea that it is essentially the rest of the orbit's angular momentum can be useful.

Taking into account perturbations from the small body, $\nabla^\mu T_{\mu\nu}=0$ now implies that the small body follows a "forced" geodesic,

$$u^\mu\hat{\nabla}_\mu u^\nu=f^\nu\,, \tag{64}$$

where $\hat{\nabla}_\mu$ is the covariant derivative in the background spacetime. The novel feature of Eq. (64) is the *self force* f^ν, a correction to the motion of order the small body's spacetime perturbation. The self force is so named because it arises from the body's interaction with its own spacetime correction.

Computing the gravitational self force near a black hole is an active area of current research. It is useful to break the self force into a *dissipative* piece, $f^\nu_{\rm diss}$, which is asymmetric under time reversal, and a *conservative* piece, $f^\nu_{\rm cons}$, which is symmetric. Dissipation causes the "conserved" quantities (E,L_z,Q) to decay, driving inspiral of the small body. Quinn and Wald [65] have shown that the rate at which E and L_z change due to $f^\nu_{\rm diss}$ is identical to what is found when one computes the fluxes of energy and angular momentum encoded by the Isaacson tensor (16).

The conservative self force does not cause orbit decay. "Conserved" constants remain conserved, but the orbits are shifted from the background geodesics. This reflects the fact that, even neglecting dissipation, the small body's motion is determined by the full spacetime, not just the background black hole. Conservative effects shift the orbital frequencies by an amount

$$\delta\Omega_x\sim\Omega_x\times(\mu/M) \tag{65}$$

[where $x \in (\phi, \theta, r)$]. Because the GWs have spectral support at harmonics of the orbital frequencies, these small but non-negligible frequency shifts are directly encoded in the waves that the binary generates. Good discussion and a toy model can be found in [66].

There has been enormous progress in understanding self forces on orbits around non-rotating holes. Barack and Sago [67] have completed an analysis of the full self force for circular orbits about a Schwarzschild black hole; generalization to eccentric orbits is in progress (L. Barack, private communication). An independent approach developed by Detweiler [68] has been found to agree with Barack and Sago extremely well; see [69] for detailed discussion of this comparison.

4.2 Gravitational waves from extreme mass ratio binaries

We now discuss the properties of GWs and GW sources as calculated using perturbation theory. Our goal is to highlight features of the Kerr inspiral waveform. We will neglect the conservative self force, which is not yet understood for the Kerr case well enough to be applied to these waves. When conservative effects are neglected, the binary can be regarded as evolving through a sequence of geodesics, with the sequence determined by the rates at which GWs change the "constants" E, L_z, and Q. Modeling compact binaries in this limit takes three ingredients: First, a description of black hole orbits; second, an algorithm to compute GWs from the orbits, and to infer how the waves' backreaction evolves us from orbit to orbit; and third, a method to integrate along the orbital sequence to build the full waveform. A description of this method is given in [70]; we summarize the main results of these three ingredients here.

4.2.1 Black hole orbits.

Motion near a black hole can be conveniently written in the coordinates of Eq. (59) as $r(t)$, $\theta(t)$, and $\phi(t)$. Because t corresponds to time far from the black hole, this gives a useful description of the motion as measured by distant observers. *Bound* orbits are confined to a region near the hole. They have $r_{\rm min} \le r(t) \le r_{\rm max}$ and $\theta_{\rm min} \le \theta(t) \le \pi - \theta_{\rm min}$, and thus occupy a torus in the 3-space near the hole's event horizon; an example is shown in Fig. 4, taken from [71]. Selecting the constants E, L_z, and Q fully determines $r_{\rm min/max}$ and $\theta_{\rm min}$. It is useful for some discussions to reparameterize the radial motion, defining an eccentricity e and a semi-latus rectum p via

$$r_{\rm min} = \frac{p}{1+e} \,, \qquad r_{\rm max} = \frac{p}{1-e} \,. \tag{66}$$

For many bound black hole orbits, $r(t)$, $\theta(t)$, and $\phi(t)$ are periodic [72, 73]. (Exceptions are orbits which plunge into the hole; we discuss these below.) Near the hole, the time to cover the full range of r becomes distinct from the time to cover the θ range, which becomes distinct from the time to cover 2π radians of azimuth. One can say that spacetime curvature splits the Keplerian orbital frequency Ω into Ω_r, Ω_θ, and Ω_ϕ. Figure 5 shows these three frequencies, plotted as functions of semi-major axis A for fixed values of e and $\theta_{\rm min}$. Notice that all three approach $\Omega \propto A^{-3/2}$ for large A.

4.2.2 Gravitational radiation from orbits.

Because their orbits are periodic, GWs from a body orbiting a black hole will have support at harmonics of the orbital frequencies. One can write the two polarizations

$$h_+ + i h_\times = \sum H_{mkn} e^{i\omega_{mkn} t} \,, \qquad \text{where} \tag{67}$$

$$\omega_{mkn} = m\Omega_\phi + k\Omega_\theta + n\Omega_r \,. \tag{68}$$

The amplitude H_{mkn} can be found by solving the Teukolsky equation (62) using the decomposition (63); details for the general case can be found in [71].

The expansion (67) does not work well for orbits that plunge into the black hole; those orbits are not periodic, and cannot be expanded using a set of real frequencies. A better way to calculate those waves is to solve the Teukolsky equation (62) *without* introducing the decomposion (63). Results for waves from

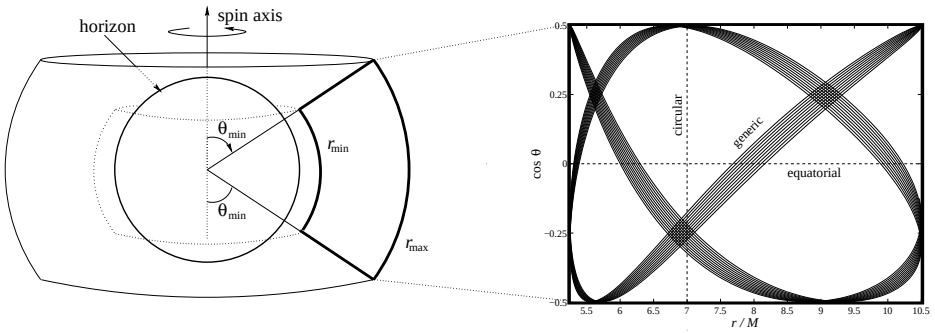

Figure 4: The geometry of a generic Kerr black hole orbit [taken from [71]]. This orbit is about a black hole with spin parameter $a = 0.998M$ (recall $a \leq M$, so this represents a nearly maximally spinning black hole). The range of its radial motion is determined by $p = 7GM/c^2$ (G and c are set to 1 in the figure) and $e = 1/3$; θ ranges from 60° to 120°. The left panel shows the torus in coordinate space this torus occupies. The right panel illustrates how a generic orbit ergodically fills this torus.

plunging orbits in the language of perturbation theory were first given by Damour, Nagar, and Tartaglia [74]; Sundararajan [75] has recently extended the cases that we can model to full generality.

As mentioned above, it is fairly simple to compute the flux of energy $\dot{E}$ and angular momentum $\dot{L}_z$ from the Isaacson tensor, Eq. (16), once the waves are known. Recent work [76] has shown that a similar result describes $\dot{Q}$. Once $\dot{E}$, $\dot{L}_z$, and $\dot{Q}$ are known, it is straightforward to evolve the orbital elements $r_{\rm min/max}$ and $\theta_{\rm min}$, specifying the sequence of orbits through which GWs drive the system. Once that sequence is known, it is straightforward to build the worldline that a small body follows as it spirals into the black hole. From the worldline, we can build a source function $\mathcal{T}(t)$ for Eq. (62) and compute the evolving inspiral waves.

4.3 Mapping black hole spacetimes

Extreme mass ratio GW events may allow a unique and powerful measurement: We may use them to "map" the spacetimes of black holes and test how well they satisfy the stringent requirements of GR. As discussed above, an extreme mass ratio inspiral is essentially a sequence of orbits. Thanks to the mass ratio, the small body moves through this sequence slowly, spending a lot of time "close to" any orbit in the sequence. Also thanks to the mass ratio, each orbit's properties are mostly determined by the larger body. In analogy to *geodesy*, the mapping of earth's gravity with satellite orbits, one can imagine *bothrodesy*[3], the mapping of a black hole's gravity by studying the orbits of inspiraling "satellites."

In more detail, consider first Newtonian gravity. The exterior potential of a body of radius R can be expanded in a set of multipole moments:

$$\Phi_N = -\frac{GM}{r} + G\sum_{l=2}^{\infty}\left(\frac{R}{r}\right)^{l+1} M_{lm}Y_{lm}(\theta,\phi)\ . \tag{69}$$

Studying orbits allows us to map the potential Φ_N, and thus to infer the moments M_{lm}. By enforcing Poisson's equation in the interior, $\nabla^2\Phi_N = 4\pi G\rho$, and then matching at the surface R, one can relate the moments M_{lm} to the distribution of matter. In this way, orbits allow us to map in detail the distribution of matter in a body like the earth.

Bothrodesy applies the same idea to a black hole. The spacetime of any stationary, axisymmetric body can be described by a set of "mass moments" M_l, similar to the M_{lm} of Eq. (69); and a set of "current moments" S_l which describe the distribution of mass-energy's *flow*. The moments of a black hole take a simple, special form: for a Kerr black hole (59) with mass M and spin parameter a,

$$M_l + iS_l = M(ia)^l\ . \tag{70}$$

[3]This name was coined by Sterl Phinney, and comes from the word $\beta o\theta\rho o\varsigma$, which refers to a sacrificial pit in ancient Greek. This author offers an apology to speakers of modern Greek.

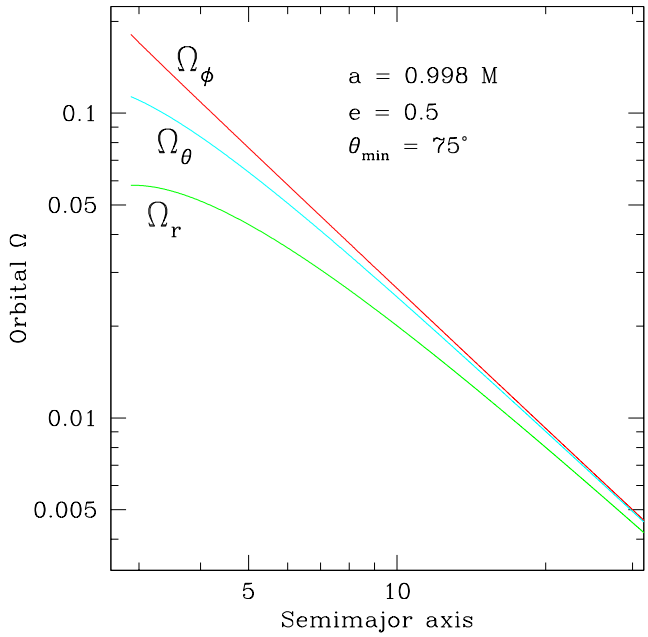

Figure 5: Orbital frequencies for generic Kerr black hole orbits. We vary the orbits' semilatus rectum p, but fix eccentricity $e = 0.5$ and inclination parameter $\theta_{\rm min} = 75°$. Our results are plotted as a function of semimajor axis $A = p/\sqrt{1-e^2}$. All three frequencies asymptote to the Keplerian value $\Omega = \sqrt{GM/A^3}$ in the weak field, but differ significantly from each other in the strong field.

A black hole has a mass moment $M_0 = M$ and a current moment $S_1 = aM$ (i.e., the magnitude of its spin is aM, modulo factors of G and c). *Once those moments are known, all other moments are fixed if the Kerr solution describes the spacetime.* This is a restatement of the "no hair" theorem [77, 78] that a black hole's properties are set by its mass and spin.

The facts that an object's spacetime and orbits are determined by its multipoles, and that the Kerr moments take such a simple form, suggests a consistency test: Develop an algorithm for mapping the multipolar structure by studying orbits, and check that the $l \geq 2$ moments satisfy Eq. (70). Ryan [79] first demonstrated that such a measurement can be done, and Brink [80] has recently clarified what must be done for such measurements to be done in practice. Collins and Hughes [81] took the first steps in formulating this question as a null experiment (with the Schwarzschild solution as the null hypothesis). Glampedakis and Babak [82] formulated a similar approach appropriate to Kerr black holes; Vigeland and Hughes [83] have recently extended the Collins and Hughes formalism in that direction.

A robust test of the Kerr solution is thus a very likely outcome of measuring waves from extreme mass ratio captures. If testing metrics is not your cup of tea, precision black hole metrology may be: In the process of mapping a spacetime, one measures with exquisite accuracy both the mass and the spin of the large black hole. Barack and Cutler [84] have found that in most cases these events will allow us to determine both the mass and the spin of the large black hole with 0.1% errors are better. GW measurements will give us a precise picture of these amazing objects.

Acknowledgments

Portions of this proceedings article were adapted from previous reviews I have written or cowritten (Refs. [3, 60]). Much of the research discussed here was done in collaboration with my collaborators Steve Drasco, Éanna Flanagan, and Gaurav Khanna, as well as my current and former graduate students Nathan Collins, Ryan Lang, Pranesh Sundararajan, and Sarah Vigeland. My group's research in gravitational waves and

compact binaries is supported by NSF Grant PHY-0449884 and NASA Grant NNX08AL42G; some of the work discussed here was also supported by NASA Grant NNG05G105G and the MIT Class of 1956 Career Development Fund. I gratefully acknowledge the support of the Adam J. Burgasser Chair in Astrophysics at MIT in completing this conference writeup.

References

[1] J. D. Jackson, *Classical electrodynamics* (Wiley, New York, 1975).

[2] A. S. Eddington, Proc. Roy. Soc. Lond. **A102**, 268 (1922).

[3] E. E. Flanagan and S. A. Hughes, New J. Phys. **7**, 204 (2005).

[4] R. A. Isaacson, Phys. Rev. **166**, 1272 (1968).

[5] S. L. Shapiro and S. A. Teukolsky, *Black Holes, White Dwarfs, and Neutron Stars: The Physics of Compact Objects* (Wiley, New York, 1983).

[6] J. M. Weisberg and J. H. Taylor, in *The Relativistic Binary Pulsa B1913+16: Thirty Years of Observations and Analysis*, Astron. Soc. of the Pac. Conf. Ser. **328**, 25 (2005).

[7] I. H. Stairs et al., Astrophys. J. **505**, 352 (1998).

[8] D. J. Nice et al., Astrophys. J. **634**, 1242 (2005).

[9] B. A. Jacoby et al., Astrophys. J. Lett. **644**, L113 (2006).

[10] M. Kramer and I. H. Stairs, Ann. Rev. Astron. Astrophys. **46**, 541 (2008).

[11] N. D. R. Bhat, M. Bailes, and J. P. W. Verbiest, Phys. Rev. D **77**, 124017 (2008).

[12] L. Kasian, AIP Conf. Ser. **983**, 485 (2008).

[13] D. Eichler, M. Livio, T. Piran, and D. N. Schramm, Nature **340**, 126 (1989).

[14] D. B. Fox et al., Nature **437**, 845 (2005).

[15] E. Nakar, A. Gal-Yam, and D. B. Fox, Astrophys. J. **650**, 281 (2006).

[16] S. Komossa et al., Astrophys. J. Lett. **582**, L15 (2003).

[17] H. L. Maness et al., Astrophys. J. **602**, 123 (2004).

[18] C. Rodriguez et al., Astrophys. J. **646**, 49 (2006).

[19] H. Zhou, T. Wang, X. Zhang, X. Dong, and C. Li, Astrophys. J. Lett. **604**, L33 (2004).

[20] B. F. Gerke, Astrophys. J. Lett. **660**, L23 (2007).

[21] M. C. Begelman, R. D. Blandford, and M. J. Rees, Nature **287**, 307 (1980).

[22] J. E. Conway and J. M. Wrobel, Astrophys. J. **439**, 98 (1995).

[23] A. P. Lobanov and J. Roland, Astron. Astrophys. **431**, 831 (2005).

[24] M. J. Valtonen et al., Nature **452**, 851 (2008).

[25] R. Narayan, T. Piran, and A. Shemi, Astrophys. J. Lett. **379**, L17 (1991).

[26] E. S. Phinney, Astrophys. J. Lett. **380**, L17 (1991).

[27] V. Kalogera, K. Belczynski, C. Kim, R. O'Shaughnessy, and B. Willems, Phys. Rep. **442**, 75 (2007).

[28] L. J. Spitzer, Astrophys. J. Lett. **148**, 139 (1969).

[29] S. F. Portegies Zwart and S. L. W. McMillan, Astrophys. J. Lett. **528**, L17 (2000).

[30] R. M. O'Leary, R. O'Shaughnessy, and F. A. Rasio, Phys. Rev. D **76**, 6 (2007).

[31] A. D. Mackey, M. I. Wilkinson, M. B. Davies, and G. F. Gilmore, Mon. Not. R. Astron. Soc. **386**, 65 (2008).

[32] K. Menou, Z. Haiman, and V. K. Narayanan, Astrophys. J. **558**, 535 (2001).

[33] Q. Yu and S. Tremaine, Mon. Not. R. Astron. Soc. **335**, 965 (2002).

[34] M. Volonteri, F. Haardt, and P. Madau, Astrophys. J. **582**, 559 (2003).

[35] Z. Haiman, L. Ciotti, and J. P. Ostriker, Astrophys. J. **606**, 763 (2004).

[36] P. F. Hopkins, T. J. Cox, D. Kereš, and L. Hernquist, Astrophys. J. Suppl. **175**, 390 (2008).

[37] T. Di Matteo, J. Colberg, V. Springel, L. Hernquist, and D. Sijacki, Astrophys. J. **676**, 33 (2008).

[38] S. Sigurdsson and M. J. Rees, Mon. Not. R. Astron. Soc. **284**, 318 (1997).

[39] C. Hopman and T. Alexander, Astrophys. J. **629**, 362 (2005).

[40] Y. Rathore, R. D. Blandford, and A. E. Broderick, Mon. Not. R. Astron. Soc. **357**, 834 (2005).

[41] K. Menou, Z. Haiman, and K. Menou, New Astron. Rev. **51**, 884 (2008).

[42] V. Faraoni, Gen. Rel. Grav. **39**, 677 (2007).

[43] L. S. Finn, Phys. Rev. D **79**, 022002 (2008).

[44] J. Hough and S. Rowan, Liv. Rev. Rel. **3**, 3 (2000).

[45] M. Tinto and S. V. Dhurandar, Liv. Rev. Rel. **8**, 4 (2005).

[46] P. Fritschel, *Second generation instruments for the Laser Interferometer Gravitational Wave Observatory (LIGO)*, SPIE Conf. Ser. **4856**, 282 (2003).

[47] D. E. McClelland, *Status of the Australian consortium for interferometric gravitational astronomy*, in Proceedings of the 9th Marcel Grossman Meeting, eds. V. G. Gurzadyan, R. T. Jantzen, and R. Ruffini, p. 1864 (2002).

[48] A. C. Searle, S. M. Scott, D. E. McClelland, and L. S. Finn, Phys. Rev. D **73**, 124014 (2006).

[49] S. Vitale, gr-qc/0504062.

[50] S. Kawamura et al., Class. Quantum Grav. **23**, 125 (2006).

[51] L. D. Landau and E. M. Lifschitz, *The classical theory of fields* (Pergamon, London, 1975).

[52] L. Blanchet, Liv. Rev. Rel. **9**, 4 (2006).

[53] K. S. Thorne and J. B. Hartle, Phys. Rev. D **31**, 1815 (1985).

[54] L. Blanchet, T. Damour, B. R. Iyer, C. M. Will, and A. G. Wiseman, Phys. Rev. Lett. **74**, 3515 (1995).

[55] R. N. Lang and S. A. Hughes, Phys. Rev. D **74**, 122001 (2006).

[56] L. Rezzolla, *Gravitational waves from perturbed black holes and relativistic stars*, in ICTP Lecture Series **3** (2003).

[57] F. J. Zerilli, Phys. Rev. D **2**, 2141 (1970).

[58] T. Regge and J. A. Wheeler, Phys. Rev. **108**, 1063 (1957).

[59] S. A. Teukolsky, Astrophys. J. **185**, 635 (1973).

[60] S. A. Hughes, Ann. Rev. Astron. Astrophys. **47**, 107 (2009).

[61] S. Mano, H. Suzuki, and E. Takasugi, Prog. Theo. Phys. **95**, 1079 (1996).

[62] R. Fujita and H. Tagoshi, Prog. Theor. Phys. **112**, 415 (2004).

[63] R. Fujita and H. Tagoshi, Prog. Theor. Phys. **113**, 1165 (2005).

[64] C. W. Misner, K. S. Thorne, and J. A. Wheeler, *Gravitation* (W. H. Freeman and Co., San Francisco, 1973).

[65] T. C. Quinn and R. M. Wald, Phys. Rev. D **60**, 064009 (1999).

[66] A. Pound, E. Poisson, and B. G. Nickel, Phys. Rev. D **72**, 124001 (2005).

[67] L. Barack and N. Sago, Phys. Rev. D **75**, 064021 (2007).

[68] S. Detweiler, Phys. Rev. D **77**, 124026 (2008).

[69] N. Sago, L. Barack, and S. Detweiler, Phys. Rev. D **78**, 124024 (2008).

[70] S. A. Hughes, S. Drasco, E. E. Flanagan, and J. Franklin, Phys. Rev. Lett. **94**, 221101 (2005).

[71] S. Drasco and S. A. Hughes, Phys. Rev. D **73**, 024027 (2006).

[72] W. Schmidt, Class. Quantum Grav. **19**, 2743 (2002).

[73] S. Drasco and S. A. Hughes, Phys. Rev. D **69**, 044015 (2004).

[74] A. Nagar, T. Damour, and A. Tartaglia, Class. Quantum Grav. **24**, 109 (2007).

[75] P. A. Sundararajan, Phys. Rev. D **77**, 124050 (2008).

[76] K. Ganz, W. Hikida, H. Nakano, and T. Tanaka, Prog. Theor. Phys. **117**, 1041 (2007).

[77] B. Carter, Phys. Rev. Lett. **26**, 331 (1971).

[78] D. C. Robinson, Phys. Rev. Lett. **34**, 905 (1975).

[79] F. D. Ryan, Phys. Rev. D **52**, 5707 (1995).

[80] J. Brink, Phys. Rev. D **78**, 102001 (2008).

[81] N. A. Collins and S. A. Hughes, Phys. Rev. D **69**, 124022 (2004).

[82] K. Glampedakis and S. Babak, Class. Quantum Grav. **23**, 4167 (2006).

[83] S. J. Vigeland and S. A. Hughes, Phys. Rev. D **81**, 024030 (2010).

[84] L. Barack and C. Cutler, Phys. Rev. D **69**, 082005 (2004).

X-Ray Observation of Black Hole Candidates

Shunji Kitamoto [1](a),(b)

(a) *Department of Physics, Rikkyo University, Toshima, Tokyo 171-8501*
(b) *Research Center for Measurement in Advanced Science, Rikkyo University, Toshima, Tokyo 171-8501*

Abstract

The observation strategy of Black Hole (BH) candidates is now changing. We are entering a new era to investigate fundamental properties of BHs. Some challenging observations have been performed. However the environmental nature of vicinity of BHs, an accretion flow around BHs, is still unclear. Recent observations reveal their further complexity.

1 Introduction

There are three kinds of black hole candidates. One is a stellar mass BH, which is an end of evolution of massive stars. Second one is a super massive BH. We now believe that majority of galaxies are hosts of a BH and have been co-evolved with the BH. Third is an intermediate mass BH. Ultra luminal sources, which we can find in some galaxies except for its nucleus, are candidates of this category, but we have not yet understood well this kind of BHs. Thus we do not discuss the intermediate mass BHs in this work, and we mainly concentrate on the stellar mass BHs.

Many of X-ray bright stars are known to be binaries. Among them some have the following three characteristics. One is a rapid time variation in its intensity. Some have a time scale of 1 ms. Second is a very bright luminosity. The luminosity is roughly 10^{38} erg s^{-1}, although the intensity is highly variable. Third is a typical temperature of $\sim$1 keV. These characteristics can be explained by a model; mass accretion onto a small and massive object. The candidates of the small and massive objects are compact stars; white dwarfs, neutron stars, and BHs. The identification, what is the small and massive object, is a very difficult problem. Especially a distinction from neutron stars to BHs, is a tough work. Tanaka & Shibazaki [1] showed a beautiful figure of X-ray energy spectra of bright X-ray stars, where X-ray spectra of some stars are explained by a combination of emissions from an accretion disk and from a surface of a neutron star, but some show very soft spectra explained by only an emission from an accretion disk lacking an emission from a surface of a neutron star. These objects, spectra of which can be explained by only an accretion disk, are called ultra soft sources and are considered to be BH candidates. There are another kind of BH candidates. They have some characteristics, which are similar to those of other BH candidates, for example power-law type energy spectra, rapid time variations and so on.

The most reliable candidates are called "dynamical BHs". Some of the binaries can be measured their orbital velocity via an observation of their Doppler shift. Although there is uncertainty due to an un-known inclination of an orbital plane, a lower limit of the mass can be estimated form their orbital motion. If a lower-limit mass, or an estimated mass, is greater than ~ 3 $M_\odot$, the object is considered to be a BH, and is called "dynamical BH". Now 20 dynamical BHs are known [2]. Distributions of the estimated mass of the dynamical BHs are plotted in figure 1. All are less than 16 $M_\odot$, and reasonably considered to be a remnant of massive stars.

In this way, compact stars with a mass of greater than ~ 3 $M_\odot$ certainly exist as celestial objects. In other word, if compact stars with a mass of more than ~ 3 $M_\odot$ are BHs, an existence of BHs as celestial objects is now beyond dispute.

[1]Email address: kitamoto@rikkyo.ac.jp

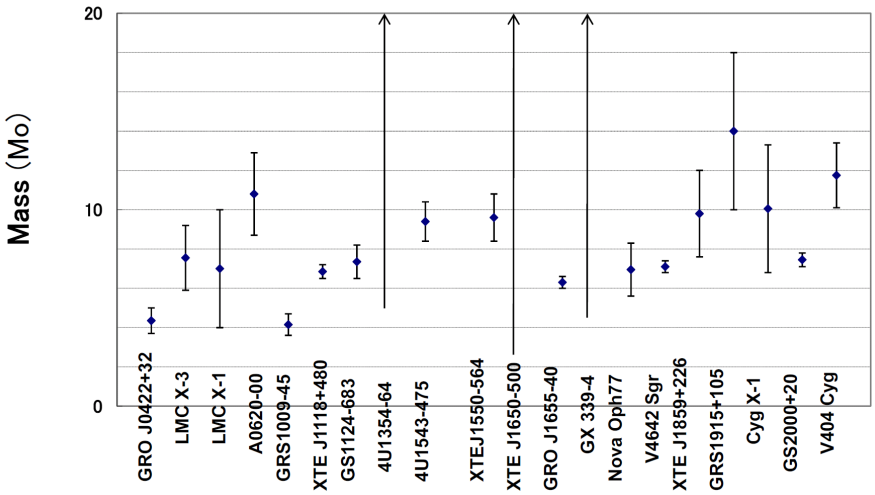

Figure 1: Mass distribution of 20 "dynamical BHs".

2 Observation of BH Properties

2.1 Radius of ISCOs

If we can measure a radius of an inner most stable circular orbit (ISCO) around a compact star, we can distinguish BHs from neutron stars. In addition, lots of information is contained in the radius of ISCO. Estimation of radii of ISCOs was reported by Ebisawa et al. [7]. They applied a general relativistic accretion disk model to two BH candidates and two neutron star sources. The model is most sensitive to a mass of a compact star, via a radius of its ISCO. The model also depends on an inclination angle of an accretion disk. A difficulty of this method is that the model depends of the mass accretion rate. The mass accretion rate is derived from a luminosity and thus we have to assume a distance to the object. They derived significant higher mass of the above two BH candidates than those of the two neutron stars.

Similar analyses were applied to intensity variable objects, LMC X-3 [6], and GS 2000+25 [8], using a more simple accretion disk model. Ebisawa et al. [6] showed that the mass of LMC X-3, determined via the above method, is almost constant against the variation of the luminosity. Terada et al. [8] showed that the inner radius of the accretion disk of GS2000+25 is almost constant during the intensity decay with more than two orders of magnitude. However these attempts are strongly model dependent, and we know that a simple accretion disk model is just an approximation and the absolute values derived from this method is not reliable.

2.2 BH Spins

The other important property of BHs is its spin. In the case of stellar mass BHs, their active life-time is less than $\sim 10^8$ yr and their accretion rate is also less than $\sim 10^{-8}$ $M_\odot$ yr^{-1}. Thus the accumulated mass via an accretion is not more than their mass. Therefore they gain most of their angular momentum at the moment of their birth. Investigation of a spin distribution of stellar mass BHs discloses a nature of super novae or a nature of first BHs in the universe. This situation is different in the case of super massive BHs. Their age is as much as the age of the universe and their accretion rate is ~ 1 $M_\odot$ yr^{-1}. Thus the accreted mass is much larger than their mass, which is $\sim 10^{7\sim 8}$ $M_\odot$. They gain most of their angular moment during their evolution. Investigation of their spin is investigation of their growing-up history. Since the accreting matter should move as an quasi-Keplerian, the most of super massive BHs should be extremely spinning.

BH spins can be measured by determining an innermost stable circular orbit (ISCO) by observing an orbiting accretion disk. A radius of an ISCO of Schwarzschild BHs is 6 R_g, but it of maximal Kerr BHs is near 1 R_g, where R_g is the gravitational radius. There are some possible methods for measurement of the

radius of an ISCO. One is a measurement of a shape of emission lines from orbiting accretion disks. The emission lines emitted from inner part of an accretion disk suffer relativistic effects; the gravitational red shift, the Doppler shift and the beaming effect. Consequently an observed shape of the emission lines are skewed and double hones shape depending on an inclination, radial distribution of the intensity and the radius of the ISCO [3, 4]. A detection of such lines are first reported by Tanaka et al. [5] from a bright Seyfert galaxy, MCG 6-30-15. An important fact for the line shape measurement is that it depends on the radius of a ISCO normalized by the gravitational radius. Therefore the shape is independent on a BH mass.

A continuum emission from an accretion disk has also information of a radius of an ISCO. The continuum emission from an accretion disk becomes hotter and more luminous, by shrinking the radius of the ISCO. High frequency QPOs also have information of a radius of an ISCO. If we know a BH mass, we can discuss its BH spin.

3 X-Ray Observation

X-rays come from an accretion disk, but its emission mechanism is not yet well understood. In general, two types of accretion disks are known. One is the standard accretion disk [9], which is optically thick and geometrically thin. An accreting matter flows as roughly Keplerian motion. The other is called as an "ADAF"[10] or a "RIAF", which is optically thin and geometrically thick. An accreting matter flows as advection dominant motion and its radiation efficiency is low. Depending on a mass accretion rate, accretion disks show typically either of these two types of accretion disks. We classify them as a "low state" and a "high state". By more higher mass accretion rate, accretion disks change to the other state, where a high temperature corona appears and becomes thick. This is, observationally, called "very high state" [11]. Between the "low state" and the "high state", sometimes an "intermediate state" appears.

In the low state, where the accretion is considered to be the "ADAF". The energy spectrum can be roughly simulated by a power law with a cut-off around 100 keV. On the other hand, the spectra in the high state can be roughly simulated by a multi color black body [12] with a high energy tail component.

In this paper, we will summarize Suzaku [13] observations of three BH candidates, GRO J1655-40, Cyg X-1 and GX 339-4. Suzaku is the fifth Japanese X-ray observatory launched on July 10, 2005. Three main instruments were installed; the X-ray Imaging Spectrometer (XIS)[16], which consists of four CCD cameras, the Hard X-ray Detector (HXD)[17, 18], consisting a Si PIN detector array and GSO scintillators and the X-Ray Spectrometer (XRS), which is a micro-calorimeter having $\sim$10 eV energy resolution[14]. The XIS and XRS were installed on focal planes of the five X-ray telescopes (XRT)[15]. Suzaku has the following three superior characteristics;

- Suzaku covers a wide energy band from 0.3 keV to 400 keV.
- The CCD cameras, covering the energy range from 0.2 keV to 10 keV, have large effective area and low background with a moderate energy resolution.
- The HXD, covering the energy range from 10 keV to 400 keV, has extremely low back ground.

3.1 GRO J1655-40 Observed with Suzaku

An X-ray energy spectrum of a micro-quasar, GRO J1655-40, was obtained by Suzaku. The results of GRO J1655-40 have been published by Takahashi et al. [19]. The spectrum was significantly detected in an extremely wide energy range from 0.6 keV to 300 keV. The overall spectra can be roughly simulated by a power-law with a high energy cut off, by taking account of an photoelectric absorption. However, the statistically good spectra cannot be fitted by such a simple model. Thus we apply more physical model which shows the high-energy cut-off. A Comptonized model of soft photons by hot electrons is one possible model. The origin of the soft photons is not identified but most general interpretation is an optically thick accretion disk. Then they tried a model consisting of a disk component and a Comptonized component. The residuals of the data from the best fit model show bump in the high energy region comparing to the best fit model. This means that the data have a concave structure around 10 keV region. Usually this structure is interpreted as a reflection by an accretion disk. By including a reflection, the fitting

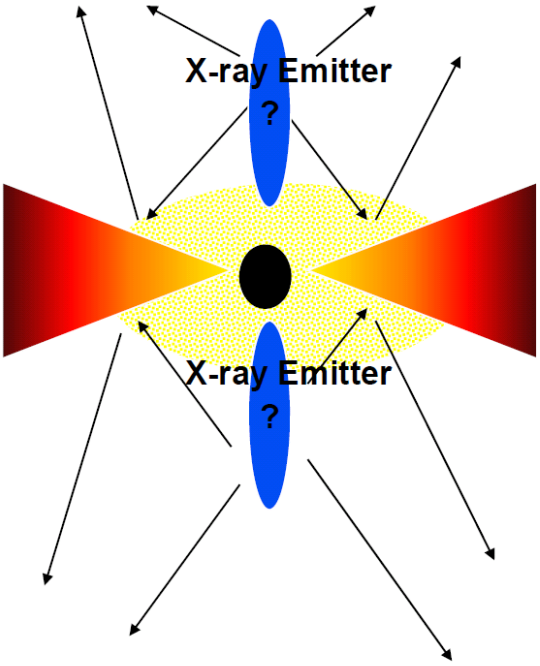

Figure 2: A cartoon of an inner region of an accretion flow. Primary X-rays are emitted from a surface of the accretion disk and also from somewhere near a BH. The inner part of the accretion disk is covered by a hot plasma, which is not spherical.

is slightly improved, but there is still a hump in the high energy region. Then they tried another Comptonization component with a different y-parameter (a different temperature or a different optical depth) of a hot plasma, instead of the reflection. The fitting becomes dramatically better. Finally they added two reflection components corresponding to the two Comptonization components. The fitting becomes slightly better. Then they obtained a reasonable fit in all the wide energy range.

Although they included a Gaussian function for a Fe-K emission line, it was not significant. The spectrum, in a narrow energy range from 5 keV to 8 keV, can be well fitted by a simple power law model with no emission or no absorption line like feature.

From the high quality spectrum obtained by Suzaku, they found that the inner part of the accretion disk is very complex. They introduced two Compotonization components. However, this should be only a simple approximation of a complex structure of the accretion disk, for example multiple component of Comptonization, or more naturally the hot plasma has a temperature distribution and/or non-spherical shape and thus has a distribution of its optical depth. A simple cartoon is shown in figure 2.

3.2 Cygnus X-1 Observed with Suzaku

Cygnus X-1 is the most famous BH candidate. Suzaku observed Cyg X-1 and obtained a wide band and high quality spectrum. Makishima et al. [20] reported its results. The similar analysis was performed for data of Cyg X-1, to that of GRO J1655-40. Consequently the spectrum was fitted by the same model; Disk component plus two Comptonization components and their reflections. The spectra of Cyg X-1 and GRO J1655-40 are essentially the same, and only their parameters are different.

The differences between them are the mass of the BHs and the inclination of the orbital plane. The mass of Cyg X-1 is $12\sim20 M_\odot$, while that of GRO J1655-40 is $\sim$6.5 $M_\odot$. The inclination angles of the Cyg X-1 and GRO J1655-40 are $\sim 40^\circ$ and $\sim 70^\circ$, respectively. Their luminosities, when Suzaku observed them, were $\sim 4.4\times10^{37}$ erg s^{-1} and $\sim 4.9\times10^{36}$ erg s^{-1}, respectively. If we compare their luminosity normalized by their Eddington luminosity, that of Cyg X-1 is larger than GRO J1655-40 by a factor of

$3 \sim 5$.

Makishima et al. [20] compared their spectra in a model independent manner, using a spectral ratio (spectrum of GRO J1655-40 divided by that of Cyg X-1). We can see some features in the ratio. Below $\sim$2 keV, the spectral ratio decreased significantly. This is mainly due to the large contribution of the disk component in Cyg X-1. The prime reason of this is a difference of their inclination angle. Since the inclination angle of GRO J1655-40 is relatively large, the disk component should be strongly occulted by the disk itself, while we can see the disk of Cyg X-1. We can find a small dip around $\sim$6.5 keV. This is due to a difference of the equivalent widths of Fe-K emission lines. An equivalent width of the Fe-K line in Cyg X-1 is $\sim$ 300 eV, but that of GRO J 1655-40 is much smaller. This small equivalent width of the Fe-K line is also attributed to the large inclination angle of GRO J1655-40, since the Fe-K line is thought to be fluorescence by the accretion disk. There is a concave structure from $\sim$5 keV to $\sim$50 keV, and this structure can be explained by the two reasons. One is the difference of the index of the power law components. GRO J1655-40 is a little flat spectrum, hence a large y-parameter of the Compotonization. This might be due to a high temperature of the hot plasma due to a small luminosity of the GRO J1655-40. Overlaying this difference of the power-law index, large contribution of the reflection component in Cyg X-1 makes a broad valley from $\sim$10 keV to $\sim$ 80 keV. This large contribution of the reflection component is again due to the smaller inclination of Cyg X-1 than that of GRO J1655-40.

Thus the spectra of GRO J1655-40 and Cyg X-1 are explained by the essentially same model. Almost all their differences are interpreted by the difference between their inclination angles. In other word, these simple interpretations suggest that the model constructed by the Suzaku observation has very high reliability.

By comparing the parameters of the best fit models of GRO J1655-40 and of Cyg X-1, we can find that relative intensities of the two Comptonization components (hard and soft components) are siginificantly different between GRO J1655-40 and Cyg X-1. The fraction of the hard Comptonization component of GRO J1655-40 is larger than that of Cyg X-1. If we consider that this is also due to the difference of the inclination angles, the hot plasma attributed to the low y-parameter component (soft) might be partially occulted in the case of GRO J1655-40.

These results of the Suzaku observation reveal a possible complex structure of the accretion disk around the BHs. The hot plasma must cover the inner region of the accretion disk. Even the shape of the hot plasma is not spherical. Furthermore it is still questionable whether the observable accretion disk continues into the ISCO or not. It is also notable that the disk truncation has been discussed in order to explain the behavior of GRS J1915-105[21], which is another famous BH candidate.

3.3 GX339-4 Observed with Suzaku

In the previous section, we discussed the results of the two BH candidates observed by Suzaku. Both were in its "low state". Thus the existence of the high temperature plasma or a corona is naturally expected. Therefore we are intrigued with results of the "high state", where the accretion disk is expected to be an optically thick standard disk. Yamada et al. [22] reported the Suzaku observation of GX 339-4, in its unfortunately "very high state". The spectra below $\sim$8 keV is dominated by the disk component, which is roughly described by the multi collar black body. The spectrum above $\sim$8 keV is described by a combination of a power law (or a Comptonization component) and a reflection component. By taking into account the Comptonizaion component, the estimation of the radius of the inner accretion disk yields $R_{in}/R_g = (5\sim32)$. A disk truncation before the ISCO might be suggested.

4 Challenge to Spin Observation

Some BH candidates are considered to be highly rotating. For example, GRO J1655-40 and GRS J1915-105 show jets with a super-luminal motion, suggesting their unusual nature. Some models for jet production in BHs involve BH spin [24].

Although there are several ways to investigate a BH spin, currently the most productive manner is by using a shape of a Fe-K line. A broad and skewed Fe-K line emission by strong relativistic effects was predicted by Fabian et al. [3]. A detection of such a broad Fe-K line was first reported by Tanaka et al. [5] in the Seyfert galaxy MCG 6-30-15. Analyzing a detailed shape of the Fe-K line from MCG 6-30-15,

Miniutti et al. [25] indicated its high spin. The best advantage of this study is the fact that the shape does not depend on BH masses and thus not depend on the distance to objects.

Similar attempts have been performed by Miller et al. [26, 27, 28], Miniutti et al. [30], and Laor [31]. Miller et al. [29] compiled results of spins of eight stellar-mass BHs, including GX339-4, GRO J1655-40 and Cyg X-1. They reported their spin distributions. Two BHs, GRO J1655-40 and GX 339-4, among them have spin parameters more than 0.9, whereas Cyg X-1 has less than 0.1.

However, Yamada et al. [22] are giving a caution for a treatment of continuum spectra. They showed that a careful data analysis lead a result of a narrow Fe-K line profile and does not requires any broad and highly skewed shape. On the detection of Fe-K line from GRO J1655-40, there is a confliction from Suzaku data by Takahashi et al. (2008), where no significant detection of the Fe-K line was reported.

GRS J1915-105 was also studies the shape of its Fe K-line[23]. Their result showed that the inner emitting orbit is larger than the ISCO, even in Schwarzschild metric, suggesting a disk truncation. Therefore the observation of BH spins from the Fe-K line shape is still keeping straying.

5 Summary

So far 20 galactic BHs have been dynamically confirmed. Now we are going to start an investigation of properties of BHs such as BH spins. A radius of an inner most stable circular orbit (ISCO) directly relate to its mass and its spin. The BH spins are also measureable by a shape of a Fe-K emission line, which depends on a normalized radius of a ISCO by a gravitational radius.

However, we have not yet well understood an X-ray emission from an accretion disk. The accretion flow into a BH is complex and thus observations of ISCOs are not easy. The existence of two Compton components probably relates to the geometrical configuration of the hot plasma around the ISCO. The inner part of the accretion disk should affected by complex situations; magnetic field, high photon density, advection dominant flow and so on. These effects might make a disk truncation at outer region than ISCO.

A shape of Fe-K lines gives us important information on the inner region of the accretion disk, if the lines originate the fluorescence of an accretion disk. However, analyses of a broad emission line strongly depend on an assumed continuum model. We require statistically better data and need understanding of an accretion flow near ISCO. The investigation of BH spin is a next future topic. One of the important scientific objects of the future satellite missions; such as Astro-H and IXO, is the “Measurement of BH Spin” [32, 33].

References

[1] Tanaka, Y., & Shibazaki, N. 1996, Annual Review of A&A, 34, 607

[2] Remillard, R. A., & McClintock, J. E. 2006, Annual Review of A&A, 44, 49

[3] Fabian, A. C., Rees, M. J., Stella, L., & White, N. E. 1989, Mon. Not. R. Astron. Soc. , 238, 729

[4] Kojima, Y. 1991, Mon. Not. R. Astron. Soc. , 250, 629

[5] Tanaka, Y., et al. 1995, Nature, 375, 659

[6] Ebisawa, K., Makino, F., Mitsuda, K., Belloni, T., Cowley, A. P., Schmidtke, P. C., & Treves, A. 1993, Astrophys. J. , 403, 684

[7] Ebisawa, K., Mitsuda, K., & Hanawa, T. 1991, Astrophys. J. , 367, 213

[8] Terada, K., Kitamoto, S., Negoro, H., & Iga, S. 2002, PASJ, 54, 609

[9] Shakura, N. I., & Sunyaev, R. A. 1976, Mon. Not. R. Astron. Soc. , 175, 613

[10] Narayan, R., & Yi, I. 1994, APJL, 428, L13

[11] Miyamoto, S., Kimura, K., Kitamoto, S., Dotani, T., & Ebisawa, K. 1991, Astrophys. J. , 383, 784

[12] Mitsuda, K., et al. 1984, PASJ, 36, 741

[13] Mitsuda, K., et al. 2007, PASJ, 59, 1

[14] Kelley, R. L., et al. 2007, PASJ, 59, 77

[15] Serlemitsos, P. J., et al. 2007, PASJ, 59, 9

[16] Koyama, K., et al. 2007, PASJ, 59, 23

[17] Takahashi, T., et al. 2007, PASJ, 59, 35

[18] Kokubun, M., et al. 2007, PASJ, 59, 53

[19] Takahashi, H. Fukazawa, Y. Mizuno, T. Hirasawa, A. Kitamoto, S. Sudoh, K. Ogita, T. Kubota, A. Makishima, K. Itoh, T. Parmar, A. N. Ebisawa, K. Naik, S. Dotani, T. Kokubun, M. Ohnuki, K. Takahashi, T. Yaqoob, T. Angelini, L. Ueda, Y. Yamaoka, K. Kotani, T. Kawai, N. Namiki, M. Kohmura, T. and Negoro, H. 2008, PASJ, 60, 69

[20] Makishima, K. Takahashi, H. Yamada, S. Done, C. Kubota, A. Dotani, T. Ebisawa, K. Itoh, T. Kitamoto, S. Negoro, H. Ueda, Y. and Yamaoka, K. 2008, PASJ, 60, 585

[21] Belloni, T., Klein-Wolt, M., Méndez, M., van der Klis, M., & van Paradijs, J. 2000, A&AP, 355, 271

[22] Yamada, S. Makishima, K. Uehara, Y. Nakazawa, K. Takahashi, H. Dotani, T. Ueda, Y. Ebisawa, K. Kubota, A. and Gandhi, P. 2009, APJL, 707, L109

[23] Martocchia, A., Matt, G., Karas, V., Belloni, T., & Feroci, M. 2002, A&AP, 387, 215

[24] Blandford, R. D., & Znajek, R. L. 1977, Mon. Not. R. Astron. Soc. , 179, 433

[25] Miniutti, G. Fabian, A. C. Anabuki, N. Crummy, J. Fukazawa, Y. Gallo, L. Haba, Y. Hayashida, K. Holt, S. Kunieda, H. Larsson, J. Markowitz, A. Matsumoto, C. Ohno, M. Reeves, J. N. Takahashi, T. Tanaka, Y. Terashima, Y. Torii, K. Ueda, Y. Ushio, M. Watanabe, S. Yamauchi, M. and Yaqoob, T. 2007, PASJ, 59, 315

[26] Miller, J. M. Fabian, A. C. Wijnands, R. Reynolds, C. S. Ehle, M. Freyberg, M. J. van der Klis, M. Lewin, W. H. G. Sanchez-Fernandez, C. and Castro-Tirado, A. J. 2002, APJL, 570, L69

[27] Miller, J. M. Fabian, A. C. and Reynolds, C. S. Nowak, M. A. Homan, J. Freyberg, M. J. Ehle, M. Belloni, T. Wijnands, R. van der Klis, M. Charles, P. A. and Lewin, W. H. G. 2004, APJL, 606, L131

[28] Miller, J. M., Raymond, J., Fabian, A., Steeghs, D., Homan, J., Reynolds, C., van der Klis, M., & Wijnands, R. 2006, Nature, 441, 953

[29] Miller, J. M., Reynolds, C. S., Fabian, A. C., Miniutti, G., & Gallo, L. C. 2009, Astrophys. J. , 697, 900

[30] Miniutti, G., Fabian, A. C., & Miller, J. M. 2004, Mon. Not. R. Astron. Soc. , 351, 466

[31] Laor, A. 1991, Astrophys. J. , 376, 90

[32] Brenneman, L. Miller, J. Nantra, P. Volonteri, M. Cappi, M. Matt, G. Kitamoto, S. Paerels, F. Mendez, M. Smith, R. Nowak, M. Garcia, M. Watson, M. Weisskopf, M. Terashima, Y. and Ueda, Y. 2009, Spin and Relativistic Phenomena Around BHs: The Astronomy and Astrophysics Decadal Survey, 2010, 26

[33] Miller, J. Uttley, Nandra, Barret, Paerels, Mandez, Diaz, Cappi, Kitamoto, Nowak, Wilms, Rothschild, Smith, Weisskopf, M. Teraschima, Y. and Ueda, Y. 2009, Stellar-Mass BHs and Their Progenitors: The Astronomy and Astrophysics Decadal Survey, 2010, 207

Boundary condition for D-brane from Wilson loop at the AdS boundary[1]

Tsunehide Kuroki[2]

Department of Physics, Rikkyo University, Toshima, Tokyo 171-8501

Abstract

We study the supersymmetric Wilson loops in the four-dimensional $\mathcal{N} = 4$ super Yang-Mills theory in the context of the AdS/CFT correspondence. In the gauge theory side, it is known that the expectation value of the Wilson loops of circular shape with winding number k, $W_k(C)$, is calculable by using a Gaussian matrix model. In the gravity side, the expectation value of the loop is conjectured to be given by the classical value of the action $S_{\rm D3}$ for a probe D3-brane with k electric fluxes as $\langle W_k(C)\rangle = \mathrm{e}^{-S_{\rm D3}}$. However, according to the spirit of the AdS/CFT correspondence, in principle we have to perform the path integral for the D3-brane action in the $\mathrm{AdS}_5\times\mathrm{S}^5$ under appropriate boundary conditions which should be given in terms of data of the Wilson loop at the AdS boundary. We clarify what kind of boundary conditions are imposed on the D3-brane from the Wilson loop. As an application, our boundary conditions provide a natural interpretation of a position of an eigenvalue in the Gaussian matrix model as an integrated flux on the D3-brane.

1 Introduction

Much progress in string theory for the last ten years suggests that quantum gravity will be formulated as the large-N limit of gauge theories or matrix models [2–4]. The key in this approach is that all the information on gravity or geometry in the bulk is encoded into gauge theory degrees of freedom on the boundary. This idea called holography is realized in the AdS/CFT correspondence. In particular, we consider a circular Wilson loop in the gauge theory in the context of the AdS/CFT correspondence as a nice and concrete realization of holography idea. In our analysis, we emphasize importance of boundary conditions the gauge theory imposes on the geometry. We hope this kind of study has some implications to the brane world scenario, cosmology, or other quantum gravity formulations.

2 Circular Wilson loop in $\mathcal{N} = 4$ $U(N)$ SYM

In this section we review the circular Wilson loop in the four-dimensional $\mathcal{N} = 4$ $U(N)$ supersymmetric Yang-Mills (SYM) theory in the large-N limit. Bosonic fields in this theory are the $U(N)$ gauge field A_μ ($\mu = 0 \sim 3$), the scalar fields Φ_i ($i = 4 \sim 9$) in the adjoint representation of $U(N)$. In terms of these fields, the circular Wilson loop is defined as

$$W_k(C) = \frac{1}{N}\mathrm{tr}P\exp\left(\int_C ds(iA_\mu\dot{x}^\mu(s) + \Phi_i\dot{y}^i(s))\right), \tag{1}$$

where C is a circle parametrized by s, k is the winding number of the Wilson loop, and $x^\mu(s)$, $y^i(s)$ represents the shape of the loop in the four-dimensional, and six-dimensional space, respectively. In particular, when we are interested in the circular Wilson loop, $x^\mu(s)$ describes the circle C, e.g. $x^\mu(s) = (\cos s, \sin s, 0, 0)$. In order to take advantage of the AdS/CFT correspondence, eventually we have to take $N \to \infty$ limit.

[1] Based on the work [1]

[2] Email address: tkuroki@rikkyo.ac.jp

In this setup, let us summarize the main result in the gauge theory side [5–7]. We are interested in the vacuum expectation value of the circular Wilson loop in the large-N limit

$$\langle W_k(C)\rangle \equiv \frac{1}{Z_{\text{gauge}}}\int \mathcal{D}(\text{all fields}) W_k(C) e^{-S_{\text{gauge}}}, \tag{2}$$

where S_{gauge} is the action of the gauge theory. The standard way to compute this is by the perturbation theory in terms of the gauge theory coupling constant g_{YM}. We choose two points on the Wilson loop s_1, s_2, and connect fields on these points by their propagators as $\langle A_\mu(x(s_1))A_\nu(x(s_2))\rangle$, $\langle \Phi_i(x(s_1))\Phi_j(x(s_2))\rangle$. However, since these fields also carry $\dot{x}^\mu$ and $\dot{y}^i$, the net contribution of the propagators becomes

$$-\langle A_\mu(x(s_1))A_\nu(x(s_2))\rangle\, \dot{x}^\mu(s_1)\dot{x}^\nu(s_2) + \langle \Phi_i(x(s_1))\Phi_j(x(s_2))\rangle\, \dot{y}^i(s_1)\dot{y}^j(s_2). \tag{3}$$

The crucial property of the circular Wilson loop is that this becomes constant, namely independent of the space-time points $x^\mu(s_1)$ and $x^\mu(s_2)$ provided that $\dot{x}^2 - \dot{y}^2 = 0$. More precisely, when this condition is satisfied, the above quantity becomes $g_{\text{YM}}^2/8\pi^2$. Thus the combined propagator loses space-time dependence. Due to this property, the computation of $\langle W_k(C)\rangle$ is greatly simplified. Therefore, in the following let us concentrate on the circular Wilson loop (1) with $\dot{x}^2 - \dot{y}^2 = 0$ satisfied. In fact, this condition is known as the one under which the Wilson loop preserves the half of supersymmetries. Furthermore, it is known that diagrams with internal vertices vanish because of the supersymmetry. Thus the computation is reduced to the sum over all planar diagrams with the constant propagator, which is just a combinatorics problem. Actually, the calculation boils down to the one-matrix model

$$\langle W_k(C)\rangle = \left\langle \frac{1}{N}\operatorname{tr} e^{kM}\right\rangle_{\text{MM}} \equiv \frac{1}{Z_{\text{MM}}}\int dM \frac{1}{N}\operatorname{tr} e^{kM} e^{-S_{\text{MM}}}, \tag{4}$$

$$S_{\text{MM}} = \frac{2N}{\lambda}\operatorname{tr} M^2, \qquad \lambda \equiv g_{YM}^2 N, \tag{5}$$

where M is an $N\times N$ Hermitian matrix. From the observations above, it is easy to see that this matrix model reproduces the calculation of $\langle W_k(C)\rangle$ in the large-N limit, because it generates all planar diagrams with the constant propagator proportional to $\lambda/N = g_{\text{YM}}^2$. Note that the operator $\frac{1}{N}\operatorname{tr} e^{kM}$ is a remnant of the Wilson loop $W_k(C)$, where the winding number k appears in the exponent. We can calculate (4) by the standard technique [8]: performing integration over angular variables, (4) can be written as integration over N eigenvalues of M

$$\begin{aligned}\langle W_k(C)\rangle &= \frac{1}{Z}\int \prod_i dm_i \exp(-NV_{\text{eff}}),\\ V_{\text{eff}} &= \sum_i \frac{2}{\lambda}m_i^2 - \sum_{i,j}\log(m_i-m_j)^2 - \frac{k}{N}m_N.\end{aligned} \tag{6}$$

This implies that the system now becomes that of N particles in the Gaussian potential with strong repulsive logarithmic force between them. Moreover, in the presence of the Wilson loop, the last eigenvalue m_N feels extra linear potential proportional to k. In particular, when k is of order N, it survives in the large-N limit. This situation is quite interesting, so henceforth let us discuss the case where k is of order N.

In the large-N limit, these eigenvalues are expected to form a continuous distribution, and the distribution function can be derived from the saddle point method in the large-N limit. The result is [1]

$$\rho(m) = \frac{2}{\pi\lambda}\sqrt{\lambda - m^2} + \frac{1}{N}\delta(m - m_*), \tag{7}$$

which is displayed in Figure 1. Here $m_* = \sqrt{\lambda(1+\kappa^2)}$ and $\kappa \equiv k\sqrt{\lambda}/4N$ which is $\mathcal{O}(1)$ when k is $\mathcal{O}(N)$. The isolated eigenvalue distribution at m_* originates from the last eigenvalue m_N. Given (7), it is easy to calculate $\langle W_k(C)\rangle$ as [1, 9]

$$\langle W_k(C)\rangle = \exp\left[N\left(2\kappa\sqrt{1+\kappa^2} + 2\operatorname{arcsinh}\kappa\right)\right]. \tag{8}$$

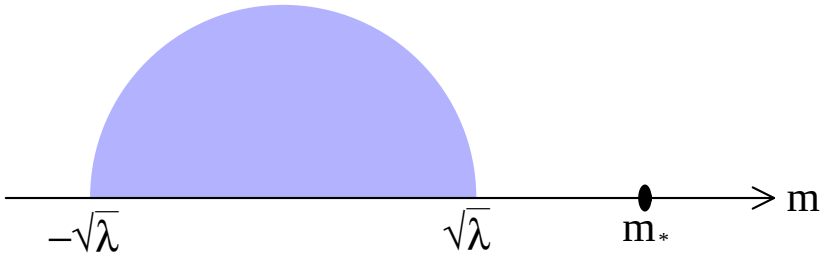

Figure 1: The eigenvalue distribution with k of $\mathcal{O}(N)$.

Conversely, detailed analysis [1] of the matrix model tells us that on general grounds, we can deduce from $\langle W_k(C)\rangle$ the position of the isolated eigenvalue as $\langle W_k(C)\rangle = \exp(-V_{\rm eff}(k)) \to m_* = -V'_{\rm eff}(k)$. In the gravity side, by a totally different method we can calculate $\langle W_k(C)\rangle$, from which we can read off a bulk interpretation of m_* by using this relation.

3 AdS/CFT for Wilson loop

In this section we review main results of the Wilson loop in the AdS/CFT correspondence. First we consider the case of the Wilson loop with winding number $k = 1$, then we turn to k of $\mathcal{O}(N)$ case.

3.1 $k = 1$ case

The statement of AdS/CFT for the Wilson loop with $k = 1$ is [10, 11]

$$\langle W_{k=1}(C)\rangle = \int_{\rm b.c.} e^{-(S_{\rm NG}+S_b)}, \tag{9}$$

where $S_{\rm NG}$ and S_b is the Nambu-Goto action and a possible boundary term, respectively. In the right hand side the path integral should be over all fields on a string world sheet in $\mathrm{AdS}_5\times\mathrm{S}^5$ attached to the loop C at the AdS boundary under appropriate boundary conditions. Here we stress importance of the boundary conditions in the right hand side in (9). First of all, from the theoretical point of view, in the spirit of the AdS/CFT correspondence a bulk or gravity quantity should be completely fixed by the boundary or gauge theory data, which should enter in the right hand side through boundary conditions. On the other hand, from the practical point of view, usually the relation (9) is applied in the case of $\lambda \gg 1$, where the path integral in the right hand side can be replaced by $e^{-S_{\rm cl}}$ with $S_{\rm cl}$ the action evaluated for the classical solution. However, in order to fix the classical solution, we have to specify appropriate boundary conditions at, for example, the AdS boundary corresponding to the presence of the Wilson loop. Thus an important issue in (9) is what kind of boundary conditions and/or boundary terms the Wilson loop impose on the bulk or geometry.

A nice argument on boundary conditions based on the T-duality is given in [12]: let us start from the 10-dimensional gauge theory, namely D9-brane world volume theory. If a string is attached to a Wilson loop in this theory, string coordinates in all directions X^μ ($\mu = 0 \sim 9$) should have the Dirichlet boundary condition because their boundary values are all fixed by the position of the Wilson loop. Then applying the T-duality in $i = 4 \sim 9$ directions, we find that X^μ ($\mu = 0 \sim 3$) still have the Dirichlet boundary condition, while X^i ($i = 4 \sim 9$) should have the Neumann boundary condition. Namely, the string coordinates have the Dirichlet boundary condition for the D3-brane world volume directions, and the Neumann boundary condition for the orthogonal directions.

The above T-duality argument implies that the right hand side in (9) will be a function of X^μ ($\mu = 0 \sim 3$) and P_i ($i = 4 \sim 9$). This requires boundary terms for the Neumann directions $i = 4 \sim 9$. In order to see this, let us parametrize a string world sheet attached to the Wilson loop by σ^1, σ^2 as

follows: the world sheet boundary exists at $\sigma^2 = 0$, while the boundary itself is parametrized by σ^1. Then variation of the classical world sheet action reads

$$\delta S\Big|_{\rm cl} = \int d^2\sigma \left[\frac{\delta S}{\delta X}\delta X + \frac{\delta S}{\delta \partial X}\delta \partial X\right]\Big|_{\rm cl} = -\oint_{\sigma^2=0} d\sigma^1 P_i \delta X^i, \tag{10}$$

where $|_{\rm cl}$ represents evaluation via a classical solution and $P_i = \delta\mathcal{L}/\delta\partial_2 X^i$ is the boundary momentum. This equation suggests that the classical action is a function of X^i. The standard way to flip the boundary condition, namely to change a function of X^i to that of P_i is the Legendre transformation. We add the boundary term as

$$\tilde{S} = S + \oint_{\sigma^2=0} d\sigma^1 P_i X^i \quad \to \quad \delta\tilde{S}\Big|_{\rm cl} = \oint_{\sigma^2=0} d\sigma^1 X^i \delta P_i, \tag{11}$$

which shows that $\tilde{S}\Big|_{\rm cl}$ is a function of P_i as expected. Thus we conclude that we have to add the boundary term $S_b = \oint_{\sigma^2=0} d\sigma^1 P_i X^i$ for the Neumann direction.

In order to give a concrete form of the above boundary conditions, let us choose the $\mathrm{AdS}_5\times\mathrm{S}^5$ metric as

$$\begin{aligned} ds^2 &= \frac{L^2}{Y^2}\left((dX^\mu)^2 + (dY^i)^2\right) \\ &= L^2\left(\left(\frac{2\pi\alpha' U}{L^2}\right)^2 (dX^\mu)^2 + \frac{(dU^i)^2}{U^2}\right), \quad (U^i)^2 = U = \frac{L^2}{2\pi\alpha' Y}, \quad U^i = U\theta^i, \end{aligned} \tag{12}$$

where $L = \lambda^{\frac{1}{4}}\sqrt{\alpha'}$, θ^i is a coordinate of the unit S^5, and the gauge theory lives in the four-dimensional space-time X^μ ($\mu = 0 \sim 3$). Then the Wilson loop (1) provides following boundary conditions [12]:

- Dirichlet: $X^\mu(\sigma^1, \sigma^2 = 0) = x^\mu(\sigma^1)$,
- Neumann: $P_i(\sigma^1, \sigma^2 = 0) = \dot{y}_i(\sigma^1)$,

where P_i is the conjugate momentum of U^i. The latter equation is nontrivial, but there are some arguments supporting it based on symmetries and constraints [12]. In the next section we derive a similar boundary condition in the case of k of $\mathcal{O}(N)$. It is worth noticing that these boundary conditions are along the spirit of AdS/CFT, namely the Wilson loop data provides the boundary conditions for the fields in the bulk.

3.2 k of $\mathcal{O}(N)$ case

Now let us turn to the case where k is of $\mathcal{O}(N)$. A crucial observation is that in this case we have to consider k world sheets, because the Wilson loop with winding number k originates from k fundamental open strings connecting N D3-branes and a probe D3-brane, which should correspond to k world sheets attached to the loop in the gravity side. However, since k is now of $\mathcal{O}(N)$, we are considering $N \sim 1/g_s$ world sheets, which means that we can no longer neglect string interactions, namely we need nonperturbative description. For this system, an interesting proposal was made in [13] that when k is of $\mathcal{O}(N)$, the string world sheet attached to the loop should be replaced by a D3-brane world volume. Namely, the basic relation for the Wilson loop in the AdS/CFT correspondence given in (9) now becomes

$$\langle W_k(C)\rangle = \int_{\rm b.c.} e^{-(S_{\rm D3}+S_b)}, \tag{13}$$

where $S_{\rm D3}$ is the Dirac-Born-Infeld action for a D3-brane including the Wess-Zumino term. Their proposal is based on the fact that a fundamental string can be regarded as a BPS configuration from the point of view of the D3-brane world volume theory [14]. In fact, as we will see later, using the relation (13), we can compute $\langle W_k(C)\rangle$ in the gravity side and it agrees exactly with the gauge theory result given in (8).

In this approach, there are apparently different points from the string world sheet ($k = 1$) case: first of all, the world volume is now four-dimensional and hence attachment to the one-dimensional loop at the

AdS boundary is somewhat nontrivial. In the following σ^a ($a = 1 \sim 4$) denote coordinates on the world volume. Secondly, apart from the scalar fields $X^\mu(\sigma^a)$, $U^i(\sigma^a)$ ($\mu = 0 \sim 3$, $i = 4 \sim 9$) which describe the position of the D3-brane in $AdS_5 \times S^5$ in terms of the coordinates given in (12), we have a $U(1)$ gauge field $A_a(\sigma^a)$. Thus we have to specify a boundary condition and a possible boundary term even for this gauge field. $A_a(\sigma^a)$ on a D3-brane world volume should not be confused with the original $U(N)$ gauge field in the gauge theory side.

For the purpose of examining boundary conditions for a D3-brane, let us parametrize the D3-brane world volume in such a way that the world volume boundary is again given by $\sigma^2 = 0$, and the one-dimensional boundary itself is parametrized by σ^1. Other directions are parametrized by σ^3, σ^4. The same argument as before yields apparent boundary conditions

1. X^μ: Dirichlet, $X^\mu(\sigma^1, \sigma^2 = 0) = x^\mu(\sigma^1)$,
   (Here by using reparametrization invariance of the Wilson loop, we make an identification $s = \sigma^1$.)
2. U^i: Neumann,
3. $\Pi^{a=1}(\sigma^1, \sigma^2 = 0) = -ik$ for each σ^1.

Several notices are in order. As for 2, it should be emphasized that we do not yet know explicitly how to specify P_{U^i} at the boundary. It is true that in the string case $P_{U^i} = \dot{y}_i$, but it is not guaranteed that this is also the case with the D3-brane. The boundary condition 3 reflects that the fact that the end point of a string attached to a D-brane can be regarded as an electric charge from the D3 world volume viewpoint and therefore if it moves along the circle to form the Wilson loop, it induces flux of $U(1)$ gauge field in the σ^1 direction. Recalling the discussion in (11), we have to add the boundary terms for fields with the Neumann boundary conditions, namely the boundary term for the transverse scalar fields $\oint_{\sigma^2=0} d\sigma^1 d\sigma^3 d\sigma^4 P_{U^i} U^i$ and that for the gauge field $\oint_{\sigma^2=0} d\sigma^1 d\sigma^3 d\sigma^4 \Pi^1 A_1$.

Now we make a short review of the explicit form of the D3-brane solution given in [13]. If we take the AdS_5 metric as

$$ds^2_{AdS_5} = L^2 \left(\left(\frac{2\pi\alpha' U}{L^2} \right)^2 \left(dr_1^2 + r_1^2 d\psi^2 + dr_2^2 + r_2^2 d\phi^2 \right) + \frac{dU^2}{U^2} \right), \tag{14}$$

then the loop can be assumed to be located at $r_1 = R$, $r_2 = 0$, which corresponds to the world volume parametrization $\sigma^1 = \psi$, $\sigma^2 = r_2$ and σ^3, σ^4 parametrize S^2 which shrinks at the boundary $\sigma^2 = r_2 = 0$. In this case, the half BPS nature is strong enough to fix the form of the classical solution uniquely once we take account of only the gauge field boundary condition $\Pi^{a=1} = -ik$. Essentially the solution takes the same form as in [14] and near the boundary $r_2 \ll 1$, it looks like

$$U \sim \frac{\kappa\sqrt{\lambda}}{2\pi r_2}, \quad A_1 \sim \frac{-iR\kappa\sqrt{\lambda}}{2\pi r_2}, \tag{15}$$

where κ is defined below (7). Plugging the solution into the action, we have

$$S_{D3} + S_b = -N \left(2\kappa\sqrt{1+\kappa^2} + 2\mathrm{arcsinh}\,\kappa \right). \tag{16}$$

Then according to (13) we can calculate $\langle W_k(C) \rangle$ as

$$\begin{aligned} \langle W_k(C) \rangle &= \int e^{-(S_{\text{D3-brane}} + S_b)} \\ &= \exp\left(-(S_{\text{D3-brane}} + S_b) \right)\big|_{\text{cl}} \\ &= \exp\left[N \left(2\kappa\sqrt{1+\kappa^2} + 2\mathrm{arcsinh}\,\kappa \right) \right], \end{aligned} \tag{17}$$

where in the second equality we have used $\lambda \gg 1$. This indeed agrees with the gauge theory result (8). Since $\langle W_k(C) \rangle$ is quite a complicated function, this agreement strongly supports the claim (13), at least in strong coupling regime $\lambda \gg 1$.

4 Boundary condition for D-brane from Wilson loop

The agreement (17) shown in [13] looks quite nice, but we emphasize here that the derivation in [13] is not completely along the spirit of AdS/CFT. Namely, in the basic relation (13), the right hand side will be a function of X^μ, Π^a and P_{U^i} and their boundary conditions should be provided in terms of the Wilson loop. Then the path integral, or the evaluation of the classical action should be done under these boundary conditions. In contrast to this, in [13] they do not take account of the boundary condition for P_{U^i} and rather they evaluate the action from the explicit form of the classical solution which can be uniquely fixed due to many supersymmetries the configuration preserves. It should be noticed that in the spirit of the AdS/CFT correspondence, the boundary term and the boundary condition should be specified in (13) in terms of the Wilson loop without referring to the equation of motion. Moreover, a prescription itself of giving boundary conditions from a Wilson loop would be generic and independent of its shape. Thus our aim is to deduce D3-brane boundary conditions for generic shape of the Wilson loop without using the equation of motion. Our problem is quite unique, because usually a D-brane specifies boundary conditions for an open string attached to it, while in the present case we are considering boundary conditions for a D-brane itself imposed by a Wilson loop.

4.1 Derivation of boundary conditions

For our purpose, let us take the (Wick rotated) $AdS_5 \times S^5$ metric as

$$ds^2 = \left(\frac{2\pi\alpha' U}{L}\right)^2 (dt^2 + d\rho^2 + \rho^2(d\theta^2 + \sin^2\theta d\phi^2)) + L^2 \frac{(dU^i)^2}{U^2}, \tag{18}$$

where the gauge theory lives in the four-dimensional space-time parametrized by t, ρ, θ and ϕ, and the AdS boundary exists at $U = \infty$. We choose t, ρ in such a way that a loop of generic shape is located at $\rho = 0$, and that it is extended into the t-direction in the four-dimensional space-time. A D3-brane is in the AdS_5, and is attached to the loop $\rho = 0$ at the AdS boundary. We take σ^a $(a = 1 \sim 4)$ as the D3-brane world volume coordinates, hence world volume fields are embedding coordinates $t = t(\sigma^a)$, $\rho = \rho(\sigma^a)$, $\cdots$, $U^i = U^i(\sigma^a)$, and the $U(1)$ gauge field $A_a(\sigma^a)$. As before, we take σ^a in such a way that the world volume boundary is at $\sigma^2 = 0$, and there the boundary itself is parametrized by σ^1. Thus $\rho \to 0$ as $\sigma^2 \to 0$. Note that at the beginning the world volume boundary has nothing to do with the AdS boundary $U = \infty$. Rather, we impose a condition later that the world volume boundary is located at the AdS boundary. As for other world volume coordinates, it is natural to set $\sigma^3 = \theta$, $\sigma^4 = \phi$. Near the world volume boundary $\sigma^2 \sim 0$, $\rho \sim 0$, then the S^2 parametrized by σ^3 and σ^4 shrinks, hence all fields become independent of them. Namely, at least near the world volume boundary, t, ρ and U^i are fields only of σ^1, σ^2: $t = t(\sigma^1, \sigma^2)$, $\rho = \rho(\sigma^1, \sigma^2)$ $U^i = U^i(\sigma^1, \sigma^2)$ for $\sigma^2 \sim 0$. As for the gauge field, at the world volume boundary it is along the σ^1-direction as we discussed above (14): $A_{a=1} = A_{a=1}(\sigma^2)$.

Using these coordinate choice, let us consider the D3-brane action. Near the world volume boundary, S^2-part can be integrated trivially and we obtain

$$S_{\rm D3}|_{\sigma^2\sim 0} = \int_{\sigma^2\sim 0} d\sigma^1 d\sigma^2 L_{\rm D3} = \int_{\sigma^2\sim 0} d\sigma^1 d\sigma^2 \sqrt{\det_{\sigma^1,\sigma^2}(g_{ab} + 2\pi\alpha' F_{ab})}. \tag{19}$$

From the effective Lagrangian $L_{\rm D3}$ we define conjugate momenta near the world volume boundary as

$$P_t = \frac{\partial L_{\rm D3}}{\partial(\partial_2 t)}, \quad P_\rho = \frac{\partial L_{\rm D3}}{\partial(\partial_2 \rho)}, \quad P_{U^i} = \frac{\partial L_{\rm D3}}{\partial(\partial_2 U^i)}, \quad \Pi^{a=1} = \frac{\partial L_{\rm D3}}{\partial(\partial_2 A_1)}. \tag{20}$$

The diffeomorphism invariance of the action implies the Hamiltonian constraint among these conjugate momenta

$$\begin{aligned} 0 = {} & (P_{U^i})^2 + (\Pi^1)^2\big((\partial_1 t)^2 + (\partial_1\rho)^2\big) - \frac{16\pi}{\lambda} N\big(P_t\partial_1\rho - P_\rho\partial_1 t\big)\rho^2 \\ & - \left(64\pi^2\lambda^{-2}N^2(U\rho)^4 - \frac{\lambda}{4\pi^2}(\Pi^1)^2\right)\left(\frac{\partial_1 U^i}{U^2}\right)^2 + \frac{\lambda}{4\pi^2}(P_t^2 + P_\rho^2)\frac{1}{U^4}. \end{aligned} \tag{21}$$

Let us examine what this equation means at the world volume boundary, i.e. $\rho \to 0$ ($\sigma^2 \to 0$)[3]. Here we make a crucial requirement that when $\sigma^2 \to 0$, $U \to \infty$. Namely, the world volume boundary lies at the AdS boundary. Then the constraint is greatly simplified to yield

$$P_{U^i}^2 + (\Pi^1)^2(\partial_1 t)^2 = 0, \quad \text{at } \sigma^2 = 0. \tag{22}$$

As discussed in subsection 3.2, a natural boundary condition for the gauge field is $\Pi^1(\sigma^1, \sigma^2 = 0) = -ik$ for each σ^1. Plugging this into the above, we get $P_{U^i} = -k\,|\partial_1 t|\,\theta_i$ with $\theta_i = U_i/U$ being S^5 coordinate, where we have used $P_{U^i} = (U^i/U)P_U$ and chosen the minus sign in order to make it consistent with the equation of motion. This is only the point we refer to information of the equation of motion. However, at $\sigma^2 = 0$, the loop is assumed to be extended along the t-direction and the D3-brane world volume is attached to it. Thus we have $|\partial_1 t| = |\dot{X}^\mu(\sigma^1)|$ at least in a local patch around a point on the loop. By using the Dirichlet boundary condition for X^μ: $X^\mu(\sigma^1, \sigma^2 = 0) = x^\mu(\sigma^1)$, we find that $|\partial_1 t|$ can be identified with $|\dot{x}^\mu|$ at least in a local patch. Thus we see that the Hamiltonian constraint (21) at the world volume boundary $\sigma^2 = 0$ under the requirement $U(\sigma^1, \sigma^2 = 0) = \infty$ implies the following boundary conditions:

$$X^\mu(\sigma^1, \sigma^2 = 0) = x^\mu(\sigma^1), \tag{23}$$

$$\Pi^1(\sigma^1, \sigma^2 = 0) = -ik, \qquad P_{U^i}(\sigma^1, \sigma^2 = 0) = -k\left|\dot{x}(\sigma^1)\right|\theta_i(\sigma^1), \tag{24}$$

where we have again identified s with σ^1 by using the reparametrization of the loop. By use of the embedding coordinates X^μ, we can convert the world volume indices of Π^a into the space-time ones like $\Pi^\mu \equiv \partial_a X^\mu \Pi^a$. Since Π^a has the only non-vanishing component for $a = 1$, Π^μ satisfies the following boundary condition

$$\Pi^\mu = \partial_1 X^\mu \Pi^1 = -ik\dot{x}^\mu, \qquad \text{at } \sigma^2 = 0, \tag{25}$$

where we have used (23). Using the second boundary condition in (24), this gives the following relation

$$(\Pi^\mu)^2 + (P_{U^i})^2 = 0\,. \tag{26}$$

It is worth noting that the boundary condition (24) thus corresponds to the BPS condition in [14], i.e., force balance between the electric charge Π^1 and the deformation of the D3-brane which is characterized by P_{U^i}, in the case of the spike solution in the flat space. Since the spike solution presented in [14] is the half BPS, it is natural that the equation (26) also implies a local BPS condition for the Wilson loop. In fact, in the gauge theory side, the local BPS condition for the Wilson loop (1) is given by

$$\dot{x}^2 = \dot{y}^2, \tag{27}$$

as commented in section 2. For the Wilson loop satisfying this condition, $\dot{y}_i = |\dot{x}|\theta_i$. Therefore, by using this relation in (24), we deduce boundary conditions in a general case as

$$\Pi^\mu(\sigma^1, \sigma^2 = 0) = -ik\dot{x}^\mu(\sigma^1), \qquad P_{U^i}(\sigma^1, \sigma^2 = 0) = -k\dot{y}_i(\sigma^1). \tag{28}$$

We find our boundary condition quite natural because once it is assumed, the local BPS conditions in both sides become equivalent. From the point of view of our general boundary conditions (28), (24) are those in a local patch along the loop where the loop can be regarded as the straight line with $\dot{x}^2 = \dot{y}^2$. In summary, the Wilson loop with winding number k of $\mathcal{O}(N)$ given in (1) provides following boundary conditions on a D3-brane in the AdS/CFT correspondence:

$$\text{Dirichlet for } X^\mu: \qquad X^\mu(\sigma^1, \sigma^2 = 0) = x^\mu(\sigma^1), \tag{29}$$

$$\text{Neumann for } A_a: \qquad \Pi^\mu(\sigma^1, \sigma^2 = 0) = -ik\dot{x}^\mu(\sigma^1), \qquad \left(\Pi^\mu = \frac{\partial X^\mu}{\partial \sigma^1}\Pi^1\right) \tag{30}$$

$$\text{Neumann for } U^i: \qquad P_{U^i}(\sigma^1, \sigma^2 = 0) = -k\dot{y}_i(\sigma^1). \tag{31}$$

[3] In $k = 1$ (string world sheet) case, relation between the Hamiltonian constraint and a boundary condition was discussed in [12].

Note that these are in accordance with the spirit of the AdS/CFT correspondence: the boundary conditions are given in terms of the data of the Wilson loop $x^\mu(s)$, $y^i(s)$ and k, namely the shape of the loop and the winding number.

There are several evidences supporting our boundary conditions. For example, they are consistent with the boundary conditions for the string world sheet ($k = 1$) case. Moreover, we can explicitly check that the D3-brane solution obtained in [13] which we briefly review in subsection 3.2 actually satisfies our boundary conditions. Here we again emphasize that in our derivation we do not refer to the equation of motion, hence this fact is an evidence for validity of our boundary conditions. Another interesting aspect of our boundary condition is that under them the Gauss' law constraint $\Pi^{a=2} = 0$ implies $\partial\sigma^2/\partial\sigma^1 = 0$, namely orthogonality relation between the tangential and perpendicular directions of the world volume boundary.

5 Bulk interpretation of the position of eigenvalue

In this section as an application of our boundary conditions (29)∼(31), we examine what happens if they are applied to the basic relation (13). As mentioned in (17), when $\lambda \gg 1$, the path integral in the right hand side in (13) can be replaced by $e^{-S^{\rm cl}_{\rm D3}-S^{\rm cl}_b}$ where the action is evaluated by its classical value under the boundary conditions (29)∼(31). Therefore, for $\lambda \gg 1$, we have

$$\langle W_k(C)\rangle = e^{-\left(S^{\rm cl}_{\rm D3}+S^{\rm cl}_b\right)\big|_{\rm b.c.}}, \tag{32}$$

where $|_{\rm b.c.}$ denotes the evaluation under (29)∼(31). Thus the exponent of $\langle W_k(C)\rangle$, $V_{\rm eff}(k)$ defined below (8) can be read from this equation as $V_{\rm eff}(k) = \left(S^{\rm cl}_{\rm D3} + S^{\rm cl}_b\right)\big|_{\rm b.c.}$. Then by using the fact we mentioned at the end of section 2, we can make a connection between the position of the isolated eigenvalue m_* and the bulk quantity as

$$m_* = -V'_{\rm eff}(k) = -\frac{\partial}{\partial k}\left(S^{\rm cl}_{\rm D3} + S^{\rm cl}_b\right)\big|_{\rm b.c.}. \tag{33}$$

In order to calculate this, it is instructive to notice that k is a part of the boundary conditions and as such variation of k gives rise to that of the classical action. However, the variation of the classical action only comes from the boundary action due to the equation of motion. More precisely, for the Dirichlet direction the variation is given as (10), while that for the Neumann direction is as (11). From the boundary conditions (29)∼(31), the variation with respect to k does not affect the Dirichlet direction X^μ. Thus as in (11) the variation comes only from the boundary term

$$S^{\rm cl}_b = \oint_{\sigma^2=0} d\sigma^1 d\sigma^3 d\sigma^4 (\Pi^1 A_1 + P_{U^i} U^i). \tag{34}$$

Now from (30) and (31), we obtain

$$S^{\rm cl}_b\big|_{\rm b.c.} = -k \oint_{\sigma^2=0} d\sigma^1 \left(iA_1\dot{x}^1 + U^i\dot{y}_i\right). \tag{35}$$

Notice here that in (29)∼(31), the integration over S^2-part (namely σ^3 and σ^4) is done as in (19) and (20). Therefore we finally find that

$$m_* = -\frac{\partial\, S^{\rm cl}_b\big|_{\rm b.c.}}{\partial k} = \oint_{\sigma^2=0} d\sigma^1 \left(iA_1\dot{x}^1 + U^i\dot{y}_i\right). \tag{36}$$

Thus we obtain a clear interpretation of the isolated eigenvalue as a bulk quantity, namely as flux of the gauge field, more precisely, an integration over the $U(1)$ gauge field plus the scalar field along the loop.

As for this result, several notes are in order: first of all, the above derivation is exactly in accordance with the spirit of the AdS/CFT correspondence in contrast to the result in [13] where they use the explicit form of the solution to the equation of motion as in (15) to get (16). On the other hand, in our derivation we do not use the explicit form of the solution. Rather, plugging it into (36), we obtain

$$\int_{\sigma^2=0} d\sigma^1 \left(iA_1\dot{x}^1 + U^i\dot{y}_i\right) = \sqrt{\lambda(1+\kappa^2)}, \tag{37}$$

which indeed reproduces the gauge theory result below (7). This is a nontrivial consistency check of our boundary conditions. It is also important to recognize that the boundary condition for U^i in (31) plays an essential role in deriving (37), which is missed in [13]. Finally we note that we again have (the exponent of) the $U(1)$ Wilson loop. It would be quite an interesting aspect of our result, although the $U(1)$ gauge field on the D3-brane in the bulk of course should not be confused with the original $U(N)$ gauge field on the N D3-brane in the gauge theory side.

6 Conclusions

We have analyzed the circular Wilson loop with winding number k of $\mathcal{O}(N)$ in the gauge theory by using a D3-brane carrying k units of charge in the context of the AdS/CFT correspondence. It is known that the calculation of the expectation value of this Wilson loop in the gauge theory side amounts to considering a Gaussian matrix model with an exponential operator insertion due to its symmetry. In this calculation an isolated eigenvalue plays an essential role. After emphasizing importance of boundary conditions the Wilson loop imposes on the gravity side, we deduce them based on the Hamiltonian constraint. We have checked that our boundary conditions pass several nontrivial tests. As an application, we have taken account of them in the AdS/CFT correspondence for the Wilson loop and succeeded in giving an interesting interpretation in terms of fields in the gravity side to the position of the eigenvalue in the matrix model.

References

[1] S. Kawamoto, T. Kuroki and A. Miwa, "Boundary condition for D-brane from Wilson loop, and gravitational interpretation of eigenvalue in matrix model in AdS/CFT correspondence," Phys. Rev. D **79**, 126010 (2009) [arXiv:0812.4229 [hep-th]].

[2] T. Banks, W. Fischler, S. H. Shenker and L. Susskind, "M theory as a matrix model: A conjecture," Phys. Rev. D **55**, 5112 (1997) [arXiv:hep-th/9610043].

[3] N. Ishibashi, H. Kawai, Y. Kitazawa and A. Tsuchiya, "A large-N reduced model as superstring," Nucl. Phys. B **498**, 467 (1997) [arXiv:hep-th/9612115].

[4] J. M. Maldacena, "The large N limit of superconformal field theories and supergravity," Adv. Theor. Math. Phys. **2**, 231 (1998) [Int. J. Theor. Phys. **38**, 1113 (1999)] [arXiv:hep-th/9711200].

[5] J. K. Erickson, G. W. Semenoff and K. Zarembo, "Wilson loops in N = 4 supersymmetric Yang-Mills theory," Nucl. Phys. B **582**, 155 (2000) [arXiv:hep-th/0003055].

[6] N. Drukker and D. J. Gross, "An exact prediction of N = 4 SUSYM theory for string theory," J. Math. Phys. **42**, 2896 (2001) [arXiv:hep-th/0010274].

[7] V. Pestun, "Localization of gauge theory on a four-sphere and supersymmetric Wilson loops," arXiv:0712.2824 [hep-th].

[8] E. Brezin, C. Itzykson, G. Parisi and J. B. Zuber, "Planar Diagrams," Commun. Math. Phys. **59**, 35 (1978).

[9] S. Yamaguchi, "Bubbling geometries for half BPS Wilson lines," Int. J. Mod. Phys. A **22**, 1353 (2007) [arXiv:hep-th/0601089].

[10] S. J. Rey and J. T. Yee, "Macroscopic strings as heavy quarks in large N gauge theory and anti-de Sitter supergravity," Eur. Phys. J. C **22**, 379 (2001) [arXiv:hep-th/9803001].

[11] J. M. Maldacena, "Wilson loops in large N field theories," Phys. Rev. Lett. **80**, 4859 (1998) [arXiv:hep-th/9803002].

[12] N. Drukker, D. J. Gross and H. Ooguri, "Wilson loops and minimal surfaces," Phys. Rev. D **60**, 125006 (1999) [arXiv:hep-th/9904191].

[13] N. Drukker and B. Fiol, "All-genus calculation of Wilson loops using D-branes," JHEP **0502**, 010 (2005) [arXiv:hep-th/0501109].

[14] C. G. Callan and J. M. Maldacena, "Brane dynamics from the Born-Infeld action," Nucl. Phys. B **513**, 198 (1998) [arXiv:hep-th/9708147].

High Energy Astrophysics and Gamma-Ray Bursts in the *Fermi* Era

Soebur Razzaque [1] [2]
On behalf of the *Fermi* Collaborations

Space Science Division, U.S. Naval Research Laboratory, Washington, D.C., USA

Abstract

With the launch of the *Fermi* gamma ray space telescope, high-energy astrophysics has entered a new era. Exciting new results on Galactic and extragalactic sources are leading to a better understanding of the physics and astrophysics of these objects. I will discuss results from the *Fermi* gamma ray space telescope on the extragalactic background light (EBL) and gamma-ray bursts (GRBs).

1 Introduction

The *Fermi* Gamma Ray Space Telescope (formerly known as *GLAST*) was launched on June, 11^{th} 2008 to provide an unprecedented view of the γ-ray Universe. The main instrument onboard *Fermi*, the Large Area Telescope (LAT), offers a broader bandpass ($\sim$ 20 MeV to over 300 GeV) [10] and its sensitivity exceeds by more than an order of magnitude that of its predecessor instrument EGRET onboard the *Compton Gamma Ray Observatory* [46], and the Italian Space Agency satellite *AGILE* [45], which was launched in 2007. The LAT observes the full sky every 3 hr in survey mode, leading to a broadly uniform exposure with less that $\sim$ 15% variation. The Gamma-ray Burst Monitor (GBM), the lower energy ($\sim$ 8 keV – 40 MeV) instrument onboard *Fermi*, observes the full unocculted sky at all time and provides alerts from transient sources such as GRBs.

The main science goal of *Fermi* is to find answers to the questions:

- How do super-massive black holes in Active Galactic Nuclei create powerful jets of material moving at nearly light speed? What are the jets made of?
- What are the mechanisms that produce Gamma-Ray Burst explosions? What is the energy budget?
- How has the amount of starlight in the Universe changed over cosmic time?
- What are the unidentified gamma-ray sources found by EGRET?
- What is the origin of the cosmic rays that pervade the galaxy?
- What is the nature of dark matter?

While answers to many of these questions are still elusive, *Fermi* is providing new insights and exciting results on the Galactic and extragalactic sources, on cosmic rays and on the total amount of starlight in the universe. GRBs and blazars (Active Galactic Nuclei with their jets pointed in our direction) constitute the primary extragalactic sources. The total amount of energy content in the form of starlight in the universe is only second to the total amount of energy content in the cosmic microwave background. Starlight photons, from infrared to ultraviolet, form a background known as the extragalactic background light (EBL) in which high-energy γ rays from extragalactic sources may be absorbed by producing an e^+e^- pair. Thus it is important to understand this background.

[1] Email address: srazzaque@ssd5.nrl.navy.mil
[2] NRC Resident Research Associate

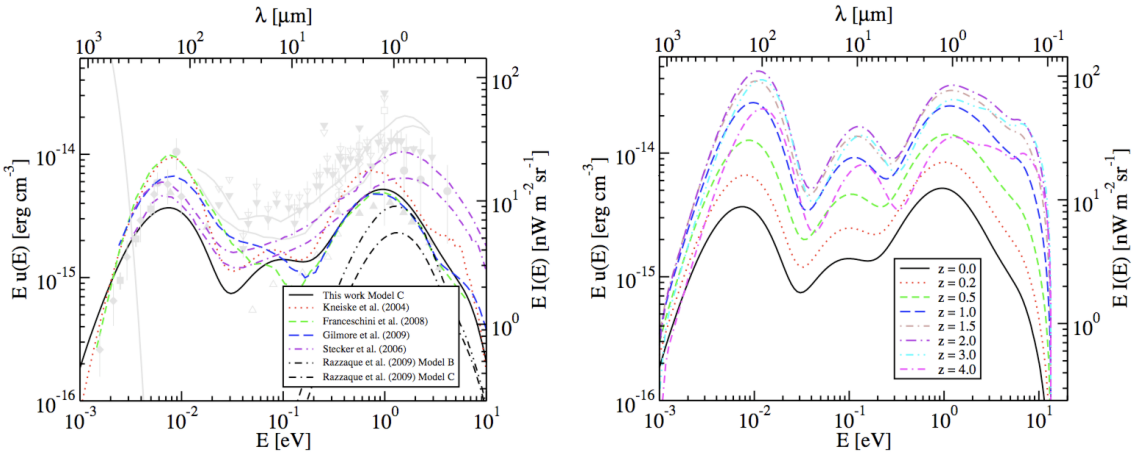

Figure 1: **Left panel** – Wavelength-dependent intensity of EBL predicted by different models (black and colored lines). Also shown are EBL measurements and limits by gray points and lines. **Right panel** – Cosmological evolution of EBL intensity for the model in Ref. [19] in a ΛCDM universe. Note that the intensity may increase by more than an order of magnitude at high redshift. Both plots are from Ref. [19].

2 Extragalactic Background Light

The extragalactic background light is the accummulated radiation from structure formation and its cosmological evolution. The knowledge of its intensity with time probes models of galaxy and star formation. The intensity of the EBL from the near-IR to ultraviolet is thought to be dominated by direct starlight emission out to large redshifts, and by optically bright AGN. At longer wavelengths the infrared background is produced by thermal radiation from dust which is heated by starlight, and also emission from polycyclic aromatic hydrocarbons.

Direct measurement of the EBL is difficult due to contamination by foreground zodiacal and Galactic light [25], and galaxy counts result in a lower limit since the number of unresolved sources is unknown [33]. A number of EBL models (see Fig. 1) have been developed over the last two decades [19, 21, 22, 28, 29, 37, 39, 42, 44], however large scatter in available EBL data does not constrain these models strongly.

The primary extragalactic sources emitting γ-ray photons are blazars, which are galaxies with relativistic jets directed along our line of sight; and GRBs, which are thought to be caused by exploding high-mass stars (long GRBs) or possibly degenerate mergers (short GRBs) with beamed emission along our line of sight for a brief period. GRBs have not been used to contrain EBL absorption during the pre-*Fermi* era mainly because of a lack of sensitivity to transient objects above a few GeV. EGRET sensitivity dropped significantly above 10 GeV while TeV instruments have a too small field-of-view to catch the prompt phase where most of the emission occurs. The new energy window ($10 - 300$ GeV) accessible by *Fermi*, and its wide FoV, makes GRBs interesting targets to constrain EBL absorption in this energy band.

2.1 Gamma Ray Opacity of the Universe

Constraining the EBL intensity from direct measurement of γ rays is difficult beacause of its evolution with cosmic time (see Fig. 1) and may only be possible for nearby TeV blazars [20]. The opacity of the universe for a high-energy γ ray, emitted from redshift z with energy E, to produce an e^+e^- pair by interacting with an EBL photon however can be calculated as [39]

$$\begin{aligned}\tau_{\gamma\gamma}(E,z) &= c\int_0^z dz_1 \left|\frac{dt}{dz_1}\right| \int_0^\infty d\epsilon_1 \int_{-1}^1 d\cos\theta \frac{1}{2}\frac{u_{\epsilon_1}}{\epsilon_1}(1-\cos\theta)\sigma_{\gamma\gamma}(s) \\ &= c\pi r_e^2 \frac{m_e^4 c^8}{E^2}\int_0^z \frac{dz_1}{(1+z_1)^2}\left|\frac{dt}{dz_1}\right| \int_{m_e^2c^4/E(1+z_1)}^\infty d\epsilon_1 \frac{u_{\epsilon_1}}{\epsilon_1}\bar{\varphi}[s_0(\epsilon_1)], \end{aligned} \quad (1)$$

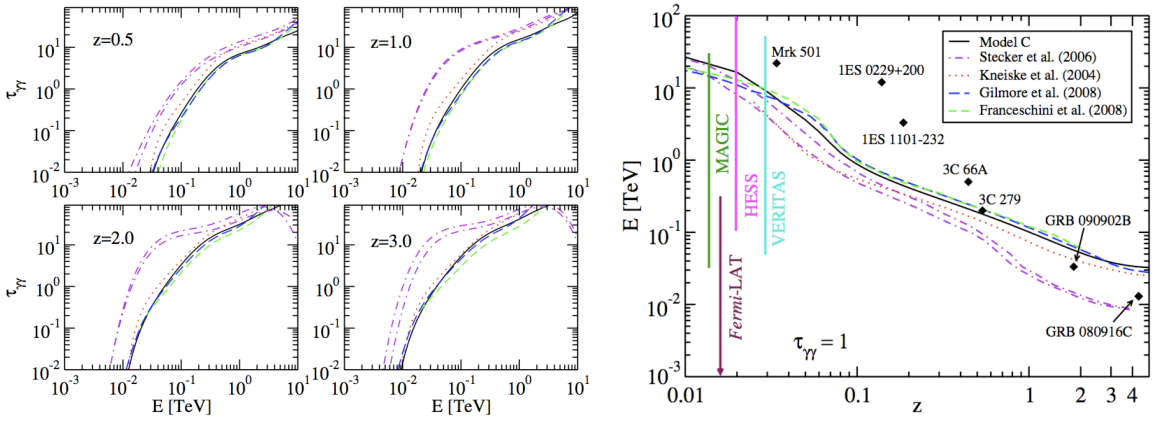

Figure 2: **Left panel** – Opacity of high-energy γ rays to produce an e^+e^- pair by interacting with an EBL photon at different redshift. The lines correspond to different EBL models shown in Fig. 1. **Right panel** – The $\gamma\gamma$ opacity $\tau_{\gamma\gamma} = 1$ curves for various EBL models in the E-z plane. Also shown are the highest-energy γ rays detected from different blazars and GRBs along with energy ranges in which different γ-ray telescopes are sensitive. The universe is predicted to be optically thin to γ rays in the E-z plane below a particular $\tau_{\gamma\gamma} = 1$ model curve. Thus high-energy data points above a model curve has potential to constrain that model. Both plots are from Ref. [19].

for an isotropic background photon field. Here u_{ϵ_1} is the specific energy density of EBL photons at redshift z_1 of interaction, $\sigma_{\gamma\gamma}(s)$ is the total $\gamma\gamma \to e^+e^-$ cross section and $s = E(1+z_1)\epsilon_1(1-\cos\theta)/2m_e^2c^4$ is the center-of-mass energy squared. The function $\bar{\varphi}[s_0]$, with $s_0 = E(1+z_1)\epsilon_1/m_e^2c^4$, is given in Ref. [24]. The threshold energy for e^+e^- pair production from the condition $s_0 = 1$ is $\epsilon_{1,\rm th} \approx m_e^2c^4/E(1+z_1)$. The lower limit of the energy integration $\epsilon_{1,\rm th} \approx 1$ eV and $\sim 250/(1+z_1)$ GeV γ-rays interact dominantly with these photons. Fig. 2 (left panel) shows the $\gamma\gamma$ opacity of the universe for different EBL models and at different redshift. The right panel of Fig. 2 shows the EBL model-dependent $\tau_{\gamma\gamma}(E,z) = 1$ curves and the highest-energy photons detected from GRBs and Blazars.

Assuming that high-energy photon absorption in EBL is the sole mechanism that affects the γ-ray flux from a source at redshift z, the observed and intrinsic fluxes can be related by the opacity as

$$F_{obs}(E) = e^{-\tau_{\gamma\gamma}(E,z)} F_{int}(E). \tag{2}$$

This expression can be used to (i) explore γ-ray flux attenuation in EBL from AGN population, assuming a fixed intrinsic spectrum for all AGNs leading to a redshift-dependent flux ratio between a low- and a high- energy band; (ii) constrain EBL models which predict $\tau_{\gamma\gamma}(E,z)$ values much higer than the opacity that would give the observed fluxes from individual blazars and GRBs; and (iii) put upper limits on γ-ray opacity calculated from observed flux of individual blazars and GRBs, and extrapolation of the intrinsic fluxes to high energies.

2.2 *Fermi* Sources Constraining EBL Models

The highest energy γ-ray emission from high redshift sources are the most effective probe of the γ-ray opacity of the universe, and consequently to contrain EBL models. In contrast to ground-based γ-ray detectors, *Fermi* has demonstrated the possibility of probing the EBL at high redshifts by the detection of blazars at ≥ 10 GeV energies out to $z > 3$, and additionally by the detection of GRB 080916C at a redshift of ~ 4.35 [1]. GRBs are known to exist at even higher redshifts (GRB 090423 is the current record holder with $z \sim 8.2$). Therefore observations of these sources with *Fermi* stand as promising candidates for probing the optical-UV EBL at high redshifts which are not accessible to Cherenkov telescopes.

Fermi LAT detected 6 GRBs to-date[3] with measured redshift. Among the detected blazars, 260 flat-spectrum radio quasars (FSRQs) and 128 BL Lacs have known redshift [7]. Highest-energy photons above

[3]Time of writing this proceedings

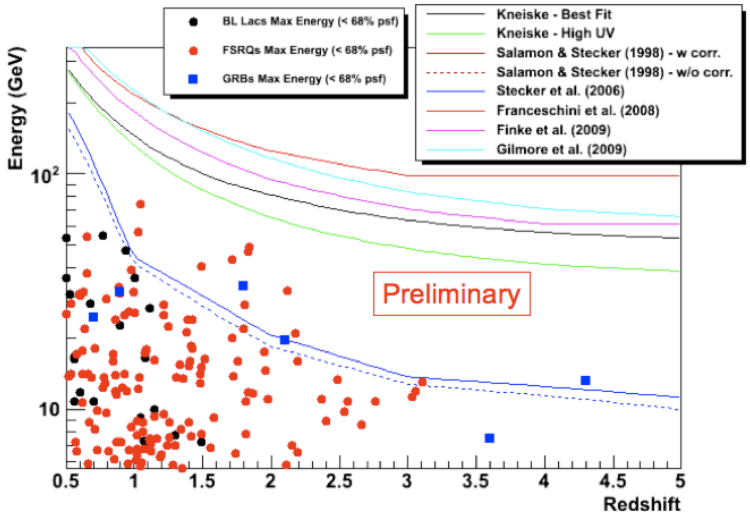

Figure 3: Highest-energy γ rays detected with *Fermi* LAT from blazars (11 month) and GRBs. Also shown are the $\tau_{\gamma\gamma} = 3$ opacity curves for different EBL models [8].

$\sim$ 6 GeV from these sources are plotted in Fig. 3 along with their redshift information. Also plotted are the $\tau_{\gamma\gamma} = 3$ opacity curves for different EBL models. Models which predict large γ-ray opacity can be potentially ruled-out from observations of the highest-energy γ rays above the model curve. The highest-energy, 31 GeV, photon from GRB 090902B at $z = 1.822$ already rules-out the EBL models of Stecker et al. [44] at 3σ confidence level [4]. Detailed results on EBL constraint using *Fermi* data will be published elsewhere [8].

3 Gamma-Ray Bursts

To date *Fermi* GBM has detected 375 GRBs (252 in the first yr). Among them 14 GRBs (9 in the first yr) have been detected with *Fermi* LAT (see Fig. 4). It is worthwhile to mention a few bright GRBs detected with *Fermi*.

- **GRB 080916C :** First bright long GRB detected with LAT (GRB 080825C is the first LAT detected GRB [2]) on 16 September 2008 at a redshift $z = 4.35 \pm 0.15$. More than 3000 LAT photons were detected within first 100 sec (see Fig. 5 left plot). With a total fluence of $f \approx 2.4 \times 10^{-4}$ erg cm^{-2}, the total apparent-isotropic energy release from this GRB is $E_{iso} = 4\pi d_L^2 f \approx 8.8 \times 10^{54}$ erg, where d_L is the luminosity distance. This is the most energetic GRB detected to-date and strongly suggests that the emission from the GRBs is jetted, covering $\gtrsim 10^{-2}$ of the total solid angle, otherwise a staggering ~ 4.9 times the solar rest energy would be needed to produce isotropic emission. No significant emission was detected in the LAT energy range for the first $\sim$ 4 sec (see Fig. 5 left plot). The first $\gtrsim$ 100 MeV and $\gtrsim$ 1 GeV photons arrive $\sim$ 4 sec and $\sim$ 6 sec after the trigger, respectively. The highest-energy, 13.2 GeV, photon from this GRB was detected 16.54 sec after the GBM trigger. While emission in the GBM energy range lasted up to $\sim$ 200 sec after the trigger, $\gtrsim$ 100 MeV emisson lasted up to $\sim$ 1400 sec after the trigger. Details are reported in Ref. [1].

- **GRB 090510 :** This is the first short GRB detected with *Fermi* LAT with a known redshift of $z = 0.903 \pm 0.003$ (GRB 081024B is the first short GRB detected with LAT [5]) [3, 6]. GBM triggered on a weak precursor of this burst, however the main emission starts ~ 0.5 sec after the trigger and extends up to 3 sec (see Fig. 8 for a light curve). Unusually large fluence of $f \approx 5 \times 10^{-5}$ erg cm^{-2} in the 10 keV – 30 GeV range from a relatively high redshift for a short burst results in $E_{iso} \approx 10^{53}$ erg, the largest for any short GRB. Note that the fluence in high-energy (100 MeV – 10 GeV) γ rays

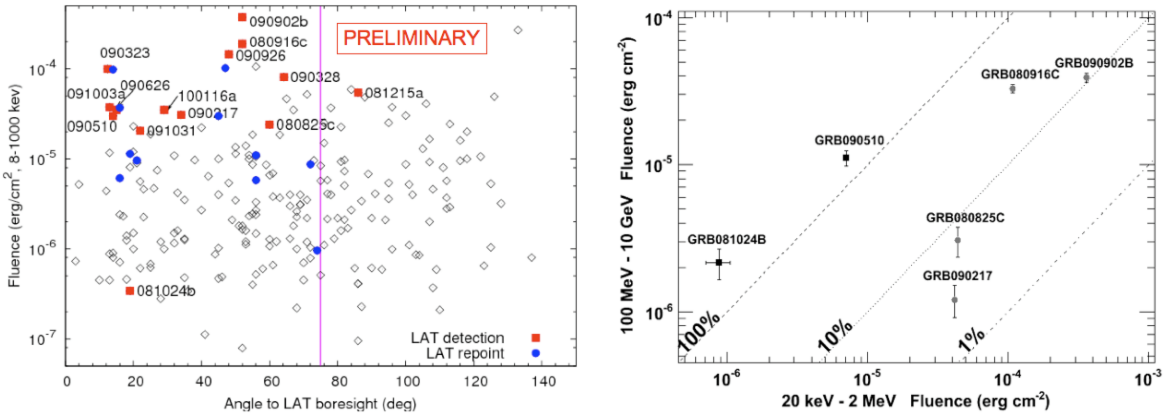

Figure 4: **Left panel** — Fluence vs. angle to LAT boresight for GRBs detected with *Fermi* GBM (open diamonds). The blue discs and red squares correspond to the GRBs to which *Fermi* slewed (automatic repoint) and detected with LAT, respectively. The vertical magenta line indicates the edge of the LAT field-of-view. Note that the fluences are preliminary and the final values will be published in the GBM catalog. **Right panel** — Ratio of high-energy (100 MeV – 10 GeV) to low-energy (20 keV – 2 MeV) γ-ray fluence for six bright GRBs detected with LAT. Note that GRBs 081024B and 090510 are short GRBs, and both show higher fluence in the high-energy component than in the low-energy component as opposed to the long GRBs [31].

is larger than the flunce in low-energy (20 keV – 2 MeV) γ rays, a feature detected in the other short GRB 081024B as well (see Fig. 4, right panel). Emission at $\gtrsim$ 100 MeV started $\sim$ 0.1 sec after the start of the main GBM emission or $\sim$ 0.6 sec after the trigger and lasted for $\sim$ 100 sec The highest-energy, 31 GeV, photon (highest for any short GRB) was detected 0.859 sec after the trigger. See Refs. [3, 6, 16] for further details.

- **GRB 090902B :** At a redshift $z = 1.822$, GRB 090902B is one of the most luminous long GRB detected with *Fermi* LAT [4]. It was detected on 2 September 2009 and the LAT repointed to its direction autonomously prompted by a GBM trigger. With a 10 keV – 10 GeV fluence of $f \approx 4.4 \times 10^{-4}$ erg cm^{-2} collected over the first 25 sec of the prompt emission, the apparent-isotropic energy release is $E_{iso} \approx 3.6 \times 10^{54}$ erg and is comparable to GRB 080916C. More than 200 photons with $\gtrsim$ 100 MeV (39 with $\gtrsim$ 1 GeV) were detected from this GRB, the first arrived $\sim$ 3 sec after the GBM trigger (see Fig. 5, right panel). The $\gtrsim$ 100 MeV emission lasted up to 1 ksec and the highest-energy, $33.4^{+2.7}_{-3.5}$ GeV (highest from any GRB), was detected 82 sec after the trigger.

Another bright long GRB 090926A shows similar characterists such as delayed onset of $\gtrsim$ 100 MeV emission as other bright GRBs mentioned above, although details are not available yet [9]. The less-bright long GRB 080825C ($\sim$ 3.4% chance probablity) and short GRB 081024B also provide hints of such delayed onset of high-energy emission, statistics of high-energy photon are low however from these GRBs. Their redshifts are unknown as well. On the other hand GRB 090217, again with low statistics, do not show any significant delay for the onset of $\gtrsim$ 100 MeV emission.

Bright LAT detected GRBs show high-energy, $\gtrsim$ 100 MeV, temporally extended emission long after keV – MeV emission in GBM falls below detection threshold. Although previous mission, *Compton Gamma Ray Observatory*, detected such extended emission from GRB 940217 [26] most LAT detected GRBs display this behavior. In case of GRB 080916C high-energy emission was detected up to 1400 sec after the trigger, while GBM emission lasted for less than 200 sec High-energy emissions from short GRB 090510 and long GRB 090902B were detected up to over 200 sec and 1000 sec after trigger, respectively (see Fig. 6). However GRBs such GRB 081215A and GRB 090217, with low photon statistics and without delayed onset of high-energy emission, do not show extended emission signatures.

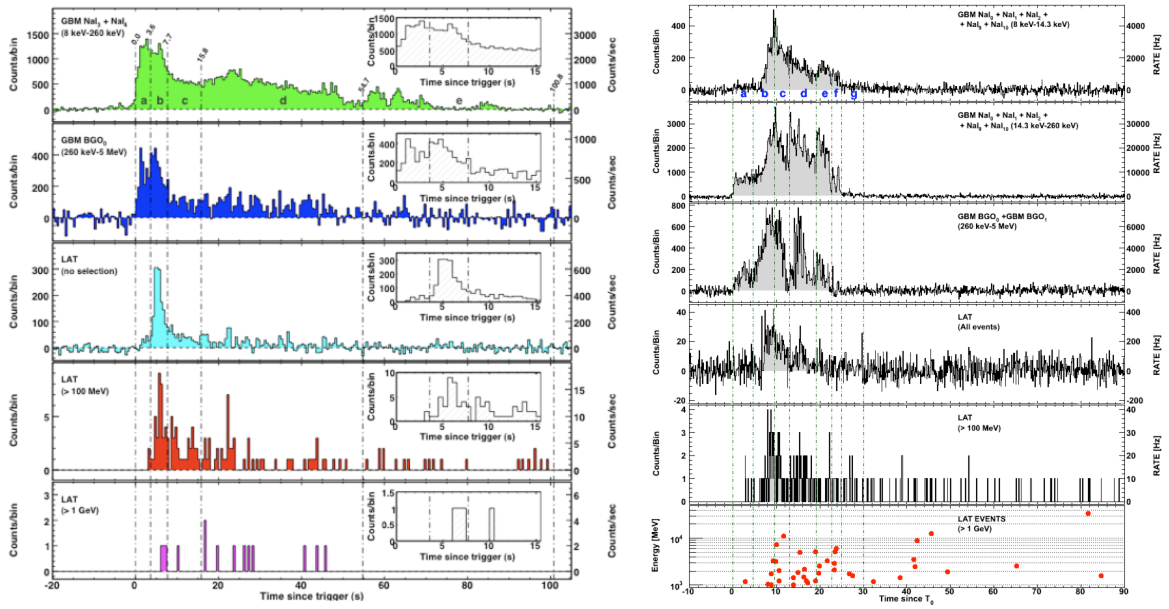

Figure 5: Light curves of two long GRBs 080916C (left plot) [1] and 090902B (right plot) [4]. The top 2 panels in the left plot and top 3 panels in the right plot are background subtracted light curve in the GBM energy range. The bottom panel in the right panel shows the arrival times of all photons with energies > 1 GeV. Note that the $\gtrsim 100$ MeV photons from both GRBs arrive delayed compared to the triggering GBM emission. This feature is detected in some other LAT GRBs as well.

Spectrum of GRB in the keV – MeV range is typically fitted with a Band function of the form [13]

$$\begin{aligned} n(E) &= A\left(\frac{E}{100\ \text{keV}}\right)^{\alpha} \exp\left(-\frac{E(2+\alpha)}{E_{\text{peak}}}\right)\ ;\ E < E_c \\ &= A\left(\frac{E_{\text{peak}}(\alpha-\beta)}{100\ \text{keV}(2+\alpha)}\right)^{\alpha-\beta} \exp(\beta-\alpha)\left(\frac{E}{100\ \text{keV}}\right)^{\beta}\ ;\ E \geq E_c \end{aligned} \tag{3}$$

where $E_c = (\alpha-\beta)E_{\text{peak}}/(2+\alpha)$ and E_{peak} is the peak photon energy in the νF_ν or energy spectrum and α and β are photon number indices below and above the peak energy. While time-resolved spectra from GRB 080916C can be fitted satisfactorily by the Band funcion, spectra from GRB 090510 and 090902B require an additional power-law component (see Fig. 7). In case of GRB 090510 the required power-law component for the time integrated (0.5 – 1.0 sec) spectrum has an index -1.62 [6]. The index remains about the same, -1.66 and -1.54, in time intervals 0.6 – 0.8 sec and 0.8 – 0.9 sec respectively. At later time (0.9 - 1.0 sec) the power-law index becomes slightly softer -1.92 ± 0.2 and a Band function component is not needed to fit spectrum as emission in the GBM range falls below detection threshold. In case of GRB 090902B the additional power-law component has roughly constant index, -1.9, throughout the burst duration and becomes slightly harder, -1.6 ± 0.2, in the interval 19.2 – 25.0 sec after the trigger [4]. An additional power-law component is also needed to fit GRB 090926A spectra [9].

Here we summarize the main properties of the *Fermi* LAT detected bright GRBs:

- Delayed onset of $\gtrsim 100$ MeV emission with respect to keV – MeV emission detected with GBM.
- Temporally extended $\gtrsim 100$ MeV emission beyond the end of the GBM emission.
- A power-law component in addition to the typical Band function is necessary to fit spectra of a number of GRBs.

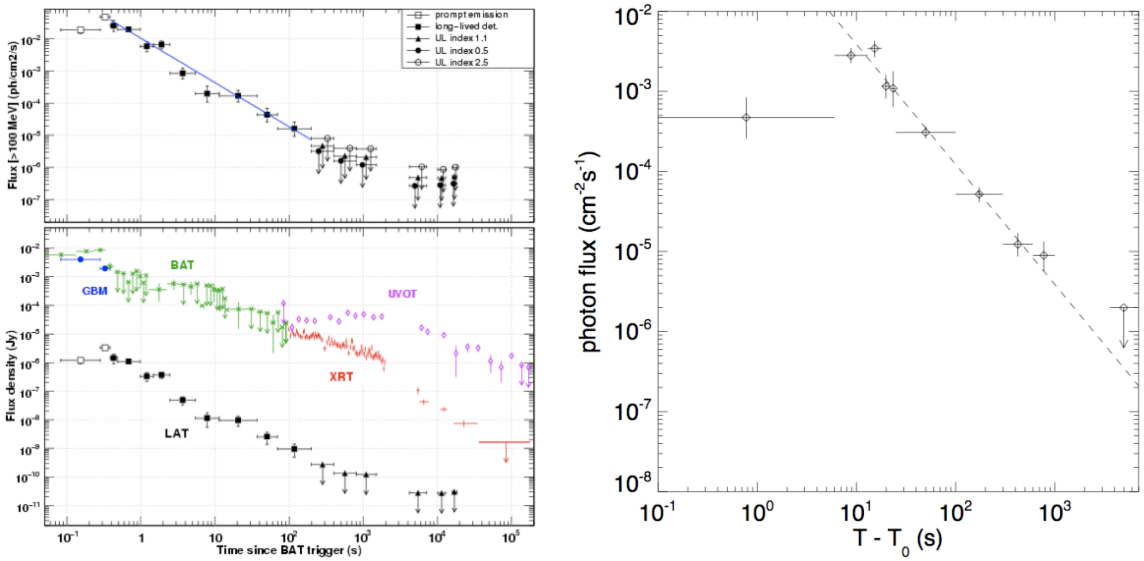

Figure 6: Extended high-energy, $\gtrsim 100$ MeV, emission from short GRB 090510 (left plot) [16] and from long GRB 090902B (right plot) [4]. The power-law decay of the flux, $\propto t^{-1.38}$ for GRB 090510 (left plot, top panel, blue line) and $\propto t^{-1.5}$ for GRB 090902B (right plot, dashed line), is a typical signature of GRB afterglow emission. Simultaneous multiwavelength data from *Swift* BAT, XRT and UVOT instruments are also shown for GRB 090510 (left plot, bottom panel) [16].

3.1 Modeling of *Fermi* LAT Detected GRBs

Gamma-ray emission detected from GRBs over six decades ($\sim$ 10 keV – 10 GeV) in energy by *Fermi* LAT and GBM has extremely important implications for understanding GRB properties such as jetted emission, relativistic outflow speed, particle acceleration, emission region size scale, emission mechanisms, etc. Detection of high-energy γ rays from GRBs is useful in non-GRB science as well, and can be used to probe the intensity of the extragalactic background light and quantum gravity.

Jetted emission: Calculation of large isotropic energy release, exceeding a few solar rest mass energy in some cases, from fluence and redshift data strongly hint that GRB emission is jetted. From observations of very high-energy photons during the prompt GRB phase, the minimum Lorentz factor of the jet bulk motion can be calculated with the constraint that the opacity for $e^{\pm}$ pair production with soft target photons is unity [14, 32, 38].

Given a γ-ray flux variability time-scale t_v, an observed broadband photon spectrum $n(\epsilon)$ and the GRB redshift z, a general formula can be written for the optical depth of a high-energy photons of energy E to $\gamma\gamma \to e^+e^-$ pair production,

$$\tau_{\gamma\gamma}(E) = \frac{3}{4}\frac{\sigma_T d_L^2}{t_v \Gamma}\frac{m_e^4 c^6}{E^2(1+z)^3}\int_{\frac{m_e^2 c^4 \Gamma}{E(1+z)}}^{\infty}\frac{d\epsilon'}{\epsilon'^2}\, n\left(\frac{\epsilon'\Gamma}{1+z}\right)\varphi\left[\frac{\epsilon' E(1+z)}{\Gamma}\right] , \tag{4}$$

where d_L is the luminosity distance and σ_T is the Thomson cross-section. The function $\varphi[\epsilon' E(1+z)/\Gamma]$ is defined in Ref. [24] The derivation of $\Gamma_{\rm min}$ usually follows from the condition $\tau_{\gamma\gamma}(E_{\rm max}) = 1$, or equivalently $\tau_{\gamma\gamma}(E < E_{\rm max}) < 1$. In case the target photon spectrum can be fitted with the Band function in Eq. (3), $\Gamma_{\rm min}$ can be calculated analytically with a delta-function approximation for the

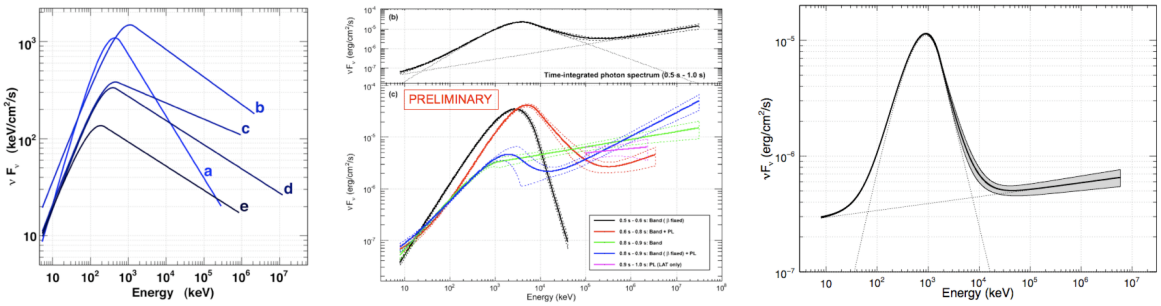

Figure 7: **Left plot** — Time-resolved νF_ν or energy spectral fits over six decades in energy (10 keV – 10 GeV) for GRB 080916C [1]. The Band function fits spectra in all 5 time intervals (a: 0.004–3.58 sec, b: 3.58 – 7.68 sec, c: 7.68 – 15.87 sec, d: 15.87 – 54.78 sec and e: 54.78 – 100.86 sec) reasonably well, although presence of a hard spectral component as suggested by evolution of the spectra cannot be ruled-out definitely. **Center plot** — Time-integrated (top panel) and time-resolved (bottom panel) spectral fits for GRB 090510 [6]. A power-law spectral component in addition to the Band function is preferred over Band function-only fit for the time-integrated spectrum and time-resolved spectra in the intervals: 0.6 –0.8 sec and 0.8 – 0.9 sec At later time, 0.9 – 1.0 sec a power-law alone fits spectrum. **Right plot** — Spectral fit to GRB 090902B data in the time interval 4.6 – 9.6 sec after the trigger [4]. A single power-law component in addition to a Band function is necessary to fit data above ~ 100 MeV and below ~ 50 keV. The slope of the power-law component do not change substantially at later time.

$\gamma\gamma \to e^+e^-$ total cross-section as

$$\Gamma_{\rm min}(E_{\rm max}) = \left[\frac{4d_L^2 A}{c^2 t_v}\frac{m_e^2c^4}{(1+z)^2E_{\rm max}}g\sigma_T\right]^{\frac{1}{2-2\beta}}\left[\frac{(\alpha-\beta)E_{\rm pk}}{(2+\alpha)100\ {\rm keV}}\right]^{\frac{\alpha-\beta}{2-2\beta}} \times \exp\left(\frac{\beta-\alpha}{2-2\beta}\right)\left[\frac{2m_e^2c^4}{E_{\rm max}(1+z)^2 100\ {\rm keV}}\right]^{\frac{\beta}{2-2\beta}} ; \quad \text{for} \quad \Gamma_{\rm min} > \sqrt{\frac{(1+z)^2E_{\rm max}E_{\rm pk}(\alpha-\beta)}{2m_e^2c^4(2+\alpha)}} , \tag{5}$$

where A, $E_{\rm pk}$, α and β are the Band function parameters, and $g\sigma_T$ is the total $\gamma\gamma$ cross-section. The factor $g \approx 0.23$ and it depends on the target photon spectrum. Eq. (5) agrees with the numerical solution to Eq. (4) for $\Gamma_{\rm min}$ to within a few percent.

The minimum bulk Lorentz factor calculated from LAT detected GRBs are rather large: $\Gamma_{\rm min} \approx 900$ for GRB 080916C [1], $\Gamma_{\rm min} \approx 1200$ for GRB 090510 [6] and $\Gamma_{\rm min} \approx 1000$ for GRB 090902B [4]. This implies that the γ ray emission region is at a radius $R \approx 2\Gamma^2 ct_v/(1+z) \gtrsim 10^{16}$ cm for a typical value of $t_v \approx 100$ ms.

Power-law spectral component: A hard spectral component producing the observed excess at low energies in GRB 090902B is difficult to explain in the context of leptonic models by the usual synchrotron self-Compton (SSC) mechanisms [35, 36] In the simplest versions of these models, the peak of the SSC emission is expected to have a much higher energy than the synchrotron peak at MeV energies, and the SSC component has a soft tail that is well below the synchrotron flux at lower energies and so would not produce excess emission below ~ 50 keV as detected in GRB 090902B [4]. Photospheric thermal emission together with power-law high-energy components may explain GRB 090902B spectra [41], although origin of the power-law component will require a separate emission mechanism. Hadronic models, either in the form of proton synchrotron radiation [40] or photohadronic interactions [12], can produce a hard component with a similar low energy excess via direct and cascade radiation (e.g., synchrotron emission by secondary pairs at low energies). However, the total energy release in hadronic models exceeds the observed gamma-ray energy significantly and may pose a challenge for the total energy budget.

Delayed onset of high-energy emission: The delayed onset of the $\gtrsim 100$ MeV emission from the GBM trigger has been modeled for GRB 080916C as arising from proton synchrotron radiation in

the prompt phase [40] and for GRB 090510 as arising from electron synchrotron radiation in the early afterglow phase [23, 30]. In order to produce the peak of the LAT emission 9 sec after the trigger in the early afterglow scenario for GRB 090902B from deceleration of the GRB fireball, a value of $\Gamma_0 \approx 1000$ is required [4]. This is similar to calculated $\Gamma_{\rm min}$ but the observed large amplitude variability on short time scales ($\approx$ 90 ms) in the LAT data, which is usually attributed to prompt emission, may argue against such models. Also, the appearance of the power-law component extending down to $\approx$ 8 keV within only a few seconds of the GRB trigger disfavors an afterglow interpretation for GRB 090902B. The proton synchrotron model, on the other hand, requires a rather large total energy budget, as mentioned previously.

Temporally extended high-energy emission: Smooth power-law decay and approximately constant spectra of the high-energy emission during the time after the end of the GBM emission (see Fig. 6) provide strong evidence that this emisson arises from early afterglow phase [34, 43]. GRB 090510 provides a unique opportunity to study simultaneous emission in the optical – UV to > GeV range up to a kilosec after the trigger [6, 16], thanks to UVOT and XRT instruments onboard *Swift* which slewed to the burst triggered by BAT independently of *Fermi*. The rich data set, however, challenges our understanding of the GRB afterglow emission model. Although GRB 090510 data can be fitted with a typical forward shock model with reasonable spectra in the UV – GeV energy range, the temporal behavior fails to satisfy the expected $F_\nu \propto t^{-\alpha}\nu^{-\beta}$ relations [16] from the simple forward shock model [43]. More complicated models such as a combined internal-external shock model [16] or a two-component jet model may be needed [15] to explain extended emission data.

3.2 Limits on Quantum Gravity Mass Scale

A number of theories leading to quantization of gravity (QG) suggest that space-time has a foamy structure that affects propagation of photons, namely their speeds become energy dependent, thus violating special relativity or Lorentz symmetry [11, 17, 18]. The dispersion relation for the photon is modified in such theories, leading to a time dispersion accumulated over cosmic length scale between photons of different energies. Cosmological distances of the GRBs make them ideal systems for such time of flight test of the Lorentz invariance violation (LIV) by detecting any arrival time difference between the high and low energy photons which were emitted simultaneously from the GRBs. The time difference is [27]

$$\Delta t = \frac{1+n}{2H_0}\frac{E_h^n - E_l^n}{(M_{QG,n}c^2)^2}\int_0^z \frac{(1+z')^n}{\sqrt{\Omega_m(1+z')^3+\Omega_\Lambda}}dz' \tag{6}$$

where n corresponds to the term in the expansion of the photon dispersion relation, $M_{QG,n}$ is the QG mass scale, E_h^n and E_l^n are the energies of a high and low energy photon respectively and H_0 is the Hubble constant.

Fermi LAT detected a $13.22^{+0.70}_{-1.54}$ GeV photon from GRB 080916C, at redshift $z = 4.35 \pm 0.15$ after 16.54 sec of the GRB trigger [1]. The chance probability that this highest-energy photon was from background is only 1.7×10^{-5}. This allowed to put a lower limit on the QG mass scale, for the first time using *Fermi* data, assuming the triggering MeV photons and the highest-energy photon were emitted simultaneously and $\Delta t = 16.54$ sec time dispersion is due to QG effect. The resulting limits, for the linear ($n = 1$) and quadratic ($n = 2$) terms are [1]

$$\begin{aligned} M_{QG,1} &> 1.51\times10^{18}\left(\frac{E_h}{13.22\ \text{GeV}}\right)\left(\frac{\Delta t}{16.54\ \text{sec}}\right)^{-1}\ \text{GeV}/c^2\ , \\ M_{QG,2} &> 9.42\times10^{9}\left(\frac{E_h}{13.22\ \text{GeV}}\right)\left(\frac{\Delta t}{16.54\ \text{sec}}\right)^{-1/2}\ \text{GeV}/c^2\ . \end{aligned} \tag{7}$$

Note that these limits were the most stringent of this kind at that time, and the linear limit was less than an order of magnitude below the Planck mass $M_P = \sqrt{\hbar c^5/G_N} = 1.22 \times 10^{19}$ GeV.

The most stringent constraint on the QG mass derived from the time of flight test however comes from the short GRB 090510 at a redshift $z = 0.9003 \pm 0.003$ [3]. The 1σ confidence range for the highest-energy, 31 GeV, photon is (27.97, 36.32) GeV which was detected 0.829 sec after the GBM trigger and 0.859 sec after an episode of weak emission or precursor (see Fig. 8). Assuming the most conservative scenario in

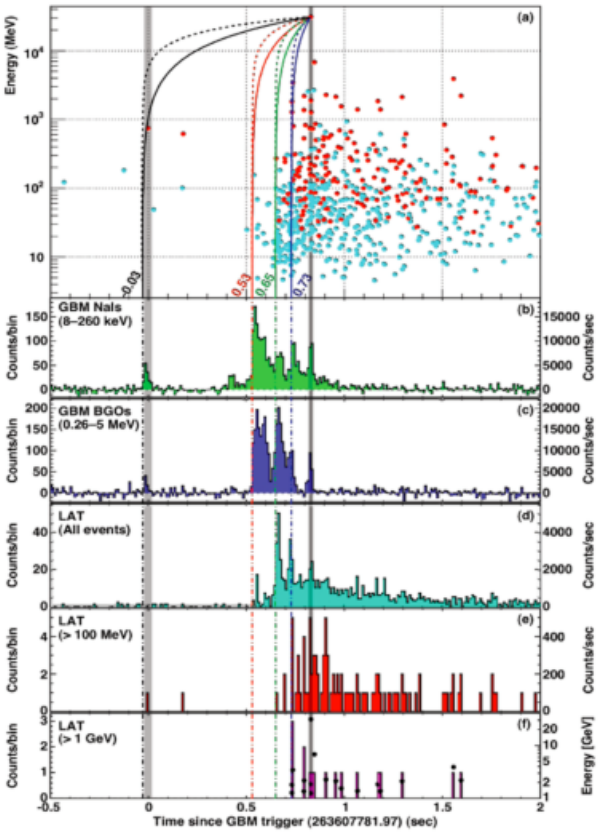

Figure 8: Arrival times of photons detected with *Fermi* LAT from GRB 090510 with two different γ-ray filters denoted with red and cyan points (top panel) [3]. The bottom five panels, (a) - (f), correspond to light curve in different energy range. The solid and dashed curves are normalized to pass through the highest energy (31 GeV) photon and represent the relation between a photon's energy and arrival time for linear ($n = 1$) and quadratic ($n = 2$) LIV, respectively, assuming it is emitted at $t_{start} - T_0 = -30$ ms (black; first small GBM pulse onset), 530 ms (red; main < MeV emission onset), 648 ms (green; > 100 MeV emission onset), 730 ms (blue; > GeV emission onset). Photons emitted at t_{start} would be located along such a line due to (a positive) LIV induced time delay. The gray shaded regions indicate the arrival time of the 31 GeV photon $\pm$10 ms (on the right) and of a 750 MeV photon (during the first GBM pulse) $\pm$20 ms (on the left), which can both constrain a negative time delay. See Ref. [3] for details.

which the highest-energy photon was emitted during the precursor or 0.03 sec prior to the GBM trigger and is given by

$$M_{QG,1} > 1.19\ M_P \left(\frac{E_h}{27.97\ \text{GeV}}\right) \left(\frac{\Delta t}{0.859\ \text{sec}}\right)^{-1}. \tag{8}$$

Less conservative estimates of the emission time for the 31 GeV photon result in larger QG mass as we note below.

- The photon was emitted after the start of main MeV emission
  $\Delta t \leq 0.299$ sec, $M_{QG,1} \geq 3.42\ M_P$.

- The photon was emitted after the start of $\gtrsim 100$ MeV emission
  $\Delta t \leq 0.199$ sec, $M_{QG,1} \geq 5.12\ M_P$.

- The photon was emitted after the start of $\gtrsim 1$ GeV emission
  $\Delta t \leq 0.099$ sec, $M_{QG,1} \geq 10.0\ M_P$.

- The photon was emitted within a 20 ms pulse, implies limit on both positive negative time dispersion $\Delta t \leq \pm 0.01$ sec, $M_{QG,1} \geq 102\ M_P$.

Assuming that the 750 MeV photon, detected 0.019 sec prior to the precursor, was emitted at the same time as the precursor emission gives another limit $M_{QG,1} \geq 1.33\ M_P$ from negative time delay

Finally, an independent method called DisCan or Dispersion Cancellation was used to extract time lag from all LAT photons in the 35 MeV – 31 GeV range. Using this method results in a QG upperlimit of $M_{QG,1} \geq 1.22\ M_P$, consistent with the most conservative limit.

4 Conclusions

Fermi gamma ray space telescope is providing exciting new data in the relatively less explored ~ 100 MeV to > 100 GeV energy range. Galactic sources such as pulsars, supernova remnants, and extragalactic sources such as GRBs, blazars, radio galaxies and starburst galaxies are the main astrophysical objects detected with *Fermi* LAT. Together with *Fermi* GBM, LAT is discovering new results on GRBs such as (i) a delayed onset of $\gtrsim 100$ MeV emisson and (ii) a hard spectral component, as well as collecting more data on temporally extended high-energy emission. High-energy data collected with *Fermi* LAT show that the GRB jet velocity can be rather high, a jet bulk Lorentz factor of the order of 1000 or more in a few cases. This result together with the delayed onset and hard spectral component affects emission modeling, and no satisfactory model has been found yet to explain all these features. The highest-energy photons from GRBs are, however, shown to constrain models of the extragalactic background light that pervades the universe and quantum gravity models which violate Lorentz invariance.

References

[1] Abdo, A., et al. 2009a, Science, 323, 1688

[2] Abdo, A., et al. 2009b, Astrophys. J. , 707, 580

[3] Abdo, A., et al. 2009c, Nature (London), 462, 331

[4] Abdo, A., et al. 2009d, Astrophys. J. , 706, L138

[5] Abdo, A., et al. 2009e, Astrophys. J. , in press

[6] Abdo, A., et al. 2010a, Astrophys. J. , submitted

[7] Abdo, A., et al. 2010b, Astrophys. J. , submitted

[8] Abdo, A., et al. 2010c, in prep.

[9] Abdo, A., et al. 2010d, in prep.

[10] Atwood, W. B., et al. 2009, Astrophys. J. Supp., 697, 1071

[11] Amelino-Camelia, G., Ellis, J., Mavromatos, N. E., Nanopoulos, D. V. & Sarkar, S. 1998, Nature (London), 393, 763

[12] Asano, K., Guiriec, S., & Mészáros, P. 2009, Astrophys. J. , 705, L191

[13] Band, D., et al. 1993, Astrophys. J. , 413, 281

[14] Baring, M. G., & Harding, A. K. 1997, Astrophys. J. , 491, 663

[15] Corsi, A., Guetta, D., & Piro, L. 2009, arXiv:0911.4453

[16] De Pasquale, M., et al. 2010, Astrophys. J. , 709, L146

[17] Ellis, J., Mavromatos, N. E., Nanopoulos, D. V. & Sakharov, A. S. 2003, A&A, 402, 409

[18] Ellis, J., Mavromatos, N. E., Nanopoulos, D. V., Sakharov, A. S. & Sarkisyan, E. K. G. 2006, Astropart. Phys., 25, 402

[19] Finke, J. D., Razzaque, S., & Dermer, C. D. 2009, Astrophys. J. , in press, arXiv:0905.1115

[20] Finke, J. D., & Razzaque, S. 2009, Astrophys. J. , 698, 1761

[21] Franceschini, A., Rodighiero, G., & Vaccari, M. 2008, A&A, 487, 837

[22] Gilmore, R. C., Madau, P., Primack, J. R., Somerville, R. S., & Haardt, F. 2009, Mon. Not. R. Astron. Soc. , 399, 1694

[23] Ghirlanda, G., Ghisellini, G., & Nava, L. 2009, ArXiv e-prints

[24] Gould, R. J. & Shréder, G. 1966, Phys. Rev. Lett. 16, 252

[25] Hauser, M. G., & Dwek, E. 2001, ARA&A, 39, 249

[26] Hurley, K., et al. 1994, Nature (London), 372, 652

[27] Jacob, U., & Piran, T. 2008, J. Cosmol. Astropart. Phys. 01, 031

[28] Kneiske, T. M., Mannheim, K. & Hartmann, D. H. 2002, A&A 386, 1

[29] Kneiske, T. M., Bretz, T., Mannheim, K. & Hartmann, D. H. 2004, A&A 413, 807

[30] Kumar, P., & Barniol Duran, R. 2009, ArXiv e-prints

[31] Le, T., & Dermer, C. D. 2009, Astrophys. J. , 700, 1026

[32] Lithwick, Y., & Sari, R. 2001, Astrophys. J. , 555, 540

[33] Madau, P., & Pozzetti, L. 2000, Mon. Not. R. Astron. Soc. , 312, L9

[34] Meszaros, P., & Rees, M. J. 1997, Astrophys. J. , 476, 232

[35] Mészáros, P. 2006, Reports on Progress in Physics, 69, 2259

[36] Piran, T. 2005, Reviews of Modern Physics, 76, 1143

[37] Primack, J. R., Bullock, J. S., & Somerville, R. S. 2005, in AIP Conf. Ser. 745, High Energy Gamma-Ray Astronomy, ed. F. A. Aharonian, H. J. Völk, & D. Horns (Melville, NY: AIP), 23

[38] Razzaque, S., Mészáros, P., & Zhang, B. 2004, Astrophys. J. , 613, 1072

[39] Razzaque, S., Dermer, C. D., & Finke, J. D. 2009, Astrophys. J. , 697, 483

[40] Razzaque, S., Dermer, C. D., & Finke, J. D. 2009, ArXiv e-prints

[41] Ryde, F., et al. 2010, Astrophys. J. , 709, L172

[42] Salamon, M. H., & Stecker, F. W. 1998, Astrophys. J. , 493, 547

[43] Sari, R., Piran, T. & Narayan, R. 1998, Astrophys. J. , 497, L17

[44] Stecker, F. W., Malkan, M. A. & Scully, S. T. 2006, Astrophys. J. , 648, 774

[45] Tavani, M., et al. 2008, Nucl. Instrum. Methods Phys. Res. A, 588, 52

[46] Thompson, D. J., et al. 1993, Astrophys. J. Supp., 86, 629

Gauge-invariant construction of quantum cosmology

Fumitoshi Amemiya[1] and Tatsuhiko Koike[2]

Department of Physics, Keio University, 3-14-1 Hiyoshi, Kohoku-ku, 223-8522 Yokohama, Japan

Abstract

We present and analyze a gauge-invariant quantum theory of the Friedmann-Robertson-Walker universe with dust. We construct the reduced phase space spanned by gauge-invariant quantities by using the so-called relational formalism at the classical level. The reduced phase space thereby obtained can be quantized in the same manner as an ordinary mechanical system. This quantization procedure realizes a possible resolution to the problem of time and observables in canonical quantum gravity. We analyze the classical initial singularity of the theory by evolving a wave packet backward in time and evaluating the expectation value of the scale factor. It is shown that the initial singularity of the universe is avoided by the quantum gravitational effects.

1 Introduction

The quantum gravitational effects would be dominant at the Planck scale, where the Universe itself must be treated as a quantum object. One thus needs a quantum theory of the Universe in order to understand what happens near the initial singularity. In general, the Dirac quantization method has been used to quantize cosmological models. Unfortunately, this method causes the "problem of time" (see, e.g., [1] and references therein), that is, time evolution is lost in the following two senses. The first is the dynamics of the wave function Ψ. The canonical formulation of GR leads to a constrained system and a Hamiltonian is of the form $H = \Sigma_i N^i C_i$, where $C_i = 0$ are first-class constraints and N^i are arbitrary functions. Since the classical constraints are translated into the quantum constraints $\hat{C}_i\Psi = 0$ by the Dirac method, the Schrödinger equation becomes trivial for the physical state: $i\hbar\frac{\partial\Psi}{\partial t} = \hat{H}\Psi = 0$. The second is concerned with observables. In ordinary gauge theories, observables are gauge-invariant quantities. Since a gauge-invariant quantity O is defined as having vanishing Poisson brackets with all constraint functions $\{C_i, O\} = 0$, the quantity O becomes a constant of motion by the Hamilton equation $\dot{O} = \{H, O\} = 0$. Thus, the dynamics of observables is lost in both classical and quantum theories if one restricts observables to gauge-invariant quantities.

A possible way to overcome these problems is that one finds gauge-invariant quantities and a method to extract their physical evolution at the classical level, and then constructs a quantum theory based on them. The idea for constructing gauge-invariant quantities which has been stressed in [2, 3] is that the relation between dynamical variables is gauge invariant even if they are gauge variant, respectively. As the realization of the idea, a formal expression of gauge-invariant quantities in constrained systems was recently presented [4, 5]. This method is often called the relational formalism. If one applies the relational formalism to a deparametrized theory, one can construct the reduced phase space coordinatized by gauge-invariant quantities and obtain a physical Hamiltonian which generates the time evolution thereof.

In the present work, we construct and analyze a gauge-invariant quantum theory of the Friedmann-Robertson-Walker (FRW) universe without the problem of time. We consider the case when the matter involves dynamical dust introduced by Brown and Kuchař [6]. The advantage of the dust is that one can deparametrize the Hamiltonian constraint and extract a natural time variable which corresponds to the cosmological proper time when one solves equations of motion. Therefore, we can apply the relational formalism to construct the reduced phase space of the FRW universe with dust, and then quantize the reduced system without dealing with the constraint. In order to investigate what happens near the classical initial singularity, we find and analyze the solutions of the constructed quantum theory of the

[1]Email address: famemiya@rk.phys.keio.ac.jp
[2]Email address: koike@phys.keio.ac.jp

Universe. As a consequence, it is shown that the initial singularity is replaced by a big bounce by the quantum gravitational effectsD

In this paper, we adopt the following unit for the speed of light: $c = 1$.

2 Relational formalism

The key observation of the relational formalism to define gauge-invariant quantities is as follows. Take two functions F and T on the phase space. Then, the value of F at $T = \tau$ is gauge invariant even if F and T themselves are gauge variant. That is, one can interpret one of the function T as a clock and consider the relation between T and other variables as time evolution. If we denote a phase space point by $x = (q^a, p_a)$, the mathematical definition of the gauge-invariant quantity $O^\tau_F(x)$ as a phase space function is given by

$$O^\tau_F(x) := \alpha^t_C(F)(x)|_{\alpha^t_C(T)(x)=\tau}. \tag{1}$$

Here, α^t_C denotes the action of the gauge transformation generated by C, and t is a parameter along the gauge orbits. The action of α^t_C on a function is given by $\alpha^t_C(F)(x) = F\left(\alpha^t_C(x)\right)$, which is written as a series $\alpha^t_C(F)(x) = \sum_{n=0}^{\infty} \frac{t^n}{n!}\{C, F\}_{(n)}(x)$, where $\{C, F\}_{(0)} := F$ and $\{C, F\}_{(n+1)} := \left\{C, \{C, F\}_{(n)}\right\}$.

A constraint equation $C = 0$ is said to be of deparametrized form if it is written as

$$C = P + h(q^a, p_a) = 0 \tag{2}$$

with some phase space coordinates $\{q^a, T; p_a, P\}$. In the deparametrized theories, the reduced phase space is spanned by the gauge-invariant quantities $\left(O^\tau_{q^a}(x), O^\tau_{p_a}(x)\right)$ associated with q^a and p_a with the simple symplectic structure

$$\left\{O^\tau_{q^a}(x), O^\tau_{p_b}(x)\right\} = \delta^a_b. \tag{3}$$

The physical Hamiltonian H is obtained by replacing q^a and p_a in $h(q^a, p_a)$ with $O^\tau_{q^a}(x)$ and $O^\tau_{p_a}(x)$,

$$H\left(O^\tau_{q^a}(x), O^\tau_{p_a}(x)\right) := h\left(O^\tau_{q^a}(x), O^\tau_{p_a}(x)\right), \tag{4}$$

which generates the time evolution of the gauge-invariant quantities:

$$\frac{\partial O^\tau_F(x)}{\partial \tau} = \left\{H, O^\tau_F(x)\right\}. \tag{5}$$

3 Friedmann-Robertson-Walker universe with dust

The total action of the flat FRW universe with the dust is written as

$$S_{\rm tot} = S_{\rm grav} + S_{\rm dust} = \int dt \int_\Sigma d^3x \left(p_a \dot{a} + P\dot{T} - NC_{\rm tot}\right), \tag{6}$$

where the Hamiltonian constraint takes the form

$$C_{\rm grav} = -\kappa \frac{p_a^2}{12a} + \frac{\Lambda a^3}{\kappa} + \frac{R}{a}, \quad C_{\rm dust} = P. \tag{7}$$

Here, a is the scale factor, p_a is its conjugate momentum defined as $p_a := -\frac{6a\dot{a}}{\kappa N}$, T is the proper time along the flow-lines of the dust particle when the equations of motion hold, P is canonically conjugate to T, Λ is the cosmological constant, $R = \rho_{\rm rad} a^4$ is a constant associated with the kinematically incorporated radiation with energy density $\rho_{\rm rad}$. The total Hamiltonian constraint has the deparametrized form.

Let us apply the relational formalism to the system and obtain the reduced phase space coordinatized by gauge-invariant quantities. In the present case, T becomes the clock, that is, the evolution of all gauge-invariant quantities are measured by relative relation with respect to T. As explained in Sec.2, the reduced phase space is coordinatized by

$$A(\tau) := O^\tau_a(x), \ P_A(\tau) := O^\tau_{p_a}(x). \tag{8}$$

Recall that, the meaning of $O_a^\tau(x)$ is the value of a at $T=\tau$. The symplectic structure is written as

$$\{A(\tau), P_A(\tau)\} = 1. \tag{9}$$

As can be seen from (4), the Hamiltonian which generates the time evolution of the gauge-invariant quantities is obtained by replacing a' and p'_a in $h(a', p'_a)$ with $A(\tau)$ and $P_A(\tau)$:

$$H = h(A, P_A) = -\kappa \frac{P_A^2}{12A} + \frac{\Lambda A^3}{\kappa} + \frac{R}{A}. \tag{10}$$

Hereafter, we call the gauge-invariant quantity $A(\tau)$ the scale factor.

4 Quantization

Let us now quantize the system obtained in the previous section. In the ordinary procedure of the canonical quantization, the Poisson bracket is replaced by the commutation relation among the operators corresponding to canonical variables:

$$[\hat{A}, \hat{P}_A] = i\hbar. \tag{11}$$

We take the ordinary Schrödinger representation of the canonical commutation relation:

$$\hat{A}\Psi(A) = A\Psi(A), \ \ \hat{P}_A\Psi(A) = -i\hbar \frac{\partial}{\partial A}\Psi(A). \tag{12}$$

In general, there are many ambiguities in the choices of canonical variables, the Hilbert space and the operator ordering. As for the first one, we have chosen the most natural phase space variables, the scale factor and its conjugate momentum. Although this choice leads to negative values of the scale factor by von Neumann's theorem, one can consider the restriction of the range of the scale factor $A \geq 0$ in the quantum system. Under the restriction, $\hat{P}_A$ fails to be self-adjoint in general. However, one can ensure the self-adjointness of the Hamiltonian by imposing boundary conditions on wave functions. Thus, we first define the operator ordering of the Hamiltonian (10) and the measure on the space of wave functions, and then derive the boundary conditions on wave functions. In this paper, we only consider the ordering $\frac{P_A^2}{A} \to \hat{P}_A \frac{1}{A} \hat{P}_A$ for simplicity. Other orderings are discussed in Ref. [7].

In this case, the Schrödinger equation $i\hbar \frac{\partial \Psi}{\partial \tau} = \hat{H}\Psi$ takes the form

$$i\hbar \frac{\partial \Psi}{\partial \tau} = \frac{\kappa \hbar^2}{12} \left(\frac{1}{A} \frac{\partial^2 \Psi}{\partial A^2} - \frac{1}{A^2} \frac{\partial \Psi}{\partial A} \right) + \left(\frac{\Lambda A^3}{\kappa} + \frac{R}{A} \right) \Psi. \tag{13}$$

We define the Hilbert space as $\mathcal{H} = L^2(\mathbb{R}_+, dA)$ where $\mathbb{R}_+$ represents the set of non-negative real numbers. With this inner product, $\hat{P}_A$ is Hermitian and in fact symmetric, but not self-adjoint. The condition for the Hamiltonian to become Hermitian $\langle \Psi_1 | \hat{H} | \Psi_2 \rangle = \langle \Psi_1 | \hat{H}^\dagger | \Psi_2 \rangle$ is satisfied when $\Psi_1^* \frac{1}{A} \frac{d\Psi_2}{dA} \Big|_0^\infty = \frac{d\Psi_1^*}{dA} \frac{1}{A} \Psi_2 \Big|_0^\infty$. If we assume the wave functions vanish at infinity, the relation holds if each of the wave functions Ψ_1 and Ψ_2 satisfies the condition

$$\frac{1}{\sqrt{A}} \left(\Psi - \gamma \frac{d\Psi}{dA} \right) \Big|_{A=0} = 0, \tag{14}$$

where γ is a real number. The Hamiltonian is indeed self-adjoint if its domain is restricted to wave functions which satisfy the boundary condition (14). In Sec. 4, we shall use the simplest boundary condition corresponding to $\gamma = 0$:

$$\frac{\Psi(A)}{\sqrt{A}} \Big|_{A=0} = 0. \tag{15}$$

5 Dynamics of the Universe

In this section, we shall analyze the dynamics of the Universe. We perform numerical calculations in order to solve the Schrödinger equation (13). The procedure of the numerical calculations is as follows. We first set the initial wave function sharply peaked at some value of A. We next evolve it backward in time and evaluate the expectation value of the scale factor. The boundary condition considered here is (15). The numerical methods used here are the fourth-order Runge-Kutta method in the time integration and the midpoint difference method for the spatial differentiation. We choose the initial wave function as a wave packet. Fig. 1(a) shows the comparison between the expectation values of the scale factor for the four cases $(r, \lambda) = (0, 0), (0, 1), (1, 0)$, and $(1, 1)$, where $r := \left(\frac{3}{2\pi}\right)^{\frac{1}{3}} \frac{R}{\hbar}$ and $\lambda := \frac{\hbar G}{12}\Lambda$. The absolute values of the wave function when $r = \lambda = 1$ are plotted in Fig. 1(b). The effect from the radiation is so small that the plots for the models with or without the radiation almost completely overlap. Therefore, we only show the two cases when the matter involves the radiation, with or without the cosmological constant, in Fig.1(a). As the figure indicates, the expectation value of the scale factor has a nonzero minimum, that is, the initial singularity is replaced by a big bounce.

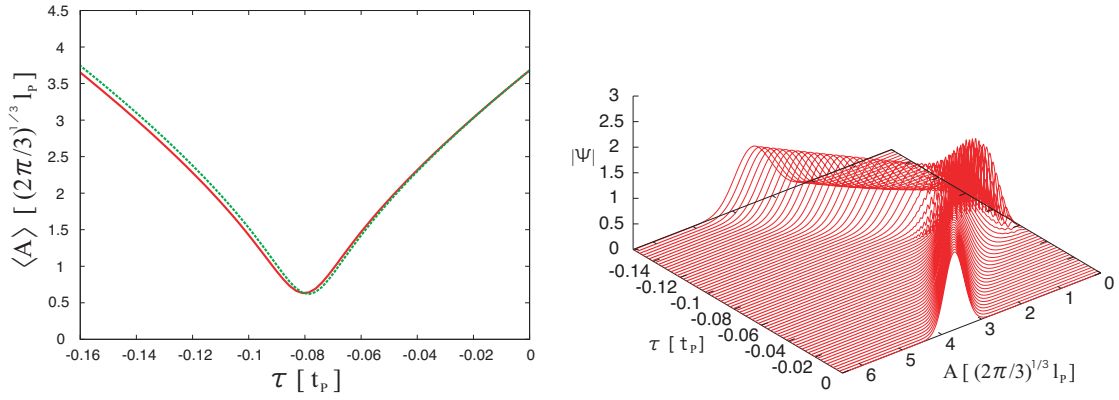

(a) (b)

Figure 1: Fig.(a) shows the expectation value of the scale factor $\langle A \rangle$ as a function of time τ. The solid line represents the cases with the cosmological constant, while the dashed line is for the cases without the cosmological constant. Fig.(b) shows the absolute value of the wave function as a function of the time τ and the scale factor A in the case when $(r, \lambda) = (1, 1)$

References

[1] C. J. Isham, gr-qc/9210011.

[2] P. G. Bergmann, Rev. Mod. Phys. **33** 510 (1961).

[3] C. Rovelli, Class. Quantum Grav. **8** 1895 (1991).

[4] B. Dittrich, Gen. Rel. Grav. **39** 1891 (2007), gr-qc/0411013.

[5] T. Thiemann, Class. Quantum Grav. **23** 1163 (2006).

[6] J. D. Brown and K. V. Kuchař, Phys. Rev. D **51** 5600 (1995).

[7] F. Amemiya and T. Koike, Phys. Rev. D **80**, 103507 (2009).

Cosmological Influence on Gravitationally Bound Local System: Case of Lemaître–Tolman–Bondi Spacetime and its Application to Secular Increase of Astronomical Unit

Hideyoshi Arakida[1]

School of Education, Waseda University

Abstract

We investigated the influence of inhomogeneity of the Universe on the gravitationally bound local system such as the solar system based on the Lemaître–Tolman–Bondi (LTB) solution. In this study, we concentrated on the dynamical perturbation to the planetary motion and derived the leading order effect arisen from LTB model in the straightforward way; first we expressed the perturbation attributed to LTB model in the standard comoving coordinates (t, r, θ, ϕ), then transformed it into the curvature or proper coordinates $(t, \mathcal{R}, \theta, \phi)$, imposing the approximate relation between r and $\mathcal{R}$. It was shown that not only the familiar cosmological contribution arisen from the homogeneous and isotropic Friedmann–Lemaître–Robertson–Walker (FLRW) Universe but also the correction due to the radial inhomogeneity of LTB model are considerably weak and currently undetectable. We also applied the results to the problem of secular increase in the astronomical unit reported by Krasinsky and Brumberg (2004) and found that the inhomogeneity of the Universe dose not cause the significant effect for explaining the observed $d\mathrm{AU}/dt = 15 \pm 4$ [m/century].

1 Dynamical Perturbation in LTB Model

We will obtain the cosmological perturbation attributed to the LTB model, which is analogous to $F_R^{(\mathrm{FLRW})}, F_\phi^{(\mathrm{FLRW})}$ in previous section. The metric of LTB spacetime in the standard comoving form is given by [3, 12, 16, 19],

$$ds^2 = -c^2dt^2 + \frac{1}{1+2\mathcal{E}(r)}\left(\frac{\partial \mathcal{R}}{\partial r}\right)^2 dr^2 + \mathcal{R}^2 d\Omega^2, \tag{1}$$

here $\mathcal{R}$ is the function of t and r, and

$$\mathcal{E}(r) = \frac{1}{2c^2}\left(\frac{\partial \mathcal{R}}{\partial t}\right)^2 - \frac{\mathcal{M}(r)}{\mathcal{R}} - \frac{1}{6}\Lambda\mathcal{R}^2, \tag{2}$$

$$\mathcal{M}(r) = \frac{4\pi G}{c^2}\int \rho(t,r)\mathcal{R}^2\frac{\partial \mathcal{R}}{\partial r}dr, \tag{3}$$

in which Λ is the cosmological constant, $\rho(t,r)$ is the density of the cosmological pressureless particles, and $\mathcal{E}(r)$ and $\mathcal{M}(r)$ are the arbitrary functions of r; $\mathcal{E}(r)$ can be considered as the generalization of curvature parameter k in the FLRW model and $\mathcal{M}(r)$ is the active gravitational mass that generates the gravitational field. $\mathcal{R}$ has the dimension of physical length, namely, the source area distance or the luminosity distance, while r is the coordinate value then dimensionless, see Plebański and Krasiński [16] for more details.

[1]Email address: arakida@edu.waseda.ac.jp

Making use of (1), the equations of motion for r, ϕ become,

$$\begin{aligned}\frac{d^2r}{dt^2} &= -\left[2\frac{\partial^2\mathcal{R}}{\partial t\partial r}\frac{dr}{dt}+\frac{\partial^2\mathcal{R}}{\partial r^2}\left(\frac{dr}{dt}\right)^2\right.\\ &\quad\left.-(1+2\mathcal{E})\mathcal{R}\left(\frac{d\phi}{dt}\right)^2\right]\frac{1}{\frac{\partial\mathcal{R}}{\partial r}}\\ &\quad+\frac{1}{1+2\mathcal{E}}\frac{d\mathcal{E}}{dr}\left(\frac{dr}{dt}\right)^2, \qquad (4)\\ \frac{d^2\phi}{dt^2} &= -\frac{2}{\mathcal{R}}\left[\frac{\partial\mathcal{R}}{dt}+\frac{\partial\mathcal{R}}{\partial r}\frac{dr}{dt}\right]\frac{d\phi}{dt}, \qquad (5)\end{aligned}$$

where we dropped the $\mathcal{O}(c^{-2})$ and higher order terms. When the flat FLRW limit, $\mathcal{R}\to R=ra(t), \mathcal{E}\to k=0$,

In order to relate between r and $\mathcal{R}$ explicitly, we suppose that the background LTB spacetime is the regular at the origin $r=0$ where the central body is located, and that the test particle, such as a planet, moves around $r=0$ then the redshift z in this area is sufficiently small, $z\ll 1$. So according to Mashhoon et al. [13], we adopt the following expansion forms for $\mathcal{R}, \mathcal{E}, \mathcal{M}$ around $r=0$ as,

$$\begin{aligned}\mathcal{R}(t,r) &= ra(t)\left[1+\frac{1}{2}\frac{1}{a(t)}\Delta(t)r+\mathcal{O}(r^2)\right],\\ &\quad \Delta(t)=\left.\frac{\partial^2\mathcal{R}}{\partial r^2}\right|_{r=0}\ll 1, \qquad (6)\\ \mathcal{E}(r) &= \frac{1}{2}\epsilon r^2+\mathcal{O}(r^3), \quad \epsilon=\left.\frac{d^2\mathcal{E}}{dr^2}\right|_{r=0}\ll 1, \qquad (7)\\ \mathcal{M}(r) &= \frac{1}{6}mr^3+\mathcal{O}(r^4), \quad m=\left.\frac{d^3\mathcal{M}}{dr^3}\right|_{r=0}\ll 1, \qquad (8)\end{aligned}$$

in which the scale factor $a(t)$ is defined as,

$$a(t)\equiv\left.\frac{\partial\mathcal{R}}{\partial r}\right|_{r=0}. \qquad (9)$$

Using these relations, (4) and (5) are rewritten as,

$$\begin{aligned}\frac{d^2\mathcal{R}}{dt^2}-\mathcal{R}\left(\frac{d\phi}{dt}\right)^2 &= \mathcal{F}_{\mathcal{R}}^{(\mathrm{LTB})}, \qquad (10)\\ \frac{d}{dt}\left(\mathcal{R}^2\frac{d\phi}{dt}\right) &= \mathcal{F}_{\phi}^{(\mathrm{LTB})}, \qquad (11)\end{aligned}$$

where the leading order dynamical perturbations, $\mathcal{F}_{\mathcal{R}}^{(\mathrm{LTB})}$ and $\mathcal{F}_{\phi}^{(\mathrm{LTB})}$ are expressed as,

$$\begin{aligned}\mathcal{F}_{\mathcal{R}}^{(\mathrm{LTB})} &= \left[\frac{\ddot{a}}{a}+\left(\frac{1}{\Delta}\frac{d\Delta}{dt}\right)^2\right]\mathcal{R}-\frac{2\epsilon}{\Delta}\left[\frac{\mathcal{R}\dot{a}^2}{a^2}-\frac{\dot{a}}{a}\dot{\mathcal{R}}\right]\\ &= \left[-q\left(\frac{\dot{a}}{a}\right)^2+\left(\frac{1}{\Delta}\frac{d\Delta}{dt}\right)^2\right]\mathcal{R}\\ &\quad-\frac{2\epsilon}{\Delta}\left[\frac{\mathcal{R}\dot{a}^2}{a^2}-\frac{\dot{a}}{a}\dot{\mathcal{R}}\right], \qquad (12)\\ \mathcal{F}_{\phi}^{(\mathrm{LTB})} &= 0. \qquad (13)\end{aligned}$$

In (12), we used the standard relation in the FLRW model,

$$\frac{\ddot{a}}{a}=-q\left(\frac{\dot{a}}{a}\right)^2, \qquad (14)$$

in which q is the deceleration parameter. The first term in (12) is $F_R^{(\mathrm{FLRW})}$, the second to forth terms are corrections arisen from the LTB model. It may be possible to consider that the second term in (12) is analogous to $F_R^{(\mathrm{FLRW})} = -q(\dot{a}/a)^2$.

In (12), we need to evaluate not only ϵ determining the geometry or curvature of the Universe but also $\Delta(t)$ characterizing the radial inhomogeneity. Since current observations indicate the flat Universe then we let $\epsilon \to 0$ here. While, $\Delta(t)$ may be in principle obtained from the modified luminosity-redshift relation [15],

$$d_{\mathrm{L}} = c\left[\frac{z}{H} + \frac{z^2}{2H}(1-q-C)\right], \quad C = \frac{1}{aH^2}\frac{d\Delta}{dt}. \tag{15}$$

Finally, the Newtonian equation of motion may be given by,

$$\frac{d^2\mathcal{R}}{dt^2} - \mathcal{R}\left(\frac{d\phi}{dt}\right)^2 = -\frac{GM}{\mathcal{R}} + \mathcal{F}_{\mathcal{R}}^{(\mathrm{LTB})}, \tag{16}$$

$$\frac{d}{dt}\left(\mathcal{R}^2\frac{d\phi}{dt}\right) = \mathcal{F}_{\phi}^{(\mathrm{LTB})}. \tag{17}$$

2 Application to Secular Increase in Astronomical Unit

In this section, as the application of (16) and (17), we consider the secular increase in the astronomical unit reported by Krasinsky and Brumberg [11] (see also Standish [18] and section 5 of Arakida [1]). They found that from the analysis of planetary radar and martian orbiters/landers, the astronomical unit (AU) increase with respect to meters as $d\mathrm{AU}/dt = 15 \pm 4$ [m/century]. This secular trend currently cannot be related to any theoretical predictions and so far the origin of this secular increase is far from clear.

Krasinsky and Brumberg suggested one possibility as the future work, namely, the inhomogeneity of the Universe may induce the observable effect and explain $d\mathrm{AU}/dt$. Then, in terms of LTB model, let us give consideration to this possibility. Since current cosmological observations assist the flat geometry of the Universe. then we adopt $\epsilon = 0$. In this case, the cosmological contribution is governed by,

$$\mathcal{F}_{\mathcal{R}}^{(\mathrm{LTB})} = \left[-q\left(\frac{\dot{a}}{a}\right)^2 + \left(\frac{1}{\Delta}\frac{d\Delta}{dt}\right)^2\right]\mathcal{R}. \tag{18}$$

In our approximation, $(\ddot{a}/a)\mathcal{R}$ or $-q(\dot{a}/a)\mathcal{R}$ is a dominant cosmological effect, nevertheless, this contribution is considerably small, see Arakida [1], Adkins and McDonnell [2], Carrera and Giulini [4], Cooperstock et al. [5], Faraoni and Jacques [6], Järnefelt [7, 8, 9], Klioner and Soffel [10], Noerdlinger and Ptroesian [14], Sereno and Jetzer [17]. From the assumption (6), Δ may be regarded as the correction to scale factor, $a(t)$. And its time variation $d\Delta/dt$ may be also smaller than da/dt. Further, it is known that the deviation in the observed Cosmic Microwave Background (CMB) radiation is of the order of 10^{-5}, then the inhomogeneity of the Universe also causes only negligibly weak contribution.

Therefore, it is currently difficult to detect the cosmological contribution attributed to not only the FLRW model but also the inhomogeneity of the Universe, and then an inhomogeneity of the background cosmological matter distribution cannot causes the detectable effect and explain the observed $d\mathrm{AU}/dt$.

References

[1] Arakida, H.: New Astron., **14**, 264 (2009)

[2] Adkins, G.S., McDonnell, J.: Phys. Rev. D, **75**, id 082001 (2007)

[3] Bondi, H.: MNRAS, **107**, 410 (1947)

[4] Carrera, M., Giulini, D.: arXiv:0810.2712 (2008)

[5] Cooperstock, F.I., Faraoni, V., Vollick, D.N.: ApJ, **503**, 61 (1998)

[6] Faraoni, V., Jacques, A.: Phys. Rev. D, **76**, id 063510 (2006)

[7] Järnefelt, G.: Ann. Acad. Soc. Sci. Fennicae, **A45**, 3 (1940)

[8] Järnefelt, G.: Arkiv Matem. Astron. Fys., **27**, 1 (1940)

[9] Järnefelt, G.: Ann. Acad. Soc. Sci. Fennicae, **A45**, 12 (1942)

[10] Klioner, S.A., Soffel, M.H.: Proc. of the Symposium "The Three-Dimensional Universe with Gaia", 305 (2004)

[11] Krasinsky, G.A., Brumberg, V.A.: Celest. Mech. Dyn. Astrn., **90**, 267 (2004)

[12] Lemaître, G.: Ann. Soc. Sci. Bruxelles A, **53**, 51 (1933)

[13] Mashhoon, B., Mobed, N., Singh, D.: Class. Quant. Grav., **24**, 5031 (2007)

[14] Noerdlinger, P.D., Petrosian, V.: ApJ, **168**, 1 (1972)

[15] Partovi, M.H., Mashhoon, B.: ApJ, **276**, 2 (1984)

[16] Plebański, J., Krasiński, A.: An Introduction to General Relativity and Cosmology, Cambrigde Univ. Press (2006)

[17] Sereno, M., Jetzer, P.: Phys. Rev. D, **75**, id 064031 (2007)

[18] Standish, E.M.: Proc. IAU Colloq., **196**, 163 (2005)

[19] Tolman, R.C., Proc. Nat. Acad. Sci., **20**, 410 (1934)

Inverse problem for gravitational waves by three-body system in Lagrange's orbit

Hideki Asada[1]

Faculty of Science and Technology, Hirosaki University, Hirosaki 036-8561, Japan

Abstract

We study an inverse problem for gravitational waves by three-body systems in Lagrange's orbit. We present a method of determining the parameters such as each mass, source distance and orbital inclination angle from gravitational waves observations alone. A binary source test is also discussed.

1 Introduction

"*Can one hear the shape of a drum?*" is a well-known question posed by Mark Kac in 1966 [1], where to "hear" the shape of a drum is to infer information about the shape of the drumhead from the sound it makes. This question can be traced back to Hermann Weyl [2, 3]. Now, it is interesting to pose a gravitational-wave *inverse* problem for the forthcoming gravitational-wave astronomy by ground-based or space-borne detectors. To "hear" a source through gravitational-wave observations is to extract the information about the source from the gravitational waves it makes.

It is of general interest to ask "*can one tell how many apples are falling in the dark of night?*" One simpler question is how and whether two-body and three-body gravitating systems can be distinguished through observations of gravitational waves that are made by these sources.

Continuing work initiated in an earlier publication [Torigoe et al. Phys. Rev. Lett. **102**, 251101 (2009)], gravitational wave forms for a three-body system in Lagrange's orbit are considered especially in an analytic method. We derive an expression of the three-body wave forms at the mass quadrupole, octupole and current quadrupole orders. By using the expressions, we solve a gravitational-wave *inverse* problem of determining the source parameters to this particular configuration (three masses, a distance of the source to an observer, and the orbital inclination angle to the line of sight) through observations of the gravitational wave forms alone. We discuss also whether and how a binary source can be distinguished from a three-body system in Lagrange's orbit or others.

2 Three-body system and gravitational waves

We consider a three-body system in Lagrange's orbit, where $m_{\rm tot}$ denotes the total mass, a denotes the length of an equilateral triangle, ν_i means mass ratios, ω is the orbital angular frequency, r is a source distance from an observer, and i defines the orbital inclination angle [5]. We obtain the quadrupolar part of gravitational waves as [5]

$$\begin{aligned} r \times h^{+}_{\rm Q} &= -m_{\rm tot} a^2 \omega^2 (1+\cos^2 i) \\ &\quad \times \left[\Big(\nu_1(\nu_2+\nu_3) - 2\nu_2\nu_3 \Big) \cos 2\omega t + \sqrt{3}\nu_1(\nu_2-\nu_3) \sin 2\omega t \right], \end{aligned} \tag{1}$$

$$\begin{aligned} r \times h^{\times}_{\rm Q} &= -2m_{\rm tot} a^2 \omega^2 \cos i \\ &\quad \times \left[\Big(\nu_1(\nu_2+\nu_3) - 2\nu_2\nu_3 \Big) \sin 2\omega t - \sqrt{3}\nu_1(\nu_2-\nu_3) \cos 2\omega t \right]. \end{aligned} \tag{2}$$

[1]Email address: asada@phys.hirosaki-u.ac.jp

We also obtain the plus and cross modes of the mass octupolar waves as

$$
\begin{aligned}
r \times h^{+}_{\mathrm{Oct}} &= -\frac{1}{12} m^2_{\mathrm{tot}} \omega \sin i \\
&\times \Big[27(1+\cos^2 i) \Big(3^{3/2} \nu_1 \nu_2 \nu_3 \cos 3\omega t + (\nu_1-\nu_2)(\nu_2-\nu_3)(\nu_3-\nu_1) \sin 3\omega t \Big) \\
&+ (1-3\cos^2 i) \left(\frac{\sqrt{3}}{2} \nu_1 \{ \nu_2(\nu_2-\nu_1) + \nu_3(\nu_3-\nu_1) \} \cos \omega t \right. \\
&\left. - \frac{1}{2}(\nu_2-\nu_3)\{(\nu_1-\nu_2)(\nu_1-\nu_3) - 3\nu_2\nu_3\} \sin \omega t \right) \Big], \qquad (3)
\end{aligned}
$$

$$
\begin{aligned}
r \times h^{\times}_{\mathrm{Oct}} &= -\frac{1}{12} m^2_{\mathrm{tot}} \omega \sin 2i \\
&\times \Big[27 \Big(3^{3/2} \nu_1 \nu_2 \nu_3 \sin 3\omega t - (\nu_1-\nu_2)(\nu_2-\nu_3)(\nu_3-\nu_1) \cos 3\omega t \Big) \\
&- \left(\frac{\sqrt{3}}{2} \nu_1 \{ \nu_2(\nu_2-\nu_1) + \nu_3(\nu_3-\nu_1) \} \sin \omega t \right. \\
&\left. + \frac{1}{2}(\nu_2-\nu_3)\{(\nu_1-\nu_2)(\nu_1-\nu_3) - 3\nu_2\nu_3\} \cos \omega t \right) \Big]. \qquad (4)
\end{aligned}
$$

Here, we consider current quadrupolar waves.

$$
\begin{aligned}
r \times h^{+}_{\mathrm{C}} &= \frac{4}{3} m^2_{\mathrm{tot}} \omega \sin i \\
&\times \Big[\frac{\sqrt{3}}{2} \nu_1 \{ \nu_2(\nu_2-\nu_1) + \nu_3(\nu_3-\nu_1) \} \cos \omega t \\
&- \frac{1}{2}(\nu_2-\nu_3)\{(\nu_1-\nu_2)(\nu_1-\nu_3) - 3\nu_2\nu_3\} \sin \omega t \Big], \qquad (5)
\end{aligned}
$$

$$
\begin{aligned}
r \times h^{\times}_{\mathrm{C}} &= \frac{2}{3} m^2_{\mathrm{tot}} \omega \sin 2i \\
&\times \Big[\frac{\sqrt{3}}{2} \nu_1 \{ \nu_2(\nu_2-\nu_1) + \nu_3(\nu_3-\nu_1) \} \sin \omega t \\
&+ \frac{1}{2}(\nu_2-\nu_3)\{(\nu_1-\nu_2)(\nu_1-\nu_3) - 3\nu_2\nu_3\} \cos \omega t \Big]. \qquad (6)
\end{aligned}
$$

Both the mass octupolar and current quadrupolar parts are proportional to $m^2_{\mathrm{tot}}\omega$. Hence they can be combined as

$$
\begin{aligned}
r \times h^{+}_{\mathrm{Oct+C}} &= -\frac{1}{4} m^2_{\mathrm{tot}} \omega \sin i \\
&\times \Big[9(1+\cos^2 i) \Big(3^{3/2} \nu_1 \nu_2 \nu_3 \cos 3\omega t + (\nu_1-\nu_2)(\nu_2-\nu_3)(\nu_3-\nu_1) \sin 3\omega t \Big) \\
&- (5+\cos^2 i) \left(\frac{\sqrt{3}}{2} \nu_1 \{ \nu_2(\nu_2-\nu_1) + \nu_3(\nu_3-\nu_1) \} \cos \omega t \right. \\
&\left. - \frac{1}{2}(\nu_2-\nu_3)\{(\nu_1-\nu_2)(\nu_1-\nu_3) - 3\nu_2\nu_3\} \sin \omega t \right) \Big], \qquad (7)
\end{aligned}
$$

and

$$
\begin{aligned}
r \times h^{\times}_{\mathrm{Oct+C}} &= -\frac{1}{4} m_{\mathrm{tot}}^2 \omega \sin 2i \\
&\times \Big[9 \Big(3^{3/2} \nu_1 \nu_2 \nu_3 \sin 3\omega t - (\nu_1 - \nu_2)(\nu_2 - \nu_3)(\nu_3 - \nu_1) \cos 3\omega t \Big) \\
&-3 \left(\frac{\sqrt{3}}{2} \nu_1 \{ \nu_2 (\nu_2 - \nu_1) + \nu_3 (\nu_3 - \nu_1) \} \sin \omega t \right. \\
&\left. + \frac{1}{2} (\nu_2 - \nu_3) \{ (\nu_1 - \nu_2)(\nu_1 - \nu_3) - 3 \nu_2 \nu_3 \} \cos \omega t \right) \Big]. \qquad (8)
\end{aligned}
$$

Here, we can find (in principle) measurable quantities: Phase differences and amplitudes of each wave mode [5].

3 Conclusion

Figure shows a schematic flowchart toward the parameter determinations and binary source test. Further investigations are needed in order to extend to arbitrary number of particles, other orbits or alternative theories of gravity more interestingly.

References

[1] M. Kac, Am. Math. Mon. **73**, 1 (1966).

[2] H. Weyl, Gött. Nach. 110 (1911).

[3] H. Weyl, Math. Ann. **71** 441 (1912).

[4] Y. Torigoe, K. Hattori and H. Asada, Phys. Rev. Lett. **102**, 251101 (2009).

[5] H. Asada, Phys. Rev. D **80**, 064021 (2009).

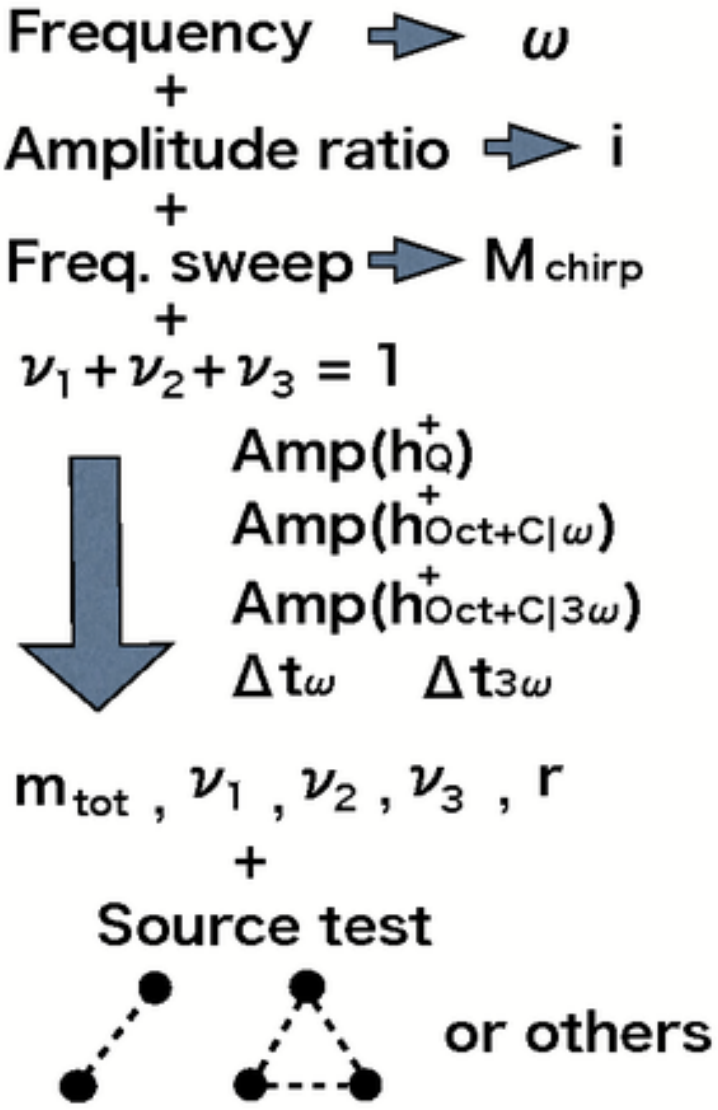

Figure 1: Flow chart of the parameter determinations and source tests. By using equations derived in [5], the source parameters can be determined through gravitational-wave observations alone. In addition, a binary source can be distinguished from a three-body system in Lagrange's orbit or others.

Equilibrium description of thermodynamics in modified gravitational theories

Kazuharu Bamba[1(a)], Chao-Qiang Geng[2(a)] and Shinji Tsujikawa[3(b)]

[(a)] *Department of Physics, National Tsing Hua University, Hsinchu, Taiwan 300*
[(b)] *Department of Physics, Faculty of Science, Tokyo University of Science, 1-3, Kagurazaka, Shinjuku-ku, Tokyo 162-8601, Japan*

Abstract

We demonstrate that it is possible to obtain a picture of equilibrium thermodynamics on the apparent horizon in the expanding cosmological background for a wide class of modified gravity theories with the Lagrangian density $f(R, \phi, X)$, where R is the Ricci scalar and $X = -(\nabla\phi)^2/2$ is the kinetic energy of a scalar field ϕ. In this framework, the horizon entropy S corresponding to equilibrium thermodynamics is proportional to the horizon area A with a constant coefficient, as in the Einstein gravity. We show that for a flat cosmological background with a decreasing Hubble parameter, S globally increases with time.

1 Introduction

The discovery of black hole entropy has opened up a window for a profound physical connection between gravity and thermodynamics [1]. The gravitational entropy S in the Einstein gravity is proportional to the horizon area A of black holes, such that $S = A/(4G)$, where G is gravitational constant. A black hole with mass M obeys the first law of thermodynamics, $T\mathrm{d}S = \mathrm{d}M$ [2], where $T = \kappa/(2\pi)$ is a Hawking temperature determined by the surface gravity κ [3]. Since black hole solutions follow from Einstein field equations, the first law of black hole thermodynamics implies some connection between thermodynamics and Einstein equations. In fact, it was shown [4] that Einstein equations can be derived by using the Clausius relation $T\mathrm{d}S = \mathrm{d}Q$ on all local acceleration horizons in the Rindler space-time together with the relation $S \propto A$, where $\mathrm{d}Q$ and T are the energy flux across the horizon and the Unruh temperature seen by an accelerating observer just inside the horizon, respectively.

In the theories where the Lagrangian density f is a non-linear function in terms of the Ricci scalar R (so called "$f(R)$ gravity"), it was pointed out [5] that a non-equilibrium treatment is required such that the Clausius relation is modified to $\mathrm{d}S = \mathrm{d}Q/T + \mathrm{d}_i S$. Here the horizon entropy S is defined by $S = F(R)A/(4G)$ with $F(R) = \partial f/\partial R$ and $\mathrm{d}_i S$ describes a bulk viscosity entropy production term. The variation of the quantity $F(R)$ gives rise to the non-equilibrium term $\mathrm{d}_i S$ that is absent in the Einstein gravity. The appearance of a non-equilibrium entropy production term $\mathrm{d}_i \hat{S}$ is intimately related to the theories in which the derivative of the Lagrangian density f with respect to R is not constant. It is of interest to see whether an equilibrium description of thermodynamics is possible in such modified gravity theories. In the present paper, we review our results in Ref. [6] and show that equilibrium thermodynamics does exist for the general Lagrangian density $f(R, \phi, X)$, where f is function of R, a scalar field ϕ, and a field kinetic energy $X = -(\nabla\phi)^2/2$. Note that this analysis covers $f(R)$ gravity and scalar-tensor theories as special cases.

2 Thermodynamics in modified gravity

We start with the following action:

$$I = \int \mathrm{d}^4x\sqrt{-g}\left[\frac{f(R, \phi, X)}{16\pi G} + \mathcal{L}_{\mathrm{matter}}\right], \tag{1}$$

[1]Email address: bamba@phys.nthu.edu.tw
[2]Email address: geng@phys.nthu.edu.tw
[3]Email address: shinji@rs.kagu.tus.ac.jp

where g is the determinant of the metric tensor $g_{\mu\nu}$ and $\mathcal{L}_{\rm matter}$ is the matter Lagrangian. R is the scalar curvature, ϕ is a scalar field, $X \equiv -(1/2)\, g^{\mu\nu}\nabla_\mu\phi\nabla_\nu\phi$ is a kinetic term of ϕ (∇_μ is the covariant derivative operator associated with $g_{\mu\nu}$). The action (1) can describe many modified gravity theories, e.g., $f(R)$ gravity, Brans-Dicke theories, scalar-tensor theories, and dilaton gravity. In addition, it also includes scalar field theories such as quintessence and k-essence.

From the action (1), the gravitational field equation and the equation of motion for ϕ are derived as

$$FG_{\mu\nu} = 8\pi G T^{(\rm matter)}_{\mu\nu} + \frac{1}{2}g_{\mu\nu}(f - RF) + \nabla_\mu\nabla_\nu F - g_{\mu\nu}\Box F + \frac{1}{2}f_{,X}\nabla_\mu\phi\nabla_\nu\phi\,, \tag{2}$$

$$\frac{1}{\sqrt{-g}}\partial_\mu\left(f_{,X}\sqrt{-g}g^{\mu\nu}\partial_\nu\phi\right) + f_{,\phi} = 0\,, \tag{3}$$

where $F \equiv \partial f/\partial R$, $f_{,X} \equiv \partial f/\partial X$, $f_{,\phi} \equiv \partial f/\partial\phi$. $G_{\mu\nu} = R_{\mu\nu} - (1/2)\, g_{\mu\nu}R$ is the Einstein tensor and $\Box \equiv g^{\mu\nu}\nabla_\mu\nabla_\nu$ is the covariant d'Alembertian for the scalar field. For the matter energy momentum tensor $T^{(\rm matter)}_{\mu\nu}$, we consider perfect fluids of ordinary matter (radiation and non-relativistic matter) with total energy density ρ_f and pressure P_f.

We consider the 4-dimensional Friedmann-Lemaître-Robertson-Walker (FLRW) space-time with the metric, $\mathrm{d}s^2 = h_{\alpha\beta}\mathrm{d}x^\alpha\mathrm{d}x^\beta + \tilde{r}^2\mathrm{d}\Omega^2$, where $\tilde{r} = a(t)r$ and $x^0 = t, x^1 = r$ with the two dimensional metric $h_{\alpha\beta} = \mathrm{diag}(-1, a^2(t)/[1-Kr^2])$. Here, $a(t)$ is the scale factor, K is the cosmic curvature, and $\mathrm{d}\Omega^2$ is the metric of two-dimensional sphere with unit radius. In the FLRW background, we obtain the following field equations from Eqs. (2) and (3):

$$3F\left(H^2 + \frac{K}{a^2}\right) = f_{,X}X + \frac{1}{2}(FR - f) - 3H\dot{F} + 8\pi G\rho_f\,, \tag{4}$$

$$-2F\left(\dot{H} - \frac{K}{a^2}\right) = f_{,X}X + \ddot{F} - H\dot{F} + 8\pi G\left(\rho_f + P_f\right)\,, \tag{5}$$

$$\frac{1}{a^3}\left(a^3\dot{\phi}f_{,X}\right)^{\cdot} = f_{,\phi}\,, \tag{6}$$

where $H = \dot{a}/a$ is the Hubble parameter and the dot denotes the time derivative of $\partial/\partial t$, and the scalar curvature is given by $R = 6\left(2H^2 + \dot{H} + K/a^2\right)$. The perfect fluid satisfies the continuity equation $\dot{\rho}_f + 3H\left(\rho_f + P_f\right) = 0$.

Equations (4) and (5) can be written as

$$H^2 + \frac{K}{a^2} = \frac{8\pi G}{3F}\left(\hat{\rho}_d + \rho_f\right)\,, \quad \dot{H} - \frac{K}{a^2} = -\frac{4\pi G}{F}\left(\hat{\rho}_d + \hat{P}_d + \rho_f + P_f\right)\,, \tag{7}$$

$$\hat{\rho}_d \equiv \frac{1}{8\pi G}\left[f_{,X}X + \frac{1}{2}(FR - f) - 3H\dot{F}\right]\,, \quad \hat{P}_d \equiv \frac{1}{8\pi G}\left[\ddot{F} + 2H\dot{F} - \frac{1}{2}(FR - f)\right]\,. \tag{8}$$

Note that a hat denotes quantities in the non-equilibrium description of thermodynamics. If we define the density $\hat{\rho}_d$ and the pressure $\hat{P}_d$ of "dark" components in this way, we find that they obey the following equation

$$\dot{\hat{\rho}}_d + 3H\left(\hat{\rho}_d + \hat{P}_d\right) = \frac{3}{8\pi G}\left(H^2 + \frac{K}{a^2}\right)\dot{F}\,, \tag{9}$$

where we have used Eq. (6). For the theories with $\dot{F} \neq 0$, the right-hand side (r.h.s.) of Eq. (9) does not vanish, so that the standard continuity equation does not hold. This happens for the theories such as $f(R)$ gravity and scalar-tensor theories.

Let us proceed to the thermodynamical property of the theories given above. First of all, the apparent horizon is determined by the condition $h^{\alpha\beta}\partial_\alpha\tilde{r}\partial_\beta\tilde{r} = 0$, which means that the vector $\nabla\tilde{r}$ is null on the surface of the apparent horizon. For the FLRW space-time, the radius $\tilde{r}_A$ of the apparent horizon is given by $\tilde{r}_A = \left(H^2 + K/a^2\right)^{-1/2}$. In the Einstein gravity, the horizon entropy is given by $S = A/(4G)$, where $A = 4\pi\tilde{r}_A^2$ is the area of the apparent horizon [1–3]. In the context of $f(R)$ gravity and scalar-tensor theories, the entropy has been defined as $\hat{S} = FA/(4G)$ in most of past works [5]. By using this definition, we obtain

$$\frac{1}{2\pi\tilde{r}_A}\mathrm{d}\hat{S} = 4\pi\tilde{r}_A^3 H\left(\hat{\rho}_d + \hat{P}_d + \rho_f + P_f\right)\mathrm{d}t + \frac{\tilde{r}_A}{2G}\mathrm{d}F\,. \tag{10}$$

The apparent horizon has the following Hawking temperature

$$T = \frac{|\kappa|}{2\pi}, \quad \kappa = -\frac{1}{\tilde{r}_A}\left(1 - \frac{\dot{\tilde{r}}_A}{2H\tilde{r}_A}\right), \tag{11}$$

where κ is expressed as $\kappa = -\left(\tilde{r}_A/2\right)\left(2H^2 + \dot{H} + K/a^2\right) = -2\pi G/\left(3F\right)\tilde{r}_A\left(\hat{\rho}_T - 3\hat{P}_T\right)$, with $\hat{\rho}_T \equiv \hat{\rho}_d + \rho_f$ and $\hat{P}_T \equiv \hat{P}_d + P_f$. As long as the total equation of state $w_T = \hat{P}_T/\hat{\rho}_T$ satisfies $w_T \leq 1/3$ it follows that $\kappa \leq 0$, which is the case for the standard cosmology. Then, Eq. (10) can be written as

$$T\mathrm{d}\hat{S} = 4\pi\tilde{r}_A^3 H\left(\hat{\rho}_d + \hat{P}_d + \rho_f + P_f\right)\mathrm{d}t - 2\pi\tilde{r}_A^2\left(\hat{\rho}_d + \hat{P}_d + \rho_f + P_f\right)\mathrm{d}\tilde{r}_A + \frac{T}{G}\pi\tilde{r}_A^2\mathrm{d}F\,. \tag{12}$$

In the Einstein gravity the Misner-Sharp energy [7] is defined to be $E = \tilde{r}_A/\left(2G\right)$. In $f(R)$ gravity and scalar-tensor theory this may be extended to the form $\hat{E} = \tilde{r}_A F/\left(2G\right)$ [8]. Using this latter expression for the $f(R,\phi,X)$ gravity theory, it follows that

$$\hat{E} = \frac{\tilde{r}_A F}{2G} = V\frac{3F(H^2 + K/a^2)}{8\pi G} = V\left(\hat{\rho}_d + \rho_f\right), \tag{13}$$

where $V = 4\pi\tilde{r}_A^3/3$ is the volume inside the apparent horizon. This gives

$$\mathrm{d}\hat{E} = -4\pi\tilde{r}_A^3 H\left(\hat{\rho}_d + \hat{P}_d + \rho_f + P_f\right)\mathrm{d}t + 4\pi\tilde{r}_A^2\left(\hat{\rho}_d + \rho_f\right)\mathrm{d}\tilde{r}_A + \frac{\tilde{r}_A}{2G}\mathrm{d}F\,. \tag{14}$$

The Combination of Eqs. (12) and (14) leads to

$$T\mathrm{d}\hat{S} = -\mathrm{d}\hat{E} + \hat{W}\mathrm{d}V + \frac{\tilde{r}_A}{2G}\left(1 + 2\pi\tilde{r}_A T\right)\mathrm{d}F\,, \tag{15}$$

where the work density $\hat{W}$ is defined by $\hat{W} = \left(\hat{\rho}_d + \rho_f - \hat{P}_d - P_f\right)/2$. This equation can be written in the form

$$T\mathrm{d}\hat{S} + T\mathrm{d}_i\hat{S} = -\mathrm{d}\hat{E} + \hat{W}\mathrm{d}V\,, \tag{16}$$

where

$$\mathrm{d}_i\hat{S} = -\frac{1}{T}\frac{\tilde{r}_A}{2G}\left(1 + 2\pi\tilde{r}_A T\right)\mathrm{d}F = -\left(\frac{\hat{E}}{T} + \hat{S}\right)\frac{\mathrm{d}F}{F} = -\frac{\pi}{G}\frac{4H^2 + \dot{H} + 3K/a^2}{\left(H^2 + K/a^2\right)\left(2H^2 + \dot{H} + K/a^2\right)}\mathrm{d}F\,, \tag{17}$$

which agrees with the result of Ref. [8] for $K = 0$ obtained in $f(R)$ gravity and scalar-tensor theories.

The new term $\mathrm{d}_i\hat{S}$ can be interpreted as a term of entropy production in the non-equilibrium thermodynamics. The theories with $F =$ constant lead to $\mathrm{d}_i\hat{S} = 0$, which means that the first-law of equilibrium thermodynamics holds. Meanwhile the theories with $\mathrm{d}F \neq 0$, including $f(R)$ gravity and scalar-tensor theories, give rise to the additional term (17).

The existence of a non-equilibrium entropy production term $\mathrm{d}_i\hat{S}$ is related to the fact that $\hat{\rho}_d$ and $\hat{P}_d$ defined in Eq. (8) obey Eq. (9) whose r.h.s. does not vanish for $\dot{F} \neq 0$. If it is possible to define energy density and pressure of dark components satisfying the standard continuity equation, then we anticipate that the non-equilibrium description of thermodynamics may not be necessary. We will show that such a treatment is indeed possible. We rewrite Eqs. (4) and (5) in the following forms:

$$3\left(H^2 + \frac{K}{a^2}\right) = 8\pi G\left(\rho_d + \rho_f\right), \quad -2\left(\dot{H} - \frac{K}{a^2}\right) = 8\pi G\left(\rho_d + P_d + \rho_f + P_f\right), \tag{18}$$

$$\rho_d \equiv \frac{1}{8\pi G}\left[f_{,X}X + \frac{1}{2}\left(FR - f\right) - 3H\dot{F} + 3\left(1 - F\right)\left(H^2 + \frac{K}{a^2}\right)\right], \tag{19}$$

$$P_d \equiv \frac{1}{8\pi G}\left[\ddot{F} + 2H\dot{F} - \frac{1}{2}\left(FR - f\right) - \left(1 - F\right)\left(2\dot{H} + 3H^2 + \frac{K}{a^2}\right)\right]. \tag{20}$$

If we define ρ_d and P_d in this way, they obey the following continuity equation $\dot{\rho}_d + 3H(\rho_d + P_d) = 0$, where we have used Eq. (6). Introducing the horizon entropy S in the form $S = A/(4G)$, it follows that

$$\frac{1}{2\pi\tilde{r}_A}\mathrm{d}S = 4\pi\tilde{r}_A^3 H(\rho_d + P_d + \rho_f + P_f)\,\mathrm{d}t\,. \tag{21}$$

Using the horizon temperature given in Eq. (11), we obtain

$$T\mathrm{d}S = 4\pi\tilde{r}_A^3 H(\rho_d + P_d + \rho_f + P_f)\,\mathrm{d}t - 2\pi\tilde{r}_A^2(\rho_d + P_d + \rho_f + P_f)\,\mathrm{d}\tilde{r}_A\,. \tag{22}$$

Defining the Misner-Sharp energy to be $E = \tilde{r}_A/(2G) = V(\rho_d + \rho_f)$, we find

$$\mathrm{d}E = -4\pi\tilde{r}_A^3 H(\rho_d + P_d + \rho_f + P_f)\,\mathrm{d}t + 4\pi\tilde{r}_A^2(\rho_d + \rho_f)\,\mathrm{d}\tilde{r}_A\,. \tag{23}$$

Due to the conservation equation, the r.h.s. does not include an additional term proportional to $\mathrm{d}F$. Combining Eqs. (22) and (23), we get

$$T\mathrm{d}S = -\mathrm{d}E + W\mathrm{d}V\,, \tag{24}$$

where the work density W is defined by $W = (\rho_d + \rho_f - P_d - P_f)/2$. Equation (24) corresponds to the first law of equilibrium thermodynamics. This shows that the equilibrium form of thermodynamics can be derived by introducing the energy density ρ_d and the pressure P_d in a suitable way. From Eq. (24), we find

$$T\dot{S} = V\left(3H - \frac{\dot{V}}{2V}\right)(\rho_f + \rho_d + P_f + P_d)\,. \tag{25}$$

Using $V = 4\pi\tilde{r}_A^3/3$ and Eq. (11), it follows that

$$\dot{S} = 6\pi HV\tilde{r}_A(\rho_d + \rho_f + P_d + P_f) = -\frac{2\pi}{G}\frac{H\left(\dot{H} - K/a^2\right)}{\left(H^2 + K/a^2\right)^2}\,. \tag{26}$$

The horizon entropy increases as long as the null energy condition $\rho_T + P_T \equiv \rho_d + \rho_f + P_d + P_f \geq 0$ is satisfied. The realization of the above equilibrium picture of thermodynamics comes from the fact that (i) there is an energy momentum tensor $T_{\mu\nu}^{(d)}$ satisfying the local conservation law $\nabla^\mu T_{\mu\nu}^{(d)} = 0$ and (ii) the entropy S is given by $S = CA$, where C is constant (as in the standard Einstein gravity).

3 Summary

We have shown that it is possible to obtain a picture of equilibrium thermodynamics on the apparent horizon in the expanding cosmological background for a wide class of modified gravity theories with the Lagrangian density $f(R, \phi, X)$, such as $f(R)$ gravity and scalar-tensor theories, for the case in which the horizon entropy S in equilibrium thermodynamics is proportional to the horizon area A with a constant coefficient. This comes from a suitable definition of an energy momentum tensor of the "dark" component that respects to a local energy conservation.

References

[1] J. D. Bekenstein, Phys. Rev. D **7**, 2333 (1973).

[2] J. M. Bardeen, B. Carter and S. W. Hawking, Commun. Math. Phys. **31**, 161 (1973).

[3] S. W. Hawking, Commun. Math. Phys. **43**, 199 (1975) [Erratum-ibid. **46**, 206 (1976)].

[4] T. Jacobson, Phys. Rev. Lett. **75**, 1260 (1995).

[5] C. Eling, R. Guedens and T. Jacobson, Phys. Rev. Lett. **96**, 121301 (2006).

[6] K. Bamba, C. Q. Geng and S. Tsujikawa, arXiv:0909.2159 [gr-qc].

[7] C. W. Misner and D. H. Sharp, Phys. Rev. **136**, B571 (1964).

[8] S. F. Wu, B. Wang, G. H. Yang and P. M. Zhang, Class. Quant. Grav. **25**, 235018 (2008).

Numerical simulations of the accretion process in Kerr space-times with arbitrary value of the Kerr parameter

Cosimo Bambi[1]

Institute for the Physics and Mathematics of the Universe,
The University of Tokyo,
Kashiwa, Chiba 277-8568, Japan

Abstract

According to the Cosmic Censorship Conjecture, all the singularities produced by the collapsing matter must be hidden behind an event horizon. In 4D general relativity, this implies that the final product of the collapse is a Kerr-Newman black hole. Here I consider the possibility that the Cosmic Censorship Conjecture can be violated. I present the results of some numerical simulations of the accretion process onto Kerr black holes (objects with event horizon) and Kerr super-spinars (fast-rotating objects without event horizon). This is a preliminary study to investigate how the Cosmic Censorship Conjecture can be tested by astrophysical observations.

1 Introduction

Today gravity is relatively well tested in the weak field limit, while little or nothing is known when it becomes strong [1]. Strong gravitational fields can be found around astrophysical compact objects and could be probed by studying the radiation emitted in the accretion process. However, that turns out to be a very difficult job: the radiation emitted by the falling gas depends significantly on the accretion model and it is apparently impossible to constrain gravity without several model-dependent assumptions. For such a reason, today we know some "black hole candidates", but actually we do not know if these objects have an event horizon or if the space-time around them is described by the Kerr metric. In astrophysics, one assumes that these candidates are Kerr black holes and studies different scenarios of accretion in order to explain observations. Here I am instead interested in testing the actual nature of these objects. In particular, I consider the possibility that some black hole candidates rotate too fast to have an event horizon and I show that the accretion process onto them would be so much different that hopefully future theoretical studies and astrophysical observations will be able to confirm or rule out such a possibility.

2 The Cosmic Censorship Conjecture

In general relativity, under apparently reasonable assumptions, the collapsing matter leads inevitably to the formation of singularities. Here there are two possibilities: *i*) the singularity is hidden behind an event horizon and the final product is a black hole, *ii*) the singularity is not hidden behind an event horizon and therefore is naked. Since space-times with naked singularities typically have pathologies, usually some form of the Cosmic Censorship Conjecture is assumed and naked singularities are forbidden [2]. Neglecting the electric charge, it turns out that, in four dimensions, the final product of the gravitational collapse of matter is a Kerr black hole [3, 4].

The Kerr metric is completely characterized by two parameters; that is, the mass M and the spin J. The latter is often replaced by the Kerr parameter a, defined as $a = J/M$. Using Boyer-Lindquist coordinates, the position of the horizon of a Kerr black hole is given by

$$r_H = M + \sqrt{M^2 - a^2}\,, \tag{1}$$

which demands the well known constraint $|a| \leq M$. For $|a| > M$, there is no horizon and the space-time contains a naked singularity. In absence of horizon, it is possible to reach the physical singularity at $r = 0$

[1]Email address: cosimo.bambi@ipmu.jp

from some large r in finite time, enter the ring singularity, go to the region with negative values of r, and eventually come back to the starting point at an earlier time. So, the theory allows for the existence of closed time-like curves and causality can be violated.

However, it is widely believed that the Planck scale, $E_{Pl} \sim 10^{19}$ GeV, is the natural UV cut-off of classical general relativity. In other words, the theory would be unable to describe phenomena with a characteristic energy exceeding E_{Pl}. If we apply this general idea to the case of the Kerr space-time with $|a| > M$, where observer-independent quantities like the scalar curvature diverge at the singularity, it is at least questionable to expect that the prediction of the existence of closed time-like curves is reliable. New physics could instead replace the singularity with something else and Nature may conserve causality, not because it is impossible to create an object with $|a| > M$, but because there is no singularity in the full theory. On the basis of this argument, super-spinning Kerr objects with no event horizon, or "super-spinars", might exist in the Universe [5].

3 Accretion process

3.1 Model and assumptions

The first step to study the radiation emitted in the accretion process onto a compact object is to investigate the accretion process itself. In Ref. [6], I discussed the accretion process of a test fluid in a background Kerr space-time; that is, I neglected the back-reaction of the fluid to the geometry of the space-time, as well as the increase in mass and the variation in spin of the central object due to accretion. Such an approximation is surely reasonable to describe the accretion onto a stellar mass compact object in a binary system, because in this case the matter captured from the stellar companion is typically small in comparison with the total mass of the compact object. The results of these simulations should instead not be applied to long-term accretion onto a super-massive object at the center of a galaxy, where accretion makes the mass of the compact object increase by a few orders of magnitude from its original value.

The calculations are made with the relativistic hydrodynamics module of the public available code PLUTO [7], properly modified for the case of curved space-time, as described in [6]. The computational domain is the 2D axisymmetric space $r_{in} < r < 20\,M$ and $0 < \theta < \pi$, where r_{in} is set just outside the event horizon in the case of black hole, and $r_{in} = 0.5\,M$ in the case of super-spinar. The choice of $r_{in} = 0.5\,M$ may appear arbitrary, but it was checked that does not significantly alter the final result for any value of $|a|/M$, as long as $r_{in} \lesssim 0.7\,M$.

Here the accretion process is spherically symmetric and the gas is injected from the outer boundary at a constant rate[2]. Because of the simple treatment of the accreting matter, the gas temperature is not under control. In [6] I simply imposed a maximum temperature: the aim was not to find an accurate description of the accretion process, but to catch some peculiar features of the accretion process onto Kerr objects with $|a| > M$. The code was run with $T_{max} = 10$ keV, 100 keV, and 1 MeV, obtaining essentially the same result. Such a range of T_{max} is the one suggested by observations of galactic black hole candidates: the hard X-ray continuum (10 – 200 keV) is a typical feature of all these objects and is often explained with a hot inner disk or a hot corona, in which the electron temperature is around 100 keV (see e.g. Ref. [8]). Let us notice that in this case the accretion process is not the simple Bondi accretion. In the Bondi accretion, the temperature of the gas (ions) at the horizon (in the case of black holes) is about 100 MeV and the proper velocity of the flow is close to 1.

3.2 Results

The results of the simulations are summarized in Fig. 1, where it is shown the rest-mass energy density of the accretion flow around a Kerr black hole with $a/M = 0.9$ (top left panel) and super-spinars with $a/M = 1.1$ (top right panel), 1.4 (bottom left panel), and 2.0 (bottom right panel). The peculiar feature of the case with $|a|/M > 1$ is that the gravitational force near the massive object can be repulsive.

There are three qualitatively different cases determined by the value of $|a|/M$ (for more details, see Ref. [6]):

[2] Spherical or quasi-spherical accretion flows are expected when the compact object accretes from the stellar medium or when it belongs to a binary system in which the companion is massive and has a strong stellar wind.

1) Black hole with $|a|/M \leq 1$. We have the usual accretion picture: the injected matter always reaches a quasi-steady state configuration, in which matter is lost behind the event horizon at the same rate as it enters the computational domain.
2) Super-spinars with $|a|/M > 1$. The gravitational force in the neighborhood of the center $r = 0$ can be repulsive (because of the singularity, not of the rotation of the gas) and thus makes the accretion process harder. The critical radius where the gravitational force changes from attractive to repulsive can be estimated analytically. In Boyer-Lindquist coordinates, it is roughly determined by the sign of the quantity $r^2 - a^2 \cos^2\theta$, i.e. the force is attractive (repulsive) if $r^2 - a^2 \cos^2\theta > 0$ (< 0), where θ is the polar angle[3]. There are two different super-spinar regimes:
2*a*) Super-spinars with $|a|/M < 1.4$. The accretion process is extremely suppressed and only a small amount of the accreting gas can reach the center. Most of the gas is accumulated around the object, forming a high density cloud that continues to grow. Apparently, no quasi-steady state exists.
2*b*) Super-spinars with $|a|/M \geq 1.4$. In this case the repulsive force is not capable of preventing a regular accretion of the object. The flow reaches the center by forming a sort of high density disk on the equatorial plane. A quasi-steady state configuration is possible.

The origin of the critical value $|a|/M = 1.4$ can be understood with an analytical argument, as the maximum value for which there are stable marginally bound orbits on the equatorial plane with zero angular momentum at infinity.

4 Final remarks

It is widely believed that the final product of the gravitational collapse of matter is a Kerr black hole. However such a conclusion is based on a set of unproved assumptions, including the Cosmic Censorship Conjecture. In this talk I discussed the possibility that the Cosmic Censorship Conjecture can be violated and I presented some astrophysical implications. I showed that the accretion process in Kerr space-time onto objects with event horizon (black holes) and without event horizon (super-spinars) is quite different and hopefully the two scenarios can be distinguished observationally with no model-dependent assumptions.

Two comments are in order here. First, if the Cosmic Censorship Conjecture is violated, there is no uniqueness theorem guaranteeing that the space-time is described by the Kerr metric. And indeed other axisymmetric solutions of the Einstein equations in vacuum with naked singularities are known (e.g. the Weyl space-times). Here I discussed the case of super-spinar because it is likely the simplest example. Second, we do not know if super-spinars are stable objects and this question is presumably difficult to address, because we do not know how the singularity is solved in the full theory.

The study of the accretion process onto objects with and without event horizon is the first step to figure out possible observational signatures of the radiation emitted in the accretion process which can be used to test the Cosmic Censorship Conjecture. For example, an application of this work will be the predictions of the "direct image" of super-spinars [9, 10].

Acknowledgments

I wish to thank my collaborators, Katherine Freese, Tomohiro Harada, Rohta Takahashi, and Naoki Yoshida. This work was supported by World Premier International Research Center Initiative (WPI Initiative), MEXT, Japan.

References

[1] C. M. Will, Living Rev. Rel. **9**, 3 (2005).

[2] R. Penrose, Riv. Nuovo Cim. **1**, 252 (1969) [Gen. Rel. Grav. **34**, 1141 (2002)].

[3] This simple criterion works better for higher values of $|a|/M$ and cannot explain some important features of the case $1 < |a|/M < 1.4$.

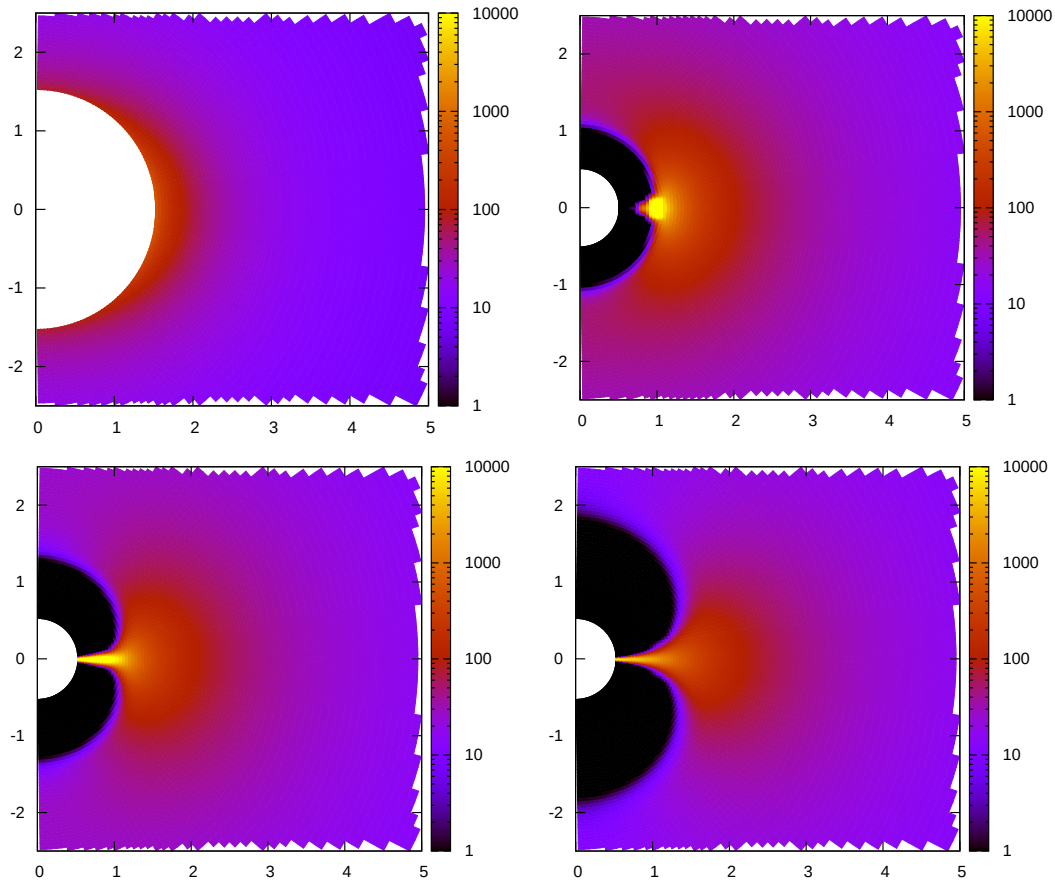

Figure 1: Density plot of the accretion flow around a Kerr BH with $a_* = 0.9$ (top left panel) and super-spinars with $a_* = 1.1$ (top right panel), $a_* = 1.4$ (bottom left panel), and $a_* = 2.0$ (bottom right panel). The density scale (shown on the right hand side of each panel) is in arbitrary units. The unit of length along the x and y axes is M. The white area is out of the domain of computation. The peculiar feature of the super-spinar case is that most of the space-time around the central object is almost empty (the black regions in the pictures): that is the result of the repulsive force at short distance from the center. For more details, see Ref. [6].

[3] B. Carter, Phys. Rev. Lett. **26**, 331 (1971).

[4] D. C. Robinson, Phys. Rev. Lett. **34**, 905 (1975).

[5] E. G. Gimon and P. Horava, Phys. Lett. B **672**, 299 (2009).

[6] C. Bambi, K. Freese, T. Harada, R. Takahashi and N. Yoshida, Phys. Rev. D **80**, 104023 (2009).

[7] A. Mignone, G. Bodo, S. Massaglia, T. Matsakos, O. Tesileanu and C. Zanni, Astrophys. J. Suppl. **170**, 228 (2007).

[8] E. P. Liang, Phys. Rep. **302**, 67 (1998).

[9] C. Bambi and K. Freese, Phys. Rev. D **79**, 043002 (2009).

[10] C. Bambi, K. Freese and R. Takahashi, arXiv:0908.3238 [astro-ph.HE].

Singular and non-singular endstates in massless scalar field collapse

Swastik Bhattacharya[1]

Department of Astronomy and Astrophysics, Tata Institute of Fundamental Research, Mumbai 400005, India

Abstract

We study the collapse of a massless scalar field coupled to gravity. A class of blackhole solutions are identified. We also report on a class of solutions where collapse starts from a regular spacelike surface but then the collapsing scalar field freezes. As a result, in these solutions, a black hole does not form, neither is there any singularity in the future.

1 Introduction

The endstate of gravitational collapse is of great interest in gravitational physics. The formation of spacetime singularities in gravitational collapse and formation of black holes is an issue, which has been investigated in much detail in Einstein's theory. The occurrence of singularities indicates the breakdown the known laws of physics and offers a regime where the quantum gravity effects would be important. As is well known, dynamical evolution of matter fields in a spacetime generically yields a singularity, provided reasonable physical conditions are satisfied such as the causality, a suitable energy condition ensuring the positivity of energy density, and formation of trapped surfaces. This result tells us what might happen in those stars, where continual collapse occurs. Therefore it is important to investigate whether continual collapse always leads to a singular endstate or any other possibility also exists.

The case of gravitational collapse of a massless scalar field is of particular interest in both collapse situations as well as cosmological scenarios. In cosmology, special importance is attached to the evolution of a scalar field, which has attracted a great deal of attention in past decades. In gravitational collapse studies, the nature of singularity for massless scalar fields has been examined and a number of numerical and analytical works have been done in recent years on spherical collapse models from the perspective of the cosmic censorship hypothesis. The issues that have been raised above regarding gravitational collapse, can be investigated for massless scalar field models. This would provide us with some insight into a collapsing matter field in general.

In the present study, we outline a mathematical structure to deal with the evolution of massless scalar fields in a spherically symmetric spacetime in comoving coordinates. For massless scalar field, this coordinate system breaks down when the gradient of the scalar field becomes null. However, as will be shown later, in models satisfying some physically reasonable conditions, the gradient of the scalar field always remains timelike. So our analysis holds for this class of models. In this case, the energy-momentum tensor of the massless scalar field has exact correspondence with that of a stiff fluid. So this analysis is applicable to stiff fluid collapse also.

Using this formalism, we then examine the classes of collapsing models. In particular we find a class of black hole solutions where the future singularity is spacelike. We also point out a class of models where the collapse starts from a regular initial surface but with time the rate of collapse decreases so that neither any trapped surface nor any singularity is formed in the future.

2 The Basic Formalism

In this section, we set up the Einstein equations for the massless scalar field in comoving coordinates.

[1]Email address: swastik@tifr.res.in

2.1 Matter field and coordinate system

The energy-momentum tensor for the massless scalar field is

$$T_{ab} = \phi_{;a}\phi_{;b} - \frac{1}{2}g_{ab}(\phi_{;c}\phi_{;d}g^{cd}). \tag{1}$$

In this case, the strong energy condition is always satisfied. We choose the comoving coordinate system, in which $T_{\mu\nu}$ and $g_{\mu\nu}$ are diagonal. The coordinates are t, r, θ and ϕ. This implies that there are only two choices: $\phi = \phi(t)$ or $\phi = \phi(r)$. Here we shall consider only the case, where $\phi = \phi(t)$. The equation of state is $\rho = P_r = P_\theta$, which is that of a stiff fluid. The coordinate system breaks down when $\phi_{,\mu}$ is null. The metric is

$$ds^2 = e^{2\nu}dt^2 - e^{2\psi}dr^2 - R^2d\theta^2 - R^2sin^2\theta d\phi^2 \tag{2}$$

2.2 Einstein equations

The Einstein equations are

$$R_{\mu\nu} - \frac{1}{2}Rg_{\mu\nu} = -\kappa T_{\mu\nu} \tag{3}$$

We work in such units so that κ is one. We define a function F by

$$G - H = 1 - \frac{F}{R} \tag{4}$$

where G and H are given by

$$G = e^{-2\psi}R'^2 \tag{5}$$

and

$$H = e^{-2\nu}\dot{R}^2. \tag{6}$$

Then we can write down the Einstein equations in the form [1]

$$\rho = \frac{F'}{R^2R'}, P_r = -\frac{\dot{F}}{R^2\dot{R}}, \tag{7}$$

$$\nu'(\rho + P_r) = 2(P_\theta - P_r)\frac{R'}{R} - P_r', \tag{8}$$

$$-2\dot{R}' + R'\frac{\dot{G}}{G} + \dot{R}\frac{H'}{H} = 0 \tag{9}$$

where the density ρ is given by

$$\rho = \frac{1}{2}e^{-2\nu}\dot{\phi}^2 \tag{10}$$

3 Collapse of the scalar field

The massless scalar field collapses from a regular initial spacelike surface. At the initial time t_i, the following functions of the comoving radius r are specified.

$$\nu(t_i, r) = \nu_0(r), \psi(t_i, r) = \psi_0(r), R(t_i, r) = r, \phi(t_i), F(t_i, r) = F_0(r) \tag{11}$$

Since we are considering a collapse solution, we discuss only the cases where $\dot{R} \leq 0$, i.e. the area radius gets smaller with time. For convenience, we define a quantity v by the relation $v = \frac{R}{r}$. There would be a strong curvature singularity at $v = 0$.

3.1 Regularity conditions

Here we consider those solutions that satisfy the following regularity conditions. A physically reasonable collapse solution satisfies these conditions. All the metric functions are C_2 at any non-singular spacetime point. Also ρ , P_r and P_θ are finite at any regular spacetime point. Further we take $R' > 0$ for all regular spacetime points. This corresponds to the condition that there are no shell-crossings in the spacetime. Since $|\phi_{,\mu}\,\phi^{,\mu}| \propto \rho$, as long as $\rho > 0$, the comoving coordinates can be used. We consider here only those cases where $\rho(r, t_2) \leq \rho(r, t_1)$ if $t_2 < t_1$. This means that during the collapse, the density should not decrease with time. Then if the collapse starts from a regular spacelike surface where the gradient of the scalar field is timelike, then throughout the collapse, the gradient remains timelike. The F.R.W. solutions are examples of this type.

3.2 A class of blackhole solutions

The variables r and t can be interchanged to r and v in all the equations. For convenience, we define a new function M by the relation

$$F = r^3 M \tag{12}$$

Then the system of the Einstein equations can be reduced to the two equations.

$$v' = -\frac{3M + rM_{,r} + vM_{,v}}{2rM_{,v}}; \tag{13}$$

and

$$\dot{v} = -\frac{e^\nu}{\sqrt{v}}\sqrt{[\frac{v}{r^2}(G-1) + M]}. \tag{14}$$

where $e^\nu = \frac{v}{\sqrt{-2M_{,v}}}$ and $G = -\frac{v^2 M_{,v}(v + rv')^2}{f^2(r)}$ and $f(r)$ is a function of integration. The last two equations constitute a integrable Pfaffian when M satisfies the equation,

$$\frac{\partial \dot{v}}{\partial r} + v'\frac{\partial \dot{v}}{\partial v} - \dot{v}\frac{\partial v'}{\partial v} = 0 \tag{15}$$

This is a Monge-Ampere type 2nd order p.d.e. for M. However since the expression for $\dot{v}$ has square roots in it, sometimes it would be more convenient for us to consider the equation,

$$\frac{\partial \dot{v}^2}{\partial r} + v'\frac{\partial \dot{v}^2}{\partial v} - 2\dot{v}^2\frac{\partial v'}{\partial v} = 0 \tag{16}$$

The solutions of (16) are solutions of (15) also; except when $\dot{v} = 0$. Now we are in a position to analyze the consequences of the Einstein equations.

The time taken for a comoving shell r to reach the singularity is given by $t_s(r) = \int_1^0 \frac{1}{\dot{v}} dv$. It can be shown that the regularity conditions imply that M must be of the form $M = \frac{m_0}{v^3} + r^n g(r, v)$, where $n \geq 2$. In terms of M and v, the density can be expressed as $\rho = -\frac{M_{,v}}{v^2}$. From these relations, it can be shown that if $t_s(r)$ is continuous, then $t_s(r) = constant$. Which means that, only spacelike singularities are formed. Therefore this would give us a class of black hole solutions [2].

3.3 Collapse without formation of singularity in the future

Using the formalism that we have presented here so far, we can prove an interesting result [2].
If there is a solution which satisfies the regularity conditions, and for which $\dot{v} \leq 0$ and $v'(r, t) \geq b$, where $b > 0$ for $r_1 \leq r \leq r_2$ for some $r_1 > 0$ and r_2, and $t \in (t_i, \infty)$, then the comoving shells never become singular.

For these solutions, it can be shown that $\dot{v} < l$ for any $l > 0$ for an infinite interval of coordinate time. This means that the collapsing matter would freeze eventually. It is important to note though that this result does not guarantee the existence of such singularity-free solutions. To see whether such solutions

are there or not we consider (15) and find out an appropriate boundary condition which would result in the freezing of collapse.

To this end, we set the following Cauchy boundary condition for equation (15) for M. On the surface, $v = \chi(r)$, where $\chi(r)$ is some regular function of r, $M(v, r)$ and $\frac{\partial M(v,r)}{\partial n}$, i.e. M and its derivative normal to the surface are given. We set the boundary condition in such a way that both of them are analytic functions. Also they are chosen so as to satisfy $[\frac{v}{r^2}(G-1)+M] \mid_{v=\chi(r)} = 0$ and $\chi'(r) \neq v'(v,r) \mid_{v=\chi(r)}$. From this, it can be shown that $[\frac{v}{r^2}(G-1)+M]_{,v} \mid_{v=\chi(r)} = 0$. Partial differentiation of both the sides of (15) with respect to v, gives us $\frac{\partial^3 M}{\partial^3 v} \mid_{v=\chi(r)}$ in terms of $M(v,r) \mid_{v=\chi(r)}$ and $\frac{\partial M(v,r)}{\partial n} \mid_{v=\chi(r)}$. Then $[\frac{v}{r^2}(G-1)+M]_{,vv} \mid_{v=\chi(r)}$ can also be found out. We choose the two given functions in such a way so that $[\frac{v}{r^2}(G-1)+M]_{,vv} \mid_{v=\chi(r)} > 0$. Further they have to satisfy

$$[\frac{\partial \dot{v}}{\partial r} + v' \frac{\partial \dot{v}}{\partial v}] \mid_{v=\chi(r)} = 0 \tag{17}$$

(17) is the condition that guarantees that the solution to (16) would also be a solution to (15). Now using Cauchy-Kovalevsky theorem, it can be proved that a solution of (16) exists in some neighbourhood of the curve $v = \chi(r)$. The $v = \chi(r)$ curve divides this neighbourhood into two parts. In one part, v increases along any line $r = r_2$. For the collapse solution, we need to consider only this part. Since this is a solution to (15) as well, such a solution to the Einstein equations exist.

Now we show that this solution does not have a future singularity. For some value of $r = r_1$, $\dot{v}$ can be written as

$$\dot{v} = -a_1(r_1)(v - v_c) + O[(v - v_c)^2] \tag{18}$$

where $a_1(r_1) > 0$. Now it can be shown that the time $t(v_1, r_1)$ taken by the comoving shell r_1 to reach $v_1 = \chi(r_1)$ is infinite. The proper time taken by a comoving shell r_1 to reach v_1 is $\tau(v_1, r_1) = \int_{t_i}^{t(v_1,r_1)} e^{\nu} dt$. Since $e^{\nu}(t, r_1)$ has a positive minimum in the range (t_i, ∞), $\tau(v_1, r_1)$ is also infinite. So collapse does not lead to a singularity in the future. It can also be shown that the proper time for the formation of trapped surface is also infinite. This is consistent with the singularity theorems as formation of trapped surfaces implies that singularity would form eventually because the strong energy condition is satisfied.

The above analysis tells us that there would be solutions where the scalar field collapses from a regular spacelike hypersurface and ultimately the collapse stops. Trapped surfaces do not form, neither is there any future singularity. However the present analysis does not tell us whether it would be possible to extend these solutions in the past from the regular spacelike hypersurface mentioned earlier.

4 Discussion

The formalism described here is effective in finding out about the endstate of the collapse of massless scalar fields and stiff fluids. Using this formalism, it is possible to identify a class of black hole solutions. For massless scalar fields, there can be collapse models where collapse ultimately stops. Trapped surfaces do not form and the endstate is non-singular. However it is not clear whether these solutions can be extended in the past indefinitely. They might be of interest as examples of collapse models where collapse slows down, there is no bounce, still neither a black hole forms nor is there any singularity in the future. If time-reversed, these models might be of interest in cosmology as the initial singularity would be absent in that case. It would be of interest to see whether it is possible to find out about the endstate of collapsing matter proceeding in the way described here with different equations of state.

References

[1] R. Goswami and P. S. Joshi, Phys. Rev. D **76**, p.084026 (2007)

[2] S. Bhattacharya, R. Goswami and P. S. Joshi, Arxiv: 0807.1985.

Asymptotic iteration method for spheroidal harmonics of higher-dimensional Kerr-(A)dS black holes

H. T. Cho[1(a)], A. S. Cornell[2(b)], Jason Doukas[3(c)], and Wade Naylor[4(d)]

[(a)] *Department of Physics, Tamkang University, Tamsui, Taipei, Taiwan, Republic of China,*
[(b)] *National Institute for Theoretical Physics; School of Physics, University of the Witwatersrand, Wits 2050, South Africa,*
[(c)] *Yukawa Institute for Theoretical Physics, Kyoto University, Kyoto, 606-8502, Japan,*
[(d)] *Department of Physics, Ritsumeikan University, Kusatsu, Shiga 525-8577, Japan.*

Abstract

In this work we calculate the angular eigenvalues of the $(n+4)$-dimensional *simply* rotating Kerr-(A)dS angular equation using the Asymptotic Iteration Method (AIM). We then compare this method with the Continued Fraction Method (CFM) thereby checking our results.

1 Introduction

Recently a new method for obtaining solutions of second order ordinary differential equations has been developed called the asymptotic iteration method (AIM) [1]. The AIM provides a simple approach to obtaining eigenvalues of bound state problems, even for spheroidal harmonics with c a general complex number, large or small [1], and even to quasinormal mode (QNM) calculations [2]. It has also been shown that the AIM is closely related to the continued fractions method (CFM)[4] derived from an exact solution to the Schrödinger equation via a WKB ansatz [5], where a related CFM is often employed in numerical calculations of spheroidal eigenvalues and QNM of black hole equations [6].

In this letter we will demonstrate that the AIM can also be applied to the generalized scalar hyper-spheroidal equation, $S_{kjm}(\theta)$, derived from an $(n+4)$-dimensional *simply* rotating Kerr-(A)dS angular separation equation [3, 7, 8]:

$$\frac{\partial_\theta\Big((1+\alpha\cos^2\theta)\sin\theta\cos^n\theta\partial_\theta S\Big)}{\sin\theta\cos^n\theta}+\left(A_{kjm}-\frac{m^2(1+\alpha)}{\sin^2\theta}-\frac{c^2\sin^2\theta}{1+\alpha\cos^2\theta}-\frac{j(j+n-1)}{\cos^2\theta}\right)S \quad =0 \quad (1)$$

where we have defined $\alpha = a^2\Lambda$ with a the angular rotation parameter, and that the frequency ω is contained in the dimensionless parameter $c = a\omega$.

Higher dimensional spheroids have already been discussed by Berti et al. [9], who use a 3-term CFM to solve the angular eigenvalues, however, the generalized scalar hyper-spheroidal equation under investigation here contains four regular singular points[5] which leads to a 4-term recurrence relation [10]. The simplest brute force approach to deal with an n-term recurrence relation is to use n Gaussian eliminations to reduce the problem to a tri-diagonal matrix form [11] but this can often be very tedious.

Even in four-dimensions the Kerr-(A)dS case does not allow for a simple 3-term continued fraction relation nevertheless an elegant method has been developed to deal with situations of this type [8], where such techniques can only be applied if there are exactly four regular singular points. In contrast to this the appeal of the AIM is that it can be applied somewhat independently of the singularity structure of the ordinary differential equation and thus to a larger class of equations.

[1] Email address: htcho@mail.tku.edu.tw
[2] Email address: alan.cornell@wits.ac.za
[3] Email address: jasonad@yukawa.kyoto-u.ac.jp
[4] Email address: naylor@se.ritsumei.ac.jp
[5] Unlike the asymptotically flat limit ($\Lambda = 0$) which only has three.

2 The Asymptotic Iteration Method

To write the angular equation in a form suitable for the AIM we substitute $x = \cos\theta$ and obtain:

$$(1-x^2)(1+\alpha x^2)S''(x) + \left(\frac{n(1-x^2)-x^2}{x} + \alpha x(n+2-(n+3)x^2) - x(1+\alpha x^2)\right) S'(x) + \left(A_{kjm} - \frac{c^2(1-x^2)}{1+\alpha x^2} - \frac{m^2(1+\alpha)}{1-x^2} - \frac{j(j+n-1)}{x^2}\right) S(x) = 0 \ . \quad (2)$$

Note that the separation constant A_{kjm} above corresponds to a simple eigenvalue shift in the asymptotically flat cases studied thus far [9], as can be verified by setting $\alpha = 0$.

The AIM can be implemented by multiplying S_{kjm} by the characteristic exponents; however, we have found that the most suitable form (fastest converging) is obtained by multiplying the angular mode function by [1]:

$$S_{kjm}(x) = (1-x^2)^{\frac{|m|}{2}} y_{kjm}(x) \ , \quad (3)$$

which leads to a differential equation in the AIM form:

$$y'' = \lambda_0 y' + s_0 y \ , \quad (4)$$

where (for Kerr-(A)dS) λ_0 and s_0 are given in Ref. [3], and where the primes of y denote derivatives with respect to x. Differentiating equation (4) p times with respect to x, leads to:

$$y^{(p+2)} = \lambda_p y' + s_p y \ , \quad (5)$$

where the superscript p indicates the p-th derivative with respect to x and

$$\lambda_p = \lambda'_{p-1} + s_{p-1} + \lambda_0\lambda_{p-1} \qquad \text{with} \qquad s_p = s'_{p-1} + s_0\lambda_{p-1} \ . \quad (6)$$

For sufficiently large p the asymptotic aspect of the "method" is introduced, that is:

$$\frac{s_p(x)}{\lambda_p(x)} = \frac{s_{p-1}(x)}{\lambda_{p-1}(x)} \equiv \beta(x) \ , \quad (7)$$

which leads to the general eigenfunction solution given in Ref. [1]. Within the framework of the AIM, a sufficient condition for imposing termination of the iterations is when $\delta_p(x) = 0$, for a given choice of x, where $\delta_p(x) = s_p(x)\lambda_{p-1}(x) - s_{p-1}(x)\lambda_p(x)$ [1]. For each value of m and k (or j), in a given $(n+4)$-dimensions, the roots of δ_p lead to a tower of eigenvalues $(m, \ell_1, \ell_2, \dots)$, where larger iterations give more roots and better convergence for higher ℓ modes in the tower.

It has also been noticed that the AIM converges fastest at the maximum of the potential [1], which in four dimensions occurs at $x = 0$ (even with $\alpha \neq 0$ and for general spin-s). However, in the higher dimensional case we could not determine the relevant Schrödinger like form and thus the maximum of the potential could not be analytically obtained. Nevertheless, as can be seen from the plots in Fig. 1 we found that the point $x = \frac{1}{2} = \cos\frac{\pi}{3}$, in general, gave the fastest convergence.

3 Heun's method for de-Sitter case

As we mentioned earlier we could also work with a 4-term recurrence relation directly and use Gaussian elimination to obtain a 3-term recurrence, which then allows for the eigenvalues to be solved using the CFM. However, if we write the angular equation (1) in terms of the variable $x = \cos(2\theta)$ [8]:

$$(1-x^2)(2+\alpha(1+x))S''(x) + \left(n-1-(n+3)x + \frac{\alpha}{2}(1+x)(n+1-(n+5)x)\right) S'(x) + \left(\frac{A_{klm}}{2} + \frac{c^2(x-1)}{2(2+\alpha(1+x))} + \frac{m^2(1+\alpha)}{x-1} - \frac{j(j+n-1)}{x+1}\right) S(x) = 0 \quad (8)$$

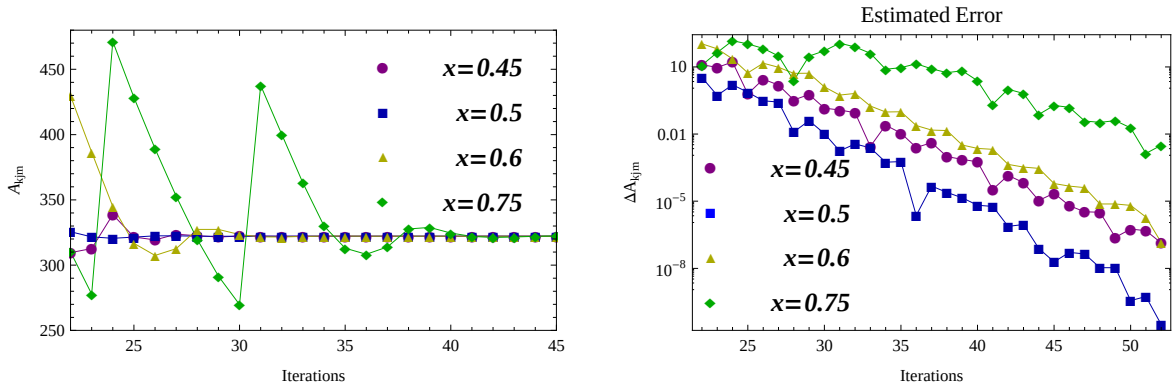

Figure 1: *Plot of the convergence of a typical eigenvalue* A_{711} *(*$n = 1$*,* $c = 1$ *and* $\alpha = 1$*) under* p *iterations of the AIM for various choices of* $x = \{0.45, 0.5, 0.6, 0.75\}$*. Shown on the left is the eigenvalue verses* p*, while on the right is a* log *plot of the estimated error,* $|A_{kjm}(p) - A_{kjm}(\infty)|$*.*

Table 1: *Comparison of selected eigenvalues,* A_{kjm}*, the Kerr-AdS case with* $c = 1$*,* $\alpha = -0.05$*,* $n = 1$ *(extra dimensions) and* $m = 0$*. Numbers in brackets represent the number of iterations required to reach convergence at the quoted precision, where subscript* A *and* C *are shorthand for AIM and CFM respectively.*

k	$j = 0$	$j = 1$
0	$0.4978643318\ (14)_A\ (3)_C$	$3.317784170\ (14)_A\ (3)_C$
1	$8.304871188\ (15)_A\ (4)_C$	$15.12466814\ (15)_A\ (4)_C$
2	$23.89847347\ (16)_A\ (5)_C$	$34.63440913\ (17)_A\ (5)_C$
3	$47.29227791\ (17)_A\ (6)_C$	$61.93248179\ (19)_A\ (6)_C$
4	$78.48442957\ (20)_A\ (8)_C$	$97.02600365\ (21)_A\ (8)_C$
5	$117.4747381\ (23)_A\ (9)_C$	$139.9165956\ (23)_A\ (9)_C$
6	$164.2631560\ (25)_A\ (10)_C$	$190.6047952\ (24)_A\ (10)_C$
7	$218.8496664\ (27)_A\ (11)_C$	$249.0908236\ (27)_A\ (11)_C$

and define $x = 2z - 1$, with the mode functions scaled by the characteristic exponents:

$$Q(x) = 2^{\frac{|m|}{2}}(z-1)^{\frac{|m|}{2}}(2z)^{\frac{j}{2}}\left(z+\frac{1}{\alpha}\right)^{\pm\frac{ic}{2\sqrt{\alpha}}} y(z)\ , \tag{9}$$

then the angular mode equation can now be written in the Heun form [8]:

$$\left[\frac{d^2}{dz^2} + \left(\frac{\gamma}{z} + \frac{\delta}{z-1} + \frac{\epsilon}{z+\frac{1}{\alpha}}\right)\frac{d}{dz} + \frac{\alpha\beta z - q}{z(z-1)(z+\frac{1}{\alpha})}\right] y(z) = 0\ , \tag{10}$$

where α, β, γ, δ, ϵ and q are given in Ref. [3], and where these results are identical to the Kerr-AdS case considered in Ref. [8] by choosing $\alpha = -a^2/R^2$.

To compare with the AIM method we shall use the fact that a three-term recurrence relation is guaranteed for any solution to Heun's differential equation [8]:

$$\alpha_0 c_1 + \beta_0 c_0 = 0\ , \tag{11}$$

$$\alpha_p c_{p+1} + \beta_p c_p + \gamma_p c_{p-1} = 0\ , \qquad (p = 1, 2, \dots)\ , \tag{12}$$

where for the Kerr-(A)dS case α_p, β_p and γ_p are given in Ref. [8]. Once a 3-term recurrence relation is obtained the eigenvalue A_{kjm} can be found (for a given ω) by solving a continued fraction of the form [6, 9]:

$$\beta_0 - \frac{\alpha_0\gamma_1}{\beta_1 -}\frac{\alpha_1\gamma_2}{\beta_2 -}\frac{\alpha_2\gamma_3}{\beta_3 -}\dots = 0\ . \tag{13}$$

Table 2: *Comparison of selected eigenvalues between the AIM and the CFM for different numbers of dimensions of the Kerr-dS case with* $c = 1$, $\alpha = 1$, $m = j = k = 0$.

n	2	3	4	5
A_{CFM}	0.284	0.2254	0.1861	0.1581
A_{AIM}	0.284049	0.225367	0.18606	0.158068

4 Analysis & Discussion

We have calculated the eigenvalues shown in Table 1 of the $(n + 4)$-dimensional *simply* rotating Kerr-(A)dS angular separation equation using the AIM and the CFM. Although we only considered a real parameter $c = a\omega$, we could also have used a purely imaginary or complex value of c, see Ref. [2]. For brevity we presented results for $n = 1$ extra dimensions only, but we have also checked the dependence on dimension, as can be seen in Table 2 for the fundamental $k = 0$ mode.

We found that the CFM eigenvalue solutions converged very quickly with accurate results even after a continued fraction depth of only $p = 15$. One point worth mentioning is that the $\alpha \to 0$ limit cannot be taken via Heun's method, because the recurrence relation (and hence the continued fraction) diverges for this case. In contrast the AIM has no such problem. The AIM also gives an alternative approach to obtaining the eigenfunctions in terms of simple integrals, which may be useful for symbolic computations.

In conclusion, we have highlighted how the AIM can be applied to higher-dimensional scalar or tensor gravitational (for $n \geq 3$) spheroidal harmonics, which arise in the separation of metrics. We have seen that the AIM requires very little manipulation in order to obtain a fast route to the angular eigenvalues, which may be useful for cases where Heun's method may not apply. However, the AIM does have some shortfalls. Note that while we did not attempt to optimise either algorithm, our implementation of the AIM was found to be much slower than that of the CFM. Considering that the CFM essentially involves expanding out p nested fractions, whereas the AIM involves taking p^{th} order derivatives, this behaviour is not surprising. However, for most of the cases we considered only a few seconds were required to reach the desired level of accuracy and thus the time was not a large concern.

References

[1] H. Ciftci, R. L. Hall and N. Saad, J. Phys. **A 36** (2003) 11807; T. Barakat, K. Abodayeh and A. Mukheimer, J. Phys. A: Math. Gen. **38** (2005) 1299-1304; T. Barakat, K. Abodayeh, B. Abdallah and O. M. Al-Dossary, Can. J. Phys. **84**, (2006) 121-129.

[2] H. T. Cho, A. S. Cornell, J. Doukas and W. Naylor, arXiv:0912.2740 [gr-qc].

[3] H. T. Cho, A. S. Cornell, J. Doukas and W. Naylor, Phys. Rev. D **80**, 064022 (2009) [arXiv:0904.1867 [gr-qc]].

[4] A. R. Matamala, F. A. Gutierrez and J. Díaz-Valdés, Phys. Lett. **A 361** (2007) 16-17.

[5] S.C. Miller, Phys. Rev. D **12** (1975) 3838; M. Jameel, Phys. Rev. D **15** (1977) 2409.

[6] E. W. Leaver, Proc. Roy. Soc. Lond. A **402** (1985) 285.

[7] Gibbons, G. W., Lü, H., Page, D. N. and Pope, C. N.: *J. Geom. Phys.* **53** (2005) 49–73.

[8] H. Kodama, R. A. Konoplya and A. Zhidenko, arXiv:0812.0445 [hep-th]; H. Suzuki, E. Takasugi and H. Umetsu, Prog. Theor. Phys. **100** (1998) 491. [arXiv:gr-qc/9805064].

[9] E. Berti, V. Cardoso and M. Casals, Phys. Rev. D **73** (2006) 024013 [Erratum-ibid. D **73** (2006) 109902] [arXiv:gr-qc/0511111].

[10] M. Giammatteo and I. G. Moss, Class. Quant. Grav. **22** (2005) 1803. [arXiv:gr-qc/0502046].

[11] E. W. Leaver, Phys. Rev. D **41**, 2986 (1990).

Cosmological perturbations of a perfect fluid and non-commutative geometry

Antonio De Felice[1]

Department of Physics, Faculty of Science, Tokyo University of Science, 1-3, Kagurazaka, Shinjuku-ku, Tokyo 162-8601

Abstract

I provide an action that describes the linear cosmological perturbations of a perfect fluid. This action is suited not only to perfect fluids with a barotropic equation of state, but also to those for which the pressure depends on two thermodynamical variables. By quantizing the system we find that 1) some perturbation fields exhibit a non-commutativity quite analogous to the one observed for a charged particle moving in a strong magnetic field, 2) curvature and pressure perturbations cannot be measured at the same time at the same point, 3) ghosts appear if the null energy condition is violated.

1 Action

In this proceeding I will report the work done in collboration with Jean-Marc Gérard and Teruaki Suyama [1].

The action considered here has been introduced by Schutz [3] and is defined as follows

$$S = \int d^4x\sqrt{-g}\left[\frac{R}{16\pi G} + p(\mu, s)\right]. \tag{1}$$

Alternative functionals have been proposed, all being physically equivalent as shown in [4]. We chose the version (1) as it was the most convenient for our purpose. The four-velocity of the perfect fluid is defined via potentials:

$$u_\nu = \frac{1}{\mu}\left(\partial_\nu\ell + \theta\partial_\nu s + A\partial_\nu B\right), \tag{2}$$

where ℓ, θ, A and B are all scalar fields. The normalization for the four-velocity, $u^\nu u_\nu = -1$, gives μ in terms of the other fields. The fundamental fields over which the action (1) will be varied are $g_{\mu\nu}$, ℓ, θ, s, A, and B.

Having chosen the Lagrangian for gravity to be the one of GR, we recover $G_{\mu\nu} = 8\pi G\, T_{\mu\nu}$ by varying with respect to the metric field. Besides the conservation of particle number and entropy already discussed, the other equations of motion derived from Eq. (1) are

$$u^\alpha\partial_\alpha\theta = T, \quad u^\alpha\partial_\alpha A = 0, \quad u^\alpha\partial_\alpha B = 0. \tag{3}$$

In a FLRW universe, $u_i = 0$ and $u_0 = -1$ such that the solutions to Eq. (3) are simply

$$A = A(\vec{x}), \quad B = B(\vec{x}), \quad \theta = \int^t T(t')\mathrm{d}t' + \tilde{\theta}(\vec{x}). \tag{4}$$

There is a complete freedom for the functions A, B, and $\tilde{\theta}$ [2], any choice leading to the same physical background. We will take advantage of this freedom to simplify our study of the scalar and vector perturbations.

[1] Email address: defelice@rs.kagu.tus.ac.jp

[2] Since $u_\nu = (-1, \vec{0})$, we also have that $\ell = -\int^t \mu(t')\mathrm{d}t' + \tilde{\ell}$, and $\vec{\nabla}\tilde{\ell} = -A\vec{\nabla}B$, which implies that $\vec{\nabla}A \times \vec{\nabla}B = 0$.

1.1 Scalar type perturbations

Let us simply consider the choice $A = B = \tilde{\theta} = 0$, to remove the vector perturbations arising from W_i. Regarding the metric, δg_{00} and δg_{0i} are auxiliary fields such that the only scalar component which will be dynamical is the curvature perturbation ϕ defined by $\delta g_{ij} = 2a^2\phi\,\delta_{ij}$.

We make a field redefinition, $v = \delta\ell + \theta(t)\delta s$, and introduce two gauge invariant fields, $\Phi = \phi + Hv/\mu$ and $\delta\bar{\theta} = \delta\theta + Tv/\mu$, to expand the action (1) at second order:

$$S_S = \int \mathrm{d}t\mathrm{d}^3\vec{x}\left\{\frac{a^3Q_S}{2}\left[\dot{\Phi}^2 - \frac{c_s^2}{a^2}(\vec{\nabla}\Phi)^2\right] + C\delta s\dot{\Phi} - \frac{D}{2}\delta s^2 - E(\delta\bar{\theta}\dot{\delta s} - \delta s\dot{\delta\bar{\theta}} + \delta A\dot{\delta B} - \delta B\dot{\delta A})\right\}. \tag{5}$$

The coefficients for Φ are given by $Q_S = \frac{\rho+p}{c_s^2H^2}$, $c_s^2 \equiv \frac{\dot{p}}{\dot{\rho}} = \left(\frac{\partial p}{\partial\rho}\right)_s$, whereas the remaining coefficients are

$$C = \frac{na^3}{H}\left[\mu\left(\frac{\partial T}{\partial\mu}\right)_s - T\right], \quad E = \frac{na^3}{2}, \quad D = na^3\left[T\left(\frac{\partial T}{\partial\mu}\right)_s + \left(\frac{\partial T}{\partial s}\right)_\mu\right]. \tag{6}$$

The general solution for δs, δA, and δB is their initial values since Eq. (5) forces them to be time-independent. As a consequence, the non trivial equations of motion are

$$\frac{1}{a^3Q_S}\frac{\mathrm{d}}{\mathrm{d}t}(a^3Q_S\dot{\Phi}) - \frac{c_s^2}{a^2}\nabla^2\Phi = -\frac{\dot{C}}{a^3Q_S}\,\delta s\,, \tag{7}$$

$$na^3\dot{\delta\bar{\theta}} - D\delta s + C\dot{\Phi} = 0\,. \tag{8}$$

If $T = f(s)\,\mu$, which is equivalent to having a barotropic equation of state $p = p(\rho)$ [3], then $C = 0$. Both radiation and dust fulfill this condition. In these cases, the field Φ completely decouples from δs and propagates with a sound speed c_s, if $c_s^2 > 0$. Note that a cosmological constant has vanishing Q_S so that no contribution for perturbations arises, as is well known.

1.2 Vector type perturbations

To arrive at the desired action via the shortest path, let us first assume that all the perturbation variables propagate only in one direction, say the z-direction. This should be allowed, as we know that perturbations with different wavenumber vectors do not mix in a FLRW universe. Once we obtain the action for this particular mode, we can then easily infer the general action.

Taking again advantage of the freedom to select these background functions, we can make the simplest choice that contains all the information needed for the vector modes, namely $A = \tilde{\theta} = 0$, $B_{,i} = b_i$, where $\vec{b} = (b, 0, 0)$ is a constant vector orthogonal to the z-direction.

We find

$$S_V = \int \mathrm{d}^4x\left[\frac{a}{32\pi G}\,(\partial_jV_i)\,(\partial_jV_i) + a^3(\rho+p)\dot{C}_i\delta u_i + a^2(\rho+p)V_i\delta u_i - \tfrac{1}{2}\,a\,(\rho+p)\delta u_i\delta u_i\right], \tag{9}$$

where we substituted δu_i for $b_i\delta A/\mu$. Variations with respect to V_i and C_i yield the following equations,

$$\triangle V_i = 16\pi Ga(\rho+p)\delta u_i, \qquad \frac{\mathrm{d}}{\mathrm{d}t}[(\rho+p)a^3\delta u_i] = 0, \tag{10}$$

respectively. Again, these equations exactly coincide with those derived by perturbing the Einstein equations and the energy-momentum conservation law.

2 Quantization

The most important advantage of the action approach proposed in this letter is that it allows us to quantize the system. Although the inhomogeneities of the present universe, such as the galaxy distribution, are

[3] In this case, we obtain $(\partial\mu/\partial s)_\rho = T$ such that $(\partial p/\partial s)_\rho = n[(\partial\mu/\partial s)_\rho - T] = 0$.

clearly described by the classical theory, the quantization of a perfect fluid may have something to do with the early universe if the seeds for structure formation are provided by quantum fluctuations of fields generated during inflation. Yet, besides its practical utility, our action approach also opens new theoretical prospects, as discussed below. In the following, we will again treat the quantization for the scalar and vector type perturbations separately.

2.1 Scalar type perturbations

To quantize the scalar perturbations, let us first introduce the canonical field $\psi \equiv \sqrt{a^3 Q_S}\Phi$. To avoid the appearance of a ghost, we assume that Q_S is positive. This means that $(\rho+p)/c_s^2 > 0$. Such a constraint, together with the stability of the perturbations, $c_s^2 > 0$, lead to the null energy condition $\rho+p > 0$. Using the new variable ψ, the action (5) is rewritten as

$$S_S = \int \mathrm{d}^4x \left[\frac{\dot{\psi}^2}{2} - \frac{c_s^2}{2a^2}(\vec{\nabla}\psi)^2 + C_1 \delta s \dot{\psi} + C_2 \delta s \psi - \frac{N}{2}(\delta\bar{\theta}\dot{\delta s} - \delta s \dot{\delta\bar{\theta}}) - \frac{D}{2}\delta s^2 \right], \tag{11}$$

where we have neglected δA and δB as they do not contribute to the Hamiltonian. The field ψ has a canonical kinetic term, whereas the quadratic terms for δs and $\delta\bar{\theta}$ are at most linear in their time derivatives. Yet, it is known [6] that a consistent quantization of such a singular Lagrangian can be done provided one introduces the following commutation conditions,

$$\left[\hat{\psi}(t,\vec{x}), \hat{\pi}(t,\vec{y})\right] = i\delta(\vec{x}-\vec{y})\,, \tag{12}$$

$$\left[\hat{\delta s}(t,\vec{x}), \hat{\delta\bar{\theta}}(t,\vec{y})\right] = -\frac{i}{N}\delta(\vec{x}-\vec{y})\,. \tag{13}$$

All the other commutators are zero and π is the canonical conjugate momentum of ψ. The corresponding Hamiltonian is given by

$$\hat{H} = \int \mathrm{d}^3\vec{x} \left[\frac{1}{2}\left(\hat{\pi} - C_1\hat{\delta s}\right)^2 + \frac{c_s^2}{2a^2}(\vec{\nabla}\hat{\psi})^2 - C_2\hat{\delta s}\hat{\psi} + \frac{D}{2}\hat{\delta s}^2 \right]. \tag{14}$$

One can easily check that the Heisenberg equations, with the help of the commutation relations, yield the same equations of motion as the classical ones derived from the variation of Eq. (11).

The commutation relation (13) shows that $\hat{\delta s}$ and $\hat{\delta\bar{\theta}}$ are non-commuting variables. At this level, it is quite interesting to compare the action (11) with the one of the Landau problem, an archetype of non-commutative geometry. Regarding $\hat{\delta s}$ and $\hat{\delta\bar{\theta}}$, the action (11) is essentially the same as the one for a charged particle moving on a two-dimensional surface with a constant magnetic field background in the transverse direction:

$$S = \int \mathrm{d}t \left[\frac{m}{2}(\dot{x}^2+\dot{y}^2) - \frac{\mathcal{B}}{2}(\dot{x}y - \dot{y}x) - V(x,y) \right]. \tag{15}$$

Within this analogy, the perturbation fields $(\delta s, \delta\bar{\theta})$ correspond to the (x,y) space coordinates for the particle, and the number of particles $N = na^3$ plays the role of the constant magnetic field $\mathcal{B}$. Interestingly enough, while the non-commutative relation $[\hat{x},\hat{y}] = -i/\mathcal{B}$ in the Landau problem [6] holds only in the absence of the kinetic term in Eq. (15), which is valid in the large magnetic field limit, the non-commutative relation (13) of a perfect fluid is exact for any finite number of particles. So, perfect fluids provide a nice example of non-commutativity.

The non-commutation relation (12) leads to another interesting physical consequence. By using once more the Einstein equations and the energy-momentum conservation law, we find that the pressure perturbation in the comoving gauge ($v = 0$) is given by $\hat{\delta p} = -(\rho+p)\dot{\hat{\phi}}/H$. Then, the commutator between ϕ and δp becomes

$$\left[\hat{\phi}(t,\vec{x}), \hat{\delta p}(t,\vec{y})\right] = -ic_s^2 H\delta(\vec{x}-\vec{y})/a^3. \tag{16}$$

Consequently, curvature and pressure perturbations cannot be measured at the same time, at the same point.

2.2 Vector type perturbations

Time derivatives of V_i and δu_i do not appear in the action (9). Therefore, those are auxiliary fields which can be eliminated through their equations of motion. The action (9) becomes then a functional which depends only on C_i. To make this action canonical, we introduce a new variable $F_i(\vec{k},t) = \sqrt{a^3 Q_V(k,t)} C_i^{\parallel}(\vec{k},t)$, where $C_i^{\parallel}(\vec{k},t)$ is the Fourier transform of $C_i^{\parallel}(\vec{x},t)$ and Q_V is given by

$$Q_V(k,t) = \frac{a^2 k^2 (\rho + p)}{k^2 + 16\pi G a^2 (\rho + p)}. \tag{17}$$

To avoid the appearance of ghosts, Q_V must be positive. So, as for the scalar modes we require $\rho + p > 0$, i.e. the null energy condition to hold. In terms of F_i, the canonical action in Fourier space is given by

$$S_V = \int \mathrm{d}t \mathrm{d}^3 k \left(\tfrac{1}{2} \dot{F}_i^* \dot{F}_i - \tfrac{1}{2} m_k^2 F_i^* F_i \right), \tag{18}$$

with

$$m_k^2 = -\frac{1}{2} \frac{\mathrm{d}^2}{\mathrm{d}t^2} \log(a^3 Q_V) - \frac{1}{4} \left(\frac{\mathrm{d}}{\mathrm{d}t} \log a^3 Q_V \right)^2. \tag{19}$$

Now the quantization is done by imposing the following canonical condition for F_i and its conjugate momentum

$$\left[\hat{F}_i(t,\vec{k}), \hat{\pi}_j{}^{\dagger}(t,\vec{k}') \right] = i\delta(\vec{k} - \vec{k}') \left(\delta_{ij} - \frac{k_i k_j}{k^2} \right). \tag{20}$$

The corresponding Hamiltonian is given by

$$\hat{H} = \int \mathrm{d}^3 k \left(\tfrac{1}{2} \hat{\pi}_i^{\dagger} \hat{\pi}_i + \tfrac{1}{2} m_k^2 \hat{F}_i^{\dagger} \hat{F}_i \right), \tag{21}$$

and the evolution of the operators is given by the Heisenberg equation with the help of the commutation relation (20). The quantum version of Eq. (10) implies $\left[\hat{V}_i(t,\vec{x}), \delta\hat{u}_j(t,\vec{y}) \right] = 0$. Therefore, the gauge invariant metric perturbation and the vorticity of the perfect fluid can be measured at the same time, at the same point.

I have introduced a new frame to study the theory of cosmological perturbations for a perfect fluid. Starting from the action itself, first reproduced the known results derived from the equations of motion. Quantizing then the perturbation fields we found that some of them do not commute, leading thus to a non-commutative field-geometry. I also concluded that a simultaneous measurement of curvature perturbations and pressure inhomogeneities is not allowed. Finally I proved that both the null energy condition and a positive $c_s^2 = \dot{p}/\dot{\rho}$ have to hold at all times in order to avoid ghost degrees of freedom.

References

[1] A. De Felice, J. M. Gerard and T. Suyama, arXiv:0908.3439 [gr-qc].

[2] C. W. Misner, K. S. Thorne and J. A. Wheeler, *San Francisco 1973, 1279p*

[3] B. F. Schutz, Phys. Rev. D **2**, 2762 (1970).

[4] B. F. Schutz and R. Sorkin, Annals Phys. **107** (1977) 1.

[5] J. Garriga and V. F. Mukhanov, Phys. Lett. B **458**, 219 (1999).

[6] L. Faddeev and R. Jackiw, Phys. Rev. Lett. **60**, 1692 (1988).

Graviton emission from simply rotating Kerr black holes: Transverse traceless tensor graviton modes

Jason Doukas[1(a)], H. T. Cho[2(b)], A. S. Cornell[3(c)] Wade Naylor[4(d)]

[(a)] *Yukawa Institute for Theoretical Physics, Kyoto University, Kyoto, 606-8502, Japan.*
[(b)] *Department of Physics, Tamkang University, Tamsui, Taipei, Taiwan, Republic of China*
[(c)] *National Institute for Theoretical Physics; School of Physics, University of the Witwatersrand, Wits 2050, South Africa* (d)*Department of Physics, Ritsumeikan University, Kusatsu, Shiga 525-8577, Japan*

Abstract

In this article we present greybody factors and Hawking radiation for tensor graviton modes (in seven dimensions and greater, $n \geq 3$) from simply rotating $(n+4)$-dimensional Kerr black holes.

1 Introduction

The reduction of the graviton perturbation equations into master variable equations for higher-dimensional rotating black holes has been one of the great challenges in recent years,[1, 2]. The method based upon the gauge invariant formalism, developed in reference [3] has allowed for the separation of the tensor mode decomposition of simply rotating Myers-Perry-(A)dS black holes [1, 4, 5], which has recently been used for a stability analysis of Kerr-AdS black holes [6, 7]. In this work we shall focus on a simply rotating black hole in $(n+4)$-dimensional Kerr spacetime.

The wave equation for the tensorial mode of the gravitational perturbation for $n \geq 3$ is equivalent to the wave equation of a massless free scalar field [1, 6] where the determinant is given by the product of the base metric [6] and higher-dimensional spherical harmonics [10]. The separation of the wave equation is implemented by making the ansatz:

$$\Phi = e^{i\omega t - im\varphi} R(r) S_{jlm}(\theta) Y_{j,i_1,i_2,\ldots,i_{n-1}}(\theta_{n-1}, \phi) \ , \tag{1}$$

where $Y_{j,i_1,i_2,\ldots,i_{n-1}}(\theta_{n-1}, \phi)$ are the hyperspherical harmonics on the n-sphere with eigenvalues $-j(j+n-1)$. This separation ansatz leads to a generalized hyper-spheroidal equation for the $S_{jlm}(\theta)$ functions and an equation for $R(r)$ with separation constant A_{ljm}. These equations are coupled via ω. The restrictions on m, j and l [8] are:$l > j + |m|$; $\frac{l-j+|m|}{2} \in \{0, 1, 2...\}$, with $j = 2, 3, \ldots, l$ and $|m| = 0, 1, \ldots, l-j$. The degeneracy for a traceless symmetric tensor on an n-sphere [9] is given by:

$$D_j^T = \frac{(n+1)(n-2)(j+n)(j-1)(2j+n-1)(j+n-3)!}{2(n-1)!(j+1)!} \ . \tag{2}$$

For dimensions $n \geq 3$ we can parameterize the black hole mass, M, in terms of the horizon radius r_h: $2M = r_h^{n-1}(r_h^2 + a^2)(1 - \lambda r_h^2)$. By defining the transform: $R(r) = r^{-n/2}(r^2 + a^2)^{-1/2}\Phi(r)$, and tortoise coordinates [6]:$dy = \frac{r^2+a^2}{\Delta_r} dr$, where $\frac{\Delta_r}{r^2+a^2} = 1 - \frac{2M}{(r^2+a^2)r^{n-1}} - \frac{2\Lambda}{(n+2)(n+3)} r^2$. After defining the dimensionless variables: $x = r/r_h$, $\omega_\star = \omega r_h$, $y_\star = y/r_h$, $\Delta_\star = \Delta/r_h^2$, $a_\star = a/r_h$, $\lambda_\star = \lambda r_h^2$ and $\Lambda_\star = \Lambda r_h^2$, the radial equation takes the WKB form [6]:

$$\frac{d^2\Phi}{dy_\star^2} + Q(x)\Phi = 0 \ , \tag{3}$$

The CFM for the flat case was implemented using the input parameters described in reference [8].

[1] j.doukas@ms.unimelb.edu.au
[2] htcho@mail.tku.edu.tw
[3] alan.cornell@wits.ac.za
[4] naylor@se.ritsumei.ac.jp

In the near the horizon limit, $x \to 1$, the radial solution Φ has the following form (for *IN* modes [6, 10]):

$$\Phi_{\rm NH} \quad = \quad A^{(H)}_{\rm in} e^{-i\tilde{\omega}_\star x_\star} + A^{(H)}_{\rm out} e^{-i\tilde{\omega}_\star x_\star} \ , \tag{4}$$

where $\tilde{\omega}_\star = \omega_\star - m\Omega_\star$, $\Omega_\star = \frac{a_\star(1-\lambda_\star)}{(1+a_\star^2)}$. Imposing that there are no outgoing modes at the black hole horizon $A^{(H)}_{\rm out} = 0$, we obtain the IVP:

$$\Phi_{\rm NH}(x_0) = 1 \ , \quad \Phi'_{\rm NH}(x_0) = -i\tilde{\omega}_\star \frac{x_0^2 + a_\star^2}{\Delta_\star(x_0)} \ , \tag{5}$$

where $x_0 = 1 + \epsilon$ with $\epsilon \sim 10^{-5}$. The greybody factor can be determined numerically with the above horizon IVP matched onto the appropriate far-field form. The solutions have a far field (FF) form at spatial infinity, where $x_\star \to x$ (for $x \to \infty$):

$$\Phi_{\rm FF} \approx x^{-\frac{n+1}{2}} \left(A^{(\infty)}_{\rm in} e^{-i\omega_\star x} + A^{(\infty)}_{\rm out} e^{i\omega_\star x} \right) \ . \tag{6}$$

The NH solution can then be matched onto the FF equation (6) [11], where the reflection coefficient is then defined as the ratio $|\mathcal{R}_{ljm}|^2 = |A^{(\infty)}_{\rm out}|^2 / |A^{(\infty)}_{\rm in}|^2$, and the relationship between the absorption and reflection coefficient is:

$$|\mathcal{A}_{ljmn}|^2 = 1 - |\mathcal{R}_{ljmn}|^2 = 1 - \left| \frac{A^{(\infty)}_{\rm out}}{A^{(\infty)}_{\rm in}} \right|^2 \ . \tag{7}$$

Some typical examples of the absorption probability as a function of $\omega_\star$ ($=\omega r_h^2$) in the asymptotically flat limit are shown in the top two panels of Fig. 1. Solutions with charge or rotation undergo super-radiance

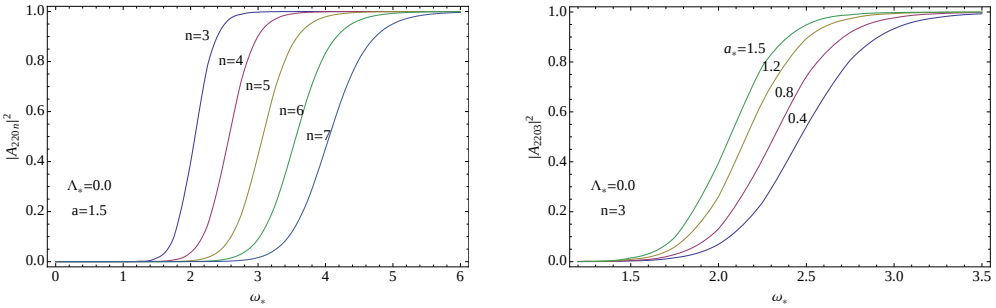

Figure 1: *Various plots of absorption probabilities in the asymptotically flat case, where unless stated all plots are for $n = 3$. Note that on the scale of these plots superradiance is too small to discern.*

[12], where the condition for super-radiance to occur is that the absorption probability becomes negative. Some plots of the superradiance regime are shown in Fig. 2. An interesting feature of black holes in Kerr-dS spacetimes is that the superradiance effect is enhanced by the strength of the cosmological constant, this can be seen from Fig. 2.

2 Conclusion

This note is based on our more expanded paper [13] which was the first time that the Hawking emission of these perturbations was been calculated. Some of the results can be seen in Figs. 3. The results are consistent with those of other works [10], where they considered the bulk emission of scalar spin-0 fields on the Kerr-AF background. An important difference is that because the modes start from $j = 2, 3, 4, \ldots$ the spectrum is shifted to the right (larger j corresponds to larger scattering energies ω). For spin-0 fields the sums start from $j = 0$, which implies lower energy emissions. The lack of $j = 0, 1$ modes has another effect, which can be seen from Fig. 4.

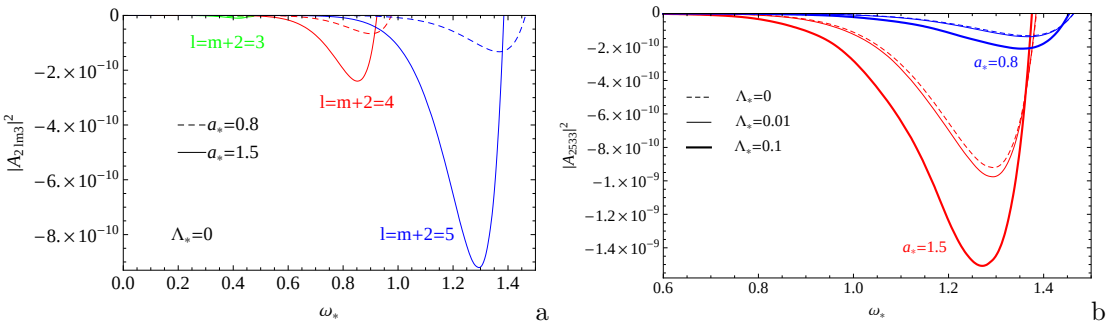

Figure 2: *Absorption probability plots in the superradiance regime for the asymptotically flat case. In (b) superradiance plots for various choices of the cosmological constant (Λr_h^2), for the rotations $a_\star = 0.8$ (blue) and $a_\star = 1.5$ (red).*

Perhaps the most interesting result from our investigation of the Kerr-dS case is the effect that the cosmological constant has on enhancing superradiance a larger cosmological constant leads to more superradiance and hence will cause the black hole to spin down more quickly. Hopefully, within this decade, a separable set of Master equations for all the graviton perturbations will be obtained.

References

[1] H. Kodama, Lect. Notes Phys. **769**, 427 (2009) [arXiv:0712.2703 [hep-th]].

[2] H. Kodama and A. Ishibashi, Prog. Theor. Phys. **110**, 701 (2003) [arXiv:hep-th/0305147].

[3] H. Kodama, A. Ishibashi and O. Seto, Phys. Rev. D **62**, 064022 (2000) [arXiv:hep-th/0004160].

[4] H. Kodama, Prog. Theor. Phys. Suppl. **172**, 11 (2008) [arXiv:0711.4184 [hep-th]].

[5] R. C. Myers and M. J. Perry, Annals Phys. **172**, 304 (1986).

[6] H. Kodama, R. A. Konoplya and A. Zhidenko, Phys. Rev. D **79**, 044003 (2009) [arXiv:0812.0445 [hep-th]].

[7] H. Kodama, R. A. Konoplya and A. Zhidenko, arXiv:0904.2154 [gr-qc].

[8] E. Berti, V. Cardoso and M. Casals, Phys. Rev. D **73**, 024013 (2006) [Erratum-ibid. D **73**, 109902 (2006)] [arXiv:gr-qc/0511111].

[9] M. A. Rubin and C. R. Ordonez, J. Math. Phys. **26**, 65 (1985); M. A. Rubin and C. R. Ordonez, J. Math. Phys. **25**, 2888 (1984), URL http://link.aip.org/link/?JMP/25/2888/1

[10] M. Casals, S. R. Dolan, P. Kanti and E. Winstanley, JHEP **0806**, 071 (2008) [arXiv:0801.4910 [hep-th]].

[11] D. Ida, K. y. Oda and S. C. Park, Phys. Rev. D **71**, 124039 (2005) [arXiv:hep-th/0503052].

[12] B. S. DeWitt, Phys. Rept. **19**, 295 (1975).

[13] Doukas, Jason and Cho, H. T. and Cornell, A. S. and Naylor, Wade, Phys. Rev.D80(2009) 045021.

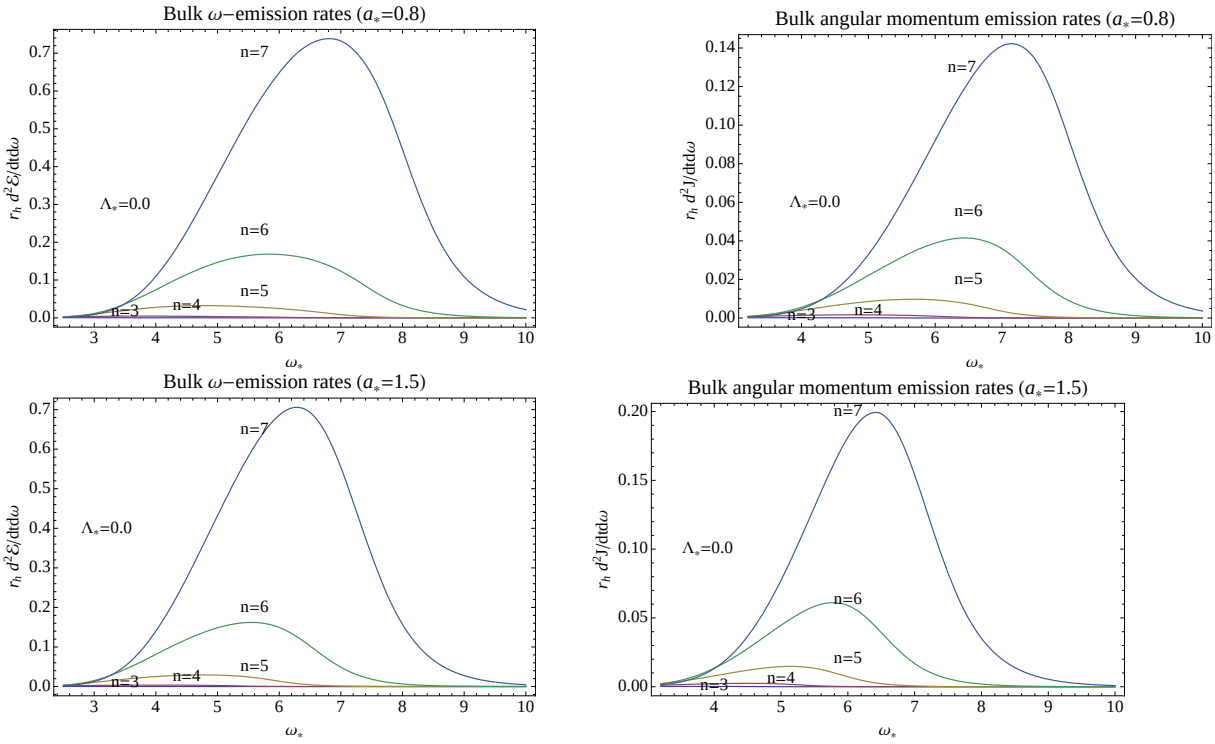

Figure 3: *Energy and angular momentum emissions in asymptotically flat space ($\Lambda = 0$) for different dimensions $n + 4$ with $a/r_h = 0.8$ (top) and with $a/r_h = 1.5$ (bottom).*

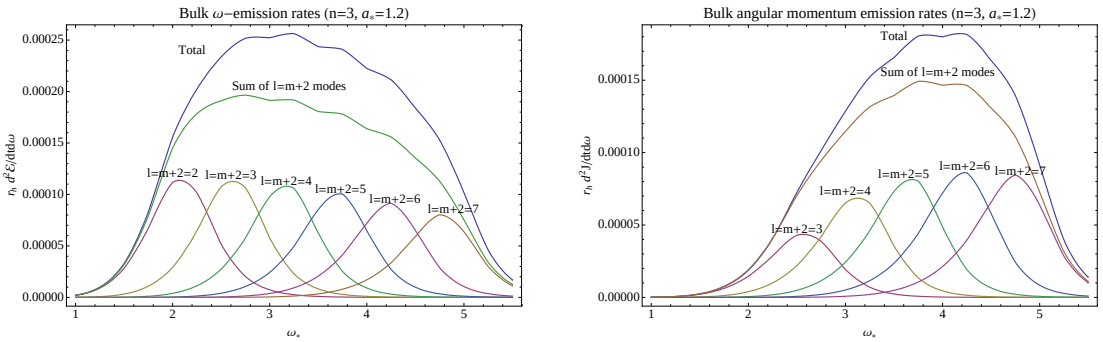

Figure 4: *Contribution to energy and angular momentum emissions from the dominant $l = m+2 = 3, \ldots$ modes for $n = 3$ and $a_\star = 1.2$ (with $\Lambda = 0$).*

Beyond the Dirac-Nambu-Goto approximation in Brane-Black Hole systems[1]

Viktor G. Czinner[2(a)] and Antonino Flachi[3(b)]

[(a)] *KFKI Research Institute for Particle and Nuclear Physics, Department of Theoretical Physics, Budapest, Hungary*
[(b)] *Yukawa Institute for Theoretical Physics, Kyoto University, Japan*

Abstract

We consider curvature corrections to static, axisymmetric Dirac-Nambu-Goto membranes embedded into a spherically symmetric black hole spacetime with arbitrary number of dimensions. Since the next to leading order corrections in the effective brane action are quadratic in the brane thickness ℓ, we adopt a linear perturbation approach in ℓ^2. The perturbations are general in the sense that they are not restricted to the Rindler zone nor to the near-critical solutions of the unperturbed system. As a result, an unexpected asymmetry in the perturbed system is found. In configurations, where the brane does not cross the black hole horizon, the perturbative approach used here does not lead to regular solutions of the perturbation equation if the number of the brane's spacetime dimensions $D > 3$. This condition, however, does not hold for the horizon crossing solutions. Consequently we argue that the perturbative approaches used here breaks down for subcritical type solutions near the axis of the system for $D > 3$. Nevertheless, we can discuss topology-changing phase transitions in cases when $D = 2$ or 3, i.e. when the brane is a 1-dimensional string or a 2-dimensional sheet, respectively. In the general case, a different approach should be sought. Based on the energy properties of those branes that are quasi-statically evolved from the equatorial configuration, we illustrate the results of the phase transition in the case of a $D = 3$ brane. It is found that small thickness perturbations do not modify the order of the transition, i.e. it remains first order just as in the case of vanishing thickness.

1 Notice

Higher dimensional black objects and branes are of importance and interest in several areas of present days physics. The classical black hole uniqueness theorems are known to fail in higher dimensions, and it turns out that a whole menagerie of black objects (black strings, rings, cigars, etc.) appear to exist. The study of new types of black objects became a very active research field recently, and among many other interesting aspects, the properties of possible transitions between the different types, or *phases*, is of special interest. For example, during the transition between a caged black hole and a black string phase, Kol demonstrated that the Euclidean topology of the system changes. This type of transition is called *merger* transition, and Kol found a strong similarity in its properties with the Choptuik critical collapse phenomena.

Recently, Frolov suggested a simple toy model with many features in common with merger and topology changing transitions. The model consists of a bulk N-dimensional black hole and a test D-dimensional brane in it ($D \leq N-1$), called *brane-black hole* (BBH) system. The black hole is spherically symmetric, static and can be neutral or charged. The brane is infinitely thin, and it is described by the Dirac-Nambu-Goto action. It is also static, spherically symmetric and it is assumed to reach asymptotic infinity in the form of a $(D-1)$-dimensional plane. Due to the gravitational attraction of the black hole, the brane is deformed and there are two types of equilibrium configurations. The brane either

[1] This is a very brief summary of [1]. We refer the reader to the original reference for details and complete list of references.

[2] Email address: czinner@rmki.kfki.hu
[3] Email address: flachi@yukawa.kyoto-u.ac.jp

crosses the black hole horizon, or it lies totally outside of the black hole (see FIG. 1). In between the two types of configurations there exists a critical solution that separates the two phases. Frolov studied the transition between the so called *subcritical phase* (when the brane does not intersect the black hole horizon) and *supercritical phase* (when the brane crosses the horizon), and found a close similarity both with the merger transition in a caged black hole - black string system and with the Choptuik critical collapse phenomena.

The AdS/CFT correspondence also provides motivation to study the above BBH system. In fact, according to the correspondence, at sufficiently high temperature, a small number of flavors (N_f) of fundamental matter in strongly coupled gauge theories with a large number of colors ($N_c \gg N_f$), may be described, in the holographic dual, by probe Dq-branes in the gravitational background of a black hole. Using the tool of the gauge/gravity correspondence, Mateos *et al.* studied the phase transition of quark-antiquark bound states (mesons). They showed that in the case of an infinitely thin brane, the system generally undergoes a first order phase transition characterized by a change in the meson spectrum. The corresponding phase diagram in the vicinity of the critical solution exhibits a self similar structure, and this critical behavior and the first order transition are essentially universal to all Dp/Dq systems.

Importantly, it was pointed out, that higher order corrections to the brane effective action may cause, in principle, modifications to the above picture and it is likely that they spoil the system's scaling symmetry and self-similar behavior. Indeed, higher-derivative corrections to the D-brane action correspond to finite 't Hooft coupling corrections in the holographic dual, and provide a more realistic description of the system. These corrections may become important in the vicinity of the phase transition, since the curvature of the brane becomes large there.

In the context of low-scale gravity theories, the possibility that a micro black hole may form in high energy collisions, like those at the LHC, re-creates a setup similar to the BBH system described above. In particular, the question whether a black hole may escape into the extra dimensional bulk has raised some attention, due to the potential phenomenological relevance. Clarifying the role of the thickness of the brane in that context is also an important issue.

The dynamics of branes keeps also attracting attention in the context of higher dimensional generalizations of the Bernstein conjecture and the study of the stability of brane-black hole systems.

For all the above reasons, it is important to go beyond the approximation of zero thickness and consider higher order, curvature corrections coming from small thickness perturbations in the BBH system. Curvature corrections to the dynamics of domain walls without self-gravitation, in the case of non-zero thickness have been investigated earlier by Carter and Gregory. They demonstrated that the next to leading order contribution is quadratic in the wall width (the brane thickness) and they obtained an exact, analytic expression for the corresponding effective action in terms of the intrinsic Ricci scalar R and the extrinsic curvature scalar K.

In the present paper we consider thickness perturbations to the BBH system using the general curvature corrected effective brane action of Carter and Gregory. To analyze this system we followed a perturbative treatment, in the sense that we treated the curvature corrections as small perturbations in the effective action (they are indeed very small as being quadratic in the perturbation parameter). To obtain the dynamical equation for the perturbations, we used the quadratic perturbation parameter to expand the $4th$-order Euler-Lagrange equation and kept the linear terms only. As a result, a second order, linear equation was found to describe the perturbations, with a very complicated source term. We analyzed the asymptotics of the perturbation equation, and found that there is no subcritical solution regular on the axis of the system above a certain dimension. This implies that our perturbation method is not appropriate in this region. We argued that the full non-perturbative solution may cure the problem. Although we do not report them in this brief summary, we have presented the analytic solution for far distances and the numerical solution in the near horizon region of the perturbation equation for various dimensions. We also addressed the question of the phase transition in the case of a $D = 3$ dimensional brane. For this purpose we have used the approach of Flachi *et al.* based on the energy properties of a quasi-static brane evolution from the equatorial configuration.

Small thickness perturbations to the brane dynamics are derived from higher-order, curvature corrections to the effective action of the brane. In the present model we do not consider the self-gravitation of the brane, hence the curvature scalars are completely determined by the embedding black hole spacetime. In the approximation when all the relevant dynamical length scales L of the system are very large com-

pared to the parameter ℓ that characterizes the thickness of the brane, the BBH system can be described by the following exact, analytic expression for the effective action:

$$S = \int d^D\zeta \sqrt{-\det\gamma_{\mu\nu}} \left[-\frac{8\mu^2}{3\ell}(1 + C_1 R + C_2 K^2) \right], \tag{1}$$

where R is the Ricci scalar, K is the extrinsic curvature scalar and the coefficients C_1 and C_2 are expressed by the wall thickness parameter as $C_1 = (\pi^2 - 6)\ell^2/24$ and $C_2 = -\ell^2/3$. The parameter μ is related to the thickness as $\ell = (\mu\sqrt{2\lambda})^{-1}$ which originates from a field theoretical domain-wall model, where μ is the mass parameter and λ is the coupling constant of the scalar field. The details of the Euler-Lagrange equation are very lengthy and will be omitted here. In brief, we studied thickness perturbations to static, D-dimensional, Dirac-Nambu-Goto branes embedded into higher dimensional, spherically symmetric, black hole spacetimes. The perturbations originate from higher order, curvature corrections added to the thin brane action, and are quadratic in the thickness of the brane. Applying a linear perturbation method with the perturbation parameter ℓ^2/L^2, we derived the general form of the perturbation equation for a brane that is axisymmetric and has a form of a $(D-1)$-dimensional plane at asymptotic infinity.

From the analysis of the asymptotic behavior of the perturbation equation, we found that there is no regular solution of the perturbed problem in the Minkowski embedding case, unless the brane is a string, or a sheet. This restriction, however does not hold for the black hole embedding solutions, which are always regular within our perturbative approach. The $D = 3$ case should not be too different from branes with larger dimensionality as long as additional symmetries are imposed on the brane angular directions.

From this result, we concluded that the absence of regular solutions above the dimension $D = 3$ implies, that the problem can not be solved within our perturbative approach around the thin solution, which is not smooth on the axis of the system. Hence, for a general discussion, one needs to find a new, exact solution of the curvature corrected problem, that is expected to behave differently from the thin solution and it is smooth on the axis. After the above conclusions, we provided the solution of the perturbation equation for various brane (D) and bulk (N) dimensions. The far distance equations are integrated analytically, while the near horizon solutions are obtained by numerical computations. The deformations of the perturbed brane configurations are plotted and a comparison is made with the corresponding thin brane configurations with identical boundary conditions, for both types of solution. A sample result is illustrated in Fig. 1, where the thick (red) brane configurations are shown together with their thin (blue) counterparts in a cylindrical coordinate system, in the case of an $N = 5$, $n = 2$ black hole embedding.

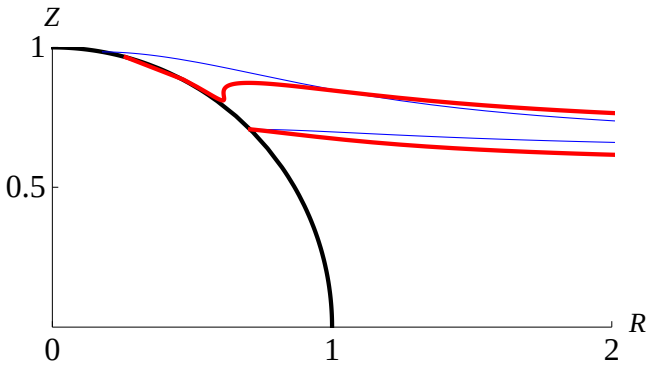

Figure 1: The picture shows the thick (red) brane configurations together with their thin (blue) counterparts in a cylindrical coordinate system, in the case of an $N = 5$, $n = 2$ black hole embedding. The initial conditions are $\theta_0 = \frac{\pi}{4}$ (bottom curves) and $\frac{\pi}{17.5}$ (top curves), and the thickness parameter ℓ is chosen to be large for the purpose of making the effects visible. The black curve represents the black hole's event horizon.

One motivation of this paper was to consider the effects of higher derivative, curvature corrections on the first order phase transition between the Minkowski and black hole branch, that is present in the unperturbed system. With the solution of the perturbed problem we found that within a perturbative

approach, one can consider a phase transition between the two branches only in the cases of $D = 2$ or 3. We investigated the properties of this transition in the case of a $D = 3$ brane, and found that small thickness perturbations do not modify the qualitative behavior of the phase transition, i.e. it remains a first order one, just as in the case of zero thickness.

Since our perturbative approach does not provide a regular thick brane solution for dimensions $D > 3$, we cannot answer in the most general way the question whether higher order, curvature corrections in the effective brane action can change the order of the phase transition in the BBH system or not. Although we expect that small corrections may not change the picture too much, as they are quadratic in the thickness of the brane, a definitive answer can only be given within a non-perturbative approach. Further study to address this question is in progress.

2 References

References

[1] V.G. Czinner and A. Flachi, Phys. Rev. D **80**, 104017 (2009).

Post-Newtonian gravitational wave polarisations and spherical harmonic components for a particle in circular orbit around a Schwarzschild black hole

Ryuichi Fujita[1] and Bala Iyer[2]

Theoretical Physics, Raman Research Institute, Bangalore 560 080, India

Abstract

We derive the post-Newtonian expansion of gravitational waves for a test particle in circular orbit of radius r_0 around a Schwarzschild black hole of mass M. We calculate the gravitational wave forms up to v^{11} order beyond Newtonian, where $v = (M/r_0)^{1/2}$. Although the results in this paper are limited to the case of test particle, they should also improve post-Newtonian expansion for the case of a finite mass ratio, which is currently known up to v^7.

1 Introduction

One of the most important sources of gravitational waves for the laser interferometer detectors is the inspiral and merger of a compact binary system. To extract physical information of the source, accurate and efficient theoretical templates are needed to be matched with observed data. The early inspiral phase is accurately described by the analytic post-Newtonian approximation, while the late inspiral and the subsequent merger phases are described by full numerical solution of the Einstein equation.

Since the recent breakthrough in numerical relativity [1], a number of the simulations have computed gravitational waves through inspiral, merger and ringdown with sufficient accuracy that one can compare its wave forms with post-Newtonian approximation. One can use the comparison to investigate the region of validity of post-Newtonian approximation in the inspiral phase. Additionally, it is also important to investigate whether higher post-Newtonian terms broaden the region of validity because computational cost of numerical simulation is very high.

We derive the post-Newtonian expansion of gravitational waves for a test particle in circular orbit around a Schwarzschild black hole of mass. We solve the Teukolsky equation to compute the gravitational waves. The Teukolsky equation is the fundamental equation in black hole perturbation formalism. Although it is limited to test particle limit, black hole perturbation formalism has a big advantage that one can go to higher post-Newtonian order systematically. In the case of finite mass ratio, the amplitude of gravitational waves and the orbital phase are known up to v^6 and v^7 respectively [2] for quasi-circular orbits. In the case of test particle limit, gravitational wave form and energy flux to infinity are known up to v^8 and v^{11} respectively for a circular orbit around Schwarzschild black hole [3, 4]. In Ref. [4]. gravitational wave form is not derived but energy flux up to v^{11}. Thus, we derive the gravitational wave forms up to v^{11} order beyond Newtonian. In this paper, we derive the wave forms projected onto spin-weighted spherical harmonics, which are suitable for the comparison with the results of numerical simulations. In the case of Schwarzschild black hole, it is easy to derive the plus and cross polarisation wave forms, which are suitable for data analysis, from spin-weighted spherical harmonics components. Thus, we omit the plus and cross polarisation wave forms in this paper. Throughout this paper, we use geometrized units, $c = G = 1$.

2 Teukolsky formalism

In the Teukolsky formalism, the gravitational perturbation of a Kerr black hole is described in terms of the Newman-Penrose variables, Ψ_0 and Ψ_4, which satisfy the master equation. The Weyl scalar Ψ_4 is

[1]Email address: draone@rri.res.in
[2]Email address: bri@rri.res.in

related to the amplitude of the gravitational wave at infinity as

$$\Psi_4 \to \frac{1}{2}(\ddot{h}_+ - i\,\ddot{h}_\times), \quad \text{for } r \to \infty. \tag{1}$$

The master equation for Ψ_4 can be separated into radial and angular parts if we expand Ψ_4 in Fourier harmonic modes as

$$\rho^{-4}\Psi_4 = \sum_{\ell m}\int_{-\infty}^{\infty} d\omega e^{-i\omega t + im\varphi}\ {}_{-2}S^{a\omega}_{\ell m}(\theta)R_{\ell m\omega}(r), \tag{2}$$

where $\rho = (r - ia\cos\theta)^{-1}$, the angular function ${}_{-2}S^{a\omega}_{\ell m}(\theta)$ is the spin-weighted spheroidal harmonic with spin $s = -2$, and M and aM are the mass and angular momentum of the black hole, respectively. In the followings, we focus on a Schwarzschild black hole case. Then the spin-weighted spheroidal harmonic ${}_{-2}S^{a\omega}_{\ell m}(\theta)$ is reduced to the spin-weighted spherical harmonic ${}_{-2}Y_{\ell m}(\theta)$. It is straightforward to compute the spin-weighted spherical harmonic, so we will show how to solve the radial Teukoslky equation,

$$\left[\Delta^2\frac{d}{dr}\left(\frac{1}{\Delta}\frac{d}{dr}\right) + U(r)\right]R_{\ell m\omega}(r) = T_{\ell m\omega}(r), \tag{3}$$

where

$$U(r) = \frac{r^2}{\Delta}\left[\omega^2 r^2 - 4i\omega(r-3M)\right] - (\ell-1)(\ell+2), \quad \Delta = r(r-2M), \tag{4}$$

and $T_{\ell m\omega}$ is the source term which is contraction of the energy momentum tensor of the small particle and null tetrad.

We solve Eq. (3) using the Green function method. For this purpose, we need a homogeneous solution $R^{in}_{\ell\omega}$ of Eq. (3) which satisfies the boundary conditions

$$R^{\rm in}_{\ell m\omega} = \begin{cases} B^{\rm trans}_{\ell m\omega}\Delta^2 e^{-i\omega r^*} & \text{for} \quad r^* \to -\infty, \\ r^3 B^{\rm ref}_{\ell m\omega}e^{i\omega r^*} + r^{-1}B^{\rm in}_{\ell m\omega}e^{-i\omega r^*} & \text{for} \quad r^* \to +\infty, \end{cases} \tag{5}$$

where $r^* = r + 2M\ln(r/2M - 1)$. Then the outgoing-wave solution of Eq. (3) at infinity with appropriate boundary conditions at horizon is given by

$$\begin{aligned} R_{\ell m\omega}(r\to\infty) = & \quad \frac{r^3 e^{i\omega r^*}}{2i\omega B^{\rm in}_{\ell m\omega}}\int_{2M}^{\infty} dr R^{\rm in}_{\ell m\omega}T_{\ell m\omega}(r)\Delta^{-2} \\ = & \quad r^3 e^{i\omega r^*}\tilde{Z}_{\ell m\omega}. \end{aligned} \tag{6}$$

In the case of a circular orbit, the frequency spectrum of $T_{\ell m\omega}$ becomes discrete. Then $\tilde{Z}_{\ell m\omega}$ in Eq. (6) takes the form

$$\tilde{Z}_{\ell m\omega} = Z_{\ell m\omega}\delta(\omega - m\Omega), \tag{7}$$

where

$$\begin{aligned} Z_{\ell m\omega} = & \quad \frac{\pi}{i\omega r_0^2 B^{in}_{\ell\omega}}\Bigg\{\Bigg[-{}_0b_{\ell m} - 2i\,{}_{-1}b_{\ell m}\left(1 + \frac{i}{2}\omega r_0^2/(r_0-2M)\right) \\ & + i\,{}_{-2}b_{\ell m}\omega r_0(1-2M/r_0)^{-2}\left(1 - M/r_0 + \frac{1}{2}i\omega r_0\right)\Bigg]R^{in}_{\ell m} \\ & + \left[i\,{}_{-1}b_{\ell m} - {}_{-2}\,b_{\ell m}\left(1 + i\omega r_0^2/(r_0-2M)\right)\right]r_0 R^{in\,\prime}_{\ell\omega}(r_0) \\ & + \frac{1}{2}\,{}_{-2}b_{\ell m}r_0^2 R^{in\,\prime\prime}_{\ell\omega}(r_0)\Bigg\}\quad , \end{aligned} \tag{8}$$

and ${}_sb_{\ell m}$ are defined by

$${}_0b_{\ell m} = \frac{1}{2}\left[(\ell-1)\ell(\ell+1)(\ell+2)\right]^{1/2}{}_0Y_{\ell m}\left(\frac{\pi}{2},0\right)\tilde{E}r_0/(r_0-2M),$$

$$
\begin{aligned}
{}_{-1}b_{\ell m} &= [(\ell-1)(\ell+2)]^{1/2}\, {}_{-1}Y_{\ell m}\left(\frac{\pi}{2},0\right)\tilde{L}/r_0, \\
{}_{-2}b_{\ell m} &= {}_{-2}Y_{\ell m}\left(\frac{\pi}{2},0\right)\tilde{L}\Omega.
\end{aligned} \tag{9}
$$

Here, $\Omega = (M/r_0^3)^{1/2}$ is the angular frequency of the particle, $\tilde{E}$ and $\tilde{L}$ are the specific energy and angular momentum of the particle respectively, which are given by

$$
\tilde{E} = (r_0 - 2M)/\sqrt{r_0(r_0-3M)}, \tag{10}
$$

and

$$
\tilde{L} = \sqrt{Mr_0}/\sqrt{1-3M/r_0}, \tag{11}
$$

where r_0 is the orbital radius.

In terms of the amplitudes $Z_{\ell m}$, the gravitational wave luminosity and the gravitational wave forms are respectively given by

$$
\frac{dE}{dt} = \sum_{\ell=2}^{\infty}\sum_{m=-\ell}^{\ell} |Z_{\ell m}|^2/2\pi\omega^2, \tag{12}
$$

and

$$
h_+ - i\,h_\times = -\frac{2}{r}\sum_{l,m}\frac{Z^{\infty}_{lm\omega}}{\omega^2}\frac{{}_{-2}Y^{a\omega}_{lm}(\theta)}{\sqrt{2\pi}}\, e^{i\omega(r^*-t)+im\phi}. \tag{13}
$$

where $\omega = m\Omega$. We calculate the gravitational wave forms in the post-Newtonian expansion, that is, in the expansion with respect to $v = (M/r_0)^{1/2}$. In order to compute $Z^{\infty}_{lm\omega}$, we need the series expansion of the ingoing-wave Teukolsky function $R^{in}_{\ell\omega}$ in terms of $\epsilon = 2M\omega = O(v^3)$ and $z = \omega r = O(v)$ and the asymptotic amplitudes $B^{in}_{\ell m}$ in terms of ϵ. We use the formalism developed by Mano, Suzuki and Takasugi to compute them, but omit to explain it here. For the reader who would like to know the details, see the review Ref. [5].

3 Results

For the comparisons between the post-Newtonian expansion and numerical simulations, we decompose $h^+_{\ell m}$ and $h^\times_{\ell m}$ into the modes of spin-weighted spherical harmonics as

$$
h^+_{\ell m} - i\,h^\times_{\ell,m} = \sum_{\ell m} h_{\ell m}\, {}_{-2}Y_{lm}(\theta,\phi). \tag{14}
$$

Comparing Eqs. (13) and (14), $h_{\ell m}$ is expressed as

$$
h_{\ell m} = -\frac{2}{r}\frac{Z^{\infty}_{lm\omega}\, e^{i\omega(r^*-t)}}{\omega^2}, \tag{15}
$$

where $\omega = m\Omega$.

We introduce the factorization defined in Ref. [2] as,

$$
h_{\ell m} = -\frac{2\,v^2}{r}H_{\ell m}, \tag{16}
$$

$$
H_{\ell m} = \sqrt{\frac{16\pi}{5}}\hat{H}_{\ell m}e^{-im\psi_{\ell m}}. \tag{17}
$$

Then the amplitude $\hat{H}_{22}$ up to $O(v^{11})$ and the phase ψ_{22} up to $O(v^9)$ are derived respectively as,

$$\begin{aligned}\hat{H}_{2,2} &= 1-\frac{107}{42}v^2+2\pi v^3-\frac{2173}{1512}v^4-\frac{107}{21}\pi v^5\\ &+v^6\left(-\frac{856}{105}\,\mathrm{eulerlog}(2,v)+\frac{27027409}{646800}+\frac{2}{3}\pi^2\right)-\frac{2173}{756}\pi v^7\\ &+v^8\left(-\frac{846557506853}{12713500800}-\frac{107}{63}\pi^2+\frac{45796}{2205}\,\mathrm{eulerlog}(2,v)\right)\\ &+v^9\left(\frac{27027409}{323400}\pi-\frac{4}{3}\pi^3-\frac{1712}{105}\pi\,\mathrm{eulerlog}(2,v)\right)\\ &+v^{10}\left(-\frac{866305477369}{9153720576}-\frac{2173}{2268}\pi^2+\frac{232511}{19845}\,\mathrm{eulerlog}(2,v)\right)\\ &+v^{11}\left(-\frac{846557506853}{6356750400}\pi+\frac{214}{63}\pi^3+\frac{91592}{2205}\pi\,\mathrm{eulerlog}(2,v)\right),\end{aligned}$$

$$\psi_{22}=\Omega(t-r^*)+4v^3\left(\frac{17}{12}-\gamma-\ln(8v)\right)-\frac{428\pi v^6}{105}+v^9\left(\frac{64}{3}\zeta(3)-\frac{1712}{315}\pi^2+\frac{259}{81}\right),$$

where

$$\mathrm{eulerlog}(m,v)=\gamma+\ln(2mv).$$

and γ is Euler constant and $\zeta(n)$ is zeta function.

These results are consistent with Ref. [2] up to $O(v^6)$. Using Eq. (14), we can derive the plus and cross polarisations and compare them with Ref. [3]. Then we find that our results are consistent with Ref. [3] up to $O(v^8)$. However, we note that the factorized wave forms in this paper are simpler than literature since we completely factored out the phase. The other modes of the amplitude $\hat{H}_{\ell m}$ and the phase $\psi_{\ell m}$ will appear elsewhere.

4 Summary

We derived the post-Newtonian expansion of gravitational waves up to v^{11} for a test particle in circular orbit around a Schwarzschild black hole of mass. The wave forms are projected onto spin-weighted spherical harmonics and useful to be compared with numerical relativity.

One of the future works is comparison of phase with full numerical calculation of black hole perturbation, which can be used to investigate whether one needs higher post-Newtonian order than v^{11}. And another application is a circular orbit around a Kerr black hole. Unlike a Schwarzschild black hole, the wave forms in the Teukolsky formalism are expressed in terms of spin-weighted spheroidal harmonics in the case of a Kerr black hole. Although it is straightforward, the transformation from the plus and cross polarisations to spin-weighted spherical harmonics components is not simpler than that of Schwarzschild black hole. All of them will be discussed elsewhere.

References

[1] F. Pretorius, Phys. Rev. Lett. **95**, 121101 (2005); M. Campanelli, C. O. Lousto, P. Marronetti, and Y. Zlochower, Phys. Rev. Lett. **96**, 111101 (2006); J. G. Baker, J. Centrella, D.-I. Choi, M. Koppitz, and J. van Meter, Phys. Rev. Lett. **96**, 111102 (2006).

[2] L. Blanchet, G. Faye, B. R. Iyer and S. Sinha, Class. Quant. Grav. **25**, 165003 (2008)

[3] H. Tagoshi and M. Sasaki, Prog. Theor. Phys. **92** (1994), 745.

[4] T. Tanaka, H. Tagoshi, and M. Sasaki, Prog. Theor. Phys. **96** (1996), 1087.

[5] M. Sasaki and H. Tagoshi, Living Rev. Relativity **6**, (2003), 6.

Gravitational Lensing Effects in the LTB Model

Hajime Goto[1](a) and Hideo Kodama(a),(b)

(a) *Department of Particle and Nuclear Physics, Graduate University for Advanced Studies, Tsukuba, Ibaraki 305-0801*
(b) *KEK, Tsukuba, Ibaraki 305-0801*

Abstract

In this talk, we discuss how to estimate the gravitational lensing effect of a local void on the CMB polarization by using the LTB model.

1 Introduction

Type Ia supernova (SNIa) observations imply an acceleration of the cosmic expansion if the universe is homogeneous and isotropic on scales larger than 200Mpc. If we abandon this assumption called the Cosmological Principle, then other explanations become possible. The most interesting model of such a nature is the local void model, which was first proposed by Kenji Tomita in 2000 [1]. This model assumes that we are around the center of a low density spherically symmetric void and the spacetime is well described by the Lemaître-Tolman-Bondi (LTB) model. In this model, the cosmic expansion rate decreases outward at each constant time slice, which produces an apparent acceleration of the universe when observed along the past light cone. Although this model violates the Cosmological Principle and requires the accidental situation concerning our location in the universe, it does not require any dark energy or a modification of gravity theory. Further, as far as the redshift-luminosity distance relation obtained by the SNIa observations is concerned, this model can reproduce the observational results with any accuracy because it contains at least one arbitrary function of the radius. Actually, it has passed all observational tests so far. Therefore, it is of crucial importance to find observational tests that enable us to discriminate this void model from the FLRW-based models, in order to establish the necessity of dark energy or a modification of gravity.

One possible such test is to observe effects of the inhomogeneity on CMB temperature and polarization. For example, gravitational lensing is expected to generate B-mode and the $\langle EB \rangle$ correlation for an off-center observer in the local void model. In this talk, we explain how to calculate such gravitational lensing effects on CMB in the LTB model.

2 CMB Polarization

2.1 How to Represent Polarizations

First of all, we explain the standard method to represent the polarization of radiations. Let us consider an quasi-monochromatic plane electromagnetic wave propagating toward an observer, and take an orthonormal xy-basis that is orthogonal to the wave propagation direction. Then, the electric field of the wave is represented as $\boldsymbol{E} = E_x \boldsymbol{e}_x + E_y \boldsymbol{e}_y$, with $E_x = a_x \sin(\omega t - \epsilon_x)$ and $E_y = a_y \sin(\omega t - \epsilon_y)$.

In this setup, one can define parameters that represent polarization as follows: $I := \langle a_y^2 \rangle + \langle a_x^2 \rangle$, $Q := \langle a_y^2 \rangle - \langle a_x^2 \rangle$, $U := \langle 2a_y a_x \cos(\epsilon_y - \epsilon_x) \rangle$, and $V := \langle 2a_y a_x \sin(\epsilon_y - \epsilon_x) \rangle$. These are called the Stokes parameters. Physically, I represents intensity (temperature), Q and U represent linear polarization, and V represents circular polarization. We ignore V because circular polarization is never generated by Thomson scattering in the early universe.

If the orthonormal basis is rotated in the wave plane, Q and U are linearly transformed. Since this is inconvenient, we will introduce new quantities below that are independent of the choice of the orthonormal basis.

[1]Email address: gotohaji@post.kek.jp

2.2 Polarization Distribution Patterns

Up to this point, we have considered a wave propagating only in one direction, whose polarization can be described by the Stokes parameters (I, Q, U). In real observations, this set of parameters is measured for photons of each direction, and the result is represented by three functions on the sky, $I(\boldsymbol{\theta}_{\rm obs})$, $Q(\boldsymbol{\theta}_{\rm obs})$ and $U(\boldsymbol{\theta}_{\rm obs})$, where $\boldsymbol{\theta}_{\rm obs}$ represents the position on the sky.

In the present article, for simplicity, let us work in the flat-sky approximation. This approximation is valid when we consider only a small part of the whole sky. Let us define a tensor from Q and U as

$$P_{ab}(\boldsymbol{x}) = \frac{1}{2}\begin{pmatrix} Q(\boldsymbol{x}) & U(\boldsymbol{x}) \\ U(\boldsymbol{x}) & -Q(\boldsymbol{x}) \end{pmatrix}, \tag{1}$$

where the subscripts of P run over x and y ($x \equiv 1$, $y \equiv 2$). This tensor is called the polarization tensor.

The polarization tensor field can be used to define the two functions on the sky, $E(\boldsymbol{x})$ and $B(\boldsymbol{x})$, which are independent of the choice of the orthonormal basis, by $\nabla^2 E(\boldsymbol{x}) = \partial_a \partial_b P_{ab}(\boldsymbol{x})$, $\nabla^2 B(\boldsymbol{x}) = \epsilon_{ac}\partial_b \partial_c P_{ab}(\boldsymbol{x})$. Because these represent the 'gradient' and 'curl' (or 'rotation') components of the linear polarization distribution, respectively, they are called the E-modes and the B-modes, respectively.

The power spectra and correlation functions are defined in terms of their Fourier transformations $\tilde{E}(\boldsymbol{\ell})$ and $\tilde{B}(\boldsymbol{\ell})$ as

$$\langle \tilde{X}_1(\boldsymbol{\ell}) \tilde{X}_2(\boldsymbol{\ell}') \rangle = (2\pi)^2 \delta(\boldsymbol{\ell} + \boldsymbol{\ell}') C_\ell^{\mathrm{X_1 X_2}}, \tag{2}$$

with $\tilde{X}_1,\ \tilde{X}_2 \in \{\tilde{\Theta},\ \tilde{E},\ \tilde{B}\}$ and $\mathrm{X}_1,\ \mathrm{X}_2 \in \{\mathrm{T},\ \mathrm{E},\ \mathrm{B}\}$, where Θ represents the intensity (temperature) fluctuation around the sky average ('2.7K'). If physics and the ensemble for averaging are invariant under a parity inversion, it turns out that $C_\ell^{\rm TB} = C_\ell^{\rm EB} = 0$.

In the real, spherical-sky case, a similar argument holds. For details, the reader is referred to Ref. [2].

3 Gravitational Lensing Effects

Inhomogeneous gravitational fields produce two effects on photon propagation. The first is a bending of its trajectory, and the second is the change of the photon energy in addition to the standard redshift by cosmic expansion. The latter is the so-called Sachs-Wolfe effect, which we do not consider in this article. Intuitively speaking, as far as CMB measurements by a fixed observer are concerned, the former—called 'shear field effect'—can be further divided into two parts: (*i*) the change of the photon direction in the sky and (*ii*) the displacement of the intersection sphere of the past light cone and the last scattering surface in the direction perpendicular to this sphere. In order to give a definite meaning to this distinction, we need to introduce some reference FLRW model to define 'unperturbed' photon trajectories and past light cones. However, this procedure introduces the gauge freedom corresponding to the mapping between the real universe and the reference model, and thus make that distinction obscure. In fact, for the FLRW model with small perturbations, the displacement of the last scattering sphere can be set to be zero by an appropriate gauge choice, and in this gauge, the shear field effect can be represented only in terms of (*i*), namely, the 'gravitational lensing effect'. In the local void model, it is not so certain whether the same argument holds when the non-linearity of inhomogeneities is large. In the present article, we simply assume that the shift of the last scattering point in the direction normal to the last scattering sphere can be set to zero by a gauge choice.

3.1 General formula

Under this assumption, the gravitational lensing effect on the CMB anisotropy can be simply determined by the two-dimensional shift vector $\boldsymbol{d}$ on the sky representing the difference between the observed direction of a photon and its initial direction on the last scattering sphere (Fig. 1a). The same formula holds for the LTB model as that for the FLRW model [3], [4], [5], and [6].

In the flat-sky approximation, let us represent the CMB temperature and polarization that would be observed in the reference exact FLRW model without gravitational lensing as $\tilde{\Theta}$, $\tilde{Q}$ and $\tilde{U}$ ($\tilde{E}$ and $\tilde{B}$).

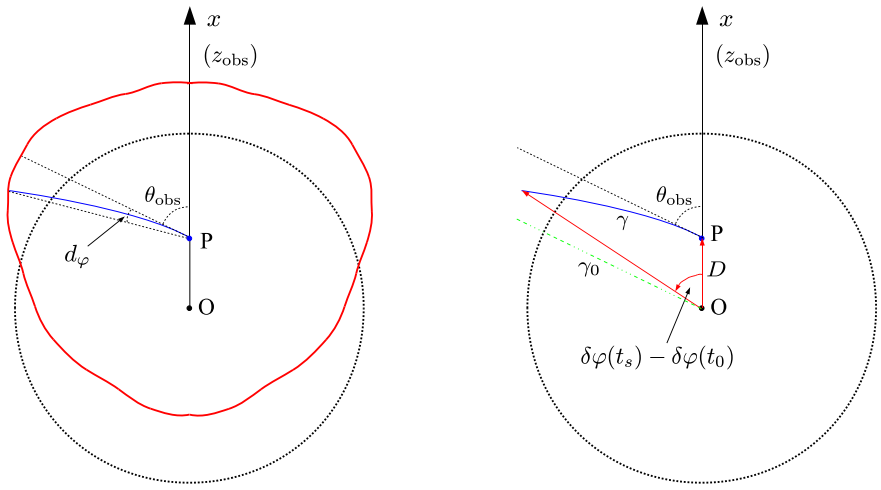

Fig. 1a Fig. 1b

Figure 1: (a) Photon propagation in the LTB model. The black circle (dashed line) represents the last scattering sphere for the observer at the center O, and the red curve (solid line) represents that for an off-center observer P. The blue curve (arriving at P) is the photon trajectory. (b) The photon trajectory γ in the (r, φ) coordinates. Each trajectory is contained in the unique two-plane passing through O, P and the last scattering point. The green line (dashed-dotted line) represents the reference radial null geodesic γ_0.

Then, the corresponding quantities observed with gravitational lensing are given by

$$\Theta(\boldsymbol{\theta}_{\rm obs}) = \tilde{\Theta}(\boldsymbol{\theta}_{\rm obs}+\boldsymbol{d}) = \int \frac{d^2\boldsymbol{\ell}}{(2\pi)^2} e^{i\boldsymbol{\ell}\cdot(\boldsymbol{\theta}_{\rm obs}+\boldsymbol{d})}\tilde{\Theta}(\boldsymbol{\ell}) \ , \tag{3}$$

$$Q(\boldsymbol{\theta}_{\rm obs}) = \tilde{Q}(\boldsymbol{\theta}_{\rm obs}+\boldsymbol{d}) = \int \frac{d^2\boldsymbol{\ell}}{(2\pi)^2} e^{i\boldsymbol{\ell}\cdot(\boldsymbol{\theta}_{\rm obs}+\boldsymbol{d})}\{\tilde{E}(\boldsymbol{\ell})\cos 2\phi_{\boldsymbol{\ell}} - \tilde{B}(\boldsymbol{\ell})\sin 2\phi_{\boldsymbol{\ell}}\} \ , \tag{4}$$

$$U(\boldsymbol{\theta}_{\rm obs}) = \tilde{U}(\boldsymbol{\theta}_{\rm obs}+\boldsymbol{d}) = \int \frac{d^2\boldsymbol{\ell}}{(2\pi)^2} e^{i\boldsymbol{\ell}\cdot(\boldsymbol{\theta}_{\rm obs}+\boldsymbol{d})}\{\tilde{E}(\boldsymbol{\ell})\sin 2\phi_{\boldsymbol{\ell}} + \tilde{B}(\boldsymbol{\ell})\cos 2\phi_{\boldsymbol{\ell}}\} \ , \tag{5}$$

where $\phi_{\boldsymbol{\ell}}$ is the angle between the vector $\boldsymbol{\ell}$ and the x-direction on the sky. From this, the Fourier transformation of the differences are

$$\delta\Theta(\boldsymbol{\ell}) = \int \frac{d^2\boldsymbol{\ell}'}{(2\pi)^2}\tilde{\Theta}(\boldsymbol{\ell}')W(\boldsymbol{\ell}', \boldsymbol{L}) \ , \tag{6}$$

$$\delta E(\boldsymbol{\ell}) = \int \frac{d^2\boldsymbol{\ell}'}{(2\pi)^2}\{\tilde{E}(\boldsymbol{\ell}')\cos 2\phi_{\boldsymbol{\ell}'\boldsymbol{\ell}} - \tilde{B}(\boldsymbol{\ell}')\sin 2\phi_{\boldsymbol{\ell}'\boldsymbol{\ell}}\}W(\boldsymbol{\ell}', \boldsymbol{L}) \ , \tag{7}$$

$$\delta B(\boldsymbol{\ell}) = \int \frac{d^2\boldsymbol{\ell}'}{(2\pi)^2}\{\tilde{E}(\boldsymbol{\ell}')\sin 2\phi_{\boldsymbol{\ell}'\boldsymbol{\ell}} + \tilde{B}(\boldsymbol{\ell}')\cos 2\phi_{\boldsymbol{\ell}'\boldsymbol{\ell}}\}W(\boldsymbol{\ell}', \boldsymbol{L}) \ , \tag{8}$$

where $W(\boldsymbol{\ell}, \boldsymbol{L}) = -\boldsymbol{\ell}\cdot\boldsymbol{d}(\boldsymbol{L})$, $\boldsymbol{L} = \boldsymbol{\ell} - \boldsymbol{\ell}'$, $\phi_{\boldsymbol{\ell}'\boldsymbol{\ell}} := \phi_{\boldsymbol{\ell}'} - \phi_{\boldsymbol{\ell}}$, and $\boldsymbol{d}(\boldsymbol{L})$ is the Fourier transformation of $\boldsymbol{d}(\boldsymbol{\theta}_{\rm obs})$.

3.2 Null Geodesics in the LTB Model and the Shift Vector $\boldsymbol{d}$

Thus, the investigation of the gravitational lensing effect of a local void on CMB is reduced to determine $\boldsymbol{d}$ as a function of the photon direction. For that, we have to solve the null geodesic equation in the LTB model, whose metric can be written $ds^2 = -dt^2 + S^2dr^2 + R^2(d\theta^2 + \sin^2\theta d\varphi^2)$. Here R is a function of t and r, and S is written in terms of R and the curvature function $k(r)$ as $S = R'/(1-k(r)r^2)^{1/2}$.

In terms of the photon 4-momentum $p^\mu = dx^\mu/d\lambda$ with affine parameter λ, the geodesic equation can be written as $dp^\mu/d\lambda = -\Gamma^\mu_{\nu\rho}p^\nu p^\rho$. Because of the spherical symmetry, this set of equations can be

reduced to the coupled ODEs for ω, μ and $p_\perp$ defined by $p^t = \omega$, $p^r = \mu\omega/S$, and $p_\perp^2 = \omega^2(1-\mu^2)$, where $p_\perp := R\{(p^\theta)^2 + (p^\varphi)^2 \sin^2\theta\}^{1/2}$. Without loss of generality, we can assume that the photon propagate on the 2-plane with $\theta = \pi/2$, and therefore $p^\theta = 0$ (Fig. 1b). Then, the geodesic equations are reduced to the set of four ODEs for $\omega(t)$, $r(t)$, $\varphi(t)$, and $\mu(t)$.

It is impossible to express the general solution to this set of equations in terms of known functions. However, if we restrict the consideration to null geodesics passing through a point P close to the symmetry center O, we can find explicit expression for the solution in terms of integrals of known functions. Such a geodesic γ stays close to some radial null geodesic γ_0. Hence, we can solve the geodesic equation perturbatively with respect to the deviation of the two geodesics γ and γ_0. One subtle point in this perturbative approach is that $\delta\mu$ turns out to show bad behavior near the observer. This problem can be avoided by introducing the variables b & c defined as $b := r\sqrt{1-\mu^2}$ and $c := r\mu$ instead of r and μ.

The final result reads

$$\delta c(t) = \delta c(t_0) \exp \int_{t_0}^{t} dt_1 \left(\frac{S'}{S^2}\right)_{t_1} , \tag{9}$$

$$\delta\omega(t) = \left[\delta\omega(t_0) - \delta c(t_0) \int_{t_0}^{t} dt_1 \left\{\omega\left(-\frac{\dot{S}'}{S} + \frac{\dot{S}S'}{S^2}\right)\right\}_{t_1} \exp \int_{t_0}^{t_1} dt_2 \left(\frac{S'}{S^2} + \frac{\dot{S}}{S}\right)_{t_2}\right] \cdot \exp\left(-\int_{t_0}^{t} dt_1 \left(\frac{\dot{S}}{S}\right)_{t_1}\right) , \tag{10}$$

$$\delta b(t) = \delta b(t_0) \exp \int_{t_0}^{t} dt_1 \left(\frac{R'}{SR} - \frac{\dot{R}}{R} + \frac{\dot{S}}{S} + \frac{1}{cS}\right)_{t_1} , \tag{11}$$

$$\delta\varphi(t) = \delta\varphi(t_0) \pm \delta b(t_0) \int_{t_0}^{t} dt_1 \left(\frac{1}{|c|R}\right)_{t_1} \exp \int_{t_0}^{t_1} dt_2 \left(\frac{R'}{SR} - \frac{\dot{R}}{R} + \frac{\dot{S}}{S} + \frac{1}{cS}\right)_{t_2} . \tag{12}$$

In Fig. 1b, we can take the null geodesic passing through O in the direction $\theta_{\rm obs}$ as the reference geodesic γ_0. Then, it is easy to see that the values of δb and δc at present $t = t_0$ can be expressed as

$$\delta b(t_0) = D\sqrt{1-\mu_0^2} , \quad \delta c(t_0) = D\mu_0 , \tag{13}$$

where D is the distance of the observer P from O and $\mu_0 = -\cos(\theta_{\rm obs})$. Then, (12) determines the shift vector $\boldsymbol{d} = (d_\theta, d_\varphi)$, $d_\theta = 0$, $d_\varphi = \delta\varphi(t_s) - \delta\varphi(t_0)$.

4 Summary and Future Work

In this paper, we developed a formulation to calculate the gravitational lensing effects on the CMB temperature and polarization for an off-center observer in a spherically symmetric void described by the LTB model. Explicit estimations of these effects are under investigation [7].

References

[1] Tomita, K. 2000, Astrophys. J. , 529, 26; Tomita, K. 2000, Astrophys. J. , 529, 38

[2] Cabella, P., & Kamionkowski, M. 2004, arXiv:astro-ph/0403392

[3] Seljak, U. 1996, Astrophys. J. , 463, 1

[4] Zaldarriaga, M., & Seljak, U. 1998, Phys. Rev. D , 58, 023003

[5] Hu, W. 2000, Phys. Rev. D , 62, 043007

[6] Lewis, A., & Challinor, A. 2006, Phys. Rep., 429, 1

[7] Goto, H., & Kodama, H. work in progress.

The Geodesic Properties of the Hypercylindrical Spacetime

Bogeun Gwak[1(a)], Hyeong-Chan Kim[2(b)], Bum-hoon Lee[3(a)], Wonwoo Lee[4(a)]

[(a)] *Department of Physics and BK21 Division, and Center for Quantum Spacetime, Sogang University, Seoul 121-742, Korea*
[(b)] *Division of Liberal Arts, Chungju National University, Chungju 380-702, Korea*

Abstract

We study the geodesic properties of the static hypercylindrical spacetimes in (4+1) dimensions. The effective potential analysis and gravitational lensing effects are studied in the static spacetime. We give the marginal orbits by the effective potential in timelike case. This article is prepared for the proceedings of The Nineteenth Workshop on General Relativity and Gravitation in Japan (JGRG19), 2009.

1 Introduction

Our study is geodesic properties about 5-dimensional hypercylindrical spacetimes. It is a static spacetime. The spacetime is described by two ADM parameters the mass and tension densities. As the parameters changes, the properties of the solution shows many different behaviors. Most of this article is based on [1].

2 Hypercylindrical Spacetime

The static hypercylindrical spacetime is a class of solutions parameterized by 5-dimensional string tension and mass per length [2–4]. The metric is written as,

$$\begin{aligned} ds^2 &= -F(\rho)dt^2 + G(\rho)(d\rho^2 + \rho^2 d\theta^2 + \rho^2 \sin^2\theta d\phi^2) \\ &\quad + H(\rho)dz^2\,, \\ F &= \left(1-\frac{K_a}{\rho}\right)^{s}\left(1+\frac{K_a}{\rho}\right)^{-s}\,, \\ G &= \left(1-\frac{K_a}{\rho}\right)^{2-\frac{(1+a)s}{2-a}}\left(1+\frac{K_a}{\rho}\right)^{2+\frac{(1+a)s}{2-a}}\,, \\ H &= \left(1-\frac{K_a}{\rho}\right)^{\frac{(-1+2a)s}{2-a}}\left(1+\frac{K_a}{\rho}\right)^{\frac{(1-2a)s}{2-a}}\,, \end{aligned} \tag{1}$$

where a is the string tension to mass ratio, $s = \frac{2(2-a)}{\sqrt{3(1-a+a^2)}}$, and $K_a = \sqrt{\frac{1-a+a^2}{3}}G_5\zeta$. Hypercylindrical spacetime gives 5-dimensional cylindrical solution in which the spherically symmetric 3+1 dimensions are orthogonal to the 1-dimensional line like 5^{th} coordinate. For specific values of a, we have well known solutions. For $a = 0.5$, the metric (1) becomes the Schwarzschild solution, and for $a = 2$ a Kaluza-Klein bubble solution. The position of horizon is given by K_a in the Schwarzschild case. Except for $a = 0.5$, the $\rho = K_a$ corresponds to a naked singularity [5]. In the effective potential level, the naked singularities can be classified by two types, weakly and strongly naked singularity [6, 7].

The physical importance of these facts is the observable quantities of the weakly naked singularity in $-1 \le a \le 2$ which has the maximum point in the effective potential which gives the unstable circular

[1]Email address: rasenis@sogang.ac.kr
[2]Email address: hckim@chungju.ac.kr
[3]Email address: bhl@sogang.ac.kr
[4]Email address: warrior@sogang.ac.kr

orbits and Schwarzschild case. The observation quantities such as the deflection angles of lightlike orbits are not easy to distinguish one from the other in this case.

On the other hand, the strongly naked singularity shows qualitatively different behaviors in $a \geq -1$ or $2 \leq a$. These behaviors can be shown in the effective potential of lightlike case comparing to the weakly naked singularity.

The effective potential can be obtained from the geodesic Lagrangian. The metric components are only dependent on coordinate ρ. It gives conserved quantities E for time, L for angle, and W for 5th direction momentum. Without loss of generality, we choose the coordinate θ equals to $\frac{\pi}{2}$ using spherical symmetry of the metric. The effective potential is given [1],

$$V_{eff} = \frac{1}{2}\frac{F(\rho)L^2}{\rho^2 G(\rho)}\,. \tag{2}$$

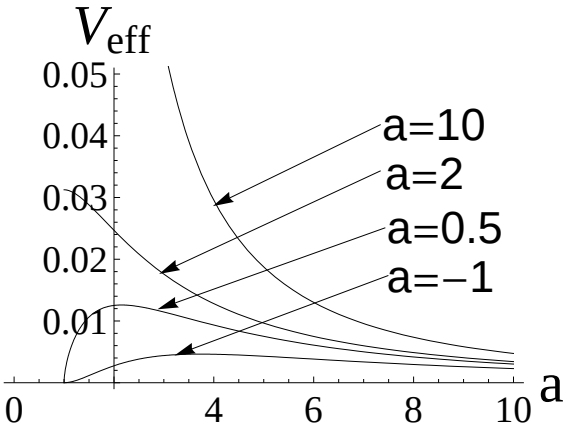

Figure 1: The effective potential at specific value of parameter a.

In the range of $-1 \leq a \leq 2$, the effective potentials have maximum point which light can make unstable circular orbit named photon sphere which partly covers their naked singularity like horizon. The other values of parameter a give no maximum point like as shown in Figure 1, so the naked singularity is exposed completely. The size of horizon is related to the capture-cross section which light cannot escape from gravity of the spacetime. In the Figure 2, the maximum value is achieved for the Schwarzschild case, and as the parameter value a becomes farther away from the Schwarzschild case, the capture-cross section becomes smaller. Briefly, the deflection angles for spacetimes with $-1 \leq a \leq 2$ are qualitatively

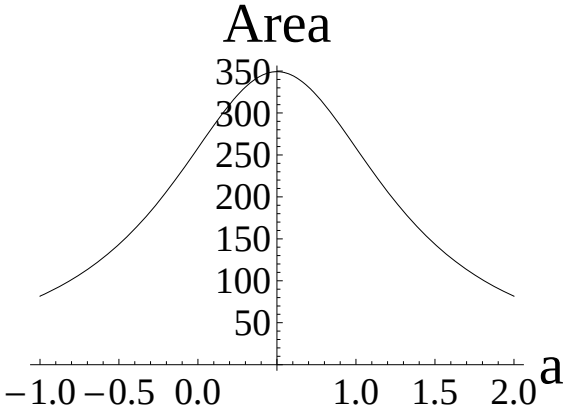

Figure 2: The effective potential at specific value of parameter a.

a	-1	-0.5	0	0.5	1	1.5
L	2.9	4.8	6.4	7	5.2	3
ρ	1.56673	4.59308	7.54371	8.38068	9.07818	5.48575

Table 1: The relations of a, L, ρ are shown. For each value of the constant a, the angular momentum L and radius ρ for marginal orbit are shown. In these analysis, objects which are not $a = \frac{1}{2}$ have different geodesic properties, which Schwarzschild black string has.

similar to each other. It means that distinguishing Schwarzschild and weakly naked singularity case is not easy. On the other hand, the strongly one gives very different values of deflection angle. The weakly naked spacetime have unstable circular orbits at the maximum point in the effective potential, capture-cross section, and similar effect in gravitational lensing as those of the Schwarzschild case. It gives same properties in [6–8].

In the timelike geodesics, there are unstable circular orbits at the maximum point of effective potential like Schwarzschild case. In the range of $-1 < a < 2$, the orbit can exist only for $r \geq 6M$ as in the Schwarzschild spacetime case if $a = \frac{1}{2}$. The orbit at $r = 6M$ is called the marginal stable circular orbit or the innermost stable circular orbit. Some examples are shown in Fig. 3.

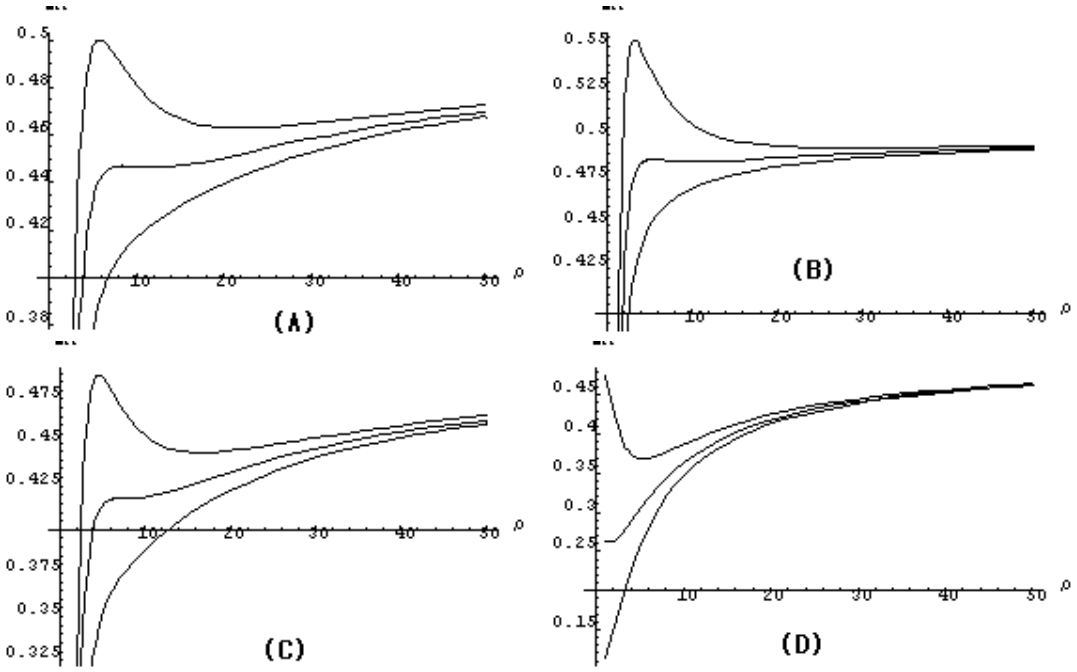

Figure 3: (A) The case of the Schwarzschild black string, $a = \frac{1}{2}$. In (A), upper curve is at $L = 8$, and the middle is at $L = 7$, and the lower is at $L = 6$(all figures are some ordering.). The marginal orbit appears at middle curve. (B) is of $a = \frac{3}{2}$. The angular momentums, L, are 4, 3, 2. (C) is for $a = 0$. From above table 1, the radius of marginal orbit is moved to left side and does not change its shape. (D) is for $a = -1$. In this case, the shape of potential is different from other case.

From the Fig. 3, we see that there are finite potential barrier due to the angular momentum for the cases of $a = 0$, $a = \frac{1}{2}$ and $a = \frac{3}{2}$. On the other hand, the potential barrier preventing a particle reaching deep inside appears appeared for the case of $a = -1$.

3 CONCLUSIONS

In this paper, we have studied the geodesic motions and the orbits of both a massive particle and light ray. The geometry of the hypercylindrical solution is dependent on single constant a, a ratio of tension and mass density. This geometry becomes that of the Schwarzschild black string for $a = \frac{1}{2}$, and the static Kaluza-Klein bubble for $a = 2$. There exist five conserved quantities corresponding to translation symmetry of time, angle, 5th dimension coordinate, and two quantities which give equatorial plane $\theta = \frac{1}{2}\pi$. The light can move around a unstable circular orbit in $-1 \leq a \leq 2$. The radial range of the unstable circular orbit is related to area of light capture. The capture cross section is formed in $-1 \leq a \leq 2$, and the largest area case is $a = \frac{1}{2}$ Schwarzschild black string. We calculate the timelike geodesic equations and the range of the constant a which gives stable circular orbits in $a < -1$. One of the characteristics of the timelike case is that there exist a marginal stable circular orbit in $-1 < a < 2$. The angular momentum and radius of this marginal orbit is numerically obtained, and the shapes of the effective potentials are similar to Schwarzschild black string in $-1 < a < 2$.

Acknowledgments

This work was supported by the National Research Foundation of Korea(NRF) grant funded by the Korea government(MEST)through the Center for Quantum Spacetime(CQUeST) of Sogang University with grant number 2005-0049409. BG is supported by the scholarship of Korea Science and Engineering Foundation (Scholarship Number:S2-2008-000-00800-1). WL was supported by the Korea Research Foundation Grant funded by the Korean Government(MOEHRD)(KRF-2007-355-C00014).

References

[1] B. Gwak, B.-H. Lee, and W. Lee, J. Korean Phys. Soc. **54**, 2202 (2009), [arXiv:0806.4320].

[2] D. Kramer, Acta Phys. Polon. B **2**, 807 (1971); A. Chodos and S. Detweiler, Gen. Rel. Grav. **14**, 879 (1982); J. Gross and M. M. Perry, Nucl. Phys. B **226**, 29 (1983); A. Davidson and D. A. Owen, Phys. Lett. B **155**, 247 (1985).

[3] C. H. Lee, Phys. Rev. D **74**, 104016 (2006), hep-th/0608167.

[4] S. Yun, arXiv:0905.4338 [gr-qc].

[5] I. Cho, G. Kang, S. P. Kim and C. H. Lee; J. Korean Phys. Soc. **53**, 1089 (2008), [arXiv:0709.1021]; *in preparation.*

[6] K. S. Virbhadra and G. F. R. Ellis, Phys. Rev. D **65**, 103004 (2002).

[7] C. M. Claudel, K. S. Virbhadra and G. F. R. Ellis, J. Math. Phys. **0142**, 818 (2001) [arXiv:gr-qc/0005050].

[8] K. S. Virbhadra, Phys. Rev. D **79**, 083004 (2009) [arXiv:0810.2109 [gr-qc]].

Interior of a charged black hole with an exotic scalar field

A. Doroshkevich[(a)], Jakob Hansen[1(b)], D.I. Novikov[(a)], I.D. Novikov[(b)] & A. Shatskiy[(a)]

[(a)] *Astro Space Center, Lebedev Physical Institute, Russian Academy of Sciences, Moscow, Russia*
[(b)] *KISTI, 335 Gwahak-ro, Yuseong-gu, Daejeon, 305-806, Republic of Korea*

Abstract

We use a numerical code to investigate the nonlinear processes arising when a Reissner-Nordström black hole (RNBH) is irradiated by an exotic scalar field beam. These processes are quite different from the processes arising in the case of the same black hole being irradiated by a beam of a normal scalar field. For full results and detailed analyses, see [1].

1 Introduction

The internal structure and physics of black holes (BH) has been the subject of researches during many years. A powerful tool for such investigations is to consider a Reissner-Nordström BH (RNBH) which is nonlinearly perturbed by a selfgravitating scalar field. This toy BH model is not very realistic but it shares many properties, including causal structure, with the more realistic rotating BHs.

This toy model has been used in the paper [2] to analyze the physics of the interior of a BH in the case of irradiation by a normal massless scalar field. Recent astrophysical observations suggests that a considerable part of the matter in the Universe consists of a hypothetical dark energy, exotic matter, which violates at least the strong and perhaps also the weak energy condition. These discoveries and other theoretical investigations put a question about the physics of the interior of a BH nonlinearly perturbed by exotic matter.

The goal of this work is to perform such an analysis by using numerical methods. Our numerical code was described and tested in details in [1, 3]. We will see that the physics of the interior of a BH with an exotic scalar field is quite different from the physics of a BH with a normal scalar field.

Due to space requirements, only a summary of results can be presented in this text. For full discussions and complete results, please see [1].

2 Our model

We investigate the evolution of a spherical BH with a fixed electric charge $q = 0.95m0$ (i.e. Reissner-Nordström metric) and initial mass $m0 = 1$, which is under the action of pulses of an exotic scalar field Ψ (modelled as a massless, selfgravitating scalar field with a negative kinetic energy term, i.e. it has a negative energy density, $\varepsilon < 0$ [1, 3]).

For our model and numerical analysis, we use double null coordinates. The line element in double null coordinates can be written as

$$ds^2 = -2e^{2\sigma(u,v)}du\,dv + r^2(u,v)d\Omega^2, \tag{1}$$

where $\sigma(u,v)$ and $r(u,v)$ are functions of the null coordinates u and v (in- and out-going respectively).

The energy-momentum tensor can be written as a sum of contributions from the exotic scalar field Ψ and from the ordinary magnetic field, i.e. : $T_{\mu\nu} = T^{\Psi}_{\mu\nu} + T^{em}_{\mu\nu}$.

The full non-linear Einstein equations in this case become rather simple and are easily written out in their complete form. They reduce to a set of evolution equations which are supplemented by two constraint equations (for the full explicit expressions, see [1]).

We wish to numerically evolve the unknown functions $r(u,v)$, $\sigma(u,v)$ and $\Psi(u,v)$ throughout some computational domain. We do this by following the approach described in [2, 3] (and references therein)

[1]Email address: jakobidetsortehul@gmail.com

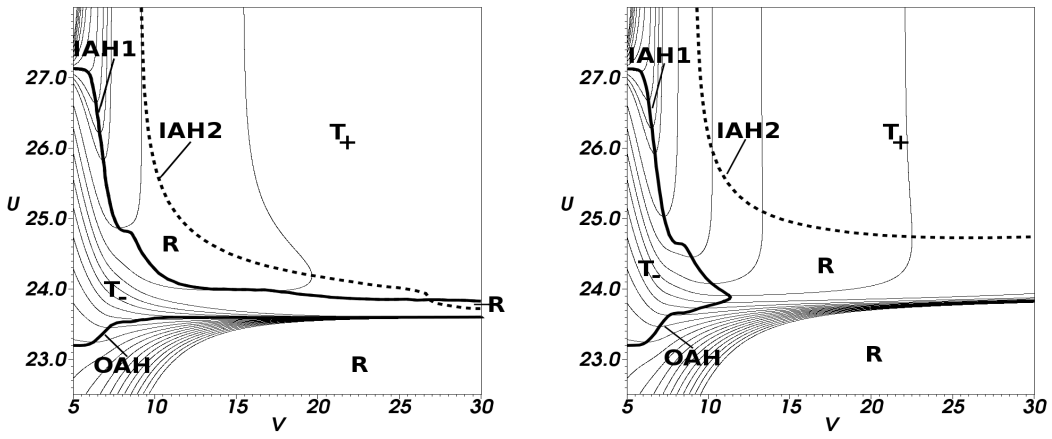

(a) Case of weak exotic pulse (BH survives).

(b) Case of strong exotic pulse (BH vanishes).

Figure 1: Thin lines are lines of constant r, thick lines marks the apparent horizons. Also shown are positions of R- and T-regions.

to numerically integrate the evolution equations. These equations form a well-posed initial value problem in which we can specify initial values of the unknown functions on two initial null segments, namely an ingoing ($v = v_0 = constant$) and an outgoing ($u = u_0 = constant$) segment. We impose the constraint equations on the initial segments, consistency of the evolving fields with the constraint equations is then ensured via the contracted Bianchi identities [4]. However we use the constraint equations throughout the domain of integration to check the accuracy of the numerical simulation.

Our choice of initial values corresponds to the following physical situation; There is a Reissner-Nordström BH and at some distance from the horizon, at the initial moment there is a rather narrow spherical layer of an in-falling exotic scalar field (see [1] for details).

3 The case of survival of the BH (weak pulse)

We start from the case when the power of the exotic beam is rather weak. We shall see that in this case, the BH survives but the positions of the horizons change.

In fig. 1(a) is shown the causal structure for the case of weak pulse, including location of R and T regions and positions of the horizons. As was shown in [2], sending a pulse of the normal scalar field into a RNBH causes the positions of the horizons change, the outer apparent horizont (OAH) in that case will go to larger r and the inner apparent horizon (IAH1) will go to smaller r. In fig. 1(a), we see that the opposite effect takes place when the pulse is an exotic scalar field. I.e. instead of diverging, the two horizons (OAH and IAH1) now converge towards each other. This is a direct effect of the negative energy content of the exotic scalar field. However, the two horizons do not meet and thus the BH is not destroyed.

Fig. 2(a) shows the mass function, i.e. the total mass (without the magnetic field) in a sphere of radius $r(u, v)$ (see [2] and refs. therein). It is seen that for small v, when the pulse enters the RNBH (between $5 \leq v \leq 9$), the mass function decreases as a direct result of the negative mass being sent into the BH. This is also opposite to the effect of a positive energy pulse[2]. Soon thereafter, however, the mass function increases for those lines of constant u which are inside of the BH (for $u \geq 24$). This increase of the mass function is partly related to scattering of the exotic field, partly related to the mass inflation effect (see [5]), which also works in the case of an exotic scalar field. The mass function along $u = 0$ (border of our computational domain) is seen to be smaller than 0.95 which would normally indicate that the RNBH (with charge $q = 0.95m0$) would vanish. However, because of scattering effects, not all the radiation from $u = 0$ reaches the BH (around $u = 23$), but is scattered away due to the curvature of the

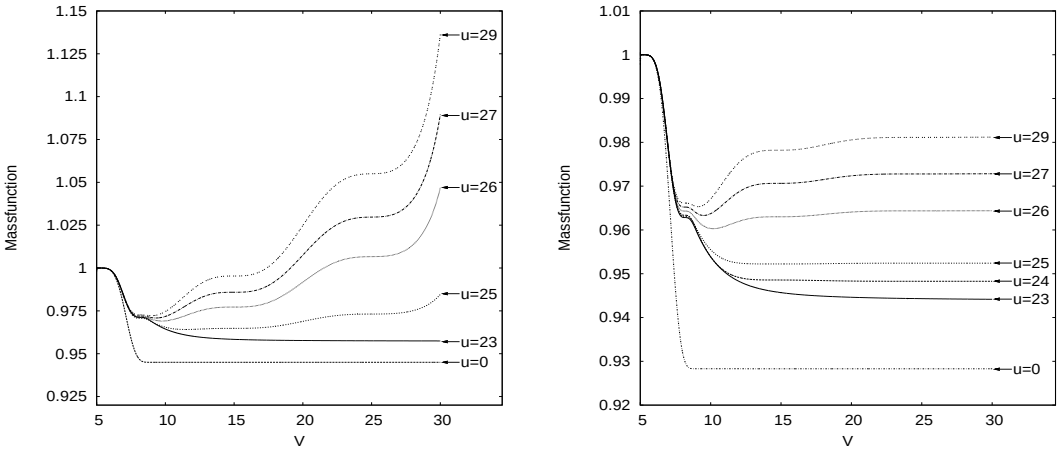

(a) Case of weak exotic pulse (BH survives).

(b) Case of strong exotic pulse (BH vanishes).

Figure 2: The mass function along lines of constant u.

space-time. Thus, the mass near the OAH is "only" reduced to approx. 0.96, which (in agreement with fig. 1(a), indicated that the BH survives the pulse of exotic radiation.

Our analysis allows us to guess at the Penrose diagram for the case when a pulse of exotic scalar radiation is sent into a RNBH which is weak enough that the BH survives the pulse. This Penrose diagram can be seen in fig. 3(a).

4 The case of destruction of the BH (strong pulse)

Next we consider a pulse which has a higher negative energy. Fig. 1(b) shows the further evolutions of the general picture of the R and T regions for this case.

Now, total power of the exotic beam is large enough to reduce the mass of the object in the critical region $u \approx [23.2; 23.9]$ (where the OAH formed for the previous case), to below the critical value $m_{crit} = q = 0.95$, see Fig. 2(b). Thus even after the reduction of the power of the beam during the propagation from $u = 0$ to $u \approx 23.2$ due to the scattering, it is strong enough to destroy the BH. This means that the inner and out horizons should meet and disappear. This process is seen in Fig. 1(b).

For this case, for high v, the BH is converted into an object where the outer R and inner R-regions are connected. Now the test photons $u = const$ for all value of u go to bigger r, when $v \to \infty$.

The mass function for big v and big u becomes greater than $m = 0.95$ but still the BH vanishes. It is related to the scattering of the exotic scalar field outside to bigger r. Of cause this is possible in the case of dynamical BHs. In this region (big v and big u) we are at big r, definitely outside the (dynamical) BH which is at smaller v.

Fig. 3(b) represents the Penrose diagram that is confirmed by our numerical simulations for the cases when the BH was destroyed by the radiation.

At the end of this section we note the following. When the Reissner-Nordström BH is irradiated by a pulse of the exotic scalar radiation, the OAH becomes smaller (or disappears completely) and part of the outgoing radiation from the T_- region can go to the outer R'-region in our Universe. This radiation may come into the T_- region from the R''-region that belongs to another Universe, which is the counterpart of the outer R'-region of Fig. 3(b) in our Universe (from the left hand side of Fig. 3(b) outside the computational domain). This means that it is possible for some radiation from the other Universe to come to our R'-region. The propagation of the radiation in the opposite direction, from our R'-region to the R''-region in the other Universe, is still impossible. We call such an object a semi-traversable wormhole.

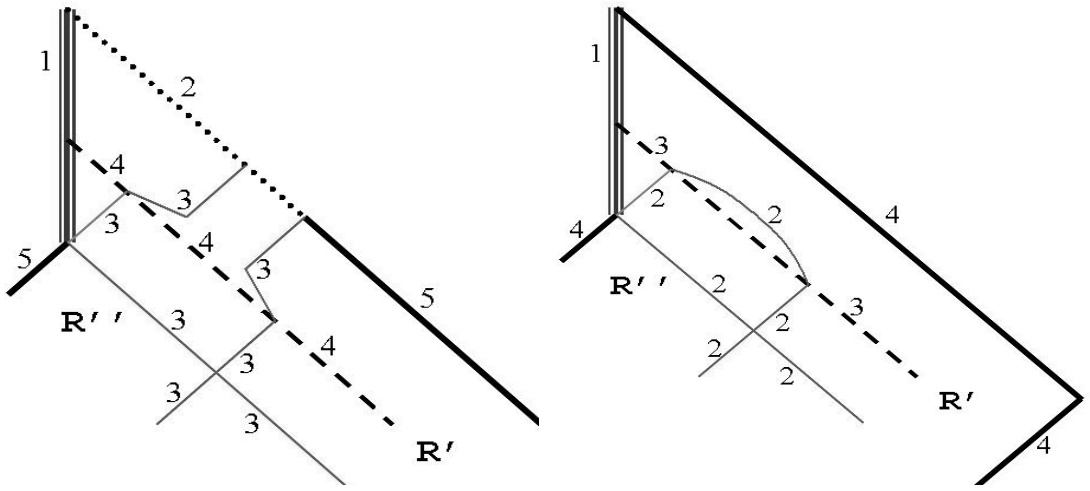

(a) 1 – strong timelike singularity $r = 0$, 2 – weak singularity, 3 – horizons, 4 – narrow beam of the exotic scalar field, 5 – light infinity, R' – our universe, R'' – another universe.

(b) BH is destroyed after being irradiated by a beam of the exotic scalar field. Here: 1 – strong singularity $r = 0$, 2 – horizons, 3 – narrow beam of the exotic scalar field, 4 – light infinity, R' – our universe, R'' – another universe.

Figure 3: Penrose diagrams for case : a) BH surives after being irradiated by a beam of the exotic scalar field, b) BH is destroyed after being irradiated by a beam of the exotic scalar field

5 Conclusions

The processes arising when a Reissner-Nordström BH is irradiated by a beam of an exotic scalar field with a negative energy density have been analyzed. We performed the corresponding numerical computations using a numerical code specially designed for the purpose. It was demonstrated that these processes are quite different from the processes arising in the case of the irradiation of a Reissner-Nordström BH by a beam of a normal scalar field.

The evolution of the mass function demonstrate that in the case of the exotic scalar field, the evolution does not lead to the origin of a strong space-like singularity $r = 0$ in the T-region as was the seen in the case of irradiation by the normal scalar field [2].

The numerical calculations demonstrate the manifestation of the antifocusing effects in the gravity field of an exotic scalar field with a negative energy density.

When the power of the exotic beam with a negative energy density is great enough, the mass function becomes less than the charge q near the outer horizon. As a result the BH disappears.

Again, we note that for full results and detailed analyses, see [1] in which we analyse a greater number of cases in detail (including the case of simultaneous normal and exotic scalar fields).

References

[1] A. Doroshkevich, J. Hansen, D. Novikov, I. Novikov, and A. Shatskiy. *arXiv: 0908.1300.*

[2] J. Hansen, A. Khokhlov, and I. Novikov. *Phys. Rev. D*, 71:064013, 2005.

[3] A. Doroshkevich, J. Hansen, I. Novikov, and A. Shatskiy. *Int. J. Mod. Phys. D*, 71:064013, 2009.

[4] L. M. Burko and A. Ori. Late-time evolution of nonlinear gravitational collapse. *Phys. Rev. D*, 56:7820, 1997.

[5] E. Poisson and W. Israel. *Phys. Rev. D*, 41:1796, 1990.

Einstein-Rosen waves and self-similarity

Tomohiro Harada[1]

Department of Physics, Rikkyo University, Toshima, Tokyo 171-8501, Japan

Abstract

The validity of the self-similarity hypothesis in nonspherical geometry is a very interesting problem as there may exist gravitational waves. In this article we briefly review the recent results about self-similar vacuum solutions to the Einstein equation in the so-called whole-cylinder symmetry based on Harada, Nakao and Nolan (2009) [1].

1 Introduction

Classical general relativity has no characteristic scale in the theory, whereas it contains two dimensional constants, the gravitational constant G and the speed of light c. This means that the theory may admit self-similar solutions. Self-similar solutions reproduce their spatial configuration scaled in their time evolution as schematically shown in Fig. 1.

Although self-similar solutions are special solutions of Einstein's field equations, they are very important in gravitational physics. In particular, it has been explicitly conjectured that in the cosmological context spherically symmetric fluctuations might naturally evolve from complex initial conditions via the Einstein equations to a self-similar form in certain circumstances (Carr 1993 [2, 3]). This is called the similarity hypothesis.

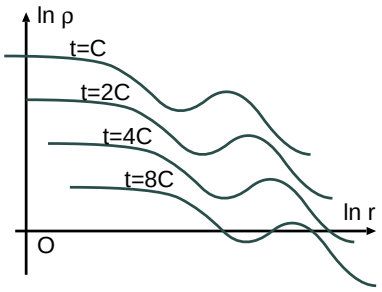

Figure 1: Self-similar density field

As above the similarity hypothesis was originally proposed for spherically symmetric systems. On the other hand, it is well known that there is no dynamical degree of freedom in gravity in spherical symmetry due to Birkoff's theorem. This means that the original hypothesis is not relevant to the physical properties of gravitational field. This motivates us to generalise the hypothesis to nonspherical systems. Among nonspherical systems, we here choose cylindrically symmetric spacetimes because it provides one of the simplest systems with gravitational waves. The vacuum Einstein equation there essentially reduces to the "1+1" wave equation. It is therefore interesting to ask whether there is any nontrivial vacuum self-similar solutions in cylindrical symmetry and what role the self-similar solutions play if any.

2 Einstein-Rosen waves

Here we consider the so-called whole-cylinder symmetry. The line element is given by

$$ds^2 = e^{2\gamma-2\psi}(-dt^2+dx^2) + e^{-2\psi}r^2d\varphi^2 + e^{2\psi}dz^2, \tag{1}$$

where $\gamma = \gamma(t,x)$, $\psi = \psi(t,x)$, $r = r(t,x)$ and $\varphi = 0$ and $\varphi = 2\pi$ are identified. In this spacetime, we can introduce the C energy associated with each cylinder (t,x), which is defined by $E = \left(1 - e^{-2\psi}\nabla^a r \nabla_a r\right)/8$ [4]. A cylinder (t,x) is trapped, marginally trapped and untrapped if $E > 1/8$, $E = 1/8$ and $E < 1/8$, respectively. It can be also seen that the constant r hypersurface is spacelike, null and timelike if $E > 1/8$, $E = 1/8$ and $E < 1/8$, respectively. A cylindrical trapping horizon is defined as a hypersurface foliated by marginally trapped cylinders [5].

[1]Email address: harada@rikkyo.ac.jp

The vacuum solutions in whole-cylinder symmetry are called Einstein-Rosen waves. One component of Einstein's equations implies $r = f(t-x) + g(t+x)$, where f and g are arbitrary functions. Here we mainly concentrate on the untrapped case. In this case, we can choose f and g such that $r = x$ by rescaling t and x. Thus, the line element reduces to

$$ds^2 = e^{2(\gamma-\psi)}(-dt^2 + dx^2) + e^{-2\psi}x^2 d\varphi^2 + e^{2\psi}dz^2. \tag{2}$$

In this setting, the C energy is given by

$$E = (1 - e^{-2\gamma})/8. \tag{3}$$

Another component of Einstein's equations require ψ to satisfy the cylindrically symmetric wave equation in a flat spacetime, i.e.,

$$-\psi_{,tt} + \psi_{,xx} + \frac{1}{x}\psi_{,x} = 0. \tag{4}$$

γ is fully determined from ψ up to a constant.

3 Self-similar Einstein-Rosen waves

3.1 The orthogonal case

If a vector field $\mathbf{v}$ satisfies $\mathcal{L}_{\mathbf{v}} g_{ab} = 2g_{ab}$, it is called a homothetic vector. If a spacetime admits a homothetic vector field, it is called a self-similar spacetime. We consider a self-similar spacetime with whole-cylinder symmetry and first assume that the homothetic vector $\mathbf{v}$ is orthogonal to the cylinders of symmetry, i.e.,

$$\mathbf{v} = A(t,x)\frac{\partial}{\partial t} + B(t,x)\frac{\partial}{\partial x}. \tag{5}$$

Then, it turns out that Einstein-Rosen waves are compatible with self-similarity. For the compatibility, the following condition must be satisfied:

$$\psi(t,x) = \Psi(\xi) + \frac{1}{2}\ln|x| \quad \gamma(t,x) = \Gamma(\xi), \tag{6}$$

where $\xi \equiv t/x$. Under the above condition, Einstein's equations reduce to the ordinary differential equations, which are integrated to give

$$\psi = \frac{1}{2}\ln|\xi \pm \sqrt{\xi^2 - 1}| + \frac{1}{2}\ln|x| + \Psi_0, \tag{7}$$

$$\gamma = \frac{1}{2}\ln\left|\frac{1}{2}\left(\frac{\xi}{\sqrt{\xi^2-1}} \pm 1\right)\right| + \lambda, \tag{8}$$

where $t > x \geq 0$, Ψ_0 is gauge, and $\lambda \neq 0$ implies a conical singularity.

In fact, we can easily show that the above solutions have the Riemann tensor vanishing and hence correspond to flat spacetimes. In particular, the solution with $\lambda = 0$ has no conical singularity and is what we should call a "cylindrical Milne universe". The line element can be written in a standard form:

$$ds^2 = -d\tau^2 + dp^2 + dq^2 + d\zeta^2, \tag{9}$$

for $\lambda = 0$, where we have put

$$\tau^2 - \zeta^2 = t + \sqrt{t^2 - x^2} \quad p^2 + q^2 = t - \sqrt{t^2 - x^2}. \tag{10}$$

Although this class of solutions are shown to be flat, they are still worth to study. From Eqs. (3), (8) and (10), we can find that the C energy is given by

$$E = \frac{1}{8}\frac{t - \sqrt{t^2-x^2}}{t + \sqrt{t^2-x^2}} = \frac{1}{8}\frac{p^2+q^2}{\tau^2 - \zeta^2}, \tag{11}$$

and hence nonvanishing even though the spacetime is flat. We can also easily show that the light cone, given by

$$t^2 = x^2 \quad \text{or} \quad \tau^2 = p^2 + q^2 + \zeta^2 \tag{12}$$

for the flat spacetime, is a cylindrical trapping horizon, where $E = 1/8$.

3.2 The nonorthogonal case

The wave equation (4) for $\psi(t,x)$ is linear and has a static solution $\ln|x|$. This means that the linear combination of $\Psi(\xi)$ and $\ln|x|$ is also a solution, where $\Psi(\xi)$ is the solution given by Eq. (7). Assuming a regular or conically singular axis, we obtain

$$\psi = \kappa\left[\ln(\xi+\sqrt{\xi^2-1})+\ln|x|\right], \tag{13}$$

$$\gamma = 2\kappa^2\ln\left|\frac{1}{2}\left(\frac{\xi}{\sqrt{\xi^2-1}}+1\right)\right|+\lambda, \tag{14}$$

where κ and λ are constants of integration. $\lambda\neq 0$ just introduces a conical singularity, while κ parametrises the physical properties of the solutions. For $\kappa\neq 1$, we find a homothetic vector which is not orthogonal to the cylinders unless $\kappa=1/2$. This means that the solutions are self-similar. For $\kappa=1$, we instead find a Killing vector.

For the solutions obtained above, the line element can be written as

$$ds^2 = \frac{(t+\sqrt{t^2-x^2})^{2\kappa(2\kappa-1)}}{2^{4\kappa^2}(t^2-x^2)^{2\kappa^2}}e^{2\lambda}(-dt^2+dx^2)+\frac{x^2}{(t+\sqrt{t^2-x^2})^{2\kappa}}d\varphi^2+(t+\sqrt{t^2-x^2})^{2\kappa}dz^2 \tag{15}$$

$$= \frac{T^{4\kappa(2\kappa-1)}}{(T^2-X^2)^{4\kappa^2-1}}e^{2\lambda}(-dT^2+dX^2)+\frac{X^2}{T^{2(2\kappa-1)}}d\varphi^2+T^{4\kappa}dz^2, \tag{16}$$

where $T^2=t+\sqrt{t^2-x^2}$, $X^2=t-\sqrt{t^2-x^2}$ and $T>X\geq 0$. From the above expressions, we can easily see that the solution is Minkowski for $\kappa=0$, cylindrical Milne for $\kappa=1/2$, and cylindrical Kasner for $\kappa=-1/2$.

4 Physical interpretation

Because of the page limit we only sketch how to obtain the global structure of the self-similar spacetimes obtained above. The readers who are interested in the details of the analysis are encouraged to read Harada, Nakao and Nolan (2009) [1]. To study the global structure of the spacetime, we measure the spacetime with the affine length and examine the boundaries of the solutions. The boundary point may be infinity, singularity or extendible boundary. Using the obtained metric, we can explicitly show the following features: $T=0$ is finite for $\kappa<1$ but timelike infinity for $\kappa\geq 1$; $T=\infty$ is timelike infinity for $\kappa<1$ but finite for $\kappa\geq 1$; $T+X=\infty$ is null infinity for any κ; $T=X$ is finite for $0<\kappa^2<1/2$ but null infinity for $\kappa^2\geq 1/2$; $T=X$ is scalar polynomial singularity for $0<\kappa^2<1/4, 1/4<\kappa^2<3/8$, but regular for $3/8<\kappa^2<1/2$. Figure 2 shows the domain originally given by the self-similar Einstein-Rosen wave solutions in the TX plane.

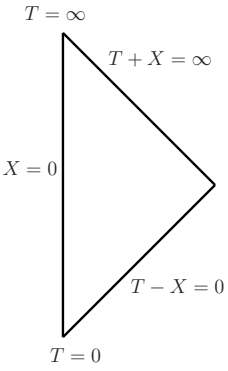

Figure 2: The domain of the solutions

The case of $3/8<\kappa^2<1/2$ is particularly interesting. In this case, using u and v defined by $T=(v^n+u^n)/2, X=(v^n-u^n)/2$, where $n=1/[2(1-2\kappa^2)]$, the line element is given by

$$ds^2 = -[2(1-2\kappa^2)]^{-2}e^{2\lambda}\left(\frac{v^n+u^n}{2}\right)^{4\kappa(2\kappa-1)}dudv + \left(\frac{v^n+u^n}{2}\right)^{2(1-2\kappa)}\left(\frac{v^n-u^n}{2}\right)^2 d\varphi^2+\left(\frac{v^n+u^n}{2}\right)^{4\kappa}dz^2. \tag{17}$$

Thus, we can find an analytical extension beyond $u=0$ or $T=X$ if and only if n is a natural number. In this case, $u=0$ is a cylindrical trapping horizon. On the other hand, if $3/8<\kappa^2<1/2$ but n is not integer, the extension beyond $u=0$ is only finitely differentiable at $u=0$. If n is a positive odd number but not unity, there appears spacelike curvature singularity on

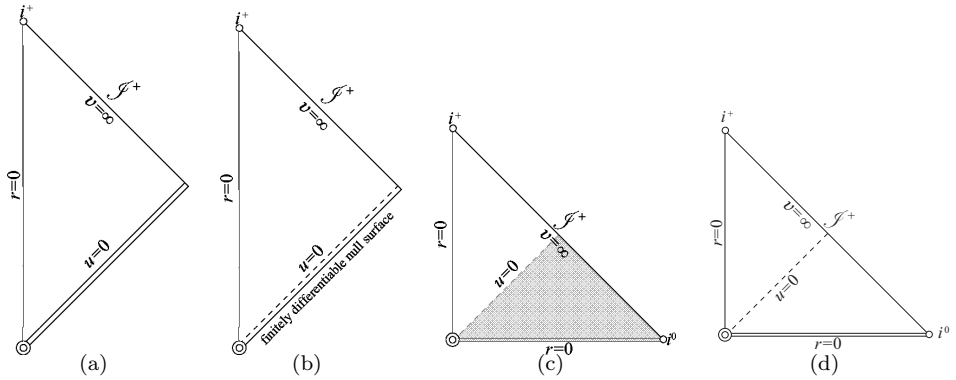

Figure 3: The conformal diagrams for (a) $0 < \kappa^2 < 1/4, 1/4 < \kappa^2 < 3/8$, (b) $3/8 < \kappa^2 < 1/2$ but $n(> 2)$ noninteger, (c) odd $n \geq 3$ and (d) even $n \geq 2$. The single and double circles denote infinity and singularity, respectively.

which $r = 0$. If n is a positive even number, the spacetime instead has spacelike quasi-regular singularity on which $t = 0$.

There is a strong numerical evidence which suggests that the self-similar solution obtained here describes the asymptotic behaviour of more general Einstein-Rosen waves emitted from the collapse of cylindrically symmetric dust collapse. Figure 8 of Nakao et al. [6] shows the snapshots of $\psi = \psi(t, x)$ in the numerical simulations of cylindrically symmetric dust collapse. In that figure, it is seen that the gravitational waves emitted from the dust collapse gradually approach an exact self-similar solution with particular values of κ and λ as time proceeds.

5 Summary

We have studied self-similar vacuum solutions in whole-cylinder symmetry. We have found the following results. If the homothetic vector is orthogonal to the cylinders of symmetry, the spacetime must be flat and is cylindrical Milne. This solution admits nonvanishing C energy and a cylindrical trapping horizon. If the homothetic vector is allowed not to be orthogonal, we instead find a two-parameter family of nonflat solutions with a regular or conically singular axis. A generic member of the family describes the dynamics of cylindrical gravitational waves, involving spacetime singularities. There is a convincing numerical evidence that the self-similar solution obtained here describes the asymptotic behaviour of more general Einstein-Rosen waves. Thus, the similarity hypothesis which was originally proposed for spherical symmetry can be naturally generalised to cylindrically symmetric spacetimes. It should be stressed that the self-similarity hypothesis can apply to the genuine gravitational dynamical degrees of freedom.

References

[1] T. Harada, K. Nakao and B. C. Nolan, Phys. Rev. D**80**, 024025 (2009); Erratum-ibid. D **80**, 109903(E) (2009).

[2] B. J. Carr, unpublished.

[3] B. J. Carr and A. A. Coley, Gen. Relativ. Gravit. **37**, 2165 (2005).

[4] K. S. Thorne, Phys. Rev. **138**, B251 (1965).

[5] S. A. Hayward, Class. Quantum Grav. **17**, 1749 (2000).

[6] K. Nakao, T. Harada, Y. Kurita, and Y. Morisawa, Prog. Theor. Phys. **122**, 521 (2009).

Toroidal Spiral Strings in Higher-dimensional Spacetime

Takahisa Igata[1] and Hideki Ishihara[2]

Department of Mathematics and Physics, Graduate School of Science, Osaka City University, Osaka 558–8585, Japan

Abstract

We report on our progress in research of separability of the Nambu-Goto equation for test strings with a symmetric configuration in a shape of toroidal spiral in a five-dimensional Kerr-AdS black hole. In particular, for a '*Hopf loop*' string which is a special class of the toroidal spirals, we show the complete separation of variables occurs in two cases, Kerr background and Kerr-AdS background with equal angular momenta. We also obtain the dynamical solution for the Hopf loop around a black hole and for the general toroidal spiral in Minkowski background.

1 INTRODUCTION

Recently, much attention has been focused on the study of higher-dimensional spacetime. One of our important task is revealing properties of higher-dimensional black hole because identification of the spacetime dimension could be done by observations of phenomena concerning to black holes.

When we study black hole physics, a test particle plays an crucial role as a probe of black hole spacetime because it gives us information of the geometry around it. In addition a test string would be also a powerful tool to understand the black hole physics.

Here we discuss dynamics of a test string around a higher-dimensional spacetime. As is known that Kerr-AdS black hole spacetimes are typical exact solutions of the Einstein equation in arbitrary dimension. Now we consider the five-dimensional one, which corresponding metric is given by

$$ds^2 = -\frac{\Delta_\theta \Xi_r dt^2}{\Xi_a \Xi_b} + \frac{2M}{\Sigma}\left(\frac{\Delta_\theta dt}{\Xi_a \Xi_b} - \nu\right)^2 + \frac{\Sigma dr^2}{\Delta_r} + \frac{\Sigma d\theta^2}{\Delta_\theta} + \frac{r^2+a^2}{\Xi_a}\sin^2\theta d\Phi^2 + \frac{r^2+b^2}{\Xi_b}\cos^2\theta d\Psi^2, \quad (1)$$

with

$$\Delta_r = \frac{(r^2+a^2)(r^2+b^2)(1+\lambda^2 r^2)}{r^2} - 2M, \qquad \Delta_\theta = 1 - a^2\lambda^2\cos^2\theta - b^2\lambda^2\sin^2\theta\ , \quad (2)$$

$$\nu = a\sin^2\theta\frac{d\Phi}{\Xi_a} + b\cos^2\theta\frac{d\Psi}{\Xi_b}, \qquad \Sigma = r^2 + a^2\cos^2\theta + b^2\sin^2\theta, \quad (3)$$

$$\Xi_a = 1 - a^2\lambda^2, \qquad \Xi_b = 1 - b^2\lambda^2, \qquad \Xi_r = 1 + \lambda^2 r^2, \quad (4)$$

where M is the mass parameter, and a and b are two independent rotational parameters. The parameter λ is connected with the cosmological constant Λ as $\lambda^2 = -\Lambda/6$. We should note that the spacetimes have a remarkable common property in arbitrary dimension, that is, separability in the geodesic Hamilton-Jacobi equation [1–3]. It is expected that a string motion could be also separable due to the geometrical property. In fact, separability is also shown for a string in a class of stationary string in [4–6]. Hence, we concentrate on the dynamical string in the five-dimensional Kerr-AdS black hole.

We discuss a special string which has a symmetry of configuration. We assume that one of the Killing vector fields, say ξ, on a target spacetime is tangent to a worldsheet of the string. We call it a *cohomogeneity-one string* associated with ξ. A stationary string is in a class of a cohomogeneity-one string where the Killing vector is timelike. It is known that the Nambu-Goto action for a cohomogeneity-one

[1]E-mail:igata@sci.osaka-cu.ac.jp
[2]E-mail:ishihara@sci.osaka-cu.ac.jp

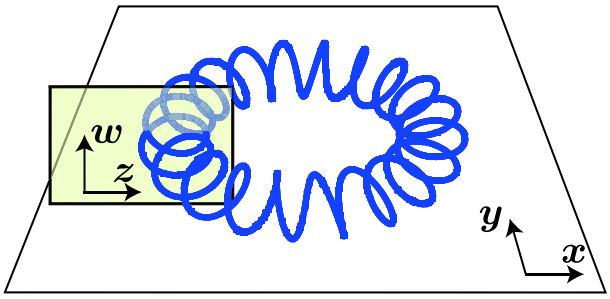

Figure 1: A toroidal spiral string coils around a torus embedded in the four-dimensional space on a snap shot.

string reduces to a geodesic action in a quotient space $\mathcal{O}$, constructed by the isometry group generated by ξ, with a norm weighed metric $Fh_{\mu\nu}$ as follows,

$$S_{NG} = -\mu\,\Delta\sigma \int_{\mathcal{C}} \sqrt{-F\,h_{\mu\nu}\,\frac{dx^\mu}{d\tau}\,\frac{dx^\nu}{d\tau}}\,d\tau, \tag{5}$$

where μ is a tension of string, τ and σ are the coordinates of the string worldsheet, $\mathcal{C}$ is a curve on $\mathcal{O}$, F is a norm of ξ, and $h_{\mu\nu}$ is natural projection metric of $\mathcal{O}$ defined as $h_{\mu\nu} = g_{\mu\nu} - \xi_\mu\xi_\nu/F$. Therefore, the problem for finding solution of motion of cohomogeneity-one strings associated with ξ in the five-dimensional Kerr-AdS black hole reduces to the problem for solving geodesic equations in a four-dimensional space $(\mathcal{O}, Fh_{\mu\nu})$.

We concentrate on dynamics of a class of cohomogeniety-one strings, *toroidal spiral strings* [7, 8]. The string is associated with the Killing vector field

$$\xi = \partial_\Phi + \alpha\partial_\Psi, \tag{6}$$

where Ψ and Φ are correspond to the azimuthal angles on the independent two-dimensional planes in the four-dimensional spatial section and ∂_Φ and ∂_Ψ are the commutable rotational Killing vector fields. The constant α describes winding ratio of the string. The string have a spiral shape along a circle on a time slice as shown in Figure 1.

We stress that the special class of the toroidal spiral strings with $\alpha^2 = 1$ behaves "good" as discussed later. The string in this class lies along a fiber of Hopf fibration S^3 which is a constant surface of the radial coordinate on a timeslice in the Kerr-AdS black hole, after which we name the string as a *Hopf loop*. We will see that the Hopf loop has a special nature in the following section.

2 SEPARABILITY

Let us discuss the separability in the geodesic equation in $(\mathcal{O}, Fh_{\mu\nu})$ for a toroidal spiral string. In order to solve the geodesic equation, we use the Hamilton-Jacobi method. The Hamilton-Jacobi equation in our case is written by

$$\begin{aligned}
&\left[\frac{(r^2+a^2)(r^2+b^2)\Xi_a\Xi_b - 2M(r^2+a^2b^2\lambda^2)}{r^2\Delta_r} + \frac{2(1-a^2\lambda^2)(1-b^2\lambda^2)}{\lambda^2(a^2+b^2)+\lambda^2(a^2-b^2)\cos 2\theta - 2}\right]\frac{E^2}{\lambda^2} \\
&+\left[4abM\alpha\Xi_r + (\alpha^2-1)(b^2-a^2)r^2\Xi_r + a^2b^2\Xi_r\Big[(\alpha^2-1)(1+\lambda^2(a^2-b^2)) - 2\alpha^2\Big]\right. \\
&\left.+a^2(1+\alpha^2r^2\lambda^2)(a^2\Xi_r - 2M) + b^2(\alpha^2+r^2\lambda^2)(b^2\Xi_r - 2M) + \left(\frac{\alpha^2\Xi_a}{\sin^2\theta} + \frac{\Xi_b}{\cos^2\theta}\right)\right]L^2 \\
&+\frac{4M[-b(r^2+a^2)+\alpha a(r^2+b^2)]}{r^2\Delta_r}EL + \Delta_r\left(\frac{dS_r}{dr}\right)^2 + \Delta_\theta\left(\frac{dS_\theta}{d\theta}\right)^2 = -\mu^2F\Sigma,
\end{aligned} \tag{7}$$

where S_r and S_θ, each term of the Hamilton's principal function, are functions r and θ, respectively, and E and L are conserved quantities correspond to the energy and the angular momentum of the string. We find that separation of variables does not occur for a general toroidal spiral string because the right-hand side of (7), which has the explicit form

$$\begin{aligned}\mu^2 F\Sigma &= \mu^2(r^2+a^2\cos^2\theta+b^2\sin^2\theta)\Big[\frac{(r^2+b^2)\alpha^2\cos^2\theta}{\Xi_b}+\frac{(r^2+a^2)\sin^2\theta}{\Xi_a}\Big]\\ &\quad +2M\mu^2\Big(\frac{\alpha b\cos^2\theta}{\Xi_b}+\frac{a\sin^2\theta}{\Xi_a}\Big)^2,\end{aligned} \tag{8}$$

does not allow the separation of variables. The complete separability in the Hamilton-Jacobi equation depends on the parameter α, and parameters of the background geometry.

When we consider a Hopf loop, $\alpha = 1$, around the black hole, we see that the Hamilton-Jacobi equation can be separable for two cases:

(A) vanishing cosmological constant *i.e.*, the background is a Kerr black hole,

(B) the black hole with non-zero cosmological constant and two equal angular momenta.

The complete separability implies that the metric $Fh_{\mu\nu}$ admits Killing tensor fields. One obtains the irreducible and reducible Killing tensor field on the quotient space $(\mathcal{O}, Fh_{\mu\nu})$ in the case of (A) and (B), respectively(see ref.[9] for detail discussion).

3 DYNAMICS

Let us see dynamics of a Hopf loop around the Kerr-AdS black hole in the case of (B). The metric $Fh_{\mu\nu}$ has SO(3) symmetry because the base space of the Hopf bundle becomes round S^2, and F is a function of r. Therefore, without loss of generality, we can restrict our attention to study geodesics confined in the equatorial plane, *i.e.*, $\theta = \pi/4$.

Then, with appropriate choice of the Lagrange multiplier N, the radial equation of motion becomes $\dot{r}^2 + V_{\text{eff}} = E^2$, with the effective potential given by

$$V_{\text{eff}} = \frac{\mu^2 r^2 \Delta_r}{(r^2+a^2)\Xi_a^2} + \frac{4r^2\Delta_r\Xi_a L^2}{[(r^2+a^2)^2\Xi_a + 2Ma^2](r^2+a^2)}. \tag{9}$$

Typical shapes of the effective potential for the case (B) are given in Figure 2. The figure shows that the radial motion of the Hopf loop is classified into two types, bounded or unbounded. This nature is understood that the motions of Hopf loops are driven by the three forces; tension of string, centrifugal force, and gravitational force, and the orbits are determined by the competition of these forces [8]. The existence of bounded orbits for the Hopf loop is analogous to the case of a free particle around a four-dimensional black hole. We note that this is particular nature of the string because there is no bounded orbit for test particles around the five-dimensional Kerr black hole [2].

Stationary Hopf loop solution exists at the local minimum of V_{eff}. By the effect of the gravitational force, there exists a critical radius of Hopf loop for each black hole such that no stable Hopf loop is inside the radius, namely, the innermost stable orbit exists. In addition, in the case of $\Lambda > 0$, Hopf loops can grow up to infinite radius by the de Sitter expansion, and the outermost stable orbit exists.

We have also studied dynamics of a toroidal spiral string in the five-dimensional Minkowski background and shown that

- For a general toroidal spiral, *i.e.*, for all α, the Hamilton-Jacobi equation is completely separable

In addition, we can obtain the general solution which describes harmonic oscillations of radii of torus which is coiled by the toroidal spiral explicitly (see ref.[9] for detail discussion).

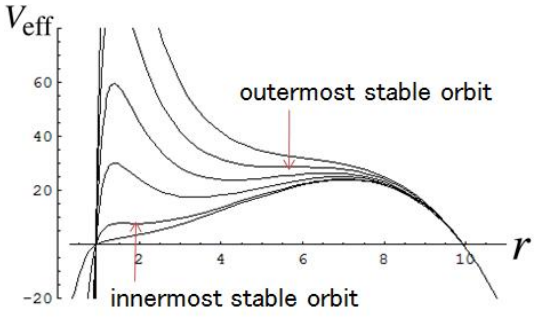

Figure 2: The effective potentials for radial motion of a Hopf loop with respect to each L in the five-dimensional Kerr-AdS black hole with equal angular momenta. The parameter choice is $r_g = 2M = 1$, $\Lambda/6 = -\lambda^2 = 0.01$, and $a = 1/4$.

4 SUMMARY

In this proceeding, we have discussed the separability of the Nambu-Goto equations for a toroidal spiral string in the five-dimensional spacetime. We have found that the equation admits the separation of variables for a Hopf loop in a Kerr black hole and a Kerr-AdS black hole with two equal angular momenta.

We have also shown the dynamical properties of the Hopf loop strings in the five-dimensional black hole. There exist bounded orbits and unbounded orbits in the quotient space, and also exist the innermost or outermost stable orbit. Since the motions of Hopf loops are driven by three forces: tension of string, the centrifugal force, and force of gravity, the orbits are determined by the competition of these forces. The stationary configurations are achieved by the balance of these forces.

The existence of the bounded orbits of the Hopf loops around five-dimensional black holes makes us recall the free particles around a four-dimensional black hole. These results shows that the toroidal spiral string is a candidate of observational probe in place of a test particle in higher-dimensional spacetime. The existence of the stationary configuration and the bounded orbits of the string shows that there are prospects for long life of the closed string in the higher-dimensional universe.

References

[1] B. Carter, Commun. Math. Phys. **10**, 280 (1968).

[2] V. P. Frolov and D. Stojkovic, Phys. Rev. D **68**, 064011 (2003) [arXiv:gr-qc/0301016].

[3] V. P. Frolov, P. Krtous and D. Kubiznak, JHEP **0702**, 005 (2007) [arXiv:hep-th/0611245].

[4] V. P. Frolov and K. A. Stevens, Phys. Rev. D **70**, 044035 (2004) [arXiv:gr-qc/0404035].

[5] D. Kubiznak and V. P. Frolov, JHEP **0802**, 007 (2008) [arXiv:0711.2300 [hep-th]].

[6] H. Ahmedov and A. N. Aliev, Phys. Rev. D **78**, 064023 (2008) [arXiv:0805.1594 [hep-th]].

[7] J. J. Blanco-Pillado, R. Emparan and A. Iglesias, JHEP **0801**, 014 (2008) [arXiv:0712.0611 [hep-th]].

[8] T. Igata and H. Ishihara, arXiv:0911.0266 [hep-th].

[9] T. Igata and H. Ishihara, arXiv:0911.5549 [hep-th].

All Near-Horizon Geometries of Extremal Vacuum Black Holes

Akihiro Ishibashi[1]

KEK Theory Center, IPNS, KEK

Abstract

This talk is aimed at introducing the paper of [arXiv:0909.3462] by S. Hollands and the present author, which addresses the classification problem of all vacuum near-horizon geometries in D-dimensions with $(D-3)$ commuting rotational symmetries. Here we present some of the key formulas and main results of the paper.

1 Key formulas and main results

We are concerned with the classification problem of higher dimensional black hole solutions: Given a higher dimensional gravity theory, we wish to first (i) identify all (physical) parameters that uniquely determine black hole solutions of the theory, and then (ii) construct explicitly all possible black hole solutions characterized by the parameters. In this generality, however, the black hole classification problem appears to be difficult to address, so we restrict attention to some interesting subclass of solutions.

Many known families of black hole solutions possess a limit wherein the black hole horizon becomes degenerate; such black holes are called *extremal*. Due to the limiting procedure, extremal black holes are in some sense at the fringe of the space of all black holes, and therefore possess special properties which make them easier to study in various respects. It is known that any extremal black hole with a degenerate Killing horizon admits the *near-horizon geometry*, which is obtained by taking a suitable scaling process to the metric in an immediate vicinity of the degenerate horizon. More precisely, for any spacetime with a degenerate Killing horizon, one can introduce, in a neighborhood of the horizon, *Gaussian-null coordinates*, (v, u, y^a), such that the metric takes the form

$$\mathrm{d}s^2 = 2\mathrm{d}v(\mathrm{d}u + u^2\alpha\mathrm{d}v + u\beta_a\mathrm{d}y^a) + \gamma_{ab}\mathrm{d}y^a\mathrm{d}y^b\,, \tag{1}$$

where the horizon is located at $u = 0$ and where v is the Killing parameter and at the same time, an affine parameter along the null generators of the horizon. The metric functions $\alpha, \beta_a, \gamma_{ab}$, which are independent of v, can be seen as functions on horizon cross section, H, at $u = 0 = v$. We consider diffeomorphism $v \mapsto v/\epsilon,\ u \mapsto \epsilon u$, leaving y^a unchanged, and then take $\epsilon \to 0$. The obtained near-horizon metric looks exactly like the original one, but now the new metric functions $\alpha, \beta_a, \gamma_{ab}$ depend on neither v nor u. The near horizon metric satisfies the same dynamics as the original black hole solution. It is, in fact, this near-horizon geometry that enters many interesting applications, such as the arguments pertaining to the derivation of the Bekenstein-Hawking entropy.

The purpose of the paper [1] is to classify all near-horizon geometries which can arise from D-dimensional extremal, stationary vacuum black holes. We assume further that the geometries admit $D-3$ commuting rotational symmetries, generated by axial Killing vector fields, $\psi_i = \partial/\partial\varphi^i,\ i = 1, ..., D-3$. Then, the metric functions for such a near-horizon geometry depend only on a single coordinate, say x, which may correspond to a polar coordinate and can be chosen $x \in [-1, 1]$. Furthermore, it can be shown that a near horizon geometry possesses more symmetries, $O(2,1) \times U(1)^{D-3}$, than the original solution does [2]. Previously, Kunduri-Lucietti [3] gave a classification of such near-horizon geometries in $D = 4, 5$. However, their method does not appear to be generalized to higher dimensional case $D \geq 6$. We use a different method based on a matrix (sigma-model) formulation of the vacuum Einstein equations that works in arbitrary dimensions. In the following we briefly explain our method. First, as a consequence of

[1]Email address: akihiro.ishibashi@kek.jp

our symmetry assumption and the dynamics (part of the vacuum Einstein equations) we can find a new coordinate system, (v, r, x, φ^i), in which the near-horizon metric, (1), are rewritten as

$$\mathrm{d}s^2 = \frac{1-x^2}{\det f}(2\mathrm{d}v\mathrm{d}r - C^2r^2\mathrm{d}v^2) + \frac{\mathrm{d}x^2}{C^2\det f} + f_{ij}(\mathrm{d}\varphi^i + rCk^i\mathrm{d}v)(\mathrm{d}\varphi^j + rCk^j\mathrm{d}v)\,, \tag{2}$$

where k^i and C are some constants and $f_{ij} := \mathrm{d}s^2(\psi_i, \psi_j)$ depends only on x. The horizon is now at $r = 0$ and v is the Killing parameter as before. In obtaining the above form of the metric, we have used up all but the ij-components of the Einstein equations. We use the remaining Einstein equations to determine the matrix of functions, f_{ij}. For this purpose, we introduce *twist potentials*, χ_i, defined up to a constant by $\mathrm{d}\chi_i = \star(\psi_1 \wedge \cdots \wedge \psi_{D-3} \wedge \mathrm{d}\psi_i)$, and then set the matrix

$$\Phi = \begin{pmatrix} (\det f)^{-1} & -(\det f)^{-1}\chi_i \\ -(\det f)^{-1}\chi_i & f_{ij} + (\det f)^{-1}\chi_i\chi_j \end{pmatrix}. \tag{3}$$

The matrix elements are functions of only x. Then, the content of the remaining vacuum Einstein equations is expressed as the *ordinary* differential equations

$$\partial_x[(1-x^2)\Phi^{-1}\partial_x\Phi] = 0\,. \tag{4}$$

This matrix equation is easily integrated to

$$\Phi(x) = Q\left(\frac{1+x}{1-x}\right)^L, \tag{5}$$

where $Q = \Phi(0)$, $L = (1/2)(1-x^2)\Phi(x)^{-1}\partial_x\Phi(x)$ are both constant real $(D-2)\times(D-2)$ matrices. Since the matrix, Φ, is symmetric, unimodular, and positive definite, one can show that $\det Q = 1$, $\mathrm{Tr}L = 0$, $Q = Q^T > 0$, $L^TQ = QL$, and further that $Q = S^TS$ for some real invertible matrix $S = (s_{IJ})$ of $\det S = \pm 1$. Using these properties, the matrix Φ is given by

$$\Phi_{IJ}(x) = \sum_{K=0}^{D-3}\left(\frac{1+x}{1-x}\right)^{\sigma_K} s_{KI}s_{KJ}\,. \tag{6}$$

This is the most general solutions to eq. (4) with the real parameters s_{IJ}, σ_I, subject to the constraints $\det S = \pm 1$, $\sum_{I=0}^{D-3}\sigma_I = 0$. This solution determines f_{ij} and χ_i and in turn fix the constants k^i and C, thus completely fixing the near-horizon geometry. It turns out that the smoothness of the near-horizon metric implies further constraints on s_{IJ} and σ_I. The results are summarized as follows:

$$\sigma_I = \begin{cases} 0 & \text{if } I \le D-5, \\ -1 & \text{if } I = D-4, \\ 1 & \text{if } I = D-3, \end{cases} \tag{7}$$

and

$$k^i = \frac{2c_+c_-}{c_+ - c_-}\left(\frac{a_+^i}{\mu_j a_+^j} + \frac{a_-^i}{\mu_j a_-^j}\right), \quad C = \frac{4c_+^2}{(c_+-c_-)\mu_i a_+^i} = \frac{4c_-^2}{(c_+-c_-)\mu_i a_-^i}\,, \tag{8}$$

where

$$\mu_i = s_{(D-3)i} = s_{(D-4)i}\,, \quad c_+ = s_{(D-3)0}\,, \quad c_- = s_{(D-4)0}\,, \tag{9}$$

and $a_\pm^i \in Z$ are real integer parameters taken so that the linear combination $\sum a_\pm^i\psi_i$ vanishes at the boundary points $x = \pm 1$. It turns out that $a_\pm^i$ determine the horizon topology as commented later on.

Thus, we have determined all quantities C, k^i, f_{ij} in the near-horizon metric (2). Making the final coordinate change $x = \cos\theta\,, \quad 0 \le \theta \le \pi$, and performing some algebraic manipulations, we get the following result:

Theorem 1. *All vacuum, non-static, near horizon metrics (except topology type $H \cong T^{D-2}$) with assumed symmetry are parametrized by the real parameters $c_\pm, \mu_i, s_{Ii}$, and the integers $a^i_\pm$ where $I = 0, \dots, D-5$ and $i = 1, \dots, D-3$, and* g.c.d.$(a^i_\pm) = 1$. *The explicit form of the near horizon metric in terms of these parameters is*

$$\begin{aligned} g &= \mathrm{e}^{-\lambda}(2\mathrm{d}v\mathrm{d}r - C^2 r^2 \mathrm{d}v^2 + C^{-2}\,\mathrm{d}\theta^2) + \mathrm{e}^{+\lambda}\Bigg\{ (c_+ - c_-)^2 (\sin^2\theta)\,\Omega^2 \\ &\quad + (1+\cos\theta)^2 c_+^2 \sum_I \left(\omega_I - \frac{s_I\cdot a_+}{\mu\cdot a_+}\Omega\right)^2 + (1-\cos\theta)^2 c_-^2 \sum_I \left(\omega_I - \frac{s_I\cdot a_-}{\mu\cdot a_-}\Omega\right)^2 \\ &\quad + \frac{c_\pm^2 \sin^2\theta}{(\mu\cdot a_\pm)^2} \sum_{I<J} \Big((s_I\cdot a_\pm)\omega_J - (s_J\cdot a_\pm)\omega_I\Big)^2 \Bigg\}. \end{aligned} \tag{10}$$

Here, the sums run over I, J from $0, \dots, D-5$, the function $\lambda(\theta)$ is given by

$$\exp[-\lambda(\theta)] = c_+^2(1+\cos\theta)^2 + c_-^2(1-\cos\theta)^2 + \frac{c_\pm^2 \sin^2\theta}{(\mu\cdot a_\pm)^2}\sum_I (s_I\cdot a_\pm)^2\,, \tag{11}$$

C is given by $C = 4c_\pm^2[(c_+ - c_-)(\mu\cdot a_\pm)]^{-1}$, and we have defined the 1-forms

$$\Omega(r) = \mu\cdot\mathrm{d}\varphi + 4Cr\frac{c_+c_-}{c_+-c_-}\mathrm{d}v \tag{12}$$

$$\omega_I(r) = s_I\cdot\mathrm{d}\varphi + \frac{r}{2}C^2(s_I\cdot a_+ + s_I\cdot a_-)\,\mathrm{d}v\,. \tag{13}$$

We are also using the shorthand notations such as $s_{Ii}a^i_+ = s_I\cdot a_+$, or $\mu\cdot\mathrm{d}\varphi = \mu_i\mathrm{d}\varphi^i$, etc. The parameters are subject to the constraints $\mu\cdot a_\pm \neq 0$ and

$$\frac{c_+^2}{\mu\cdot a_+} = \frac{c_-^2}{\mu\cdot a_-}\,, \quad \frac{c_+(s_I\cdot a_+)}{\mu\cdot a_+} = \frac{c_-(s_I\cdot a_-)}{\mu\cdot a_-}\,, \quad \pm 1 = (c_+ - c_-)\,\epsilon^{ijk\dots m}s_{0i}s_{1j}s_{2k}\cdots\mu_m \tag{14}$$

but they are otherwise free. The coordinates φ^i are 2π-periodic, $0 \le \theta \le \pi$, and v, r are arbitrary. When writing "$\pm$", we mean that the formulae hold for both signs.

Remarks: (i) The meaning of the parameters are as follows. The parameters $a^i_\pm \in \mathbb{Z}$ are related to the horizon topology. Up to a globally defined coordinate transformation of the form $\varphi^i \mapsto \sum A^i_j\varphi^j \mod 2\pi$, $A \in SL(\mathbb{Z}, D-3)$, we have

$$a_+ = (1,0,0,\dots,0)\,, \quad a_- = (q,p,0,\dots,0)\,, \quad p,q\in\mathbb{Z}\,, \quad \text{g.c.d.}(p,q) = 1\,. \tag{15}$$

A general analysis of compact manifolds with a cohomogeneity-one torus action implies that the topology of H is

$$H \cong \begin{cases} S^3\times T^{D-5} & \text{if } p=\pm1, q=0, \\ S^2\times T^{D-4} & \text{if } p=0, q=1, \\ L(p,q)\times T^{D-5} & \text{otherwise.} \end{cases} \tag{16}$$

The constants $\mu_i, c_\pm, a^i_\pm$ are directly related to the horizon area by

$$A_H = \frac{(2\pi)^{D-3}(c_+-c_-)^2(\mu\cdot a_\pm)^2}{8c_\pm^4}\,, \tag{17}$$

and we also have

$$J_i := \frac{1}{2}\int_H \star(\mathrm{d}\psi_i) = (2\pi)^{D-3}\,\frac{c_+-c_-}{2c_-c_+}\mu_i\,. \tag{18}$$

In an asymptotically flat or Kaluza-Klein black hole spacetime with a single horizon H, J_i would be equal to the Komar expressions for the angular momentum. The near horizon limits that we consider do not of

course satisfy any such asymptotic conditions, and hence this cannot be done. Nevertheless, if the near horizon metric under consideration arises from an asymptotically flat or asymptotically Kaluza-Klein spacetime, then the J_i are the angular momenta of that spacetime. Hence, we see that the parameters $c_\pm, \mu_i, a^i_\pm$ are directly related to geometrical/topological properties of the metric. This seems to be less clear for the remaining parameters s_{Ii}.

(ii) The number of continuous parameters on which our metric depend can be counted as follows. First, the matrix s_{Ii} has $(D-3)(D-4)$ independent components, μ_i has $(D-3)$ and $c_\pm$ has 2 components. These parameters are subject to the $(D-2)$ constrains, eqs. (14). However, changing s_{Ii} to $\sum_{J=0}^{D-5} R^J{}_I s_{Ji}$, with $R^J{}_I$ an orthogonal matrix in $O(D-4)$, does not change the metric. Since such a matrix depends on $(D-4)(D-5)/2$ parameters, our metrics depend only on $(D-3)(D-4)+(D-3)+2-(D-2)-(D-4)(D-5)/2 = (D-2)(D-3)/2$ real continuous parameters.

(iii) By contrast to the case $D \leq 5$ given in [3], not all near horizon metrics that we have found can be obtained as the near horizon limits of known black hole solutions in dimensions $D \geq 6$. It is conceivable that there are further extremal black hole solutions—to be found—which give our metrics in the near horizon limit, but it is also possible that some of our metrics in $D \geq 6$ simply do not arise in this way.

References

[1] Hollands, S. and Ishibashi, A.: "All Vacuum Near-Horizon Geometries in D-dimensions with $(D-3)$ Commuting Rotational Symmetries" [arXiv:0909.3462[gr-qc]] to be published in Ann. Henri Poincaré

[2] Kunduri, H. K., Lucietti, J. and Reall, H. S.: "Near-horizon symmetries of extremal black holes," Class. Quant. Grav. **24** (2007) 4169 [arXiv:0705.4214 [hep-th]].

[3] Kunduri, H. K. and Lucietti, J.: "A classification of near-horizon geometries of extremal vacuum black holes," J. Math. Phys. **50** (2009) 082502 [arXiv:0806.2051 [hep-th]].

No Static Star Solution in Horava Gravity

Keisuke Izumi[1] and Shinji Mukohyama[2]

IPMU, The University of Tokyo, Kashiwa, Chiba 277-8582, Japan

Abstract

In Hořava-Lifshitz gravity, regularity of a solution requires smoothness of not only the spacetime geometry but also the foliation. As a result, the regularity condition at the center of a star is more restrictive than in general relativity. Assuming that the energy density is a piecewise-continuous, non-negative function of the pressure and that the pressure at the center is positive, we prove that the momentum conservation law is incompatible with the regularity at the center for any spherically-symmetric, static configurations. Therefore, we conclude that a spherically-symmetric star should include a time-dependent region near the center. This supports the picture that Hořava-Lifshitz gravity does not recover general relativity at low energy but can instead mimic general relativity plus cold dark matter.

1 Introduction and Summary

Recently, a power-counting renormalizable gravity theory was proposed by Hořava [1, 2]. The essential reason for the power-counting renormalizability is that in the ultraviolet (UV), the theory exhibits the Lifshitz-type anisotropic scaling

$$t \to b^z t, \ \vec{x} \to b\vec{x}, \tag{1}$$

with the dynamical critical exponent $z \geq 3$. Because of the Lifshitz scaling, this theory is often called Hořava-Lifshitz gravity. Although power-counting renormalizability does not necessarily imply renormalizability, there is a good possibility that the theory is unitary and renormalizable.

In Hořava-Lifshitz gravity, regularity of a solution requires smoothness of not only the spacetime geometry but also the foliation. As a result, the regularity condition at the center of a star is more restrictive than in general relativity. Under the assumptions that the energy density is piecewise-continuous non-negative function of the pressure and that the pressure at the center is positive, we have proved that the momentum conservation law is incompatible with the regularity at the center for any spherically-symmetric, globally-static configurations [6]. The proof is totally insensitive to the structure of higher spatial curvature terms and, thus, holds for any values of the dynamical critical exponent z. Therefore, under the assumption we made on the matter sector, we conclude that a spherically-symmetric star should include a time-dependent region, presumably near the center.

The assumptions we made are physically natural. For example, a polytropic fluid satisfies them. Note that our proof does not assume asymptotic flatness and that a cosmological constant Λ can be included in the gravity action. Shifting ρ, $-P$ and $-M_{Pl}^2\Lambda$ with the same amount does not change the physical system but may validate/invalidate some of the assumptions of the proof. In order to construct a static star solution, we need to violate at least one of the assumptions for all possible choices of such a shift. One possibility is to introduce an exotic matter such as a quintessence field. Introduction of an exotic matter is, however, not necessarily sufficient for the existence of a static star solution.

One must not consider our result, i.e. nonexistence of static star, as a serious problem of Hořava-Lifshitz theory. It is known that this theory does not recover general relativity at low energy but can instead mimic general relativity plus cold dark matter [3] [3] The existence of built-in "cold dark matter" is an inevitable prediction of the theory and might solve the mystery of dark matter in the universe. Our result is totally consistent with this picture: as in the standard cold dark matter scenario, the "cold

[1]Email address: keisuke.izumi@ipmu.jp
[2]Email address: shinji.mukohyama@ipmu.jp
[3]The constraint algebra is smaller than in general relativity since the time slicing is synchronized with the rest frame of cold dark matter in the theory level.

dark matter" accretes toward a star and thus inevitably makes the stellar center dynamical. This is the physical reason why there is no static star in Hořava-Lifshitz theory and, thus, our result strongly supports the "dark matter as an integration constant" scenario [3].

2 Definition and basic feature of Hořava-Lifshitz gravity

Basic quantities in the gravity sector are the lapse function $N(t)$, the shift vector $N^i(t,\vec{x})$ and the three-dimensional spatial metric $g_{ij}(t,\vec{x})$. These variables can be combined to form a four-dimensional metric in the Arnowitt-Deser-Misner (ADM) form:

$$ds^2 = -N^2dt^2 + g_{ij}(dx^i + N^i dt)(dx^j + N^j dt). \tag{2}$$

Since the lapse function is roughly speaking a gauge freedom associated with the space-independent time reparametrization, it is rather natural to restrict the lapse function to be space-independent. This condition, called the projectability condition, is not only natural but also mandatory, as pointed out in Hořava's original paper [1]. Indeed, if we abandoned the projectability condition then we would face phenomenological obstacles [4] and theoretical inconsistencies [5]. On the other hand, with the projectability condition (and without the detailed balance condition), the theory is free from those problems [3]. Therefore, we impose the projectability condition and demand that the lapse function be space-independent. The Hamiltonian constraint is, as a result, not a local equation satisfied at each spatial point but an equation integrated over a whole space.

The action is

$$\begin{aligned} I &= I_g + I_m, &(3)\\ I_g &= \frac{M_{Pl}^2}{2}\int dtdx^3 N\sqrt{g}(K^{ij}K_{ij} - \lambda K^2 \\ &\qquad +\Lambda + R + L_{z>1}), &(4)\end{aligned}$$

where

$$K_{ij} = \frac{1}{2N}(\partial_t g_{ij} - D_i N_j - D_j N_i), \quad K = g^{ij}K_{ij}, \tag{5}$$

D_i is the covariant derivative compatible with g_{ij}, Λ is a cosmological constant, R is the Ricci scalar of g_{ij}, $L_{z>1}$ represents higher spatial curvature terms and I_m is the matter action. Here, we have rescaled the time coordinate so that the coefficients of $K^{ij}K_{ij}$ and R agree. Note that not only the gravitational action I_g but also the matter action I_m should be invariant under the foliation-preserving diffeomorphism.

The invariance of I_α under the infinitesimal transformations $\delta t = f(t)$ and $\delta x^i = \zeta^i(t,x)$ leads to the following conservation equations, where α represents g or m.

$$\begin{aligned} 0 &= N\partial_t H_{\alpha\perp} \\ &\quad + \int dx^3 \left[N^i\partial_t(\sqrt{g}\mathcal{H}_{\alpha i}) + \frac{1}{2}N\sqrt{g}\mathcal{E}_\alpha^{ij}\partial_t g_{ij}\right], &(6)\\ 0 &= \frac{1}{N}(\partial_t - N^j D_j)\mathcal{H}_{\alpha i} + K\mathcal{H}_{\alpha i} \\ &\quad - \frac{1}{N}\mathcal{H}_{\alpha j}D_i N^j - D^j\mathcal{E}_{\alpha ij}. &(7)\end{aligned}$$

3 No spherically symmetric and static solution

Surprisingly enough, we have found a no-go result [6]: a spherically-symmetric, globally static solution can not be constructed in Hořava-Lifshitz gravity under the assumption that the energy density is a piecewise-continuous, non-negative function of the pressure and that the pressure at the center is positive. This section provides a proof of this statement.

3.1 Painlevé-Gullstrand coordinate and Matter sector

We consider spherical-symmetric and static configurations. Since the lapse function does not depend on spatial coordinates, we can set it to unity by space-independent time reparametrization:

$$N = 1. \tag{8}$$

For a spherically symmetric, static configuration, we can express the shift vector and the spatial metric as

$$N^i\partial_i = \beta(x)\partial_x, \quad g_{ij}dx^idx^j = dx^2 + r^2(x)d\Omega_2^2, \tag{9}$$

where $d\Omega_2^2$ is the metric of the unit sphere and x is the proper distance from the center. Non-vanishing components of the Ricci tensor and Ricci scalar for the three-dimensional geometry are

$$R^x_x = -\frac{2r''}{r}, \quad R^\theta_\theta = \frac{1}{r^2}\left[1 - rr'' - (r')^2\right], \tag{10}$$

$$R = \frac{2}{r^2}\left[1 - 2rr'' - (r')^2\right], \tag{11}$$

and the extrinsic curvature and its trace are

$$K_{ij}dx^idx^j = -\beta' dx^2 - \beta rr' d\Omega_2^2, \quad K = -\frac{(r^2\beta)'}{r^2}, \tag{12}$$

where a prime denotes derivative w.r.t. x. The corresponding ADM metric is

$$g^{(4)}_{\mu\nu}dx^\mu dx^\nu = -dt^2 + [dx + \beta(x)dt]^2 + r^2(x)d\Omega_2^2. \tag{13}$$

This is an analogue of the Painlevé-Gullstrand coordinate system. Note that

$$\xi^\mu = \left(\frac{\partial}{\partial t}\right)^\mu \tag{14}$$

is a timelike Killing vector. Global staticity requires ξ^μ to be globally timelike, i.e. $1-\beta^2 > 0$ everywhere. The unit vector n^μ normal to the constant time hypersurface is given by

$$n_\mu dx^\mu = -dt, \quad n^\mu\partial_\mu = \partial_t - \beta\partial_x. \tag{15}$$

As for (real) matter, for simplicity we consider the perfect-fluid form which is at rest w.r.t. the Killing vector ξ^μ:

$$T_{\mu\nu} = \rho(x)u_\mu u_\nu + P(x)\left[g^{(4)}_{\mu\nu} + u_\mu u_\nu\right], \tag{16}$$

$$u^\mu = \frac{\xi^\mu}{\sqrt{1-\beta^2}}. \tag{17}$$

Its components relevant for the ADM decomposition are

$$T_{\mu\nu}n^\mu n^\nu = (1-\beta^2)^{-1}(\rho + P) - P, \tag{18}$$

$$T_{\mu i}n^\mu dx^i = (1-\beta^2)^{-1}(\rho + P)\beta dx, \tag{19}$$

$$T_{ij}dx^idx^j = [\beta^2\rho + P]dx^2 + Pr^2 d\Omega_2^2. \tag{20}$$

3.2 Inconsistency near the center

In this subsection, we show that a spherically-symmetric compact object cannot be globally-static under a set of reasonable assumptions in the matter sector. We assume that the energy density ρ is a piecewise-continuous [4] non-negative function of the pressure P and that the pressure at the center P_c is positive. The three-dimensional spatial geometry and the extrinsic curvature must be regular at the center because

[4] We assume piecewise-continuity instead of continuity, in order to allow $dP/d\rho$ to vanish in a finite interval of ρ.

the constant-time surfaces are physically embeded in Hořava-Lifshitz gravity. We prove that the regularity condition at the center is incompatible with the momentum conservation law of the matter under the above assumptions. Since the momentum conservation equation does not include higher spatial curvature terms in the gravity action, our proof is totally insensitive to the structure of higher spatial curvature terms and holds for any values of the dynamical critical exponent z.

In the following argument, we make the proposition that there exists a spherically-symmetric, globally-static, regular solution, and show contradiction. As commented after eq. (14), the global-staticity implies that $(1-\beta^2)$ is positive everywhere.

The momentum conservation equation, (7) with $\alpha = m$, becomes

$$P'(1-\beta^2) + (\rho + P)(1-\beta^2)' = 0. \tag{21}$$

The regularity of the extrinsic curvature (12) implies that β' is finite. This and (21) imply that P' is also finite. As a corollary, β and P are continuous functions of x. Since ρ is assumed to be a piecewise continuous function of P, this means that $\rho + P$ is a piecewise continuous function of x.

Let x_c be the value of x at the center. Since we have assumed that ρ is non-negative everywhere and that $P_c > 0$, the continuity of $P(x)$ implies that $\rho + P$ is positive in a neighborhood of the center. Now let us define x_0 as the minimal value for which at least one of $(\rho+P)|_{x=x_0}$, $\lim_{x\to x_0-0}(\rho+P)$ and $\lim_{x\to x_0+0}(\rho+P)$ is non-positive.

Dividing eq. (21) by $(\rho+P)(1-\beta^2)$ and integrating it over the interval $x_c \le x < x_0$, we obtain

$$\ln(1-\beta_0^2) - \ln(1-\beta_c^2) = -\int_{x_c}^{x_0-0} \frac{P'}{\rho+P} dx, \tag{22}$$

where $\beta_c \equiv \beta(x = x_c)$ and $\beta_0 \equiv \beta(x = x_0)$. The regularity of the Ricci scalar (11) and the extrinsic curvature (12) at the center implies that ${r'}_c = 1$ and $\beta_c = 0$, where ${r'}_c$ is the value of r' at the center. Therefore, the left hand side of eq. (22) is non-positive.

Since P is a differentiable function of x, the right hand side of eq. (22) can be transformed as

$$-\int_{x_c}^{x_0-0} \frac{P'}{\rho+P} dx = -\int_{P_c}^{P_0} \frac{dP}{\rho(P)+P}, \tag{23}$$

where $P_0 \equiv P(x = x_0)$. The definition of x_0 implies that at least one of $(\rho+P)|_{x=x_0}$, $\lim_{x\to x_0-0}(\rho+P)$ and $\lim_{x\to x_0+0}(\rho+P)$ is non-positive. Since we have assumed that ρ is non-negative everywhere, $P_0 = \lim_{x\to x_0-0} P = \lim_{x\to x_0+0} P$ is non-positive. Thus, we have

$$P_0 \le 0 < P_c. \tag{24}$$

This implies positivity of the right hand side of (23) since from the definition of x_0 the integrand is positive in the domain of integration. This leads to an contradiction with the previous statement that the left hand side of (22) should be non-positive.

References

[1] P. Horava, Phys. Rev. D **79**, 084008 (2009) [arXiv:0901.3775 [hep-th]].

[2] P. Horava, Phys. Rev. Lett. **102**, 161301 (2009) [arXiv:0902.3657 [hep-th]].

[3] S. Mukohyama, Phys. Rev. D **80**, 064005 (2009) [arXiv:0905.3563 [hep-th]]. S. Mukohyama, arXiv:0906.5069 [hep-th].

[4] C. Charmousis, G. Niz, A. Padilla and P. M. Saffin, JHEP **0908**, 070 (2009) [arXiv:0905.2579 [hep-th]].

[5] M. Li and Y. Pang, arXiv:0905.2751 [hep-th].

[6] K. Izumi and S. Mukohyama, arXiv:0911.1814 [hep-th].

Gravitational waves and Q-ball formation[1]

Kohei Kamada[2 (a),(b)], Takeshi Chiba[(c)] and Masahide Yamaguchi[(d)]

[(a)] *Department of Physics, Graduate School of Science, The University of Tokyo, Tokyo 113-0033, Japan*
[(b)] *Research Center for the Early Universe (RESCEU), Graduate School of Science, The University of Tokyo, Tokyo 113-0033, Japan*
[(c)] *Department of Physics, College of Humanities and Sciences, Nihon University, Tokyo 156-8550, Japan*
[(d)] *Department of Physics and Mathematics, Aoyama Gakuin University, Sagamihara 229-8558, Japan*

Abstract

The detectability of the gravitational waves (GWs) from the Q-ball formation associated with the Affleck-Dine (AD) mechanism is studied. We take into account both of the dilution effect due to Q-ball domination and of finite temperature effects. We find that there is a finite but small parameter region where such GWs may be detected by future detectors such as DECIGO or BBO, only in the case when the thermal logarithmic potential dominates the potential of the AD field. Unfortunately, for such parameter region the present baryon asymmetry of the universe can hardly be explained unless one fine-tunes A-terms in the potential.

1 Introduction

Primordial gravitational waves (GWs) provide us with a lot of important information of the early universe. Recently, a new interesting mechanism to produce GWs was proposed in Refs. [1, 2], in which it is shown that significant GWs are generated during the Q-ball formation associated with Affleck-Dine (AD) mechanism of baryogenesis [3]. The AD mechanism implies the formation of non-topological solitons, Q-balls, whose existence and stability are guaranteed by a conserved charge, Q [4]. The Q-balls are formed by the amplification of fluctuation around homogeneous scalar fields that carry baryon or lepton number. Since this formation process of such Q-balls is inhomogeneous and not spherical, GWs can be generated during the formation.

In order to calculate the present properties of such GWs, one has to not only estimate the amount of GWs at the formation of Q-balls but also take into account the cosmic history after the production of the GWs. The energy density of the GWs at the Q-ball formation is proportional to some powers of the field value of the AD condensate, which implies that the initial energy density of the GWs becomes large if the typical charge Q of Q-balls is large. On the other hand, the lifetime of Q-balls becomes longer for larger Q because the temperature at the decay of Q-balls is typically proportional to the inverse square-root of the charge Q. Therefore, Q-balls with large Q can quickly dominate the energy density of the universe and hence dilute the GWs significantly. Thus, the detectability of such GWs is determined by the balance of the above two competing effects. In this study, we consider the decay of Q-balls without exotic effects by which Q-balls decay quickly and calculate the amplitude and frequency of GWs from Q-balls taking into account of the dilution factor correctly, which results in dramatic changes in the present amplitude of the GWs from the Q-ball formation.

The properties of the Q-balls depend on shape of the effective potential, which varies with the supersymmetry (SUSY) breaking mechanism and other effects. Thus, there are many types of Q-balls. Among them, thermal log type Q-balls that are formed by thermal (logarithmic) effects have an interesting feature. The energy density of this type of Q-balls decreases at least as rapid as radiation. This is because the thermal logarithmic potential itself also decreases with the cosmic expansion while the number of Q-balls in a comoving volume does not change. Hence, this type of Q-balls cannot dominate the energy density of the universe and do not dilute GWs. This is favorable for the detection of the

[1] This talk is based on [5].
[2] Email address: kamada@resceu.s.u-tokyo.ac.jp

GWs from the Q-ball formation because the dilution during the Q-ball dominated era is the main obstacle for the detection. Therefore, in this study, we concentrate on the thermal log type Q-balls and estimate the present amplitudes and frequencies of the GWs at the formation of such Q-balls. We show that such GWs may be detected by the next-generation gravitational detectors like DECIGO and BBO if particular conditions of reheating temperature, the initial field value of the AD field, gravitino mass and messenger mass are realized in the gauge mediated SUSY breaking model. However, we also find that such a condition spans a very small region in the parameter space. Moreover, we also find that it is difficult to explain the present baryon asymmetry for such a parameter region unless one fine tunes the CP-violating A-terms in the potential.

2 Affleck-Dine mechanism and Q-ball

In supersymmetric theories, there are many flat directions along which the scalar potentials become flat in the global SUSY limit and some of them carry baryon and/or lepton number. In the realistic world, SUSY is broken and the potentials for the flat directions are slightly lifted, the way of which depends on the SUSY breaking mechanism. Moreover, in the presence of thermal plasma [3], it also acquires thermal corrections. Thus, scalar fields that moves along a flat direction feels a force from the potentials. Their dynamics can be expressed in terms of a scalar field Φ (AD field). Hereafter we only consider the dynamics of a AD field $\Phi = \phi e^{i\theta}/\sqrt{2}$.

In the early universe, the AD field can acquire large field values. Then it starts to rotate around the origin when the Hubble parameter reaches its effective mass. The angular velocity is provided by CP-violating A-terms from the SUSY breaking effects. If the AD field carries baryon or lepton charge β_c, the angular momentum of the motion in the complex plane of the AD field represents the baryon or lepton number density given by

$$n_B(t_{\rm osc}) = i\beta_c(\dot{\Phi}^*\Phi - \Phi^*\dot{\Phi}) \simeq \beta_c a_m m_{3/2}\phi_{\rm osc}^2, \tag{1}$$

which implies that baryon or lepton asymmetry is generated in the universe. Here a_m is a CP-violating parameter of the order of unity in general, $m_{3/2}$ is the gravitino mass and $\phi_{\rm osc} = |\Phi_{\rm osc}|/\sqrt{2}$ is the amplitude of the AD field at the onset of the rotation around the origin.

Next we consider the Q-ball formation. Fluctuations around the homogeneous mode feel spatial instabilities and grow nonlinearly during the oscillation of the AD field and eventually form clumpy objects, Q-balls, if $V(\phi)/\phi^2$ has a global minimum at $\phi = \phi_{\rm min} \neq 0$ [4]. In many cases, Q-balls are formed just after the onset of the rotation of the AD field.

The way of amplification of fluctuations and the properties of Q-balls are different with the potential for the AD field. When thermal logarithmic potential,

$$V_{\rm thermal} \simeq \alpha_g^2 T^4 \log\left(\frac{|\Phi|^2}{T^2}\right), \tag{2}$$

dominates the potential for the AD field, these thermal log type Q-balls have an interesting character. Since the dominant contribution to the potential depends on the temperature which changes with the cosmic time, the properties of Q-balls change as well. Moreover, for some temperatures, other contributions can dominate the thermal logarithmic contribution in the potential, which implies that the properties of Q-balls may drastically change and Q-balls may disappear if the dominant contribution of the potential does not allow a Q-ball solution. In the gauge mediated SUSY breaking mechanism, for example, the potentials that dominate the potential for the AD field afterwards should be

$$V_{\rm grav} = m_{3/2}^2\left[1 + K\log\left(\frac{|\Phi|^2}{M_G^2}\right)\right]|\Phi|^2 \quad \text{and} \quad V_{\rm gauge} = M_F^4\left(\log\frac{|\Phi|^2}{M_S^2}\right)^2. \tag{3}$$

Here M_F is the messenger mass in the gauge mediated SUSY breaking models. When $V_{\rm grav}$ with positive K dominates first, the fate of Q-balls is rather complicated. This potential does not allow a Q-ball

[3] Thermal plasma can exist even before the reheating from inflaton decay, because its partial decay products are easily thermalized.

solution and hence the almost homogeneous AD field is recovered. After this transition, the value of the AD field decreases due to the cosmic expansion. Thus, $V_{\rm gauge}$ dominates $V_{\rm grav}$ gradually, which implies that Q-balls are formed again.

Q-balls or the homogeneous AD field can dominate the energy density of the universe from when $V_{\rm grav}$ dominates the potential. Thus, it is important to estimate the time when they dominate the energy density of the universe and their decay rate. The Q-ball domination time can be evaluated by the energy density of the Q-balls at the Q-ball formation and the Q-ball transformation time. In the case described above, the Hubble parameter at the Q-ball domination is given by [5]

$$H_{\rm dom} \simeq 10^{-3} \frac{m_{3/2}^2 \phi_{\rm osc}^8}{M_G^7 T_R^2}, \tag{4}$$

where M_G is the reduced Planck mass and T_R is the reheating temperature.

Then we consider the decay rate of Q-balls. Q-balls can decay into light fermions if the decay processes are kinematically allowed. However, in their interiors the Pauli exclusion principle forbids their decays into fermions [6]. Therefore Q-balls can decay only from their surfaces. This sets the upper bound on the decay rate of Q-balls, and in fact, it is almost saturated for the cases we are interested in [6]. In the case described above, the Hubble parameter at the Q-ball domination is given by [5]

$$H_{\rm dec} \simeq 0.3 \times \frac{m_{3/2}^5}{M_F^4}. \tag{5}$$

3 Gravitational waves from Q-ball formation

Now we consider the generation of the GWs. As mentioned before, the process of formation of Q-balls is inhomogeneous and not spherical. Thus, GWs are emitted at that time. In the case of the thermal log type Q-balls, the density parameter of the GWs from Q-balls and their typical frequency are given by [5]

$$\Omega_{\rm GW}^* \simeq 2 \times 10^{-6} \left(\frac{\phi_{\rm osc}}{M_G} \right)^4, \quad \text{and} \quad f_* \simeq 0.04 \times \frac{T_{\rm osc}^2}{\phi_{\rm osc}}. \tag{6}$$

The energy density of the GWs can be rather large if $\phi_{\rm osc}$ is large.

The density parameter of GWs are diluted during the inflaton oscillation dominated era, the Q-ball dominated era and recent matter and dark energy dominated era, and their frequency is also redshifted by cosmic expansion. Thus, the present properties of the GWs from the Q-ball formation are given by [5],

$$\Omega_{\rm GW}^0 \simeq \Omega_{\rm GW}^* \times \begin{cases} \left(\dfrac{H_R}{H_*} \right)^{2/3} \left(\dfrac{H_{\rm dec}}{H_{\rm dom}} \right)^{2/3} \dfrac{a_{eq}}{a_0} & (\text{with Q} - \text{ball domination}), \\ \left(\dfrac{H_R}{H_*} \right)^{2/3} \dfrac{a_{eq}}{a_0} & (\text{without Q} - \text{ball domination}), \end{cases} \tag{7}$$

$$f_0 \simeq f_* \times \begin{cases} \dfrac{T_0}{T_R} \left(\dfrac{H_{\rm dec}}{H_{\rm dom}} \right)^{1/6} \left(\dfrac{H_R}{H_*} \right)^{2/3} & (\text{with Q} - \text{ball domination}), \\ \dfrac{T_0}{T_R} \left(\dfrac{H_R}{H_*} \right)^{2/3} & (\text{without Q} - \text{ball domination}). \end{cases} \tag{8}$$

Here T_0 is temperature at present and $a_{\rm eq}$ and a_0 are the scale factors at the matter-radiation equality and at present, respectively.

When in the gauge mediated SUSY breaking mechanism with $V_{\rm grav}(K > 0)$, we find that when

$$M_F \simeq 10^4 {\rm GeV}, \quad m_{3/2} \simeq 10 {\rm GeV}, \quad \phi_{\rm osc} \simeq M_G \quad \text{and} \quad T_R \simeq 10^{10} {\rm GeV}., \tag{9}$$

there is Q-ball dominated era and we have $\Omega_{\rm GW} \simeq 10^{-16}$ for $f_0 \simeq 10$ [Hz] [5]. This is on the edge of the DECIGO or BBO sensitivity range. Thus, it is difficult but not impossible to detect such GWs by the

next generation detectors. Moreover there is no other parameter set to realize GW emissions suitable for detection [5]. One should notice that though gravitino does not overclose the universe because of large entropy production from Q-ball decay, the next-to-lightest supersymmetric particle (NLSP) decay may spoil the success of the BBN in some cases since the hadronic decay product of NLSP would destroy the light elements.

Here we comment on the present baryon and lepton asymmetry. In the situation where the GWs from the Q-ball formation might be detected, both present baryon/lepton asymmetry and radiation are generated by the Q-ball decay. The present baryon/lepton-to-entropy ratio would be rather large and be of the order of unity unless the parameter in the A-term, a_m, is strongly suppressed. In the case of Q-ball with baryonic charge, it is far beyond the experimental bound on the present baryon asymmetry. Even in the case of L-balls, that is, Q-balls with lepton charge but without baryon charge, the situation does not change since the decay temperature of Q-ball is about 500 GeV and hence the lepton asymmetry is converted to baryon asymmetry by sphaleron process that conserves $B-L$ charge. The way to avoid such large baryon/lepton asymmetry in this scenario is that the Q-balls are made of the AD field with $B-L=0$. In this case, however, we need other baryogenesis mechanisms.

4 Conclusion

In this study, we have discussed the detectability of the GWs from the Q-ball formation. At the Q-ball formation, Q-balls with large Q can produce a large amount of GWs. However, such Q-balls decay slowly and they may dominate the energy density of the universe so that GWs are significantly diluted. Therefore the detectability of the GWs is determined by these two competing effects.

We have shown that in the gauge mediated SUSY breaking model, if the reheating temperature is $T_R \simeq 10^{10}$ GeV and the initial field value of the AD field is $\phi_{\rm osc} \simeq M_G$ with $m_{3/2} \simeq 10$GeV and $M_F \simeq 10^4$ GeV, the present density parameter of the GWs from the Q-ball formation can be as large as $\Omega^0_{\rm GW} \simeq 10^{-16}$ and their frequency is $f_0 \simeq 10$ Hz. Thus, it is difficult but not impossible to detect them by next-generation gravitational detectors like DECIGO or BBO, but the parameter region for detectable GWs is very small. In other cases, it is shown that it is almost impossible to detect GWs from Q-ball formation [5].

Moreover, there are difficulties in this successful parameter region. One is that such parameter region predicts too large baryon asymmetry. Thus, once the GWs from the Q-ball formation are detected, we have the following two possibilities. In the case that such Q-balls are responsible for the present baryon asymmetry, the A-terms are suppressed by symmetry reason. The second option is that Q-balls are irrelevant for baryogenesis, which is realized for the AD fields with $B-L=0$. Another is the identification of such GWs. A first order phase transition in the early universe would produce similar spectrum of GWs. However, in our case, the gravitino mass must be around 10 GeV for the detection of the GWs from the Q-ball formation. Thus, if collider experiments could determine the gravitino mass by measuring the lifetime of the NLSP, that would provide complemental information or even rule out this scenario.

References

[1] A. Kusenko and A. Mazumdar, Phys. Rev. Lett. **101**, 211301 (2008) [arXiv:0807.4554 [astro-ph]].

[2] A. Kusenko, A. Mazumdar and T. Multamaki, Phys. Rev. D **79**, 124034 (2009) [arXiv:0902.2197 [astro-ph.CO]].

[3] I. Affleck and M. Dine, Nucl. Phys. B **249**, 361 (1985).

[4] S. R. Coleman, Nucl. Phys. B **262**, 263 (1985) [Erratum-ibid. B **269**, 744 (1986)].

[5] T. Chiba, K. Kamada and M. Yamaguchi, arXiv:0912.3585 [astro-ph.CO].

[6] A. G. Cohen, S. R. Coleman, H. Georgi and A. Manohar, Nucl. Phys. B **272**, 301 (1986).

Boson Stars under Deconstruction

Nahomi Kan[1(a)] and Kiyoshi Shiraishi[2(b)]

[(a)] *Yamaguchi Junior College, Hofu-shi, Yamaguchi 747-1232, Japan*
[(b)] *Yamaguchi University, Yamaguchi-shi, Yamaguchi 753-8512, Japan*

Abstract

We study solutions for boson stars in multiscalar theory. We start with simple models with N scalar theories. Our purpose is to study the models in which the mass matrix of scalars and the scalar couplings are given by an extended method of dimensional deconstruction. The properties of the boson stars are investigated by the Newtonian approximation with the large coupling limit.

1 Introduction

Boson Stars (BSs) have been studied in expectation of solving the rotation curve (RC) problem. Many authors have attempted to explain RC of galaxies by assuming the existence of the galactic scale BS. In order to fit the observable data, the mass density of BS needs to be widely distributed. This configuration can be constructed by the models such as BSs with scalar particles in excited states or the rotating BSs, but these BSs are unstable. Whereas Newtonian BSs with all the particles in only one ground state is stable, it is difficult to illustrate the realistic RC. Alternative models to solve these problems have been studied by Matos and Ureña-López [1], and recently by Bernal *et al.* [2]. They considered the multi-state BS, *i. e.* scalar fields both in ground and in excited states, with no (quadratic) self-couplings.
In the present work, We consider multi-kind scalar BS, not multi-states. We suggest several models. The first model contains two scalar particles with self- and mutual-couplings. [3] The second model is build up under dimensional deconstruction (DD). This model contains N scalar particles interacting with oneself and with adjacent scalars. DD has an aspect of latticized extra dimensions, and the latter model could be an alternative to a higher dimensional BS. In each model, we examine BS with large coupling limit. We also consider BSs under extended DD. In this model, DD is generalized to field theory based on a *graph*, and the interactions between scalar particles are restricted by supersymmetry (SUSY).

2 Non-Relativistic Multi-scalar Boson Star

We consider a BS model, in which two scalar particles ψ_1 and ψ_2 with self- and mutual-couplings g_{ij}, described by the Hamiltonian:

$$\begin{aligned} H-\mu_1\tilde{N}_1-\mu_2\tilde{N}_2 &= \frac{\hbar^2}{2m_1}|\nabla\psi_1|^2+\frac{\hbar^2}{2m_2}|\nabla\psi_2|^2+\left(m_1|\psi_1|^2+|\psi_2|^2\right)\phi+\frac{1}{8\pi G}(\nabla\phi)^2 \\ &\quad -\mu_1|\psi_1|^2-\mu_2|\psi_2|^2+\frac{1}{4}\frac{\hbar^3}{c}\left(\frac{g_{11}}{{m_1}^2}|\psi_1|^4+2\frac{g_{12}}{m_1m_2}|\psi_1|^2|\psi_2|^2+\frac{g_{22}}{{m_2}^2}|\psi_2|^4\right), \end{aligned} \tag{1}$$

where $\tilde{N}_i$ and μ_i are the number density and the chemical potential of the i-th scalar, respectively, whereas ϕ is the gravitational potential. We also normalize the particle number to $N_i=\int d^3r|\psi_i|^2$. In the large coupling limit [6], the equations of motion are as follows:

$$\nabla^2\phi=4\pi G(m_1|\psi_1|^2+m_2|\psi_2|^2), \tag{2}$$

$$m_1\phi\psi_1+\frac{1}{2}\left(\frac{g_{11}}{{m_1}^2}|\psi_1|^2+\frac{g_{12}}{m_1m_2}|\psi_2|^2\right)=\mu_1\psi_1, \tag{3}$$

$$m_2\phi\psi_2+\frac{1}{2}\left(\frac{g_{22}}{{m_2}^2}|\psi_2|^2+\frac{g_{12}}{m_1m_2}|\psi_1|^2\right)=\mu_2\psi_2, \tag{4}$$

[1]Email address: kan@yamaguchi-jc.ac.jp
[2]Email address: shiraish@yamaguchi-u.ac.jp
[3]Interacting boson stars and Q-balls have been studied by Brihaye *et al.* [3–5].

where $\hbar = c = 1$. In the core of the BS, where $\psi_1 \neq 0, \psi_2 \neq 0$, the gravitational potential becomes

$$\phi + const. \propto -\frac{\sin(\omega r)}{r}, \tag{5}$$

where r is the distance from the center of the BS, and

$$\omega^2 = 8\pi G \frac{{m_2}^4 g_{11} - 2{m_1}^2{m_2}^2 g_{12} + {m_1}^4 g_{22}}{g_{11}g_{22} - {g_{22}}^2}. \tag{6}$$

The outside of the BS, where $\psi_1 \neq 0, \psi_2 = 0$, the gravitational potential is

$$\phi + const. \propto -\frac{\sin(\omega_1 r + \delta)}{r}, \tag{7}$$

with $\omega_1 = 8\pi G {m_1}^4/{g_{11}}^2$. The typical structure of BS are shown in Fig. 1 and the rotational curves in Fig. 2. We can find that the gravitational potential is spread out by the existence of Ψ_1, and which leads to an improvement of RC. If a single scalar field model is considered, which realized by $\Psi_2 = 0$ in (1), the

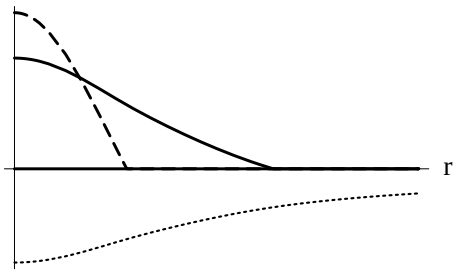

Figure 1: The behavior of the scalar fields Ψ_1, Ψ_2 and the gravitational potential ϕ as the function of the rescaled distance r. The solid line, the broken line and the dotted line represent Ψ_1, Ψ_2 and ϕ, respectively. The potential is spread out by the existence of Ψ_1.

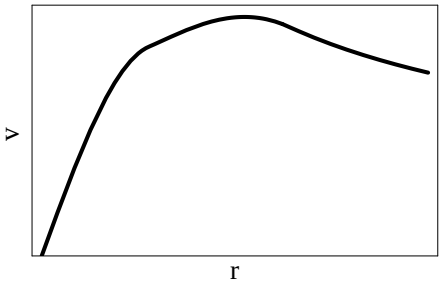

Figure 2: The behavior of the rotational velocity v as the function of the rescaled distance r. The multi-scalar configuration improve RC.

range of the gravitational potential becomes narrow (Fig. 3), and the RC looks far from a satisfactory explanation of the observational data (Fig. 4).

3 General-Relativistic Boson Star under Deconstruction

We propose three models of BSs under the DD scheme.

3.1 Static and Spherical Boson Star

We consider self-interacting $U(1)$ scalar field theory in DD. This model is described by the action:

$$S_B = \int d^4x\sqrt{-g}\sum_{i=1}^{N}\left\{|\partial_\mu\phi_i|^2 - m^2|\phi_i|^2 - f^2|\phi_{i+1} - \phi_i|^2 - \frac{\tilde{\lambda}N}{2}|\phi_i|^4\right\}. \tag{8}$$

If $f = 0$, $[U(1)]^N$ symmetry recovers. Ansatz for a static and spherical BS: $\phi_i(x) = \frac{1}{\sqrt{N}}\phi(r)e^{-i\omega t + i\theta_i}$, where θ_i is a constant number, leads to the square of a scalar boson mass:

$$m^2 + \frac{f^2}{N}\sum_{i=1}^{N}|1 - \mathrm{e}^{i(\theta_{i+1}-\theta_i)}|^2 \equiv m_b^2, \tag{9}$$

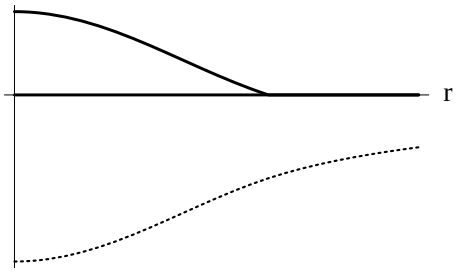

Figure 3: The behavior of the scalar field and the gravitational potential as the function of the rescaled distance r. The solid line represents the scalar field, whereas the dotted line represents the gravitational potential. Compared to the two scalar field model (Fig. 1), the range of the potential becomes narrow.

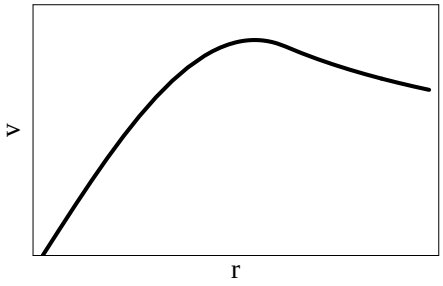

Figure 4: The behavior of the rotational velocity v as the function of the rescaled distance r. The RC looks far from a satisfactory explanation of the observational data.

and to the charge density:

$$\sum_{i=1}^{N} i(\phi_i^* \partial_0 \phi_i - \phi_i \partial_0 \phi_i^*) = 2\omega\phi(r)^2, \tag{10}$$

where the charge are equally distributed on each site. The BS mass made of a single scalar with mass m_b becomes $M_{BS} \sim \frac{M_{pl}^2}{m_b}$ for no coupling, whereas $M_{BS} \sim \sqrt{\tilde{\lambda}}\frac{M_{pl}^3}{m_b^2}$ for large coupling, where we use the convention of Jetzer [7]. Stars with these maximum masses are stable. If $\theta_1 = \cdots = \theta_N$, or $N \to \infty$, Kaluza-Klein (KK) theory is recovered and BSs are made of the zero-mode field with a minimum mass $(m_b^2)_{min} = m^2$.

3.2 Boson Star under Generalized Deconstruction –SUSY-inspired model–

We extend DD to the model based on graph theory. In this model, a continuum limit is not necessary, and $U(1)$ interactions at each site (vertex) of an arbitrary graph is still invariant. We also assume SUSY in order to restrict the other interactions [8], and then simplify the interaction terms. This model is described by the action:

$$S_B = \int d^4x\sqrt{-g} \sum_{i,j=1}^{N} \left\{ |\partial_\mu \phi_i|^2 - m^2|\phi_i|^2 - f^2 \phi_i^* \triangle_{ij} \phi_j - \frac{N\Lambda_{ij}}{2}|\phi_i|^2|\phi_j|^2 \right\}, \tag{11}$$

where $\lambda = \sum_{i,j} \Lambda_{ij}$, and $\triangle$ is graph laplacian. Unfortunately, this model also describes a single $U(1)$ charge in general. Thus the most probable BS in this model is made of a scalar field with the minimum mass.

3.3 Graph-oriented model

Characteristic matrices associated with a graph are the graph laplacian $\triangle$ and identity matrix. We expand the scalar field by the eigenvector of the graph laplacian, such as $\vec{\phi} = \{\phi_1, \phi_2, \cdots, \phi_N\} = \sum_{a=1}^{N} \phi_a \vec{x}_a$, where $\triangle \vec{x}_a = \lambda_a \vec{x}_a$, and $\vec{x}_a \cdot \vec{x}_b = \delta_{ab}$, as usual. In this notations, BS based on the graph with p vertices and q edges is described by the action:

$$S_B = \int d^4x\sqrt{-g} \left\{ \partial\vec{\phi}^\dagger \cdot \partial\vec{\phi} - m^2|\vec{\phi}|^2 - f^2 \vec{\phi}^\dagger \triangle \vec{\phi} - \frac{\Lambda_p}{2}(|\vec{\phi}|^2)^2 - \Lambda_q |\vec{\phi}|^2 \vec{\phi}^\dagger \triangle \vec{\phi} - \frac{\Lambda_r}{2}(\vec{\phi}^\dagger \triangle \vec{\phi})^2 \right\}. \tag{12}$$

If $\phi_3 = \cdots = \phi_N = 0$ and $\lambda_1 = 0$, a boson mass becomes $m_a = \sqrt{m^2 + f^2\lambda_a}$ and interaction terms are

$$-\frac{\Lambda_p}{8}\left(\frac{|\psi_1|^2}{m_1} + \frac{|\psi_2|^2}{m_2}\right)^2 - \frac{\Lambda_q}{4}\lambda_2\frac{|\psi_2|^2}{m_2}\left(\frac{|\psi_1|^2}{m_1} + \frac{|\psi_2|^2}{m_2}\right) - \frac{\Lambda_r}{8}{\lambda_2}^2\frac{|\psi_2|^4}{m_2}, \tag{13}$$

where $\psi_a \equiv \sqrt{2m_a}\phi_a e^{im_a t}$. Self- and mutual-couplings g_{ij} can be read from (13), such as $g_{11} = \Lambda_q/4$, and so on. By similar ways, we can obtain systematic construction of many-scalar models with several conserved charges.

4 Summary and Outlook

We have examined the Newtonian boson star with two $U(1)$ charges in the large-coupling limit. The understanding of rotation curves of galaxies are improved in this model. We have also examined BSs under deconstruction. In the continuum limit, it is found that the possible BS is made of "zero mode" field. We have suggested two models of BSs based on graph theory.
As future work, we will consider general relativistic BSs and graph-oriented models with many charges or arbitrary couplings. We will also investigate excited states under the condition of fixing the mass and size of BSs. Time dependent solutions or oscillations are also interesting. We wish to study these subjects, elsewhere.

Acknowledgements

The authors would like to thank K. Kobayashi for useful comments, and also the organizers of JGRG19.

References

[1] T. Matos and L. Arturo Ureña-López, Gen. Rel. Grav. **39**, 1279 (2007).

[2] A. Bernal, J. Barranco, D. Alic and C. Palenzuela, [arXiv:0908.2435 [gr-qc]].

[3] Y. Brihaye, T. Caebergs, B. Hartmann and M. Minkov, Phys. Rev. D **80**, 064014 (2009).

[4] Y. Brihaye and B. Hartmann, Phys. Rev. D **79**, 064013 (2008).

[5] Y. Brihaye and B. Hartmann, Nonlinearity **21**, 1937 (2008).

[6] M. Colpi, S. L. Shapiro and I. Wasserman, Phys. Rev. Lett. **57**, 2485 (1986).

[7] P. Jetzer, Phys. Rep. **220**, 163 (1992).

[8] N. Kan, K. Kobayashi and K. Shiraishi, Phys. Rev. D **80**, 045005 (2009); [arXiv:0901.1168 [hep-th]].

Quantum Back Reaction to asymptotically AdS Black Holes

Kazumi Kashiyama[1(a)], Norihiro Tanahashi[2(a)], Antonino Flachi[3(b)], and Takahiro Tanaka[4(b)]

[(a)] *Department of Physics, Kyoto University, Kyoto 606-8502*
[(b)] *Yukawa Institute for Theoretical Physics, Kyoto University, Kyoto 606-8502*

Abstract

We analyze the effects of the back reaction due to a conformal field theory (CFT) on a black hole spacetime with negative cosmological constant. We study the geometry numerically and take into account the energy momentum tensor of CFT approximated by a radiation fluid. We find a sequence of configurations without a horizon in thermal equilibrium (*CFT stars*), followed by a sequence of configurations with a horizon. We discuss the thermodynamic properties of the system and how back reaction effects alter the space-time structure. We also provide an interpretation of the above sequence of solutions in terms of the AdS/CFT correspondence. The dual five-dimensional description is given by the Karch-Randall model, in which a sequence of five-dimensional floating black holes followed by a sequence of brane localized black holes correspond to the above solutions.

In this brief note, we will report on our study of quantum back reaction effects for black hole spacetime with negative cosmological constant. For brevity we limit our selves to present the main results and invite the interested reader to consult the Ref. [1] for details.

The main issue that triggerd our attention in the problem is that in the Randall-Sundrum model [2] (RS) no *large*, stable, static black hole solution localized on the brane or floating in the bulk have so far been found, whereas *small* localized solutions have been constructed numerically [3] for black holes with size smaller than the curvature scale l. The above situation is in tune with the prediction of the AdS/CFT correspondence [4] and suggests the absence of static 4D black holes that would evaporate due to the presence of the CFT. The absence of 4D static solutions, according to the correspondence, would imply the existence of a 5D classical dynamical process analogous to the 4D quantum evaporation, clarifying why 5D solutions cannnot be found [5, 6].

It is clearly difficult to provide any relevant (numerical) proof, and it makes sense to take an indirect approach by considering modifications to the RS model. A natural thing to do is to relax the asymptotic structure of the branes, and consider the Karch-Randall model (KR) where branes are asymptotically AdS [7].

Contrary to the RS model, in the KR model a stable small black hole solution is expected to exist at a certain distance from the brane. This *floating* black hole is infinitely far from the brane in the RS limit of the KR model [8]. As in the RS model, the AdS/CFT correspondence works also in the KR model, but with a very different outcome. As we have mentioned, in the RS model the CFT back reaction causes the black hole to evaporate preventing the staticity of the solution. (For clarity, we mention that, since we are interested in equilibrium configurations, the vacuum state that we consider throughout the paper refers to the Hartle-Hawking state.) In the KR model, the branes are asymptotically AdS, and the presence of a non-zero cosmological constant changes the situation dramatically. Since the lapse function in AdS behaves at large distances as r/L (L is the 4D AdS curvature scale), the temperature and hence the energy density of (thermal) CFT decrease rapidly for $r \gg L$, reducing the effects of the back reaction. If the black hole size is large, the energy density due to CFT will stay negligiblly small at any radius. On the other hand, if the size of the black hole is small, the back reaction becomes important and a

[1]Email address: kashiyama@tap.scphys.kyoto-u.ac.jp
[2]Email address: tanahashi@tap.scphys.kyoto-u.ac.jp
[3]Email address: flachi@yukawa.kyoto-u.ac.jp
[4]Email address: tanaka@yukawa.kyoto-u.ac.jp

static black hole solution becomes non-trivial. Roughly speaking, such a small black hole will be unstable against the CFT back reaction and should evaporate into a CFT star of the same mass.

The sequence of the CFT stars can be tagged by the central density, and the end-point of the sequence corresponds to a star with singular central density and lapse vanishing at the center. Thus, this sequence of the CFT stars will naturally flow into the sequence of quantum corrected black holes, whose starting-point corresponds to a small black hole in the limit of zero horizon radius.

According to the AdS/CFT correspondence, we may expect that a five-dimensional black hole in the KR model will be dual to the above sequence of 4D CFT stars and quantum black holes [8]. Naive expectation is that a brane-localized black hole and a floating black hole in the KR model are, respectively, dual to a four-dimensional black hole with back reaction of CFT halo and a star composed of CFT, which we refer to as quantum black hole and CFT star. If it is really the case, we can examine black holes in the KR model by analyzing the four-dimensional system. Thus, we can interpret the sequence, the lapse vanishes at the center of the system. This four-dimensional configuration corresponds to a five-dimensional black hole floating in the bulk and just touching the brane, since the lapse vanishes at the touching point for this five-dimensional configulation too. In this way, we may speculate that the sequence of black holes corresponds to the sequence of CFT stars, while the sequence of brane-localized black holes corresponds to the sequence of quantum black holes.

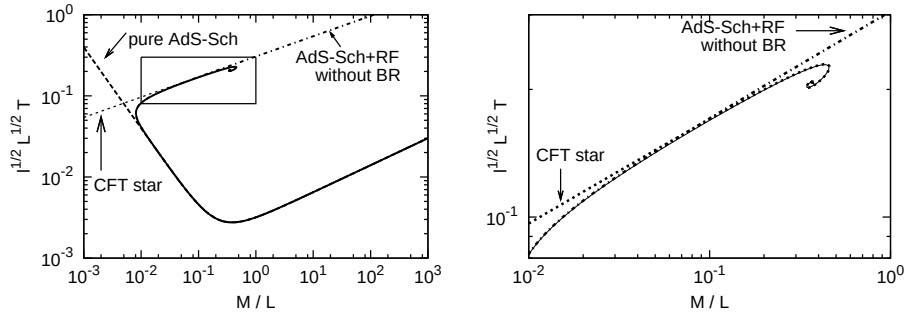

(a) Phase diagram of quantum corrected black hole and CFT star

(b) Closeup of the transition point

Figure 1: Relation between M and T for CFT stars (dotted line) and quantum black holes (solid line). For the black hole system, we set $\ell/L = 10^{-4}$. To understand the back reaction effect more clearly we add temperature-energy relation for Schwarzschild AdS space with (dotted-dashed line) and without (dashed line) the contribution of the radiation fluids. The right panel shows the closeup around the transition point.

In Ref. [1] we have studied the relevant quantum back reaction problem and illustrated explicitly the above picture. Hence, for brevity, we will only report the results for the thermodynamical quantities.

Figure 1 shows the relation between the total mass M and temperature of the system T. The dotted line refers to the star sequence, while the solid line to the quantum black hole sequene. In order to clarify the back reaction effects, two additional reference curves are also shown in the same figure. The dashed line refers to the purely Schwarzschild AdS black hole case, and the dotted-dashed line refers to the sum of the black hole mass and the energy due to the CFT without taking into account the back reaction to the geometry. The smooth transition between the sequences of CFT stars and quantum black holes is evident.

Figure 2 shows the total entropy of CFT stars (left panel) and quantum black holes (right panel) with respect to the central density of the star and black hole horizon radius, respectively. In the right panel we set the parameter $\ell/L = 10^{-3}$(solid line), 10^{-4} (dashed line) and 10^{-5} (dotted line). Again, the two sequences are connected in the limit of infinite central density for the star configuration sequence, and in the limit of vanishing horizon radius for the black hole sequence. A CFT star with large central density 'becomes' a small mass black hole at the connection point. The transition occurs at

$$M/L = 0.36\ ,\ \ell^{1/2}L^{1/2}T = 0.21\ ,\ \ell^{-1/2}L^{-3/2}S = 2.0\ . \tag{1}$$

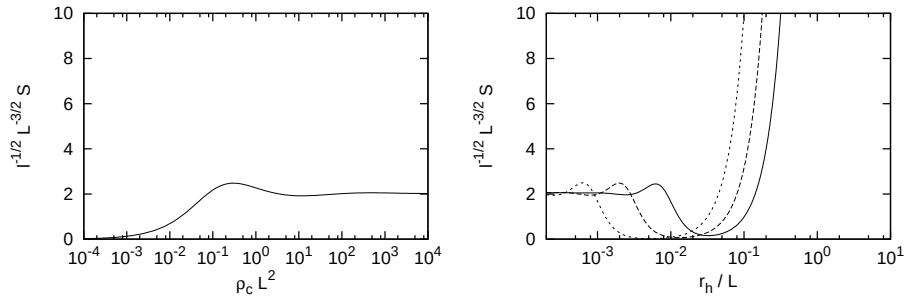

(a) CFT star (b) Black hole + CFT

Figure 2: Total entropy of CFT stars (left panel) and quantum black holes (right panel) with respect to the central density of the star and black hole horizon radius, respectively. In the right panel we set the parameter $\ell/L = 10^{-3}$ (solid line), 10^{-4} (dashed line) and 10^{-5} (dotted line).

These critical values do not depend on the ratio ℓ/L.

The AdS/CFT correspondence relates the above sequence of 4D CFT stars and quantum black holes, to a sequence of classical 5D floating and localized black holes in KR model. For instance, one can estimate the expected size of the classical black hole on the 5D side and the transition points, by relating the entropy to the area of black hole horizon. Here, we spare the details of the discussion that can be found in Ref.[1] and conclude by summarizing the expected phase diagram of black hole solutions in the KR model in Figure 3. We claimed that (i) there are stability changing points along the sequence of brane-localized black hole solutions. The first transition corresponding to the minimum total mass of the system occurs when the five-dimensional horizon radius is $\approx 0.7 \cdot (\ell^3 L^2)^{1/5}$; (ii) the sequence of bulk floating black holes leads to the sequence of brane-localized black holes and this transition between these two sequences occurs when the black hole temperature is $\approx 0.21 \cdot (\ell L)^{-1/2}$ and the five-dimensional black hole horizon radius is $\approx 0.7 \cdot (lL)^{1/2}$.

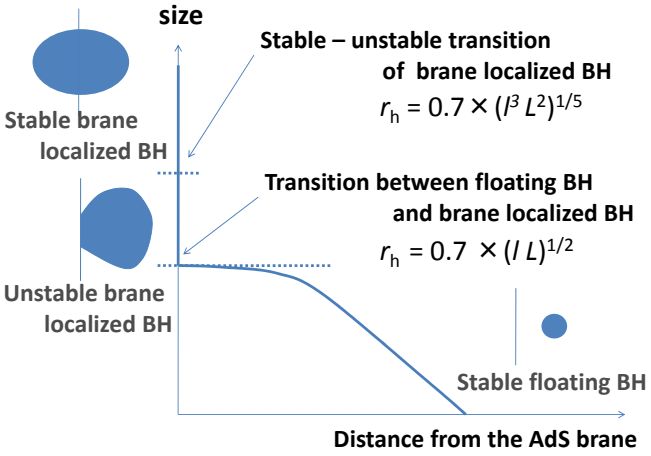

Figure 3: Phase diagram of BH solutions in the KR model.

acknowledgments

This work is supported by the JSPS through Grants Nos. 19540285, 19GS0219, 2056381, 20740133, 21244033. We also acknowledge the support of the Global COE Program "The Next Generation of Physics, Spun from Universality and Emergence" from the Ministry of Education, Culture, Sports, Science and Technology (MEXT) of Japan.

References

[1] K.Kashiyama et al., J. High Energy Phys. **01** 099 (2010).

[2] L. Randall, R. Sundrum, Phys. Rev. Lett. **83** 4690 (1999).

[3] H. Kudoh, T. Tanaka, N. Nakamura, Phys. Rev. D **68** 024035 (2003).

[4] J. M. Maldacena, Adv. Theor. Math. Phys. **2** 231 (1998).

[5] T. Tanaka, Prog. Theor. Phys. Suppl. **148** 307 (2003).

[6] R. Emparan, A. Fabbri, N. Kaloper, J. High Energy Phys. **0208** 043 (2002).

[7] A. Karch, L. Randall, J. High Energy Phys. **05** 008 (2001).

[8] T. Tanaka, Prog. Theor. Phys. Suppl. **121** 1133 (2009)

Dynamical Black Rings with a Positive Cosmological Constant

Masashi Kimura[1]

Department of Mathematics and Physics, Graduate School of Science, Osaka City University, 3-3-138 Sugimoto, Sumiyoshi, Osaka 558-8585, Japan

Abstract

We construct dynamical black ring solutions in the five dimensional Einstein-Maxwell system with a positive cosmological constant and investigate the geometrical structure. The solutions describe the physical process such that a thin black ring at early time shrinks and changes into a single black hole as time increase.

1 Introduction

Recently, higher dimensional black holes have attracted much attention in the context of string theory and the brane world scenario. In particular, the black ring solution [1] is one of the most important discovery because that means the uniqueness theorem does not hold in higher-dimensional space-time unlike the case of four-dimensional space-time and the shape of black objects can take various topology in higher-dimension. In fact, many solutions which have more complicated structure have been constructed (see [2, 3]).

It is interesting to have black ring solution with a cosmological constant in the context of AdS/CFT correspondence. However, by now, attempts to obtain regular black ring solution with a cosmological constant did not succeed [4, 5]. This might be because the co-existence of the scales of the diameter of black ring and the cosmological constant is difficult. In [6], Caldarelli et al. constructed solutions for thin black rings in dS and AdS space-times using approximate methods, and they mentioned static black ring can exist in the case of positive cosmological constant because of the force balance between gravitational force and repulsive force by cosmological constant.

We consider a possibility that solution is dynamical by the existence of positive cosmological constant unlike the other works so far. In general, it is difficult to obtain dynamical black hole solutions, however we can easily construct such the black hole solution in the case of the mass equal to the charge as is constructed by Kastor and Traschen [7]. Kastor-Traschen solution [7] was generalized to higher-dimension in [8] and coalescing black holes on Gibbons-Hawking space in [9, 10]. In this presentation, we discuss the dynamical black ring solution in a variation of the Kastor-Traschen solutions based on the paper [11].

2 Construction of Dynamical Black Ring Solutions

We consider five dimensional Einstein-Maxwell system with a positive cosmological constant, which is described by the action

$$S = \frac{1}{16\pi G_5}\int dx^5\sqrt{-g}(R - 4\Lambda - F_{\mu\nu}F^{\mu\nu}), \tag{1}$$

where R is the five dimensional scalar curvature, $F_{\mu\nu}$ is the Maxwell field strength tensor, Λ is the positive cosmological constant and G_5 is the five-dimensional Newton constant. From this action, we write down the Einstein equation

$$R_{\mu\nu} - \frac{1}{2}Rg_{\mu\nu} + 2g_{\mu\nu}\Lambda = 2\left(F_{\mu\lambda}F_{\nu}{}^{\lambda} - \frac{1}{4}g_{\mu\nu}F_{\alpha\beta}F^{\alpha\beta}\right), \tag{2}$$

and the Maxwell equation

$$F^{\mu\nu}{}_{;\nu} = 0. \tag{3}$$

[1]E-mail:mkimura@sci.osaka-cu.ac.jp

In this system, we consider the following metric and the gauge 1-form

$$ds^2 = -H^{-2}dt^2 + He^{-\lambda t}ds^2_{\mathrm{E}^4}, \tag{4}$$

$$A = \pm\frac{\sqrt{3}}{2}H^{-1}dt, \tag{5}$$

where $ds^2_{\mathrm{E}^4}$ is a four-dimensional Euclid space and $\lambda = \sqrt{4\Lambda/3}$ and the function H is

$$H = 1 + \frac{1}{e^{-\lambda t}}\Psi, \tag{6}$$

and the function Ψ is independent of time coordinate t. As shown in [7, 8], if the function Ψ is the solution of the Laplace equation on $ds^2_{\mathrm{E}^4}$

$$\triangle_{\mathrm{E}^4}\Psi = 0, \tag{7}$$

the metric (4) and the gauge-1-form (5) become solutions of five-dimensional Einstein-Maxwell system with a positive cosmological constant.[2]

In [8], the function Ψ was chosen as point source harmonics, and then the solution describes coalescence of multi-black holes with the topology of S^3. In construct, in this presentation, we focus on the ring source solutions of (7) given by

$$\Psi = \sum_i \frac{m_i}{\sqrt{(r_1+a_i)^2+r_2^2}\sqrt{(r_1-a_i)^2+r_2^2}} + \sum_i \frac{n_i}{\sqrt{r_1^2+(r_2+b_i)^2}\sqrt{r_1^2+(r_1-b_i)^2}}, \tag{8}$$

where we use the coordinate of $ds^2_{\mathrm{E}^4}$ as

$$ds^2_{\mathrm{E}^4} = dr_1^2 + r_1^2d\phi_1^2 + dr_2^2 + r_2^2d\phi_2^2, \tag{9}$$

and Ψ satisfies

$$\triangle\Psi = \sum_i \frac{m_i}{2\pi a_i}\delta(r_1-a_i)\delta(r_2) + \sum_i \frac{n_i}{2\pi b_i}\delta(r_1)\delta(r_2-b_i). \tag{10}$$

3 Global structure of single black ring solution

In this presentation, we focus on a single black ring solution, namely the harmonics Ψ takes the form

$$\Psi = \frac{m}{\sqrt{(r_1+a)^2+r_2^2}\sqrt{(r_1-a)^2+r_2^2}}. \tag{11}$$

In this case, the solution is dynamical because the topologies of the spatial cross section of the event horizon change from $\mathrm{S}^2\times\mathrm{S}^1$ at early time into S^3 at late time as shown in the following subsection.

3.1 Event Horizon

At $r := \sqrt{r_1^2+r_2^2} \to \infty$, the metric (4) behaves

$$ds^2 \simeq -\left(1+\frac{1}{e^{-\lambda t}}\frac{m}{r_1^2+r_2^2}\right)^{-2}dt^2 + \left(1+\frac{1}{e^{-\lambda t}}\frac{m}{r_1^2+r_2^2}\right)e^{-\lambda t}(dr_1^2+r_1^2d\phi_1^2+dr_2^2+r_2^2d\phi_2^2). \tag{12}$$

We can see the geometry described by (4) at large radius asymptotes to that of Reissner-Nordström-de Sitter solution. If $m < m_{\mathrm{ext}} = 16/(27\lambda^2)$, the metric (12) have a black hole horizon at $r\to\infty, t\to\infty$ s.t. $e^{-\lambda t}r^2 = x_h$ where x_h is a constant safisfies the equation

$$\lambda^2(x_h+m^3) - 4x_h^2 = 0. \tag{13}$$

So we can find event horizon of the metric (4) locally at late time around large radius.

Similar to the discussion in [13], by solving null geodesics from each point of the event horizons on $t =$ const. surface at late time to the past, we can get null geodesic generators of the event horizons, namely we can find the locations of the event horizons approximately. We plot coordinate value of event horizon in $r_1 - r_2$ plane at each time in Fig.1. From this, we can see that the topology of spatial cross section of event horizon at late time is S^3 and the topology of that at early time is $\mathrm{S}^1\times\mathrm{S}^2$.

[2] In [9, 12] the case of Gibbons-Hawking base space is discussed.

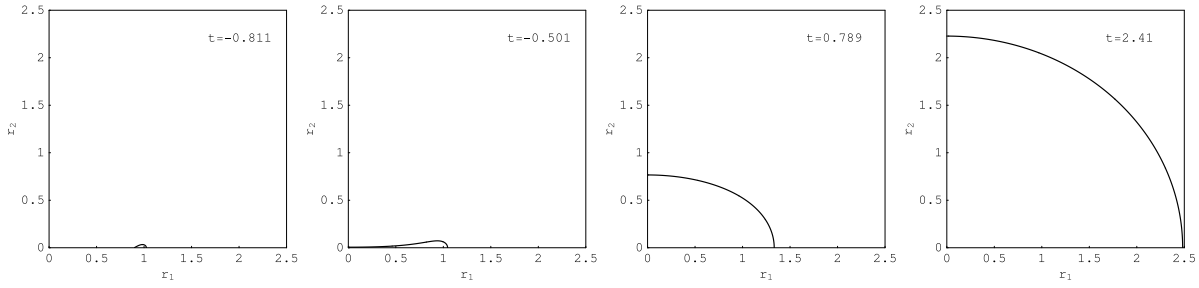

Figure 1: Time evolution of the event horizon for a single black ring in $r_1 - r_2$ plane. Coordinate values of event horizon of each time slices are plotted. We set parameters $\lambda = 1,\ m = 1/2,\ a = 1$.

3.2 Early Time Behavior

From Fig.1, at early time, we can see the event horizon locate on near the points of ring source of harmonics $r_1 = a, r_2 = 0$. So in this section, we study the geometrical structure near $r_1 = a,\ r_2 = 0$ analytically. Near the points $r_1 = a, r_2 = 0$, the metric (4) behaves

$$ds^2 \simeq -\left(1 + \frac{1}{e^{-\lambda t}}\frac{m}{2a\rho}\right)^{-2} dt^2 + \left(1 + \frac{1}{e^{-\lambda t}}\frac{m}{2a\rho}\right) e^{-\lambda t}\left(d\rho^2 + \rho^2(d\theta^2 + \sin^2\theta d\phi^2) + a^2 d\phi_1^2\right), \quad (14)$$

where we introduce new coordinate $\rho,\ \theta,\ \phi$ as

$$\rho\sin\theta\cos\phi = r_1 - a, \qquad \rho\sin\theta\sin\phi = r_2\sin\phi_2, \qquad \rho\cos\theta = r_2\cos\phi_2. \quad (15)$$

From this, we can see that the early time behavior is like black string. The metric (4) describes the physical process such that a thin black ring at early time shrinks and changes into a single black hole as time increase.

If we take $\lambda = 0$ limit of the metric (14), it reduce to the charged black string solution with the mass equal to the charge [14]. The charged black string solution [14] is regular solution which has two horizon if the mass is greater then the charge, but it has naked singularity at degenerated horizon if the mass equal to the charge. One may worry about that the metric (14) also has naked singularity. So, we investigate whether the singularities are hidden by the horizon, i.e., whether the null geodesic generators of event horizon reach $r_1 = a, r_2 = 0$ at a finite past time.

To do this we study null geodesics in the metric (14). The geometry of (14) has $SO(3) \times U(1)$ symmetry, so it is sufficient to focus on $t - \rho$ part of the metic (14). The null geodesics $\rho = \rho(t)$ which goes inward from the future to the past satisfies

$$\frac{d\rho}{dt} = \frac{1}{\sqrt{e^{-\lambda t}}}\left(1 + \frac{1}{e^{-\lambda t}}\frac{m}{2a\rho}\right)^{-3/2}. \quad (16)$$

The solution of this equation (16) asymptotes to

$$\rho(t) \to \frac{1}{e^{-2\lambda t}}\frac{\lambda^2 m^3}{2a^3}, \quad (17)$$

as $t \to -\infty$. So, we can see that the singularity is hidden by event horizon at least finite past time. However, in the $t \to -\infty$ limit along the event horizon (17), the curvature behaves

$$R_{\alpha\beta\mu\nu}R^{\alpha\beta\mu\nu} \sim e^{-4\lambda t} \to \infty, \quad (18)$$

but we consider this singularity is not so wrong as long as we focus on the region in which the time coordinate t takes finite values.

4 Summary and Discussion

In this presentation, we have discussed the dynamical black ring solutions in the five dimensional Einstein-Maxwell system with a positive cosmological constant. Our solution has constructed by use of ring source harmonics on four-dimensional Euclid space and this is analogous to the case of super-symmetric black ring solution [15]. In the case of single ring source harmonics, the solutions describe the physical process such that a thin black ring at early time shrinks and changes into a single black hole as time increase. In general, our solution can describe coalescence of multi black rings.

All regular black ring solutions so far found have angular momenta to keep balance between gravitational force and centrifugal force, otherwise there exist some singularities. On the other hand, our solutions do not rotate, i.e., do not have angular momentum, but clearly this has no conical singularity because of the way of the construction of the solution. We consider that this is because of the balance between gravitational force and electric force.

One of important point in this presentation is that if we set $\lambda = 0$ our solutions are static singular solutions which have curvature singularities at the points Ψ diverge, but in the case of $\lambda \neq 0$ our solutions become regular in the region in which the time coordinate t takes finite values since the event horizon encloses the singularities. This suggest that other harmonics which were not focused on so far also give regular solutions with various horizon topologies. It may be also interesting that this way applies to the case of dimensions higher than five.

Acknowledgements

The author would like to thank Hideki Ishihara for useful discussions. This work is supported by the JSPS Grant-in-Aid for Scientific Research No. 20·7858.

References

[1] R. Emparan and H. S. Reall, Phys. Rev. Lett. **88**, 101101 (2002) [arXiv:hep-th/0110260].

[2] R. Emparan and H. S. Reall, Class. Quant. Grav. **23**, R169 (2006) [arXiv:hep-th/0608012].

[3] R. Emparan and H. S. Reall, Living Rev. Rel. **11**, 6 (2008) [arXiv:0801.3471 [hep-th]].

[4] C. S. Chu and S. H. Dai, Phys. Rev. D **75**, 064016 (2007) [arXiv:hep-th/0611325].

[5] H. K. Kunduri, J. Lucietti and H. S. Reall, JHEP **0702**, 026 (2007) [arXiv:hep-th/0611351].

[6] M. M. Caldarelli, R. Emparan and M. J. Rodriguez, JHEP **0811**, 011 (2008) [arXiv:0806.1954 [hep-th]].

[7] D. Kastor and J. H. Traschen, Phys. Rev. D **47**, 5370 (1993) [arXiv:hep-th/9212035].

[8] L. A. J. London, Nucl. Phys. B **434**, 709 (1995).

[9] H. Ishihara, M. Kimura and S. Tomizawa, Class. Quant. Grav. **23**, L89 (2006) [arXiv:hep-th/0609165].

[10] C. M. Yoo, H. Ishihara, M. Kimura, K. Matsuno and S. Tomizawa, Class. Quant. Grav. **25**, 095017 (2008) [arXiv:0708.0708 [gr-qc]].

[11] M. Kimura, Phys. Rev. D **80**, 044012 (2009) [arXiv:0904.4311 [gr-qc]].

[12] D. Ida, H. Ishihara, M. Kimura, K. Matsuno, Y. Morisawa and S. Tomizawa, Class. Quant. Grav. **24**, 3141 (2007) [arXiv:hep-th/0702148].

[13] D. Ida, K. i. Nakao, M. Siino and S. A. Hayward, Phys. Rev. D **58**, 121501 (1998).

[14] G. T. Horowitz and K. Maeda, Phys. Rev. D **65**, 104028 (2002) [arXiv:hep-th/0201241].

[15] J. P. Gauntlett and J. B. Gutowski, Phys. Rev. D **71**, 045002 (2005) [arXiv:hep-th/0408122].

Emergence of Spacetimes and Noncommutativity

Shinpei Kobayashi[1](a) and Tsuguhiko Asakawa[2](b)

(a) *Department of Physics, Gunma National College of Technology, 580 Toribacho, Maebashi, 371-8530*
(b) *Department of Physics, Graduate School of Science, Tohoku University, Sendai 980-8578*

Abstract

We investigate a three-dimensional gravitational theory on a noncommutative space which has a cosmological constant term only [1]. We found various kinds of nontrivial solutions, by applying a similar technique which was used to seek noncommutative solitons in noncommutative scalar field theories. Some of those solutions correspond to bubbles of spacetimes, or represent dimensional reduction. The solution which interpolates $G_{\mu\nu} = 0$ and Minkowski metric is also found. All solutions we obtained are non-perturbative in the noncommutative parameter θ, therefore they are different from solutions found in other contexts of noncommutative theory of gravity and would have a close relation to quantum gravity.

1 Introduction

The construction of a consistent theory of spacetime at the Planck scale is one of the main issue in fundamental physics. There is an expectation that a noncommutativity among spacetime coordinates

$$[x^\mu, x^\nu] = i\theta^{\mu\nu} \tag{1}$$

emerges in such a scale. In fact, there are so many attempts to make this idea manifest, that is, to construct a consistent theory of gravity with noncommutativity to be taken into account. For example, a noncommutative extension of the gauge theory of gravitation[2], that of the correspondence between the three-dimensional Einstein gravity and the three-dimensional Chern-Simons theory[3], and the noncommutative effects to gravitational sources[4] have been investigated intensively. Also, the authors of [5] proposed a theory of gravity on noncommutative spaces from the viewpoint of twisting the diffeomorphism (you can find more references in [1]). Some solutions for such noncommutative theories have been already found, but they are also the solutions for the ordinary Einstein gravity. Namely, we have not had any nontrivial solutions particular to the gravitational theories on noncommutative spaces so far.

As for this point, we take a rather different approach to investigate the effect of the noncommutativity, by finding classical solutions that can not be obtained as the deformation of solutions of commutative theories but are non-perturbative in the noncommutativity θ. To this end, we would like to work with a three-dimensional noncommutative gravitational theory that consists of a cosmological constant term only, that is to say, a noncommutative gravitational theory without the Ricci scalar. We adopt the first order (vielbein) formalism, and the action of our theory reduces to just the three-dimensional determinant of the vielbein. One reason to work with this situation is that the cosmological constant term is made by the $\star$-multiplication only and that would be common for many approaches to noncommutative gravity, i.e., it is model independent.

This set up is also motivated by the idea of [6], where some noncommutative solitons have been derived in noncommutative scalar field theories. Our case, as the determinant is made of the $\star$-multiplication of vielbein, is analogous to the noncommutative ϕ^3-theory investigated in [6], and we can apply a similar technique to find nontrivial solutions, namely, by switching to the operator formulation and using projection operators or their generalization.

[1]Email address: shimpei@nat.gunma-ct.ac.jp
[2]Email address: asakawa@tuhep.phys.tohoku.ac.jp

2 The Noncommutative Gravity of Cosmological Constant

We would like to consider a three-dimensional noncommutative plane $\mathbb{R}^3$ with coordinates $x^\mu(\mu = 0, 1, 2)$ or (t, x, y). The star product is defined for any functions on $\mathbb{R}^3$ as

$$(f \star g)(x) = \exp\left(\frac{i}{2}\frac{\partial}{\partial x^\mu}\theta^{\mu\nu}\frac{\partial}{\partial y^\nu} f(x)g(y)\big|_{y\to x}\right), \tag{2}$$

where $\theta^{\mu\nu}$ is a constant, anti-symmetric matrix which represents the noncommutativity. In order to avoid a conceptual problem of causality, we introduce the noncommutativity purely in the spatial coordinates $[x, y]_\star \equiv x \star y - y \star x = i\theta$, by choosing $\theta^{0i} = 0(i = 1, 2)$ and $\theta^{12} \equiv \theta$.

We exploit the first order formulation of a three-dimensional theory of gravity on a noncommutative $\mathbb{R}^3$ which has a cosmological constant term only,

$$S = -\frac{\Lambda}{\kappa^2}\int dtd^2x\ E^\star = -\frac{\Lambda}{3!\kappa^2}\int dtd^2x\epsilon^{\mu\nu\rho}\epsilon_{abc}E^a_\mu \star E^b_\nu \star E^c_\rho, \tag{3}$$

where Λ is a cosmological constant and $E^a_\mu(x)$ is a vielbein. We denote spacetime indices by μ, ν, ρ and tangent space indices by a, b, c. All indices run from 0 to 2. The metric is defined as

$$G_{\mu\nu} = \frac{1}{2}\left(E^a_\mu \star E^b_\nu + E^b_\nu \star E^a_\mu\right)\eta_{ab}, \tag{4}$$

where η_{ab} is an $SO(1, 2)$ invariant metric of the local Lorentz frame. We do not assume that E^a_μ or $G_{\mu\nu}$ are invertible as 3×3 matrices, that is, we allow degenerate metrics. $G_{\mu\nu}$ is assumed to be real for simplicity and solutions we discuss later will not contradict with this assumption, but complex metrics can also be treated in a similar manner.

Varying the action (3) with respect to E^a_μ and using the cyclic symmetry of the star product, we have nine equations of motion for ${}^\forall\mu$ and ${}^\forall a$,

$$\epsilon^{\mu\nu\rho}\epsilon_{abc}\{E^b_\nu, E^c_\rho\}_\star = 0. \tag{5}$$

Here we used the star-anticommutator defined by $\{f, g\}_\star \equiv \frac{1}{2}(f \star g + g \star f)$.

In order to find solutions of (5), we exploit the recipe used in [6], i.e., the usage of the connection between the star product and the operator formulation, an analogue of the Weyl-Wigner correspondence in quantum mechanics. The creation and the annihilation operator are defined by

$$\hat{a} = \frac{\hat{x} + i\hat{y}}{\sqrt{2\theta}}, \quad \hat{a}^\dagger = \frac{\hat{x} - i\hat{y}}{\sqrt{2\theta}}. \tag{6}$$

The Hilbert space $\mathcal{H}$ is now spanned by orthonormal basis $|\, n\,\rangle$ $(n = 0, 1, 2, \cdots)$, which is the energy eigenstate of the one-dimensional harmonic oscillator given in (6). Thus a general operator O acting on $\mathcal{H}$ can be written as the linear combination of the matrix elements of the form

$$O = \sum_{i,j=0}^{\infty} O^i_j\, |\, i\,\rangle\langle\, j\,|\,. \tag{7}$$

In particular, the projection operator $|\, i\,\rangle\langle\, i\,|$ will be important to construct solutions. The function (symbol) ϕ_i corresponding to the projection operator (that is $O_{\phi_i} = |\, i\,\rangle\langle\, i\,|$) can be expressed as

$$\phi_i(x, y) = 2(-1)^i e^{-r^2/\theta} L_i\left(\frac{2r^2}{\theta}\right), \tag{8}$$

where $L_i(x)$ is the i-th Laguerre polynomial and $r^2 = x^2 + y^2$. By construction, ϕ_i is the orthogonal projection $\phi_i \star \phi_j = \delta_{ij}\phi_i$ and satisfy the completeness relation $\sum_{i=0}^{\infty}\phi_i = 1$.

3 Noncommutative Solitons by Projection Operators

We have found that there is an infinite numbers of nontrivial solutions for (5) by expanding the vielbein as

$$E^a_\mu = \sum_{i,j=0}^{\infty} (C^a_\mu)^i_j \,|\, i \,\rangle \langle\, j \,|\,. \tag{9}$$

Here $(C^a_\mu)^i_j$ is a (complex) number. In this proceeding we would like to show the easiest solution as an example (general solutions are given in [1]), that is, the solution of diagonal vielbein. For this case, the equation of motion becomes very simple and we can easily check that the following vielbein solves (5):

$$E^b_\nu = \mathrm{diag}(\alpha_0\phi_0, \alpha_1\phi_1, \alpha_2\phi_2), \tag{10}$$

where α_0, α_1 and α_2 are arbitrary complex numbers. The solution (10) gives the line element

$$ds^2 = 2e^{-r^2/\theta}\left(-\alpha_0^2 dt^2 - \alpha_1^2\left(1-\frac{2r^2}{\theta}\right)dx^2 + \alpha_2^2\left(1-\frac{4r^2}{\theta}+\frac{2r^4}{\theta^2}\right)dy^2\right). \tag{11}$$

Once we switch to the metric formalism, we can evaluate the Ricci scalar and other scalar invariants to understand this spacetime intuitively. All of them diverge at $r=\infty$ coming from the overall factor $e^{-r^2/\theta}$ appeared in (11), and also diverge at several values of r which comes from the zero points of the Laguerre polynomials, so the spacetime is divided into several radial regions by the walls of curvature singularities. The divergent points agree with those satisfy $\det G = 0$. In each region, the Ricci scalar evaluated by ordinary GR method is meaningful because $\det G \neq 0$. When we take the commutative limit $\theta \to 0$, all of the walls shrink to $r=0$ and only one curvature singularity will appear there. This solution suggests that the bubbles of several spacetimes with small cosmological constants would emerge from this solution.

Also, some solutions found in similar way indicate dimensional reduction, that is, they are effectively one- or two-dimensional because of the degeneracy $\det_\star G = 0$. In the context of quantum gravity, the possibility of dimensional reduction have been intensively discussed, so it would be interesting to investigate the relation of our theory to them.

4 Noncommutative Solitons by Clifford Algebras

There is another class of solutions for (5), that is represented by various dimensional Clifford algebras. All solutions of this type we found are proportional to the Minkowski metric and satisfy $\det_\star G \neq 0$, as opposed to the ones in the previous section.

To be more precise, let us for example focus on the indices $i = 0, 1$ and define the $SO(3)$ gamma matrices (Pauli matrices) as

$$\begin{aligned}
\gamma^0 &= \sigma^3 = |\,0\,\rangle\langle\,0\,| - |\,1\,\rangle\langle\,1\,|\,,\\
\gamma^1 &= \sigma^1 = |\,1\,\rangle\langle\,0\,| + |\,0\,\rangle\langle\,1\,|\,,\\
\gamma^2 &= \sigma^2 = i\,|\,1\,\rangle\langle\,0\,| - i\,|\,0\,\rangle\langle\,1\,|\,.
\end{aligned} \tag{12}$$

They satisfies the Clifford algebra relation $\{\gamma^\mu, \gamma^\nu\} = 2\delta^{\mu\nu}\mathbf{1}_2$. Here $\mathbf{1}_2 = |\,0\,\rangle\langle\,0\,| + |\,1\,\rangle\langle\,1\,|$ is a unit matrix in the two dimensional subspace spanned by $|\,0\,\rangle$ and $|\,1\,\rangle$, which is equivalent to the projection operator $\phi_0 + \phi_1$ in the full Hilbert space. Then the vielbein of the form

$$E^a_\mu = \begin{pmatrix} \gamma^0 & 0 & 0 \\ 0 & \gamma^1 & 0 \\ 0 & 0 & \gamma^2 \end{pmatrix} \tag{13}$$

is evidently a solution for (5). The metric for this vielbein is

$$G_{\mu\nu} = \eta_{\mu\nu}\left(|\,0\,\rangle\langle\,0\,| + |\,1\,\rangle\langle\,1\,|\right) = \eta_{\mu\nu}\left(\phi_0+\phi_1\right) \tag{14}$$

$$= \frac{4r^2}{\theta} e^{-r^2/\theta}\eta_{\mu\nu}. \tag{15}$$

Remarkably, this metric is proportional to the three-dimensional Minkowski metric, so that it is natural to regard this solution as a soliton that interpolates two vacua $G_{\mu\nu} = 0$ and $G_{\mu\nu} = \eta_{\mu\nu}$. We might be able to say that this solution expresses the emergence of the Minkowski spacetime from the cosmological constant term and the noncommutativity.

5 Summary

We considered the three-dimensional gravity only with the cosmological constant term on the noncommutative space. This theory has an infinite number of nontrivial solutions and the solutions we have shown here can be classified into two classes, i.e., the solutions constructed by using the projection operators and the ones constructed by applying the Clifford algebra.

All solutions in the former class satisfy $\det_\star G = 0$ but $\det G \neq 0$, so we could calculate commutative scalar curvatures produced by the metrics based on the solutions of the vielbein. In [1] we also give other solutions that are effectively one- or two-dimensional because of the degeneracy $\det_\star G = 0$ which would have close relation to quantum gravity.

The solutions in the latter class are noncommutative solitons interpolating $G_{\mu\nu} = 0$ and $G_{\mu\nu} = \eta_{\mu\nu}$. They satisfy $\det_\star G \neq 0$ and $\det G \neq 0$ and they are regarded as either a bubble of ordinary spacetime around the nothing $G_{\mu\nu} = 0$, or a hole (bubble of nothing) in the Minkowski space, where their regions with different scalar curvatures are partitioned by the wall of the curvature singularity.

Now we would like to propose a new point of view for the cosmological constant term: the action we gave here is already a full theory though there is no scalar curvature term. When we adopt this idea, the metric, the Ricci scalar and other physical quantities can be constructed after the vielbein is obtained by solving the equation of motion (5). In other words, we switch the second order formalism effectively. In this case, the vielbein which solves (5) can be regarded as a "meta" spacetime or a seed vielbein that can work as a source for the commutative Ricci scalar R or the noncommutative one $R_\star$. We would like to emphasize that this point of view have never appeared. One of the reasons for that is that on commutative spaces, a cosmological constant term itself can not give a nontrivial solution, but it needs a kinetic term.

This is the first trial that suggest the emergence of "meta" spacetimes only from a cosmological constant and noncommutativity. In this respect, this scenario gives also a new direction about the cosmological constant problem, that is, the cosmological constant is necessary for spacetimes to emerge. As a next step, extending our theory to include spin connections and studying the symmetries of this theory would be interesting. Both fundamental and phenomenological questions on this model have to be investigated further.

References

[1] T. Asakawa and S. Kobayashi, [arXiv:0911.2136].

[2] A. H. Chamseddine, *Phys. Lett.* **B504** (2001) 33–37 [hep-th/0009153];

[3] M. Banados, O. Chandia, N. E. Grandi, F. A. Schaposnik and G. A. Silva, *Phys. Rev.* **D64** (2001) 084012 [hep-th/0104264];

[4] P. Nicolini, A. Smailagic and E. Spallucci, *Phys. Lett.* **B632** (2006) 547–551 [gr-qc/0510112].

[5] P. Aschieri, M. Dimitrijevic, F. Meyer and J. Wess, *Class. Quant. Grav.* **23** (2006) 1883–1912 [hep-th/0510059]; P. Aschieri *et. al.*, *Class. Quant. Grav.* **22** (2005) 3511–3532 [hep-th/0504183].

[6] R. Gopakumar, S. Minwalla and A. Strominger, *JHEP* **05** (2000) 020 [hep-th/0003160]; J. A. Harvey, P. Kraus and F. Larsen, *JHEP* **12** (2000) 024 [hep-th/0010060]; J. A. Harvey, [hep-th/0102076].

Curvatons in Warped Throats

Takeshi Kobayashi[1 (a)] and Shinji Mukohyama[2 (b)]

[(a)] *Institute for Cosmic Ray Research, The University of Tokyo, 5-1-5 Kashiwanoha, Kashiwa, Chiba 277-8582, Japan*
[(b)] *Institute for the Physics and Mathematics of the Universe (IPMU), The University of Tokyo, 5-1-5 Kashiwanoha, Kashiwa, Chiba 277-8582, Japan*

Abstract

We present a curvaton model from type IIB string theory compactified on a warped throat with approximate isometries. Considering an (anti-)D3-brane sitting at the throat tip as a prototype standard model brane, we show that the brane's position in the isometry directions can play the role of curvatons. The basic picture is that the fluctuations of the (anti-)D3-brane in the angular isometry directions during inflation eventually turns into the primordial curvature perturbations, and subsequently the brane's oscillation excites other open string modes on the brane and reheat the universe. We find in the explicit case of the KS throat that a wide range of parameters allows a consistent curvaton scenario. It is also shown that the oscillations of branes at throat tips are capable of producing large non-Gaussianity, either through curvature or isocurvature perturbations. Since such setups naturally arise in warped (multi-)throat compactifications and are constrained by observational data, the model can provide tests for compactification scenarios. This work gives an explicit example of string theory providing light fields for generating curvature perturbations. Such mechanisms free the inflaton from being responsible for the perturbations, thus open up new possibilities for inflation models. The discussions in this paper are based on [1].

1 Introduction

An important feature of string cosmology is its high sensitivity to the physics of string compactification. This imposes stringent restrictions on string inflationary models, and it is nontrivial whether the inflaton can generate the primordial curvature perturbations. However, one can expect some field(s) other than the inflaton to have generated the curvature perturbations, as in the case of the curvaton scenario [2–5]. In this paper, we present a simple curvaton model from string theory compactified on a warped throat with approximate isometries. A good example of such throats is the deformed conifold [6] in type IIB string theory, where it has been shown that fluxes and nonperturbative effects can stabilize all its moduli [7, 8]. Considering an (anti-)D3-brane sitting at the throat tip as a prototype standard model brane, we show that the brane's position in the isometry directions can play the role of the curvaton. The basic picture is that the fluctuations of the (anti-)D3-brane in the angular isometry directions during inflation eventually turns into the primordial curvature perturbations, and subsequently the brane's oscillation excites other open string modes on the brane and reheat our universe. We find in the explicit case of the Klebanov-Strassler (KS) throat [6] that a wide range of parameters allows a consistent curvaton scenario. The discussions in this paper are based on [1].

2 Effective Action

Let us consider the six-dimensional internal space to be compactified to a (conformally) Calabi-Yau (CY) space which includes warped deformed conifold throat regions, whose leading order background geometry takes the following form,

$$ds^2 = h(r)^2 g^{(4)}_{\mu\nu} dx^\mu dx^\nu + h(r)^{-2} \left(dr^2 + r^2 g^{(5)}_{mn} d\theta^m d\theta^n \right), \tag{1}$$

[1]Email address: takeshi.kobayashi@ipmu.jp
[2]Email address: shinji.mukohyama@ipmu.jp

where r is the radial coordinate which decreases as one approaches the tip of the throat, and θ^m are the five-dimensional angular coordinates. $h(r)$ is the warp factor, which is to leading order independent of the angular coordinates.

Assuming that we are living on an $\overline{\text{D3}}$-brane sitting at the tip of the conifold throat, the angular position of the $\overline{\text{D3}}$ in the isometry directions plays the role of curvatons. However, since the throat is glued to the bulk CY which in general do not preserve such isometries, the throat isometries are broken. Also, nonperturbative effects that stabilize the Kähler moduli confine the $\overline{\text{D3}}$ to certain loci on the tip. The warping of the throat suppresses all such effects at the tip, and consequently the angular position of the $\overline{\text{D3}}$ receives small mass and couplings to other open string modes on the brane. As a consequence, one can obtain the curvaton action from the DBI and CS terms of a probe $\overline{\text{D3}}$-brane inside a GKP[7]-type warped throat,

$$\frac{\mathcal{L}}{\sqrt{-g^{(4)}}} \simeq -(\partial\sigma)^2 + \bar{\psi} i \not{D} \psi - (m_{\rm bulk}^2 + m_{\rm np}^2)\sigma^2 + \frac{g_s M^{1/2} \alpha'^{3/2}}{h_0^3} \frac{m_{\rm bulk}^2 m_{\rm np}^2}{m_{\rm bulk}^2 + m_{\rm np}^2} \sigma \bar{\psi} i \not{D} \psi, \tag{2}$$

where g_s is the string coupling, α' is the string scale, M is the R-R flux number of the throat, and h_0 is the warp factor at the throat tip. Here we have focused on the flattest angular direction θ (among the three angular directions of the S^3 tip), and assumed that the $\overline{\text{D3}}$ is stabilized in the other directions. The curvaton σ is obtained by canonically normalizing this direction,

$$\sigma \equiv \sqrt{T_3} r_0 \theta, \tag{3}$$

where r_0 is the IR cutoff of the deformed conifold and $T_3 \sim 1/(g_s \alpha'^2)$ is the D3 ($\overline{\text{D3}}$) tension. Also, ψ is the world-volume fermion, into which the angular degrees of freedom (i.e. the curvaton) decay first. (We assume that (some of) the world-volume fermions are significantly lighter than the curvaton.)[3] We have dropped numerical factors and will carry out order-of-magnitude estimations in this paper.

The masses arising from bulk and nonperturbative effects are defined as follows, respectively,

$$m_{\rm bulk}^2 \equiv \frac{h_0^\Delta}{r_0^2} \sim \frac{h_0^{\Delta-2}}{g_s M \alpha'}, \qquad m_{\rm np}^2 \equiv \frac{h_0^{\lambda-2}}{g_s M \alpha'}, \tag{4}$$

The symbols Δ and λ respectively denote how much the bulk and nonperturbative effects are suppressed in terms of the warp factor. By comparing Δ and λ, one can measure the relative strength of the bulk and nonperturbative effects at the throat tip, e.g., $\Delta \sim 5.3$ for a KS throat [9], and $\lambda \sim 5.5$ for simple cases of the Kuperstein embedding of wrapped D7-branes [10]. The point we would like to emphasize is that various effects with different angular dependence misalign the (local) minima of the potential and interaction terms, hence providing decay channels to the curvaton.

Since the field range of σ is restricted by the radius of the S^3 tip, one statistically expects that the field value of the curvaton during inflation is

$$\sigma_* \sim \frac{h_0 M^{1/2}}{\alpha'^{1/2}}. \tag{5}$$

3 Cosmological Perturbations

Equipped with the information on the angular position of the $\overline{\text{D3}}$-brane discussed in the previous section, let us look into the parameter space and show that the angular oscillation of the $\overline{\text{D3}}$ at the throat tip actually plays the role of the curvaton. We assume that the SM particles are realized on the curvaton $\overline{\text{D3}}$-brane. How the SM particles are realized on the world-volume of the D-brane is out of the scope of this paper, though one naively expects that the interactions among the open string modes on the brane is suppressed by the local string scale. The decay rate from the curvaton to the world-volume fermions is further suppressed by the warp factor. Therefore, after the curvaton decay into world-volume fermions,

[3] One can check that the decay of the curvaton into world-volume fermions induced by the three-point term in (2) is the most important interaction. The curvaton also interacts with world-volume gauge fields, gravitons, and Kaluza-Klein modes in the throat, but those interactions have no major effect on the curvaton dynamics, perturbatively nor through parametric resonance.

we can expect the fermions to soon decay into or thermalize with the SM particles (or particles that eventually turn into SM particles). For the cosmic inflation, we do not specify its details. However, we assume that the inflaton energy is transferred to radiation right after the end of inflation. In cases where the curvaton dominates the universe before it decays, the reheating of the universe is sourced by the decay of the curvaton. On the other hand, if the curvaton is subdominant at decay, then reheating should rely on the remnants of inflation. We require the curvaton to decay before BBN, but if one also wants to incorporate baryogenesis, then the decay time should be corrected according to the baryogenesis scenario.

In addition to such cosmological requirements, several microscopic constraints need to be satisfied. In order to trust our action (2), the curvaton brane has to be moving nonrelativistically. Furthermore, the Hubble parameter during inflation should be smaller than the local string scale of the throat to avoid stringy corrections to the throat. For the same reason, the curvaton's oscillation energy also should be smaller than the local string scale.

We illustrate the parameter space on the Δ-λ plane in Figure 1. The remaining four parameters (i.e. g_s, M, h_0, and the length scale of the internal bulk $L/\alpha'^{1/2}$) are fixed to the values explained in the caption. One sees that as Δ or λ increase, i.e. the bulk or nonperturbative effects weaken, the decay rate of the curvaton is suppressed and the curvaton comes closer to dominating the universe before decay. The figure clearly shows that when either the bulk or nonperturbative effect is absent, i.e. Δ or $\lambda \to \infty$, the curvaton cannot decay, and one crosses the orange line which is the BBN constraint. As we take different values for the four parameters g_s, M, $L/\alpha'^{1/2}$, and h_0, the consistent region (the yellow region in the figure) deforms and shifts in the Δ-λ plane. Though we have shown only a single example, one can check that consistent curvaton scenarios are allowed for broad ranges of the parameters.

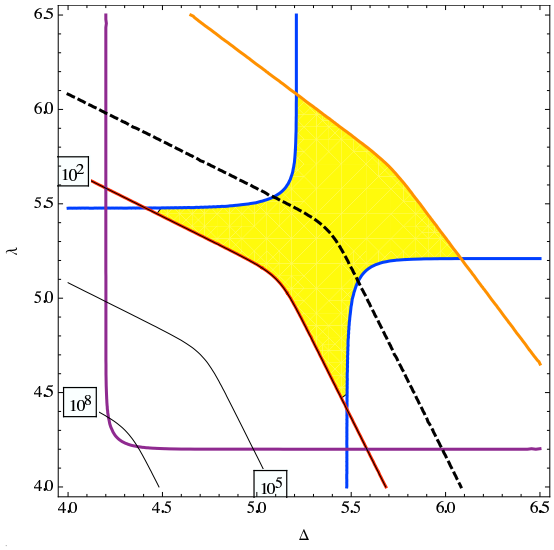

Figure 1: The consistency conditions for the curvaton scenario on the Δ-λ plane, where the other parameters are set to $g_s = 0.1$, $M = 300$, $L/\alpha'^{1/2} = 3$, $h_0 = 10^{-5}$ (hence $N \sim 50000$, $K \sim 200$, $M_{\rm Pl}\alpha'^{1/2} \sim 300$). The lines denote where each condition is saturated, blue: masslessness of the curvaton, orange: decay before BBN, red: $f_{\rm NL} \lesssim 100$, purple: curvaton oscillation energy bound. The yellow region satisfies all four conditions. (In this case, these four conditions include other cosmological and microscopic requirements.) On the right (left) side of the dashed line, the curvaton dominates (subdominates) the universe at the decay epoch. The produced non-Gaussianities are also shown as contour lines for $f_{\rm NL}$. Here the inflation scale can be estimated from $H_{\rm inf}/M_{\rm Pl} \sim 10^{-11} f_{\rm NL}$.

4 Conclusions

We have proposed a model for generating the primordial perturbations and reheating our universe from angular oscillations of D-branes at the tip of throats. The geometrical features of throats – warping and (approximate) isometries – yielded curvaton scenarios. We have also seen that effects that break the force-free condition of the D-brane in the isometry directions, such as the isometry breaking bulk effects and moduli stabilizing nonperturbative effects played an important role in our model. Depending on the (un)balance between the various features of the background geometry, the curvaton model shows different behaviours, e.g., the curvaton may contribute mainly to non-Gaussianity, or survive until now and contribute to dark matter, generating non-Gaussian isocurvature perturbations. These cases of interest are further studied in [1], where it is shown that each scenario can be realized in a wide range of parameter space. In other words, our model may be considered as generally arising from compactification scenarios containing warped throats with isometries. Therefore, it may serve as a test for discussing the validness of (multi-)throat compactification scenarios. The curvaton model is capable of producing large non-Gaussianity, and upcoming CMB experiments are expected to allow us to give more rigorous arguments.

One of the general lessons of our work is that in string theory, one finds it quite natural to consider fields other than the inflaton for generating the primordial perturbations. Such light fields can be realized in string theory, thus giving rise to mechanisms which may have seemed too intricate from the phenomenological point of view. It is fair to say that top-down approaches to inflationary cosmology can provide us with rich ideas beyond the standard slow-roll inflation pictures.

Acknowledgements

The work of T.K. was supported by Grant-in-Aid for JSPS Fellows No. 21·8966. The work of S.M. was supported in part by MEXT through a Grant-in-Aid for Young Scientists (B) No. 17740134, by JSPS through a Grant-in-Aid for Creative Scientific Research No. 19GS0219, and by the Mitsubishi Foundation. This work was supported by World Premier International Research Center Initiative (WPI Initiative), MEXT, Japan.

References

[1] T. Kobayashi and S. Mukohyama, JCAP **0907**, 032 (2009) [arXiv:0905.2835 [hep-th]].

[2] A. D. Linde and V. F. Mukhanov, Phys. Rev. D **56**, 535 (1997) [arXiv:astro-ph/9610219].

[3] K. Enqvist and M. S. Sloth, Nucl. Phys. B **626**, 395 (2002) [arXiv:hep-ph/0109214].

[4] D. H. Lyth and D. Wands, Phys. Lett. B **524**, 5 (2002) [arXiv:hep-ph/0110002].

[5] T. Moroi and T. Takahashi, Phys. Lett. B **522**, 215 (2001) [Erratum-ibid. B **539**, 303 (2002)] [arXiv:hep-ph/0110096].

[6] I. R. Klebanov and M. J. Strassler, JHEP **0008**, 052 (2000) [arXiv:hep-th/0007191].

[7] S. B. Giddings, S. Kachru and J. Polchinski, Phys. Rev. D **66**, 106006 (2002) [arXiv:hep-th/0105097].

[8] S. Kachru, R. Kallosh, A. D. Linde and S. P. Trivedi, Phys. Rev. D **68**, 046005 (2003) [arXiv:hep-th/0301240].

[9] O. Aharony, Y. E. Antebi and M. Berkooz, Phys. Rev. D **72**, 106009 (2005) [arXiv:hep-th/0508080].

[10] O. DeWolfe, L. McAllister, G. Shiu and B. Underwood, JHEP **0709**, 121 (2007) [arXiv:hep-th/0703088].

Large scale evolution of the curvature perturbation in Hořava-Lifshitz cosmology

Tsutomu Kobayashi,[1(a)] Yuko Urakawa,[2(a)] and Masahide Yamaguchi[3(b)]

[(a)] *Department of Physics, Waseda University, Okubo 3-4-1, Shinjuku, Tokyo 169-8555, Japan*
[(b)] *Department of Physics and Mathematics, Aoyama Gakuin University, Sagamihara 229-8558, Japan*

Abstract

In the non-relativistic theory of gravity recently proposed by Hořava, the Hamiltonian constraint is not satisfied locally at each point in space. The absence of the local Hamiltonian constraint allows the system to have an extra dark-matter-like component as an integration constant. We discuss consequences of this fact in the context of cosmological perturbations, paying a particular attention to the large scale evolution of the curvature perturbation. The curvature perturbation is defined in a gauge invariant manner with this "dark matter" taken into account. We then clarify the conditions under which the curvature perturbation is conserved on large scales. This is done by using the evolution equations.

1 Introduction

A power-counting renormalizable theory of gravity, proposed recently by Hořava [1], has attracted much attention. The essential aspect of the theory is broken Lorentz invariance in the ultraviolet (UV), where it exhibits a Lifshitz-like anisotropic scaling, $t \to \ell^z t$, $\vec{x} \to \ell \vec{x}$, with the dynamical critical exponent $z = 3$. Several versions of Hořava gravity have been known, which are classified according to whether or not the detailed balance and the projectability conditions are imposed. Among them the theory with projectability and without detailed balance is argued to evade the problems pointed out in the literature. The most distinguished feature of projectable Hořava gravity is that the Hamiltonian constraint is not a local equation satisfied at each point in space, but rather a global equation integrated over the whole space. Since the global Hamiltonian constraint is less restrictive than the local one, it allows for a wider class of solutions which contain an additional dust-like component as an integration constant, as was clearly remarked in [2]. In this paper, we discuss consequences of the absence of the local Hamiltonian constraint within the context of cosmological perturbations based on [3].

2 Hořava gravity

We consider the projectable version of Hořava gravity without detailed balance. The dynamical variables are $\mathcal{N}$, $\mathcal{N}_i$, and γ_{ij} The projectability condition states that the lapse function depends only on the time coordinate, $\mathcal{N} = \mathcal{N}(t)$, while $\mathcal{N}_i$ and γ_{ij} may depend on t and $\vec{x}$. The theory is invariant under the foliation-preserving diffeomorphism: $t \to \tilde{t}(t)$, $x^i \to \tilde{x}^i(t, \vec{x})$. The dynamical variables are subject to the action [1, 4]

$$S = \frac{1}{16\pi G} \int \mathrm{d}t \mathrm{d}^3x \mathcal{N}\sqrt{\gamma} \left(K_{ij}K^{ij} - \lambda K^2 + R + \mathcal{L}_{V2} \right) + \int \mathrm{d}t \mathrm{d}^3x \mathcal{N}\sqrt{\gamma}\mathcal{L}_{\mathrm{m}}, \tag{1}$$

where $\mathcal{L}_{\mathrm{m}}$ is the Lagrangian for matter fields, K_{ij} is the extrinsic curvature, $R = \gamma^{ij}R_{ij}$ is the trace of the Ricci scalar (the spatial curvature scalar), and $\mathcal{L}_{V2}$ is the higher spatial curvature Lagrangian which is not relevant in this paper.

Variation with respect to $\mathcal{N}$ yields the Hamiltonian constraint. In the projectable version of Hořava gravity, the Hamiltonian constraint is not satisfied locally at each spatial point, but rather a global

[1]Email address: tsutomu"at"gravity.phys.waseda.ac.jp
[2]Email address: yuko"at"gravity.phys.waseda.ac.jp
[3]Email address: gucci"at"phys.aoyama.ac.jp

equation integrated over the whole space because $\mathcal{N}$ is a function of t only. The global Hamiltonian constraint reads

$$\int \mathrm{d}^3x\sqrt{\gamma}\left[K_{ij}K^{ij} - \lambda K^2 - R - \mathcal{L}_{V2} + 16\pi G\, E\right] = 0, \tag{2}$$

where $E := -\mathcal{L}_\mathrm{m} - \mathcal{N}\delta\mathcal{L}_\mathrm{m}/\delta\mathcal{N}$. Variation with respect to $\mathcal{N}_i$ leads to the momentum constraint, and variation with respect to γ_{ij} gives the evolution equations: $\ldots = 8\pi G T_{ij}$.

3 Background evolution

The background evolution of Hořava cosmology can be derived by setting $\mathcal{N} = 1$, $\mathcal{N}_i = 0$, and $\gamma_{ij} = a^2(t)\delta_{ij}$. The evolution equation at zeroth order reads

$$\frac{1-3\lambda}{2}\left(3H^2 + 2\dot{H}\right) = 8\pi G p, \tag{3}$$

where $H := \dot{a}/a$, and $T_{ij} = p\gamma_{ij}$ has been assumed.

Let us *define* $\mathcal{E}(t)$ by

$$8\pi G\left[\mathcal{E}(t) + \rho\right] = -\frac{3}{2}(1-3\lambda)H^2, \tag{4}$$

where ρ is the background value of the matter energy density E. In the case of $\lambda = 1$, the meaning of $\mathcal{E}$ becomes more transparent by noticing that $8\pi G\mathcal{E} = 8\pi G T_0{}^0 - G_0{}^0$, where $G_0{}^0$ is the $(0\,0)$ component of the usual Einstein tensor: $\mathcal{E}$ arises because the local Hamiltonian constraint is absent in Hořava gravity. This term corresponds to "dark matter as an integration constant" in Refs. [2].

We emphasize that in this paper the homogeneous background is assumed at least in our observable patch of the universe because nobody can tell what happens beyond the present horizon scale. Under this assumption we can conclude from the global Hamiltonian constraint that $\mathcal{E}$ does not necessarily vanish in the local patch. For example, we may have $\mathcal{E} > 0$ in our patch of the universe, but $\mathcal{E}$ may be negative in a different patch. Our assumption is in contrast to Ref. [5].

In terms of $\mathcal{E}$, Eq. (3) can be written in the form of a conservation equation: $\dot{\mathcal{E}} + \dot{\rho} + 3H\left(\mathcal{E} + \rho + p\right) = 0$. This does not guarantee the local conservation of the matter energy density. If the matter action respects general covariance, we have an additional conservation equation, $\dot{\rho} + 3H(\rho + p) = 0$. Using the local conservation of matter energy, we obtain $\dot{\mathcal{E}} + 3H\mathcal{E} = 0$, implying that $\mathcal{E}$ indeed shows a dust-like behavior [2].

4 Large scale cosmological perturbations

Let us study linear perturbations around the cosmological background. The perturbed metric is given by

$$\mathcal{N}^2 = 1 + 2A(t), \quad \mathcal{N}_i = a^2 B_{,i}, \quad \gamma_{ij} = a^2\left[(1-2\psi)\delta_{ij} + 2D_{,ij}\right]. \tag{5}$$

Since we are imposing the projectability condition, the perturbation of the lapse function A does not depend on $\vec{x}$. Under the scalar gauge transformation, $t \to t + \chi^0(t)$, $x^i \to x^i + \partial^i\chi(t,\vec{x})$, the metric perturbations transform as $A \to A - \dot{\chi}^0$, $\psi \to \psi + H\chi^0$, $B \to B - \dot{\chi}$, and $D \to D - \chi$. Since χ^0 depends only on t, inhomogeneous ψ cannot be gauged away, while A can be set to zero by the gauge transformation. This point is in contrast to general relativity. It is convenient to define $\sigma := \dot{D} - B$, which is gauge invariant.

The evolution equations take the form

$$-(1-3\lambda)\left[\ddot{\psi} + 3H\dot{\psi} + H\dot{A} + \left(3H^2 + 2\dot{H}\right)A\right] + \mathcal{O}(\nabla^2) = 8\pi G\delta p, \tag{6}$$

where δp is the isotropic pressure perturbation and $\nabla^2 := \delta^{ij}\partial_i\partial_j$. (We do not consider the case in which higher spatial derivative terms are much larger than $\mathcal{O}(\nabla^2)$ terms, though $\mathcal{O}(\nabla^6)$ terms have an interesting effect on the spectrum of perturbations.)

Analogously to $\mathcal{E}$ defined in the previous section, let us now *define* $\varepsilon(t,\vec{x})$ by

$$-8\pi G\left[\varepsilon(t,\vec{x})+\delta\rho\right]=-3(1-3\lambda)H\left(\dot{\psi}+HA\right)-2\nabla^2\left(\frac{\psi}{a^2}+H\sigma\right), \tag{7}$$

where $\delta\rho$ is the perturbation of the matter energy density E. In the case of $\lambda=1$ we have $8\pi G\varepsilon = 8\pi G\delta T_0^{\ 0}-\delta G_0^{\ 0}$, from which it is clear again that ε is a consequence of the absence of the local Hamiltonian constraint. Thus, ε may be regarded as a energy density perturbation of "dark matter as an integration constant." It is easy to check that ε transforms as $\varepsilon\to\varepsilon-\dot{\mathcal{E}}\chi^0$ under the gauge transformation. In terms of ε, the trace part of the evolution equations can be written as

$$\dot{\varepsilon}+\dot{\delta\rho}+3H\left(\varepsilon+\delta\rho+\delta p\right)-3\dot{\psi}\left(\mathcal{E}+\rho+p\right)=\frac{1}{8\pi G}\nabla^2\left[2\frac{\dot{\psi}}{a^2}+2\dot{H}\sigma+3H(1-\lambda)\left(\dot{\sigma}+3H\sigma\right)\right]+\mathcal{O}\left(\nabla^4\right), \tag{8}$$

which reminds us of the perturbed energy conservation equation. *If the matter energy density is conserved locally at perturbative order on large scales,* one has, in addition to Eq. (8), $\dot{\delta\rho}+3H\left(\delta\rho+\delta p\right)-3\dot{\psi}(\rho+p)=\mathcal{O}(\nabla^2)$. Note, however, that Eq. (8) does not necessarily imply the local conservation of the matter energy density. In the following we assume that $\mathcal{E}\neq 0$.

Formally, one can define the following gauge invariant quantities:

$$\zeta:=(1-f)\zeta_{\rm HL}+f\zeta_{\rm m},\quad \zeta_{\rm HL}:=-\psi-H\frac{\varepsilon}{\dot{\mathcal{E}}},\quad \zeta_{\rm m}:=-\psi-H\frac{\delta\rho}{\dot{\rho}}, \tag{9}$$

with $f(t):=\frac{\dot{\rho}}{\dot{\mathcal{E}}+\dot{\rho}}$. *Only when the matter energy density is conserved locally at zeroth order,* we may rewrite Eq. (4) to have $f=\frac{\rho+p}{\mathcal{E}+\rho+p}$. Using the definition (7), ζ can be written more explicitly as

$$\zeta=-\psi+\frac{H}{\dot{H}}\left(\dot{\psi}+HA\right)+\frac{2\nabla^2\left(\psi/a^2+H\sigma\right)}{3(1-3\lambda)\dot{H}}, \tag{10}$$

so that ζ can be expressed solely in terms of the metric perturbations. Using the variables defined above and neglecting the $\mathcal{O}(\nabla^2)$ terms, we can rewrite Eq. (8) in a suggestive form as

$$\dot{\zeta}\simeq-\frac{H}{\mathcal{E}+\rho+p}\delta p_{\rm nad}+Hc_s^2f(1-f)\mathcal{S}_{\rm HL}, \tag{11}$$

where we have introduced the non-adiabatic pressure perturbation of matter, $\delta p_{\rm nad}:=\delta p-c_s^2\delta\rho$, with $c_s^2:=\dot{p}/\dot{\rho}$, and the isocurvature fluctuation between "dark matter as an integration constant" and ordinary matter, $\mathcal{S}_{\rm HL}:=3\left(\zeta_{\rm HL}-\zeta_{\rm m}\right)$. We emphasize that Eq. (11) has been derived only by using the evolution equations.

Equation (11) however tells nothing about the large scale evolution of ζ unless the evolution of $\zeta_{\rm m}$ and $\zeta_{\rm HL}$ is specified (except for the special case $c_s^2f(1-f)\simeq 0$). If the matter energy is conserved locally, one finds that $\dot{f}+3Hc_s^2f(1-f)=0$ at zeroth order and $\dot{\zeta}_{\rm m}\simeq 0$ on large scales at perturbative order, assuming that $\delta p_{\rm nad}=0$. In this case it can be shown that $\dot{\zeta}_{\rm HL}\simeq 0$ on large scales, but ζ is not conserved in general. Indeed, it follows immediately from the definition that $\zeta(t,\vec{x})=[1-f(t)]\zeta_{\rm HL}^{(0)}(\vec{x})+f(t)\zeta_{\rm m}^{(0)}(\vec{x})$, where $\zeta_{\rm HL}^{(0)}$ and $\zeta_{\rm m}^{(0)}$ are the initial conditions for the corresponding variables. For dust-like matter with $\rho\propto a^{-3}$, f is constant since $\mathcal{E}$ also scales as a^{-3}, and hence ζ is conserved. This fact was already clear in Eq. (11) with $c_s^2=0$. Another case in which ζ is conserved on large scales is $\mathcal{S}_{\rm HL}=0$, that is, $\zeta_{\rm m}=\zeta_{\rm HL}$. Whether this "adiabatic relation" between "dark matter" and usual matter is likely or not depends upon the specific scenario in the early universe.

Interesting cases with $f\simeq 0$ and $f\simeq 1$ can be studied without knowing the evolution of $\mathcal{S}_{\rm HL}$ and hence without relying on the local conservation of the ordinary matter energy density. If radiation dominates the energy density of the universe at early times, we have $(1-f)\simeq 0$, which leads to the conservation of ζ during that period. On the other hand, if "dark matter as an integration constant" accounts for a significant portion of real dark matter and dominates the energy density of the universe at late times, we have $f\simeq 0$, which again leads to the conservation of ζ. However, in the intermediate regime,

$f(1-f) = \mathcal{O}(1)$, so that the curvature perturbation grows provided that $\mathcal{S}_{\rm HL} \neq 0$. This property is in accordance with what is found in a conventional multi-fluid system. One should also notice that in the case where "dark matter as an integration constant" constitutes a large portion of real dark matter, $\mathcal{S}_{\rm HL}$ represents the isocurvature fluctuation between dark matter and radiation, which is strongly constrained by the cosmic microwave background (CMB) anisotropy. Thus, the scenario in which "dark matter as an integration constant" is really a dark matter component and there is no natural reason to explain $\mathcal{S}_{\rm HL} = 0$ gives rise to a large isocurvature fluctuation, which could be incompatible with the present constraint.

5 Conclusions

In this paper, we have studied the large scale evolution of the cosmological curvature perturbation in projectable Hořava gravity, emphasizing the effect of "dark matter as an integration constant" [2] that appears as a consequence of the global Hamiltonian constraint. Our view is that we cannot tell the cosmological dynamics far outside the present Hubble horizon, and hence the global Hamiltonian constraint does not provide any information in our observable patch of the universe. This assumption makes the impact of "dark matter as an integration constant" rather non-trivial. The curvature perturbation ζ has been defined in a gauge invariant manner with this "dark matter" component taken into account. We then clarified the conditions under which ζ is conserved on large scales by invoking the evolution equations. In particular, we pointed out that ζ is sourced by the relative entropy perturbation $\mathcal{S}_{\rm HL}$ between "dark matter as an integration constant" and ordinary matter. This source term is effective during the period when $c_s^2 f(1-f)$ is not negligible. In that period, we need to know the evolution of $\mathcal{S}_{\rm HL}$ in order to know the evolution of ζ. This is made possible by assuming the local conservation of the energy density of ordinary matter.

If the "dark matter" component constitutes a large portion of real dark matter, $\mathcal{S}_{\rm HL}$ corresponds to the isocurvature fluctuation between radiation and dark matter, which is strongly constrained by the cosmic microwave background anisotropy. In this case, one therefore needs a natural reason to explain $\mathcal{S}_{\rm HL} \simeq 0$, which is a challenge in Hořava cosmology.

References

[1] P. Horava, Phys. Rev. D **79**, 084008 (2009).

[2] S. Mukohyama, Phys. Rev. D **80**, 064005 (2009).

[3] T. Kobayashi, Y. Urakawa and M. Yamaguchi, JCAP **0911**, 015 (2009).

[4] T. P. Sotiriou, M. Visser and S. Weinfurtner, Phys. Rev. Lett. **102**, 251601 (2009); T. P. Sotiriou, M. Visser and S. Weinfurtner, JHEP **0910**, 033 (2009).

[5] A. Wang and R. Maartens, arXiv:0907.1748 [hep-th].

Generalized GRMHD equations and their implications

Shinji Koide[1]

Department of Physics, Kumamoto University, Kurokami, Kumamoto 860-8555

Abstract

We derived a set of 3+1 formalism of generalized general relativistic magnetohydrodynamic (GRMHD) equations to study phenomena of plasmas around rotating black holes. One of the equations with respect to the generalized Ohm's law shows electromotive forces due to gravitation, centrifugal force, and frame-dragging effect in a plasma around a black hole. In this paper, we summarize the equations briefly, and also mention the gravitational magnetic reconnection which can be caused by the gravitational electromotive force and charge separation even in a case of zero resistivity.

1 Introduction

Numerical simulations of general relativistic magnetohydrodynamics (GRMHD) of plasmas around black holes have confirmed a mechanism of a magnetically driven relativistic jet from a disk around a black hole [1, 2]. All of these GRMHD simulations of jet formation showed artificial appearance of magnetic islands, which are caused through magnetic reconnections due to numerical resistivity. In spite of the numerical inconsistency, these numerical results clearly suggested spontaneous formation of anti-parallel magnetic configuration, which means magnetic reconnection is caused easily in the black hole magnetospheres. The magnetic reconnection would change the global magnetic configuration drastically and influence the global dynamics of plasmas around the black holes. Thus, calculations including resistivity, the cause of magnetic reconnection, are highly expected. It is noted that causality is broken and artificial wave instability is caused when we use the standard Ohm's law, where an inertia of charge and moment of current are neglected [3]. To guarantee causality, we have to use generalized GRMHD including generalized relativistic Ohm's law [3, 4]. The generalized GRMHD equations were introduced on the basis of two-fluid approximation of plasma in Kerr metric by Khanna [5]. A more generalized equations from the general relativistic Vlasov-Boltzmann equation in time-varying space-time were formulated by Meier [6]. It was proofed that causality is satisfied for plasmas whose plasma parameter is much greater than unity [3, 7]. In this paper, we summarize the generalized GRMHD equations derived by Koide [7]. We show the electromotive forces due to gravitation, centrifugal force, and frame-dragging effect around the black hole, which are indicated by the generalized Ohm's law of plasmas around rotating black holes. The gravitational electromotive force can cause the magnetic reconnection even in a case of zero resistivity.

2 Generalized GRMHD equations

We summarize the generalized GRMHD equations of plasmas in the space-time, $x^\mu = (t, x^1, x^2, x^3)$ around a black hole where metric ds^2 is given by $ds^2 = g_{\mu\nu}dx^\mu dx^\nu$ (Equations (18), (24), and (59) with Equations (25) and (58) of Koide [7]). Throughout this paper, we use the unit system, where light speed is unity. The generalized GRMHD equations are as follows:

$$\nabla_\nu(\rho U^\nu) = 0, \tag{1}$$

$$\nabla_\nu T^{\mu\nu} = 0, \tag{2}$$

$$\frac{1}{ne}\nabla_\nu K^{\mu\nu} = \frac{1}{2ne}\nabla^\mu(\Delta\mu p - \Delta p) + \left(U^\nu - \frac{\Delta\mu}{ne}J^\nu\right)F^\mu{}_\nu - \eta\left[J^\mu - \rho'_{\rm e}(1+\Theta)U^\mu\right], \tag{3}$$

[1]Email address: koidesin@sci.kumamoto-u.ac.jp

and Maxwell equations

$$\nabla_\nu {}^*F^{\mu\nu} = 0, \tag{4}$$
$$\nabla_\nu F^{\mu\nu} = J^\mu, \tag{5}$$

where

$$T^{\mu\nu} \equiv pg^{\mu\nu} + hU^\mu U^\nu + \frac{\mu h^\ddagger}{(ne)^2} J^\mu J^\nu + \frac{2\mu\Delta h}{ne}(U^\mu J^\nu + J^\mu U^\nu) + F^\mu{}_\sigma F^{\mu\sigma} - \frac{1}{4} g^{\mu\nu} F^{\kappa\lambda} F_{\kappa\lambda}, \tag{6}$$

$$K^{\mu\nu} \equiv \frac{\mu h^\ddagger}{ne}(U^\mu J^\nu + J^\mu U^\nu) + \frac{\Delta h}{2} U^\mu U^\nu - \frac{\mu \Delta h^\sharp}{(ne)^2} J^\mu J^\nu. \tag{7}$$

Here, we used the two-fluid model, where we assumed the plasma consists of positively charged particles with charge e and mass m_+ and negatively charged particles with charge $-e$ and mass m_-. We used the typical mass of plasma particle $m = m_+ + m_-$, normalized reduced mass $\mu = m_+ m_-/m^2$, and normalized mass difference $\Delta\mu = (m_+ - m_-)/m$. The variables ρ, h, p, $n \equiv \rho/m$, Δp, and Δh are mass density, enthalpy density, pressure, number density, pressure difference of two fluids, and difference of two fluid enthalpy densities. Furthermore, ∇_μ, U^μ, and J^μ are covariant derivative, 4–velocity, and 4–current density, respectively, and $F_{\mu\nu}$ is the electromagnetic strength tensor and ${}^*F_{\mu\nu}$ is dual tensor of $F_{\mu\nu}$. We also use the variables related to enthalpy density,

$$h^\ddagger = h - \Delta\mu h \qquad \text{and} \qquad \Delta h^\sharp = \Delta\mu h - \frac{1-3\mu}{2\mu}\Delta h. \tag{8}$$

The variable η indicates resistivity and Θ is the rate of equipartition with respect to the thermalized energy due to friction (for detail, see Appendix A of Koide [4]). It is noted that Equation (5) yields the equation of continuity with respect to the current,

$$\nabla_\nu J^\nu = 0. \tag{9}$$

In addition, we assume the plasma consists of two perfect fluids with the equal specific heat ratio, Γ. The equations of states are

$$h = n^2 \left[\frac{m_+}{n_+} + \frac{m_-}{n_-} + \frac{\Gamma}{2(\Gamma-1)} \left\{ \left(\frac{1}{n_+^2} + \frac{1}{n_-^2} \right) p + \left(\frac{1}{n_+^2} - \frac{1}{n_-^2} \right) \Delta p \right\} \right], \tag{10}$$

$$\Delta h = 2\mu m n^2 \left[\frac{1}{n_+} - \frac{1}{n_-} + \frac{\Gamma}{2(\Gamma-1)} \left\{ \left(\frac{1}{m_+ n_+^2} - \frac{1}{m_- n_-^2} \right) p + \left(\frac{1}{m_+ n_+^2} + \frac{1}{m_- n_-^2} \right) \Delta p \right\} \right], \tag{11}$$

where

$$n_\pm \equiv \left[n^2 \mp \frac{2 m_\mp n}{em} U^\nu J_\nu - \left(\frac{m_\mp}{em} \right)^2 J^\nu J_\nu \right]^{1/2} \tag{12}$$

corresponds to the particle number density of each charged fluid (see Equations (74) – (78) of Koide [7]).

In the generalized GRMHD equations and the Maxwell equations, there are three types of terms including covariant derivatives: (i) contravariant vector like ρU^μ and J^μ, (ii) anti-symmetric 2nd rank tensor like $F_{\mu\nu}$ and ${}^*F_{\mu\nu}$, and (iii) symmetric 2nd rank tensor like $T^{\mu\nu}$ and $K^{\mu\nu}$. With respect to any contravariant vector A^μ and any anti-symmetric 2nd rank tensor $A^{\mu\nu}$, we have

$$\nabla_\nu A^\nu = \frac{1}{\sqrt{-g}} \partial_\nu \left(\sqrt{-g} A^\nu \right), \tag{13}$$

$$\nabla_\nu A^{\mu\nu} = -\frac{1}{\sqrt{-g}} \partial_\nu \left(\sqrt{-g} A^{\mu\nu} \right), \tag{14}$$

where g is the determinant of the metric $(g_{\mu\nu})$. As for an arbitrary symmetric 2nd rank tensor $S^{\mu\nu}$, the derivative is written by the Christoffel symbol, $\Gamma^\lambda_{\mu\nu} = \frac{1}{2} g^{\lambda\sigma}(-\partial_\sigma g_{\mu\nu} + \partial_\mu g_{\nu\sigma} + \partial_\nu g_{\sigma\mu})$ as

$$\nabla_\nu S^{\mu\nu} = \frac{1}{\sqrt{-g}} \partial_\nu \left(\sqrt{-g} S^{\mu\nu} \right) + \Gamma^\mu_{\sigma\nu} S^{\sigma\nu}. \tag{15}$$

We assume that off-diagonal spatial elements of the metric $g_{\mu\nu}$ vanish, $g_{ij} = 0$ $(i \neq j)$. Writing non-zero components by

$$g_{00} = -h_0^2, \qquad g_{ii} = h_i^2, \qquad g_{i0} = g_{0i} = -h_i^2 \omega_i, \tag{16}$$

we have

$$ds^2 = g_{\mu\nu} dx^\mu dx^\nu = -h_0^2 dt^2 + \sum_{i=1}^{3} \left[h_i^2 (dx^i)^2 - 2h_i^2 \omega_i dt dx^i \right]. \tag{17}$$

When we define the lapse function α and shift vector β^i by

$$\alpha = \left[h_0^2 + \sum_{i=1}^{3} (h_i \omega_i)^2 \right]^{1/2}, \quad \beta^i = \frac{h_i \omega_i}{\alpha}, \tag{18}$$

the line element ds is written by

$$ds^2 = -\alpha^2 dt^2 + \sum_{i=1}^{3} (h_i dx^i - \alpha \beta^i dt)^2. \tag{19}$$

Using "zero-angular-momentum observer (ZAMO) frame" $\hat{x}^\mu$, where the line element is $ds^2 = -d\hat{t}^2 + \sum_i (\hat{x}^i)^2 = \eta_{\mu\nu} dx^\mu dx^\nu$, we have the 3+1 formalism of the generalized GRMHD and the Maxwell equations. As for equations including only derivatives with respect to contravariant vector or anti-symmetric 2nd rank tensor, we obtain their 3+1 formalism easily using Equations (13) and (14). With respect to an equation including terms of derivative of symmetric 2nd rank tensor like Equation (15),

$$\nabla_\nu S^{\mu\nu} = H^\mu, \tag{20}$$

the 3+1 formalism is given by

$$\begin{aligned}
&\frac{\partial}{\partial t} \hat{S}^{00} + \frac{1}{h_1 h_2 h_3} \sum_j \frac{\partial}{\partial x^j} \left[\frac{\alpha h_1 h_2 h_3}{h_j} \left(\hat{S}^{0j} + \beta^j \hat{S}^{00} \right) \right] + \sum_j \frac{1}{h_j} \frac{\partial \alpha}{\partial x^j} \hat{S}^{j0} \\
&+ \sum_{j,k} \alpha \beta^k (G_{kj} \hat{S}^{kj} - G_{jk} \hat{S}^{jj}) + \sum_{j,k} \sigma_{jk} \hat{S}^{jk} = \alpha \hat{H}^0,
\end{aligned} \tag{21}$$

$$\begin{aligned}
&\frac{\partial}{\partial t} \hat{S}^{i0} + \frac{1}{h_1 h_2 h_3} \sum_j \frac{\partial}{\partial x^j} \left[\frac{\alpha h_1 h_2 h_3}{h_j} \left(\hat{S}^{ij} + \beta^j \hat{S}^{i0} \right) \right] + \frac{1}{h_i} \frac{\partial \alpha}{\partial x^i} \hat{S}^{00} \\
&- \sum_j \alpha \left[G_{ij} \hat{S}^{ij} - G_{ji} \hat{S}^{jj} + \beta^j (G_{ij} \hat{S}^{0i} - G_{ji} \hat{S}^{0j}) \right] + \sum_j \sigma_{ji} \hat{S}^{0j} = \alpha \hat{H}^i,
\end{aligned} \tag{22}$$

where the alphabetic index (i, j, and k) runs from 1 to 3, $G_{ij} \equiv -\frac{1}{h_i h_j} \frac{\partial h_i}{\partial x^j}$, and $\sigma_{ij} \equiv \frac{1}{h_j} \frac{\partial}{\partial x^j} (\alpha \beta^i)$ (see Appendix A of Koide [7]).

3 Discussion

Using Equations (3) and (22), we obtain the intuitive 3+1 form of spatial part of the generalized general relativistic Ohm's law,

$$\begin{aligned}
&\frac{1}{ne} \frac{\partial}{\partial t} \left(\frac{\mu h^\ddagger}{ne} \hat{J}^{\dagger j} \right) = -\frac{1}{ne} \left[\frac{1}{h_1 h_2 h_3} \sum_j \frac{\partial}{\partial x^j} \left[\frac{\alpha h_1 h_2 h_3}{h_j} (\hat{K}^{ij} + \beta^j \frac{\mu h^\ddagger}{ne} \hat{J}^{\dagger i}) \right] \right. \\
&\left. + \frac{2\mu h^\ddagger}{ne} \frac{1}{h_i} \frac{\partial \alpha}{\partial x^i} \rho_{\rm e}^\dagger - \sum_j \alpha \left\{ G_{ij} \hat{K}^{ij} - G_{ji} \hat{K}^{jj} + \beta^j \frac{\mu h^\ddagger}{ne} \left(G_{ij} \hat{J}^{\dagger i} - G_{ji} \hat{J}^{\dagger j} \right) \right\} + \sum_j \frac{\mu h^\ddagger}{ne} \sigma_{ji} \hat{J}^{\dagger j} \right] \\
&+ \alpha \left[\frac{1}{2ne} \frac{1}{h_i} \frac{\partial}{\partial x^i} (\Delta \mu p - \Delta p) + \left(\hat{U}^\nu - \frac{\Delta \mu}{ne} \hat{J}^\nu \right) \hat{F}_{i\nu} - \eta [\hat{J}^i - \rho_{\rm e}' (1 + \Theta) \hat{U}^i] \right],
\end{aligned} \tag{23}$$

where we defined the modified current density and modified charge density as,

$$\hat{J}^{\dagger i} \equiv \frac{ne}{\mu h^{\ddagger}}\hat{K}^{i0} = \gamma\hat{J}^i + \hat{\rho}_{\rm e}\hat{U}^i - \frac{\Delta h^{\sharp}}{neh^{\ddagger}}\hat{\rho}_{\rm e}\hat{J}^i + \frac{ne\Delta h}{2\mu h^{\ddagger}}\gamma U^i \approx \gamma\tilde{J}^i + (\tilde{\rho}_{\rm e} - \gamma\tilde{\rho}'_{\rm e})U^i, \tag{24}$$

$$\hat{\rho}^{\dagger}_{\rm e} \equiv \frac{ne}{2\mu h^{\ddagger}}\hat{K}^{00} = \hat{\rho}_{\rm e}\left(\gamma - \frac{\Delta h^{\sharp}}{2neh^{\ddagger}}\hat{\rho}_{\rm e}\right) + \frac{ne\Delta h}{4\mu h^{\ddagger}}\hat{\gamma}^2 \approx \gamma(\tilde{\rho}_{\rm e} - \gamma\tilde{\rho}'_{\rm e}/2). \tag{25}$$

The last three terms in the last bracket of the right-hand side of Equation (23) correspond the electromotive forces due to gravity, centrifugal force, and frame-dragging effect, respectively. The gravitational electromotive 3-force,

$$\boldsymbol{E}_{\rm grv} = \frac{2\mu h}{(ne)^2}\nabla(\ln\alpha)\rho^{\dagger}_{\rm e}\frac{1}{\gamma} \tag{26}$$

may cause the magnetic reconnection, while frame dragging and centrifugal electromotive forces never change the topology of the magnetic field configuration. The magnetic reconnection will be induced by the gravitational electromotive force in the following situation as an example. Let us consider a current sheet in an accretion disk around a black hole, which is thin and localized near the equatorial plane and whose current is directed radially. When the net electric charge is distributed at the equatorial current sheet locally, the local radial electric field is induced by the gravitational electromotive force $\boldsymbol{E} = \boldsymbol{E}_{\rm grv}$. When the direction of the gravitational electromotive force $\boldsymbol{E}_{\rm grv}$ is the same as that of the current density $\boldsymbol{J}$ of the current sheet, we can define the positive effective resistivity $\eta_{\rm grv}$, which satisfies $\boldsymbol{E}_{\rm grv} = \eta_{\rm grv}\boldsymbol{J}$. We recognize that this effective resistivity induces the magnetic reconnection. The sign of $\eta_{\rm grv}$ depends on the charge separation $\rho^{\dagger}_{\rm e}$ and the directions of current and gravity. This process shows that the charge causes the magnetic reconnection in the gravity. It is natural to consider that the charge separation is not kept stationary because of plasma oscillation and the gravitational magnetic reconnection is transient. With respect to the charge separation of plasmas around black holes, we found an new instability of charge separation using linear analysis of the generalized GRMHD equations [8]. This instability causes the charge separation with small-scale length in a disk around a black hole. Thus, the gravitational electromotive force due to the small-scale charge separation is expected to induce the magnetic reconnection in average.

I am grateful to Mika Koide for her helpful comments on this paper. I thank Kunihito Ioka for his fruitful discussion during the conference.

References

[1] S. Koide, K. Shibata, & T. Kudoh, Phys. Rev. D **74**, 044005 (2006) .

[2] J. C. McKinney, Mon. Not. R. Astron. Soc. **368**, 1561 (2006).

[3] S. Koide, Phys. Rev. D **78**, 125026 (2008).

[4] S. Koide, Astrophys. J. **696**, 2220 (2009).

[5] R. Khanna, Mon. Not. R. Astron. Soc. **294**, 673 (l998).

[6] D. L. Meier, Astrophys. J. **605**, 340 (2004).

[7] S. Koide, Astrophys. J. **708**, 1459 (2010).

[8] Koide, S. Astrophys. J. , submitted

Black Hole Magnetosphere for Two-fluid Flows

Yasufumi Kojima[1]

Department of Physics, Hiroshima University, Higashi-Hiroshima 739–8526, Japan

Abstract

A numerical approach to construct a black hole magnetosphere is given. The stationary axisymmetric structures of electromagnetic fields and plasma flows in Schwarzschild spacetime are assumed. The charge density and current as the source terms of the Maxwell's equations are calculated by solving motions of positively and negatively charged particles for which electromagnetic forces are determined by global electromagnetic fields. The two-fluid approach without using an ideal MHD condition is discussed.

1 Introduction

Magnetosphere around a black hole has been studied for more than three decades. See e.g.,[1, 2] for a review. The energy extraction from central supermassive black hole may be important as a model of AGNs[3]. The numerical construction of global electromagnetic structure is not easy even if stationary and axially symmetries are assumed. Normally, an ideal MHD condition is also assumed everywhere. There are five constants along the field line, and the global structure of magnetic flux function $G(r,\theta)$ is determined by the trans-field equation, so-called the Grad-Shafranov equation. It is not easy to obtain a consistent solution, since the equation is highly non-linear and contains unknown functionals, $\Phi(G)$,$S(G)$. For example, a poor choice of the functionals leads to a singularity of the function $G(r,\theta)$. It is therefore necessary to determine $G(r,\theta)$ and $(\Phi(G),S(G))$. We here consider the problem in term of two-fluid approximation, by relaxing the ideal MHD condition. The method is applied to construction of pulsar magnetosphere[4].

2 Formalism

We consider a stationary, axially symmetric electromagnetic field in the Schwarzschild metric,

$$ds^2 = -\alpha^2 dt^2 + \alpha^{-2} dr^2 + r^2 d\theta^2 + (r\sin\theta)^2 d\phi^2, \tag{1}$$

where $\alpha = 1 - 2M/r$ and M is the mass of the black hole. It is not difficult to extend the Kerr metric, which is necessary to examine the Blandford-Znajek process[3]. The 3+1 split formalism[5] is used in this paper, and electromagnetic fields $(\vec{E},\vec{B})$, charge density ρ_e, and current $\vec{j}$ mean the quantities measured by fiducial observer at each point. Electromagnetic fields are generally expressed by three scalar functions $\Phi(r,\theta)$,$G(r,\theta)$,$S(r,\theta)$ as

$$\vec{E} = -\frac{1}{\alpha}\vec{\nabla}\Phi, \tag{2}$$

$$\vec{B} = \frac{1}{r\sin\theta}\vec{\nabla}G \times \vec{e}_\phi + \frac{S}{\alpha r\sin\theta}\vec{e}_\phi, \tag{3}$$

where $\vec{e}_\phi$ is the azimuthal unit vector. A set of Maxwell equations in stationary, axisymmetric case

$$\nabla\cdot\vec{E} = 4\pi\rho_e, \qquad \nabla\cdot\vec{B} = 0, \qquad \vec{\nabla}\times(\alpha\vec{E}) = 0, \qquad \vec{\nabla}\times(\alpha\vec{B}) = 4\pi\vec{j} \tag{4}$$

are reduced to

$$\frac{\alpha}{r^2}\frac{\partial}{\partial r}\left(r^2\frac{\partial\Phi}{\partial r}\right) + \frac{1}{\alpha r^2\sin\theta}\frac{\partial}{\partial\theta}\left(\sin\theta\frac{\partial\Phi}{\partial\theta}\right) = -4\pi\rho_e, \tag{5}$$

[1]Email: kojima@theo.phys.sci.hiroshima-u.ac.jp

$$\frac{\partial}{\partial r}\left(\alpha^2\frac{\partial G}{\partial r}\right)+\frac{\sin\theta}{r^2}\frac{\partial}{\partial\theta}\left(\frac{1}{\sin\theta}\frac{\partial G}{\partial\theta}\right)=-4\pi r\sin\theta j_\phi, \tag{6}$$

and

$$\frac{1}{r\sin\theta}\vec{\nabla}S\times\vec{e}_\phi=4\pi\alpha\vec{j}_p. \tag{7}$$

The ideal MHD condition, $\vec{E}\cdot\vec{B}=0$ leads to $\Phi=\Phi(G)$. The electric current should be along the magnetic field line, so that we have $S=S(G)$. These functional relations are used in the MHD approach, but are not assumed here.

We adopt a treatment in which the plasma is modeled as a two-component fluid. Each component, consisting of positively or negatively charged particles, is described by a number density $n_\pm$ and velocity $\vec{v}_\pm$. We assume that the positive particle has mass m and charge q, while the negative one has mass m and charge $-q$. The charge density and current are given as

$$\rho_e=q(n_+-n_-), \tag{8}$$

$$\vec{j}=q(n_+\vec{v}_+-n_-\vec{v}_-). \tag{9}$$

Continuity equation for each component in the stationary condition is

$$\vec{\nabla}\cdot(\alpha n_\pm\vec{v}_\pm)=0. \tag{10}$$

This equation is satisfied by introducing a stream function $F_\pm(r,\theta)$ as

$$\alpha n_\pm\vec{v}_\pm=\frac{1}{r\sin\theta}\vec{\nabla}F_\pm\times\vec{e}_\phi. \tag{11}$$

The number density is given by

$$n_\pm=\frac{|\nabla F_\pm|}{\alpha r\sin\theta(v_{\pm r}^2+v_{\pm\theta}^2)^{1/2}}. \tag{12}$$

The current function S in eq.(7) can be solved as

$$S=4\pi q(F_+-F_-). \tag{13}$$

The interaction between two-component fluids is assumed only through the global electromagnetic fields, i.e, collision and thermal pressure are ignored. The gravity is expressed by the derivative of α in the Schwarzschild spacetime. The equation of motion for each component with mass m and charge $\pm q$ in the stationary state is given by

$$\left(\vec{v}_\pm\cdot\vec{\nabla}\right)\gamma_\pm\vec{v}_\pm=-\gamma_\pm\vec{\nabla}\ln\alpha\pm\frac{q}{m}\left[\vec{E}+\vec{v}_\pm\times\vec{B}\right]. \tag{14}$$

There are two conserved quantities along each stream line, i.e, generalized angular momentum $J_\pm$ and Bernoulli integral $K_\pm$:

$$J_\pm=\gamma_\pm v_{\pm\phi}r\sin\theta\pm\frac{q}{m}G, \tag{15}$$

$$K_\pm=\alpha\gamma_\pm\pm\frac{q}{m}\Phi. \tag{16}$$

These quantities depend on the stream functions $F_\pm$ only, and the spatial distributions are therefore determined by $F_\pm$ which is specified at the injection point in our model. The stream functions are determined by

$$\begin{aligned}&\frac{\partial}{\partial r}\left(\alpha^2\frac{\partial F_\pm}{\partial r}\right)+\frac{\sin\theta}{r^2}\frac{\partial}{\partial\theta}\left(\frac{1}{\sin\theta}\frac{\partial F_\pm}{\partial\theta}\right)\\&=\vec{\nabla}\ln\left(\frac{n_\pm\alpha^2}{\gamma_\pm}\right)\cdot\vec{\nabla}F_\pm\pm\frac{q}{mc}\frac{n_\pm}{\gamma_\pm}S+\frac{\alpha n_\pm^2r^2\sin^2\theta}{\gamma_\pm}\left(K'_\pm-\frac{\alpha v_{\pm\phi}}{r\sin\theta}J'_\pm\right),\end{aligned} \tag{17}$$

where $J'_\pm$ and $K'_\pm$ are derivatives of $J_\pm$ and $K_\pm$ with respect to $F_\pm$.

3 Summary

The global structure of electromagnetic fields and plasma flows is determined by four partial differential equations of elliptic type, i.e, eqs. (5),(6) and (17). They should be subject to appropriate boundary conditions. There are two integrals along the stream line for each fluid component. The details of numerical method and results will be given elsewhere.

References

[1] V. S. Beskin, Phys.-Usp., **40**, 659 (1997).

[2] B. Punsly, *Black hole gravitohydromagnetics* Springer (2001).

[3] R. D. Blandford and R. L. Znajek, Mon. Not. R. Astron. Soc. , **179**, 433 (1977).

[4] Y. Kojima and J. Oogi, Mon. Not. R. Astron. Soc. , **398**, 271 (2009).

[5] K. S. Thorne, R. H. Price and D. A .MacDonald, *Black holes: The membrane paradigm* Yale University Press (1986).

Black hole-neutron star binaries in numerical relativity

Koutarou Kyutoku[1(a)], Masaru Shibata[2(a)], Tetsuro Yamamoto[(b)], Keisuke Taniguchi[3(c)]

[(a)] *Yukawa Institute for Theoretical Physics, Kyoto University, Kyoto 606-8502*
[(b)] *Yugen Club, Toyama, Shinjuku, Tokyo 162-0052*
[(c)] *Graduate School of Arts and Sciences, The University of Tokyo, Komaba, Meguro, Tokyo 153-8902*

Abstract

Gravitational waves from the mergers of the compact object binaries including neutron stars are believed to give us unique information about the equation of state at high density, which cannot be constrained from the terrestrial experiments. We investigate the dependence of the gravitational waveforms from the mergers of the black hole-neutron star binaries on the equation of state of the neutron stars by numerical relativistic simulations, and show that it is possible that the gravitational wave spectrum from the black hole-neutron star binary gives us an opportunity for the observation of the compactness or the radius of the neutron star through the tidal disruption of the neutron star.

1 Introduction

The mergers of the compact object binaries such as black hole-neutron star (hereafter BH-NS) binaries are the most promising sources of the gravitational waves (hereafter GW) for ground-based laser-interferometric detectors. Furthermore, it is possible that the massive-hot accretion disks are formed after the mergers of BH-NS binaries, which are the ones of the possible progenitors of the short gamma-ray bursts. To predict realistic gravitational waveforms and to investigate the remnants of the binary mergers, we must perform fully general relativistic simulations, or numerical relativity.

The final fates of the BH-NS mergers are classified into two cases, in which the tidal disruptions of the NS occurs during the inspiral or not. Whether the tidal disruption occur or not is determined mainly by two parameters; the mass ratio of the binary, $Q \equiv M_{\rm BH}/M_{\rm NS}$, and the compactness of the NS, $\mathcal{C} \equiv GM_{\rm NS}/Rc^2$, where $M_{\rm BH}$ is the mass of the BH, $M_{\rm NS}$ is the mass of the NS and R is the radius of the NS in isolation. In our previous work [3] it is found that the features of the tidal disruption is cleary seen in the gravitational waveforms if the mass ratio of the binary Q is small and the compactness of the NS $\mathcal{C}$ is also small, since the tidal force of the BH acting on the NS is significant in such cases and truncates the GW suddenly.

For the fixed mass NS, the radius and equivalently the compactness of the NS in isolation is determined by the adopted equation of state (hereafter EOS). When the EOS in the high density region is stiff, the pressure inside the NS is so strong that it easily circumvents the NS to contract due to its strong self gravitational forces and the radius of the NS tends to be larger than the case in which the EOS in the NS is softer. One important role of the gravitational wave astronomy is to constrain or determine the EOS in such high density region, which is not well constrained both by the theory and the terrestrial experiments, from the observation of the GWs from the NS.

In this work, we investigated the effects of the realistic EOS on the gravitational waves emitted during the mergers of BH-NS binaries by the numerical relativistic simulations, using the piecewise polytropic EOS [5], which analytically mimics the nuclear-theory based EOS at high density. In section 2, we describe the method of our calculation. In sectoin 3 we show our numerical results, especially focusing on the dependence of the gravitational waveforms on the adopted EOS. Section 4 is devoted to a summary.

[1]Email address: kyutoku@yukawa.kyoto-u.ac.jp
[2]Email address: mshibata@yukawa.kyoto-u.ac.jp
[3]Email address:keisuke@ea.c.u-tokyo.ac.jp

2 Methods

Initial conditions of the dynamical simulations are computed as solutions of the initial value problem of general relativity. Almost all assumptions and methods for the computation of quasiequilibrium state of the BH-NS binary are the same as described in Ref. [2]; the BH are modeled as a puncture with zero spin and the matter inside NS is assumed to have irrotational velocity field. The difference is the implementatoin of the piecewise polytropic EOS [5] for the NS matter to analytically represent the nuclear-theory based, zero-temparature EOS. Piecewise polytropic EOS with N pieces has the form of

$$P = \kappa_i \rho^{\Gamma_i} \ (\rho_{i-1} < \rho < \rho_i), \tag{1}$$

where $\rho_0 = 0$ and $\rho_N \to \infty$. Here P denotes the pressure and ρ is the rest-mass density. The specific internal energy and the specific enthalpy are calculated using the first law of thermodynamics under the assumption of the zero-temparature. Recently it is reported that the piecewise polytropic EOS with four pieces are adequate to represent most of the realistic EOS [5], however, we use only two pieces EOS in this work for the sake of simplicity. Our two pieces EOS is still useful to clarify how the EOS affects the gravitational waveforms through the difference in the NS compactness $\mathcal{C}$. We also fix the EOS at low density, which corresponds to the relatively well-constrained EOS in the crust region, and vary the EOS at high density, which corresponds to the core region. In this paper we used eight EOS to represent the EOS in the core region.

Our current interest is to clarify the difference in the GW due to the tidal disruption of the NS and it is shown that such features are not present in the case of high mass-ratio binaries with $Q \gtrsim 4$ in our previous work [3]. According to this result, we focus on the binaries with the canonical mass NS, $M_{\rm NS} = 1.35 M_\odot$, and the relatively low mass-ratio binary with $Q \equiv M_{\rm BH}/M_{\rm NS} = 2$. Numerical computation of the initial conditions are performed using the multi-domain spectral method library LORENE [4].

Our dynamical simulations are performed using fully relativistic, adaptive-mesh refinement code SACRA [1] developed in our group. The formulation, gauge conditions and chosen schemes are almost the same as described in Refs. [1, 3] except for the implementation of the piecewise polytropic EOS for the cold part of the EOS. For the thermal part of the EOS, we employed simple Γ-law EOS as a rough approximation. While the implematation of more realistic, finite temparature EOS is important to elucidate the features of the remnant BH-disk systems, this approximation seems to be adequate for our current interest, i.e. to clarify the effect of tidal disruption on the GW, since the finite temparature effect does not seem to play an important role on the tidal features of the NS. We also note that the detailed microphysics such as neutrino emisson and the effect of the magnetic fields may be important ingredients controlling the features of the remnatns after the merger. The implementation of such effects will be essential to clarify if the BH-NS binary mergers can actually be the progenitors of the short gamma-ray bursts, and we do not go into detail of that issue in this paper.

3 Results

In Fig. 1, we show the GW spectra from the mergers of the face-on BH-NS binary at the 100Mpc distance from us, calculated in our simulations. We also show the GW spectra calculated with the quadrupole formula and with the post-Newtonian, so-called Taylor-T4 formula [6] for the comparison. Numerically calculated GW spectra at the earlier stages of the mergers coincides with the spectrum calculated with the Taylor-T4 formula within high precision, since the point particle approximation to the NS is valid in that low-frequency range.

The GW spectra at high frequency range are sensitive to the compactness or the radius of the NS. This is due to the fact that the tidal disruption occurs at earlier stage of the inspiral for the binary with less compact NS, since in the merger of such binary the tidal force of the BH plays more important role through the larger radius of the NS. The GW amplitude from such binary decreases suddenly at the occurence of the tidal disruption and the GW spectrum is terminated at rather smaller frequency. By contrast, if the NS is more compact the inspiral extends to rather high frequncy without tidal disruption and consequently the high frequency GW is emitted. Actually, the GW spectra shown in Fig. 1 are in order of the compactnesses or the radii of the NS; the leftmost GW spectrum shows the GW from the binary with largest NS radius and the rightmost GW spectrum shows the GW from the smallest

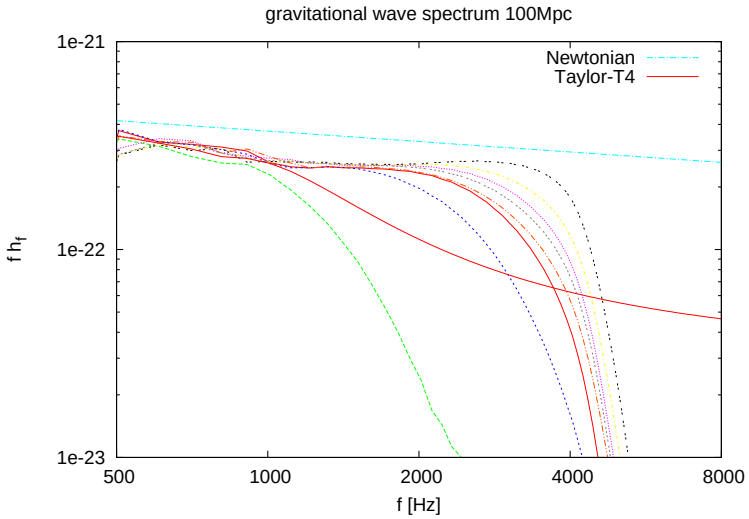

Figure 1: Several spectra of the GWs from the BH-NS binaries with $Q = 2$ and $M_{\rm NS} = 1.35M_\odot$, calculated with different EOS. All binaries are 100Mpc from us and assumed to be face-on. Upper transverse line represents the the spectrum calculated with Newtonian orbit and quadrupole formula, and lower transverse line represents the spectrum calculated with the so-called Taylor-T4 formula. The other lines are calculated by our numerical simulations and show the difference of the NS compactnesses. For the binaries with stiffer EOS and less compact NS, the GW amplitude decreases at the smaller frequency due to the tidal disruptions and higher frequency GWs are not emitted. By contrast, for softer EOS and more compact NS, inspiral extends longer and higher frequency GWs are emitted.

NS radius. We suggest that it may be possible to determine the radius of the NS accurately from the observations of the gravitational waveforms at the tidal disruptions.

Because we fix the mass of the NS $M_{\rm NS}$ in this work, we cannot determine which of the parameter can be extracted from the observations of the GW, the compactness or the radius. To clarify what parameters associated with the EOS can be well constrained, wider range of survey will be required about the mass of the NS and also the mass ratio of the binary. Moreover, it will be necessary to implement the piecewise polytropic EOS with more pieces in order to clarify to what precision we can constrain the realistic EOS from the observations.

4 Summary

We numerically calculate the gravitational waveforms from the BH-NS binaries with realistic EOS modeled as the piecewise polytropic EOS composed of two pieces. In particular we focus on the low mass-ratio binaries to investigate the effects of the tidal disruption on the GW spectra, since the tidal forces of the BH play more important roles in the mergers of the low mass-ratio binaries.

We find that the GW spectra reflect the compactness of the NS compactnesses or radii at least for the case of $Q = 2$ and $M_{\rm NS} = 1.35M_\odot$. The GW spectra from the binaries with less compact NS truncate at the smaller frequency due to the occurence of the tidal disruptions, while the spectra from the binaries with more compact NS extends to high frequncy. It is expected that from the observations of the GW from the BH-NS binary mergers, we can know the compactness or the radius of the NS accurately and it will be able to constrain the EOS at high density, core region.

More surveys on the GW from the binary of the different mass-ratio, the different mass of the NS and the piecewise polytropic EOS with more pieces are necessary to clarify systematically the dependence of the GW from the BH-NS binaries on the adopted EOS. It would also be important to incorpolate detailed microphysics and the effect of the magnetic fields to clarify the features of the merger remnants and show whether the BH-NS binaries can be the sources of the short gamma-ray bursts.

References

[1] T. Yamamoto, M. Shibata, K. Taniguchi, Phys. Rev. D **78**, 064054 (2008).

[2] K. Kyutoku, M. Shibata, K. Taniguchi, Phys. Rev. D **79**, 124018 (2009).

[3] M. Shibata, K. Kyutoku, T. Yamamoto, K. Taniguchi, Phys. Rev. D **79**, 044030 (2009).

[4] LORENE website: http://www.lorene.obspm.fr/

[5] J. S. Read, B. D. Lackey, B. J. Owen, J. L. Friedman Phys. Rev. D **79**, 124032 (2009).

[6] A. Buonanno, G. B. Cook, F. Pretrius Phys. Rev. D **75**, 124018 (2007).

Quantitative evaluation of the amplitude of the primordial magnetic field generated at the pre-recombination era

Satoshi Maeda[1(a)], Keitaro Takahashi[2(b)], Tsutomu Kobayahi[3(c)] and Tetusya Shiromizu[4(a)]

[(a)] *Department of Physics, Kyoto University, Department of Physic, Kyoto, 606-8502*
[(b)] *Department of Physics, Nagoya University, Chikusa-ku, Nagoya, 464-8602*
[(c)] *Department of Physics, Waseda University, Okubo 3-4-1, Shinjuku, Tokyo, 169-8555*

Abstract

The origin of the large-scale magnetic fields is one of the interesting problem in modern cosmology. We explored the possibility of generating the such fields at the pre-recombination era using the second-order perturbation theory. Thomson scattering is important for generating the fields. In order to treat this process analytically, we use tight coupling approximation. Finally it was shown that the source term for the magnetic field is given by the product of the first order perturbations. In this work, we solve the evolution equation of the first-order perturbations and calculate the power spectrum of the magnetic field generated at the recombination era in order to get the quantitative evaluation of the amplitude of the generated magnetic fields.

1 Introduction

We observe the magnetic fields($\sim \mu Gauss$) in the galaxy and galaxy clusters today. The origin of such fields is not clear yet[1]. If primordial large-scale magnetic field is present, it may serve as seeds for the magnetic fields in galaxies and clusters which are amplified through the dynamo mechanism after galaxy formation[2].

There are many mechanism which give the generation of the large-scale primordial magnetic fields in the early universe. And many authors examine the possible of the magnetic fields generated at the pre-recombination era[3–6]. The standard inflationary scenario predicts the generation of the scalar (and tensor) perturbations which explain the fluctuations of the cosmic microwave background and the seeds for the large scale structure. The first-order vector perturbations like magnetic fields can not be generated in the standard inflationary scenario. However, there are the possible of the generation of the vector perturbation when we consider up to the send-order perturbations. When we consider the pre-recombination era, photons are strongly coupled with protons and electrons via the Thomson scattering. Since the proton's and electron's Thomson cross section is different, the difference of the velocities is generated. In the result, the rotational current and the magnetic field is produced. In the previous work[6], we consider the above mechanism and using the second-order cosmological perturbation theory and tight coupling approximation for the Thomson scattering and give the evolution equation of the magnetic fields:

$$(a^3 B^i)' = \frac{1-\beta^3}{1+\beta}\frac{\sigma_T}{e}a^2\bar{\rho}_\gamma^{(0)}\left[\frac{2a^2\mathcal{H}}{\bar{\alpha}^{(0)}}\omega^{(2)i} + \epsilon^{ijk}\frac{\bar{R}^{(0)}}{1+\bar{R}^{(0)}}\partial_j\Delta_b^{(I,1)}\delta v_{(\gamma b)k}^{(I,1)}\right]. \tag{1}$$

where a is the scale factor and $\mathcal{H} = a'/a$, $\beta = m_e/m_p$, $\bar{R}^{(0)} = 3\bar{\rho}_b^{(0)}/4\bar{\rho}_\gamma^{(0)}$,

$$\bar{\alpha}^{(0)} = \frac{(1+\beta^2)(1+\bar{R}^{(0)})}{1+\beta}\frac{a\sigma_T\bar{\rho}_\gamma^{(0)}}{m_p}, \quad \Delta_b^{(I,1)} = \int d\eta\partial_i\delta v_{(\gamma b)}^{(I,1)i}, \quad \delta v_{(\gamma b)i}^{(I,1)} = \frac{1}{\bar{\alpha}^{(0)}}\left[\mathcal{H}v_i^{(1)} - \frac{1}{4}\frac{\partial_i\delta\bar{\rho}_\gamma^{(1)}}{\bar{\rho}_\gamma^{(0)}}\right] \tag{2}$$

[1]Email address: smaeda@tap.scphys.kyoto-u.ac.jp
[2]Email address: keitaro@a.phys.nagoya-u.ac.jp
[3]Email address: tsutomu@gravity.phys.waseda.ac.jp
[4]Email address: shiromizu@tap.scphys.kyoto-u.ac.jp

and the prime denotes the derivative with respect to conformal time η. And $\omega^{(2)}$ represents the photon's vorticity. Furthermore, we derive the vorticity evolution equation:

$$(a^2\omega^{(2)i})' + \frac{\mathcal{H}\bar{R}^{(0)}}{1+\bar{R}^{(0)}}a^2\omega^{(2)i} = \frac{\bar{R}^{(0)})}{2(1+\bar{R}^{(0)})^2}\epsilon^{ijk}\partial_j\Delta_b^{(I,1)}\bar{\alpha}^{(0)}\delta v_{(\gamma b)k}^{(I,1)}. \tag{3}$$

We find that the vorticity itself is sourced by the product of the first-order perturbation in the vorticity evolution equation. We find from eq.(1) and eq.(3) that the sources of the magnetic fields are the product of the first-order perturbations We call the first and second term in eq.(1) as the vorticity and slip term.

Our purpose in this work is the quantitative evaluation of the magnitude of the fields. Therefore we calculate the power spectrum of the magnetic fields.

2 The time evolution of the fluctuations

We solve the linearized equation since the source of the second-order magnetic fields is the product of the first-order cosmological perturbations. Since the scalar, vector and tensor perturbations are separated in the linearized theory, we consider only scalar perturbations which are the photon's velocity perturbations $v_i = \partial_i v$ and photon's density perturbations $\delta = \delta\bar{\rho}_\gamma^{(1)}/\bar{\rho}_\gamma^{(0)}$. Let us consider the radiation dominant era and only photon's perturbations. The linearized Einstein equation gives the time evolution of the metric perturbations $\hat{\psi}^{(1)}$, which express the gravitational potential, and the relation between the metric, density and velocity perturbations:

$$\frac{d^2\hat{\psi}_{\vec{k}}^{(1)}}{d\eta^2} + \frac{4}{\eta}\frac{d\hat{\psi}_{\vec{k}}^{(1)}}{d\eta} + \frac{1}{3}k^2\hat{\psi}_{\vec{k}}^{(1)} = 0, \tag{4}$$

$$-\frac{3}{2}\mathcal{H}^2\hat{\delta}_{\vec{k}}^{(1)} = 3\mathcal{H}\left((\hat{\psi}_{\vec{k}}^{(1)})' + \mathcal{H}\hat{\psi}_{\vec{k}}^{(1)}\right) + k^2\hat{\psi}_{\vec{k}}^{(1)}, \tag{5}$$

$$-2\mathcal{H}^2\hat{v}_{\vec{k}}^{(1)} = (\hat{\psi}_{\vec{k}}^{(1)})' + \mathcal{H}\hat{\psi}_{\vec{k}}^{(1)}, \tag{6}$$

where the hat denotes the Fourier component. We consider only the radiation perturbations in the above calculation. However, the dark matter perturbations dominate on the small scale since radiation perturbations diffuse by the Silk damping. So this approximation is valid for $k < k_{silk}$. The Silk scale, k_{Silk}, is the scale where the Silk damping is important.

We can replace eq.(4) into the spherical Bessel's differential equation and have the solution

$$\hat{\psi}^{(1)}(k,\eta) \quad = \quad 3\hat{\psi}_0^{(1)}(\vec{k})\frac{j_1(k\eta/\sqrt{3})}{k\eta/\sqrt{3}}, \tag{7}$$

where $j_1(x)$ is spherical Bessel functions of order 1 and $\hat{\psi}_0^{(1)}$ is the primordial perturbation. Substituting eq.(7) into eq.(5) and eq.(6), we get the time evolution of density and velocity perturbations. Finally, the magnetic fields can be represented by the primordial perturbations.

3 The power spectrum of the magnetic fields

We define the power spectrum of the magnetic fields as the following:

$$< B_i(\vec{k},\eta)B^{*i}(\vec{K},\eta) >= \frac{2\pi^2}{k^3}P_B(k)\delta(\vec{k}-\vec{K}), \tag{8}$$

where the bracket represents an ensemble average. In order to calculate the left-hand side in the above equation, we give the magnetic fields in Fourier space from eq.(1):

$$\hat{B}^i(\vec{k},\eta) = -\frac{1-\beta^3}{1+\beta}\frac{\sigma_T\rho_{\gamma 0}^{(0)}}{ea^3}\int_0^\eta d\eta' a^{-2}(\eta')\left(\hat{\Omega}^i + \hat{S}^i\right), \tag{9}$$

where $\hat{\Omega}^i$ and $\hat{S}^i$ are the Fourier transformation of the vorticity part and the slip part. Using this equation, we take ensemble average of magnetic fields.

$$< \hat{B}_i(\vec{k},\eta)\hat{B}^{*i}(\vec{K},\eta) > = \left(\frac{1-\beta^3}{1+\beta}\frac{\sigma_T\rho^{(0)}_{\gamma 0}}{ea^3}\right)^2 \int_0^\eta d\eta_1 \int_0^\eta d\eta_2 a^{-2}(\eta_1)a^{-2}(\eta_2) \times \\ \times < \left(\hat{\Omega}_i(\vec{k},\eta_1)+\hat{S}_i(\vec{k},\eta_1)\right)\left(\hat{\Omega}^{*i}(\vec{K},\eta_2)+\hat{S}^{*i}(\vec{K}\eta_2)\right) > . \quad (10)$$

Reminded that an ensemble average of the primordial perturbations satisfy the following equation using the power spectrum of the primordial perturbations

$$< \hat{\psi}_0(\vec{k})\hat{\psi}^*_0(\vec{K}) >= \frac{2\pi^2}{k^3}P_\psi(k)\delta(\vec{k}-\vec{K}), \quad (11)$$

we calculate eq.(10) and the power spectrum of the magnetic fields is represented by one of the primordial perturbations.

After the tedious calculations we have finally the power spectrum of the magnetic fields,

$$\frac{2\pi^2}{k^3}P_B(k,\eta) = \left(\frac{1-\beta^3}{1+\beta}\frac{\sigma_T\rho_{\gamma 0}}{ea^3}\right)^2 (2\pi^2)^2 \int d^3p \int_0^\eta d\eta_1 \int_0^\eta d\eta_2 \times \\ \times|\vec{k}\times\vec{p}|^2\frac{P_\psi(p)}{p^3}\frac{P_\psi(|\vec{k}-\vec{p}|)}{|\vec{k}-\vec{p}|^3}a^{-2}(\eta_1)a^{-2}(\eta_2)\{g(\vec{k},\vec{p},\eta_1)+f(\vec{k},\vec{p},\eta_1)\}\times \\ \times\{g(\vec{k},\vec{p},\eta_2)-g(\vec{k},\vec{k}-\vec{p},\eta_2)+f(\vec{k},\vec{p},\eta_2)-f(\vec{k},\vec{k}-\vec{p},\eta_2)\}, \quad (12)$$

where $y_1 = p\eta/\sqrt{3}$, $y_2 = |\vec{k}-\vec{p}|\eta/\sqrt{3}$, $P(\eta) = \mathcal{H}\bar{R}^{(0)}/1+\bar{R}^{(0)}$,

$$f(\vec{k},\vec{p},\eta) = \frac{1}{(2\pi)^{3/2}}\frac{\bar{R}^{(0)}}{1+\bar{R}^{(0)}}\frac{1}{\bar{\alpha}^{(0)}}\frac{\eta^2}{4}p^4|\vec{k}-\vec{p}|^2\frac{j_1(y_2)}{y_2}\int_0^\eta d\eta'\left(\frac{(\eta')^2}{\bar{\alpha}^{(0)}}\frac{j_1(y_1')}{y_1'}\right), \quad (13)$$

$$g(\vec{k},\vec{p},\eta) = \frac{1}{4\eta\bar{\alpha}^{(0)}}\frac{1}{(2\pi)^{3/2}}e^{-\int_0^\eta P(\eta')d\eta'}p^4|\vec{k}-\vec{p}|^2\times \\ \times\int_0^\eta d\eta'\frac{\bar{R}^{(0)}}{(1+\bar{R}^{(0)})^2}(\eta')^2\frac{j_1(y_2')}{y_2'}\int_0^{\eta'}d\eta''\left(\frac{(\eta'')^2}{\bar{\alpha}^{(0)}}\frac{j_1(y_1'')}{y_1''}\right)e^{\int_0^{\eta'}P(\eta'')d\eta''}, \quad (14)$$

$$P_\psi(k) = \frac{9}{4}\Delta^2_{\mathcal{R}}(k_0)\left(\frac{k}{k_0}\right)^{n_s-1}. \quad (15)$$

where $j_1(x)$ is the spherical Bessel function of the first kind and order one. In recent measurements, $n_s \simeq 1.0$ and $\Delta^2_{\mathcal{R}}(k_0 = 0.002\text{Mpc}) \simeq 2.5\times 10^{-9}$.

Here we note the range of the wave-number integral. The photon's perturbations on smaller scale than the Silk scale are suppressed by the Silk damping. But we do not consider this effect in the calculation in Section 2. It causes the divergence of the wave-number integral in eq.(12). The photon's density and velocity perturbations on smaller scale than the Silk scale, k^{-1}_{Silk}, do not contribute to the generation of the magnetic fields because of the Silk damping. So we set $k_{\max} = k_{Silk}$ as the upper limit of the wave-number integral. And the contribution of the large-scale perturbation should be important when the perturbations enter the horizon. Hence the lower limit of the wave-number integral is $k_{\min} = k_{\rm H}$. We mention that the Silk scale depends on the time, $k_{Silk} \simeq 4.3\times 10^{-6}a^{-3/2}(\text{Mpc})^{-1}$ and the horizon scale depends also on the time, $k_{\rm H} = 1/\eta$.

4 Summary

We derived the evolution equation of the magnetic fields and found the product of the first-order perturbations is the source for generating the fields at the pre-recombination era in our previous work. In this

work, we estimate the power spectrum of the magnetic field in order to get the quantitative evaluation of the generated magnetic fields.

When we estimate the time evolution of the photon's fluctuations, we do not consider the Silk damping. The fluctuations are suppressed strongly on the small scale and do not contribute the generation of the magnetic fields mostly. Also, the fluctuations on the larger scale than the hubble horizon do not contribute. So we introduce the Silk scale as the upper limit and the horizon scale as the lower limit in the wave-number integral. A remaining work is the numerical integration of eq.(12). We will prepare the shape of the power spectrum soon.

References

[1] L. M. Widrow, Rev. Mod. Phys. **74**, 775 (2002); M. Giovannini, Int. J. Mod. Phys. D **13**, 391(2004).

[2] A. C. Davis, M. Lilley and O. Tornkvist, Phys. Rev. D **60**, 021301 (1999).

[3] S. Matarrese, S. Mollerach, A. Notari and A. Riotto, Phys. Rev. D **71**, 043502 (2005).

[4] K. Ichiki, K. Takahashi, N. Sugiyama, H. Hanayama and H. Ohno, Science **311**, 827 (2006); K. Ichiki, K. Takahashi, N. Sugiyama, H. Hanayama and H. Ohno, arXiv:astro-ph/0701329; K. Takahashi, K. Ichiki and N. Sugiyama, Phys. Rev. D **77**, 124028 (2008).

[5] T. Kobayashi, R. Maartens, T. Shiromizu and K. Takahashi, Phys. Rev. D **75**, 103501 (2007).

[6] S. Maeda, S. Kitagawa, T. Kobayashi and T. Shiromizu, Class. Quant. Grav. **26**, 135014 (2009).

Inflation, modulation and baryogenesis with warm directions

Tomohiro Matsuda[1]

Department of Physics, Saitama Institute of Technology, Saitama, 369-0293

Abstract

There are many flat directions in SUSY models, which may dissipate their energy and source the radiation background during inflation. However, the only possibility that has been studied in this direction is warm inflation, which uses "warm" (or "dissipative" if we consider more modest situation) direction as the inflaton. In this talk we discuss other significant possibilities of such directions which are dissipative and may or may not be "warm". Affleck-Dine (AD) mechanism and other cosmological scenarios are discussed in the light of "dissipative field", instead of using the conventional light field with mass protection. We sometimes consider Morikawa-Sasaki coefficient for the non-thermal background, which is important because the dissipation calculated for a naive thermal background with $T \to 0$ is not enough to discuss the dissipation with the non-thermal background. (This is a small extended version of the proceedings for the JGRG19.)

1 Dissipative directions for particle cosmology

Even in a non-thermal background, dissipation is generic for realistic field motion $\dot{\phi} \neq 0$ that leads to a coherent excitation of a heavy intermediate field χ that decays into light fermions ψ_d. Here we consider a typical interaction given by

$$\mathcal{L}_{int} = -\frac{1}{2}g^2\phi^2\chi^2 - h\chi\bar{\psi}\psi, \tag{1}$$

which leads to efficient decay of the intermediate field ($m_\chi \propto \phi$) with the decay rate

$$\Gamma_\chi \simeq \frac{N_\psi}{8\pi}h^2 m_\chi \simeq \frac{N_\psi}{8\pi}h^2 g\phi, \tag{2}$$

where N_ψ is the number of the light fermions. The dissipation coefficient is given by [1, 2]

$$\Upsilon \sim N_\chi \frac{\sqrt{2}g^3 N_\psi h^2 \phi}{8^3\pi^2}, \tag{3}$$

which is proportional to Γ_χ.

The strength of the "friction" caused by the dissipation is measured by the rate $r_\Upsilon \equiv \frac{\Upsilon}{3H}$. Then the field equation for the dissipative motion is given by

$$\ddot{\phi} + 3H(1 + r_\Upsilon)\dot{\phi} + V_\phi = 0, \tag{4}$$

where the subscript denotes the derivative with respect to the field. The effective slow-roll parameters are suppressed when r_Υ is large ("strongly dissipating");

$$\epsilon_{eff} = \frac{\epsilon}{(1 + r_\Upsilon)^2}, \qquad \eta_{eff} = \frac{\eta}{(1 + r_\Upsilon)^2}. \tag{5}$$

Our claim is very simple. **Dissipative motion is a generic phenomenon, which must be considered not only for the specific inflation model but also for other generic cosmological scenarios.** A **modest** assumption is that the background is **not** thermal, because "warm" background is not essential for the dissipative motion. Of course dissipation may be more significant when the background is thermal, but the required conditions for the thermalization are sometimes very severe. We thus

[1]Email address: matsuda@sit.ac.jp

consider non-thermal background during inflation because thermal conditions may spoil the generality of the dissipative scenario. On the other hand, thermal background is natural after reheating. We thus consider thermal background for the field motion after reheating. Assuming a thermal background, Υ can be given by

$$\Upsilon \propto \frac{T^n}{\phi^{n-1}}, \tag{6}$$

where $n = 1$ for high-temperature SUSY and $m = 3$ for low-temperature SUSY.

1.1 Natural dissipation in SUSY hybrid inflation

The first example[3] is SUSY hybrid inflation, for which we will argue that the conventional interaction $\mathcal{L}_I \sim -\frac{1}{2}g^2\phi^2\chi^2$ between the inflaton ϕ and the trigger field χ may cause significant dissipation that leads to slow-roll inflation. Namely, $O(H)$ correction from the supergravity may not spoil slow-roll in SUSY hybrid inflation.

The key in this scenario is the gravitational decay $\chi \to 2\psi_{3/2}$ of the intermediate (trigger) field, which leads to an inevitable decay rate

$$\Gamma_{\chi\to 2\psi_{3/2}} \simeq \frac{m_\chi^3}{M_p^2} \sim \frac{g^3\phi^3}{M_p^2}, \tag{7}$$

which is larger than the Hubble parameter H when $\phi > (HM_p^2)^{1/3}/g$. The dissipation coefficient of the inflaton mediated by the heavy trigger field χ is

$$\Upsilon \sim 10^{-2}\left(\frac{m_\chi}{M_p}\right)^2 \phi, \tag{8}$$

which gives the minimal value of Υ caused by the least channel of the gravitational decay. Surprisingly, $r_\Upsilon \gg 1$ is generic for the chaotic initial condition $\phi_{ini} \sim M_p$.

1.2 Dissipative Affleck-Dine field

Considering typical situation for the dissipative motion of the AD field, it is not appropriate to disregard thermal background $T \neq 0$. However, **in contrast to warm inflation** [4, 5], the thermal background is not always due to the dissipation caused by the field motion. Namely, the dissipation coefficient $\Upsilon(\phi, T)$ of the AD field may depend on the environment, temperature of the Universe, which depends on cosmological events other than the Affleck-Dine baryogenesis. Typically, MSSM directions couple to heavy directions that can decay into light fermions. Therefore, non-thermal dissipation would be significant at large distance, and thermal dissipation may be significant during a period depending on the field interaction and the temperature of the Universe. In any case, it is very important to consider dissipation of the AD field before the AD baryogenesis. If the dissipation is large enough to ensure the slow-roll, the AD-field is "trapped" at $\phi_{AD} \neq 0$. **The situation is in contrast with the conventional scenario, in which the "flip" of the potential is responsible for $\phi_{AD} \neq 0$.** If the AD field is trapped due to dissipation, the time when oscillation begins is not determined by the usual condition $m_\phi \sim H$.

The situation related to dissipation of the AD field can be summarized as follows.

1) The time when oscillation starts may be different from the conventional (non-dissipating) scenario.

2) The amplitude of the AD-field oscillation may be different.

These differences are expected to lead to crucial discrepancies in the results.

1.3 Dissipation before preheating

Above in section 1.1, we considered hybrid inflation in which the typical interaction (inflaton-trigger field interaction) leads to inevitable dissipation. A similar argument may apply to preheating scenario [6–8] in which the typical interaction (oscillating field-preheat field interaction) may lead to significant dissipation and slow-roll before the oscillation. Here we consider "instant preheating" scenario for simplicity, in which instant decay after preheating is assumed. Significant dissipation before the onset of oscillation typically

leads to a **delay of the oscillation**. To show explicitly the dissipative effect, we consider a potential with a mass

$$V(\phi) = \frac{1}{2}m^2\phi^2, \tag{9}$$

and the dissipation based on the non-thermal background. The interaction with the preheat field is given by

$$\mathcal{L}_{int} \simeq \frac{g_{PR}^2}{2}\phi^2\chi^2, \tag{10}$$

where **preheat field** χ plays the role of the **intermediate** field for the dissipation. The decay into light fermions, which is needed for the preheating scenario followed by the instant decay, is induced by the term

$$\mathcal{L}_{\psi\chi} = h\chi\bar{\psi}\psi. \tag{11}$$

Obviously, for $g \sim h \sim O(1)$, the dissipative process $\phi \to \chi \to \psi$ is efficient for the model of instant preheating. In fact, based on the non-thermal dissipation, it is very easy to show the slow-roll conditions that delays the preheating and reduces the amplitude of the oscillation. The dissipation coefficient is

$$\Upsilon \simeq 10^{-2}g_{PR}^2h^2m_\varphi \simeq 10^{-2}g_{PR}^3h^2\phi. \tag{12}$$

Then the effective slow-roll conditions are

$$\epsilon_w \simeq M_p^2\left(\frac{m^2\phi_I}{V}\right)^2\frac{1}{(1+r)^2} \sim \left(\frac{m}{10^{-2}\times\phi_I}\frac{1}{g_{PR}^3h^2}\right)^2 < 1 \tag{13}$$

$$\eta_w \simeq \frac{m^2}{H^2}\frac{1}{(1+r)^2} \sim \frac{m^2}{10^{-4}\times\phi^2}\frac{1}{g_{PR}^6h^4} < 1, \tag{14}$$

which lead to a simple slow-roll condition $\phi_I > 10^2\times m/g_{PR}^3h^2$, where the field motion is **not** oscillationary but simply slow-rolling. Therefore, the usual requirement for instant preheating followed by the instant decay now leads to a new condition for the model, which **affects the initial condition of the oscillation** that determines the amplitude of the oscillation; dissipation leads to a delay of the end of chaotic inflation. In fact, in conventional scenario of preheating after chaotic inflation, the amplitude was simply assumed that $\phi \sim M_p \gg \phi_I$. In contrast to the usual assumption, typical interaction of the scenario may lead to dissipative motion that may lead to significant slow-roll during $M_p > \phi > \phi_I$.

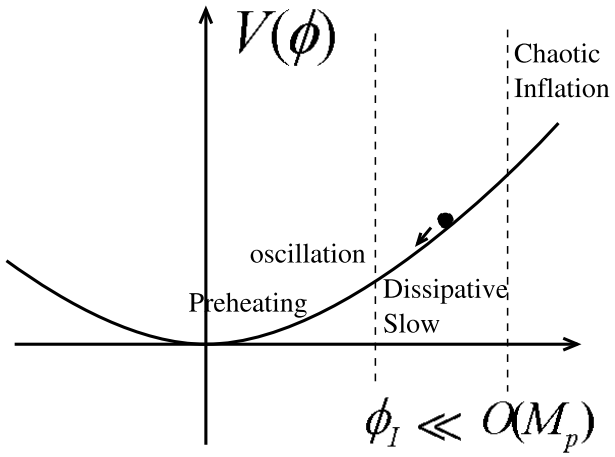

Figure 1: Without dissipation, chaotic inflation is expected to end at $\phi \sim O(M_p)$. However, interactions required for instant preheating suggests that non-thermal dissipation is common in such models and that an error may not be negligible.

1.4 Remote inflation (Thermal inflation sourced continuously by dissipation)

If dissipation is generic for many cosmological fields that acquire $O(H)$ mass during inflation, these fields may lead to thermal background during inflation. Note that there are at least **two** significant models in which thermal background is used for inflationary scenario: warm inflation and thermal inflation. In fact, warm inflation is based on the thermal background sourced by the dissipation, while no source mechanism has been considered for thermal inflation. Our idea is based on a naive question: **What happens if radiation in thermal inflation is sourced continuously by (many) cosmological fields that acquire $O(H)$ mass and dissipate their energy during inflation?** Namely, background radiation sourced by dissipation may cause symmetry restoration in a remote sector [9, 10], where thermal inflation occurs.

1.5 Conclusions and discussions

In this talk we considered simple examples of cosmological scenarios in which dissipation may change the usual argument based on cold (non-dissipating) scenario. I believe the situation is now obvious suggesting why the dissipation is very important for particle cosmology. The study related to the cosmological dissipation may give us a key to understand the interactions in the particle model in terms of the cosmological observations. In previous studies dissipation has been studied only for the inflaton in the very early Universe (warm inflation). However, in the light of particle cosmology, dissipation is very important in understanding interactions in the SUSY model [11], GUT or the string theory [12].

References

[1] M. Morikawa and M. Sasaki, "Entropy Production In The Inflationary Universe," Prog. Theor. Phys. **72**, 782 (1984).

[2] A. Berera and R. O. Ramos, "Dynamics of interacting scalar fields in expanding space-time," Phys. Rev. D **71**, 023513 (2005),[hep-ph/0406339].

[3] T. Matsuda, "A new perspective on supersymmetric inflation," JCAP **0911**, 022 (2009) [arXiv:0911.2350 [hep-ph]].

[4] A. Berera, "The warm inflationary universe," Contemp. Phys. **47**, 33 (2006) [arXiv:0809.4198].

[5] T. Matsuda, "Evolution of the curvature perturbations during warm inflation," JCAP **0906**, 002 (2009) [arXiv:0905.0308]

[6] E. W. Kolb, A. Riotto and A. Vallinotto, "Curvature perturbations from broken symmetries," Phys. Rev. D **71**, 043513 (2005) [astro-ph/0410546].

[7] T. Matsuda, "Generating the curvature perturbation with instant preheating," JCAP **0703**, 003 (2007) [hep-th/0610232].

[8] T. Matsuda, "Generating curvature perturbations with MSSM flat directions," JCAP **0706**, 029 (2007) [hep-ph/0701024].

[9] T. Matsuda, "Remote Inflation as hybrid-like sneutrino/MSSM inflation," [arXiv:0905.4328].

[10] T. Matsuda, "Remote Inflation: Hybrid-like inflation without hybrid-type potential," JCAP **0907**, 003 (2009) [arXiv:0904.2821].

[11] T. Matsuda, "Successful D-term inflation with moduli," Phys. Lett. B **423**, 35 (1998) [hep-ph/9705448].

[12] T. Matsuda, "Modulated Inflation," Phys. Lett. B **665**, 338 (2008) [arXiv:0801.2648]. [hep-ph/0202209].

Cosmic acceleration and higher-dimensional gravity

Masato Minamitsuji[1 (a)]

[(a)] *Center for Quantum Spacetime, Sogang University, Shinsu-dong 1, Mapo-gu, Seoul, 121-742 South Korea*

Abstract

The self-accelerating branch of the Dvali-Gabadadze-Porrati (DGP) five-dimensional braneworld has provided a compelling model for the current cosmic acceleration. Recent observations, however, have not favored it so much. We discuss the solutions which contain a de Sitter 3-brane in the cascading DGP braneworld model, which is a kind of higher-dimensional generalizations of the DGP model, where a p-dimensional brane is placed on a $(p+1)$-dimensional one and the p-brane action contains the $(p+1)$-dimensional induced scalar curvature term. In the simplest six-dimensional model, we derive the solutions. Our solutions can be classified into two branches, which reduce to the self-accelerating and normal solutions in the limit of the original five-dimensional DGP model. In the presence of the six-dimensional bulk gravity, the 'normal' branch provides a new self-accelerating solution. The expansion rate of this new branch is generically lower than that of the original one, which may alleviate the fine-tuning problem.

Recent observational data with high precision suggest that our Universe is currently in an accelerating phase [1, 2]. They are consistent with the presence of a nonzero cosmological constant or quantum vacuum energy, but its value must be extremely tiny. In the context of the braneworld, the Dvali-Gabadadze-Porrati (DGP) five-dimensional model has been a compelling model for the cosmic acceleration [3–5]. The DGP model contains a mechanism to modify the gravitational law just on cosmological scales by the effects of the four-dimensional Einstein-Hilbert term put into the action of our 3-brane Universe. Such an intrinsic curvature term would be induced due to quantum loops of the matter fields which are localized on the 3-brane. The effect of the four-dimensional intrinsic curvature term on the 3-brane recovers the Einstein gravity on small scales but on large distance scales gravitational law becomes five-dimensional. The DGP model realizes the so-called self-accelerating Universe that features a four-dimensional de Sitter phase even though our 3-brane Universe is completely empty. Recent studies, however, have indicated that the observational data have not favored the self-accelerating branch of DGP (see e.g., Ref. [6] of [6]). The self-accelerating solutions have also faced the disastrous issue of ghost excitations (see e.g., Ref. [7] of [6]): The energy is not bounded from below and therefore the theory is already pathological even at the classical level.

There are possibilities that the realistic cosmological model may be obtained by generalizing the five-dimensional DGP model to a higher-dimensional spacetime. An interesting model is so-called the cascading DGP model [7]. The model is constructed by a set of branes of the different dimensionality, where a p-brane is placed on a $(p+1)$-dimensional brane and the p-brane action contains the $(p+1)$-dimensional induced scalar curvature term. For instance, in the simplest six-dimensional model, a 3-brane Universe whose action contains an induced four-dimensional scalar curvature term is placed on a 4-brane whose action contains an induced five-dimensional scalar curvature term, embedded into a (possibly infinitely extended) six-dimensional spacetime. An extension to the case of an arbitrary number of spacetime dimensions is straightforward in principle. It is expected that in such kind of model, in the infrared region the gravitational force falls off sufficiently fast to exhibit 'degravitation' [7]. The linearized analysis has confirmed this idea in part at the level of the linearized theory [7].

One of crucial questions is the viability of the cascading DGP model. To answer to this question, of course, one should go beyond the linearized analysis and in particular investigate the cosmology. Non-linearities may detect effects which may not appear in the linearized treatment. In addition, cosmology can help to have a better understanding of the model and of the idea of gravity localized through

[1] Email address: minamituzi@sogang.ac.kr

intrinsic curvature terms on the 3-brane and 4-brane. As the first step to this direction, we will look for the solutions which contain a de Sitter 3-brane. They may give rise to the self-accelerating cosmological solutions in the simplest six-dimensional cascading DGP model.

The system of our interest is that our 3-brane Universe Σ_4 is placed on a 4-brane Σ_5, embedded into the six-dimensional bulk $\mathcal{M}_6$. For simplicity, we suppress the matter terms in the bulk and on the branes. The total action is given by

$$S = \frac{M_6^4}{2}\int_{\mathcal{M}_6} d^6X\sqrt{-G}^{(6)}R + \frac{M_5^3}{2}\int_{\Sigma_5} d^5y\sqrt{-q}^{(5)}R + \frac{M_4^2}{2}\int_{\Sigma_4} d^4x\sqrt{-g}^{(4)}R, \tag{1}$$

where G_{AB}, q_{ab} and $g_{\mu\nu}$ represent metrics in $\mathcal{M}_6$, on Σ_5 and Σ_4, respectively. ${}^{(i)}R$ $(i = 6, 5, 4)$ are Ricci scalar curvature terms associated with respect to G_{AB}, q_{ab} and $g_{\mu\nu}$. For the later discussion, it is useful to introduce the crossover mass scales $m_5 := M_5^3/M_4^2$ and $m_6 := M_6^4/M_5^3$, which determines the energy scale where the five-dimensional and six-dimensional physics appear, respectively. We assume that $m_5 > m_6$. Then, it is natural to expect that the effective gravitational theory becomes four-dimensional for $H > m_5$, five-dimensional for $m_5 > H > m_6$, and finally six-dimensional for $H < m_6$, where H is the cosmic expansion rate.

We consider the six-dimensional Minkowski spacetime, which is covered by the following choice of the coordinates

$$ds_6^2 = G_{AB}dX^A dX^B = dr^2 + d\theta^2 + H^2r^2\gamma_{\mu\nu}dx^\mu dx^\nu, \tag{2}$$

where $\gamma_{\mu\nu}$ is the metric of the four-dimensional de Sitter spacetime with the expansion rate H. The r and θ coordinates represent two extra dimensions and x^μ $(\mu = 0, 1, 2, 3)$ do the ordinary four-dimensional spacetime. The surface of $r = 0$ corresponds to a (Rindler-like) horizon and only the region of $r \geq 0$ is considered. Note that the boundary surface of $r = 0$ does not cause any pathological effect because it is not a singularity. We consider a 4-brane located along the trajectory $(r(|\xi|), \theta(|\xi|))$, where the affine parameter ξ gives the proper coordinate along the 4-brane. The 3-brane is placed at $\xi = 0$, and for decreasing value of $|\xi|$ one approaches the 3-brane. We assume the Z_2-symmetry across the 4-brane and hence an identical copy is glued to the opposite side. Along the trajectory of the 4-brane $\dot{r}^2 + \dot{\theta}^2 = 1$, where the dot represents the derivative with respect to ξ. The induced metric on the 4-brane is given by

$$ds_5^2 = q_{ab}dy^a dy^b = d\xi^2 + H^2r(|\xi|)^2\gamma_{\mu\nu}dx^\mu dx^\nu. \tag{3}$$

The point where $r(\xi) = 0$ on the 4-brane corresponds to a horizon and the 4-brane is not extended beyond it. The 3-brane geometry is exactly de Sitter spacetime with the normalization condition $Hr(0) = 1$,

$$ds_4^2 = g_{\mu\nu}dx^\mu dx^\nu = \gamma_{\mu\nu}dx^\mu dx^\nu. \tag{4}$$

The nonvanishing components of the tangential and normal vectors to the 4-brane are given by $u^r = \dot{r}$,$u^\theta = \dot{\theta}$,$n^r = \epsilon\dot{\theta}$,and $n^\theta = -\epsilon\dot{r}$. We restrict that the region to be considered is to be $r > 0$ and the 3-brane is sitting on r-axis $(\theta = 0)$. The 4-brane trajectory is Z_2-symmetric across the 3-brane. $\dot{\theta} > 0$ for increasing ξ. In the case of $\epsilon = 1$, the bulk space is in the side of increasing r, while in the case of $\epsilon = -1$, the bulk space is the side of decreasing r.

The extrinsic curvature tensor is defined by $K_{ab} := \nabla_a n_b$. The junction condition is given by

$$M_6^4\Big[K_{ab} - q_{ab}K\Big] = \Big(M_5^{3\,(5)}G_{ab} + M_4^{2\,(4)}G_{\mu\nu}\delta_a^\mu\delta_b^\nu\delta(\xi)\Big). \tag{5}$$

where the square bracket denotes the jump of a bulk quantity across the 4-brane.By taking the Z_2-symmetry across the 4-brane into consideration, the matching condition becomes

$$-M_6^4\epsilon\frac{4}{r}\big(1-\dot{r}^2\big)^{1/2} = -3M_5^3\frac{1-\dot{r}^2}{r^2}, \quad M_6^4\epsilon\Big(-\frac{3}{r}\big(1-\dot{r}^2\big)^{1/2} + \frac{\ddot{r}}{(1-\dot{r}^2)^{1/2}}\Big) = \frac{3M_5^3}{2}\frac{\dot{r}^2 + r\ddot{r} - 1}{r^2} \tag{6}$$

The way to construct the solution is essentially the same as the case of a tensional 3-brane on a tensional 4-brane (See Appendix).

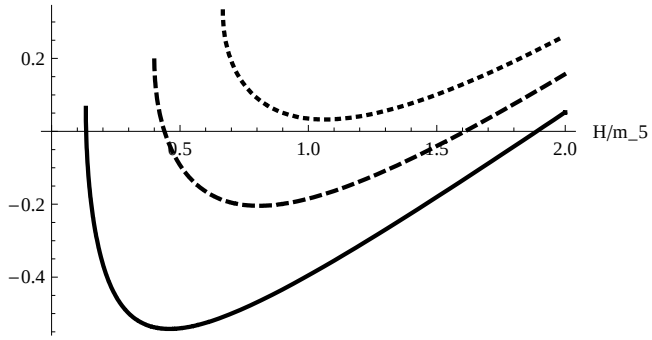

Figure 1: The left-hand-side of Eq. (11) is shown as a function of H/m_5 for fixed ratio m_6/m_5. The solid, dashed and dotted curves correspond to the cases of $m_6/m_5 = 0.1, 0.3, 0.5$, respectively. In the last case, in which m_6/m_5 is above the critical value $\left(m_6/m_5\right)_{\rm crit} = 0.46978$, there is no solution.

In our case, it is suitable to take $\epsilon = +1$ branch. Then, the junction condition tells that the trajectory of the 4-brane is given by $r(\xi) = a^{-1}\cos(a|\xi| - a\xi_0)$ with

$$a = \frac{4m_6}{3}. \tag{7}$$

where we assume $0 < a\xi_0 < \pi/2$. $r(\xi)$ vanishes at $|\xi| = |\xi_{\rm max}| = \pi/(2a) + \xi_0$. Note that, as mentioned before, the surface of $r = 0$ corresponds to a horizon and on the 4-brane there are horizons at $|\xi| = |\xi_{\rm max}|$, namely at a finite proper distance from the 3-brane. The 4-brane is not extended beyond them [8]. Now an identical copy is attached across the 4-brane. The normalization of the overall factor of the metric function at the 3-brane place requires $\cos(a\xi_0) = a/H \leq 1$. Note that

$$H \geq \frac{4m_6}{3}. \tag{8}$$

The $\ddot{r}$ term gives rise to the contribution proportional to $\delta(\xi)$. Here, by noting that

$$\frac{d}{d\xi}\arctan\left(\frac{\dot{r}}{\sqrt{1-\dot{r}^2}}\right) = \frac{\ddot{r}}{\sqrt{1-\dot{r}^2}}, \tag{9}$$

and integrating the (μ,ν)-component of the junction equation Eq. (6) across $\xi = 0$, one finds

$$M_6^4(4a\xi_0) = 6M_5^3 a\tan(a\xi_0) - 3H^2M_4^2, \tag{10}$$

which with Eq. (7) leads to

$$\frac{H}{2m_5} - \left(\sqrt{1-\frac{16m_6^2}{9H^2}} - \frac{2m_6}{3H}\arctan\left(\sqrt{\frac{9H^2}{16m_6^2}-1}\right)\right) = 0\,. \tag{11}$$

The solution of Eq. (11) determines the value of the expansion rate H. The 3-brane induces the deficit angle $4a\xi_0$ in the bulk. The configuration of the bulk space is shown in Fig. 1. The bulk space is outside the curve of the 4-brane and has an infinite volume. As mentioned before, the surface of $r = 0$ corresponds to a horizon and, in particular, on the 4-brane there are horizons at a finite proper distance from the 3-brane. The 4-brane is not extended beyond them. Note that this surface does not cause any pathological effect (see [6] for the detailed configuration of the bulk space).

For generic values of m_6, in Fig 1, the left-hand-side of Eq. (11) is shown as a function of H/m_5 for each fixed ratio m_6/m_5. It is found that below the critical ratio $m_6/m_5 < \left(m_6/m_5\right)_{\rm crit} \approx 0.46978$, there are two branches of solutions, which are here denoted by $H_+ > H_-$. On the other hand, for $m_6/m_5 > \left(m_6/m_5\right)_{\rm crit}$, there is no solution of Eq. (11). In the marginal case of $m_6/m_5 = \left(m_6/m_5\right)_{\rm crit}$, there is the degenerate solution given by $H \approx m_5$. For generic values of m_6/m_5, in Fig. 2 and 3, the

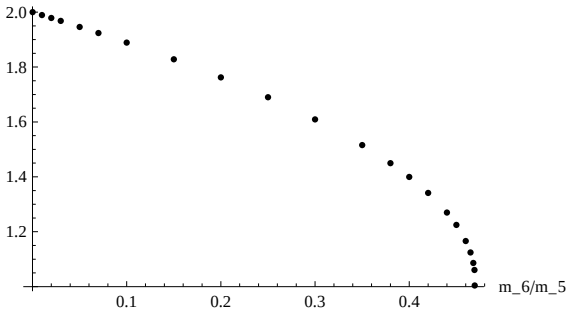

Figure 2: The larger solution H_+ is shown as a function of m_6/m_5, in the unit of m_5.

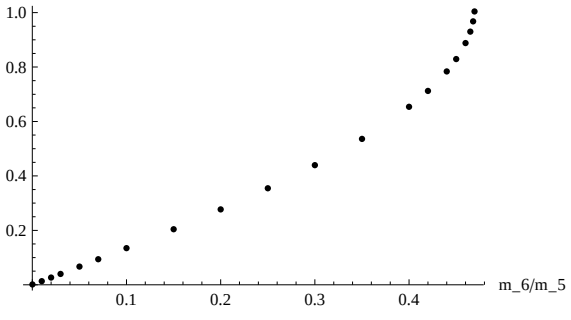

Figure 3: The smaller solution H_- is shown as a function of m_6/m_5, in the unit of m_5.

solutions H_+ and H_- are shown as functions of $m_6/m_5 (< \left(m_6/m_5\right)_{\rm crit})$, respectively. In the limit of $m_6 \ll m_5$, another solution is given approximately given by

$$H_+ \approx 2m_5, \quad H_- \approx \frac{4m_6}{3}. \tag{12}$$

In the absence of the bulk gravity, $m_6 \to 0$, the $(+)$ and $(-)$-branches coincide with the 'self-accelerating' and 'normal' solutions in the DGP model, with $H_+ = 2m_5$ and $H_- = 0$, respectively. By taking the presence of the six-dimensional bulk into consideration, the self-accelerating branch essentially remains the same. But the normal branch solution provides a new self-accelerating solution if H_-, which could be much smaller than H_+ for $m_6 \ll m_5$. Note that the existence of both of these new solutions relies on the presence of the 4-brane, since in the limit of $M_5 \to 0$ none of these solutions can exist.

As we mentioned, the self-accelerating branch of the original DGP model is not favored by recent observations and also suffers a ghost instability. What we found is that in the six-dimensional cascading DGP model, one of two branches, which corresponds to the 'normal' branch in the original DGP model, provides a new self-accelerating solution whose expansion rate could be much smaller than that in the other branch, which corresponds to the original 'self-accelerating' branch. Thus, the fine-tuning would be relaxed in some degrees. In the self-accelerating solution of the DGP model, the bulk spacetime is infinitely extended and a mode which satisfies the background solution is not normalizable. Thus, the scalar mode is hence different from the zero mode, which already implies the potential pathology about the ghost instability. In our new solutions the 4-brane where the 3-brane resides can never reach the infinity and has a finite volume. Therefore, in analogy with the case of the standard DGP, it implies that the bending mode of the 3-brane would be normalized and hence solutions could be healthy, although the detailed investigations about the stability are left for a future work.

References

[1] S. Perlmutter et al., Nature 391 (1998) 51; A. Riess et al., Astron. J., 116 (1998) 1009,

[2] D. N. Spergel et al.,Astrophys. J. Suppl. 148, 175 (2003).

[3] G. R. Dvali, G. Gabadadze and M. Porrati, Phys. Lett. B 485 (2000) 208.

[4] C. Deffayet, Phys. Lett. B 502 (2001) 199.

[5] C. Deffayet, G. R. Dvali and G. Gabadadze, Phys. Rev. D 65 (2002) 044023.

[6] M. Minamitsuji, arXiv:0806.2390 [gr-qc], to be published in Physics Letters B.

[7] G. Dvali, S. Hofmann and J. Khoury, Phys. Rev. D **76** 084006 (2007); C. de Rham, S. Hofmann, J. Khoury and A. J. Tolley, JCAP 0802 (2008)011.

[8] L. Grisa and O. Pujolas, JHEP **0806**, 059 (2008).

Physical and Mathematical Behavior of Black Diring Solutions

Takashi Mishima[1] and Hideo Iguchi[2]

Laboratory of Physics, College of Science and Technology, Nihon University, Narashinodai, Funabashi, Chiba 274-8501, Japan

Abstract

We consider some characteristics of the solutions of five-dimensional black dirings. First we confirm the equivalence of the two different solution-sets of the black dirings(one was generated by the authors with the solitonic method similar to the Backlund transformation and the other was by Evslin and Krishnan with the inverse scattering method). Then we show some physical properties of the systems of black diring: especialy the existence of thermo-dynamical systems of black diring and their properties.

1 Introduction

Previously we discovered that the five-dimensional S^1-rotating black rings appeared first in Ref. [1] can be superposed in concentric way and succeeded to construct regular black diring systems as the simplest case(called diring I) [2]. For the construction above we used the solitonic method similar to the Backlund transformation that was developed by us for the first time to generate non-trivial five-dimensional axisymmetric spacetimes with asymptotic flatness [3–5]. Following the above work, Evslin and Krishnan constructed another diring solution-set(called diring II) [6]. They used the inverse scattering method that was modified by Pomeransky to treat the higher dimensional case(hereafter abbreviated to PISM) [7]. However, because of the complexity of their expressions, the study to confirm the equivalence of these two diring solution-sets and further investigation of the physics of the diring systems still remain to be done. Here we give some answeres to these problems.

For the system of the dirings, we consider five-dimensinal spacetimes with three commuting Killing vector fields: a time-like Killing field and two axial Killing fields. We assume further that one of the axial Killing fields is orthogonal to the other Killing fields. So the line-elements adopted here is reduced to

$$ds^2 = G_{tt}(dx^0)^2 + 2G_{t\psi}dtd\psi + G_{\psi\psi}(d\psi)^2 + G_{\phi\phi}(d\phi)^2 \ + \ e^{2\nu}\left(d\rho^2 + dz^2\right) , \tag{1}$$

where the metric coefficients are the function of (ρ, z) and $\det G = -\rho^2$ is imposed. Owing to the assumptions we can say that any type of angular momentums corresponding to ϕ-rotaion is zero.

In the first half of the paper we show the complete equivalence of these two different representations with the aid of the facts established by Hollands and Yazadjiev, which concern the uniqueness of higher-dimensional black holes. In the latter half we give some physical quantities of the dirings. Using these quatities, we clarify some physical properties of the regular black diring systems. Especially we show the existence of thermo-dynamical diring systems and some peculiar properties of the thermal systems.

2 Equivalence of diring I and diring II

The strategy adopted here is the following. First, reconstructing the solution-set of diring I with the PISM we show that the difference between the diring I and diring II comes from the difference of the corresponding seeds. Then we give the moduli-parameters and physical quantities to identify the solution-sets respectively. Using these quantities we confirm the equivalence of these two solution-sets with the aid of the facts established by Hollands and Yazadjiev [8]. Once the equivalence is established, we can use the more convenient representation among the diring I and diring II according to problems we face.

[1]E-mail:tmishima@phys.ge.cst.nihon-u.ac.jp
[2]E-mail:iguchi.h@phys.ge.cst.nihon-u.ac.jp

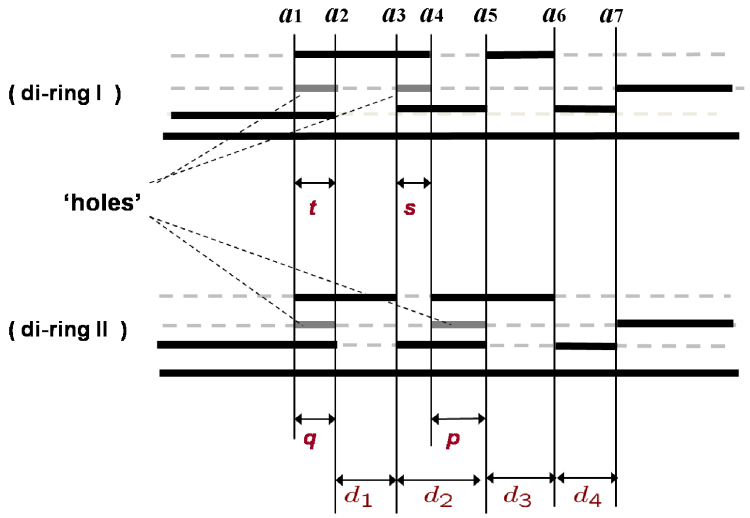

Figure 1: Rod-structures describing the seeds of the dirings. The upper and lower rod-diagrams correspond to the diring I and diring II respectively. Black rods interpreted to have 1/2 line mass density, while gray rods(holes) correspond to $-1/2$ line mass density. Two solitons are removed and recovered at the positions a_1 and a_4.

A key mathematical fact to establish the equivalence of diring I and diring II is in the work by Hollands and Yazadjiev which have discussed the uniqueness of five dimensional stationary black holes with axial $U(1)^2$-symmetry. Originally they have considered the sytems of single black hole, but their discussions can be applied to the systems of multiple black holes so that the statement is still valid with some modification. It is described that two different systems of multiple black holes are isometirc when all the rod-lengths and the Komar angular momentums coincide with each other. It should be noticed that validity of the proof seem to hold, whether conical singularities on the axes exist or not. So the above statement remains useful for the spacetimes with conical singularities. For the systems of black diring, two Komar angular momentums corresponding to the ϕ-rotation are zero so that the other two Komar angular momentums corresponding to the ψ-rotation are essential to determine the solution, once the rod-lengths are fixed. We can say further that two independent physical quantities can be used to determine the solution in place of two Komar angular momentums at least locally.

The diring I and diring II are generated by PISM from the corresponding seeds respectively. The rod structures described in Fig.1 show the seeds that are used to generate diring I and diring II. The parameters (s,t) and (p,q) inscribed on the Fig.1 mean lengths of the gray rods(holes) and have the following range:

$$0 \le s \le d_2\,,\ 0 \le t\,, \tag{2}$$

$$0 \le p \le d_2\,,\ 0 \le q\,. \tag{3}$$

Following the procedure of PISM, first two solitons with trivial BZ-parameters are removed at the positions a_1 and a_4 and then the solitons are recovered with non-trivial BZ-parameters at the same positions. Here $(b_{\rm I},\, c_{\rm I})$ and $(b_{\rm II},\, c_{\rm II})$ are assigned to BZ-parameters of diring I and II respectively. After adjusting the BZ-parameters in the following way

$$\left\{ b_{\rm I} = \pm\left(\frac{2a_{21}a_{61}a_{71}}{a_{31}a_{51}}\right)^{1/2},\ c_{\rm I} = \pm\left(\frac{2a_{42}a_{64}a_{74}}{a_{43}a_{54}}\right)^{1/2} \right\} \tag{4}$$

$$\left\{ b_{\rm II} = \pm\left(\frac{2a_{31}a_{61}a_{71}}{a_{21}a_{51}}\right)^{1/2},\ c_{\rm II} = \pm\left(\frac{2a_{43}a_{64}a_{74}}{a_{42}a_{54}}\right)^{1/2} \right\}, \tag{5}$$

we obtain the regular diring systems respectively up to conical singularities. The symbols a_{ij} is defined as $a_i - a_j$. The moduli-parameters to provide the solution-sets of diring I and II are $\{s,t,d_1,d_2,d_3,d_4\}_{\rm I}$ and $\{p,q,d_1,d_2,d_3,d_4\}_{\rm II}$ respectively. Other physical quantities of the dirings can be represented with these

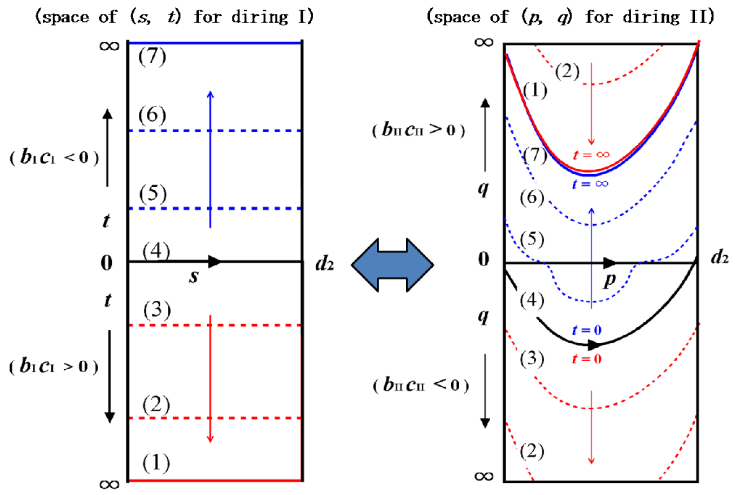

Figure 2: Correspondence between the space of (s,t) for diring I and the space of (p,q) for diring II. Each horizontal line with a number from (1) to (7) is mapped into the curve with the same number.

parameters. For example, ADM masses: $m_{\rm I}$ and $m_{\rm II}$, angles assuring regular axis for $[a_6,a_7]$: $(\Delta\phi_{\rm R})_{\rm I}$ and $(\Delta\phi_{\rm R})_{\rm II}$ and angles assuring regular axis for $[a_3,a_5]$: $(\Delta\phi_{\rm L})_{\rm I}$ and $(\Delta\phi_{\rm L})_{\rm II}$ are given as follows

$$m_{\rm I}=\frac{3\pi}{4}\left(a_{41}+a_{65}\right)+\frac{3\pi}{2}a_{41}\left[\frac{a_{41}}{(b_{\rm I}-c_{\rm I})^2}-\frac{b_{\rm I}}{b_{\rm I}-c_{\rm I}}\right],\qquad m_{\rm II}=\frac{3\pi}{4}\left(a_{31}+a_{64}\right), \tag{6}$$

$$\left(\frac{\Delta\phi_{\rm R}}{2\pi}\right)^2_{\rm I}=\frac{a_{73}^2a_{76}(a_{74}b_{\rm I}-a_{71}c_{\rm I})^2}{a_{71}^2a_{72}^2a_{74}a_{75}(b_{\rm I}-c_{\rm I})^2},\qquad \left(\frac{\Delta\phi_{\rm R}}{2\pi}\right)^2_{\rm III}=\frac{a_{71}a_{74}a_{73}a_{76}}{a_{72}^2a_{75}^2}, \tag{7}$$

$$\left(\frac{\Delta\phi_{\rm L}}{2\pi}\right)^2_{\rm I}=\frac{a_{53}^2a_{73}^2a_{62}(a_{51}a_{64}a_{74}b_{\rm I}-a_{54}a_{61}a_{71}c_{\rm I})^2}{a_{72}^2a_{51}a_{52}a_{54}a_{61}a_{63}a_{64}a_{71}a_{74}(b_{\rm I}-c_{\rm I})^2}, \tag{8}$$

$$\left(\frac{\Delta\phi_{\rm L}}{2\pi}\right)^2_{\rm II}=\left(\frac{a_{53}a_{62}a_{73}}{a_{41}^2a_{52}^2a_{63}^2a_{72}^2}\right)\left[a_{21}a_{31}a_{54}a_{64}a_{74}+a_{42}a_{51}(a_{43}a_{61}a_{71}+a_{21}a_{54}b_{\rm II}c_{\rm II})\right]. \tag{9}$$

Owing to the mathematical facts mentioned above, we can conclude that two dirings are isometrically equivalent when the coditions $(d_1,d_2,d_3,d_4)_{\rm I}=(d_1,d_2,d_3,d_4)_{\rm II}$ and $(m_{\rm I},\,(\Delta\phi_{\rm R})_{\rm I})=(m_{\rm II},\,(\Delta\phi_{\rm R})_{\rm II})$ can be imposed. Once the conditions are satisfied, remarkably simple relations between (s,t) and (p,q) are extracted from the mass equality: $m_{\rm I}(s,t)=m_{\rm II}(p,q)$ and regular angle equality: $(\Delta\phi_{\rm R})_{\rm I}=(\Delta\phi_{\rm R})_{\rm II}$ as $(p,q)=(p(s,t),q(s,t))$. Using these equations we can confirm that the correspondence between (s,t)-space and (p,q)-space is onto and one-to-one If infinities on the spaces are included. Figure 2 shows the correspondence between (s,t)-space and (p,q)-space. Finally we can say that the systems of diring I and diring II are completely equivalent.

3 Thermo-dynamical black diring

The equivalence have been established in the previous section. So we can use the more convenient representation among the diring I and diring II according to problems we face. The existence of regular dirings have been already confirmed in Ref. [2] and Ref. [6]. In the rest we show some results of physical properties of the systems of diring, especially the existence of thermo-dynamical dirings and their peculier properties. To assure that the multi-system becomes a thermal system, the surface gravities $(\kappa_L,\,\kappa_R)$ and rotational angular velocities $(\omega_L,\,\omega_R\,)$ of the inner and outer black rings of the system must be equal:

$$\kappa_L=\kappa_R\,,\qquad \omega_L=\omega_R. \tag{10}$$

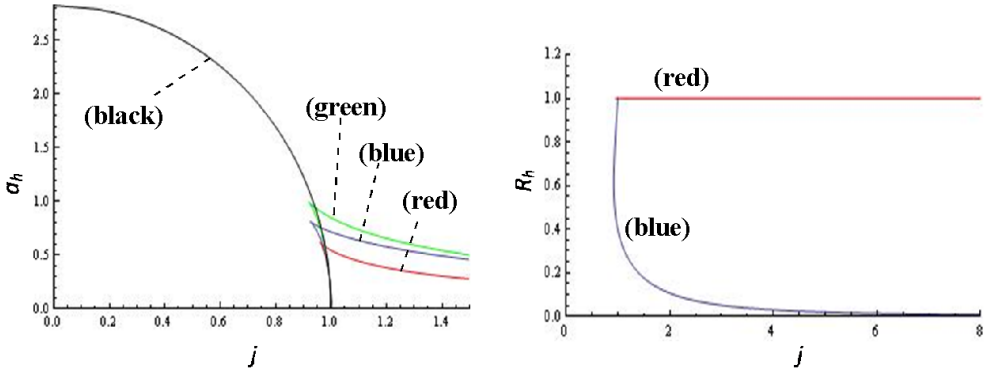

Figure 3: Left: Total area (a_h) as a function of angular momentum (j). All the quantities are normalized by ADM mass. Black, green, blue and red lines correspond to MP black hole (MP-BH), black ring (BR), black saturn (BS) and black diring (BD), respectively. Right: Ratio of the area of inner BR or BH to the area of outer BR (R_h) as a function of j. Green and blue lines correspond to BS and BR.

We investigate whether thermo-dynamical diring systems exist or not by solving the above conditions numerically. The results are shown in Figure 3. The red line in the left picture of Fig.3 shows the existence of thermo-dynamical black dirings. Other thermal systems: Meyres-Perry black holes, black rings, black saturns are also shown for comparing with the dirings. The right picture of Fig.3 shows the behavior of the ratio of the horizon-area of inner black ring or black hole to the horizon-area of outer black ring. The ratio of the system of diring holds a constant value one, while the ratio of the system of black saturn quickly vanishes as the angular momentum j increases. This means that in the system of black saturn the influence of the inner black hole quickly vanishes and in the diring the interaction of the inner and outer rings remains.

References

[1] R. Emparan and H. S. Reall, Phys. Rev. Lett. **88**, 101101 (2002).

[2] H. Iguchi and T. Mishima, Phys. Rev. D **75**, 064018 (2007).

[3] T. Mishima and H. Iguchi, Phys. Rev. D **73**, 044030 (2006).

[4] H. Iguchi and T. Mishima, Phys. Rev. D **73**, 121501 (2006).

[5] H. Iguchi and T. Mishima, Phys. Rev. D **74**, 024029 (2006).

[6] J. Evslin and C. Krishnan, Class. Quantum Phys. **26**, 125018 (2006).

[7] A. A. Pomeransky, Phys. Rev. D **73**, 044004 (2006).

[8] S. Hollands and S. Yazadjiev, Comm.Mats.Phys. **283**, 749 (2008).

A possible explanation of the secular increase of the astronomical unit

Takaho Miura[(a)], Hideki Arakida, [(b)] Masumi Kasai[(a)] and Syuichi Kuramata[(a)]

[(a)] *Faculty of Science and Technology,Hirosaki University, 3 bunkyo-cyo Hirosaki, Aomori, 036-8561, Japan*

[(b)] *Education and integrate science academy, Waseda University,1 waseda sinjuku Tokyo, Japan*

Abstract

We give an idea and the order-of-magnitude estimations to explain the recently reported secular increase of the Astronomical Unit (AU) by Krasinsky and Brumberg (2004). The idea proposed is analogous to the tidal acceleration in the Earth-Moon system, which is based on the conservation of the total angular momentum and we apply this scenario to the Sun-planets system. Assuming the existence of some tidal interactions that transfer the rotational angular momentum of the Sun and using reported value of the positive secular trend in the astronomical unit, $\frac{d}{dt}15 \pm 4$(m/s),the suggested change in the period of rotation of the Sun is about 21(ms/cy) in the case that the orbits of the eight planets have the same "expansionrate."This value is sufficiently small, and at present it seems there are no observational data which exclude this possibility. Effects of the change in the Sun's moment of inertia is also investigated. It is pointed out that the change in the moment of inertia due to the radiative mass loss by the Sun may be responsible for the secular increase of AU, if the orbital "expansion"is happening only in the inner planets system. Although the existence of some tidal interactions is assumed between the Sun and planets, concrete mechanisms of the angular momentum transfer are not discussed in this paper, which remain to be done as future investigations.

1 Introduction

The Astronomical Unit (hereafter we abbreviate AU) is one of the most essential scale in astronomy which characterizes the scale of the solar system and the standard of cosmological distance ladder. AU is also the fundamental astronomical constant that associates two length unit; one (m) in International System (SI) of Units and one (AU) in Astronomical System of Units.

In the field of fundamental astronomy e.g., the planetary ephemerides, it is one of the most important subjects to evaluate AU from the observational data. However, recently Krasinsky and Brumberg reported the positive secular trend in AU as $\frac{d}{dt}\mathrm{AU} = 15 \pm 4\,(\mathrm{m/cy})$. from the analysis of radar ranging of inner planets and Martian landers and orbiters (Krasinsky and Brumberg 2004;Standish2005).

2 Tidal Acceleration in the Earth-Moon System

In this section, we briefly summarize the tidal acceleration in the Earth-Moon system.

The conservation law of the total angular momentum in the Earth-Moon system is

$$\frac{d}{dt}\left(\ell_{\mathrm{E}} + L_{\mathrm{M}}\right) = 0, \tag{1}$$

where ℓ_{E} is the rotational angular momentum of the Earth, L_{M} is the orbital angular momentum of the Moon, and for simplicity we have neglected the rotational angular momentum of the Moon, which is about 10^{-5} times smaller than L_{M}. Then, if we assume the moment of inertia, mass, and the eccentricity of the moon's orbit are constant, the conservation of the total angular momentum Eq. (1) reads

$$\frac{\dot{T}_{\mathrm{E}}}{T_{\mathrm{E}}} = \frac{1}{2}\frac{L_{\mathrm{M}}}{\ell_{\mathrm{E}}}\frac{\dot{r}}{r} \tag{2}$$

The gradual slowing of the Earth's rotation is due to the tidal force between the orbiting Moon and the Earth, or the tidal friction.

3 Application to the Sun-Planets System

In this section, we apply the same argument in the previous section to the Sun-planets system. All we need is the conservation of the total angular momentum in the solar system. We denote the mass and the orbital elements of each planet by subscript i. The length AU, denoted by a, is used to normalize r_i, then for the Earth's radius $r_3 \equiv r_{\rm E} = a$, and for the moment it is assumed that the orbits of the all planets have the same "expansion rate," i.e.,

$$\frac{\dot{r}_i}{r_i} = \frac{\dot{a}}{a} \tag{3}$$

for each i.

In the case that the Sun's moment of inertia does not change, from the analogy to Eq. (2), we obtain the change in the period of rotation of the Sun $T_\odot$ as

$$\frac{\dot{T}_\odot}{T_\odot} = \frac{1}{2}\frac{L}{\ell_\odot}\frac{\dot{a}}{a}, \tag{4}$$

where L is the sum of the orbital angular momentums of all planets

$$L = \sum_i m_i \sqrt{GM_\odot r_i (1-e_i^2)}, \tag{5}$$

Using the value $\dot{a} \simeq 15$(m/cy) reported by Krasinsky and Brumberg, $\dot{a}/a \simeq 1.0 \times 10^{-10}$ and the right-hand-side of Eq. (4) is evaluated as

$$\frac{\dot{T}_\odot}{T_\odot} \simeq 5.7 \times \gamma_\odot^{-1} \times 10^{-10}\,({\rm cy}^{-1}). \tag{6}$$

where γ is the moment of inertia factor. The moment of inertia is

$$I_\odot = \gamma_\odot M_\odot R_\odot^2. \tag{7}$$

If we use the value $\gamma_\odot = 0.0059$ and the rotational period of the Sun as $T_\odot = 25.38$ (days), the estimated value of the change in $T_\odot$ is

$$\dot{T}_\odot \simeq 21\,({\rm ms/cy}). \tag{8}$$

The estimated value is sufficiently small and seems to be well within the observational limit.

4 Effect of the change in the moment of inertia

In the previous section, we have considered only the case that the moment of inertia $I_\odot$ is constant. If we generalize our result to the case that $I_\odot$ and $M_\odot$ are not constant, Eq. (4) changes to

$$-\frac{\dot{\gamma}_\odot}{\gamma_\odot} - \frac{\dot{M}_\odot}{M_\odot} - 2\frac{\dot{R}_\odot}{R_\odot} + \frac{\dot{T}_\odot}{T_\odot} = \frac{1}{2}\frac{L}{\ell_\odot}\left(\frac{\dot{M}_\odot}{M_\odot} + \frac{\dot{a}}{a}\right). \tag{9}$$

As a first approximation, we assume that the radiative mass loss occurs isotropically along radial direction and does not carry the angular momentum. The first term in the left-hand-side of Eq. (9) represents the effect of change in the internal density distribution of the Sun, and so far we do not have enough information on it in detail.

The second term in the left-hand-side of Eq. (9) represents the effect of mass loss, which can be evaluated in the following way. The Sun has luminosity at least $3.939\times10^{26}W$,or $4.382\times10^{9}kg/s$,including

electromagnetic radiation and contribution from neutrinos (Noerdlinger 2008). The particle mass loss rate by the solar wind is about 1.374×10^9 kg/s, according to Noerdlinger (2008). The total solar mass loss rate is then

$$-\frac{\dot{M}_\odot}{M_\odot} = 9.1 \times 10^{-12} (cy^{-1}), \tag{10}$$

which is less than a thousandth of the required value to explain the secular increase of AU (see Eq. (6)). (As pointed out by Noerdlinger (2008), Krasinsky and Brumberg (2004) unaccountably ignored the radiative mass loss $L_\odot = 3.86 \times 10^{26}$ W which is the major contribution to $\dot{M}_\odot/M_\odot$.) Therefore, we can conclude that the solar mass loss term in the left-hand-side of Eq. (9) does not make a significant contribution to the secular increase of AU, if the orbits of the eight planets have the same expansion rate.

Note that the term which is proportional to $\dot{M}_\odot/M_\odot$ also appears in the right-hand-side of Eq. (9). This term may be called as the Noerdlinger effect (Noerdlinger 2008). Noerdlinger already investigated this effect of solar mass loss, and concluded that the effect can only account for less than a tenth of the reported value by Krasinsky and Brumberg.

The third term in the left-hand-side of Eq. (9) is the contribution from the change in the solar radius. Although the very short-time and small-scale variability in the solar radius may be actually observed in the context of helioseismology, we have no detailed information on the secular change in $R_\odot$ far.

5 Case of the Sun-inner planets system

In the previous sections, we have assumed that the orbits of all the planets have the same expansion rate. However, the recent positional observations of the planets with high accuracy are mostly done within the inner planets region. Actually Krasinsky and Brumberg obtained dAU/dt by using these inner planets data, while the orbits of outer planets are given by the Russian ephemeris EPM (Ephemerides of Planets and the Moon).

Therefore, as a tentative approach, we consider the case that the expansion rates of the planetary orbits are not homogeneous but inhomogeneous in the sense that only the orbits of the inner planets expand.

In this section, we consider the case that the expansion of the planetary orbit occurs only for the inner planets.

In this case, the sum of the orbital angular momentum of all planets L is replaced by the sum of the inner planets $L_{\rm in}$:

$$L_{\rm in} \equiv \sum_{i=1}^{4} m_i \sqrt{G M_\odot r_i}. \tag{11}$$

Then Eq. (9) is now

$$-\frac{\dot{\gamma}_\odot}{\gamma_\odot} - \frac{\dot{M}_\odot}{M_\odot} - 2\frac{\dot{R}_\odot}{R_\odot} + \frac{\dot{T}_\odot}{T_\odot} = \frac{1}{2}\frac{L_{\rm in}}{\ell_\odot}\left(\frac{\dot{M}_\odot}{M_\odot} + \frac{\dot{a}}{a}\right). \tag{12}$$

Note that the sum of the angular momentum of inner planets amounts only 0.16% of the total L:

$$\frac{L_{\rm in}}{L} \simeq 1.6 \times 10^{-3}. \tag{13}$$

Therefore, under the assumption that the change in the rotational angular momentum of the Sun affects only the orbital angular momentums of the inner planets, the required values which were calculated in the previous sections to explain the secular increase of AU can now be revised to be 1.6×10^{-3} times smaller.

In particular, the right hand side of Eq. (12) is

$$\frac{1}{2}\frac{L_{\rm in}}{\ell_\odot}\frac{\dot{a}}{a} \simeq 1.5 \times 10^{-11}\,({\rm cy}^{-1}). \tag{14}$$

Interestingly, it is the same order of magnitude as (actually it is about 1.6 times larger than) $\dot{M}_\odot/M_\odot$.

Then we can conclude from Eq. (12) that the decrease of rotational angular momentum of the Sun due to the radiative mass loss has a significant contribution to the secular increase of the orbital radius of the inner planets.

6 Conclusion

In this paper, we considered the secular increase of astronomical unit recently reported by Krasinsky and Brumberg (2004), and suggested a possible explanation for this secular trend by means of the conservation law of total angular momentum. Assuming the existence of some tidal interactions that transfer the angular momentum from the Sun to the planets system, we have obtained the following results.

From the reported value $\frac{d}{dt}AU = 15 \pm 4$(m/cy),we have obtained the required value for the variation of rotational period of the Sun is about 21 (ms/cy), if we assume that eight planets in the solar system experience the same orbital expansion rate. This value is sufficiently small, and at present it seems there are no observational data which exclude this possibility.

Moreover, we have found that the effects of change in the moment of inertia of the Sun due to the radiative mass loss may be responsible for explaining the secular increase of AU. Especially, when we suppose that the orbital expansion occurs only in the inner planets region, the decrease of rotational angular momentum of the Sun has enough contribution to the secular increase of the orbital radius. Then as an answer to the question "why is AU increasing ?", we propose one possibility, namely "because the Sun is losing its angular momentum."

In present paper, we proposed the possible mechanism for explaining the secular increase of AU, nonetheless we need to verify the validity of our model by means of the some tidal dissipation models of the Sun. Moreover because the existence of dAU/dt is not confirmed robustly in terms of the independent analysis of observation by other ephemerides groups, it is important not only to perform the theoretical researches but also to re-analyze the data and to obtain more accurate value of dAU/dt adding new observations e.g., Mars Reconnaissance Orbiter, Phoenix and forthcoming MESSENGER which is cruising to the Mercury. It also seems to be meaningful to use the observations of outer planets as well, such as Cassini, Pioneer 10/11, Voyager 1/2, and New Horizons for Pluto since it is more natural situation that the variation of moment of inertia of the Sun causes the orbital changes not only of inner planets but also of outer ones. Therefore in order to reveal the origin of secular increase of AU, it is essential to investigate these sub jects in detail.

7 References

Arakida, H. 2008, arXiv:0810.282
Arakida, H. New Astron., 2009, 14, 275
Capitaine, N. and Guinot, B. 2009, arXiv:0812.2970
Dickey, J. O., Bender, P. L., Faller, J. E., Newhall, X. X.,
Ricklefs, R. L., Ries, J. G., Shelus, P. J., Veillet, C.,
Whipple, A. L., Wiant, J. R., Williams, J. G. and Yoder,
C. F. 1994, Science, 265, 482
296, 629
Krasinsky, G. A. and Brumberg, V. A. 2004, Celest. Mech.
Dyn. Astrn., 90, 267
Krasinsky, G. A. 2007, Private Communication
Mashhoon, B., Mobed, N., and Singh, D. 2007, Class. Quant.
Grav., 24, 5031
Murray, C. D. and Dermott, S. F. 1999, Solar System
Dynamics (Cambrigde University Press)
Noerdlinger, P. D. 2008, arXiv:0801.3807
Pitjeva, E. V. 2005, Solar System Research, 39, 176
Standish, E. M. 2005, Proc. IAU Colloq., 196, 163

Minimal surfaces in flat and curved spacetimes of arbitrary dimensionality

Umpei Miyamoto[1]

Department of Physics, Rikkyo University, Toshima, Tokyo 171-8501

Abstract

Minimal surfaces and domain walls play important roles in astrophysics, general relativity, and modern particle theories. First, we review the Bernstein theorem, which states that a well-defined single-valued minimal surface in 3-dimensional Euclidean flat spaces should be a plane, and its failure in general dimensions. Then, we show that this failure of Bernstein theorem in higher dimensions results in interesting consequences in the systems where the branes interact with black holes.

1 Bernstein conjecture, branes, and minimal cones

Minimal surfaces[2] in Euclidean space $\mathbb{E}^3$ have been extensively studied since the pioneering work of Thomas Young and of Laplace. In Monge, or non-parametric, gauge the surface is specified by the height function $z = z(x, y)$ above some plane. The non-parametric minimal surface equation governing the function $z(x, y)$ is

$$\partial_x \left(\frac{z_x}{\sqrt{1 + z_x^2 + z_y^2}} \right) + \partial_y \left(\frac{z_y}{\sqrt{1 + z_x^2 + z_y^2}} \right) = 0 \,. \tag{1}$$

A famous result of Bernstein asserts that the only single valued solution of Eq. (1) defined for all $(x, y) \in \mathbb{R}^2$ is a plane. It may also be shown that the planar solution is a minimizer of the area functional among compactly supported variations of the surface. In terms of brane theory, this means that the "classical ground state", *i.e.*, the static minimum of the energy functional for a membrane in three dimensional Euclidean space $\mathbb{E}^3$, which may be thought of as a static configuration in 4-dimensional Minkowski spacetime $\mathbb{E}^{3,1}$, is smooth and indeed planar. From the world volume point of view the classical ground state of the membrane preserves (2+1)-dimensional Poincaré invariance and may be thought of as a copy of (2+1)-dimensional Minkowski spacetime $\mathbb{E}^{2,1}$.

It is natural to conjecture that Bernstein's theorem remains valid for a minimal p-dimensional hypersurface in $(p + 1)$-dimensional Euclidean space $\mathbb{E}^{p+1}$. In other words, the classical ground state of a *p-brane* in $(p + 1 + 1)$-dimensional Minkowski spacetime $\mathbb{E}^{p+1,1}$ should be flat and invariant under the action of the $(p+1)$-dimensional Poincaré group $E(p, 1)$. Remarkably, although true for $p \leq 7$ it fails for $p+1 = 9$ [2]. In other words, the classical ground state of an 8-brane in 10-dimensional Minkowski spacetime spontaneously breaks 10-dimensional Poincaré invariance. The proof [2] rests on the fact that in $\mathbb{E}^8$ and above, a minimal hypersurface which is a minimizer of the p-volume functional among compactly supported variations need not be smooth. There are rather explicit counterexamples called *minimal cones*. Their existence leads to the conclusion that Bernstein's theorem fails in $\mathbb{E}^9$ [2].

As far as we aware, there has been very little discussion of the significance of this fact in the M/String theory literature. The breakdown of regularity of minimal hypersurfaces of flat space extends to minimal hypersurfaces of curved Riemannian manifolds and this has consequences for proofs of the positive energy theorem of general relativity which make essential use of minimal surfaces as a technical tool (*e.g.,* see [3] for the application to the positive mass theorem). It seems worthwhile therefore to examine the behavior of minimal surfaces in higher dimensions and in curved spaces in some explicit detail in order to understand better the situation and its possible physical implications. In particular, it is interesting to see whether the existence of various critical dimensions which has been noted in related contexts is of

[1] Email address: umpei@rikkyo.ac.jp

[2] This article is based on paper [1].

a universal nature and related to the the breakdown of Bernstein's theorem and the existence of minimal cones.

To make progress it is helpful to assume that the relevant surfaces have sufficient symmetries with which the problem may be reduced to one involving ordinary differential equations in an appropriate quotient space X, a ploy known to mathematicians as *equivariant variational theory*. Typically the brane equations of motion reduce to finding geodesics in X with respect to a suitable metric g on X, induced by the p-volume functional. The p-brane will be p-volume minimizing if the corresponding geodesic γ is length minimizing. A necessary condition that a geodesic joining points a and b be length minimizing is that γ contains no points between a and b conjugate to either. The existence of such conjugate points is governed by the Jacobi or geodesic deviation equation, solutions of which depend on the curvature of X. In the case that X is 2-dimensional, it is the sign of the Gauss curvature K which is important. If for example K is negative in the vicinity of γ, then it can contain no conjugate points and hence must be locally length minimizing. In the cases we shall consider the Gauss curvature is actually positive and a more detailed examination is required. One might have thought that positive Gauss curvature would lead to a second variation or Hessian of indefinite sign. However, the situation is more subtle since the effective metric governing the variational principle is incomplete and becomes singular near a conical point and compensatory terms can arise which in low dimension render the Hessian positive definite.

2 Branes in flat spaces

The simplest example is when a Lie group G acts isometrically on a $(p+1)$-dimensional Riemannian manifold $\{\Sigma, h\}$, thought of as "space" with orbits which are $(p-1)$-dimensional. The $X = \Sigma/G$ is (locally) 2-dimensional and a curve in X may be thought of as the projection under the action of G of a p-dimensional submanifold S of Σ. As a simple but primary example, let us consider a G-invariant submanifold $S \subset \Sigma = \mathbb{E}^{m+n+2}$ $(m, n \geq 1)$ as the configuration of p-brane $(p = n + m + 1)$. We focus on the case of $G = \mathrm{SO}(m+1) \times \mathrm{SO}(n+1) \subset \mathrm{SO}(m+n+2)$. The metric of ambient flat space is written in the form

$$h = dx^2 + x^2 d\Omega_m^2 + dy^2 + y^2 d\Omega_n^2 \,. \tag{2}$$

A projected metric $\tilde{h}$ on Σ/G is defined via a transformation of an inner product, $\tilde{h}(u_1, u_2) = h(u_1, u_2)$, where (u_1, u_2) is a pair of vectors tangent to the orbit $G(s)$, $s \in S$. Thus, in the present case $\tilde{h} = dx^2 + dy^2$. The volume function on Σ/G, which is the volume of the orbit $G(s)$, is given by $v(x, y) := \mathrm{Vol}\,(G(s)) = \Omega_m x^m \Omega_n y^n$, where Ω_n is the volume of unit n-sphere. Now, we are ready to define an effective space where the geodesic γ is to be found. The metric g of the effective space is defined as

$$g = d\ell^2 := v^{2/\lambda}(x, y)\tilde{h} = \Omega_m^2 \Omega_n^2 x^{2m} y^{2n} (dx^2 + dy^2) \,, \tag{3}$$

where λ is the co-dimension of the G-invariant surface S. For the present example, λ is given by $\lambda := \dim S - \dim G(x) = (m + n + 1) - (m + n) = 1$. The problem to find the minimal surface has been reduced to find the geodesic γ with $g = d\ell^2$. The action to be minimized is $\ell = \int x^m y^n \sqrt{dx^2 + dy^2}$. If one denotes the geodesic by $y = y(x)$ and varies the action with respect to it, one has

$$xyy'' + (myy' - nx)(1 + y'^2) = 0 \,. \tag{4}$$

One can easily see that a cone $y = \sqrt{n/m}\, x$ solves Eq. (4).

As noted before, one cannot know whether the above cone is indeed a minimizer or not until examining the second variation. Here, we introduce an alternative criterion to examine whether a geodesic is a minimizer or not. Readers are directed to [4] for an introduction to this topic. The *Jacobi equation* or *equation of geodesic deviation* is written as

$$\frac{d^2\eta}{d\ell^2} + K\eta = 0 \,, \tag{5}$$

where η and K are the geodesic deviation and Gauss curvature of metric g. For a general metric of form $g = v(x, y)^{2/\lambda}(dx^2 + dy^2)$, the Gauss curvature is given by $K = (1/2)(\text{Ricci scalar}) = -2\lambda^{-1} v^{-2/\lambda}(\partial_x^2 +$

$\partial_y^2) \ln v$. For the present case, where $v(x,y) = x^m y^n$ and $\lambda = 1$, we have

$$K = \frac{1}{x^{2m} y^{2n}} \left(\frac{m}{x^2} + \frac{n}{y^2} \right) , \tag{6}$$

which is positive definite. One can calculate the Gauss curvature and proper distance along the geodesic cone $y = \sqrt{n/m}\, x$,

$$K = \frac{2m^{n+1}}{n^n x^{2(m+n+1)}} , \quad \ell = \frac{n^{n/2}(m+n)^{1/2}}{m^{(n+1)/2}(m+n+1)} x^{m+n+1} . \tag{7}$$

Combining Eqs. (5) and (7), we have

$$\frac{d^2\eta}{d\ell^2} + \frac{c}{\ell^2}\eta = 0, \quad c = \frac{2(m+n)}{(m+n+1)^2} . \tag{8}$$

It is well known that the behavior of solution to this equation changes at $c = 1/4$. That is, Eq. (8) has a simple power solution $\eta = \ell^{\beta_\pm}$, $\beta_\pm = (1/2)\left(1 \pm \sqrt{1-4c}\right)$. Thus, the geodesic deviation oscillates (*i.e.*, there exists a conjugate point of the geodesic) for $2 \le m+n \le 5$, while not for $m+n \ge 6$ (*i.e.*, there exists no conjugate point of the geodesic). These results, and further work by Bombieri *et al.* imply that the cone as $\mathrm{SO}(m+1) \times \mathrm{SO}(n+1)$-invariant hypersurface $S \subset \mathbb{E}^{m+n+2}$ is a minimizer for $m+n+2 \ge 8$.

3 Application: Branes interacting with a black hole

So far, we have considered the Bernstein theorem and its failure in higher dimensions for minimal surfaces in flat spaces. Although not recognized well in literature, the failure of Berenstein conjecture play important roles in various context of physics, especially in higher dimensional gravitational theories. See the original paper [1] and references therein. Here, let us consider the primal gravitational system which was first investigated by Frolov [5]. Let us write the N-dimensional Schwarzschild-Tangherlini metric as

$$ds^2 = -f(r)dt^2 + f(r)^{-1}dr^2 + r^2(d\theta^2 + \sin^2\theta d\Omega_{N-3}^2), \quad f(r) = 1 - \left(\frac{r_0}{r}\right)^{N-3} . \tag{9}$$

Then, we focus on a local region near the south pole of horizon by setting $r = r_0 + \xi$, $\theta = \pi - \eta$ with small ξ/r_0 and η. At the leading order, the metric is written as

$$ds^2 = -\frac{(N-3)\xi}{r_0}dt^2 + \frac{r_0}{(N-3)\xi}d\xi^2 + r_0^2(d\eta^2 + \eta^2 d\Omega_{N-3}^2) . \tag{10}$$

Furthermore, introducing the following local coordinates $x = \sqrt{(4r_0\xi)/(N-3)}$, $y = r_0\eta$, the near horizon metric reduces to

$$ds^2 = -\kappa^2 x^2 dt^2 + dx^2 + dy^2 + y^2 d\Omega_{N-3}^2 , \tag{11}$$

where $\kappa = (N-3)/2r_0$ is the surface gravity. Thus, the near-horizon effective 2-dimensional metric in which the geodesic is to be found is

$$g = x^2 y^{2(N-3)}(dx^2 + dy^2) . \tag{12}$$

The problem has been reduced to that of $(m,n) = (1, N-3)$ in the flat-space case. Note that the factor x^2 in g comes from the time component of metric (11). Thus, the cone $y = \sqrt{N-3}\, x$ is a geodesic near the horizon, and from the analysis of geodesic deviation, this geodesic corresponds to a minimizer if $N = p+2 \ge 8$.

The work by Frolov was in part motivated by that of Kol [6] in which the "merger transition" from the Kaluza-Klein black holes to a black string was investigated. The black-hole–brane system indeed serves as a toy model of the merger transition and is shown to possess a critical dimension [7]. In addition, this system serves as the simplest (as far as we know) example of critical phenomena in gravitational

systems [8]. The cone solution separates two phases of the brane: one has a Minkowski topology and another a black hole topology. The change of stability nature of the brane appears at $p = 6$ and results in that of mass scaling of the black hole on the brane. It seems that the self similarity of the critical solution changes from discrete one to continuous one. It would be interesting to clarify why the breakdown of Bernstein conjecture is related to this change of self similarity in detail.

In addition, the black-hole–brane system has many applications to the physics of fundamental interactions via the AdS/CFT correspondence. The holographic dual of the phase transition from the Minkowski embedding to the brane embedding corresponds to the meson melting phase transition of matter in the fundamental representation (see, *e.g.*, Refs. [9]). Although the systems investigated in the literature so far correspond to the black-hole–brane systems below the critical dimension (as far as we know), it would be interesting to see in what the failure of the Bernstein conjecture results in the gauge theory side.

Acknowledgments

I would like to thank Valeri P. Frolov, Dan Gorbonos, Barak Kol, and Oleg Lunin for useful discussions and comments. I would like to acknowledge also the hospitality during my stay in Sep. 2008 at DAMTP and the Centre for Theoretical Cosmology, Cambridge University, where the work in paper [1] was started.

References

[1] G. W. Gibbons, K. i. Maeda and U. Miyamoto, "The Bernstein Conjecture, Minimal Cones, and Critical Dimensions," Class. Quant. Grav. **26**, 185008 (2009) [arXiv:0906.0264 [hep-th]].

[2] E. Bombieri, E. de Giorgi and E. Giusti, "Minimal Cones and the Bernstein Problem", *Inventiones math.* **7**, 243-268 (1969).

[3] R. Schoen and S. T. Yau, "Positivity Of The Total Mass Of A General Space-Time," Phys. Rev. Lett. **43**, 1457 (1979).

[4] H. E. Rauch, "Geodesic and Curvature in Differential Geometry in the Large", Graduate School of Mathematical Sciences, Yeshiva University, New York (1959); M. M. Postnikov, "The Variational Theory of Geodesics", Dover Publications (1983).

[5] V. P. Frolov, "Merger transitions in brane-black-hole systems: Criticality, scaling, and self-similarity," Phys. Rev. D **74**, 044006 (2006) [arXiv:gr-qc/0604114].

[6] B. Kol, "Topology change in general relativity and the black-hole black-string transition," JHEP **0510**, 049 (2005) [arXiv:hep-th/0206220].

[7] E. Sorkin, "A critical dimension in the black-string phase transition," Phys. Rev. Lett. **93**, 031601 (2004) [arXiv:hep-th/0402216]; H. Kudoh and U. Miyamoto, "On non-uniform smeared black branes," Class. Quant. Grav. **22**, 3853 (2005) [arXiv:hep-th/0506019].

[8] M. W. Choptuik, "Universality And Scaling In Gravitational Collapse Of A Massless Scalar Field," Phys. Rev. Lett. **70**, 9 (1993).

[9] D. Mateos, R. C. Myers and R. M. Thomson, "Holographic phase transitions with fundamental matter," Phys. Rev. Lett. **97**, 091601 (2006) [arXiv:hep-th/0605046]; D. Mateos, R. C. Myers and R. M. Thomson, "Thermodynamics of the brane," JHEP **0705**, 067 (2007) [arXiv:hep-th/0701132]; S. Kobayashi, D. Mateos, S. Matsuura, R. C. Myers and R. M. Thomson, "Holographic phase transitions at finite baryon density," JHEP **0702**, 016 (2007) [arXiv:hep-th/0611099].

An Earliest Black Hole Imager at Andes

Makoto Miyoshi[1 (a)], Ray S. Furuya[(b)], Noriyuki Kawaguchi[(a)], Junichi Nakajima[(c)], Yoshihisa Irimajiri[(d)], Yasuhiro Koyama[(e)], Mamoru Sekido[(e)], Hideki Ujihara[(e)], Kaname, Jose Iba, Ishitsuka[(f)], Yoshiharu Asaki [(g)], Yoshiaki Kato [(g)], Hiroshi Takeuchi [(g)], Masato Tsuboi[(g)], Takashi Kasuga[(h)], Akira Tomimatsu[(i)], Masaaki Takahashi[(j)], Yoshiharu Eriguchi[(k)], Shinichiro Yoshida[(k)], Shinji Koide[(l)], Rohta Takahashi[(m)], Tomoharu Oka[(n)]

[(a)] *Radio Astronomy Division, National Astronomical Observatory Japan, 2-21-1, Osawa, Mitaka, Tokyo 181-8588, Japan*
[(b)] *Subaru Telescope, National Astronomical Observatory of Japan, 650 North A'ohoku Place, Hilo, HI 96720, USA*
[(c)] *New Generation Wireless Communications Research Center, National Institute of Information and Communications Technology, 3-4, Hikarino-Oka, Yokosuka, Kanagawa 239-0847 Japan*
[(d)] *Applied Electromagnetic Research Center, National Institute of Information and Communications Technology, 4-2-1 Nukui-Kitamachi, Koganei, Tokyo 184-8795 Japan*
[(e)] *Kashima Space Research Center, National Institute of Information and Communications Technology, 893-1 Hirai, Kashima, Ibaraki 314-8501, Japan*
[(f)] *Instituto Geofisico del Peru, Observatorio de Ancon, Panamericana Norte, Ancon, Peru*
[(g)] *Institute of Space and Astronautical Science (ISAS), Japan Aerospace Exploration Agency (JAXA), 3-1-1 Yoshinodai, Sagamihara, Kanagawa 229-8510, Japan*
[(h)] *Department of System and Control Engineering, Hosei University, Koganei, Tokyo 184-8584, Japan*
[(i)] *Department of Physics, Nagoya University, Nagoya 464-8602, Japan*
[(j)] *Department of Physics and Astronomy, Aichi University of Education, Kariya, Aichi 448-8542, Japan*
[(k)] *Department of Earth Science and Astronomy, Graduate School of Arts and Sciences, University of Tokyo, Komaba, Meguro, Tokyo 153-8902, Japan*
[(l)] *Department of Physics, Kumamoto University, 2-39-1 Kurokami, Kumamoto 860-8555, Japan*
[(m)] *The Institute of Physical and Chemical Research (RIKEN), 2-1 Hirosawa, Wako, Saitama 351-0198, Japan*
[(n)] *Institute of Science and Technology, Keio University, 4-14-1 Hiyoshi, Yokohama, Kanagawa 223-8522, Japan*

Abstract

We are planning to construct a sub-mm VLBI system at Andes only dedicated to the detection of event horizon of SgrA*black hole. Using two of fixed large spherical dishes and a mobile small station, we sample sufficient u-v coverage, aim to image and detect the event horizon of SgrA*.

1 Introduction

Sagittarius A^* (SgrA*) is the most convincing massive black hole candidate with a mass of $4 \times 10^6 M_\odot$ hidden at the Galactic center. Because of its proximity of only 8 kpc from the sun and its quite large mass, the black hole in SgrA*has the largest apparent Schwarzschild radius of $6 \sim 10 \mu as$. Relativistic phenomena at a few Schwarzschild radii around a black hole should be observed in very near future VLBI at sub millimeter wavelength (Falcke et al. 2000, Miyoshi et al. 2004, 2007, Doeleman et al. 2008). A black hole can be seen as a shadow at the center of a bright accretion disk. Because the shadow shape depends on the physical parameters of black holes (mass, spin and charge) without their respective degeneracies, we can measure these parameters from imaging the shadow shape. SgrA*is now the most promising massive black hole for testing general relativity at strong gravity. (Takahashi 2005)

[1]Email address: makoto.miyoshi@nao.ac.jp

2 Horizon Telescope

Miyoshi et al. (2004, 2007) performed array simulations and found that a sub-mm VLBI array at the Southern Hemisphere is the best for observing SgrA*black hole[2]. It is quite natural because the SgrA*is located at -30° in declination. In Figure 2, we show the comparison of array performances of imaging SgrA*. The array simulations also showed that 10 observing stations and 8000-km array size are required to obtain a good image of SgrA*black hole shadow. In practice, however, the cost of such array construction is very expensive. We therefore have to begin with a low-cost instrument.

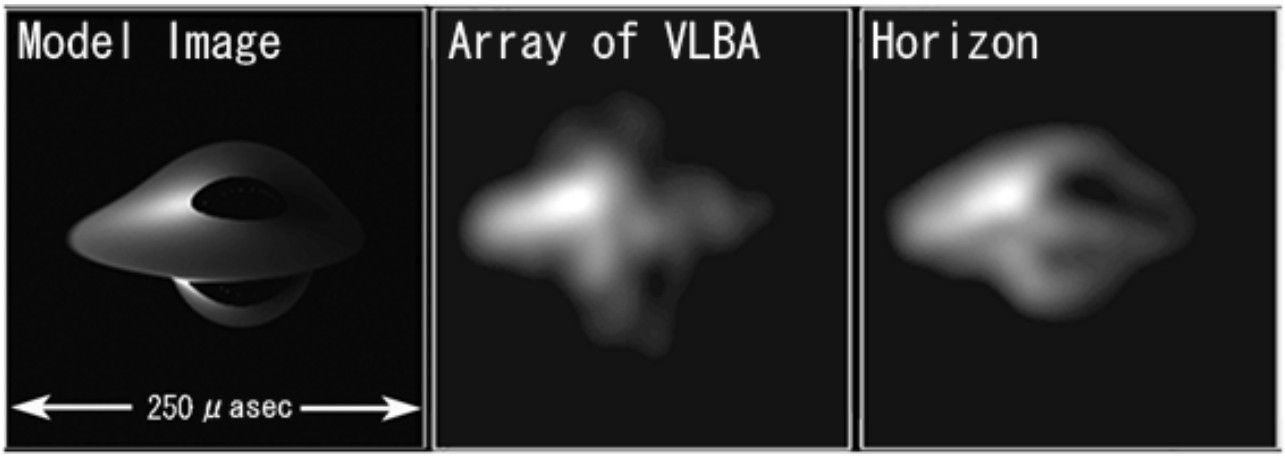

Figure 1: VLBI imaging simulations at 230GHz. Comparisons of array performances. A model image of SgrA*(center). Corresponding result by the array configuration of VLBA (center). Corresponding result by the array configuration of assumed Horizon telescope at the Southern Hemisphere. Both arrays are composed of 10 stations, and have the same array size of 8000 km (right). [The VLBA has no observing system at 230GHz and the weather conditions at the VLBA stations are not suitable for observing sub-mm wavelengths.]

3 Caravan System

In order to image the event horizon of SgrA*by sub-mm VLBI, however, it is necessary to add shorter baselines around 1000 to 2000 km to the present sub-mm VLBI stations for enhancing imaging quality. Figure 2 shows several imaging simulations indicating that the difficulty of getting correct images by a tentative present sub-mm VLBI array because of the lack of shorter baselines.
To cover shorter baselines it is appropriate to construct new stations at Andes mountains. To satisfy the technical requirement, we are planning 3-stations VLBI array at Andes, moreover with very low cost of around 10^7 US dollars, because we are in the big monetary crisis occurred once a century.
Figure 3 is an illustration showing the concept of the sub-mm VLBI, Caravan observing system. To attain cost down largely, we dare to abandon general capability and expansivity of the system and dedicate its purpose to observe SgrA*in order to detect the event horizon of SgrA*.

The Caravan is composed of two large fixed dishes and one small but mobile station. For two large fixed dishes, we are planning to use ground-fixed spherical dishes, which give us sensitivity. Spherical main reflector has no focus itself, but devising the shape of sub reflector, we can make a focus. By shifting the sub reflector, it is possible to perform tracking observations for a few hours. Because the main reflector is fixed on the ground all time, we are free from the worry about the deformation of the large

[2]Why sub-mm VLBI? Circumnuclear plasma around the SgrA*black hole blurs its intrinsic image. This effect is called as λ -square law, because the observed size of SgrA*by VLBI is proportional to the observing λ^2. At sub-mm wavelength, the law will become negligible, we can expect to observe the intrinsic figure of SgrA*.

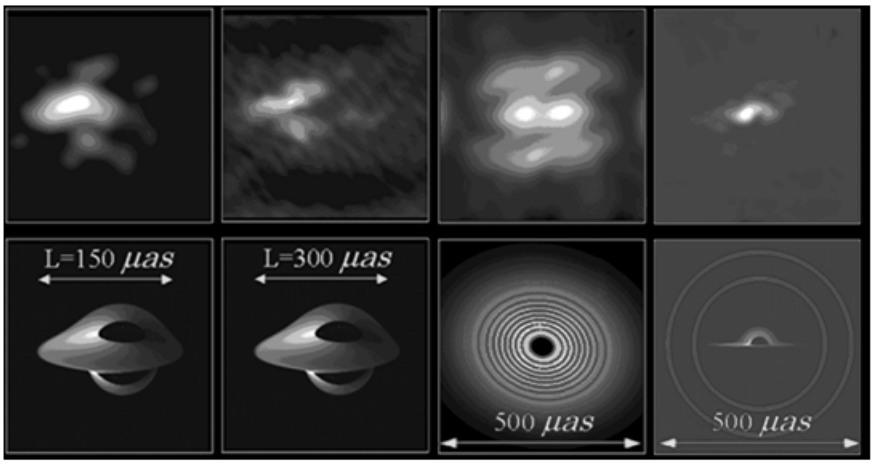

Figure 2: VLBI imaging simulations assuming with five sub-mm telescopes. At the lower panels several model images of SgrA*are shown while at the upper panels are shown corresponding resultant images. Here we assume an array including 5 stations located at Hawaii, West Coast of US, ALMA, Peru, and Closed SEST position.

main reflector due to the self weight that must be considered in cases of Az-EL mount telescopes. Unlike the surface panels of parabola, those of spherical antennas have a common curvature, we can achieve cost down by mass production of the panels. In Japan, Daishido's spherical telescopes at Waseda[3] are famous (Daishido et al. 2000). We can follow his knowledge and experience about spherical telescope.
For cost down, it is best to construct the fixed stations at existing observatory. The Huancayo observatory (IGP[4]) in Peru and the Chacaltaya Cosmic-ray Observatory[5] in Bolivia are now candidate for the location of the fixed stations of the Caravan system. These two observatories are 3300m and 5300 m in altitude respectively, suitable for sub-mm radio observations.

In order to sample various baseline vectors, we plan to make a small but mobile station, Caravan. The mobile Caravan station moves around Andes mountains, and changes its observing site position. At the new site, we open the antenna, set up the observing system. Geodetic measurement of the site position by GPS is important to obtain baseline vector. And then we perform VLBI observations between the two large fixed dishes. (We here do not mean that the observations are performed with driving the Caravan car!)

In Japan, the NICT Kashima has been developed such kinds of mobile stations for geodetic VLBI use for more than 20 years (Ichikawa et al., 2008, 2009). The sensitivity in interferometer is proportional to the product of the diameters of both antennas. If one antenna is large enough, the diameter of another can be small. We estimate the effective diameters to be 30m and 4 m for fixed and mobile stations respectively. Sampling various baseline vectors by changing observing position of the mobile Caravan will let us image the event horizon of SgrA*with better quality.

As shown in Figure 2, we cannot get a good image if the VLBI array has no sufficient uv coverage (i. e. sum of baseline vector components projected to the observing source). However, if we can assume an image model from theories and/or other observing results, an estimation of the image shape and size can be performed. Such model fittings were performed frequently at the early era of radio interferometers. Miyoshi et al.(2004, 2007) also expected the use in order to detect the black hole shadow. Actually, Doeleman et al. (2008) used the model fitting method to their data.The Caravan system will cover the dense uv coverage up to 2000 km in baseline length. Within the uv coverage, the first null point of fringe amplitude will be included, from which we can estimate the rough size of black hole shadow.

[3]http://www.astro.phys.waseda.ac.jp/index.html
[4]http://www.igp.gob.pe/
[5]http://en.wikipedia.org/wiki/Chacaltaya

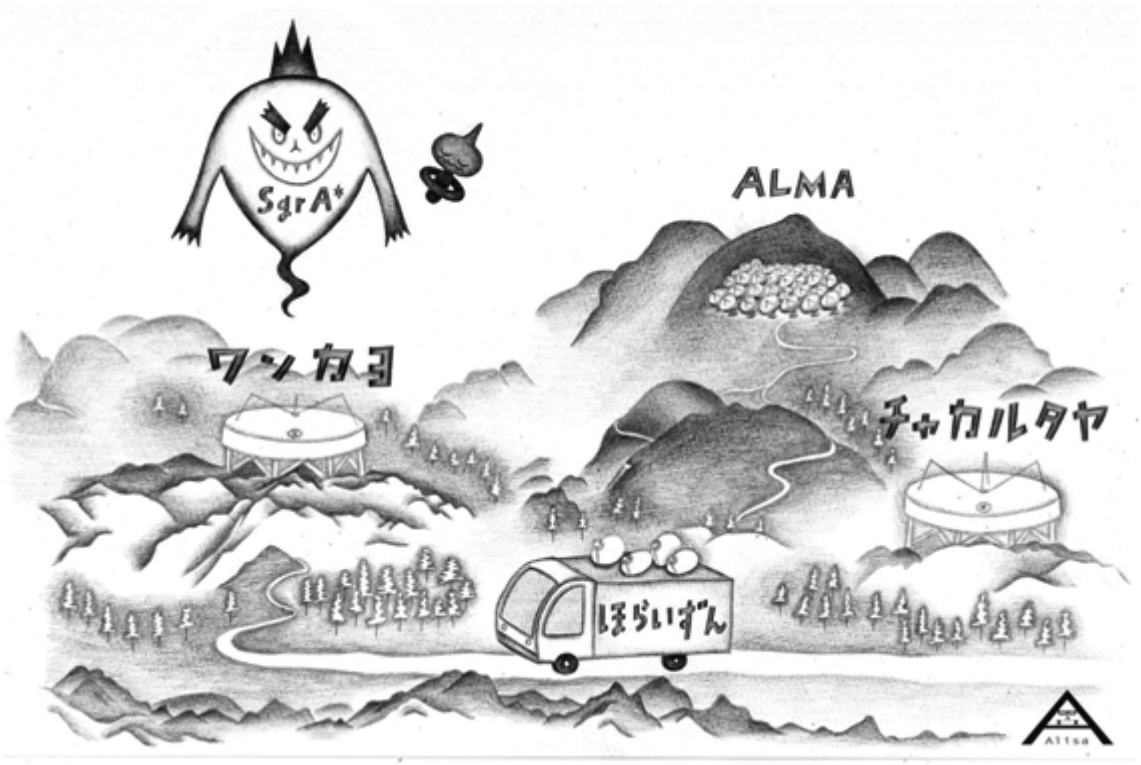

Figure 3: Concept of our sub-mm VLBI, Caravan system (illustration by A. Haba). Here we assume the Huancayo observatory (3300 m in altitude) in Peru and the Chacaltaya Cosmic-ray Observatory(5300 m) in Bolivia as the stations of the two large dishes. Practical figure of Caravan mobile station is not determined but here we illustrated like a Satellite News Gathering system in TV hookup. ALMA at Atacama (4800 m) is also drawn. Its use as VLBI station in future is also expected.

References

[1] Daishido, T., et al., Proc. SPIE 4015, 73-85, Radio Telescopes, Harvey R. Butcher; Ed. (2000)

[2] Doeleman, S. S. et al., Nature, 455, 78 (2008)

[3] Falcke, H., Melia, F., Agol, E., ApJ, 528, L13-L16, (2000)

[4] Ichikawa, R., A. et al., Proc. of the Fifth IVS General Meeting, pp.400-404, (2008)

[5] Ichikawa, R., A. et al., IVS NICT-TDC News No.30, (2009)

[6] Takahashi, R., PASJ, 57,273-277, (2005).

[7] Miyoshi, M. et al., PTPS, 155,186-189, (2004).

[8] Miyoshi, M. et al., PNAOJ, 10, 15-23, (2007), or astro-ph/0809.3548

Phantom behaviour and growth index anomalous evolution in viable $f(R)$ gravity models

Hayato Motohashi[1(a),(b)] , Alexei A. Starobinsky[2(b),(c)] and Jun'ichi Yokoyama[3(b),(d)]

(a) *Department of Physics, Graduate School of Science, The University of Tokyo, Tokyo 113-0033, Japan*
(b) *Research Center for the Early Universe (RESCEU), Graduate School of Science, The University of Tokyo, Tokyo 113-0033, Japan*
(c) *L. D. Landau Institute for Theoretical Physics, Moscow 119334, Russia*
(d) *Institute for the Physics and Mathematics of the Universe(IPMU), The University of Tokyo, Kashiwa, Chiba, 277-8568, Japan*

Abstract

We present numerical calculation of the evolution of a background space-time metric and sub-horizon matter density perturbations in viable $f(R)$ gravity models of present dark energy and cosmic acceleration. We found that viable models generically exhibit recent crossing of the phantom boundary $w_{\rm DE} = -1$. Moreover, as a consequence of the anomalous growth of density perturbations during the end of the matter-dominated stage, their growth index evolves non-monotonically with time and may even become negative.

1 Introduction

It is one of the most important issues for cosmologists and particle physicists to understand the physical origin of the dark energy (DE) which is responsible for an accelerated expansion of the current Universe. Although the standard spatially flat Λ-Cold-Dark-Matter (ΛCDM) model is consistent with all kinds of current observational data [1], some tentative deviations from it have been reported recently [2, 3]. Furthermore, in the ΛCDM model, the cosmological term is regarded as a new fundamental constant whose observed value is much smaller than any other energy scale known in physics. Hence it is natural to seek for non-stationary models of the current DE. Among them, $f(R)$ gravity which modifies and generalizes the Einstein gravity by incorporating a new phenomenological function of the Ricci scalar R, $f(R)$, can provide a self-consistent and non-trivial alternative to the ΛCDM model[4, 5].

In the previous paper [6], we calculated evolution of matter density fluctuations in viable $f(R)$ models [4, 5] for redshifts $z \gg 1$ during the matter-dominated stage and found an analytic expression for them. In this paper we extend the previous analysis and perform numerical calculations of the evolution of both background space-time and density fluctuations for the particular $f(R)$ model of Ref. [5] without such a restriction. As a result, we have found crossing of the phantom boundary $w_{\rm DE} = -1$ at an intermediate redshift $z \lesssim 1$ for the background space-time metric and an anomalous behavior of the growth index of fluctuations.

2 Background

We adopt the following action of $f(R)$ models with model parameters n, λ and R_s [5]:

$$S = \frac{1}{16\pi G}\int d^4x\sqrt{-g}f(R) + S_m, \quad f(R) = R + \lambda R_s\left[\left(1+\frac{R^2}{R_s^2}\right)^{-n} - 1\right], \tag{1}$$

[1]Email address: motohashi@resceu.s.u-tokyo.ac.jp
[2]Email address: alstar@landau.ac.ru
[3]Email address: yokoyama@resceu.s.u-tokyo.ac.jp

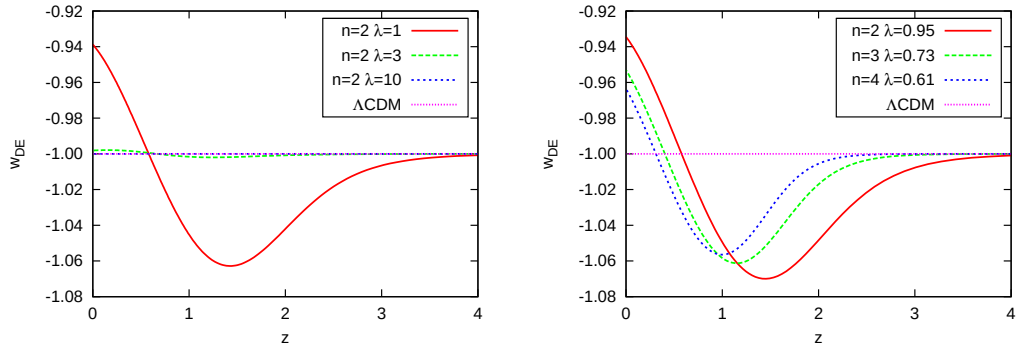

Figure 1: Evolution of the equation-of-state parameter of effective dark energy.

where S_m is the action of the matter content which is assumed to be minimally coupled to gravity. To make the late-time asymptotic de Sitter regime where $R =$ constant stable, λ has to satisfy $f'(R) > Rf''(R)$. As a result, λ has a lower limit $\lambda_{\rm min}$ for each n. Numerically we find $(n, \lambda_{\rm min})$ =(2, 0.9440), (3, 0.7259), and (4, 0.6081). From the action (1), we obtain field equations as

$$R^\mu_\nu - \frac{1}{2}\delta^\mu_\nu R = -8\pi G\left(T^\mu_{\nu(m)} + T^\mu_{\nu({\rm DE})}\right), \tag{2}$$

$$8\pi G T^\mu_{\nu({\rm DE})} \equiv (F-1)R^\mu_\nu - \frac{1}{2}(f-R)\delta^\mu_\nu + (\nabla^\mu\nabla_\nu - \delta^\mu_\nu\Box)F, \quad F(R) \equiv f'(R). \tag{3}$$

Working in the spatially flat Friedmann-Robertson-Walker (FRW) space-time with a scale factor $a(t)$,

$$3H^2 = 8\pi G\rho - 3(F-1)H^2 + \frac{1}{2}(FR - f) - 3H\dot{F}, \tag{4}$$

$$2\dot{H} = -8\pi G\rho - 2(F-1)\dot{H} - \ddot{F} + H\dot{F}, \tag{5}$$

where H is the Hubble parameter and ρ is the energy density of the material content which we assume to consist of non-relativistic matter. From (1), we can determine the DE equation of state parameter $w_{\rm DE}$,

$$w_{\rm DE} \equiv \frac{P_{\rm DE}}{\rho_{\rm DE}} = -1 + \frac{2\dot{H}(F-1) - H\dot{F} + \ddot{F}}{-3H\dot{R}F' + 3(H^2+\dot{H})(F-1) - (f-R)/2}. \tag{6}$$

We solve the evolution equation (5) numerically using (4) to check numerical accuracy. The moment when the matter density parameter $\Omega(t) = 16\pi G\rho/(16\pi G\rho + \lambda R_s)$ equals to 0.998 is chosen as the initial time t_i. We determine the current epoch $t = t_0$ by the requirement that the value of Ω takes the observed central value $\Omega_0 = 0.27$. R_s is fixed in such a way as to reproduce the current Hubble parameter $H_0 = 72$km/s/Mpc. We find the ratio R_s/H_0^2 is well fit by a simple power-law $R_s/H_0^2 = c_n\lambda^{-p_n}$ with (n, c_n, p_n) =(2, 4.16, 0.953), (3, 4.12, 0.837), and (4, 4.74, 0.702), respectively, whereas in the ΛCDM limit it would behave as $R_s/H_0^2 = 6(1-\Omega_0)/\lambda \simeq 4.38\lambda^{-1}$.

Figures 1 depict evolution of $w_{\rm DE}$ as a function of redshift z where phantom crossing is manifest. As expected, it approaches $w_{\rm DE} = -1 =$ constant as we increase λ for fixed n. For the minimal allowed values of λ, deviations from $w_{\rm DE} = -1$ are observed at 5% level on both directions in $z \lesssim 2$ independently of n. From (6), we can read off that this phantom crossing behavior is not peculiar to the specific choice of the function (1) but a generic one for models which satisfy the stability condition $F' > 0$.

3 Perturbations

We now turn to the evolution of density fluctuations. In $f(R)$ gravity, the evolution equation of density fluctuations, δ, deeply in the sub-horizon regime is given by[7]

$$\ddot{\delta} + 2H\dot{\delta} - 4\pi G_{\rm eff}\rho\delta = 0, \quad G_{\rm eff} = \frac{G}{F}\frac{1 + 4\frac{k^2}{a^2}\frac{F'}{F}}{1 + 3\frac{k^2}{a^2}\frac{F'}{F}}. \tag{7}$$

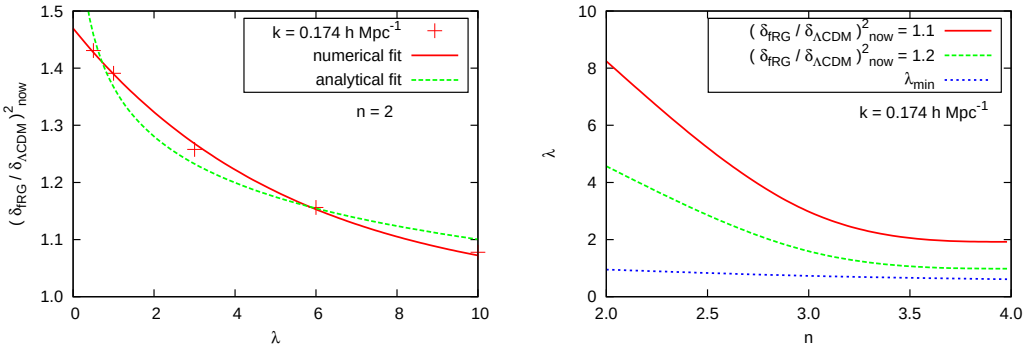

Figure 2: Constraints from the power spectrum.

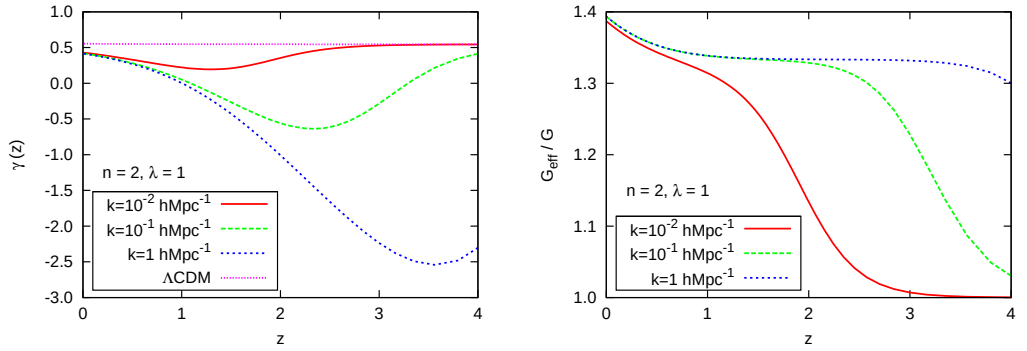

Figure 3: Evolution of $\gamma(z)$ and $G_{\rm eff}/G$.

In the previous paper[6] we obtained an analytic solution for the high-curvature regime when the scale factor evolves as $a(t) \propto t^{2/3}$ and F takes an asymptotic form $F \simeq 1 - 2n\lambda\,(R/R_s)^{-2n-1}$. In the present paper, we numerically integrate (7) up to $z = 0$ without using the approximation $|F - 1| \ll 1$.

The wavenumber of our particular interest is the scale corresponding to σ_8 normalization, for which we find $k_{\rm eff}(r = 8h^{-1}{\rm Mpc}) = 0.174h{\rm Mpc}^{-1}$. Since the standard ΛCDM model normalized by CMB data explains galaxy clustering at small scales well, $\delta_{\rm fRG}$ should not be too much larger than $\delta_{\Lambda{\rm CDM}}$ on these scales. We may typically require $(\delta_{\rm fRG}/\delta_{\Lambda{\rm CDM}})^2 \lesssim 1.1$. Although we neglect non-linear effects here, the difference between linear calculation and non-linear N-body simulation remained smaller than 5% at wavenumber $0.174h{\rm Mpc}^{-1}$[8].

The left panel of Fig. 2 represents $(\delta_{\rm fRG}/\delta_{\Lambda{\rm CDM}})^2$ as a function of λ for $n = 2$ together with two fitting functions. The solid line is from the analytic formula obtained in Ref. [6], and the broken line is numerical fitting using an exponential function $1 + b_n e^{-q_n\lambda}$. From these analysis, we can constrain the parameter space as the right panel of Fig. 2. The region which satisfy $(\delta_{\rm fRG}/\delta_{\Lambda{\rm CDM}})^2 < 1.1$ lies above the solid line. The region below the dotted line is forbidden from instability of de Sitter regime.

Next we turn to another important quantity used to distinguish different theories of gravity, namely, the gravitational growth index, $\gamma(z)$, of density fluctuations. It is defined through

$$\frac{d\ln\delta}{d\ln a} = \Omega_m(z)^{\gamma(z)}, \quad \text{or} \quad \gamma(z) = \frac{\log\left(\frac{\dot\delta}{H\delta}\right)}{\log\Omega_m}. \tag{8}$$

It takes a practically constant value $\gamma \cong 0.55$ in the standard ΛCDM model, but it evolves with time in modified gravity theories in general. We also note that $\gamma(z)$ has a nontrivial k-dependence in $f(R)$ gravity since density fluctuations with different wavenumbers evolve differently. Therefore, this quantity is a useful measure to distinguish modified gravity from ΛCDM model in the Einstein gravity.

Figures 3 show the evolution of $\gamma(z)$ together with that of $G_{\rm eff}/G$ for different values of k. In the early high-redshift regime, $\gamma(z)$ takes a constant value identical to the ΛCDM model. It gradually decreases

in time, reaches a minimum which may be even negative, and then increase again towards the present epoch. We note that recently Narikawa and Yamamoto[9] numerically calculated time evolution of $\gamma(z)$ in a simplified model which we had used in the previous paper and also obtained some analytic expansion, which behaves qualitatively the same as the numerical result but with much more exaggerated amplitudes. Our results, which satisfy all viability conditions, exhibit milder deviation from ΛCDM model than they found. At present, the constraints for the growth index is not so strict to distinguish the deviation from the ΛCDM model[10], but observations may reveal its time and wave number dependence in future.

4 Conclusion

In the present paper we have numerically calculated the evolution of both homogeneous background and density fluctuations in a viable $f(R)$ model of accelerated expansion based on the specific functional form proposed in Ref. [5]. We have found that viable $f(R)$ gravity models of accelerated expansion generically exhibit phantom behavior during the matter-dominated stage with crossing of the phantom boundary $w_{\rm DE} = -1$ at redshifts $z \lesssim 1$. The predicted time evolution of $w_{\rm DE}$ has qualitatively the same behaviour as that was recently obtained from observational data in [2].

As for density fluctuations, we have numerically confirmed our previous analytic results on a shift in the power spectrum index for large wavenumbers which exceed the scalaron mass during the matter dominated epoch[6], while for smaller wavenumbers fluctuations have the same amplitude as in the ΛCDM model.

We have also investigated the growth index $\gamma(k, z)$ of density fluctuations and have given an explanation of its anomalous evolution in terms of time dependence of $G_{\rm eff}$. Since γ has characteristic time and wavenumber dependence, future detailed observations may yield useful information on the validity of $f(R)$ gravity through this quantity, although current constraints have been obtained assuming that it is constant both in time and in wavenumber[3, 10].

Acknowledgments

HM and JY are grateful to T. Narikawa and K. Yamamoto for useful communications. AS acknowledges RESCEU hospitality as a visiting professor. He was also partially supported by the grant RFBR 08-02-00923 and by the Scientific Programme "Astronomy" of the Russian Academy of Sciences. This work was supported in part by JSPS Grant-in-Aid for Scientific Research No. 19340054(JY), JSPS Core-to-Core program "International Research Network on Dark Energy", and Global COE Program "the Physical Sciences Frontier", MEXT, Japan.

References

[1] E. Komatsu *et al.*, arXiv:1001.4538.

[2] A. Shafieloo, V. Sahni and A. A. Starobinsky, Phys. Rev. D **80**, 101301 (R) (2009) [arXiv:0903.5141].

[3] R. Bean, arXiv:0909.3853.

[4] W. Hu and I. Sawicki, Phys. Rev. D **76**, 064004 (2007) [arXiv:0705.1158].

[5] A. A. Starobinsky, JETP Lett. **86**, 157 (2007) [arXiv:0706.2041].

[6] H. Motohashi, A. A. Starobinsky and J. Yokoyama, Int. J. Mod. Phys. D **18**, 1731 (2009) [arXiv:0905.0730].

[7] S. Tsujikawa, Phys. Rev. D **76**, 023514 (2007) [arXiv:0705.1032].

[8] H. Oyaizu, M. Lima and W. Hu, Phys. Rev. D **78**, 123524 (2008) [arXiv:0807.2462].

[9] T. Narikawa and K. Yamamoto, arXiv:0912.1445.

[10] D. Rapetti, S. W. Allen, A. Mantz and H. Ebeling, arXiv:0911.1787.

Dynamical Instability of Ultra-spinning Myers-Perry Black Holes

Keiju Murata[1], Norihiro Tanahashi[2] and Takahiro Tanaka[3]

Department of Physics, Kyoto University, Kyoto 606-8502, Japan

Abstract

We study the dynamical stability of Myers-Perry black holes with single rotation parameter. We derived the gravitational perturbation equation of the most symmetric mode, which is given by a system of partial differential equations. We solve the partial differential equations by the relaxation method and find the marginally stable modes in $d = 6, 7$ dimensions. This result indicates not only the instability of Myers-Perry black holes with a large angular momentum, but also the existence of a sequence of new black hole solutions in $d \geq 6$ dimensions.

1 Introduction

Recently, various higher dimensional black holes have been found motivated by the string theory. A generalization of Kerr black holes to higher dimensions was obtained by Myers and Perry many years ago. There are also many exotic black holes in higher dimension such as black ring, etc. It is important to study the stability of these black holes in order to reveal the nature of higher dimensional gravity.

The stability of higher dimensional Schwarzschild black holes has been shown in [1]. For Myers-Perry black holes with equal angular momenta, the stability was shown for partial modes [2, 3]. On the other hand, it was predicted that Myers-Perry black holes with single rotation parameter can be unstable for $d \geq 6$ [4]. In $d \geq 6$ dimensions, Myers-Perry black holes with single rotation parameter approach black brane solutions for a sufficiently large angular momentum because of the centrifugal force. (In $d = 4, 5$ dimensions, the angular momentum of the Myers-Perry black hole has upper bound and we cannot take this limit.) It is known that the black brane solutions are unstable and, therefore, we can expect that Myers-Perry black holes with single rotation parameter are unstable for a large angular momentum. The purpose of this paper is to show the instability. The spacetime of the Myers-Perry black hole with single rotation parameter has two inhomogeneous directions. Thus, the gravitational perturbation equation is given by the system of partial differential equations in general. We will solve the partial differential equations numerically and find the instability of ultra-spinning Myers-Perry black holes.

2 Myers-Perry black holes with single rotation parameter

In this paper, we will concentrate on the Myers-Perry black holes with single angular momentum. The metric is given by

$$ds^2 = -\frac{\rho^2\Delta}{\Sigma^2}dt^2 + \frac{\Sigma^2\sin^2\theta}{\rho^2}\left(d\phi - \frac{2Ma}{\Sigma^2 r^{d-5}}dt\right)^2 + \frac{\rho^2}{\Delta}dr^2 + \rho^2 d\theta^2 + r^2\cos^2\theta d\Omega_{d-4}^2 \ , \tag{1}$$

where

$$\Delta = r^2 + a^2 - \frac{2M}{r^{d-5}} \ , \quad \rho^2 = r^2 + a^2\cos^2\theta \ , \quad \Sigma^2 = (r^2+a^2)^2 - a^2\Delta\sin^2\theta \ . \tag{2}$$

The horizon of this black holes is located at $\Delta(r_+) = 0$. The symmetry of this spacetime is $R_t \times U(1) \times SO(d-3)$, where R_t is the time translation symmetry, $U(1)$ is the rotational symmetry generated by ∂_ϕ and $SO(d-3)$ is the symmetry of $d\Omega_{d-4}^2$ part. The r and θ directions are inhomogeneous. This

[1]e-mail:murata@tap.scphys.kyoto-u.ac.jp
[2]e-mail:tanahashi@tap.scphys.kyoto-u.ac.jp
[3]e-mail:tanaka@yukawa.kyoto-u.ac.jp

symmetry is not enough to separate gravitational perturbation equations and the perturbation equations are given by partial differential equations of r and θ coordinates. Hereafter, we will use the another radial coordinate defined by $x = \int_{r_+}^{r} \frac{dr}{\Delta^{1/2}}$. In the x coordinate, the horizon is located at $x = 0$.

3 Perturbation equations

In [4], it is predicted that the Gregory-Laflamme type instability appears in the ultra-spinning Myers-Perry spacetime. Because the original Gregory-Laflamme instability appears in s-wave of the spherical part of the metric, we can expect that the instability of Myers-Perry black holes also appear in the most symmetric mode. Thus, we concentrate on the gravitational perturbation retaining the back ground symmetry, $U(1) \times SO(d-3)$. Moreover, to find the onset of the instability, we can also restrict the perturbation to the static perturbation. The metric which have the symmetry $R_t \times U(1) \times SO(d-3)$ is given by

$$ds^2 = e^{2\chi}(dx^2 + d\theta^2) - e^{\alpha-\beta+2(d-4)\gamma}dt^2 + e^{\alpha+\beta+2(d-4)\gamma}(d\phi + Adt)^2 + e^{-2\gamma}d\Omega_{d-4}^2 \ , \tag{3}$$

where functions α, β, γ, A and χ are depend on x and θ. Now, we consider the infinitesimal variation of these functions as $\alpha \to \alpha + \tilde{\alpha}$, $\beta \to \beta + \tilde{\beta}$, $\gamma \to \gamma + \tilde{\gamma}$, $A \to A + \tilde{A}$ and $\chi \to \chi + \tilde{\chi}$, where variables with tilde represent perturbed variables and background variables are given by

$$\begin{aligned} &\alpha = \frac{1}{2}\ln\left[\Delta \sin^2\theta (r^2\cos^2\theta)^{2(d-4)}\right] \ , \quad \beta = \frac{1}{2}\ln\left[\frac{\Sigma^4 \sin^2\theta}{\rho^4 \Delta}\right] \ , \\ &\gamma = -\frac{1}{2}\ln\left[r^2\cos^2\theta\right] \ , \quad A = -\frac{2Ma}{\Sigma^2 r^{d-5}} \ , \quad \chi = \ln\rho \ , \quad . \end{aligned} \tag{4}$$

The perturbation equations are given by

$$\partial^2\tilde{\alpha} + \partial(\Phi+\alpha)\cdot\partial\tilde{\alpha} + (d-4)\partial\alpha\cdot\partial\tilde{\gamma} - 4(d-4)(d-5)e^{2\gamma+2\chi}(\tilde{\gamma}+\tilde{\chi}) = 0 \ , \tag{5}$$

$$\partial^2\tilde{\beta} + \partial\Phi\cdot\partial\tilde{\beta} + (d-4)\partial\beta\cdot\partial\tilde{\gamma} + \partial\beta\cdot\partial\tilde{\alpha} + 2e^{2\beta}\partial A\cdot(\partial A\,\tilde{\beta} + \partial\tilde{A}) = 0 \ , \tag{6}$$

$$\partial^2\tilde{\gamma} + \partial\{\Phi + (d-4)\gamma\}\cdot\partial\tilde{\gamma} + \partial\gamma\cdot\partial\tilde{\alpha} + 2(d-5)e^{2\gamma+2\chi}(\tilde{\gamma}+\tilde{\chi}) = 0 \ , \tag{7}$$

$$\partial^2\tilde{A} + \partial(\Phi+2\beta)\cdot\partial\tilde{A} + (d-4)\partial A\cdot\partial\tilde{\gamma} + \partial A\cdot\partial\tilde{\alpha} + 2\partial A\cdot\partial\tilde{\beta} = 0 \ , \tag{8}$$

$$\begin{aligned} \partial^2\tilde{\chi} - \Big[&\frac{1}{2}\partial\alpha\cdot\partial\tilde{\alpha} - \frac{1}{2}\partial\beta\cdot\partial\tilde{\beta} + \frac{1}{2}e^{2\beta}(\partial A)^2\tilde{\beta} + \frac{1}{2}e^{2\beta}\partial A\cdot\partial\tilde{A} \\ &- (d-3)(d-4)\partial\gamma\cdot\partial\tilde{\gamma} - (d-4)(d-5)e^{2\gamma+2\chi}(\tilde{\gamma}+\tilde{\chi})\Big] = 0 \ . \end{aligned} \tag{9}$$

where $\Phi \equiv (d-4)\gamma + \alpha$. There are also two constraint equations,

$$\begin{aligned} C_1 \equiv &-\partial_x\partial_\theta\tilde{\Phi} + \partial_\theta\chi\partial_x\tilde{\Phi} + \partial_x\chi\partial_\theta\tilde{\Phi} - \partial_x\Phi\partial_\theta\tilde{\Phi} - \partial_\theta\Phi\partial_x\tilde{\Phi} + \partial_\theta\tilde{\chi}\partial_x\Phi + \partial_x\tilde{\chi}\partial_\theta\Phi + \tilde{\beta}e^{2\beta}\partial_x A\partial_\theta A \\ &+ \frac{1}{2}\left[\partial_x\alpha\partial_\theta\tilde{\alpha} - \partial_x\beta\partial_\theta\tilde{\beta} + e^{2\beta}\partial_x A\partial_\theta\tilde{A} - 2(d-3)(d-4)\partial_x\gamma\partial_\theta\tilde{\gamma}\right] \\ &+ \frac{1}{2}\left[\partial_\theta\alpha\partial_x\tilde{\alpha} - \partial_\theta\beta\partial_x\tilde{\beta} + e^{2\beta}\partial_\theta A\partial_x\tilde{A} - 2(d-3)(d-4)\partial_\theta\gamma\partial_x\tilde{\gamma}\right] = 0 \ , \end{aligned} \tag{10}$$

$$\begin{aligned} C_2 \equiv &-\partial_\theta^2\tilde{\Phi} - \partial_x\chi\partial_x\tilde{\Phi} + \partial_\theta\chi\partial_\theta\tilde{\Phi} - 2\partial_\theta\Phi\partial_\theta\tilde{\Phi} - \partial_x\tilde{\chi}\partial_x\Phi + \partial_\theta\tilde{\chi}\partial_\theta\Phi - \frac{1}{2}\tilde{\beta}e^{2\beta}\{(\partial_x A)^2 - (\partial_\theta A)^2\} \\ &+ \frac{1}{2}\left[\partial_\theta\alpha\partial_\theta\tilde{\alpha} - \partial_\theta\beta\partial_\theta\tilde{\beta} + e^{2\beta}\partial_\theta A\partial_\theta\tilde{A} - 2(d-3)(d-4)\partial_\theta\gamma\partial_\theta\tilde{\gamma}\right] \\ &- \frac{1}{2}\left[\partial_x\alpha\partial_x\tilde{\alpha} - \partial_x\beta\partial_x\tilde{\beta} + e^{2\beta}\partial_x A\partial_x\tilde{A} - 2(d-3)(d-4)\partial_x\gamma\partial_x\tilde{\gamma}\right] \\ &+ (d-4)(d-5)e^{2\gamma+2\chi}(\tilde{\gamma}+\tilde{\chi}) = 0 \ , \end{aligned} \tag{11}$$

The left hand sides of constraint equations C_1 and C_2 satisfy

$$\partial_\theta(e^\Phi \tilde{C}_1) - \partial_x(e^\Phi \tilde{C}_2) = 0 \ , \quad \partial_x(e^\Phi \tilde{C}_1) + \partial_\theta(e^\Phi \tilde{C}_2) = 0 \ , \tag{12}$$

where we used equations (5-9). These equations are nothing but Cauchy-Riemann equations. Therefore, if the constraint equations are satisfied at the boundary, the Eqs.(5-9) guarantee the constraint equations at whole region.

4 A method to find the instability

In this section, we explain how to solve the partial differential equations (5-11). For numerical calculation, the variables $(\tilde{\alpha}, \tilde{\beta}, \tilde{\gamma}, \tilde{A}, \tilde{\chi})$ are not good variables because some coefficients of perturbation variables in development equations (5-9) diverge at axes $\theta = 0, \pi/2$. Now, we try to eliminate the singularities at axes by changing variables and using the constraint equation (11). We define new variables $(\tilde{p}, \tilde{q}, \tilde{s})$ as

$$\tilde{p}(x,\theta) \equiv \frac{\tilde{\chi}+\tilde{\gamma}}{1+y} \ , \quad \tilde{q}(x,\theta) \equiv \frac{\tilde{\chi} - (\tilde{\alpha}+\tilde{\beta})/2 - (d-4)\tilde{\gamma}}{1-y} \ , \quad \tilde{s}(x,\theta) \equiv \frac{1}{2}\left(\tilde{\alpha} - \tilde{\beta}\right) + (d-4)\tilde{\gamma} \ , \tag{13}$$

where $y = \cos 2\theta$. In term of the new set of variables $(\tilde{p}, \tilde{q}, \tilde{s}, \tilde{A}, \tilde{\chi})$, after some appropriate linear combinations of the development equations (5-9), we obtain

$$\left[\partial_x^2 + \mathcal{M}_1\partial_y^2 + \mathcal{M}_2\partial_x + \mathcal{M}_3\partial_y + \mathcal{M}_4\right]\boldsymbol{V} = 0 \ , \tag{14}$$

where we define $\boldsymbol{V} = (\tilde{p}, \tilde{q}, \tilde{s}, \tilde{A}, \tilde{\chi})^T$ and $\mathcal{M}_i$ $(i = 1, 2, 3, 4)$ are 5×5 matrices whose components are functions of x and $y = \cos 2\theta$. Some components of $\mathcal{M}_i$ still diverge at $\theta = 0, \pi/2$. To eliminate these singularities, we use constraint equation (11). We add a vector $\boldsymbol{V}' = (-\tilde{C}_2/(1+y), -\tilde{C}_2/(1-y), -(d-3)\tilde{C}_2, 0, 0)^T$ to the left hand side of (14). Then, functional matrices are changed as $\mathcal{M}_i \to M_i$ and new matrices M_i are regularized at $\theta = 0, \pi/2$. To find stationary perturbation, we calculate the eigen value of the operator $\mathcal{O} \equiv \partial_x^2 + M_1\partial_y^2 + M_2\partial_x + M_3\partial_y + M_4$. We study the distribution of eigen values of the operator $\mathcal{O}$ with various rotation parameter a and trace the variation of eigen values. If a eigen value cross $\lambda = 0$, it means the existence of the zero mode.

5 Instability of ultra-spinning Myers-Perry black holes

We solve the eigen value of the operator $\mathcal{O}$ by the relaxation method. The domain of our calculation is $\{(x,y)|0 \le x \le x_{\max}, -1 \le y \le 1\}$, where $x_{\max}$ is given by $x_{\max}(r = r_{\max})$ where $r_{\max} = 5.0r_+$. The number of grids for x and y directions are $N_x = 30$ and $N_y = 40$, respectively.

Firstly, we consider the case of $d = 7$. The eigen value for various rotation parameter a is depicted in Figure.1. We find that the eigen value crosses $\lambda = 0$ at $a/r_+ = 1.41$ and $a/r_+ = 3.09$. The zero mode at $a/r_+ = 1.41$ is not a onset of the instability. The reason is as follows. Thermodynamical parameters of Myers-Perry black holes are given by

$$M = \frac{1}{2}r_+^{d-5}(r_+^2+a^2) \ , \quad J = \frac{1}{d-2}ar_+^{d-5}(r_+^2+a^2) \ , \quad T = \frac{(d-3)r_+^2 + (d-5)a^2}{4\pi r_+(r_+^2+a^2)} \ , \quad \Omega = \frac{a}{r_+^2+a^2} \ , \tag{15}$$

Then, the Jacobian of (T, Ω) and (M, J) is given by $\partial(T,\Omega)/\partial(M,J) \propto (d-5)(a/r_+)^2 - (d-3)$. Thus, for $a/r_+ = \sqrt{(d-3)/(d-5)}$, the transformation of (T, Ω) to (M, J) is not one to one correspondence. In our calculation, we impose conditions at the horizon that temperature and angular velocity of the stationary perturbation do not change to exclude mass and angular momentum perturbations of Myers-Perry black holes which always exist. However, these conditions are not enough to exclude trivial perturbations at $a/r_+ = \sqrt{(d-3)/(d-5)}$. Hence, the zero mode at $a/r_+ = 1.41$ is just a trivial perturbation. Thus, for $d = 7$, the onset of instability is given by $a/r_+ = 3.09$.

By the similar way, we can study the eigen value in $d = 6$ dimensions and find zero eigen values. We summarize the onset of instability as

$$a/r_+ = 4.06 \ (d = 6) \ , \quad a/r_+ = 3.09 \ (d = 7) \ . \tag{16}$$

We checked that these results do not depend on N_x, N_y and $x_{\max}$.

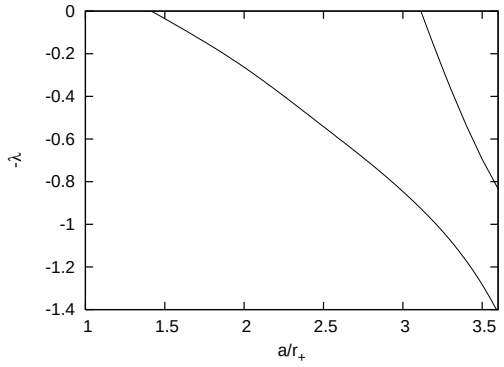

Figure 1: This is the variation of the eigen value with respect to rotation parameter a. We see the eigen value cross the $\lambda = 0$ at $a/r_+ = 1.41$ and $a/r_+ = 3.09$.

6 Summary

We studied the stability of Myers-Perry black holes with single rotation parameter. We derive the perturbation equations for the most symmetric mode. The perturbation equations are given by partial deferential equations. We solved the equations by relaxation method and find the instability in $d = 6, 7$ dimensions. We found the static perturbation of the ultra-spinning Myers-Perry black hole to see the onset of the instability. The existence of the static perturbation indicates that there exist a sequence of new black hole solutions even in non-linear regime.

Recently, the stability analysis of higher dimensional black holes becomes important beyond the gravity theory itself, because of the Gauge/Gravity duality. Since the instabilities of the AdS black holes corresponds to the phase transitions of the dual theories, the stability analysis of the AdS black holes may be the useful tool to understand the phase structure of the dual theory. The Myers-Perry black holes can be generalized to those with the cosmological constant, the so-called Kerr-AdS spacetimes. In Kerr-AdS spacetimes, an instability is also expected, which is similar to the instability found in this paper. The instability of Kerr-AdS black holes may be found using the method to show the instability of Myers-Perry black holes.

References

[1] A. Ishibashi and H. Kodama, "Stability of higher-dimensional Schwarzschild black holes," Prog. Theor. Phys. **110**, 901 (2003) [arXiv:hep-th/0305185].

[2] H. K. Kunduri, J. Lucietti and H. S. Reall, "Gravitational perturbations of higher dimensional rotating black holes: Tensor Perturbations," Phys. Rev. D **74**, 084021 (2006) [arXiv:hep-th/0606076].

[3] K. Murata and J. Soda, "Stability of Five-dimensional Myers-Perry Black Holes with Equal Angular Momenta," arXiv:0803.1371 [hep-th].

[4] R. Emparan and R. C. Myers, JHEP **0309**, 025 (2003) [arXiv:hep-th/0308056].

Consistency of Equations for the Single Scalar Field Case in Second-order Gauge-invariant Cosmological Perturbation Theory

Kouji Nakamura[1]

Optical and Infrared Astronomy Division, National Astronomical Observatory of Japan., Osawa, Mitaka, Tokyo, 181-8588, Japan.

Abstract

We derived the second-order perturbations of the Einstein equations and the Klein-Gordon equation for a generic situation in terms of gauge-invariant variables. The consistency of all the equations is confirmed. This confirmation implies that all the derived equations of the second order are self-consistent and these equations are correct in this sense. We also discuss the physical implication of these equations.

1 Introduction

The general relativistic second-order cosmological perturbation theory is one of topical subjects in the recent cosmology. Recently, the first-order approximation of our universe from a homogeneous isotropic one was revealed through the observation of the CMB by the Wilkinson Microwave Anisotropy Probe (WMAP)[1], the cosmological parameters are accurately measured, we have obtained the standard cosmological model, and the so-called "precision cosmology" has begun. These developments in observations were also supported by the theoretical sophistication of the linear order cosmological perturbation theory. To explore more detail observations, the Planck satellite was launched on the last May and its first light was reported[2]. With the increase of precision of the CMB data, the study of relativistic cosmological perturbations beyond linear order is a topical subject. The second-order cosmological perturbation theory is one of such perturbation theories beyond linear order.

In this article, we show a part of our formulation of the second-order gauge-invariant perturbation theory[3]. We give the consistency relations of the source terms in all the second-order perturbation of the Einstein equations and the Klein-Gordon equation in the single scalar field case as in the case of the perfect fluid case[4]. These consistency relations imply the all derived equations of the second order are self-consistent and these equations are correct in this sense. Further, we also discuss the physical implication of our second-order Einstein equations.

2 Metric and matter perturbations

The background spacetime for the cosmological perturbations is a homogeneous isotropic background spacetime. The background metric is given by

$$g_{ab} = a^2 \left\{ -(d\eta)_a (d\eta)_b + \gamma_{ij} (dx^i)_a (dx^j)_b \right\}, \tag{1}$$

where $\gamma_{ab} := \gamma_{ij} (dx^i)_a (dx^j)_b$ is the metric on the maximally symmetric three-space and the indices $i, j, k, ...$ for the spatial components run from 1 to 3. On this background spacetime, we consider the perturbative expansion of the metric as $\bar{g}_{ab} = g_{ab} + \lambda \mathcal{h}_{ab} + \frac{\lambda^2}{2} \mathcal{l}_{ab} + O(\lambda^3)$, where λ is the infinitesimal parameter for perturbation and h_{ab} and l_{ab} are the first- and the second-order metric perturbations, respectively. As shown in Refs. [3], the metric perturbations h_{ab} and l_{ab} are decomposed as

$$h_{ab} =: \mathcal{H}_{ab} + \pounds_X g_{ab}, \quad l_{ab} =: \mathcal{L}_{ab} + 2\pounds_X h_{ab} + \left(\pounds_Y - \pounds_X^2 \right) g_{ab}, \tag{2}$$

[1]Email address: kouji.nakamura@nao.ac.jp

where $\mathcal{H}_{ab}$ and $\mathcal{L}_{ab}$ are the gauge-invariant parts of h_{ab} and l_{ab}, respectively. The components of $\mathcal{H}_{ab}$ and $\mathcal{L}_{ab}$ can be chosen so that

$$\mathcal{H}_{ab} = a^2\left\{-2\overset{(1)}{\Phi}(d\eta)_a(d\eta)_b + 2\overset{(1)}{\nu}_i(d\eta)_{(a}(dx^i)_{b)} + \left(-2\overset{(1)}{\Psi}\gamma_{ij} + \overset{(1)}{\chi}_{ij}\right)(dx^i)_a(dx^j)_b\right\}, \tag{3}$$

$$\mathcal{L}_{ab} = a^2\left\{-2\overset{(2)}{\Phi}(d\eta)_a(d\eta)_b + 2\overset{(2)}{\nu}_i(d\eta)_{(a}(dx^i)_{b)} + \left(-2\overset{(2)}{\Psi}\gamma_{ij} + \overset{(2)}{\chi}_{ij}\right)(dx^i)_a(dx^j)_b\right\}. \tag{4}$$

In Eqs. (3) and (4), the vector-mode $\overset{(p)}{\nu}_i$ and the tensor-mode $\overset{(p)}{\chi}_{ij}$ $(p = 1, 2)$ satisfy the properties

$$D^i\overset{(p)}{\nu}_i = \gamma^{ij}D_p\overset{(p)}{\nu}_j = 0, \quad \overset{(p)}{\chi}{}^i{}_i = 0, \quad D^i\overset{(p)}{\chi}_{ij} = 0, \tag{5}$$

where γ^{kj} is the inverse of the metric γ_{ij}.

On the other hand, we also expand the scalar field as $\bar{\varphi} = \varphi + \lambda\hat{\varphi}_1 + \frac{\lambda^2}{2}\hat{\varphi}_2 + O(\lambda^3)$ and decompose $\hat{\varphi}_1$ and $\hat{\varphi}_2$ into gauge-invariant and gauge-variant parts as

$$\hat{\varphi}_1 =: \varphi_1 + \pounds_X\varphi, \quad \hat{\varphi}_2 =: \varphi_2 + 2\pounds_X\varphi_1 + \left(\pounds_Y - \pounds_X^2\right)\varphi, \tag{6}$$

respectively, where X^a and Y^a are the gauge-variant parts of the first- and the second-order metric perturbations, respectively, in Eqs. (2).

3 Equations for Perturbations

Here, we summarize the Einstein equations and the Klein-Gordon equations for the background, the first order, and the second order on the above background spacetime (1).

The background Einstein equations for a single scalar field system are given by

$$\mathcal{H}^2 + K = \frac{8\pi G}{3}a^2\left(\frac{1}{2a^2}(\partial_\eta\varphi)^2 + V(\varphi)\right), \quad 2\partial_\eta\mathcal{H} + \mathcal{H}^2 + K = 8\pi G\left(-\frac{1}{2}(\partial_\eta\varphi)^2 + a^2V(\varphi)\right), \tag{7}$$

where $\mathcal{H} := \partial_\eta a/a$, K is the curvature constant of the maximally symmetric three-space.

On the other hand, the second-order perturbations of the Einstein equation are summarized as

$$2\partial_\eta\overset{(2)}{\Psi} + 2\mathcal{H}\overset{(2)}{\Phi} - 8\pi G\varphi_2\partial_\eta\varphi = \Delta^{-1}D^k\Gamma_k, \quad \overset{(2)}{\Psi} - \overset{(2)}{\Phi} = \frac{3}{2}(\Delta + 3K)^{-1}\left\{\Delta^{-1}D^iD_j\Gamma_i{}^j - \frac{1}{3}\Gamma_k{}^k\right\}, \tag{8}$$

$$\left\{\partial_\eta^2 + 2\left(\mathcal{H} - \frac{\partial_\eta^2\varphi}{\partial_\eta\varphi}\right)\partial_\eta - \Delta - 4K + 2\left(\partial_\eta\mathcal{H} - \frac{\partial_\eta^2\varphi}{\partial_\eta\varphi}\mathcal{H}\right)\right\}\overset{(2)}{\Phi}$$
$$= -\Gamma_0 - \frac{1}{2}\Gamma_k{}^k + \Delta^{-1}D^iD_j\Gamma_i{}^j + \left(\partial_\eta - \frac{\partial_\eta^2\varphi}{\partial_\eta\varphi}\right)\Delta^{-1}D^k\Gamma_k$$
$$-\frac{3}{2}\left\{\partial_\eta^2 - \left(\frac{2\partial_\eta^2\varphi}{\partial_\eta\varphi} - \mathcal{H}\right)\partial_\eta\right\}(\Delta + 3K)^{-1}\left\{\Delta^{-1}D^iD_j\Gamma_i{}^j - \frac{1}{3}\Gamma_k{}^k\right\}, \tag{9}$$

$$\overset{(2)}{\nu}_i = \frac{2}{\Delta + 2K}\left\{D_i\Delta^{-1}D^k\Gamma_k - \Gamma_i\right\}, \quad \partial_\eta\left(a^2\overset{(2)}{\nu}_i\right) = \frac{2a^2}{\Delta + 2K}\left\{D_i\Delta^{-1}D^kD_l\Gamma_k{}^l - D_k\Gamma_i{}^k\right\}, \tag{10}$$

$$\left(\partial_\eta^2 + 2\mathcal{H}\partial_\eta + 2K - \Delta\right)\overset{(2)}{\chi}_{ij}$$
$$= 2\Gamma_{ij} - \frac{2}{3}\gamma_{ij}\Gamma_k{}^k - 3\left(D_iD_j - \frac{1}{3}\gamma_{ij}\Delta\right)(\Delta + 3K)^{-1}\left(\Delta^{-1}D^kD_l\Gamma_k{}^l - \frac{1}{3}\Gamma_k{}^k\right)$$
$$+4\left\{D_{(i}(\Delta + 2K)^{-1}D_{j)}\Delta^{-1}D^lD_k\Gamma_l{}^k - D_{(i}(\Delta + 2K)^{-1}D^k\Gamma_{j)k}\right\} = 0, \tag{11}$$

where $\Gamma_i{}^j := \gamma^{kj}\Gamma_{ik}$ and $\Gamma_k{}^k = \gamma^{ij}\Gamma_{ij}$. The source terms Γ_0, Γ_i, and Γ_{ij} are the collections of the quadratic terms of the linear-order perturbations in the second-order Einstein equations. Further, the second-order perturbation of the Klein-Gordon equation

$$\partial_\eta^2\varphi_2 + 2\mathcal{H}\partial_\eta\varphi_2 - \Delta\varphi_2 - \left(\partial_\eta \overset{(2)}{\Phi} + 3\partial_\eta \overset{(2)}{\Psi}\right)\partial_\eta\varphi + 2a^2 \overset{(2)}{\Phi}\frac{\partial V}{\partial\bar{\varphi}}(\varphi) + a^2\varphi_2\frac{\partial^2 V}{\partial\bar{\varphi}^2}(\varphi) = \Xi_{(K)}, \quad (12)$$

where the source term $\Xi_{(K)}$ is also the collections of the quadratic terms of the linear-order perturbations in the second-order Klein-Gordon equation. The explicit form of these Γ_0, Γ_i, Γ_{ij}, and $\Xi_{(K)}$ are given in Refs. [3]. The first-order perturbations of the Einstein equations are given by the replacements $\overset{(2)}{\Phi} \to \overset{(1)}{\Phi}$, $\overset{(2)}{\Psi} \to \overset{(1)}{\Psi}$, $\overset{(2)}{\nu_i} \to \overset{(1)}{\nu_i}$, $\overset{(2)}{\chi_{ij}} \to \overset{(1)}{\chi_{ij}}$, $\varphi_2 \to \varphi_1$, and $\Gamma_0 = \Gamma_i = \Gamma_{ij} = \Xi_{(K)} = 0$.

4 Consistency of equations for second-order perturbations

Now, we consider the consistency of the second-order perturbations of the Einstein equations (8) and (9) for the scalar modes, Eqs. (10) for vector mode, and the Klein-Gordon equation (12).

Since the first equation in Eqs. (10) is the initial value constraint for the vector mode $\overset{(2)}{\nu_i}$ and it should be consistent with the evolution equation, i.e., the second equation of Eqs. (10). Explicitly, these equations are consistent with each other if the equation

$$\partial_\eta\Gamma_k + 2\mathcal{H}\Gamma_k - D^l\Gamma_{lk} = 0 \quad (13)$$

is satisfied. Actually, through the first-order perturbative Einstein equations, we can directly confirm the equation (13) through the background Einstein equations, the first-order Einstein equations, and the long expressions of Γ_i and Γ_{ij} given in Refs.[3].

Next, we consider the consistency of the second-order perturbation of the Klein-Gordon equation (12) and the Einstein equations (8) and (9). From these equation, we can show that the second-order perturbation of the Klein-Gordon equation is consistent with the background and the second-order Einstein equations if the equation

$$2\left(\partial_\eta + \mathcal{H}\right)\Gamma_0 - D^k\Gamma_k + \mathcal{H}\Gamma_k{}^k + 8\pi G\partial_\eta\varphi\Xi_{(K)} = 0 \quad (14)$$

is satisfied under the background and the first-order Einstein equations. Further, we can directly confirm Eq. (14) through the background Einstein equations, the first-order perturbation of the Einstein equations, and the long expression of Γ_0, Γ_i, Γ_{ij}, and $\Xi_{(K)}$ which are given in Refs. [3].

Equation (13) comes from the consistency of the initial value constraint and evolution equation and Eq. (14) comes from the consistency between the Klein-Gordon equation and the Einstein equation. These equation should be trivially satisfied from a general viewpoint, because the Einstein equation is the first class constrained system. However, these trivial results imply that we have derived the source terms Γ_0, Γ_i, Γ_{ij}, and $\Xi_{(K)}$ are consistent with each other and are correct in this sense. We also note that these relations are independent of the details of the potential of the scalar field.

5 Summary and discussions

In this article, we summarized the second-order Einstein equation for a single scalar field system. We derived all the components of the second-order perturbation of the Einstein equation without ignoring any types modes (scalar-, vector-, tensor-types) of perturbations. As in the case of the perfect fluid[4], we derived the consistency relation between the source terms of the second-order Einstein equation and the Klein-Gordon equation.

In our formulation, any gauge fixing is not necessary and we can obtain all equations in the gauge-invariant form, which are equivalent to the complete gauge fixing. In other words, our formulation gives complete gauge-fixed equations without any gauge fixing. Therefore, equations obtained in a gauge-invariant manner cannot be reduced without physical restrictions any more. In this sense, the equations shown here are irreducible. This is one of the advantages of the gauge-invariant perturbation theory.

The resulting Einstein equations of the second order show that the mode-couplings between different types of modes appears as the quadratic terms of the linear-order perturbations owing to the nonlinear effect of the Einstein equations, in principle. Perturbations in cosmological situations are classified into three types: scalar, vector, and tensor. In the second-order perturbations, we also have these three types of perturbations as in the case of the first-order perturbations. In the scalar field system shown in this article, the first-order vector mode does not appear due to the momentum constraint of the first-order perturbation of the Einstein equation. Therefore, we have seen that three types of mode-coupling appear in the second-order Einstein equations, i.e., scalar-scalar, scalar-tensor, and tensor-tensor type of mode coupling. Since the tensor mode of the linear order is also generated due to quantum fluctuations during the inflationary phase, the mode-couplings of the scalar-tensor and tensor-tensor types may appear in the inflation. If these mode-couplings occur during the inflationary phase, these effects will depend on the scalar-tensor ratio r. If so, there is a possibility that the accurate observations of the second-order effects in the fluctuations of the scalar type in our universe also restrict the scalar-tensor ratio r or give some consistency relations between the other observations such as the measurements of the B-mode of the polarization of CMB. This will be a new effect that gives some information on the scalar-tensor ratio r.

As the current status of the second-order gauge-invariant cosmological perturbation theory, we may say that the curvature terms in the second-order Einstein tensor, i.e., the second-order perturbations of the Einstein tensor, are almost completely derived, although there remain some problems should be clarified[3]. The next task is to clarify the nature of the second-order perturbation of the energy-momentum tensor through the extension to multi-fluid or multi-field systems. Further, we also have to extend our arguments to the Einstein Boltzmann system to discuss CMB physics, since we have to treat photon and neutrinos through the Boltzmann distribution functions. This issue is also discussed in some literature[5]. If we accomplish these extension, we will be able to clarify the Non-linear effects in CMB physics.

References

[1] C. L. Bennett et al., Astrophys. J. Suppl. Ser. **148** (2003), 1. E. Komatsu et al., Astrophys. J. Suppl. Ser. **180** (2009), 330.

[2] F. R. Bouchet, arXiv:0911.3101 [astro-ph.CO].

[3] K. Nakamura, Prog. Theor. Phys. **110** (2003), 723; K. Nakamura, Prog. Theor. Phys. **113** (2005), 481; K. Nakamura, Phys. Rev. D **74** (2006), 101301(R); K. Nakamura, Prog. Theor. Phys. **117** (2005), 17; K. Nakamura, Phys. Rev. D **80** (2009), 124021; K. Nakamura, Prog. Theor. Phys. **121** (2009), 1321; K. Nakamura, arXiv:1001.2621 [gr-qc].

[4] K. Nakamura, arXiv:0901.3638 [gr-qc].

[5] N. Bartolo, S. Matarrese and A. Riotto, JCAP **0401** (2004), 003; N. Bartolo, S. Matarrese and A. Riotto, Phys. Rev. Lett. **93** (2004), 231301; N. Bartolo, E. Komatsu, S. Matarrese and A. Riotto, Phys. Rep. **402** (2004), 103; N. Bartolo, S. Matarrese and A. Riotto, JCAP **0605** (2006), 010; N. Bartolo, S. Matarrese and A. Riotto, JCAP **0606** (2006), 024; N. Bartolo, S. Matarrese and A. Riotto, JCAP **0701** (2007), 019; D. Nitta, E. Komatsu, N. Bartolo, S. Matarrese and A. Riotto, JCAP **0905** (2009), 014; C. Pitrou, J. P. Uzan and F. Bernardeau, Phys. Rev. D **78** (2008), 063526; L. Senatore, S. Tassev and M. Zaldarriaga, JCAP **0908** (2009), 031; C. Pitrou, Class. Quantum Grav. **24** (2007), 6127; *ibid.* **26** (2009), 065006.

Dark matter annihilation effects on the CMB anisotropy

Masahiro Kawasaki[1(a),(b)] and Kazunori Nakayama[2(a)]

(a) *Institute for Cosmic Ray Research, University of Tokyo, Kashiwa, Chiba 277-8582*
(b) *Institute for the Physics and Mathematics of the Universe, University of Tokyo, Kashiwa, Chiba 277-8568*

Abstract

We study the effects of dark matter annihilation during and after the cosmic recombination epoch on the cosmic microwave background anisotropy, taking into account the detailed energy deposition of the annihilation products. It is found that a fairly stringent constraint on the annihilation cross section is imposed for TeV scale dark matter masses from WMAP observations.

1 Introduction

We propose a rigorous way to constrain dark matter annihilation cross section, focusing on its effects around the recombination epoch. Dark matter annihilation injects high energy particles into thermal plasma consisting of photons, electrons, protons, neutral hydrogens and heliums. High energy particles interact with background plasma and some fraction of their energy is used for the ionization of neutral hydrogens. Therefore, dark matter annihilation affects the recombination history of the hydrogen resulting in higher residual ionization fraction (x_e) than the standard value. Even a slight shift of x_e can cause a drastic effect on the cosmic microwave background (CMB) anisotropy, and hence the annihilation rate is constrained from the precise measurements of the CMB anisotropy.

Similar analyses were carried out in several papers [1–4], especially in connection with recent anomalous cosmic-ray positron/electron fluxes [5–9]. Many of those analyses are based on the study in Ref. [10] where effects of high-energy electron/photon energy injection due to late decaying particles on CMB were investigated using the extrapolation of the result of Ref. [11] for the energy fraction going into the ionization, heating and excitation of the intergalactic medium, which was valid only for low energy electron/photon injection. Ref. [12] derived a formalism to extend this to high-energy electron/photon energy injection, but there the Hubble expansion effect was neglected. Therefore, we further extend the formalism of Ref. [12] to correctly handle the Hubble expansion, and apply it to the study of the CMB constraint on the dark matter annihilation [13]. Note that the inclusion of the Hubble expansion is essential in order to handle the effects of energy deposition on the recombination history accurately in a realistic setup in our formalism. (See Ref. [9] for a different approach to compute the details of the energy deposition.)

2 Dark matter annihilation effects on CMB

In order to calculate the effects of high-energy particle injections on the recombination history, we must first know fractions of total energy going into ionization, excitation and heating of hydrogen atom at each redshift ($d\chi_i/dz, d\chi_e/dz, d\chi_h/dz$). This was done in Refs. [12, 13]. Let us apply these results to the calculation of CMB anisotropy. In order to take into account the effects of extra ionization and heating source from dark matter annihilation, we should add the following terms for the evolution of the ionization fraction (x_e) and the gas temperature (T_b),

$$-\left[\frac{dx_e}{dz}\right]_{\rm DM} = \sum_F \int_z \frac{dz'}{H(z')(1+z')} \frac{n_\chi^2(z')\langle\sigma v\rangle_F}{n_H(z')} \frac{m_\chi}{E_{\rm Ry}} \frac{d\chi_i^{(F)}(E,z',z)}{dz}, \tag{1}$$

[1]Email address: kawasaki@icrr.u-tokyo.ac.jp
[2]Email address: nakayama@icrr.u-tokyo.ac.jp

where $E_{\rm Ry} = 13.6$ eV is the Rydberg energy, m_χ and n_χ are the mass and number density of the dark matter particle, n_H is the number density of the hydrogen atom.

$$-\left[\frac{dT_b}{dz}\right]_{\rm DM} = \sum_F \int_z \frac{dz'}{H(z')(1+z')} \frac{2n_\chi^2(z')\langle\sigma v\rangle_F}{3n_H(z')} m_\chi \frac{d\chi_h^{(F)}(E,z',z)}{dz}. \tag{2}$$

Here we have defined

$$\frac{d\chi_{i,h}^{(F)}(E,z',z)}{dz} = \int dE\ \frac{E}{m_\chi}\left[\frac{dN_F^{(e)}}{dE}\frac{d\chi_{i,h}^{(e)}(E,z',z)}{dz} + \frac{dN_F^{(\gamma)}}{dE}\frac{d\chi_{i,h}^{(\gamma)}(E,z',z)}{dz}\right], \tag{3}$$

where $dN_F^{(e,\gamma)}/dE$ denotes the spectrum of the electron and photon produced per dark matter annihilation into the mode F, and $\langle\sigma v\rangle_F$ denotes the annihilation cross section into that mode. We have included these terms in the RECFAST code [14], which is implemented in the CAMB code [15] for calculating the CMB anisotropy. It is noted that the energy integral in (3) for given final states F can be performed before solving the evolution equation once we have tables of $d\chi_{i,h}^{(e)}/dz$ and $d\chi_{i,h}^{(\gamma)}/dz$, as long as the produced particle F decays so quickly as not to lose energy by the interaction with surrounding medium, which is a valid assumption for any unstable standard model particle.

Fig. 1 shows the evolution of the ionized fraction with and without the effects of dark matter annihilation. The black solid line corresponds to the standard recombination history, without dark matter annihilation effects. Also shown are the cases of dark matter with annihilation cross section $\langle\sigma v\rangle_{e^+e^-} = 10^{-24}$ and 5×10^{-24} cm^{3}s^{-1} with m_χ=1 TeV. It is clearly seen that energy injection from dark matter annihilation works as an extra source of ionization. Then it is not hard to imagine that this modified recombination history affects the spectrum of CMB anisotropy, since large x_e implies large optical depth.

Fig. 2 shows the multipole coefficient of the CMB anisotropy (C_ℓ) of TT mode. The cases of $\langle\sigma v\rangle_{e^+e^-} = 10^{-24}$ and 5×10^{-24} cm^{3}s^{-1} with m_χ=1 TeV are also shown. It is seen that as the dark matter annihilation cross section is increased, the spectrum is more suppressed and it will deviates from the observed data.

Then we vary all cosmological parameters in the standard ΛCDM model, and derived the best fit χ^2 for each DM mass and cross section using CosmoMC code [16]. We used the observational data from WMAP [17], QUaD [18], and ACBAR [19]. The resulting 1σ and 2σ constraint on the annihilation cross section is shown in Fig. 3 [20].

3 Conclusion

We have studied the effects of dark matter annihilation on the CMB anisotropy, motivated by the fact that recent measurements of anomalous comic-ray positron/electron fluxes can be explained by the contribution from dark matter annihilation with fairly large annihilation cross section. In contrast to many preceding works, we have taken into account all the relevant energy loss processes of electrons and photons and estimated how the injected energy goes into ionization, excitation and heating of atoms. This method is applied to the calculation of CMB anisotropy, and it is found that WMAP5 results give stringent bound on the annihilation cross section.

References

[1] N. Padmanabhan and D. P. Finkbeiner, Phys. Rev. D **72**, 023508 (2005) [arXiv:astro-ph/0503486].

[2] L. Zhang, X. L. Chen, Y. A. Lei and Z. G. Si, Phys. Rev. D **74**, 103519 (2006) [arXiv:astro-ph/0603425].

[3] M. Mapelli, A. Ferrara and E. Pierpaoli, Mon. Not. Roy. Astron. Soc. **369**, 1719 (2006) [arXiv:astro-ph/0603237].

[4] A. Natarajan and D. J. Schwarz, Phys. Rev. D **78**, 103524 (2008) [arXiv:0805.3945 [astro-ph]].

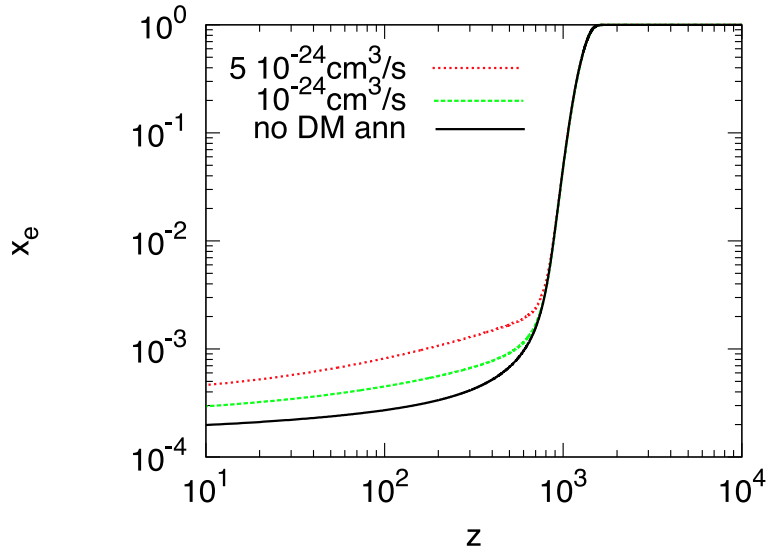

Figure 1: History of the ionization fraction as a function of redshift. The black solid line corresponds to the standard recombination history, without dark matter annihilation effects. Also shown are the cases of dark matter with annihilation cross section $\langle\sigma v\rangle_{e^+e^-} = 10^{-24}$ and 5×10^{-24} cm^{3}s^{-1} with the dark matter mass m_χ=1 TeV.

[5] A. V. Belikov and D. Hooper, arXiv:0904.1210 [hep-ph].

[6] S. Galli, F. Iocco, G. Bertone and A. Melchiorri, arXiv:0905.0003 [astro-ph.CO].

[7] G. Huetsi, A. Hektor and M. Raidal, arXiv:0906.4550 [astro-ph.CO].

[8] M. Cirelli, F. Iocco and P. Panci, arXiv:0907.0719 [astro-ph.CO].

[9] T. R. Slatyer, N. Padmanabhan and D. P. Finkbeiner, arXiv:0906.1197 [astro-ph.CO].

[10] X. L. Chen and M. Kamionkowski, Phys. Rev. D **70**, 043502 (2004) [arXiv:astro-ph/0310473].

[11] J. M. Shull and M. E. van Steenberg, Astrophys. J. **298**, 268 (1985).

[12] T. Kanzaki and M. Kawasaki, Phys. Rev. D **78**, 103004 (2008) [arXiv:0805.3969 [astro-ph]].

[13] T. Kanzaki, M. Kawasaki and K. Nakayama, arXiv:0907.3985 [astro-ph.CO].

[14] S. Seager, D. D. Sasselov and D. Scott, Astrophys. J. **523**, L1 (1999) [arXiv:astro-ph/9909275]; Astrophys. J. Suppl. **128**, 407 (2000) [arXiv:astro-ph/9912182].

[15] A. Lewis, A. Challinor and A. Lasenby, Astrophys. J. **538**, 473 (2000) [arXiv:astro-ph/9911177].

[16] A. Lewis and S. Bridle, Phys. Rev. D **66**, 103511 (2002) [arXiv:astro-ph/0205436].

[17] J. Dunkley *et al.* [WMAP Collaboration], Astrophys. J. Suppl. **180**, 306 (2009) [arXiv:0803.0586 [astro-ph]].

[18] C. Pryke *et al.* [QUaD collaboration], Astrophys. J. **692**, 1247 (2009) [arXiv:0805.1944 [astro-ph]]; M. L. Brown *et al.* [QUaD collaboration], Astrophys. J. **705**, 978 (2009) [arXiv:0906.1003 [astro-ph.CO]].

[19] C. L. Reichardt *et al.*, Astrophys. J. **694**, 1200 (2009) [arXiv:0801.1491 [astro-ph]].

[20] M. Kawasaki, K. Nakayama and T. Sekiguchi, in preparation.

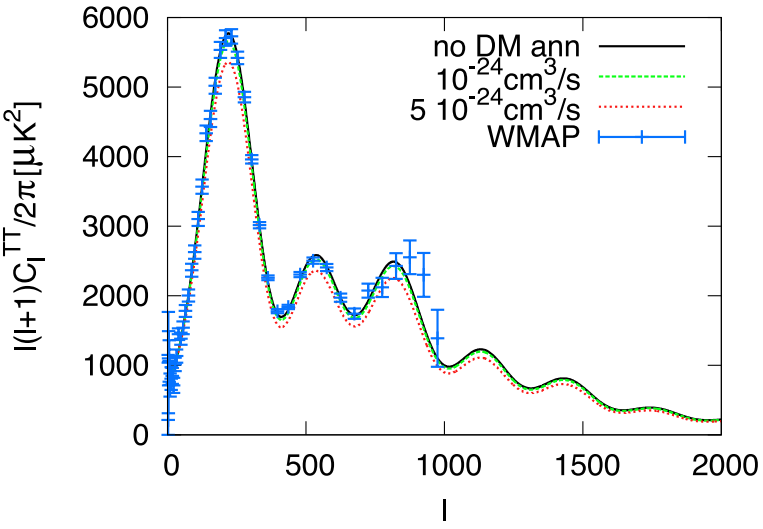

Figure 2: TT spectrum of the CMB anisotropy. The black solid line shows the WMAP5 best fit curve without dark matter annihilation. Also shown are the cases of dark matter with annihilation cross section $\langle\sigma v\rangle_{e^+e^-} = 10^{-24}$ and 5×10^{-24} cm^{3}s^{-1} with mass of m_χ =1 TeV.

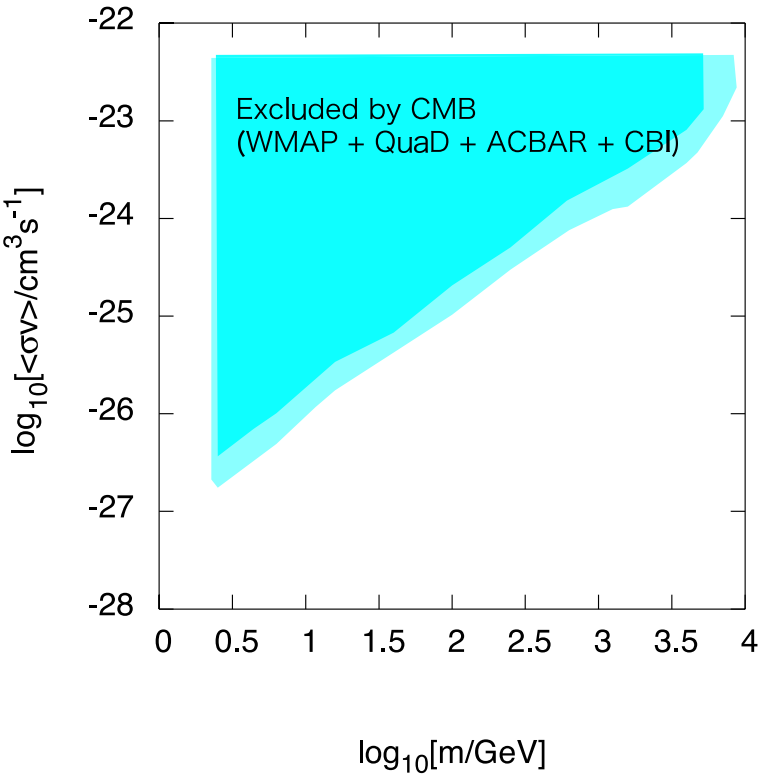

Figure 3: Constraint on the dark matter annihilation cross section with 1σ (light) and 2σ (dark) level. into e^+e^- as a function of the dark matter mass.

Characterising linear growth rate in $f(R)$ gravity

Tatsuya Narikawa[1] and Kazuhiro Yamamoto[2]

Department of Physical Science, Hiroshima University, Higashi-Hiroshima 739-8526, Japan

Abstract

We investigate the linear growth rate of cosmological matter density perturbations in a viable $f(R)$ model both numerically and analytically. We find that the growth rate in the scalar-tensor regime can be characterised by a simple analytic formula. We also investigate a prospect of constraining the Compton wavelength scale of the $f(R)$ model with a future weak lensing survey.

1 Introduction

Cosmological observations of distant Ia supernovae discovered that our universe is undergoing an accelerated expansion period, which is supported by other observations of the cosmic microwave background anisotropies and the large scale structure of galaxies. These observations are explained by the cosmological model with the cosmological constant Λ. Modification of the gravity theory is an alternative approach.

The key to distinguish between modified gravity and dynamical dark energy is the growth of cosmological perturbations. The growth history of cosmological perturbations can be tested with the large scale structure in the universe.

In the present paper, we investigate the growth history of matter density perturbations in $f(R)$ models.

2 A brief review of $f(R)$ model

We briefly review $f(R)$ model, which is defined by the action,

$$S = \frac{1}{16\pi G}\int d^4x\sqrt{-g}(R+f(R)) + \int d^4x\sqrt{-g}L^{(\mathrm{m})}, \tag{1}$$

where G is the gravitational constant, and $L^{(\mathrm{m})}$ is the matter Lagrangian density. We consider the viable models, proposed in the literatures [1, 2]. The viable models have an asymptotic formula at the late time universe ($R \gg R_c$), which can be written as $f(R) = -\lambda R_c[1-(R_c/R)^{2n}]$, where R_c is a positive constant whose value is the same order as that of the present Ricci scalar, and λ is a non-dimensional constant. Because the term λR_c plays a role of the cosmological constant, we may write $\lambda R_c = 6(1-\Omega_0)H_0^2$, where H_0 is the Hubble constant and Ω_0 is the matter density parameter. Note that we assume the spatially flat universe.

It is well known that $f_R = df(R)/dR$ plays a roll of a new degree of freedom, which behaves like a scalar field with the mass $m^2 = 1/(3f_{RR})$ where we defined $f_{RR} = d^2f(R)/dR^2$. (We have assumed $|f_R| \ll 1$ and $Rf_{RR} \ll 1$ for the viable model.)

We focus on the evolution of matter density perturbations in the $f(R)$ model, whose Fourier coefficients obey (e.g., [2])

$$\ddot{\delta} + 2H\dot{\delta} - 4\pi\left[1+\frac{1}{3}\frac{k^2/a^2}{k^2/a^2+1/(3f_{RR})}\right]G\rho\delta = 0, \tag{2}$$

where the dot denotes the differentiation with respect to the cosmic time, $H = \dot{a}/a$ is the Hubble parameter, ρ is the matter mean density, and $G_{\mathrm{eff}} = [...]G$ is the effective gravitational constant, where

[1]Email address: narikawa@theo.phys.sci.hiroshima-u.ac.jp
[2]Email address: kazuhiro@hiroshima-u.ac.jp

k is the wave number, and a is the scale factor normalised to unity at present epoch. As is noted in the above, the physical meaning of $m^2 = 1/(3f_{RR})$ is the square of the mass of the new degree of freedom which modifies the gravity force. We have the general relativity regime, $G_{\rm eff} = G$, for $k/a \ll m$, and the scalar-tensor regime, $G_{\rm eff} = 4G/3$, for $k/a \gg m$, respectively. Thus, the evolution of matter density perturbations depends on the wavenumber k, whose behaviour is determined by the mass $m^2 = 1/(3f_{RR})$.

For the Einstein de Sitter universe, the exact solution of Eq. (2) is found in the literature [3]. However, we consider the low density universe, where the solution of Eq. (2) is described in a different form in comparison with that of [3]. Using the formulas $\lambda R_c = 6(1-\Omega_0)H_0^2$ and $R = 3H_0^2\left[\Omega_0/a^3 + 4(1-\Omega_0)\right]$, we have

$$\frac{1}{3f_{RR}} = \frac{\Omega_0 H_0^2}{4n(2n+1)}\left(\frac{\lambda}{2}\right)^{2n}\left(\frac{\Omega_0}{1-\Omega_0}\right)^{2n+1}\left(\frac{1}{a^3}+\frac{4(1-\Omega_0)}{\Omega_0}\right)^{2n+2}. \tag{3}$$

Denoting the wavenumber corresponding to the Compton wavelength $1/m$ at the present epoch by k_C. Equation (3) is rewritten as

$$\frac{1}{3f_{RR}} = k_C^2\left(\frac{\Omega_0 a^{-3} + 4(1-\Omega_0)}{\Omega_0 + 4(1-\Omega_0)}\right)^{2n+2}. \tag{4}$$

We denote the growth factor by $D_1(a,k)$, which is the solution of Eq. (2) normalised so as to be $D_1(a,k) \simeq a$ at $a \ll 1$. The growth rate is defined by $f(a,k) = d\log D_1(a,k)/d\log a$. Using the growth rate $f(a,k)$, Eq. (2) is rephrased as

$$\frac{df}{d\ln a} + f^2 + \left(2 + \frac{\dot H}{H^2}\right) f = \frac{3}{2}\frac{G_{\rm eff}}{G}\Omega_m(a), \tag{5}$$

where $\Omega_m(a)$ is defined by $\Omega_m(a) = H_0^2\Omega_0 a^{-3}/H^2$. Equation (5) is useful to find an approximate solution, as we see in the next section.

3 Growth of density perturbations in $f(R)$ model

In this section, we investigate the evolution of matter density perturbations in the $f(R)$ model.

3.1 Scalar-tensor regime

In the scalar tensor regime, $k/a \gg m$, in which the wavelength is shorter than the Compton wavelength, the effective gravitational constant becomes $G_{\rm eff} = 4G/3$. In this case, we find that Eq. (5) has the solution expressed in the form

$$f(a,k) = f_0\Omega_m(a)^{\widetilde\gamma(a)}, \tag{6}$$

where f_0 obeys $f_0^2 + f_0/2 = 2$, therefore $f_0 = (-1+\sqrt{33})/4$, and $\widetilde\gamma(a) = \sum_{\ell=0}\zeta_\ell(1-\Omega_m(a))^\ell$, where ζ_ℓ is the expansion coefficients. This can be generalised to the case when $G_{\rm eff}/G(=\xi)$ is a constant value, in which the solution of Eq. (5) has the same formula as that of (6) but with $f_0 = (-1+\sqrt{1+24\xi})/4$ and

$$\begin{aligned}\widetilde\gamma(a) = {}& \frac{-41+24\xi+\sqrt{1+24\xi}}{-70+48\xi} + \frac{1}{8(-143+24\xi)(-35+24\xi)^2}\\ &\times\Big[(-41+24\xi+\sqrt{1+24\xi})\big(431+\sqrt{1+24\xi}+24\xi(-13+\sqrt{1+24\xi})\\ &-36(2+\sqrt{1+24\xi})+6(-2+3\sqrt{1+24\xi})\big)\Big](1-\Omega_m(a)) + \mathcal{O}\left((1-\Omega_m(a))^2\right).\end{aligned} \tag{7}$$

Here we assume that $G_{\rm eff}/G(=\xi)$ is constant, but we utilise this formula by replacing ξ with $G_{\rm eff}$ of Eq. (2).

Following the previous works , the growth index $\gamma(a,k)$ is introduced by $f(a,k) = \Omega_m(a)^{\gamma(a,k)}$, which is related with $\widetilde\gamma(a,k)$ by $\gamma(a,k) = \dfrac{\ln f_0}{\ln\Omega_m(a)} + \widetilde\gamma(a,k)$.

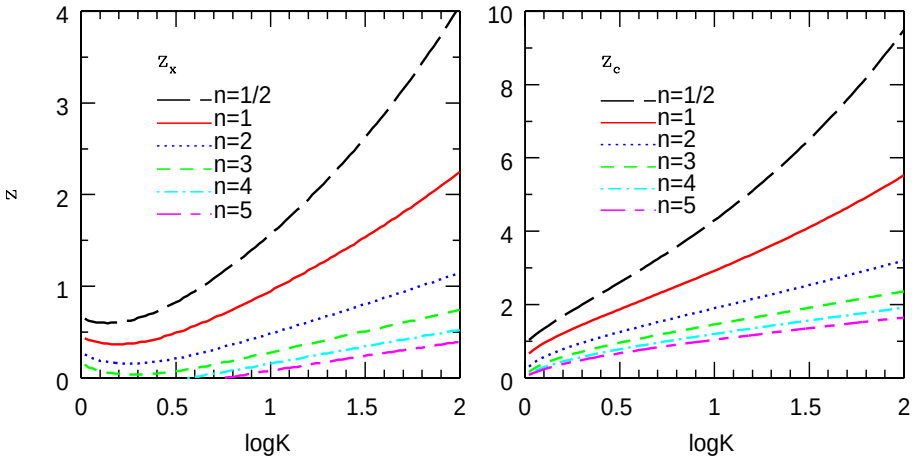

Figure 1: Left: Redshift z_x when the difference of the growth rate becomes $f^{(\mathrm{appr})} - f^{(\mathrm{exac})} = 0.03$, as a function of $K(= k/k_C)$. Right: Transition redshift z_c as a function of $K(= k/k_C)$.

Let us discuss the valid region of the approximate solution. The left panel of Fig. 1 plots the redshift z_x as a function of $K(= k/k_C)$, where z_x is defined by the redshift when the difference of the growth rate becomes $f^{(\mathrm{appr})} - f^{(\mathrm{exac})} = 0.03$. Here $f^{(\mathrm{exac})}$ is the exact solution obtained by solving Eq. (5) numerically, while $f^{(\mathrm{appr})}$ is the approximate solution. Thus, the approximate solution of the growth rate approaches the exact solution after the redshift z_x, which depends on k/k_C as well as n.

The above behaviour is related with the transition redshift z_c, when the scalar-tensor regime starts, which we defined by $k(1 + z_c) = m$, i.e.,

$$k^2(1+z_c)^2 = k_C^2 \left(\frac{\Omega_0(1+z_c)^3 + 4(1-\Omega_0)}{\Omega_0 + 4(1-\Omega_0)} \right)^{2n+2} . \tag{8}$$

The right panel of Fig. 1 plots z_c as function of $K(= k/k_C)$. Figure 1 shows $z_x < z_c$. Thus the approximate formula approaches the exact solution after the scalar-tensor regime starts. For the model with larger value of n, the Compton scale evolves rapidly. Then, the transition redshift z_c becomes small as n becomes large. For the smaller value of $K(= k/k_C)$, the transition redshift z_c becomes smaller. This is the reason why z_x is smaller, as n is larger or k/k_C is smaller. Therefore, for the case when n is large and k/k_C is smaller, the redshift when the approximate formula starts to work becomes later. For the case $n \lesssim 2$, the late-time behaviour of the growth rate can be approximated by the approximate formula as long as $K \gtrsim 1$.

4 Constraint on $f(R)$ model from weak lensing survey

Cosmological constraints on the $f(R)$ model have been investigated in Refs. [4, 5]. The weak lensing statistics is useful to obtain a constraint on the growth history of cosmological density perturbations observationally. We now consider a prospect of constraining the $f(R)$ model with a future large survey of the weak lensing. To this end, we adopt the Fisher matrix analysis, which is frequently used for estimating minimal attainable constraint on the model parameters. Here we focus on the constraint on the Compton wavenumber parameter k_C defined by Eq. (4). In this analysis, we obtained the growth rate and the growth factor by numerically solving Eq. (5).

In the present paper, the modified gravity of the $f(R)$ model is supposed to be characterised by n and k_C(or λ). We perform the Fisher matrix analysis with the 9 parameters, n, λ(or k_C), w_0, w_a, Ω_0, Ω_b, h, A, and n_s, where Ω_b is the baryon density parameter, n_s is the initial spectral index, A is the amplitude of power spectrum. w_0 and w_a characterise the background expansion history and the distance-redshift relation. And we assumed the ΛCDM model as the background expansion of the universe in the previous section.

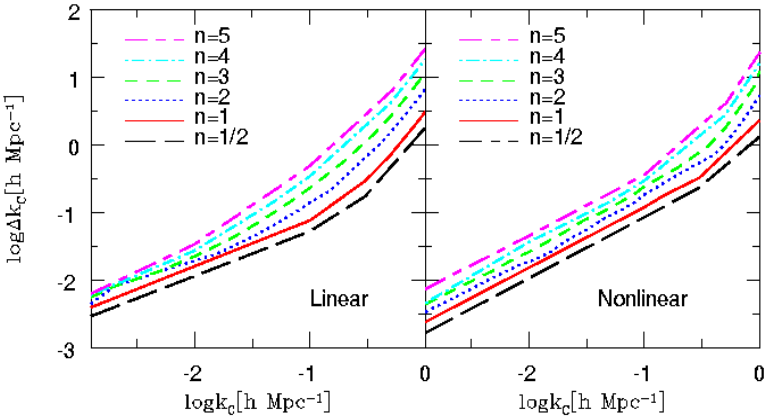

Figure 2: The 1-sigma error on k_C as a function of the target value of k_C, where the other parameters are marginalised over. The left (right) panels use the linear (nonlinear) modeling for $P_{\rm mass}(k,z)$ of the range of $10 \leq l \leq 10^3$ ($10 \leq l \leq 3 \times 10^3$).

In the Fisher matrix analysis, we assume the galaxy sample of a survey with the number density $N_g = 35$ per arcmin.^{2}, the mean redshift $z_m = 0.9$, and the total survey area, $\Delta A = 2 \times 10^4$ square degrees. We also assumed the tomography with 4 redshift bins. Figure 2 is the result of the Fisher matrix analysis of the 9 parameters, n, k_C, w_0, w_a, Ω_0, Ω_b, h, A, and n_s. Figure 2 shows the 1-sigma error on k_C as a function of the target value of k_C, where the other parameters are marginalized the Fisher matrix over. The left panels are the linear theory, while the right panels are the nonlinear model. The error of k_C is the same order of k_C for the cases $n = 1/2$ and 1, but the error becomes larger as n becomes larger.

5 Summary and conclusions

In the present paper, we have investigated the linear growth rate of cosmological matter density perturbations in the viable $f(R)$ model both numerically and analytically. We found that the growth rate in the scalar-tensor regime can be characterised by a simple analytic formula (6). This is useful to understand the characteristic behaviour of the growth index in the scalar-tensor regime. We also investigate a prospect of constraining the Compton wavelength scale of the $f(R)$ model with a future weak lensing survey. This result shows that a constraint on k_C of the same order of k_C will be obtained for the model $n = 1$ and $n = 1/2$, though the constraint is weaker as n is larger. For $k_C \gtrsim 1h{\rm Mpc}^{-1}$, the constraint is very weak. This is because the weak lensing statistics is not very sensitive to the density perturbations on the smaller scales. A more detailed explanation is presented in Ref. [6]

References

[1] A. A. Starobinsky, JETP Lett. **86**, 157 (2007) [arXiv:0706.2041].

[2] S. Tsujikawa, R. Gannouji, B. Moraes and D. Polarski, Phys. Rev. D **80**, 084044 (2009)

[3] H. Motohashi, A. A. Starobinsky and J. Yokoyama, Int. J. Mod. Phys. D **18**, 1731 (2009) [arXiv:0905.0730].

[4] F. Schmidt, A. Vikhlinin and W. Hu, Phys. Rev. D **80**, 083505 (2009)

[5] K. Yamamoto, G. Nakamura, H. Huetsi, T. Narikawa and T. Sato; (unpublished).

[6] T. Narikawa and K. Yamamoto; [arXiv:0912.1445].

Non-Gaussianity in Cosmic Microwave Background Temperature Fluctuations from Cosmic (Super-)Strings

Atsushi Naruko[1 (a)], Keitaro Takahashi[(b)], Yuuiti Sendouda[(a)], Daisuke Yamauchi[(a)], Chul-Moon Yoo[(c)] and Misao Sasaki[(a)]

[(a)] *Yukawa Institute for Theoretical Physics, Kyoto University, Kyoto 606-8502, Japan*
[(b)] *Department of Physics and Astrophysics, Nagoya University, Nagoya 464-8602, Japan*
[(c)] *Asia Pacific Center for Theoretical Physics, Pohang University of Science and Technology, Pohang 790-784, Korea*

Abstract

We compute analytically the small-scale temperature fluctuations of cosmic microwave background from cosmic (super-)strings and study the dependence on the string intercommuting probability P. We develop an analytical model which describes the evolution of a string network and calculate the numbers of string segments and kinks in a horizon volume. Then we derive the probability distribution function (pdf). The resultant pdf consists of a Gaussian part due to frequent scattering by long string segments and a non-Gaussian tail due to close encounters with kinks. It contains two phenomenological parameters which are determined by comparison with the result of numerical simulations for $P = 1$ by Fraisse et al.. We predict that the non-Gaussian feature is suppressed for small P.

1 Introduction

The imprint of cosmic strings on the cosmic microwave background (CMB) has been widely studied. Although cosmic strings are excluded as a dominant source of the observed large angular scale anisotropy, they could still be observable at small scales with new arcminute CMB experiments, such as the South Pole Telescope or the Atacama Cosmology Telescope. Because the structure of a string network is highly nonlinear, it would naturally induce a non-Gaussian feature in the CMB fluctuations. In fact, Fraisse et al. [1] found that the probability distribution function (pdf) of the temperature fluctuations has a non-Gaussian tail and negative skewness. These non-Gaussian features may help us distinguish cosmic string signals from other secondary effects and hence enhance the observability.

Recently, cosmic superstrings have attracted much attention in the context of inflation in string theory [2]. Cosmic superstrings have properties different from conventional field-theoretic cosmic strings. The intercommuting probability P can be significantly smaller than unity for superstrings while $P = 1$ for field-theoretic strings. Furthermore, a superstring network can consist of more than one type of strings and may have Y-junctions. These differences may be used to distinguish superstrings from field-theoretic strings observationally.

In this talk, we derive analytically the pdf of the small-scale CMB temperature fluctuations and study its dependence on P. At small scales where the primary fluctuations are damped, only the integrated Sachs-Wolfe (ISW) effect is relevant and, because the contribution from loops was shown to be insignificant [1], we focus on the ISW effect of long string segments and kinks.

2 Temperature fluctuations due to cosmic strings

First we summarize basic formulae for the CMB temperature fluctuations due to cosmic strings, following [3]. We denote the position of a cosmic string by $\vec{r}(t, \sigma)$ where t and σ are the time and position on

[1] Email address: naruko@yukawa.kyoto-u.ac.jp

the string worldsheet. The temperature fluctuation, $\Delta \equiv \Delta T/T$, due to a segment, in the limit that the impact parameter of a ray is much smaller than the segment length, is written as

$$\Delta(\hat{n}) = 4\pi \frac{v}{\sqrt{1-v^2}} \alpha_{\rm seg} G\mu, \qquad \alpha_{\rm seg} = \hat{n} \cdot \left(\frac{\vec{r}\,'}{|\vec{r}\,'|} \times \frac{\dot{\vec{r}}}{|\dot{\vec{r}}|} \right) \tag{1}$$

where $v = |\dot{\vec{r}}|$ is the velocity of the segment and $\alpha_{\rm seg}$ is a factor which represents the configuration of the segment and the direction of line of sight, $\hat{n}$, and the dot and prime denote the derivatives with respect to t and σ, respectively.

A kink can be modeled as a nonsmooth junction of two straight strings with different directions, $\vec{r}\,'$ [3]. Then the temperature fluctuation with the impact parameter δ is

$$\Delta(\hat{n}) = -4G\mu\alpha_{\rm kink} \log \frac{\delta}{L_{\rm kink}} \Theta(L_{\rm kink} - \delta), \qquad \alpha_{\rm kink} = \hat{n} \cdot \vec{p}, \quad \vec{p} = \left[\frac{\vec{r}\,'}{|\vec{r}\,'|^2} \right]_{\sigma_{\rm kink}-0}^{\sigma_{\rm kink}+0}, \tag{2}$$

where $L_{\rm kink}$ is a distance between kinks. The step function $\Theta(L_{\rm kink} - \delta)$ represents the effect that the fluctuation becomes negligible far from the kink, $\alpha_{\rm kink}$ represents the kink configuration, $\vec{p}$ represents the amplitude of the kink and $\sigma_{\rm kink}$ is the position of the kink.

3 Analytic model of cosmic string network

In this section, we develop an analytic model which describes the behavior of a cosmic string network. First, the interstring distance ξ and the rms velocity $v_{\rm rms}$ are calculated using a velocity-dependent one-scale model [4, 5]. Then, the number of kinks in a horizon volume is calculated. We assume that the scaling behavior is already realized by the recombination time.

For a universe with the scale factor $a(t) \propto t^{\beta}$, the evolution equations for γ and $v_{\rm rms}$ are given by [4, 5]

$$\frac{t}{\gamma}\frac{d\gamma}{dt} = 1 - \beta - \frac{1}{2}\beta\tilde{c}Pv_{\rm rms}\gamma - \beta v_{\rm rms}^2, \qquad \frac{dv_{\rm rms}}{dt} = (1 - v_{\rm rms}^2) H \left[k(v_{\rm rms})\gamma - 2v_{\rm rms} \right], \tag{3}$$

where $\tilde{c}$ is a constant which represents the efficiency of the loop formation and $k(v_{\rm rms}) \approx (2\sqrt{2}/\pi)(1 - 8v_{\rm rms}^6)/(1 + 8v_{\rm rms}^6)$ is the momentum parameter [4]. Hereafter we assume a matter-dominated universe and set $\beta = 2/3$.

It is known that a string network approaches a "scaling" regime where the characteristic scale grows with the horizon size [6]. This means that γ and $v_{\rm rms}$ are asymptotically constant in time. From (3), we obtain γ and $v_{\rm rms}$. For small $\tilde{c}P$ they can be approximately given as

$$v_{\rm rms}^2 \approx \frac{1}{2} - \frac{1}{2}\sqrt{\frac{\pi\tilde{c}P}{3\sqrt{2}}}, \quad \gamma = \frac{2v_{\rm rms}}{k(v_{\rm rms})} \approx \sqrt{\frac{\pi\sqrt{2}}{3\tilde{c}P}}. \tag{4}$$

We see that small P leads to large γ and hence large $N_{\rm seg}$ due to the inefficiency of loop formation [5].

Next, we consider the kink number evolution. Kinks are formed on string segments when they intercommute and, simultaneously, some of the existing kinks are removed through loop formation. Furthermore, kinks decay due to stretching by the cosmic expansion and the emission of gravitational waves. Here we neglect the decay due to the gravitational wave emission and focus on the decay due to cosmic expansion since it is the most efficient decay process at a matter-dominated stage [7].

According to [8], the kink amplitude, $p = |\vec{p}|$, decays with cosmic expansion as $p(t) = p_{\rm f}(t/t_{\rm f})^{-\epsilon}$, where $t_{\rm f}$ and $p_{\rm f}$ are the formation time and the amplitude at the formation respectively. We count the number of kinks with amplitude $p_{\rm min} \le p \le p_{\rm max}$. The kink number in a comoving volume $V(t) = a^3(t)V_0$ is given by the integral of the formation rate, $d\bar{N}_{\rm form}(t,p)/dtdp$. And this formation rate of kinks, which is assumed here to be independent of p, is proportional to the loop formation rate, $d\bar{N}_{\rm loop}/dt$.

$$\bar{N}_{\rm kink} = \int_{p_{\rm min}}^{p_{\rm max}} dp \int_{t_0(p)}^{t} dt \, \frac{d\bar{N}_{\rm form}(t,p)}{dtdp} = \int_{p_{\rm min}}^{p_{\rm max}} dp \int_{t_0(p)}^{t} dt \, \frac{q}{p_{\rm min}} \frac{d\bar{N}_{\rm loop}(t)}{dt} \approx \frac{2q\tilde{c}Pv_{\rm rms}\gamma^4\epsilon}{3\alpha} \left(\frac{p_{\rm max}}{p_{\rm min}} \right)^{1/\epsilon}, \tag{5}$$

where $t_0(p) = t(p/p_{\rm max})^{1/\epsilon}$, a barred quantity is a number in the comoving volume $V(t)$, q is a constant which represents the efficiency of the kink formation and α is the average loop length in units of ξ.

4 PDF of CMB fluctuations

A photon ray is scattered by segments many times through its way from the last scattering surface to an observer, hence the temperature fluctuation would behave like a random walk. If we treat a segment as a particle with the cross section ξ^2, the optical depth is

$$\tau = \int_0^{z_{\rm rec}} N_{\rm seg} H^3 \xi^2 \frac{dz}{H(1+z)} = \frac{N_{\rm seg}}{\gamma^2} \log(1+z_{\rm rec}), \tag{6}$$

where $z_{\rm rec} \approx 1100$ is the redshift at recombination. This is estimated as $7N_{\rm seg}\gamma^{-2} \approx 16$ for $P = 1$ and greater for smaller P. Therefore, remenbering Eq. (1), the pdf from segments can be approximated as Gaussian with the dispersion,

$$\sigma = 2\pi \frac{v}{\sqrt{1-v^2}} \alpha_{\rm seg} G\mu \sqrt{N_{\rm seg}\gamma^{-2}\log(1+z_{\rm rec})} \approx 2\pi\alpha_{\rm seg}\sqrt{\log(1+z_{\rm rec})} \left(\frac{\pi\sqrt{2}}{3\tilde{c}P}\right)^{1/4} G\mu, \tag{7}$$

where we have set $v = v_{\rm rms}$ and substituted (4) in the second equality.

Next, let us consider the contribution from kinks. The temperature fluctuation depends on the impact parameter as given by (2). Therefore the differential cross section with the temperature fluctuation Δ can be written as

$$\frac{d\sigma_{\rm kink}}{d\Delta} = \frac{L_{\rm kink}^2}{\Delta_0} e^{-|\Delta|/\Delta_0}, \quad \Delta_0 \equiv 2\alpha_{\rm kink} G\mu, \tag{8}$$

where $\alpha_{\rm kink}$ should be understood as the statistical average of the kink configuration. Then the pdf of temperature fluctuations due to kinks is

$$\frac{dP_{\rm kink}}{d\Delta} = \int_0^{z_{\rm rec}} N_{\rm kink} H^3 \frac{d\sigma_{\rm kink}}{d\Delta} \frac{dz}{H(1+z)} = \frac{\gamma^2}{K\Delta_0} e^{-|\Delta|/\Delta_0} \log(1+z_{\rm rec}). \tag{9}$$

We have a pdf of the form,

$$\frac{dP_{\rm tot}}{d\Delta} = \frac{dP_{\rm G}}{d\Delta} + \frac{dP_{\rm NG}}{d\Delta}, \qquad \frac{dP_{\rm G}}{d\Delta} = \frac{1}{\sqrt{2\pi}\sigma} e^{-\Delta^2/2\sigma^2}, \quad \frac{dP_{\rm NG}}{d\Delta} = \frac{\gamma^2}{K\Delta_0} \log(1+z_{\rm rec}) e^{-|\Delta|/\Delta_0}, \tag{10}$$

with σ and Δ_0 are given by Eqs. (7) and (8), respectively. $dP_{\rm G}/d\Delta$ is the Gaussian part due to frequent scattering by string segments, and $dP_{\rm NG}/d\Delta$ is the non-Gaussian tail due to rare scattering by kinks. Here, because $dP_{\rm NG}/d\Delta \ll 1$ as we see just below, we have normalized $dP_{\rm G}/d\Delta$ as $\int_{-\infty}^{\infty} d\Delta\, dP_{\rm G}/d\Delta = 1$. In the limit $P \to 1$, we have

$$\sigma \approx 14 G\mu, \quad A \approx 10\alpha_{\rm kink}^{-1} \left(\frac{p_{\rm max}}{p_{\rm min}}\right)^{-5.1} (G\mu)^{-1}, \Delta_0 = 2\alpha_{\rm kink} G\mu, \tag{11}$$

where we have set $q = 2$, $\tilde{c} = 0.23$ and $\alpha = 0.1$, as their standard values [9] and $\alpha_{\rm seg} = 1/\sqrt{2}$ for the statistical average. In addition, we have set $\alpha_{\rm kink} = 4.5$ and $p_{\rm max}/p_{\rm min} = 2.3$ as a phenomelogical parameters. On the other hand, the pdf from numerical simulations [1] can be also described as Eq. (10) with

$$\sigma_{\rm sim} \approx 12 G\mu, \ A_{\rm sim} \approx 0.03 (G\mu)^{-1}, \ \Delta_{0,\rm sim} \approx 9 G\mu. \tag{12}$$

As we see in Fig. 1, as P decreases, the Gaussian dispersion increases and the contribution of the non-Gaussian tail is suppressed. Thus the non-Gaussianity could be a probe of the cosmic string property, P. However, future observation with typical angular resolution $5'$ will not be able to resolve kinks as the non-Gaussian feature is highly suppressed even for $P = 1$. Thus we would need observation with arcminute resolution.

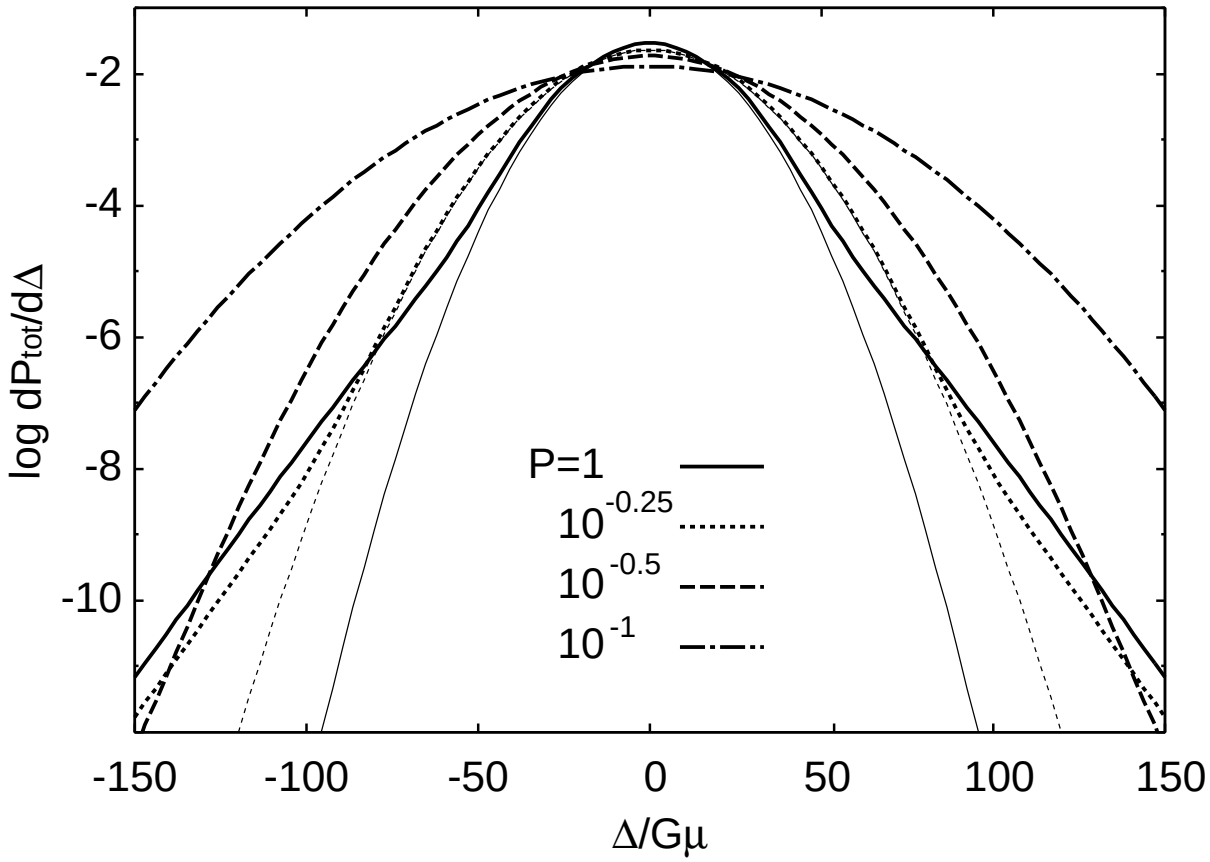

Figure 1: Dependence of the pdf on the intercommuting probability P (thick lines). The respective Gaussian parts are plotted with thin lines for comparison. For $P = 1$ and $10^{-0.25}$, the pdfs deviate significantly from the Gaussian distribution. For $P \lesssim 10^{-0.5}$, pdfs are almost Gaussian.

References

[1] A. A. Fraisse, C. Ringeval, D. N. Spergel and F. R. Bouchet, Phys. Rev. D **78**, 043535 (2008).

[2] M. Majumdar, arXiv:hep-th/0512062.

[3] A. Stebbins, Astrophys. J. **327**, 584 (1988); A. Stebbins and S. Veeraraghavan, Phys. Rev. D **51**, 1465 (1995).

[4] C. J. A. P. Martins and E. P. S. Shellard, Phys. Rev D **54**, 2535 (1996); C. J. A. P. Martins and E. P. S. Shellard, Phys. Rev D **65**, 043514 (2002).

[5] A. Avgoustidis and E. P. S. Shellard, Phys. Rev. D **73**, 041301 (2006).

[6] T. W. B. Kibble, Nucl. Phys. B **252**, 277 (1985).

[7] B. Allen and R. R. Caldwell, Phys. Rev. Lett. **65**, 1705 (1990); B. Allen and R. R. Caldwell, Phys. Rev. D **43**, R2457 (1991); B. Allen and R. R. Caldwell, Phys. Rev. D **43**, 3173 (1991).

[8] D. P. Bennett and F. R. Bouchet, Phys. Rev. D **41**, 2408 (1990).

[9] V. Vanchurin, K. Olum and A. Vilenkin, Phys. Rev. D **74** 063527 (2006); C. Ringeval and M. Sakellariadou, JCAP 0702 023 (2007); C. J. A. P. Martins and E. P. S. Shellard, Phys. Rev. D **73**, 043515 (2006).

Towards detection of motion-induced radiation?

Wade Naylor[1]

Department of Physics, Ritsumeikan University, Kusatsu, Shiga 506-8277

Abstract

We discuss the results of theoretical simulations of a proposed experiment using pulsed laser irradiation of a semi-conductor diaphragm (SCD) in a superconducting microwave cavity [4]. Because the detection apparatus uses a single photon detection Rydberg beam method the analysis can be simplified to study the number of photons emitted in a given cavity mode.

1 Introduction & motivation

Motion-induced radiation, or the dynamical Casimir effect (DCE), has been a serious theoretical research subject for about the last 40 years and is important, because it challenges the principle of relativity of motion in vacuum and has analogs with quantum gravity, see Fig. 1. Various experimental proposals now suggest that the detection of this illusive radiation may be possible. We discuss the results of theoretical simulations of a proposed experiment that generates "effective motion" using pulsed laser irradiation of a semi-conductor diaphragm (SD).

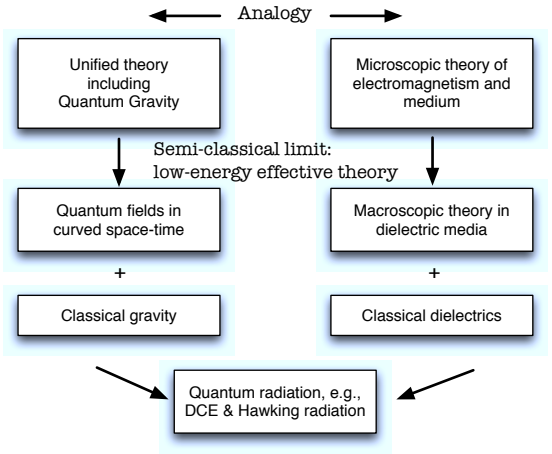

Figure 1: A diagram discussing the analogy between quantum effects in electrodynamics and in curved spacetime [1].

We have has designed (PI: Seishi Matsuki) a DCE detection system, see Figure 2, using a GHz pulsed-laser of wavelength 860nm ($E_\gamma = 1.55$eV) operating at a power $\sim 100\mu$J/pulse. The detection apparatus uses a single photon detection Rydberg beam and thus, the analysis can be simplified to study the number of photons emitted in a given cavity mode.

Questions?

- What is the best location, $\eta = d/L_z$, for the slab?
- Which frequencies dominate, dependant on pulse shape $n_s(t)$ (or relaxation time t_r)?
- Are there differences between TE and TM modes?

[1]Email address: naylor@se.ritsumei.ac.jp

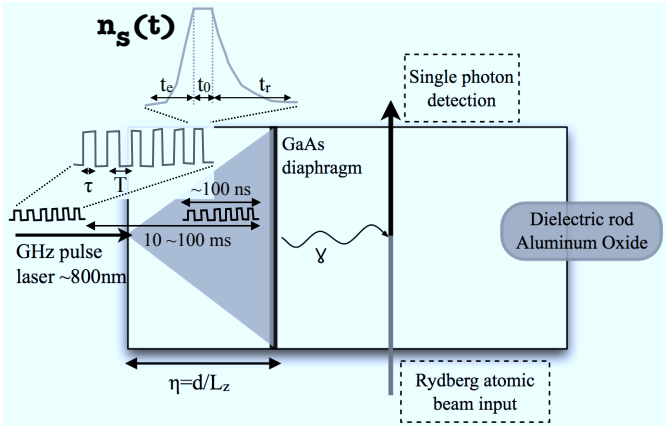

Figure 2: A laser periodically irradiates a GaAs slab ($\sim$ 0.5mm thick) inside a superconducting (high-finesse: $Q \sim 10^6$) niobium cavity at $\sim$ 100 mK. Note the single pulse duration is $T \sim$ 100ps.

2 Plasma sheet model

The Hamiltonian for a surface plasma of electrons of charge e and "effective mass" m^* on a background electromagnetic field is

$$\mathcal{H} = \frac{1}{2}\int d^3x[\mathbf{E}\cdot\mathbf{D} + \mathbf{B}\cdot\mathbf{H}] + \int d^3x \left(\frac{1}{2m^* n_s}(\mathbf{p}_\xi - en_s\mathbf{A}_\parallel)^2 + en_s\Phi\right)\delta(\mathbf{x}-\mathbf{x}_\Sigma) \tag{1}$$

where the momentum is $\dot{\boldsymbol{\xi}} = (\mathbf{p}_\xi - en_s(t)\mathbf{A}_\parallel)/m^* n_s(t)$, $n_s(t)$ is the "time dependent" surface charge density. Hamiltonian constraints imply $\mathbf{p}_\xi = 0$ [2] and thus, the electron momentum is related to the tangential vector potential by $\dot{\boldsymbol{\xi}} = -e\mathbf{A}_\parallel/m^*$, which implies that the surface current density is $\mathbf{K} = en_s(t)\dot{\boldsymbol{\xi}} = -\dfrac{e^2 n_s(t)}{m^*}\mathbf{A}_\perp$. Using surface continuity [3]: $\dot{\sigma} + n\cdot[\nabla \times n \times \mathbf{K}] = 0$ with the Fitzgerald-Lorenz gauge condition: $\partial_t\Phi + \boldsymbol{\nabla}\cdot\mathbf{A} = 0$ we arrive at

$$\dot{\sigma} = -\frac{e^2 n_s(t)}{m^*}\boldsymbol{\nabla}\cdot\mathbf{A}_\perp = \frac{e^2 n_s(t)}{m^*}\partial_t A_0 \qquad \Rightarrow \qquad \sigma = \frac{e^2 n_s(t)}{m^*}A_0\ , \tag{2}$$

where A_0 is the scalar potential. Applying the Hertz potentials Ψ for TE and Φ for TM modes to separate Maxwell's equations [4] we find the following *jump* conditions:

$$\text{disc}\ \Phi(d) = -\mu\frac{e^2 n_s(t)}{\mathbf{k}_\perp^2 m^*}\partial_z\Phi|_{z=d}, \qquad\qquad \text{disc}\ \partial_z\Psi|_{z=d} = \mu\frac{e^2 n_s(t)}{m^*}\Psi(d) \tag{3}$$

which can be derived from the wave equations below:

$$\boldsymbol{\nabla}_\perp^2\Psi + \partial_z^2\Psi - \partial_t^2\Psi = \frac{e^2 n_s(t)}{m^*}\delta(z-d)\Psi(d)\ , \qquad\qquad \boldsymbol{\nabla}_\perp^2\Phi + \partial_z^2\Phi - \partial_t^2\Phi = \frac{1}{\mathbf{k}_\perp^2}\frac{e^2 n_s(t)}{m^*}\delta'(z-d)\Phi(d)$$

From continuity of the wave-function and *jump* conditions, for TE modes we have solutions:

$$\Psi_{\mathbf{m}} = \begin{cases} A_m^{(\mathrm{TE})}\sqrt{\dfrac{1}{d}}\sin(k_{m_z}z)\sqrt{\dfrac{2}{L_x}}\cos\left(\dfrac{\pi m_x x}{L_x}\right)\sqrt{\dfrac{2}{L_y}}\cos\left(\dfrac{\pi m_y y}{L_y}\right), & 0 < z < d \\ B_m^{(\mathrm{TE})}\sqrt{\dfrac{1}{L_z-d}}\sin(k_{m_z}(L_z-z))\sqrt{\dfrac{2}{L_x}}\cos\left(\dfrac{\pi m_x x}{L_x}\right)\sqrt{\dfrac{2}{L_y}}\cos\left(\dfrac{\pi m_y y}{L_y}\right), & d < z < L_z \end{cases} \tag{4}$$

and eigenvalue relation:

$$\frac{\sin(k_{m_z}L_z)}{(k_{m_z})^{\mp 1}\sin(k_{m_z}[L_z-d])\sin(k_{m_z}d)} = \mp\frac{e^2 n_s(t)}{\mathbf{k}_\perp^2\, m^*} \tag{5}$$

where the ± signs refer to TE and TM modes respectively and for TM replace sin → cos (for TE drop the $1/k_\perp^2$ factor).

3 Particle creation

The quantum field operator expansion $\widehat{\psi}(\mathbf{r},t) = \sum_{\mathbf{m}} \left[a_{\mathbf{m}}\psi_{\mathbf{m}}(\mathbf{r},t) + a^\dagger_{\mathbf{m}}\psi^*_{\mathbf{m}}(\mathbf{r},t)\right]$ of the Hertz scalars with *instantaneous* basis ansatz (during irradiation):

$$\psi^{\text{out}}_{\mathbf{s}}(\mathbf{r},t) = \sum_{\mathbf{m}} P^{(\mathbf{s})}_{\mathbf{m}}\Psi_m(\mathbf{r},t)\ , \qquad t \geq 0 \tag{6}$$

when substituted into the wave equations leads to

$$\ddot{P}^{(s)}_n + \omega_n^2(t)P^{(s)}_n = -\sum_m^\infty \left[2M_{mn}\dot{P}^{(s)}_m + \dot{M}_{mn}P^{(s)}_m + \sum_\ell^\infty M_{n\ell}M_{m\ell}P^{(s)}_m\right] \tag{7}$$

where $\omega^2_{\mathbf{m}}(t) = c^2\Big[\left(\frac{m_x\pi}{L_x}\right)^2 + \left(\frac{m_y\pi}{L_y}\right)^2 + k^2_{m_z}(t)\Big]$ and $M_{mn} = (\Psi_n,\Psi_n)^{-1}\,\delta_{m_xn_x}\delta_{m_yn_y}\left(\frac{\partial\Psi_m}{\partial t},\Psi_n\right)$

Note, the scalar product is defined by $(\phi,\psi) = -i\int_{\text{cavity}} d^3x(\phi\,\dot{\psi}^* - \dot{\phi}\,\psi^*)$. The Bogolubov coefficients are

$$\alpha_{mn} = (\psi^{\text{out}}_m,\psi^{\text{in}}_n)\,, \qquad \beta_{mn} = -(\psi^{\text{out}}_m,[\psi^{\text{in}}_n]^*) \tag{8}$$

where in terms of the "instantaneous" mode functions

$$\beta_{mn} = \sqrt{\frac{\omega_m}{2}}P^{(n)}_m - i\sqrt{\frac{1}{2\omega_m}}\left[\dot{P}^{(n)}_m + \sum_\ell^{\ell_{max}} M_{\ell m}P^{(n)}_\ell\right] \tag{9}$$

and α_{mn} is obtained by complex conjugation. The number of photons in a given mode (for an initial vacuum state) is

$$N_m(t) = \sum_n^{\ell_{max}} |\beta_{mn}|^2 \tag{10}$$

We vary $\ell_{max} \sim 50$ until the results do not change, but an independent check is the unitarity constraint: $\sum_n^{\ell_{max}}(|\alpha_{mn}|^2 - |\beta_{mn}|^2) = 1$, see Figure 3 (left inset).

4 Results & discussion

In Figure 3 (left) is a typical example of parametric enhancement for the lowest TE modes. On the right is the dependence on different slab locations, η, for two different laser powers (unfilled triangles and circles correspond to 50μJ /pulse or $V_{\max}L_z = 5000$, while filled ones are for 0.01μJ/pulse or $V_{\max}L_z = 1$).

Answers?

- The best location for the slab is $\eta = 1/2$ for TE modes.
- The fundamental frequencies dominate, where the pulse frequency is near to twice the parametric resonance frequency (besides de-tuning effects [4]).
- For TM modes even a low laser power generates significant photon production at $\eta = 1/2$. The TM case is fairly independent of η for large laser powers.

For future work it would be interesting to use a microscopic fermion model of a plasma sheet, like that used for Graphene [5]. This would allow one to consider Ohmic losses in the slab by coupling the microscopic Lagrangian to an external set of harmonic oscillators to model losses. Although Ohmic losses are mainly due to $\mathbf{H}_\parallel$, implying a strong TM dependence, it is still unclear if the losses in the slab affect TM modes more than TE modes.

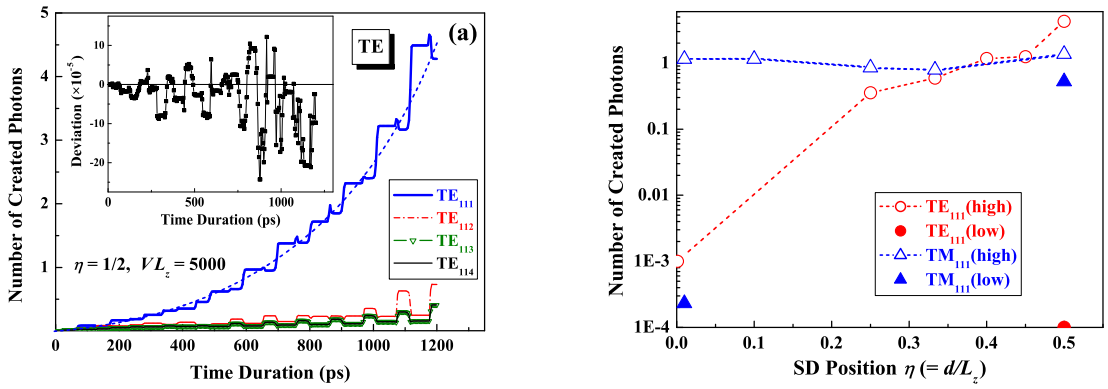

Figure 3: $N_{111}(t)$ fundamental mode. Left, TE with $\eta = 1/2$ and $V_{\max}L_z = 5000$ with higher modes giving lesser contributions (inset shows unitarity constraint). Right, TE and TM mode dependence on η.

Acknowledgements

The author acknowledges valuable discussions with Y. Kido, S. Matsuki and K. Yamamoto concerning experimental detection of motion induced radiation. This work was supported in part by Grant-in-Aid for scientific research Grant no. A20340060 under the Ministry of Education, Japan.

References

[1] Schutzhold et al., Phys. Rev. Lett. **88** (2002) 061101).

[2] G. Barton and A. Calogeracos, Annals Phys. **238**, 227 (1995).

[3] V. Namias, Am. J. Phys. **56**, 898 (1988).

[4] W. Naylor et al., Phys. Rev. A **80**, 043835 (2009).

[5] G. W. Semenoff, Phys. Rev. Lett. **53**, 2449 (1984).

Short Range Gravity Experiment in NEWTON experiment

Kazufumi Ninomiya[1] , Takashi Akiyama, Maki Hata, Hironori Nishio, Naruya Ogawa, Yuta Sekiguchi, Kentaro Watanabe, and Jiro Murata

Department of Physics, Rikkyo University, Toshima, Tokyo 171-8501

Abstract

According to the ADD model [1], deviation from Newtonfs inverse square law is expected at below sub-millimeter scale. We have developed an experimental setup using torsion balance pendulum, aiming to test the Newtonfs inverse square law at below millimeter scale. Current status and preliminary results will be presented.

1 Physics motivation

1.1 Test of Inverse Square Law

Weakness of gravitational force comparing to other three interactions is considered as one of the most severe problem in the theoretical physics. It is necessary to resolve this problem, in order to unify the three gauge interaction and gravitational force. According to a recent unified theory (super string theory, M-theory, ADD model and etc.), gravitational field may spread toward extra dimensions. In the ADD model [1], extra dimensions are predicted to exist at below mm scale. Then, an observation of a deviation from Newton's inverse square law is expected at below mm scale. If extra dimensions exist, gravitational potential should be modified. Modified gravitational potential is historically expressed using Yukawa interaction form.

$$V(r) = G\frac{Mm}{r}(1+\alpha e^{-r/\lambda}) \quad (1)$$

Here, α is coupling constant and λ is the range of the new interaction. To search for the new Yukawa term, Newton's inverse square law has been experimentally tested. However, high precision test of the inverse square law is performed at only astronomical scales [2]. Therefore, it is necessary to test the gravitational force at below mm scale.

1.2 Test of Weak Equivalence Principle

The weak equivalence principle is expressed as that, ratio between gravitational mass and inertia mass is independent of its composition. If the ratio between gravitational mass and inertia mass is constant for every material, universality of free fall must be kept. Therefore, test of the universality of free fall can be used as a test of the weak equivalence principle. Number of experimental tests confirmed that ratio between inertial mass for different compositions is same for the ratio between gravitational mass, using gravity from the earth and the sun. On the other hand, there are no experimental tests at short range below cm scale. There is also a theoretical model which predicts a violation of weak equivalence principle. Baryon number coupling force is one of such models [3]. If a new interaction which couples to baryon number, the weak equivalence principle seems to be violated. We can test the weak equivalence principle measuring the composition dependant of the gravitational constant G.

2 Experimental technique

2.1 Torsion Pendulum

In Our experiment, gravitational force is measured using torsion pendulum and online image analyzing system [7]. Principle of the measurement is shown in fig. 1.

[1]Email address: 08la013a@rikkyo.ac.jp

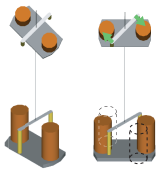

Figure 1: Torsion balance pendulum.

Angular displacement between before and after attractor position is measured as gravitational signal. It is because torsion pendulum is twisted toward balanced position where restoring force equals to the gravitational force. The torque of the torsion pendulum can be expressed using angular displacement $\Delta\theta$.

$$N = \kappa \cdot \Delta\theta \tag{2}$$

Here, N is the torque, κ is the torsional spring constant. The torsional spring constant κ is calculated using inertia moment and the periodic oscillation of the torsion pendulum.

2.2 Digital image analysis

The data taking system is originally developed for PHENIX experiment at RHIC (Relativistic Heavy Ion Collider) at Brook Heaven National laboratory, as an optical alignment system (OASys) [4]. Position resolution of 10 nanometer is achieved using the OASys. Applying this system, we developed digital image analyzing system using digital video camera for short range gravity experiment [5]. In this system, the angular displacement of the torsion pendulum can be obtained from intensity of digital images. Typical angular resolution of 1.2×10^{-6} degrees is achieved using our digital image analyzing system.

3 Experiment

3.1 Newton I experiment

In prototype experiment named Newton I, we succeeded to test the Newton's inverse square law at cm scale. To suppress the electromagnetic force, all the components used in the device are electrically connected and used non-magnetic metals (aluminum, copper, lead, brass and etc.).

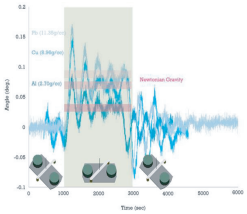

Figure 2: Time evolution of torsion pendulum.

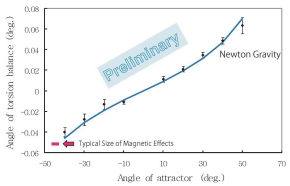

Figure 3: Inverse square law.

Typical results in Newton I are shown in fig. 2. Time evolution of torsion pendulum is plotted for lead, copper and aluminum attractors. From this result, composition dependence is confirmed. Position dependence of the torsion pendulum is shown in fig. 3, which is measured by changing the attractor angle. Solid line is Newtonian gravitational prediction. From this result, we can confirm Newton's inverse square law at cm scale.

3.2 Newton II experiment

In Newton I experiment, we have confirmed the inverse square law at cm scale. However, the largest systematic error of Newton I is caused from attractor replacement. In order to suppress this systematic effect, Newton II is developed [7]. The results of Newton II experiment is shown fig. 4 and fig. 5.

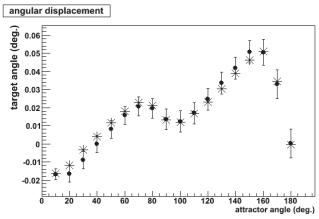

Figure 4: Gravity signal. * shows simulation data from Newtonian gravitational prediction.

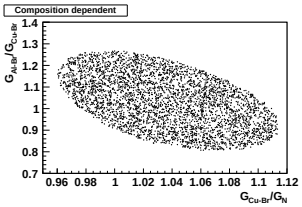

Figure 5: Composition dependence of gravitational constant G. This result is obtained at the 95% confidences level.

In Newton II, we used two materials (Cu and Al) as attractor. The gravity signal from the two materials is shown in fig.5. Using this data, Composition dependence of gravitational constant is obtained. Ratio between G_{Br-Al}/G_{Br-Cu} and G_{Br-Cu}/G_{Newton} is shown in fig.6. We have obtained the ratios, as $G_{Br-Al}/G_{Br-Cu} = 1.03 \pm 0.23$ and $G_{Br-Cu}/G_{Newton} = 1.04 \pm 0.08$. From the results, there is no composition dependence of gravitational constant G between G_{Br-Al} and G_{Br-Cu}. A new interaction coupling to the baryon number which violates the weak equivalence principle at only short range, can be parameterized as a new Yukawa term [2].

$$V(r) = G\frac{Mm}{r}(1 + \xi\frac{B_i}{\mu_i}\frac{B_j}{\mu_j}e^{-r/\lambda}) \tag{3}$$

Here, B_A is baryon number for material A, and μ_A is gravitational mass in hydrogen mass unit. Using these results, we can extract the upper limit on ξ. The results are shown in fig. 6.

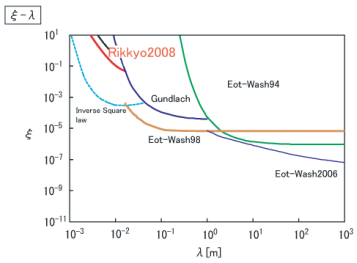

Figure 6: $\xi - \lambda$ plot. Red line is our result. This result is obtained at the 95% confidences level.

3.3 Newton SC experiment

In Newton SC experiment, new measuring method is tested, aiming high precision measurement. If moving speed of the attractor is very slow comparing to the oscillation period of the torsion pendulum, balanced position of torsion pendulum is moving with the attractor motion (forced oscillation). We have succeeded to test the inverse square law in this method. Angular displacement of the torsion pendulum is obtained for all the attractor angles from -50^o to 50^o at single measurement. Therefore, obtained data is directly used as a test of the inverse square law. Typical result from Newton SC is shown in fig. 7.

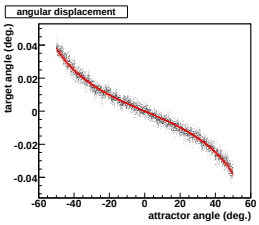

Figure 7: Time evolution of the gravity signal. Red line is Newton's gravitational prediction.

4 Summary

In Newton I experiment, we succeeded to demonstrate its ability to test the Newton's inverse square law at centimeter scale. We succeeded to confirm weak equivalence principle at mm scale in Newton II experiment. Now, we are starting new experiment named Newton III. In this experiment, we will also be able to test the inverse square law at below sum-millimeter scale.

5 Acknowledgments

Part of the present works are performed as undergraduate student experiments. The author thanks to Y. Miyano, M. Takahashi, T. Tsuneno, T. Amanuma, S. Danbara, T. Iino, S. Mizuno, Y. Araki, T. Ohmori, Y. Sakurai, S. Yamaoka, R. Tsutsui and Y. Ikeda for their vital efforts on this work. This work is supported by Grant-in-Aid for Exploratory Research (18654048, 20654024).

References

[1] Nima Arkani-Hamed, Savas Dimopoulos, Gia Dvali, Physics Letters B 429 (1998) 263-272.

[2] Ephraim Fishback, Carrick Talmadge, Nature 356 (1992) 207 . 215; "The Search for Non-Newtonian Gravity", Springer (1998) ISBN 0387984909

[3] T.D. Lee and C.N. Yang, Physical Review 98 (1955) 1501.

[4] J. Murata et. al., Nucl. Instrum. Meth. A 500(2003) 309-317.

[5] Jiro Murata, "Pico-Precision Displacement Sensor using Digital Image Analysis", IEEE Nuclear Science Symposium Conference Record 675 (2005).

[6] Maki Hata et.al., "Recent Results on Short-Range Gravity Experiment", Journal of Physics: Conference Series 189(2009)012019CIOPC2009

[7] Kazufumi Ninomiya et.al., "New Experimental Technique for Short-Range Gravity Measurement", Journal of Physics: Conference Series 189(2009)012026CIOPC2009

Searching for nontensorial polarizations of stochastic gravitational waves with laser interferometers

Atsushi Nishizawa[1](a), Atsushi Taruya(b),(c), Kazuhiro Hayama(d),(e), Seiji Kawamura(d), Masa-aki Sakagami(f)

(a) *Division of Theoretical Astronomy, National Astronomical Observatory of Japan, Mitaka, Tokyo 181-8588*
(b) *Research Center for the Early Universe, School of Science, The University of Tokyo, Tokyo 113-0033*
(c) *Institute for the Physics and Mathematics of the Universe, University of Tokyo, Kashiwa, Chiba 277-8568*
(d) *TAMA Project, National Astronomical Observatory of Japan, Mitaka, Tokyo 181-8588*
(e) *Albert-Einstein-Institut (Max-Planck-Institut für Gravitationsphysik), Callinstraße 38, D-30167 Hannover, Germany*
(f) *Graduate School of Human and Environmental Studies, Kyoto University, Kyoto 606-8501*

Abstract

In general relativity, a gravitational wave (GW) has two polarization modes, while in modified gravity, the GW is allowed to have additional polarizations. Thus, the observation of the GW polarizations can be utilized for the test of gravity theories. In this article, we investigated the mode-separability and detectability of additional polarization modes of gravitational waves, particularly focusing on a stochastic gravitational-wave background, with laser-interferometric detectors based on the ground and space. As a result, we found that the additional polarization modes can be succcesslly separated and detected.

1 Introduction

General relativity (GR) has been strictly tested in the solar system [1, 2], however, has not been strongly constrained at a cosmological scale and in a strong field regime. If the gravity theory is deviated from GR, it gives rise to various observational signatures. The properties of a gravitational wave (GW) are also altered in the propagation speed, waveforms, and polarization modes. In GR, a GW has two polarization modes (plus and cross modes), while in a general metric theory of gravitation, the GW is allowed to have, at most, six polarizations [1, 3]. Such additional polarizations appear in modified gravity and extra-dimensional theories, corresponding to extra degrees of freedom in the theories. Therefore, the observation of the GW polarizations can be utilized for the test of the gravity theory.

Currently, there are a few observational constraints on the additional polarization modes of GWs. For the scalar GWs, the observed orbital-period derivative of PSR B1913+16 agrees well with the predicted values of GR, conservatively, at a level of 1 % error [2], indicating that the contribution of scalar GWs to the energy loss is less than 1 %. On the other hand, a null result in a search for a stochastic gravitational-wave background (GWB) by LIGO [4] has given an upper limit on an energy density, $h_0^2\Omega_{\rm gw} \lesssim 3.6\times10^{-6}$. No detection can also be applied to non-Einsteinian polarizations, though a factor of the upper limit would be corrected, depending on a detector response.

In this article, we focus on the stochastic GWB here and investigate the separability of the polarization modes of the GWB with laser-interferometric detecters.

2 GW polarizations and cross-correlation analysis

Using the unit vectors $\hat{\mathbf{m}}$ and $\hat{\mathbf{n}}$ perpendicular to the unit vector pointing at the GW propagation direction $\hat{\mathbf{\Omega}}$ and to each other, the polarization tensors for $p = +, \times, b, \ell, x$, and y called plus, cross, breathing,

[1]Email address: atsushi.nishizawa@nao.ac.jp

longitudinal, vector-x, and vector-y modes, respectively, are defined by [1, 3]: $\mathbf{e}_+ = \hat{\mathbf{m}}\otimes\hat{\mathbf{m}} - \hat{\mathbf{n}}\otimes\hat{\mathbf{n}}$, $\mathbf{e}_\times = \hat{\mathbf{m}}\otimes\hat{\mathbf{n}} + \hat{\mathbf{n}}\otimes\hat{\mathbf{m}}$, $\mathbf{e}_b = \hat{\mathbf{m}}\otimes\hat{\mathbf{m}} + \hat{\mathbf{n}}\otimes\hat{\mathbf{n}}$, $\mathbf{e}_\ell = \sqrt{2}\,\hat{\mathbf{\Omega}}\otimes\hat{\mathbf{\Omega}}$, $\mathbf{e}_x = \hat{\mathbf{m}}\otimes\hat{\mathbf{\Omega}} + \hat{\mathbf{\Omega}}\otimes\hat{\mathbf{m}}$, $\mathbf{e}_y = \hat{\mathbf{n}}\otimes\hat{\mathbf{\Omega}} + \hat{\mathbf{\Omega}}\otimes\hat{\mathbf{n}}$. Each polarization mode is orthogonal to one another and is normalized so that $e^p_{ij}e^{ij}_{p'} = 2\delta_{pp'}$, $p, p' = +, \times, b, \ell, x$, and y. The angular response function of the I-th interferometer is given by contraction of the polarization tensors with the detector tensors: $F^p_I(\hat{\mathbf{\Omega}}) \equiv \mathbf{D}_I : \mathbf{e}_p(\hat{\mathbf{\Omega}})$ and $\mathbf{D}_I \equiv [\hat{\mathbf{u}}\otimes\hat{\mathbf{u}} - \hat{\mathbf{v}}\otimes\hat{\mathbf{v}}]/2$. The unit vectors $\hat{\mathbf{u}}$ and $\hat{\mathbf{v}}$ are directed to each detector arm. Note that the above expression is valid only when the arm length of the detector, L, is much smaller than the wavelength of GWs, $\lambda_{\rm g}$, in the observational frequency band we consider. This condition holds for both ground-based detectors and space-based detector such as DECICO.

We assume that a stochastic GWB is (i) isotropic, (ii) independently polarized (not correlated between polarizations), (iii) stationary, and (iv) Gaussian. Conventionally, the amplitude of GWB for each polarization is characterized by $\Omega^p_{\rm gw}(f) \equiv (d\rho^p_{\rm gw}/d\ln f)/\rho_c$, where $\rho_c = 3H_0^2/8\pi G$ and $H_0 = 100\,h_0\,{\rm km\,sec^{-1}\,Mpc^{-1}}$ [5–8]. Then, we define the GWB energy density in tensor, vector, and scalar polarization modes as $\Omega^T_{\rm gw} \equiv \Omega^+_{\rm gw} + \Omega^\times_{\rm gw}$, $\Omega^V_{\rm gw} \equiv \Omega^x_{\rm gw} + \Omega^y_{\rm gw}$, $\Omega^S_{\rm gw} \equiv \Omega^b_{\rm gw} + \Omega^\ell_{\rm gw} = \Omega^b_{\rm gw}(1+\kappa)$. Here we assume $\Omega^+_{\rm gw} = \Omega^\times_{\rm gw}$ and $\Omega^x_{\rm gw} = \Omega^y_{\rm gw}$. For the scalar mode, we introduced a model-dependent parameter, $\kappa(f) \equiv \Omega^\ell_{\rm gw}(f)/\Omega^b_{\rm gw}(f)$.

To distinguish a stochastic GWB from detector random noise, one needs to correlate detector's signals [5–8]. We assume that the amplitude of GWB is much smaller than detector noise. In the cross-correlation analysis between I-th and J-th detectors, a GW signal can be written as

$$\mu = \frac{3H_0^2}{20\pi^2}T_{\rm obs}\,\sin^2\chi\int_{-\infty}^{\infty} df|f|^{-3}\tilde{Q}(f)\left[\Omega^T_{\rm gw}(f)\gamma^T_{IJ}(f) + \Omega^V_{\rm gw}(f)\gamma^V_{IJ}(f) + \xi(f)\,\Omega^S_{\rm gw}(f)\gamma^S_{IJ}(f)\right],$$

where $T_{\rm obs}$ is observation time, $\tilde{Q}(f)$ is a filter function, which weight the correlation signal so that signal-to-noise ratio (SNR) is maximized. The parameter defined by $\xi(f) \equiv [1+2\kappa(f)]/3[1+\kappa(f)]$ takes the value in the range $1/3 \le \xi \le 2/3$, depending on the ratio of the energy density in the longitudinal mode to the breathing mode. The prefactor, $\sin^2\chi = 1 - (\hat{\mathbf{u}}\cdot\hat{\mathbf{v}})^2$, comes from the detector tensor with non-orthogonal detector arms. The sensitivity to the GWB with each polarization can be characterized by so-called overlap reduction functions (ORF) [9]

$$\gamma^M_{IJ}(f) \equiv \frac{1}{\sin^2\chi}\int_{S^2}\frac{d\hat{\Omega}}{4\pi}\,e^{2\pi i f\hat{\Omega}\cdot\Delta\vec{X}/c}\,\mathcal{R}^M_{IJ}\,,$$

with $\mathcal{R}^T_{IJ}(\hat{\mathbf{\Omega}}) \equiv (5/2)\times(F^+_I F^+_J + F^\times_I F^\times_J)$, $\mathcal{R}^V_{IJ}(\hat{\mathbf{\Omega}}) \equiv (5/2)\times(F^x_I F^x_J + F^y_I F^y_J)$, and $\mathcal{R}^S_{IJ}(\hat{\mathbf{\Omega}}) \equiv [15/(1+2\kappa)]\times(F^b_I F^b_J + \kappa F^\ell_I F^\ell_J)$. The subscript M denotes $M = T, V, S$, and $\Delta\vec{\mathbf{X}} \equiv \vec{\mathbf{X}}_I - \vec{\mathbf{X}}_J$.

3 Mode-separation and SNR

The three polarization modes, in principle, can be separated by linearly combining more than three independent correlation signals from detector pairs. In general case with arbitrarily large number $N_{\rm pair}$ of the correlation signal, an SNR by optimally combining the correlation signals is given by [10]

$$\mathrm{SNR}^M = \frac{9H_0^2}{40\pi^2}\left[2T_{\rm obs}\int_0^\infty df\,\frac{(\Omega^M_{\rm gw}(f))^2\det\mathbf{F}(f)}{f^6\mathcal{F}_M(f)}\right]^{1/2}, \tag{1}$$

$$\mathbf{F}(f) = \begin{pmatrix} F_{TT} & F_{TV} & F_{TS} \\ F_{TV} & F_{VV} & F_{VS} \\ F_{TS} & F_{VS} & F_{SS}\end{pmatrix}, \qquad F_{MM'}(f) = \sum_i \frac{\gamma^M_i(f)\gamma^{M'}_i(f)}{\mathcal{N}_i(f)},$$

where M and M' denote polarization modes, $M, M' = T, V, S$. The quantity $\mathcal{F}_M$ is the determinant of the submatrix, which is constructed by removing the M's elements from $\mathbf{F}$. The subscript i designates a detector pair (for I-th and J-th detector pair, $i = IJ$), and $\mathcal{N}_i(f)$ is defined as, say, $\mathcal{N}_{12}(f) \equiv P_1(f)P_2(f)$. The analytical fit of the noise power spectrum of a single interferometer is given by

$$P(f) = \left[6.4\times10^{-51}\left(\frac{f}{1\mathrm{Hz}}\right)^{-4} + 1.7\times10^{-48} + 5.8\times10^{-50}\left(\frac{f}{1\mathrm{Hz}}\right)^2\right]\ \mathrm{Hz}^{-1}\,.$$

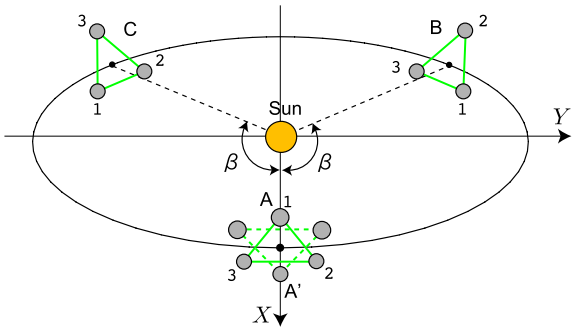

Figure 1: Four clusters, A, A', B, and C, sharing the orbit, whose radius is 1 AU.

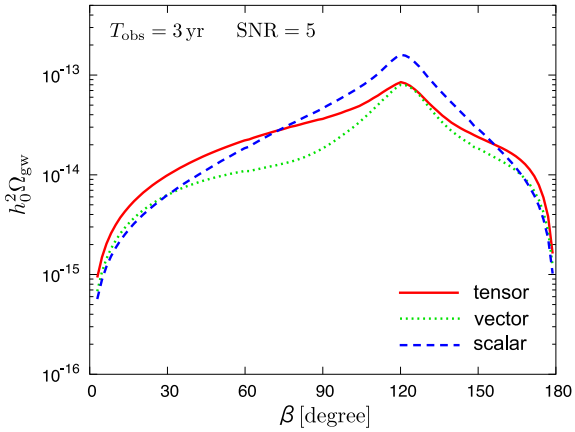

Figure 2: Detectable $h_0^2\Omega_{\rm gw}$ ($\xi h_0^2\Omega_{\rm gw}$ for the scalar mode) after the mode separation with four clusters of DECIGO.

for DECIGO and

$$P(f) = \begin{cases} 10^{-44}\left(\dfrac{f}{10\,{\rm Hz}}\right)^{-4} + 10^{-47.25}\left(\dfrac{f}{100\,{\rm Hz}}\right)^{-1.7}\ {\rm Hz}^{-1} & \text{for } 10\,{\rm Hz} \le f \le 240\,{\rm Hz}\,, \\ 10^{-46}\left(\dfrac{f}{1000\,{\rm Hz}}\right)^{3}\ {\rm Hz}^{-1} & \text{for } 240\,{\rm Hz} \le f \le 3000\,{\rm Hz}\,, \\ \infty & \text{otherwise}\,. \end{cases}$$

for advanced LIGO. The mode separability significantly affects the SNR via $\det \mathbf{F}$ in the integrand in Eq. (1). To successfully separate the modes, the condition, $\det \mathbf{F} \neq 0$, is necessary and leads to two conditions that have to be satisfied for the detector configuration: (i) the detectors have to be located at a distance more than one wavelength of the GW, (ii) detector pairs do not geometrically degenerated. If one of the two conditions fails, $\det \mathbf{F} \approx 0$ suppresses the SNR.

In the calculations below, we will assume that $\Omega_{\rm gw}^M(f)$ has a flat spectrum, *i.e.* frequency-independent, and the observation time is $T_{\rm obs} = 3\,{\rm yr}$. We set the detection threshold to SNR = 5, then it leads to the detectable $h_0^2\Omega_{\rm gw}$ ($\xi h_0^2\Omega_{\rm gw}$ for the scalar mode).

3.1 Ground-based interferometers

We perform the polarization mode separation with three detectors (minimum set needed to separate modes) among the advanced interferometers on the Earth (at $\sim 100\,{\rm Hz}$) such as AIGO, advanced LIGO at Hanford and Livingston, advanced VIRGO, and LCGT. Here we assume that all interferometers have the same noise spectrum as that of advanced LIGO, *i.e.* $P_I(f) = P(f)$. The SNR calculation is straightforward because these interferometers are located on the Earth at the distance more than one wavelength of a GW at $\sim 100\,{\rm Hz}$. Therefore, there is no problem concerning the mode degeneracy and the geometrical degeneracy of the detectors. According to [9], the set of three advanced detectors is sensitive to the GWB of $h_0^2\Omega_{\rm gw} \sim 10^{-9} - 10^{-8}$ for each polarization. This sensitivity is almost the same as that without the mode separation.

3.2 Space-based interferometers

DECIGO in the current conceptual design [11] is composed of four clusters, orbiting at 1 AU from the Sun, as shown in Fig. 1. Each cluster has three spacecrafts, which form three Fabry-Perot cavity with the armlength 10^3 km. By measuring the relative distance between a pair of the spacecrafts, three interferometer's signals are obtained in a cluster. The correlation signals that we use for the SNR

calculation are those constructed with interferometers of interclusters, because in a cluster, one cannot obtain the correlation signal sensitive enough to a GWB at low frequencies [10].

The detector configuration is shown in Fig. 1. For mathematical details of this configuration, see [10]. Since the detector separation can be approximated as the distance between the guiding centers of clusters, the distances between the clusters $D \equiv |\Delta\vec{\mathbf{X}}|$ are unchanged during their orbital motion and are given by $D_{\rm AB}(\beta) = 2R_0|\sin(\beta/2)|$ for the AB link, $D_{\rm AC}(\beta) = D_{\rm AB}(\beta)$ for AC link and $D_{\rm BC}(\beta) = 2R_0|\sin\beta|$ for the BC link. One should be noted that the only parameter in this configuration is β.

In this detector configuration, the detector separation D is typically of the order of 1 AU. This means that the ORF starts to oscillate and rapidly decay above the characteristic frequency, $f_c \equiv c/(2D) \sim 10^{-3}$ Hz. Thus, the large detector separation considerably degrades the sensitivity to the GWB in $0.1 - 1$ Hz band, however, since the ORF of each polarization mode oscillates differently in the band, the mode separability is pretty good.

The SNR as a function of β is calculated with, in total, 54 correlation signals (AA', AB, AC, A'B, A'C, BC $\times 9$ links $= 54$). The result is shown in Fig. 2. At $\beta \sim 120^\circ$, the sensitivity degrades due to the symmetry of the detector configuration, in other words, some correlation signals are degenerated. As β approach 0° and 180°, the detector sensitivity peaks, since the clusters A and B (or C), and B and C are closely located, respectively. However, such a configuration considerably loses the angular resolution to point GW sources. Thus, an optimal angle would be $\beta = 60^\circ$, which leads to $h_0^2\Omega_{\rm gw}^T = 2.2 \times 10^{-14}$, $h_0^2\Omega_{\rm gw}^V = 1.1 \times 10^{-14}$, and $\xi h_0^2\Omega_{\rm gw}^S = 1.9 \times 10^{-14}$. These sensitivities should be compared with those when the polarization modes are not separated. For two clusters that are colocated and coaligned, e.g. clusters A and A', the sensitivity is $h_0^2\Omega_{\rm gw} = 7.1 \times 10^{-17}$. The mode separation degrades the sensitivity by a few hundred times. However, the important point here is that the non-Einsteinian-polarization search does not impair the cross-correlation sensitivity to a GWB with the colocated and coaligned clusters at all, though the mode is not separated.

4 Conclusion

The GW polarizations can be utilized as a novel and accurate test of gravity. We showed that the ground-based advanced interferometers and the proposed space-based detectors such as DECIGO and BBO can successfully separate and probe the GWB with the non-Einsteinian polarization modes. The GWB search with the GW detectors is complemental to the searches at much different frequencies: CMB and pulsar timing. If the non-Einstein polarizations would be detected, it implies that GR should be extended.

References

[1] C. M. Will, *Theory and experiment in gravitational physics*, Cambridge University Press (1993).

[2] C. M. Will, Living Rev. Relativity **9**, 3 (2006).

[3] D. M. Eardley, D. L. Lee. A. P. Lightman, R. V. Wagoner, and C. M. Will, Phys. Rev. Lett. **30**, 884 (1973).

[4] The LIGO Scientific Collaboration and The Virgo Collaboration, Nature **460**, 990 (2009).

[5] N. Christensen, Phys. Rev. D **46**, 5250 (1992);

[6] E. E. Flanagan, Phys. Rev. D **48**, 2389 (1993);

[7] B. Allen and J. D. Romano, Phys. Rev. D **59**, 102001 (1999);

[8] M. Maggiore, Phys. Rep. **331**, 283 (2000).

[9] A. Nishizawa, A. Taruya, K. Hayama, K. Kawamura, and M. Sakagami, Phys. Rev. D **79**, 082002 (2009).

[10] A. Nishizawa, A. Taruya, and S. Kawamura, arXiv:0911.0525 (2009).

[11] S. Sato *et al.*, Journal of Physics: Conference Series **154**, 012040 (2009).

Dynamical black holes from intersecting M-branes

Masato Nozawa[1(a)] and Kei-ichi Maeda[2(a),(b)]

[(a)] *Department of Physics, Waseda University, Okubo 3-4-1, Shinjuku, Tokyo 169-8555, Japan*
[(b)] *Waseda Research Institute for Science and Engineering, Okubo 3-4-1, Shinjuku, Tokyo 169-8555, Japan*

Abstract

We explore the global structures of a time-dependent, spherically symmetric solution derived by compactifying intersecting M-branes. The metric we study is an exact solution of Einstein-Maxwell-dilaton system, in which four Abelian gauge fields couple to the dilation with different coupling constants. We find that the spacetime is two-parameter family and describes a charged black hole which asymptotically tends to the Friedmann-Lemaître-Robertson-Walker (FLRW) universe filled by a stiff matter.

1 Introduction

Equilibrium black holes in an isolated system are of prime importance since they are the plausible final state of the gravitational collapse modulo the cosmic censorship conjecture. According to the celebrated theorem of Hawking [1], such a stationary black hole must possess a Killing horizon. Combining with this 'rigidity theorem,' it has been established that the Kerr(-Newman) family exhausts all (electro-)vacuum black holes [2]. Moreover, it turned out that the Killing horizon exhibits laws analogous to ordinary thermodynamics, implying a deep link between classical gravity, statistical mechanics and quantum laws. Over the past 15 years, it has been successful to account for the microscopic origin of a black hole entropy within the framework of string theory (see [3] and references therein). A central ingredient responsible for reproducing the Bekenstein-Hawking entropy is to recognize the supersymmetric–thus necessarily stationary–black hole as a solution derived from *intersecting branes* in various supergravities.

One can extend these studies further into the case where the brane involves a nontrivial space-and time-coordinate dependence, for which no supersymmetry is preserved. Recently, the authors of [4] have studied intersecting brane solutions in a dynamical setting and obtained, via compactification, a number of 4-dimensional solutions with wide potential applications. Among other things, their interesting finding is the 'cosmological black hole,' which may properly describe a black hole created in the primordial fluctuations of the universe.

When a black hole is immersed in an expanding universe, the background universe becomes inhomogeneous, and the black hole will evolve by swallowing ambient matters. Hence, despite a lack of uniqueness theorem and various kinds of solutions being expected, we have been unable to find a physically convincing exact black hole solution in an FLRW universe, on which the standard cosmologically evolutionary scenario is based. Even if the exact solution is usable, it is also a formidable task to extract causal structure and physical properties thereof, since the metric is dynamical and less symmetric than isolated one. In this article, we outline the strategy for obtaining the global structure of the solution found in [4] (a detailed analysis is presented in [5]). The analysis presented here will serve as a basis for considering uncharged black holes in a more realistic astrophysical context.

2 Spacetime structure of a black hole

The spacetime metric. The authors [4] have classified the possible time-dependent intersecting brane systems in 11-dimensional supergravity and presented some interesting solutions in lower dimensions by compactification. If all branes are static in the background Minkowski spacetime, a 4-dimensional regular

[1]Email address: nozawa@gravity.phys.waseda.ac.jp
[2]Email address: maeda@waseda.jp

black hole (extremal Reissner-Nordström solution) is produced by M2-M2-M5-M5 brane system (four brane charges) or from M2-M5-W-KK brane system (two brane charges plus a Brinkmann wave and a Kaluza-Klein monopole). If the branes are allowed to move in the background expanding (11-dimensional Kasner) universe, only one brane turns out to be mobile as a consistency of metric ansatz and the field equations. By toroidal compactification of M2-M2-M5-M5 brane, one arrives at the 4-dimensional metric,

$$\mathrm{d}s^2 = -\Xi \mathrm{d}t^2 + \frac{1}{\Xi}\left(\mathrm{d}r^2 + r^2 \mathrm{d}\Omega_2^2\right) , \tag{1}$$

where $\Xi = (H_T H_S H_{S'} H_{S''})^{-1/2}$, $H_T = (t/t_0) + \bar{H}_T$ and $\{\bar{H}_T, H_S, H_{S'}, H_{S''}\}$ are arbitrary harmonics on the three-dimensional Euclid space $\mathrm{d}r^2 + r^2 \mathrm{d}\Omega_2^2$. For the sake of simplicity, we focus our attention to the case in which all branes have monopole sources with equal charge Q (> 0), i.e.,

$$H_T = \frac{t}{t_0} + \frac{Q}{r} \quad (t_0 > 0) , \qquad H_S = H_{S'} = H_{S''} = 1 + \frac{Q}{r} . \tag{2}$$

Specifically, the 4-dimensional metric is spherically symmetric.

It is easy to recognize that the metric approaches to the flat FLRW universe filled by a stiff fluid in the limit of $r \to \infty$ with t being finite, while in the limit of $r \to 0$ with t being finite, the spacetime is approximated by an $\mathrm{AdS}_2 \times \mathrm{S}^2$ metric which is a typical 'near-horizon geometry' of an extremal black hole. The above naive estimate implies that there exist a spacelike big-bang singularity at $t = 0$ and a degenerate horizon at $r = 0$. However, it is too early to say that the metric describes a black hole in the expanding universe. Indeed, as it turns out, the foregoing deduced causal properties are not true.

Viewed from four-dimensional habitant, the metric (1) with (2) solves the field equations in Einstein-Maxwell-dilaton system,

$$S = \int \mathrm{d}^4x\sqrt{-g}\left[\frac{1}{2\kappa^2}\mathcal{R} - \frac{1}{2}(\nabla_\mu \Phi)(\nabla^\mu \Phi) - \frac{1}{16\pi}\sum_A e^{\lambda_A \kappa \Phi} F^{(A)}_{\mu\nu} F^{(A)\mu\nu}\right] , \tag{3}$$

where $A = \{T, S, S', S''\}$ denotes the brane configurations and λ_A's are the respective coupling constants. This system apparently satisfies the dominant energy condition. The dilaton and the electromagnetic fields $F^{(A)} = \mathrm{d}A^{(A)}$ are given by

$$\kappa\Phi = \frac{\sqrt{6}}{4}\ln\left(\frac{H_T}{H_S}\right) , \qquad \kappa A^{(T)} = \frac{\sqrt{2\pi}}{H_T}\mathrm{d}t , \qquad \kappa A^{(S)} = \frac{\sqrt{2\pi}}{H_S}\mathrm{d}t . \tag{4}$$

Although we will be concerned with the electrically charged case, the magnetically charged one is obtainable by a duality transformation $\Phi \to -\Phi$ and $F^{(A)} \to e^{\lambda_A \Phi} * F^{(A)}$. The dilaton field drives the cosmic expansion similar to the stiff fluid.

Singularities. The dilaton profile implies that the spacetime curvature singularities exist at $r = -Q$ and $t = t_s(r) := -Q/r$, where all curvature invariant quantities indeed blow up. At these singularities the areal radius $R := r\Xi^{-1/2}$ vanishes, so that they are central singularities. Hence, far from the central inhomogeneous regions, the spacetime does not admit curvature singularity and is well-behaved. We can show that these curvature singularities are timelike and 'strong' according to the definition of Tipler, i.e., the Ricci tensor component diverges as $R_{\mu\nu}k^\mu k^\nu \propto \lambda^{-2}$, where $k^\mu = (\partial/\partial\lambda)^\mu$ denotes an affinely parametrized null vector emanating from these singularities.

Trapping horizons. Since the black hole event horizon is defined by a boundary of the causal past of future null infinity [1], we are required in principle to know the entire future evolution of spacetime in order to identify the locus of event horizon. From the practical point of view, it is more advantageous to focus on the *trapped region*, on which 'outgoing' null rays have negative expansion due to the attractive force of a black hole. As is well known, the trapped region does not arise outside the event horizon, provided the outside of a black hole is well-behaved. Hayward generalized the concept of apparent horizon and introduced a class of *trapping horizons* [6]. One strength of the use of trapping horizons is just to encompass various types of horizons associated not only with black holes but also with white holes and cosmological ones.

Defining null vectors $l^{(\pm)}_\mu = \sqrt{\Xi/2}(-\nabla_\mu t \pm \Xi\nabla_\mu r)$ which are orthogonal to metric sphere, the expansions are given by $\theta_\pm = (g_{\mu\nu} + 2l^{(+)}_{(\mu}l^{(-)}_{\nu)})\nabla^\mu l^{(\pm)\nu}$ which vanishes at $t = t^{(\mp)}_{\rm TH}(r)$, where

$$t^{(\mp)}_{\rm TH}(r) := \frac{r^2}{2t_0(H_S+3)^2}\left[H_S^5 - 6t_0^2Q(H_S+3)r^{-3} \mp H_S^3\sqrt{H_S^4 + 4t_0^2Q(H_S+3)r^{-3}}\right], \tag{5}$$

corresponds to the trapping horizon. The region $t^{(-)}_{\rm TH} < t < t^{(+)}_{\rm TH}$ with $r > 0$ denotes a past trapped region of $\theta_+ > 0$ and $\theta_- > 0$ on which even ingoing null rays have positive expansion due to the cosmic expansion. For $(t_0/Q) \lesssim 5.44$, the trapping horizon $t^{(+)}_{\rm TH}$ is spacelike, as in the background FLRW universe. Whereas, the trapping horizon $t^{(-)}_{\rm TH}$ is always timelike and encompassing the timelike singularity $t = t_s(r)$ around which $\theta_+ < 0$ and $\theta_- > 0$. The $r < 0$ region can be inferred analogously. Just inside $r = 0$, the outgoing null rays have negative expansion $\theta_+ < 0$. Thus, the $r = 0$ surface is a likely candidate of a horizon.

It is then instructive to consider the limit $r \to 0$ of trapping horizons. One easily finds that $t^{(\pm)}_{\rm TH}r$ is finite and the areal radius R approaches to constant $R_\pm$ in this limit, where

$$R_\pm = Q\left(\frac{\sqrt{1+4\tau^2}\pm 1}{2\tau}\right)^{1/2}, \qquad \tau := \frac{t_0}{Q}. \tag{6}$$

These are the infinite redshift ($t \to \infty$) and blueshift ($t \to -\infty$) surfaces for an asymptotic observer. Equation (6) gives $Q = \sqrt{R_+R_-}$ and $\tau = R_+R_-/(R_+^2 - R_-^2)$. Hence, the charge Q sets the geometrical mean of horizon radii and their relative ratio is encoded in the parameter τ.

Event horizons. We have seen that the limit $r \to \infty$ with t being finite reduces to $\mathrm{AdS}_2\times\mathrm{S}^2$ geometry. However, this limit describes only the 'throat' and fails to approximate the whole portion of the three-dimensional null surface. Since the 'throat' corresponds to infinity, it is the only candidate of the crossing point of future and past horizons, which should be infinite redshift and blueshift surfaces $t \to \pm\infty$. In order to look into the structure of these null surfaces more closely, it is most convenient to take the *near-horizon limit*, defined by

$$t \to \frac{t}{\epsilon}, \qquad r \to \epsilon r, \qquad \epsilon \to 0, \tag{7}$$

which 'zoom-up' the neighbourhood of the candidate horizon ($r \to 0$ and $t \to \pm\infty$). Taking the near-horizon limit, the near-horizon metric is given by

$$\mathrm{d}s^2_{\rm NH} = -(r/Q)^2\left(1+\frac{tr}{t_0Q}\right)^{-1/2}\mathrm{d}t^2 + (r/Q)^{-2}\left(1+\frac{tr}{t_0Q}\right)^{1/2}\left(\mathrm{d}r^2 + r^2\mathrm{d}\Omega_2^2\right). \tag{8}$$

The dilaton and the electromagnetic fields have regular limits and still solve the field equations of the Einstein-Maxwell-dilaton system, validating that the near-horizon limit (7) is well-defined. Although the metric in this coordinates is time-dependent, it turns out that the near-horizon metric (8) admits a *hypersurface-orthogonal Killing field*

$$\xi^\mu = t\left(\frac{\partial}{\partial t}\right)^\mu - r\left(\frac{\partial}{\partial r}\right)^\mu, \tag{9}$$

as a consequence of a scaling limit (7). It then turns out that the near-horizon metric (8) is static. The norm of the vector ξ^μ vanishes at $R = R_\pm$ given by (6), which coincide with the trapping horizons in the $r \to 0$ limit taken. Thus, we conclude that the null surfaces $R = R_\pm$ in the original spacetime are locally isometric to the Killing horizons in the static spacetime (8). It is notable that the vector field ξ^μ does not solve the Killing equation in the original spacetime (1). Inspecting relations in equation (6), the horizon is never degenerate for finite τ.

We are now in a position to discuss the global spacetime structure. Combining numerical calculations of null geodesic equations, we can draw the conformal diagram (figure 1). It is shown that the solution (1) have a regular event horizon with constant radius R_+. Since the event horizon is described by a Killing horizon, the black hole fails to grow.

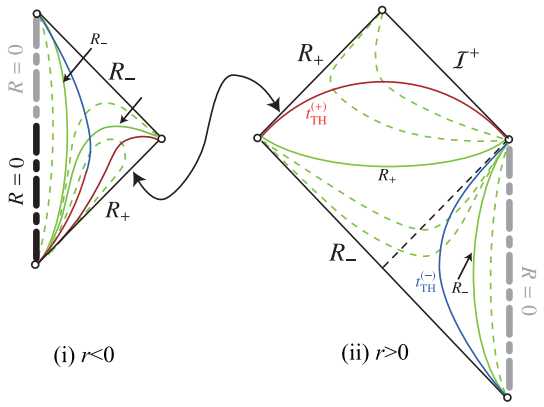

Figure 1: Conformal diagram of a black hole in an expanding universe. The green lines denote the R = constant surfaces, which change the signature across the trapping horizons. The central points $R = 0$ are the locally naked spacetime singularities.

3 Concluding Remarks

We have analyzed the spacetime structure of a time-dependent, spherically-symmetric solution obtained via dimensional reduction of the intersecting branes in 11-dimensional supergravity. We revealed that the spacetime describes a black hole immersed in an FLRW universe filled by a stiff fluid. Surprisingly, the solution admits a nondegenerate Killing horizon, so that the ambient matters fail to fall into the black hole. This distinguished property may be traced back to the fact that the overlapping brane configuration recovers supersymmetry in the static limit. The Killing symmetry of the horizon encourages us to discuss the black hole thermodynamics in an expanding universe. To proceed, we need an optimal definition of the black-hole mass, which is yet unavailable but an interesting open question.

In this article, we have focused on a spacetime that has identical monopole sources and approaches to the stiff-matter dominated expanding universe. The multi-center generalization is an interesting future work, since it plausibly describes the black-hole collision in a contracting universe. Furthermore, the authors in [7] found a more general solution–encompassing the present metric–that is asymptotically FLRW cosmos obeying arbitrary power-law expansion. The causal structure of this metric is under study.

References

[1] S. W. Hawking and G. F. R. Ellis, *"The large scale structure of space-time"* (Cambridge: Cambridge University Press, 1973).

[2] B. Carter, Black Hole Equilibrium States in Black Holes, edited by C. DeWitt and J. DeWitt (Gordon and Breach, New York, 1973).

[3] J. M. Maldacena, arXiv:hep-th/9607235.

[4] K. Maeda, N. Ohta and K. Uzawa, JHEP **0906** (2009) 051, arXiv:0903.5483 [hep-th].

[5] K. i. Maeda and M. Nozawa, arXiv:0912.2811 [hep-th].

[6] S. A. Hayward, Phys. Rev. D **49**, 6467 (1994).

[7] G. W. Gibbons and K. i. Maeda, arXiv:0912.2809 [gr-qc].

Assisted dark energy

Junko Ohashi[1] and Shinji Tsujikawa[2]

Department of Physics, Faculty of Science, Tokyo University of Science, 1-3 Kagurazaka, Shinjyuku-ku, Tokyo 162-8601, Japan

Abstract

We study cosmological dynamics of a multi-field system for a general Lagrangian density having scaling solutions. This allows the possibility that scaling radiation and matter eras are followed by a late-time cosmic acceleration through an assisted inflation mechanism. Using the bound coming from Big-Bang-Nucleosynthesis (BBN) and the condition under which each field cannot drive inflation as a single component of the universe, we find the following features: (i) a transient or eternal cosmic acceleration can be realized after the scaling matter era, (ii) a "thawing" property of assisting scalar fields is crucial to determine the evolution of the field equation of state w_ϕ, and (iii) the field equation of state today can be consistent with the observational bound w_ϕ in the presence of multiple scalar fields.

1 Introduction

The constantly accumulating observational data continue to confirm the existence of dark energy responsible for cosmic acceleration today. The cosmological constant, whose equation of state is $w = -1$, has been favored by the combined data analysis of supernovae Ia, cosmic microwave background, and baryon acoustic oscillations. Meanwhile, if the cosmological constant originates from a vacuum energy associated with particle physics, its energy scale is enormously larger than the observed value of dark energy ($\rho_{\rm DE} \approx 10^{-47}\,{\rm GeV}^4$). Hence it is important to pursue an alternative possibility to construct dark energy models consistent with particle physics.

Scalar-field models such as quintessence and k-essence have been proposed to alleviate the above problem. In particular cosmological scaling solutions are attractive to alleviate the energy scale problem of dark energy because the solutions enter the scaling regime even if the field energy density is initially comparable to the background fluid density. However the condition required for the existence of scaling solutions is incompatible with the condition for the existence of a late-time accelerated solution. Hence, in the single field case, the scaling solution cannot be followed by the scalar-field dominated solution responsible for dark energy. One of the ways to allow a transition from the scaling regime to the epoch of a late-time cosmic acceleration is to consider multiple scalar fields. For a general multi-field Lagrangian density having scaling solutions, we discuss how scaling radiation and matter eras are followed by an epoch of the late-time cosmic acceleration.

2 Dynamical system

Let us start with the following 4-dimentional action

$$S = \int d^4x\sqrt{-g}\left[\frac{R}{2} + p(\phi, X)\right] + S_f(\phi), \tag{1}$$

where R is a scalar curvature, p is a general function in terms of the field ϕ and a kinetic term $X = -g^{\mu\nu}\partial_\mu\phi\partial_\nu\phi/2$. S_f is an action for a background fluid which generally couples to the field ϕ. The existence of cosmological scaling solutions demands that the field energy density ρ_ϕ is proportional to the background fluid density ρ_f. Under this condition the Lagrangian density is restricted to take

[1]Email address: j1209610@ed.kagu.tus.ac.jp
[2]Email address: shinji@rs.kagu.tus.ac.jp

the following form with arbitrary function $g(Xe^{\lambda\phi})$ in the flat homogeneous and isotropic cosmological background [1, 2];

$$p(X,\phi) = Xg(Xe^{\lambda\phi})\,, \tag{2}$$

where λ is a constant. If we consider multiple scalar fields ϕ_i $(i = 1, 2, \cdots, n)$ with the Lagrangian density

$$p = \sum_{i=1}^{n} X_i g(X_i e^{\lambda_i \phi_i})\,, \tag{3}$$

the scaling solution can be followed by the accelerated scalar-field dominated point through the assisted inflation mechanism [3]. The multiple scalar fields evolve to give dynamics matching a single-field model with [3–5]

$$\frac{1}{\lambda_{\rm eff}^2} = \sum_{i=1}^{n} \frac{1}{\lambda_i^2}. \tag{4}$$

For the Lagrangian density (3) the dynamical field equations can cast into the form of autonomous equations [6]. In the following we study the case in which one of the fields (ϕ_1) has a large slope λ_1 to satisfy a BBN bound and other fields join the scalar-field dominated attractor at late times to give rise to cosmic acceleration. We have three fixed points relevant to radiation, matter, and accelerated epochs.

First of all, the field equation of state for the radiation-dominated scaling solution is $w_{\phi_1} = 1/3$. The constraint on the field density parameter Ω_{ϕ_1} coming from the BBN is

$$\Omega_{\phi_1} = 4p_{,X_1}/\lambda_1^2 \lesssim 0.045\,, \tag{5}$$

where $p_{,X_1} \equiv \partial p/\partial X_1$.

Second, the field equation of state for the matter-dominated scaling solution is $w_{\phi_1} = 0$. The field density parameter is

$$\Omega_{\phi} = 3p_{,X_1}/\lambda_1^2\,. \tag{6}$$

and then $\lambda_1^2 > 3p_{,X_1}$ is required [5].

Finally, in the case of the assisted field-dominated point, the field equation of state is

$$w_{\phi} = -1 + \lambda_{\rm eff}^2/3p_{,X}\,, \tag{7}$$

where $X = -g^{\mu\nu}\partial_\mu\phi\partial_\nu\phi/2$ is a kinetic energy of the effective single field ϕ. The fixed point can be responsible for the late-time acceleration for $\lambda_{\rm eff}^2 < 2p_{,X}$. Moreover, it is stable under the condition $\lambda_{\rm eff}^2 < 3p_{,X}$ [5].

3 Quintessence with multiple exponential potentials

We study multi-field cosmological dynamics for a quintessence model with exponential potentials [3]. This corresponds to the Lagrangian density $p_i = X_i - c_i e^{-\lambda_i\phi_i}$, i.e. the choice $g(X_i e^{-\lambda_i\phi_i}) = 1 - c_i/(X_i e^{\lambda_i\phi_i})$. Since $p_{,X_i} = 1$ in this model, the BBN bound and the condition for cosmic acceleration give

$$\lambda_1 > 9.42\,, \quad \text{and} \quad \lambda_{\rm eff} < \sqrt{2}\,, \tag{8}$$

respectively.

Let us consider two fields ϕ_1 and ϕ_2. In Fig. 1 we plot the evolution of the background fluid density $\rho_f = \rho_r + \rho_m$ (radiation + non-relativistic matter) and the field densities ρ_{ϕ_1}, ρ_{ϕ_2} versus the redshift z for $\lambda_1 = 10$ and $\lambda_2 = 1.5$. The cases (i), (ii), (iii) correspond to the simulations for three different initial conditions of ϕ_1. Figure 1 shows that the field ϕ_1 joins the scaling regime irrespective of initial conditions of ϕ_1. Finally the system enters the epoch in which the energy density ρ_{ϕ_2} of the second field ϕ_2 dominates the dynamics. Note that the second field density ρ_{ϕ_2} is almost frozen after the initial transient period.

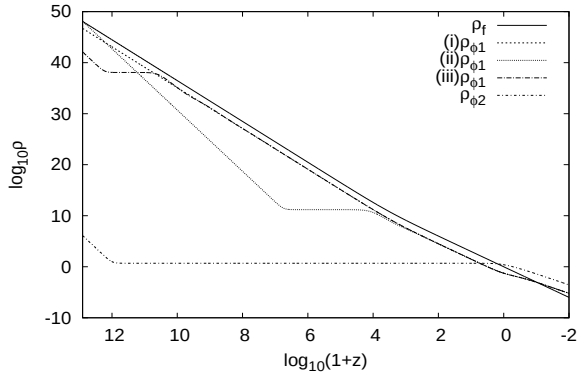

Figure 1: Example for the evolution of ρ_f, ρ_{ϕ_1}, ρ_{ϕ_2} for the qunitessence with two exponential potentials. We choose three different initial conditions for ϕ_1.

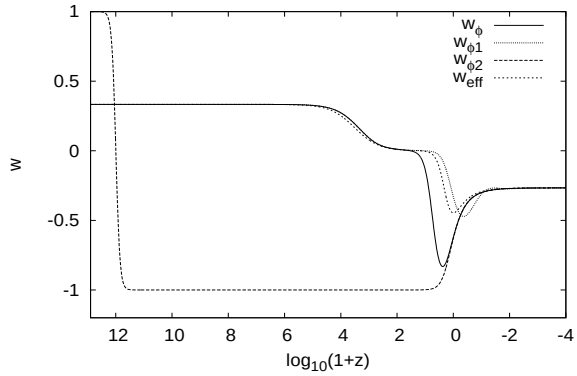

Figure 2: Example for the evolution of w_ϕ, w_{ϕ_1}, w_{ϕ_2}, and $w_{\rm eff}$ for the qunitessence with two exponential potentials.

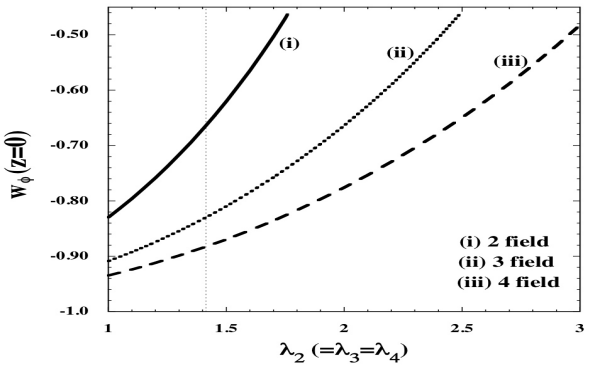

Figure 3: The equation of state w_ϕ today versus λ_i $(i \neq 1)$ for $\lambda_1 = 9.43$ in the multi-field quintessence with exponential potentials.

Figure 2 illustrates the variation of the equation of state with the same initial condition as in the case (i) of Fig. 1. Here w_ϕ and $w_{\rm eff}$ are defined by

$$w_\phi = \frac{w_{\phi_1}\Omega_{\phi_1} + w_{\phi_2}\Omega_{\phi_2}}{\Omega_{\phi_1} + \Omega_{\phi_2}}\,, \qquad w_{\rm eff} = -1 - \frac{2\dot{H}}{3H^2}\,, \tag{9}$$

where H is the Hubble expansion rate. Since $w_\phi = -0.27$ (attractor) and $w_\phi = -0.62$ $(z = 0)$ in this case, the transient acceleration occurs at the present epoch.

In Fig. 3 we show $w_\phi(z = 0)$ versus λ_i $(i \geq 2)$ for $\lambda_1 = 9.43$ in the presence of multiple scalar fields. This shows that, as we add more fields, we obtain smaller values of $w_\phi(z = 0)$. The observational bound $w_\phi(z = 0) < -0.8$ can be satisfied in the presence of more than two fields.

4 Multi-field dilatonic ghost condensate model

Next we proceed to the multi-field dilatonic ghost condensate model [1] with the Lagrangian density $p_i = -X_i + c_i e^{\lambda_i \phi_i} X_i^2$. This corresponds to the choice $g(X_i e^{\lambda_i \phi_i}) = -1 + c_i(X_i e^{\lambda_i \phi_i})$. In this model the BBN bound and the condition for cosmic acceleration translate into

$$\lambda_1 > 9.42\sqrt{2\tilde{Y}_1 - 1}\,, \qquad \lambda_{\rm eff} < \sqrt{6}/3\,, \tag{10}$$

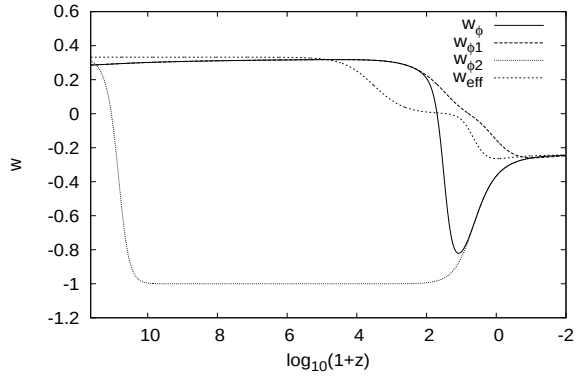

Figure 4: Example for the evolution of w_ϕ, w_{ϕ_1}, w_{ϕ_2}, and $w_{\rm eff}$ for $\lambda_1 = 40$ and $\lambda_2 = 1$ in the two-field dilatonic ghost condensate model.

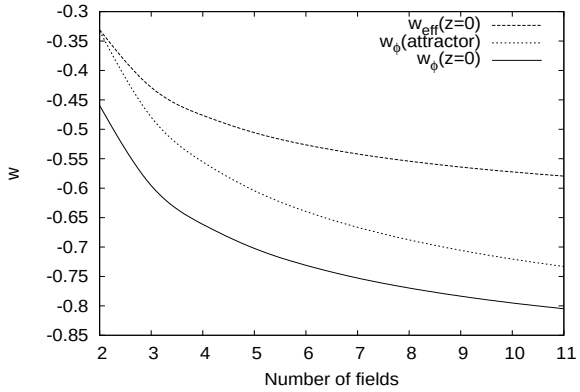

Figure 5: The equations of state versus the number n of scalar fields for $\lambda_1 = 40$ and $\lambda_i = 0.817$ $(i \geq 2)$ in the multi-field dilatonic ghost condensate model.

respectively (where $\tilde{Y}_1 = c_1 e^{\lambda_1 \phi_1} X_1$).

Figure 4 shows the evolution of the equations of state. In this model the scaling solution is absent during the radiation era (exists only in the limit $\tilde{Y}_1 \to \infty$), while it is present during the matter dominance. It takes some time for the solution to reach the scaling matter point characterized by $\tilde{Y}_1 = 1$. Hence, the period of the scaling matter era is very short. As in the case of multi-field quintessence with exponential potentials, w_ϕ first reaches a minimum and then starts to grow toward the assisted attractor. In Fig. 5 we plot $w_\phi(z = 0)$, $w_{\rm eff}(z = 0)$, and w_ϕ at the late-time attractor for $\lambda_1 = 40$ and $\lambda_i = 0.817$ $(i \geq 2)$. This shows that we require at least 10 scalar fields to realize the observational bound $w_\phi(z = 0) < -0.8$.

5 Conclusion

We have studied cosmological dynamics of assisted dark energy for the Lagrangian density (3) that possesses scaling solutions. In the presence of multiple scalar fields the scaling matter era can be followed by the phase of a late-time cosmic acceleration as long as more than one field join the assisted attractor. Since the effective slope $\lambda_{\rm eff}$ is smaller than the slope λ_i of each field, the presence of multiple scalar fields can give rise to cosmic acceleration even if none is able to do so individually. This is a nice feature from the viewpoint of particle physics because there are in general many scalar fields (dilaton, modulus, etc) with the slopes λ_i larger than the order of unity. For quintessence with exponential potentials and the multi-field dilatonic ghost condensate model, we have shown that a thawing property of assisting multiple scalar fields allows the field equation of state w_ϕ smaller than -0.8 today.

References

[1] F. Piazza and S. Tsujikawa, JCAP **0407**, 004 (2004).

[2] S. Tsujikawa and M. Sami, Phys. Lett. B **603**, 113 (2004).

[3] A. R. Liddle, A. Mazumdar and F. E. Schunck, Phys. Rev. D **58**, 061301 (1998).

[4] S. A. Kim, A. R. Liddle and S. Tsujikawa, Phys. Rev. D **72**, 043506 (2005).

[5] S. Tsujikawa, Phys. Rev. D **73**, 103504 (2006).

[6] J. Ohashi and S. Tsujikawa, Phys. Rev. D **80**, 103513 (2009).

The Riemannian Penrose inequality and a virtual gravitational collapse

Seiju Ohashi[1](a),(b), Tetsuya Shiromizu[2](b), and Sumio Yamada[3](c)

(a) *Department of Physics, Tokyo Institute of Technology, Tokyo 152-8551, Japan*
(b) *Department of Physics, Kyoto University, Kyoto 606-8502, Japan*
(c) *Mathematical Institute, Tohoku University, Sendai 980-8578, Japan*

Abstract

We reinterpret the proof of the Riemannian Penrose inequality by H. Bray. The modified argument turns out to have a nice feature so that the flow of Riemannian metrics appearing Bray's proof gives a Lorentzian metric of a spacetime. We also discuss a possible extension of our approach to charged black holes.

1 Introduction

The issue of cosmic censorship is still an unsolved problem. Closely related to this, Penrose proposed the following inequality for the black hole [1]

$$\sqrt{A/16\pi} \leq m, \tag{1}$$

where A is the area of the horizon and m is the ADM mass for an asymptotically flat spacetime. This inequality is also yet to be proved and remains an important problem.

In a Riemannian/time-symmetric space, Huisken and Ilmanen proved this inequality where the area A is that of a single black hole by using the inverse mean curvature flow [2]. At almost the same time, Bray proved it for multi black holes using a conformal flow method [3]. For the general, non-time-symmetric case, the Penrose inequality is still an open question.

As we review in the next section, Bray's proof is a bit of a mystery. This is because it is difficult to have a physical reasoning why the proof works. In this paper, we introduce a normalised conformal flow and then we regard it as a model of the time evolution, formulating a Lorentzian metric. As a result, we have a rather natural interpretation of Bray's proof. We also discuss some implications of our line of reasoning to the charged black hole case [4].

2 Brief sketch of Bray's proof

We consider a time-symmetric initial data (Σ, q_0) where q_0 is a Riemannian metric. The time-symmetric initial data is defined by a hypersurface in a spacetime with the zero extrinsic curvature. We suppose that the apparent horizons H_0 exist in the spacetime. It is known that the apparent horizon corresponds to the minimal surface in (Σ, q_0).

We introduce the following conformal transformation

$$q_t = u_t^4 q_0 \tag{2}$$

and define v_t as the "time" derivative of u_t ,$v_t = \dot{u}_t$, where dot stands for the derivative with respect to the parameter t. We then require that v_t is a harmonic function with respect to q_0

$$\Delta_{q_0} v_t = 0 \tag{3}$$

[1]Email address: ohashi@th.phys.titech.ac.jp
[2]Email address: shiromizu@tap.scphys.kyoto-u.ac.jp
[3]Email address: yamada@math.tohoku.ac.jp

with the boundary condition

$$v_t(x)|_{H_t} = 0 \quad , \quad v_t \to -e^{-t} \quad \text{as} \quad r \to \infty. \tag{4}$$

We require that H_t is the minimal surface in (Σ, q_t). From the definition of v_t, we have

$$u_t = 1 + \int_0^t v_s(x) ds \to e^{-t} \quad (\text{as } r \to \infty). \tag{5}$$

Now we have a conformal flow defined by the sequence of (Σ, q_t, H_t).

In this conformal flow, we can show that $\dot{A}_t = 0$ and $\dot{m}_t \leq 0$. Here A_t is the area of H_t and m_t is the ADM mass for (Σ, q_t). When we show $\dot{m}_t \leq 0$, an idea of Bunting and Masood-ul-Alam [5] was used in a crucial way. From these we have $A_\infty = A_0$ and $m_\infty \leq m_0$.

In the limit of $t = \infty$, we can also show that (Σ, q_t) becomes the Schwarzschild slice. Therefore $\sqrt{A_\infty/16\pi} = m_\infty$ holds. Thus,

$$\sqrt{A_0/16\pi} = \sqrt{A_\infty/16\pi} = m_\infty \leq m_0 \tag{6}$$

is proven. This is the Riemannian Penrose inequality.

It is difficult to see why this proof works. So we will modify the proof which is just a reformulation of the conformal flow. Although the new argument requires rather minor technical modifications from Bray's one, we gain a new insight, which in turn offers a physical interpretation to the conformal flow.

3 Normalized conformal flow

Let us introduce the following conformal transformation

$$\tilde{q}_t = \tilde{u}_t^4 q_0, \tag{7}$$

where $\tilde{u}_t$ is defined by $\tilde{u}_t = \left(\dfrac{m_0}{m_t}\right)^{1/2} u_t$. u_t is the same with the previous one in Eq. (2). Now we have a new flow $(\Sigma, \tilde{q}_t, H_t)$. Note that the surface H_t remains minimal after the dilation of the metric. It is easy to show $\dot{\tilde{m}}_t = 0$. In addition, it is easy to show $\dot{\tilde{A}}_t \geq 0$.

We can show that the space becomes the Schwarzschild slice in the $t = \infty$ limit as well as the case of the conformal flow. Thus, $16\pi\tilde{m}_\infty^2 = \tilde{A}_\infty$ holds. Finally we can show the Riemannian Penrose inequality again as

$$16\pi m_0^2 = 16\pi\tilde{m}_\infty^2 = \tilde{A}_\infty \geq A_0. \tag{8}$$

Namely over this normalized conformal flow, the ADM mass is conserved and the area of the apparent horizon is increasing. The former corresponds to the well-known fact that the ADM mass is a conserved quantity in asymptotically flat spacetimes. The latter corresponds to the area theorem of black holes (See Ref. [6] for the area theorem of apparent horizon). These features offers a nice physical interpretation of the normalized conformal flow. In the next section, we will look at this context more closely.

4 Physical Interpretation

From now on, we will regard the normalised conformal flow as a time evolution. We suppose that the time evolution is given by

$$\begin{aligned} ds^2 &= g_{\mu\nu} dx^\mu dx^\nu = -\alpha^2(t,x) dt^2 + \tilde{q}_t \\ &= -\alpha^2(t,x) dt^2 + \tilde{q}_{tij} dx^i dx^j, \end{aligned} \tag{9}$$

where α is the lapse function and $\tilde{q}_{tij}$ is the component of $\tilde{q}_t$. In this case the extrinsic curvature of $t =$const. hypersurfaces becomes

$$K_{ij} = \frac{1}{2\alpha} \partial_t \tilde{q}_{tij} = 2 \frac{\dot{\tilde{u}}_t}{\alpha \tilde{u}_t} \tilde{q}_{tij}. \tag{10}$$

Then it turns out that the expansion rate θ of the outgoing null geodesic congruence on H_t is non-negative

$$\theta|_{H_t} \propto (k + K - K_{ij}r^i r^j)|_{H_t} = -2\frac{\dot{m}_t}{\alpha m_t} \geq 0. \tag{11}$$

where r^μ is the unit normal vector to H_t in $(\Sigma, \tilde{q}_t)$. This is because of $\dot{m}_t \leq 0$. Here k is the trace of extrinsic curvature of H_t with respect to $\tilde{q}_t$ and $K = K^i_i$. Thus H_t is located outside an apparent horizon/marginally trapped surface in a virtual spacetime (M, g).

In the time evolution of H_t, we can see that H_t approaches to the apparent horizon

$$\theta|_{H_t} \propto -2\dot{m}_t/m_t \to 0, \tag{12}$$

because we know that the final state at $t = \infty$ is Schwarzschild slice, the convergence implies $\dot{m}_t \to 0$ as $t \to \infty$.

Let us suppose that (M, g) satisfies the four dimensional Einstein equation

$$R_{\mu\nu} - \frac{1}{2}g_{\mu\nu}R = 8\pi T_{\mu\nu}, \tag{13}$$

where $R_{\mu\nu}$ and R are the Ricci curvature and scalar curvature of g. Here we do not yet have the above equation determining the virtual spacetime. The stress tensor $T_{\mu\nu}$ needs to be chosen so that the above equation is satisfied.

To do so, let us focus on the Hamiltonian and momentum constraints,

$$^t\tilde{R} + K^2 - K_{ij}K^{ij} = 16\pi\rho \tag{14}$$

$$\tilde{D}^i K_{ij} - \tilde{D}_j K = -8\pi J_j, \tag{15}$$

where $\rho = T_{\mu\nu}t^\mu t^\nu$, $J_i = T_{\mu i}t^\mu$. $^t\tilde{R}$ and $\tilde{D}_i$ are the Ricci scalar the covariant derivative with respect to $\tilde{q}_t$, respectively. From the Hamiltonian constraint, we can calculate ρ

$$16\pi\rho = 16\pi\Big(\frac{m_t}{m_0}\Big)^2 u_t^{-4}\rho_0 + 24\frac{1}{\alpha^2}\Big(\frac{\dot{\tilde{u}}_t}{\tilde{u}_t}\Big)^2 \geq 0. \tag{16}$$

In the above we used $^0\tilde{R} = 16\pi\rho_0$, where ρ_0 is the energy density of real matters in the physical initial data. Note that ρ_0 is not one computed from virtual matters $T_{\mu\nu}$ here. Then we see that ρ comes out to be non-negative. This is a nice feature in the physical sense.

Next we can calculate J_i on H_t and the result is

$$2\pi J_i|_{H_t} = \partial_i v_t/(\alpha u_t)|_{H_t}. \tag{17}$$

Since $v_t(x)$ is the harmonic function, the maximum principle tells us $\partial_i v_t \leq 0$ outward direction of H_t. More precisely, if one introduces the outward normal vector r^i of H_t in $t =$const. slices, $r^i\partial_i v_t \leq 0$. Thus we can see the ingoing energy flux of artificial matters, that is, $r^i J_i \leq 0$.

As a consequence, we have the following physical picture for the normalised conformal flow. The virtual time evolution corresponds to the gravitational collapse. From the behavior of virtual matters characterized by $T_{\mu\nu}$, the 3-dimensional hypersurface $\cup_t H_t$ looks like a horizon. Moreover, the area of H_t is increasing with time. We recall in Bray's construction that the topological type of the surface H_t may change, as the surface may jump across some singular times. And H_t approaches to the horizon because the expansion rate of null congruence on H_t is decaying to zero at $t = \infty$. Thus, the normalized conformal flow gives us a virtual gravitational collapse. Since the final state is promised to be Schwarzschild slice in this evolution, it is natural to have the Penrose inequality. If we know that the final state is Schwarzschild slice, the area theorem implies the Penrose inequality.

5 Implication to charged black holes

Although our new proof is just a rearrangement of Bray's proof, there is a possibility to apply it to other issues. For example, one may want to address the Penrose inequality for charged black holes. According

to Ref. [7], Bray's argument is hoped to be generalized so that

$$m_0 \geq m_\infty = \frac{1}{2}\Big(R + \frac{Q^2}{R}\Big) \tag{18}$$

holds where Q is the charge of black holes. The Reissner-Nordström slice realizes the equality. Introducing the area radius by $R = \sqrt{A_0/4\pi} = \sqrt{A_\infty/4\pi}$, the above is rewritten by

$$m_0 - \sqrt{m_0^2 - Q_0^2} \leq R \leq m_0 + \sqrt{m_0^2 - Q_0^2}. \tag{19}$$

However, in Ref. [7], a counterexample to the lower bound was constructed. Because of the evidence, it is unlikely that Bray's proof works for charged black holes in the way presented above.

On the other hand, we may expect that the upper bound for the area radius holds. Namely we hope to show that the inequality

$$4\pi\Big(m_0 + \sqrt{m_0^2 - Q_0^2}\Big)^2 = A_\infty \geq A_0 = 4\pi R^2 \tag{20}$$

(that is $m_0 + \sqrt{m_0^2 - Q_0^2} \geq R$) holds. The lesson to be learned from the counterexample is that in Bray's original flow, the area radius was fixed while the mass was decreased via the flow, though physically the area should be increased till it reaches the maximal value set by the fixed mass. This is what we have done with the normalization. So with charge in play, we may hope to prove with m and Q fixed, the area can be increased till it reaches that of Reissner-Nordström's specified by the parameters (m_0, Q_0).

6 Summary

In this article, we proposed a proof of the Riemannian Penrose inequality which is a modification of Bray's proof (Ref.[3].) In the original proof by Bray, a conformal flow of the Riemannian metrics was employed, so that the mass is decreasing while the area of the horizon is fixed. However, it is difficult to see the physical reason why the proof works. Hence we proposed a dual viewpoint by normalizing the conformal flow. It is a family of conformal transformations so that now the mass is fixed while the area is increasing. Then we observed that the behaviors of the dual flow enjoy some plausible physical features, that is, the normalised conformal flow corresponds to a virtual time evolution of gravitational collapse, satisfying a non-vacuum Einstein equation. In addition, our new approach may shed some new light to prove the following Penrose type inequality for charged black holes.

$$4\pi\Big(m_0 + \sqrt{m_0^2 - Q_0^2}\Big)^2 \geq A_0, \tag{21}$$

which is consistent with a picture (Ref.[8]) resulting from the cosmic censorship as well as the so-called no-hair theorem where an evolving black hole is expected to settle down to a Kerr(-Newman) spacetime with the parameters (m_0, Q_0) specified by the initial slice. This is left for future study.

References

[1] For example, H. L. Bray and P. T. Chrusciel, arXiv:gr-qc/0312047.

[2] G. Huisken and T. Ilmanen, J. Deff. Geo. **59**, 353(2001).

[3] H. L. Bray, J. Diff. Geo. **59**, 177(2001)[arXiv:math/9911173]; arXiv:0902.3241.

[4] S. Ohashi, T. Shiromizu and S. Yamada, Phys. Rev. D **80**, 047501 (2009)[arXiv:0906.2042 [gr-qc]].

[5] G. Bunting and A. Masood-ul-Alam, Gen. Rel. Grav. **19**, 147(1987).

[6] S. A. Hayward, Phys. Rev. D **49**, 6467 (1994).

[7] G. Weinstein and S. Yamada, Comm. Math. Phys. **257**, 703(2005).

[8] R. Penrose, *Unsolved Problems in General Relativity*, Ann. Math. Study **102**, 663(1982).

Entanglement between two points separated by the sound horizon scale in the inflationary universe

Yuji Ohsumi[1] and Yasusada Nambu[2]

Department of Physics, Graduate School of Science
Nagoya University, Chikusa, Nagoya 464-8602, Japan

Abstract

Entanglement is the purely quantum correlation and does not exist in the classical mechanics. It is considered that the quantum fluctuations of a field which occur in the inflationary era become classical by the effect of the accelerated expansion, so their entanglement must disappear in this stage. We investigated the entanglement for a coarse-grained scalar field in 2 neighboring regions on the expanding spacetime [1]. As the result, it is indicated that the entanglement disappears when the distance between the 2 points exceeds the sound horizon. In this presentation, we discuss the relation between the entanglement of the field and the scale of sound horizon.

1 Introduction

According to inflation scenario, the large scale structure in the universe arose from the quantum fluctuation of a field during the inflation. While this fluctuation is quantum variable, cosmological perturbations are treated as classical stochastic variables in the theory of structure formation [2, 3]. Here, we say that variables are classical stochastic variables if their statistical quantities are given by normalized positive definite distribution functions. We call such distribution functions as classical distribution functions. Bell's theorem claims that if the system has a quantum correlation, entanglement, there exist some correlation which cannot be represented by a classical distribution [4, 5]. Hence it is necessary that the entanglement of the field disappears in order for the behavior of the field to be described using the classical distribution. Our main goal is to express the condition of it in the context of cosmology.

We have considered a minimally coupling test scalar field on the FRW spacetime undergoing an accelerated expansion, and investigated the entanglement in the field. It is well known that in such a model, the frequencies of the Fourier modes with the wave length longer than some scale become 0 and that the oscillations of the modes are frozen. In general, this scale does not coincide with the Hubble horizon scale and depends on the expansion law of the background spacetime or the mass parameter of the field. Let us call such a scale that the frequencies of the modes become 0 sound horizon scale[3].

In our previous calculation, we chose two neighboring degrees of freedom from the coarse-grained scalar field and investigated the entanglement between them. We treated a massless scalar field on the power model ($a = t^p$ with $p > 1$) and a massive scalar field on the de Sitter field ($a = \exp Ht$. $H = \text{const.}$: Hubble parameter). As coarse-graining, we inserted the ultraviolet and infrared cutoff. Our result indicated that the entanglement disappears when the physical distance between the two points becomes the sound horizon scale [1]. Let us call it "sound horizon crossing" that the physical distance between the 2 points exceeds the sound horizon. In this argument, we investigate the relation between the scale on which the entanglement disappears and the sound horizon scale for the massive scalar field on the de Sitter spacetime in the special case in which the physical distance r between the 2 points saticefies $r \lesssim 1/H$. As a result, we find that the entanglement disappears after the sound horizon crossing. Except in the next section, we use the units such that $\hbar = c = 1$.

[1]Email address: osumi@gravity.phys.nagoya-u.ac.jp
[2]Email address: nambu@gravity.phys.nagoya-u.ac.jp

[3]This "sound horizon scale" is different from the sound horizon scale defined by using the sound velocity, $c_s := \sqrt{dP/d\rho}$, of the matter field. (P: the pressure, ρ: the mass-energy density)

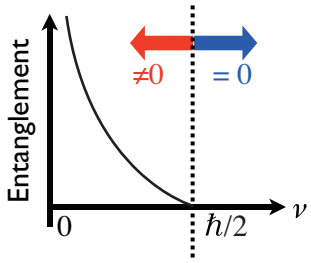

Figure 1: Degree of entanglement vs. symplectic eigenbvalue ν of the partially transposed covariance matrix of the system. The smaller ν is, the stronger the entanglement becomes.

2 Entangelment

Let us consider a bipartite system consisting of the subsystems X and Y. If the state of the total system $|\Psi\rangle$ can be written in the direct product of the states of X and Y, we say that the system is separable:

$$|\Psi\rangle = |\psi\rangle_{\mathrm{X}}|\phi\rangle_{\mathrm{Y}}. \tag{1}$$

Conversely, if the state of the total system cannot be written in such a form, we call the state is entangled. For a bipartite canonical system in a Gaussian state, we can estimate the degree of entanglement by using the following method. Let us denote the canonical variables as (q, p) and (Q, P) with $[q, p] = [Q, P] = i\hbar$ and (other) $= 0$. Then, we define the covariance matrices A, A', B, V of the system as

$$A = \begin{pmatrix} \langle\{\Delta q,\ \Delta q\}\rangle & \langle\{\Delta q,\ \Delta p\}\rangle \\ \langle\{\Delta p,\ \Delta q\}\rangle & \langle\{\Delta p,\ \Delta p\}\rangle \end{pmatrix} \qquad A' = \begin{pmatrix} \langle\{\Delta Q,\ \Delta Q\}\rangle & \langle\{\Delta Q,\ \Delta P\}\rangle \\ \langle\{\Delta P,\ \Delta Q\}\rangle & \langle\{\Delta P,\ \Delta P\}\rangle \end{pmatrix} \tag{2}$$

$$B = \begin{pmatrix} \langle\{\Delta q,\ \Delta Q\}\rangle & \langle\{\Delta q,\ \Delta P\}\rangle \\ \langle\{\Delta p,\ \Delta Q\}\rangle & \langle\{\Delta p,\ \Delta P\}\rangle \end{pmatrix} \qquad V = \begin{pmatrix} A & B \\ B^T & A' \end{pmatrix}, \tag{3}$$

where $\Delta x := x - \langle x\rangle$ and $\{x, y\} := (xy + yx)/2$. For the simplicity, we assume that $A = A'$ and $B = B^T$. In our model, the scalar field saticefies these conditions. The degree of entanglement, ν, is defined as

$$\nu := \sqrt{\det A - \det B - \sqrt{(\det A - \det B)^2 - \det V}}. \tag{4}$$

The system is entangled iff $\nu < \hbar/2$ (Fig. 1).

3 Model

We consider a minimally coupling massive test scalar field on the de Sitter spacetime.

$$ds^2 = -dt^2 + e^{2Ht}d\vec{x}^2 \qquad S = \int \frac{1}{2}(-\partial_\mu\phi\partial^\mu\phi - m^2\phi^2)\sqrt{-g}dx^4, \tag{5}$$

where t is the cosmic time and H is the Hubble parameter. Introducing the conformal time $\eta := \int 1/adt$ and the conformal variable $\chi := a\phi$, we can write down the general solution of the field as follows:

$$\chi = \frac{1}{(2\pi)^{3/2}}\int \left(a_{\vec{k}}\varphi_k e^{i\vec{k}\cdot\vec{x}} + \text{h.c.}\right)dk^3 \qquad \varphi_k = \sqrt{-\eta}H_\alpha^{(1)}(-k\eta). \tag{6}$$

We assume that the field is in the Bunch-Davies vacuum state, i.e., $a_{\vec{k}}|0\rangle = 0$.

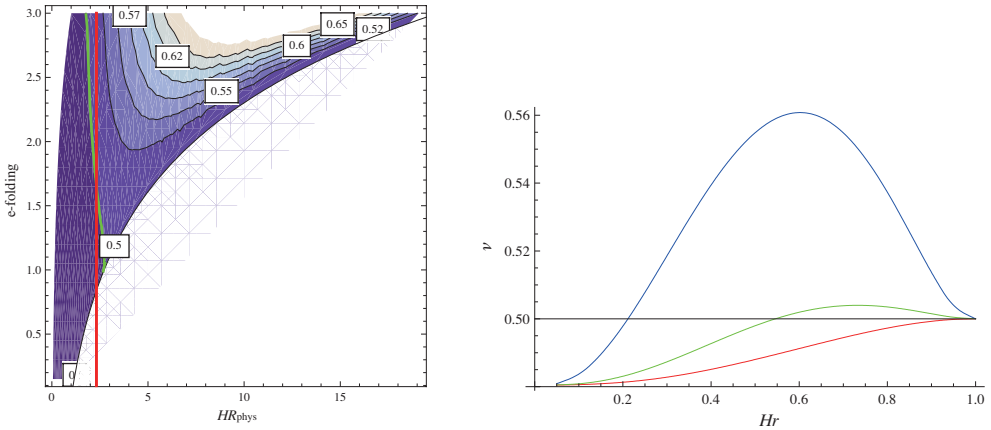

Figure 2: Spece and time dependence of the degree of entanglement ν between the two points. (a) The contour plot of ν. The horizontal axis is the physical distance $HR_{\rm phys}$; the vertical axis is the e-folding number. The thick red line represents the sound horizon. (b) The degree of entanglement ν vs. the comoving distance Hr at fixed times. The time evolves in the order of red, green and blue lines.

To the next, we introduce the coarse-grained field:

$$\tilde{\chi} := \frac{1}{(2\pi)^{3/2}}\sqrt{\frac{3(2\pi)^2}{k_c^3-k_0^3}}\int \theta(k_c-k)\theta(k-k_0)\big(a(\vec{k})\varphi_k(\eta)e^{i\vec{k}\cdot\vec{x}}+\text{h.c.}\big)dk^3 \tag{7}$$

$$\tilde{\pi} := \frac{1}{(2\pi)^{3/2}}\sqrt{\frac{3(2\pi)^2}{k_c^3-k_0^3}}\int \theta(k_c-k)\theta(k-k_0)\big(a(\vec{k})\varphi_k'(\eta)e^{i\vec{k}\cdot\vec{x}}+\text{h.c.}\big)dk^3, \tag{8}$$

where $k_c = \pi\varepsilon aH, k_0 = \pi H$ and $\varepsilon > 0$. We inserted the factor $\sqrt{3(2\pi)^2/(k_c^3-k_0^3)}$ in order for the commutation relation $[\tilde{\chi}(\vec{x}),\tilde{\pi}(\vec{x})]$ to be i. Indeed, the equal time commutation relation is

$$[\tilde{\chi}(\vec{x},\eta),\tilde{\pi}(\vec{y},\eta)] = \frac{3i}{k_c^3-k_0^3}\int_{k_0}^{k_c} k^2\frac{\sin kr}{kr}dk \qquad\qquad r := |\vec{x}-\vec{y}|, \tag{9}$$

and RHS becomes i in the limit of $r \to 0$.

Let us regard the set of the field variables $(\tilde{\chi}(\vec{x}),\tilde{\pi}(\vec{x})),(\tilde{\chi}(\vec{y}),\tilde{\pi}(\vec{y}))$ for spatial two points $\vec{x},\vec{y}$ as a bipartite system. Since the degree of entanglement introduced in the last section is available only when the variable of the two bodies commute, the coordinate $\tilde{\chi}(\vec{x})$ and the momentum $\tilde{\pi}(\vec{y})$ must commute. Hence the distance between these points r and the ultraviolet cutoff k_c saticefy the condition

$$k_0 r\cos k_0 r - \sin k_0 r = k_c r\cos k_c r - \sin k_c r. \tag{10}$$

As $k_0 = \pi H = \text{const.}$, r depends only on k_c. Since sign and cosign are periodic funcions, r takes discrete values. Hence, if k_c is fixed, we cannot calculate the entanglement for any distance between the 2 points. To make it possible, we choose the minimum value not equal zero from the discrete values of r. This corresponds to that we choose the neighboring two regions from the coarse-grained regions. Then, since there exists one-to-one correspondence between r and k_c, and we can regard k_c as a function of r conversely. This corresponds to that we change the coarse-graining scale for any given r.

Fig. 2 - (a) is the space and time dependence of the degree of entanglement ν between the two points for $m/H = 0.2$. The horizontal axis is the physical distance $R_{\rm phys} := ar$ between the two points and the vertical axis is the e-folding number. The thick red line represents the sound horizon scale. As the system is separable if $\nu > 1/2$, we can see that the entanglement disappears near the sound horizon.

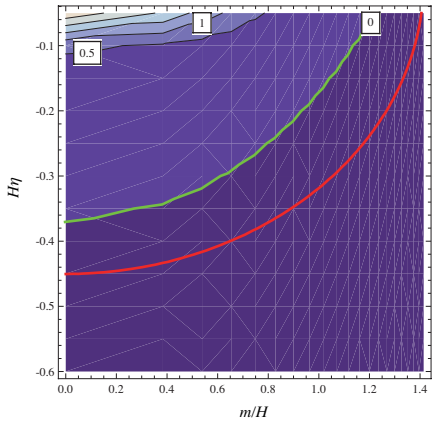

Figure 3: The plot of the second order coefficient of ν. The system is separable in the upper region of the thick green curve. The thick red curve represents the time of the sound horizon crossing.

Let us investigate analytically the relation between the separability and the sound horizon scale. Mathematically, the problem is to solve the equation $\nu = 1/2$ for the time for given k_c. However, this equation is very complex, so we must employ some approximation to deal with this equation analytically. Fig. 2 - (b) is the space dependence of ν in comoving scale at fixed time. The time evolves in the order of red, green and blue. We can see that $\nu = 1/2$ for any time at $Hr = 1$. Hence, expanding ν around $Hr = 1$, its 0th order is the constant $1/2$, and we can expect that the equation becomes easy to solve. As $Hr = 1$ corresponds to $k_c = k_0 = \pi H$, we expand ν around $k_c = k_0$:

$$\nu \sim \frac{1}{2} + \frac{1}{2}\frac{\partial^2 \nu}{\partial k_c^2}\bigg|_{k_c=k_0} (k_c - k_0)^2 + \mathcal{O}(k_c - k_0)^3. \tag{11}$$

Since $k_c \neq k_0$, the solution of the equation is $\partial^2\nu/\partial k_c^2|_{k_c=k_0} = 0$. Thus, the problem is reduced to solve this equation for the time. However, this equation is also very complex and cannot be solved analytically. Therefore, we estimate LHS numerically. The result is Fig. 3. The horizontal axis is the mass of the field m/H and the vertical axis is the conformal time $H\eta$. The thick red line represents the time of the sound horizon crossing and is given by $\pi^2 H^2\eta^2 + m^2/H^2 = 2$. We can see that the entanglement disappears after the sound horizon crossing for any m/H. Futhermore, the form of the curve of the sound horizon crossing and that of the separability are qualitatively the same. Therefore, we can think that the time when the entanglement disappears is determined by the time of the sound horizon crossing.

Acknowledgments

This research was supported by the Grant-in-Aid for Nagoya University Global COE Program, "Quest for Fundamental Principles in the Universe: from Particles to the Solar System and the Cosmos", from the Ministry of Education, Culture, Sports, Science and Technology of Japan.

References

[1] Y. Nambu and Y. Ohsumi, Phys. Rev. D **80**, 124031 (2009).

[2] A. H. Guth and S. Y. Pi, Phys. Rev. D **32**, 1899 (1985)

[3] D. V. Polarski and A. A. Starobinsky, Class. Quantum Phys. **13**, 377 (1996)

[4] J. S. Bell, *Speakable and Unspeakable in Quantum Mechanics*, Cambridge University Press (1987)

[5] E. G. Cavalcanti, C. J. Foster, M. D. Reid, P. D. Drummond, Phys. Rev. Lett. **99**, 210405 (2007)

Gravitational self-force effect on the periastron shift in Schwarzschild spacetime

Norichika Sago[1](a) and Leor Barack(b)

(a) *Yukawa Institute for Theoretical Physics, Kyoto University, Kyoto 606-8502*
(b) *School of Mathematics, University of Southampton, Southampton, SO17 1BJ, United Kingdom*

Abstract

Recently we developed a time-domain code to calculate the gravitational self-force on a point particle moving around a Schwarzschild black hole. To know how the force affects the particle's motion, it is useful to estimate the self-force correction of some characteristic variables of the orbits (e.g. ISCO frequency, periastron shift). In this work, we focus on the self-force effect on the periastron shift and investigate how to evaluate the correction from the numerical results of the self-force with our time-domain code.

1 Introduction

The problem of the motion of a point particle in black hole spacetime is one of the fundamental issues in general relativity, which recently has been studied well, motivated by the requirement of a bank of gravitational wave templates for the gravitational wave observation. To predict the motion acculately, we need to calculate the *self-force* (or back-reaction force) exerted on the particle and incorporate it to the equation of motion correctly. A breakthrough in the self-force problem has been made by Mino, Sasaki and Tanaka [1] and Quinn and Wald [2], since then a lot of effort to devise a practical method of calculating the self-force based on their works has been done. The "mode-sum scheme" [3] is considered as a promising way to derive the self-force. This scheme is based on multipole decomposition of the retarded field, and relies on standard methods of black hole perturbation theory. This has since been implemented by various authors on a case-by case basis (See [4] for a review of the recent progress in this issue).

At the early stage, the self-force of scalar-field toy model, instead of the gravitational self-force, was mainly investigated and proved that the mode-sum scheme does work well. In extending the analysis from the scalar-field case to the gravitational case, we face the difficulty associated with the gauge dependence of the gravitational self-force. The gravitational perturbation in the vicinity of the point particle, which is required to derive the self-force, is best described using the *Lorenz* gauge, which preserves the local isotropic nature of the point singularity. Therefore, the mode-sum scheme is originally constructed under the Lorenz gauge condition. On the other hand, the field equations that govern the global evolution of the metric perturbation are more tractable in gauges which comply well with the global symmetry of the black hole background, like the Regge-Wheeler gauge [5] for the Schwarzschild geometry or the "radiation" gauges [6] for the Kerr geometry. Now, in calculating the local self-force we need, essentially, to subtract a suitable local, divergent piece of the perturbation from the full (retarded) perturbation field. In doing so, both fields (local and global) must be given in the same gauge; the "gauge problem" arises since the two fields are normally calculated in different gauges.

There are two strategies to settle the problem. One is that we derive the equation of motion in a convenient gauge for calculating the metric perturbation [7, 8]. This idea is based on the work by Detweiler and Whiting [9], in which the motion is depicted as the geodesic of a smooth perturbed spacetime. Another one, which we adopt here, is that we solve the perturbation equations directly in the Lorenz gauge. The calculation is therefore done entirely within the Lorenz gauge, the mode-sum scheme is implemented in a straightforward way. This "all-Lorenz-gauge" strategy is made possible (at least for the Schwarzschild case) following a recent work by Barack and Lousto [10]. They provided a practical formulation of the Lorenz-gauge perturbation equations in Schwarzschild spacetime and demonstrated their formulation is

[1]Email address: sago@yukawa.kyoto-u.ac.jp

suitable for numerical calculation. In our recent works [11, 12], based on their formulation, we developed a code to calculate the gravitational self-force for bound orbits in Schwarzschild geometry.

Our next step is to consider the effect of the gravitational self-force on the particle's orbit. The self-force corrections in some characteristic variables of the orbit are good indicators to estimate the self-force effect and also to compare with the results of other approaches (e.g. post-Newtonian or numerical relativity, and so on). In our previous work [13], as the first example, we reported the self-force-induced shifts in the location and frequency of the inner most circular orbit (ISCO) in Schwarzschild spacetime. The result for the ISCO frequency shift is supported by the recent work on the Effective One Body formalism by Damour [14]. In this work, we focus on the periapsis advance of eccentric orbits, which is one of the characteristic variables, and give the formula of the correction in terms of the components of the self-force.

Throughout this work, we denote the masses of a orbiting point particle and a central Schwarzschild black hole as μ and M, respectively. Also we use standard geometrized units with $c = G = 1$ and metric signature $(-+++)$.

2 Periapsis advance: geodesic case

First, we review the periapsis advance in the geodesic case. The radial component of the geodesic equations in Schwarzschild spacetime is given

$$\left(\frac{dr_p}{d\tau}\right)^2 = R(r_p); \quad R(r) \equiv \mathcal{E}_0^2 - f(r)\left(1 + \frac{\mathcal{L}_0^2}{r^2}\right), \tag{1}$$

where $f(r) = 1 - 2M/r$, τ is the proper time along the orbit, $r_p(\tau)$ is the orbital radius. $\mathcal{E}_0$ and $\mathcal{L}_0$ are the specific energy and angular momentum parameters of the particle, which conserve along the geodesic orbit. An eccentric orbit is bounded in the range of $r_{\rm min} \le r \le r_{\rm max}$, where $r_{\rm min/max}$ satisfy $R(r_{\rm min}) = R(r_{\rm max}) = 0$ and $4M < r_{\rm min} \le r_{\rm max}$. $r_{\rm min}$ and $r_{\rm max}$ correspond to the periastron and apastron radius respectively. We can define a parametrization of eccentric orbits, the (dimensionless) semi-latus rectum, p, and the eccentricity, e, so that

$$p \equiv \frac{2r_{\rm min}r_{\rm max}}{M(r_{\rm min} + r_{\rm max})}, \quad e \equiv \frac{r_{\rm max} - r_{\rm min}}{r_{\rm max} + r_{\rm min}}. \tag{2}$$

With this parametrization, the orbital radius is given by

$$r_p(\chi) = \frac{pM}{1 + e\cos\chi}, \tag{3}$$

where χ is a monotonically increasing parameter ("radial phase") along the worldline [15]. By using χ, we reexpress the t and φ components of the geodesic equations as

$$\begin{aligned} \frac{dt_p}{d\chi} &= \frac{\mathcal{E}_0}{f(r_p)}\left[\mathcal{E}_0^2 - f(r_p)\left(1 + \frac{\mathcal{L}_0^2}{r_p^2}\right)\right]^{-1/2}\left(\frac{dr_p}{d\chi}\right) \equiv W_t(r_p; \mathcal{E}_0, \mathcal{L}_0), \\ \frac{d\varphi_p}{d\chi} &= \frac{\mathcal{L}_0}{r_p^2}\left[\mathcal{E}_0^2 - f(r_p)\left(1 + \frac{\mathcal{L}_0^2}{r_p^2}\right)\right]^{-1/2}\left(\frac{dr_p}{d\chi}\right) \equiv W_\varphi(r_p; \mathcal{E}_0, \mathcal{L}_0). \end{aligned} \tag{4}$$

By integrating Eq. (4) over χ, we define the radial period and the increase of the phase for one radial period as

$$T_r \equiv \int_0^{2\pi} \frac{dt_p}{d\chi} d\chi, \quad \Delta\varphi \equiv \int_0^{2\pi} \frac{d\varphi_p}{d\chi} d\chi. \tag{5}$$

Now we can define the periapsis advance

$$\delta_0(p, e) \equiv \Delta\varphi - 2\pi, \tag{6}$$

which represents the fractional difference between two frequencies

$$\Omega_\varphi = \left(1 + \frac{\delta_0}{2\pi}\right)\Omega_r, \tag{7}$$

where $\Omega_r \equiv 2\pi/T_r$ and $\Omega_\varphi = \Delta\varphi/T_r$ are the radial and azimuthal frequencies respectively.

3 Self-force correction in periapsis advance

Next, we consider the conservative correction in the periapsis advance caused by the self-force. In the same manner as [16], the conservative pieces of t and φ components of the force are given by

$$F_t^{\rm cons}(\chi) = \frac{1}{2}[F_t(\chi) - F_t(-\chi)], \quad F_\varphi^{\rm cons}(\chi) = \frac{1}{2}[F_\varphi(\chi) - F_\varphi(-\chi)], \tag{8}$$

where we treat F_t and F_φ as functions of χ. From the equations of motion, we find the rates of change of the specific energy and angular momentum

$$\frac{d\mathcal{E}}{d\tau} = -F_t, \quad \frac{d\mathcal{L}}{d\tau} = F_\varphi. \tag{9}$$

Integrating Eq. (9) over χ, we obtain the corrected energy and angular momentum

$$\mathcal{E}(\chi) = \mathcal{E}_0 + \Delta\mathcal{E}_0 + \delta\mathcal{E}(\chi), \quad \mathcal{L}(\chi) = \mathcal{L}_0 + \Delta\mathcal{L}_0 + \delta\mathcal{L}(\chi), \tag{10}$$

where $\Delta\mathcal{E}_0$ and $\Delta\mathcal{L}_0$ represent the conservative shifts in $\mathcal{E}$ and $\mathcal{L}$ at $\chi = 0$, and

$$\delta\mathcal{E}(\chi) = -\int_0^\chi F_t^{\rm cons}(\chi')\left(\frac{d\tau}{d\chi'}\right)d\chi', \quad \delta\mathcal{L}(\chi) = -\int_0^\chi F_\varphi^{\rm cons}(\chi')\left(\frac{d\tau}{d\chi'}\right)d\chi'. \tag{11}$$

All $\Delta\mathcal{E}_0$, $\Delta\mathcal{L}_0$, $\delta\mathcal{E}(\chi)$ and $\delta\mathcal{L}(\chi)$ are in the order of μ. In a similar manner to the geodesic case, we can define the periapsis advance

$$\delta(p,e) \equiv \int_0^{2\pi} W_\varphi(r_p,;\mathcal{E},\mathcal{L})d\chi - 2\pi, \tag{12}$$

and then taking the $O(\mu)$ terms from the above equation gives us the self-force correction as

$$\delta_{SF}(p,e) \equiv \int_0^{2\pi} \delta W_\varphi(r_p,;\mathcal{E}_0,\mathcal{L}_0)d\chi, \tag{13}$$

where

$$\begin{aligned}
\delta W_\varphi(r_p,;\mathcal{E}_0,\mathcal{L}_0) &= \left.\frac{\partial W_\varphi}{\partial\mathcal{E}}\right|_0[\Delta\mathcal{E}_0 + \delta\mathcal{E}(\chi)] + \left.\frac{\partial W_\varphi}{\partial\mathcal{L}}\right|_0[\Delta\mathcal{L}_0 + \delta\mathcal{L}(\chi)] \\
&= \frac{p(p-3-e^2)^{1/2}[(p-2)^2-4e^2]^{1/2}}{e^2(p-6-2e\cos\chi)^{3/2}}\left[\frac{\mathcal{E}(\pi)}{4\cos^2(\chi/2)} - \frac{\mathcal{E}(\chi)}{\sin^2\chi}\right] \\
&\quad -\frac{p^{-1/2}(p-3-e^2)^{1/2}}{Me^2(p-6-2e\cos\chi)^{3/2}}\left[\frac{(1-e)^2(p-2+2e)\mathcal{L}(\pi)}{4\cos^2(\chi/2)}\right. \\
&\quad \left. -\frac{[p(1+e^2)-2(1+3e^2)+2e(p-3-e^2)\cos\chi]\mathcal{L}(\chi)}{\sin^2\chi}\right].
\end{aligned} \tag{14}$$

Equation (14) may seem singular at $\chi = 0, \pi$, but that is not the case. Local analysis around these points shows that δW_φ is regular, although the direct implementation may require special care near $\chi = 0, \pi$.

4 Summary and discussion

In this work, we considered the self-force effect on the periapsis advance of an eccentric orbit in Schwarzschild spacetime. We gave a formula of the correction induced by the conservative piece of the self-force, which can by calculated numerically by our time-domain code. In practice, however, it is not easy to implement the formula numerically because it contains double integrals of the force and then the numerical accuracy gets worse. One way to improve it is to use integration by parts. Although it makes the formula more complicated, it may reduce the loss of the numerical accuracy. To do so, again, we have to take care on the singular behavior of each term in Eq. (14) at $\chi = 0, \pi$. This reduction is left for future study.

So far we considered only the conservative piece of the self-force, and we assume that the orbital parameters (p, e) are constant. In reality, however, the dissipation also affects the particle's orbit in the secular evolution and the parameters change in time. Even in this case, we can define the periapsis shift as

$$\delta_{SF}^{\rm actual}(t_1) = \int_{t_1}^{t_2} \frac{d\varphi}{dt} dt - \delta_0(p_1, e_1), \tag{15}$$

where t_1 and t_2 are consecutive radial turning points, and (p_1, e_1) are the orbital parameters at $t = t_1$. If the orbit evolve adiabatically, the actual correction of the periapsis shift can be given approximately as the time average of the instantaneous (conservative) correction over the orbital period,

$$\delta_{SF}^{\rm actual}(t_1) \simeq \frac{1}{(t_2 - t_1)} \int_{t_1}^{t_2} \delta_{SF}(p, e) = \delta_{SF}\left(\frac{p_1 + p_2}{2}, \frac{e_1 + e_2}{2}\right) + O(\mu^2). \tag{16}$$

The proof and feasibility of this relation should be surely investigated.

Acknowledgements

We acknowledge support from PPARC/STFC through grant number PP/E001025/1. NS also acknowledges support from Monbukagaku-sho Grant-in-Aid for the global COE program "The Next Generation of Physics, Spun from Universality and Emergence".

References

[1] Y. Mino, M. Sasaki and T. Tanaka, Phys. Rev. D **55**, 3457 (1997) [arXiv:gr-qc/9606018].

[2] T. C. Quinn and R. M. Wald, Phys. Rev. D **56**, 3381 (1997) [arXiv:gr-qc/9610053].

[3] L. Barack, Y. Mino, H. Nakano, A. Ori and M. Sasaki, Phys. Rev. Lett. **88**, 091101 (2002) [arXiv:gr-qc/0111001].

[4] L. Barack, Class. Quant. Grav. **26**, 213001 (2009) [arXiv:0908.1664 [gr-qc]].

[5] T. Regge and J. A. Wheeler, Phys. Rev. **108**, 1063 (1957).

[6] P. L. Chrzanowski, Phys. Rev. D **11**, 2042 (1975).

[7] H. Nakano, N. Sago and M. Sasaki, Phys. Rev. D **68**, 124003 (2003) [arXiv:gr-qc/0308027].

[8] S. Detweiler, Phys. Rev. D **77**, 124026 (2008) [arXiv:0804.3529 [gr-qc]].

[9] S. Detweiler and B. F. Whiting, Phys. Rev. D **67**, 024025 (2003) [arXiv:gr-qc/0202086].

[10] L. Barack and C. O. Lousto, Phys. Rev. D **72**, 104026 (2005) [arXiv:gr-qc/0510019].

[11] L. Barack and N. Sago, Phys. Rev. D **75**, 064021 (2007) [arXiv:gr-qc/0701069].

[12] L. Barack and N. Sago, in preparation.

[13] L. Barack and N. Sago, Phys. Rev. Lett. **102**, 191101 (2009) [arXiv:0902.0573 [gr-qc]].

[14] T. Damour, Phys. Rev. D **81**, 024017 (2010) [arXiv:0910.5533 [gr-qc]].

[15] C. Cutler, D. Kennefick and E. Poisson, Phys. Rev. D **50**, 3816 (1994).

[16] T. Hinderer and E. E. Flanagan, Phys. Rev. D **78**, 064028 (2008) [arXiv:0805.3337 [gr-qc]].

Relativistic Dissipative Accretion Flow onto Black Hole

Hiromi Saida[1(a)], Rohta Takahashi[2(b)] and Hiroki Nagakura[3(c)]

(a) *Department of Physics, Daido University, Nagoya, Japan*
(b) *Cosmic Radiation Laboratory, the Institute of Physical and Chemical Research, Saitama, Japan*
(c) *Department of Science and Engineering, Waseda University, Tokyo, Japan*

Abstract

Dissipations, e.g. heat flow and bulk and shear viscosities, cause the transport of energy, momentum and angular momentum, which is the essence of accretion of matters onto celestial objects. Dissipations are usually described by the Fourier and Navier-Stokes laws (*classic laws* of dissipations). However the classic laws result in an infinitely fast propagation of dissipations. In relativistic formulation, the classic laws of dissipations violate the causality, and hence no relativistic theory of accretion flow onto celestial object is formulated. In this short report, we summarize the causal dissipative hydrodynamics, so-called *Extended Irreversible Thermodynamics* (EIT), with a supplemental comment which the original works of EIT are not aware of, and then show two theorems about relativistic dissipative flows around a Schwarzschild black hole. By these theorems, an advantage of EIT in comparison with classic laws of dissipations is clarified, and a dissipative instability of an exact solution of relativistic perfect fluid flow is also obtained.

1 Extended Irreversible Thermodynamics (EIT)

We begin with summarizing the basis of perfect fluid and classic laws of dissipations (e.g. Fourier and Navier-Stokes laws) in order to clarify the basis and need for EIT. The perfect fluid is a phenomenology assuming the *local equilibrium* of fluid, which requires that each fluid element is in a thermal equilibrium state. By the local equilibrium assumption, any fluid element in perfect fluid evolves adiabatically and no entropy production arises in the fluid element. This contradicts the dissipative phenomena which are essentially the irreversible and entropy producing processes. Therefore, the basic equations of perfect fluid can not include any dissipation. Then we notice that *the local equilibrium assumption is inconsistent with the irreversible nature of dissipative phenomena*. In other words, dissipations can not exist in local equilibrium systems. On the other hand, recall that the classic laws of dissipations are also the phenomenologies assuming the local equilibrium. Hence the classic laws lead inevitably an unphysical conclusion; an infinitely fast propagation of dissipations. While the infinitely fast propagation may be harmless to Newtonian theories, however, in relativistic theories, it gives rise to a serious problem; the violation of causality. The classic laws of dissipations can not be accepted as basic laws of relativistic dissipations. (See [1] for details of the violation of causality by the local equilibrium assumption.)

From the above, it is recognized that we should abandon the local equilibrium assumption in order to obtain a consistent dissipative hydrodynamics. Therefore the idea of *local non-equilibrium* is necessary, which means that the fluid element is in a non-equilibrium state. A physically consistent phenomenology of dissipative hydrodynamics, which is based on the local *non*-equilibrium idea, is already formulated. It is called the *Extended Irreversible Thermodynamics* (EIT). As precisely explained in [1], because of the local non-equilibrium idea, EIT describes the entropy production inside each fluid element, which results in a finite speed of propagation of dissipations in both non-relativistic and relativistic situations. The relativistic EIT is a causally consistent dissipative hydrodynamics [2–4]. [4]

[1]Email address: saida@daido-it.ac.jp
[2]Email address: rohta@riken.jp
[3]Email address: hiroki@heap.phys.waseda.ac.jp

[4] Although the EIT is a dissipative "hydrodynamics", it is called "thermodynamics". This name puts emphasis on the replacement of local equilibrium idea with local *non*-equilibrium one, which is a revolution in thermodynamic treatment of fluid element. The terminology "EIT" is found in [1] which is developed by experts in non-equilibrium physics. Contrary,

Before showing the basic equations of EIT, we list the basic quantities;

$$
\begin{aligned}
u^\mu(x) &: \text{velocity field of fluid (four-velocity of fluid element)} \\
\rho(x)\ \left(=\frac{1}{V(x)}\right) &: \text{mass density } (\rho) \text{ and specific volume (volume per unit mass, } V) \\
\varepsilon_{\rm ne}(x) &: \text{non-equilibrium specific internal energy (internal energy per unit mass)} \\
p_{\rm ne}(x) &: \text{non-equilibrium pressure} \\
T_{\rm ne}(x) &: \text{non-equilibrium temperature} \\
q^\mu(x) &: \text{heat flux vector} \\
\Pi(x) &: \text{bulk viscosity} \\
\widetilde{\Pi}^{\mu\nu}(x) &: \text{shear viscosity tensor} \\
g_{\mu\nu}(x) &: \text{spacetime metric}
\end{aligned}
$$

Here x denotes the dependence on spacetime point. All of the above quantities except for u^μ and $g_{\mu\nu}$ are the *non-equilibrium thermodynamic state variables* which characterize the non-equilibrium state of each fluid element. The non-equilibrium state variables are classified into two categories: The quantities $\varepsilon_{\rm ne}$, $p_{\rm ne}$, $T_{\rm ne}$ and ρ are the state variables which exit even at the local equilibrium limit, while the quantities q^μ, Π and $\widetilde{\Pi}^{\mu\nu}$ are the state variables which should vanish at the local equilibrium limit. We call the first category ($\varepsilon_{\rm ne}$, $p_{\rm ne}$, $T_{\rm ne}$, ρ) the *non-equilibrium scalars*, and call the second category (q^μ, Π, $\widetilde{\Pi}^{\mu\nu}$) the *dissipative fluxes*. The dissipative fluxes are the origin of dissipative phenomena and make the fluid being non-equilibrium. The suffix "ne" for non-equilibrium scalars denotes "non-equilibrium", and the variables with this suffix have different value from an equilibrium case. Note that the definition of ρ (or V) is the same for both equilibrium and non-equilibrium cases; to count the number of composite particles or measure the mass per unit volume. So the suffix "ne" is not given to ρ and V.

As the basic assumption of EIT, it is required that the dissipative fluxes are *independent* non-equilibrium state variables. Furthermore, concerning the non-equilibrium scalars, it is also assumed that, as in the ordinary equilibrium thermodynamics, the number of independent non-equilibrium scalars is two for *closed* systems which conserve the number of composite particles, and three for *open* systems in which the number of composite particles changes. The remaining state variables are expressed as functions of the independent variables through the equations of state, e.g. the non-equilibrium specific entropy $\varepsilon_{\rm ne}$ is a function of independent state variables $\varepsilon_{\rm ne} = \varepsilon_{\rm ne}(\varepsilon_{\rm ne}, V, q^\mu, \Pi, \widetilde{\Pi}^{\mu\nu})$, where $\varepsilon_{\rm ne}$ and V are chosen as independent non-equilibrium scalars.

Here note the fact that EIT, at least in its present status, is not necessarily applicable to any non-equilibrium state of dissipative fluid [1]. The consistent basic equations of EIT can be formulated for sufficiently weak dissipative fluxes, which means that the strength of non-equilibrium nature should not be so strong. For example, it is shown in [4] that the EIT preserves causality of heat flow if $\sqrt{q^\mu q_\mu}/\varepsilon_{\rm ne} \lesssim 0.08$ for non-viscous fluid ($\Pi = 0$, $\widetilde{\Pi}^{\mu\nu} = 0$) under stationary and homogeneous (spatially one-dimensional) condition. We can recognize that the amount of energy transported by dissipative fluxes should be less than a few percent of the internal energy which includes mass energy. This efficiency of dissipative energy transfer is larger than the efficiency of hydrogen burning in a star ($\sim O(10^{-3})$). Therefore, although the EIT is applicable to a dissipative fluid whose local non-equilibrium states are not so far from local equilibrium states, it is expected that the EIT is applicable to many astrophysical systems.

In the present status of EIT, the above restriction is reflected in the equations of state. The equations of state, e.g. $s_{\rm ne}(\varepsilon_{\rm ne}, V, q^\mu, \Pi, \widetilde{\Pi}^{\mu\nu})$, are expanded up to second order of dissipative fluxes about the *fiducial equilibrium state*. Here the *fiducial equilibrium state* is defined as an equilibrium state of fluid element of imaginary perfect fluid possessing the same fluid velocity $u^\mu(x)$ and mass density $\rho(x)$ with our actual dissipative fluid. Then, as explained in [1], the evolution equations of dissipative fluxes are obtained under two requirements; (i) positivity of entropy production rate at each fluid element, and (ii) consistency with experimentally determined phenomenology of relaxation processes of dissipations.

the original works of relativistic dissipative hydrodynamics [2–4] put emphasis not on the thermodynamic revolution but on the preservation of causality. Here let us dare to use the term "EIT" since the local non-equilibrium nature of dissipative fluid is the physical origin of preservation of causality.

The resultant evolution equations are;

$$\tau_{\rm h}\,\dot{q}^{\,\mu} = -q^{\mu} - \lambda T\,\dot{u}^{\,\mu} + \tau_{\rm h}\,(q^{\nu}\dot{u}_{\nu})\,u^{\mu} - \lambda\,\Delta^{\mu\nu}\left(T_{,\nu} - T^{2}\left(\beta_{\rm hb}\,\Pi_{,\nu} + \beta_{\rm hs}\,\widetilde{\Pi}_{\nu}{}^{\alpha}{}_{;\alpha}\right)\right) \tag{1}$$

$$\tau_{\rm b}\,\dot{\Pi} = -\Pi - \zeta\,u^{\mu}{}_{;\mu} + \beta_{\rm hb}\,\zeta\,T\,q^{\mu}{}_{;\mu} \tag{2}$$

$$\tau_{\rm s}\left(\widetilde{\Pi}^{\,\mu\nu}\right)^{\cdot} = -\widetilde{\Pi}^{\,\mu\nu} + 2\,\tau_{\rm s}\,\dot{u}_{\alpha}\,\widetilde{\Pi}^{\,\alpha(\nu}\,u^{\nu)} - 2\,\eta\left[\,u^{\mu;\nu} - T\,\beta_{\rm hs}\,q^{\mu;\nu}\,\right]^{\circ}, \tag{3}$$

where T is the temperature of fiducial equilibrium state. Here, definitions of mathematical symbols are; $\dot{Q} := u^{\mu}Q_{;\mu}$, $\Delta^{\mu\nu} := u^{\mu}u^{\nu} + g^{\mu\nu}$ and $[A_{\mu\nu}]^{\circ} := \Delta^{\mu\alpha}\Delta^{\nu\beta}A_{(\alpha\beta)} - (1/3)\Delta^{\mu\nu}\Delta^{\alpha\beta}A_{\alpha\beta}$. And the meaning of coefficients are; τ's are relaxation times of dissipative fluxes, λ is heat conductivity, ζ and η are respectively bulk and shear viscous rates, and $\beta_{\rm hb}$ and $\beta_{\rm hs}$ are interaction coefficients between q^{μ} and Π or $\widetilde{\Pi}^{\,\mu\nu}$. For example, $\beta_{\rm hs}$ means that the heat flow arises in a shear viscous flow, also shear viscosity arises in a flow with heating. $\beta_{\rm hb}$ means the same between q^{μ} and Π. Furthermore note that, because dissipative phenomena are not time reversal, these evolution equations of dissipative fluxes are also not time reversal.

The others of EIT's basic equations are given by the conservation of mass current, $(\rho\,u^{\mu})_{;\mu} = 0$, and that of stress-energy-momentum tensor, $T^{\mu\nu}{}_{;\nu} = 0$;

$$\dot{\rho} + \rho\,u^{\mu}{}_{;\mu} = 0 \tag{4}$$

$$\rho\left(\dot{\varepsilon} + p\,\dot{V}\right) = -q^{\mu}{}_{;\mu} - q^{\mu}\,\dot{u}_{\mu} - \left(\Pi\,\Delta^{\mu\nu} + \widetilde{\Pi}^{\,\mu\nu}\right)u_{\mu\,;\,\nu} \tag{5}$$

$$(\,\rho\,\varepsilon + p + \Pi\,)\,\dot{u}^{\,\mu} = -\dot{q}^{\,\mu} + q_{\alpha}\,\dot{u}^{\,\alpha}\,u^{\mu} - u^{\alpha}{}_{;\alpha}\,q^{\mu} - q^{\alpha}\,u^{\mu}{}_{;\alpha} - \Delta^{\mu\alpha}\left((p+\Pi)_{,\alpha} + \widetilde{\Pi}_{\alpha}{}^{\beta}{}_{;\beta}\right), \tag{6}$$

where ε, p and T are the state variables of fiducial equilibrium state. The above equations (1) $\sim$ (6) and the Einstein equation are the basic equations of EIT.

Finally let us make a comment which the original works of EIT [1–4] are not aware of: The EIT can not be applied to radiation fluids as shown in [5]. Non-equilibrium radiation fluids need a special treatment different from the other matters. However, although the inconsistency of EIT with radiation fluid has been revealed, no satisfactory non-equilibrium phenomenology of radiation fluid exits at present.

2 Dissipative Accretion Flow onto a Schwarzschild Black Hole

As a preliminary report, we show two theorems, without precise proof, on dissipative flows around a Schwarzschild black hole. Both theorems can be proven by solving the basic equations of EIT without solving the Einstein equation and fixing the metric on Schwarzschild spacetime. The use of fixed background metric means that our analysis does not include the self-gravity of the dissipative fluid. Therefore the theorems shown below are applicable to non-self-gravitating dissipative flows, i.e. to the dissipative fluid whose total energy is sufficiently less than the mass of central black hole, however "non-self-gravitating" dissipative fluid is usually assumed in Newtonian accretion disk theories [6].

For the first, let us consider the spherically symmetric dissipative accretion flow onto a Schwarzschild black hole:

Theorem 2. *Shear viscosity must vanish in both non-stationary and stationary spherically symmetric dissipative accretion flows onto Schwarzschild black hole.*

Although the statement of this theorem seems to be physically natural and trivial, but let us emphasize that the classic laws of dissipations (Navier-Stokes and Fourier laws) do not yield this theorem even in non-relativistic situation [7]. Theorem 1 is one of the advantage of EIT, which yields a very physically acceptable conclusion. Now I am trying to extend this theorem to a spherical dissipative flow on general non-stationary spherical spacetime which includes the self-gravity of dissipative fluid.

For the second, let us consider the stationary and axisymmetric dissipative flow around a Schwarzschild black hole:

Theorem 3. *For stationary and axisymmetric flow with no mass accretion onto black hole, any flow of finite temperature is impossible, but only a rigid toroidal rotation of zero-temperature is possible. The fluid velocity and disspative fluxes of the possible zero-temperature flow are*

$$u^t = \frac{1}{\sqrt{f(r) - \Omega^2 r^2 \sin^2\theta}} \quad , \quad u^r = u^\theta = 0 \quad , \quad u^\phi = \Omega\, u^t \qquad \textit{and} \quad q^\mu = \Pi = \widetilde{\Pi}^{\mu\nu} = 0\,, \tag{7}$$

where (t, r, θ, ϕ) is the Schwarzschild coordinate, $f(r) := 1 - 2M/r$ with M as the black hole mass, and Ω is the angular velocity measured by a rest observer. Since Ω is constant and dissipations vanish even when they are switched on, the velocity u^μ in equation (7) expresses a rigid rotation. And the thermodynamic state variables of this flow are

$$T = p = \varepsilon = 0 \quad , \quad \rho(r,\theta) = \textit{arbitrary in the region } f(r) > \Omega^2 r^2 \sin^2\theta \tag{8}$$

Here recall that the internal energy $\varepsilon(x)$, for a fluid element at x, includes the mass energy, kinetic energy and the potential energy by external gravity due to black hole. Therefore the vanishing internal energy $\varepsilon = 0$ means that, for each fluid element, the potential energy due to black hole cancels out the kinetic and mass energies of fluid element.

This theorem together with the third law of thermodynamics implies that any flow of finite temperature is non-stationary and/or non-axisymmetric, and never relaxes to the flow given in equations (7) and (8). Hence, although a differentially rotating and stationary axisymmetric flow of finite temperature is possible for "perfect" fluid [8], such stationary flow becomes unstable once the dissipations are switched on. Theorem 2 implies the dissipative instability of an exact solution of relativistic perfect fluid.

The dissipative instability, the EIT's effect, may describe a formation of out-flow from an accretion disk without introducing a magnetic field (so-called MRI), while the "acceleration" of out-flow to form a jet will be explained with magnetic fields. In (near) future, it is expected to apply the EIT to a plasma composing an accretion disk.

References

[1] Jou D., Casas-Vazquez J. and Lebon G., 1988, *Extended Irreversible Thermodynamics*, Rep.Prog.Phys.51, 1105.
Jou D., Casas-Vazquez J., Lebon G., 2001, *Extended Irreversible Thermodynamics (3rd Edition)*, Springer Verlag, Berlin.

[2] Israel W., 1976, *Nonstationary Irreversible Thermodynamics: A Causal Relativistic Theory*, Ann.Phys.100, 310.
Israel W. and Stewart J.M., 1979, *Transient Relativistic Thermodynamics and Kinetic Theory*, Ann.Phys.118, 341.

[3] Hiscock W.A. and Lindblom L., 1983, *Stability and Causality in Dissipative Relativistic Fluids*, Ann.Phys.151, 466.

[4] Hiscock W.A. and Lindblom L., 1988, *Nonlinear pathologies in relativistic heat-conducting fluid theories*, Phys.Lett.A131, 509.

[5] Essex C., 1984, *Radiation and the violation of bilinearity in the thermodynamics of irreversible processes*, Planet.Space.Sci.32, 1035.
Essex C., 1990, *Radiation and the Continuing Failure of the Bilinear Formalism*, Advances in Thermodynamics 3, 435.
Saida H., 2005, *Two-temperature steady state thermodynamics for a radiation field*, Physica A356, 481.

[6] Kato S., Fukue J. and Mineshige S., 2008, *Black-Hole Accretion Disks*, Kyoto Univ. Press.

[7] Ray A.K., 2003, *Viscosity in spherically symmetric accretion*, Mon.Not.R.Astron.Soc.344, 1085.

[8] Fishbone L.G. and Moncrief V., 1976, *Relativistic fluid disks in orbit around Kerr black hole*, Astrophys.J.207, 962.

Formation of Rapidly Rotating Dynamic Black Holes

Motoyuki Saijo[1 (a),(b)]

[(a)] *Department of Physics, Rikkyo University, Toshima, Tokyo 171-8501*
[(b)] *Research Center for Measurement in Advanced Science, Rikkyo University, Toshima, Tokyo 171-8501*

Abstract

We investigate the formation of rapidly rotating dynamic black hole through gravitational collapse of rotating relativistic stars by means of 3+1 hydrodynamic simulations in general relativity. We succeed in producing a dynamic black hole of $a = 0.98M$ through the collapse of differentially rotating supermassive stars, and find the following three issues. Firstly, the estimated ratio of the mass between the black hole and the surrounding disk from the equilibrium star is roughly the same as the results from numerical simulation. This suggests that the picture of axisymmetric collapse is adequate, in the absence of nonaxisymmetric instabilities, to illustrate the final state of the collapse. Secondly, quasi-periodic gravitational waves continue to be emitted after the quasinormal mode frequency has decayed. Finally, when the newly formed black hole is almost extreme Kerr, the amplitude of the quasi-periodic oscillation is enhanced during the late stages of the evolution. Geometrical features, shock waves, and instabilities of the fluid are suggested as a cause of this amplification behaviour. This alternative scenario for the collapse of differentially rotating supermassive stars might be observable by LISA.

There exists plenty of evidence that supermassive black holes (SMBHs) exists in the centre of galaxies, and that they seem to rotate very rapidly [1]. There are two main categories for forming dynamic black holes (BHs) promptly. One is the merger of the binary object, while the other is gravitational collapse of an object. At the present status of the binary BHs, the highest spin of the newly formed BH is $J/M^2 = 0.69$ (J: total angular momentum of the hole; M: total gravitational mass of the hole) for the non-spinning, individual BHs, while $J/M^2 = 0.93$ for the spinning BHs. As for the collapse of a rotating relativistic star to a BH, there exists a maximum spin of the newly formed BH for the collapse of uniformly rotating relativistic stars. In fact, the collapse of uniformly rotating supermassive stars (SMSs) produces a hole of $J/M^2 = 0.75$ [2].

There are two categories of collapsing rotating SMSs based on their angular momentum distribution. One is the collapse of a uniformly rotating SMS. This happens when momentum transport is large, either through viscous turbulence or magnetic process, which drives the star to rotate uniformly. The other is the collapse of differentially rotating SMSs. This happens when the viscous and the magnetic effects are small, which allows the star to rotate differentially. One of the representative scenarios for forming a differentially rotating star is as follows. First, a gas cloud gathers in an almost spherical configuration with some amount of angular momentum in the system. Next the almost spherical star contracts, conserving the specific angular momentum due to the lack of viscosity, to form a differentially rotating star, and possibly a disk at the end of the contraction.

During the contraction of the differentially rotating SMS, prior to forming a supermassive disk, two possible instabilities may arise that terminate the contraction. One is the post-Newtonian gravitational instability, which leads the star to collapse dynamically. The other is the dynamical bar mode instability, which changes the angular momentum distribution of the star to form a bar, and possibly leads to the central core of the star collapsing to a BH due to the angular momentum loss.

Here we focus on the post-Newtonian gravitational instability in differentially rotating SMSs. We particularly focus on the case where the final estimated BH is very close to the extreme Kerr BH, which potentially leads to rotational instabilities if they occur. In particular, we plan to answer the following questions. Does the BH form coherently? What are the features of the dynamics? Does the newly formed

[1] Email address: saijo@rikkyo.ac.jp

Table 1: Four different rotating equilibrium SMSs for evolution

Model	J/M^{2} (a)	$M/R^{(b)}$	$m_{\rm disk}^{(c)}$	$(a/M)^{\rm (BH)}$ (d)
I	0.99	2.56×10^{-2}	0.044	0.98
II	1.03	2.63×10^{-2}	—	$\gtrsim 1$
III	1.07	2.78×10^{-2}	—	—
IV	1.10	3.47×10^{-2}	—	—

(a): M: gravitational mass; J: total angular momentum
(b): R: circumferential equatorial radius
(c): $m_{\rm disk}$: ratio of the estimated rest mass of the disk to the rest mass of the equilibrium star
(d): $(a/M)^{\rm (BH)}$: estimated Kerr parameter of the final hole

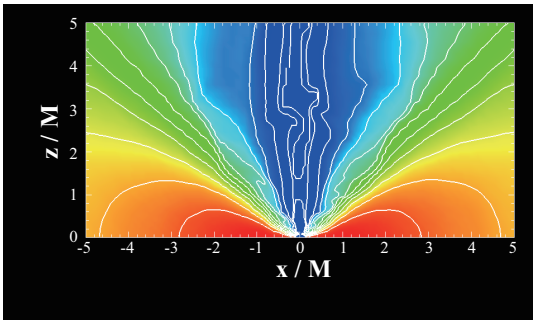

Figure 1: Snapshot of the rest mass density in the meridional plane for model II at $t = 9.30\times10^{2}M$. The contour lines denote rest mass densities $\rho/\rho_{\rm max} = 10^{-(15-i)d}$ $(i = 1, \cdots, 14)$, where $\rho_{\rm max} = 6.12\times10^{-6}$, $\rho_{\rm cut} = 1.56\times10^{-13}$, $d = (\log\rho_{\rm max} - \log\rho_{\rm cut})/15$. Note that the apparent horizon exists after $t = 7.70\times10^{2}M$, and the coordinate radius of the apparent horizon in the equatorial plane are $r_{\rm hrz} = 1.75\times10^{-1}M$.

disk lead to contain various instabilities? Can this system act as an efficient source of gravitational waves (GWs)? In order to answer these questions, three dimensional general relativistic hydrodynamics are desirable. A more detailed discussion is presented in Ref. [3]. Throughout this paper, we use the geometrized units with $G = c = 1$ and adopt Cartesian coordinates (x, y, z) with the coordinate time t.

We perform 3+1 hydrodynamic simulations in general relativity using CACTUS (gravitational physics), CARPET (mesh refinement of space and time), WHISKY (general relativistic hydrodynamics). Spacetime is evolved using the BSSN formulation with generalised hyperbolic K-driver for the lapse and generalised hyperbolic $\tilde{\Gamma}$-driver for the shift (e.g. [3]). We set the outermost boundary of the computational grid for all direction as $x_{\rm max} = 126M$, $131M$, imposing plane symmetry across the $z = 0$ plane, and use 10 refinement levels.

We first investigate the onset of collapse by evolving four differentially rotating equilibrium stars. We use the perfect fluid approximation with a Γ-law equation of state, choosing $\Gamma = 4/3$ to represent a SMS (the pressure is dominated by radiation). We also impose a high degree of differential rotation, $\Omega_{\rm c}/\Omega_{\rm e} \approx 10$, to construct the equilibrium star, where Ω_c and Ω_e represents the angular velocity at the center and the equatorial surface, respectively. We choose the z-axis as the rotational one of the equilibrium star. The character of the equilibrium stars is summarized in Table 1. Since we use the polytropic equation of state $P = \kappa\rho_0^{\Gamma}$ (P: pressure, κ: constant, ρ_0: rest mass density, Γ: adiabatic exponent) when constructing initial data sets, all physical quantities are rescalable in terms of κ. Therefore, we represent all physical quantities in a nondimensional one ($\kappa = 1$). To trigger collapse we deplete pressure by 1%. Checking the maximum rest mass density of the rotating stars throughout the evolution, we conclude that models I and II are radially unstable, while models III and IV are stable [3].

The radially unstable stars first collapse to form a BH. After that, there is a significant amount of mass ejection due to the large amount of angular momentum of the hole. It is indeed like a flare. Finally the system settles down to a quasi-stationary state; central BH with a disk (Fig. 1). Fluid elements in

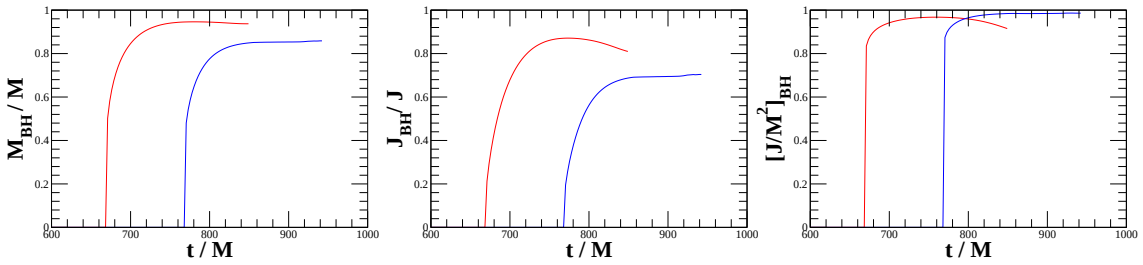

Figure 2: Gravitational mass ($M_{\rm BH}$), total angular momentum ($J_{\rm BH}$) and Kerr parameter ($(J/M^2)_{\rm BH}$) of a newly formed BH as a function of time. Red and blue line represent models I and II, respectively.

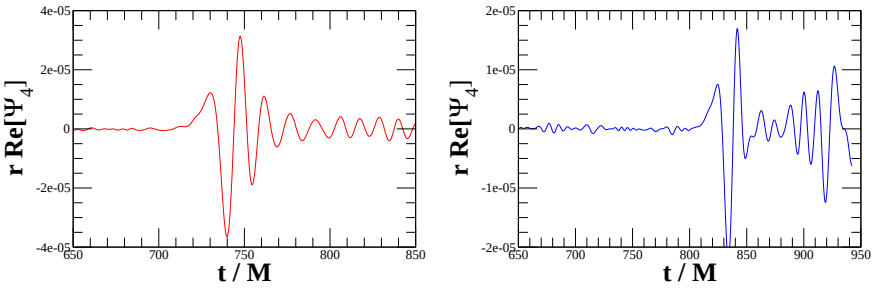

Figure 3: Gravitational waveform measured with the Weyl scalar Ψ_4 observed along the x-axis in the equatorial plane at $r = 6.55 \times 10^1 M$ for models I and II. Note that the time at which the apparent horizon is first detected is $t = 6.70 \times 10^2 M$ for model I (red line) and $t = 7.70 \times 10^2 M$ for model II (blue line). Taking the wave propagation time from the source to the observer into account, the apparent horizon formation in the waveform is roughly just before the peak due to the burst. Initially a standard burst and ringdown signal are seen, but sustained gravitational wave emission indicate additional dynamics after BH formation.

the equilibrium star are balanced by its self gravity, the pressure gradient and centrifugal force. When the BH forms, some fluid elements act as a particle which is free from the interaction. In this case, the material can spread out to a larger radius than the equilibrium radius of the star.

Next we monitor the gravitational mass, total angular momentum and the Kerr parameter of the newly formed BH throughout the evolution as shown in Fig. 2. The BH mass, the spin and the Kerr parameter increase monotonically after the BH has formed, by swallowing much of the surrounding material. This stage lasts roughly until all of the matter located inside the radius of the innermost stable circular orbit of the final BH is swallowed.

We furthermore study the formation of a massive disk from the collapse of differentially rotating SMSs. We trace the rest mass of the disk for models I and II. The rest mass of the disk monotonically decreases once the BH has formed, since the newly formed BH grows monotonically by swallowing the surrounding materials. One noticeable feature is that there is a plateau at the final stage of model II [3]. This indicates that there is a strong angular momentum barrier that a fluid fragments are prohibited to fall into a hole.

We extract gravitational waveform through gravitational collapse (Fig. 3). We find that the waveform contains three different stages. The first stage is the burst. This occurs around the time when the apparent horizon of the SMS forms. The dominant contribution of the burst comes from the axisymmetric mode due to collapse. The second stage is the quasinormal ringing of the newly formed BH. Since the dominant frequency in the spectrum is $M\omega \approx 0.4$ [3], the dominant contribution is the axisymmetric one, using the fact that quasinormal mode frequency of $l = 2$, $m = 0$ is $M\omega \approx 0.40 - 0.42$ for a BH with Kerr parameter $a \gtrsim 0.8M$ [4], where l, m denotes the indices of spin -2-weighted spheroidal harmonics. The final stage has a quasi-stationary wave. The amplitude of the waveform for model II seems to increase at late times. For model I, the quasi-stationary waveform remains for at least $\Delta t \sim 70M$, and the frequency region of $M\omega \gtrsim 0.5$ plays a role in the quasi-periodic waveform.

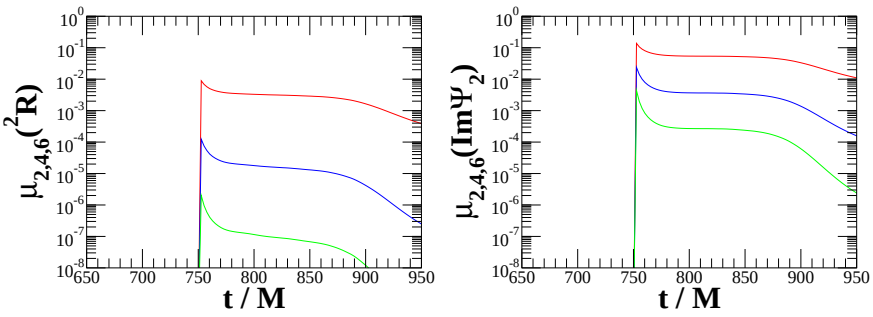

Figure 4: Multipole moments of the newly formed dynamic BH of model II. Red, blue and green lines denote the multipole moment of $l = 2$, 4 and 6.

We finally show our results of computing multipole moments of the dynamic BH in Fig. 4. Note that ${}^2R$ represents the mass multipole moment and $\Im\Psi_2$ represents the current multipole moment. Although the present computational results are preliminary, we find the following two features. One is that the quadrupole moment takes the dominant role of all multipole moments throughout the BH formation. The other is that the quadrupole moment still remains at later stage from the BH formation, although the higher moments dies out at the late stage.

We have investigated the collapse of differentially rotating SMSs, especially focusing on the post BH formation stage, by means of three dimensional hydrodynamic simulations in general relativity. We particularly focus on the onset of collapse to form a rapidly rotating BH as a final outcome.

We have found that the qualitative results of the evolution for the mass and spin of the final BH and disk are quite similar to the estimates that can be computed from the equilibrium configuration when the estimated, final BH has $J_{(\mathrm{BH})}/M^2_{(\mathrm{BH})} < 1$. This result suggests that in the absence of a nonaxisymmetric instability, the estimate of the BH mass and the disk mass agree with a simple axisymmetric picture that the specific angular momentum is conserved throughout the evolution, and the newly formed BH swallows the matter up to the radius of the innermost stable circular orbit.

We have also found that a quasi-periodic wave occurs after the ringdown of a newly formed BH. As we would normally expect the ringdown waveform to damp, it seems likely that the cause of this waveform is due to the presence of the disk in some form. Furthermore, when the newly formed BH is sufficiently close to extreme Kerr with sufficient surrounding matter we have found that the wavesignal may be significantly amplified.

We have discussed several possibilities for the origin of these amplified waves. The most likely possibilities seem to be (a) corotation resonance between the disk and the BH, (b) long-lived gravitational waves from the near-extreme BH amplified by perturbations in the disk, or (c) shocks from the infalling, accreting matter.

Finally we have shown multipole moments of the dynamic BHs. They potentially shows us the dynamics of the horizon and helps us identifying the source of the quasi-periodic gravitational waves either generated by the dynamic spacetime like BH or by the matter like disk element.

References

[1] M. Rees, in *The Future of Theoretical Physics and Cosmology*, edited by G. W. Gibbons, E. P. S. Shellard and S. J. Rankin (Cambridge Univ. Press, Cambridge, 2003), 17.

[2] M. Shibata and S. L. Shapiro, Astrophys. J. **572**, L39 (2002).

[3] M. Saijo and I. Hawke, Phys. Rev. D **80**, 64001 (2009).

[4] E. W. Leaver, Proc. R. Soc. London A **402**, 285 (1985).

[5] M. Jasiulek, Class. Quantum Phys. **26**, 245008 (2009).

Analytic formulae for CMB anisotropy in LTB cosmology

Keiki Saito[1(a)], Akihiro Ishibashi[(b)] and Hideo Kodama[(b)]

[(a)] *Department of Particles and Nuclear Physics,*
The Graduate University for Advanced Studies (SOKENDAI),
1-1 Oho, Tsukuba, Ibaraki 305-0801, Japan
[(b)] *KEK Theory Center, Institute of Particle and Nuclear Studies, KEK,*
1-1 Oho, Tsukuba, Ibaraki, 305-0801, Japan

Abstract

The local void model has lately attracted considerable attention since it can explain the present apparent accelerated expansion of the universe without introducing dark energy. However, in order to justify this model as an alternative cosmological model to the standard ΛCDM model (FLRW universe plus dark energy), one has to test the model by various observations, such as CMB temperature anisotropy, other than the distance-redshift relation of SNIa. For this purpose, we derive some analytic formulae that can be used to rigorously compare consequences of this model with observations of CMB anisotropy and to place constraints on the position of observers in the void model.

1 Introduction

In standard cosmology, we assume that our universe is isotropic and homogeneous, and accordingly is described by the Friedmann-Lemaître-Robertson-Walker (FLRW) metric. Recent observation of Cosmic Microwave Background (CMB) temperature distribution on the celestial sphere shows that the spatial curvature is flat. Furthermore, the distance-redshift relation of type Ia supernovae indicates that the expansion of the present universe is accelerated. Then, we are led to introduce, within the flat FLRW model, "dark energy," which has negative pressure and behaves just like a positive cosmological constant. However, no satisfactory model that explains the origin of dark energy has so far been proposed.

As an attempt to explain the SNIa distance-redshift relation without invoking dark energy, Tomita proposed a "local void model" [1]. In this model, our universe is no longer assumed to be homogeneous, having instead an underdense local void in the surrounding overdense universe. The isotropic nature of cosmological observations is realized by assuming the spherical symmetry and demanding that we live near the center of the void. Furthermore, the model is supposed to contain only ordinary dust like cosmic matter. Since such a spacetime can be described by Lemaître-Tolman-Bondi (LTB) spacetime [2]-[4], we also call this model the "LTB cosmological model." Since the rate of expansion in the void region is larger than that in the outer overdense region, it can explain the observed dimming of SNIa luminosity. In fact, many recently numerical analysis [5]-[9] have shown that this LTB model can accurately reproduce the SNIa distance-redshift relation.

However, in order to verify the LTB model as a viable cosmological model, one has to test the LTB model by various observations—such as CMB temperature anisotropy—other than the distance-redshift relation[2]. For this purpose, in this paper, we derive some analytic formulae that can be used to rigorously compare consequences of the LTB model with observations of CMB anisotropy. More precisely, we derive analytic formulae for CMB temperature anisotropy for dipole and quadrupole momenta, and then use the dipole formula to place the constraint on the distance between an observer and the symmetry center of the LTB model. We also check the consistency of our formulae with some numerical analysis of the CMB anisotropy in the LTB model, previously made by Alnes and Amarzguioui [10].

[1] Email address: saitok@post.kek.jp

[2] Recently, some constraints on the LTB model from BAO and kSZ effects have also been discussed, see e.g. [9]. Still, the possibility of the LTB model is not completely excluded.

In Sec. 2, we briefly summarize the LTB metric. In Sec. 3, we derive analytic formulae for CMB anisotropy in the LTB model. In Sec. 4, we obtain some constraints concerning the position of the observer. Sec. 5 is denoted to a summary.

2 LTB spacetime

A spherically symmetric spacetime with only non-relativistic matter is described by Lemaître-Tolman-Bondi (LTB) metric [2]-[4]

$$ds^2 = -dt^2 + \frac{\{R'(t,r)\}^2}{1-k(r)r^2}dr^2 + R^2(t,r)d\Omega_2^2, \tag{1}$$

where $' \equiv \partial_r$, $k(r)$ is an arbitrary function of only r. The Einstein equations reduce to

$$\left(\frac{\dot{R}}{R}\right)^2 = \frac{2GM(r)}{R^3} - \frac{k(r)r^2}{R^2}, \tag{2}$$

$$4\pi\rho(t,r) = \frac{M'(r)}{R^2R'}, \tag{3}$$

where $\dot{} \equiv \partial_t$, $M(r)$ is an arbitrary function of only r, and $\rho(t,r)$ is an energy density. The general solution for the Einstein equations in this model admits two arbitrary functions $k(r)$ and $M(r)$. By appropriately choosing the profile of these functions, one can construct some models which can reproduce the distance-redshift relation of SNIa in this model.

3 Analytic formulae for CMB anisotropy in LTB model

In this section, we derive analytic formulae for the CMB anisotropy in the LTB model. First, we assumed that the universe was locally in thermal equilibrium (that is, the distribution function F was Planck distribution Φ) at the last scattering surface, and the direction of the CMB photon traveling is fixed. In this case, F can be written as $F = \Phi(\omega/T)$, where $\omega \equiv p^t$, and T is the temperature. Then, the CMB temperature anisotropy $\delta T/T$ is defined by

$$\delta F = -\frac{\delta T}{T}\omega\partial_\omega F. \tag{4}$$

Second, supposing that an observer lives at a distance of δx^i from the center of the void, it follows that

$$(\delta F)^{(1)} = \delta x^i(\partial_i F)_0, \tag{5}$$

$$(\delta F)^{(2)} = \frac{1}{2}\delta x^i\delta x^j(\partial_i\partial_j F)_0, \tag{6}$$

where the subscript 0 means the value at the center ($r=0$) at the present time ($t=t_0$). From these, the CMB temperature anisotropy dipole $(\delta T/T)^{(1)}$ and quadrupole $(\delta T/T)^{(2)}$ are written as

$$\left(\frac{\delta T}{T}\right)^{(1)} = -\frac{\delta x^i(\partial_i F)_0}{\omega\partial_\omega F_0}, \tag{7}$$

$$\left(\frac{\delta T}{T}\right)^{(2)} = -\frac{1}{2}\frac{\delta x^i\delta x^j(\partial_i\partial_j F)_0}{\omega\partial_\omega F_0} + \frac{1}{2}\left\{\left(\frac{\delta T}{T}\right)^{(1)}\right\}^2\frac{(\omega\partial_\omega)^2F_0}{\omega\partial_\omega F_0}. \tag{8}$$

We assume that the distribution function $F(x,p)$ itself is spherically symmetric. Then, F can be written as $F(x,p) = F_0(t,r,\omega,\mu)$, where $\mu \equiv R'p^r/(\sqrt{1-kr^2}\omega)$. This implies that $\partial_i F = (\partial_i r)\partial_r F_0 + (\partial_i\omega)\partial_\omega F_0 + (\partial_i\mu)\partial_\mu F_0$. Then, we can derive analytic formulae for the CMB anisotropy dipole by solving the Boltzmann equation $\mathscr{L}[F_0] = \partial_t F_0 + \dot{r}\partial_r F_0 + \dot{\omega}\partial_\omega F_0 + \dot{\mu}\partial_\mu F_0 = 0$. The result is

$$\left(\frac{\delta T}{T}\right)^{(1)} = \delta L n^j\Omega_j\left\{\frac{\sqrt{1-k(r_i)r_i^2}}{R_0'}e^{-\tilde{P}(t_0,t_i)}\left(\frac{\partial_r F_0}{\omega\partial_\omega F_0}\right)_i + \int_0^{r_i}drH_{//}'\exp\left[\int_{t_0}^{t}dt_1H_{//}(t_1)\right]\right\}, \tag{9}$$

where $\delta L n^j$ is the position vector of the observer, $\Omega^j \equiv x^j/r$, $\tilde{P}(t_0, t_i) \equiv \int_0^{r_i} dr R''/R'$, $H_{//} \equiv \dot{R}'/R'$, and the subscript i denotes the value at the last scattering surface. By a similar method, we also derive the CMB anisotropy quadrupole formula

$$\begin{aligned}\left(\frac{\delta T}{T}\right)^{(2)} &= -\frac{\delta x^i \delta x^j}{2(\omega\partial_\omega F_0)_i}\left[(\delta_{ij}-\Omega_i\Omega_j)\left(\frac{\partial_r F_0}{r}-\mu\frac{\partial_\mu F_0}{r^2}\right)_0+\Omega_i\Omega_j(\partial_r^2 F_0)_0\right.\\ &\qquad\left.+\left\{\frac{a_\perp''}{a_\perp}\delta_{ij}+a_\perp\left(\frac{R'}{\sqrt{1-kr^2}}-a_\perp\right)''\frac{\Omega_i\Omega_j}{(R')^2}\right\}_0(\omega\partial_\omega F_0)_i\right]\\ &\quad+\frac{1}{2}\left\{\left(\frac{\delta T}{T}\right)^{(1)}\right\}^2\frac{(\omega\partial_\omega)^2 F_0}{\omega\partial_\omega F_0},\end{aligned} \tag{10}$$

where $a_\perp \equiv R/r$.

4 Constraint on LTB model

In this section, we derive some constraints concerning the position of the off-center observers in the LTB model from the CMB dipole formula (9). In general, the CMB temperature anisotropy is decomposed in spherical harmonics Y_{lm}:

$$\frac{\delta T}{T} = \sum_{l,m} a_{lm} Y_{lm}, \tag{11}$$

where the amplitudes in the expression are recovered as

$$a_{lm} = \int_0^{2\pi} d\phi \int_0^{\pi} d\theta \sin\theta \frac{\delta T}{T} Y_{lm}. \tag{12}$$

We are interested in a_{10} as the dipole moment. We estimate the CMB dipole formula (9) numerically by using the profile considered in [10] (Fig. 1),

$$M(r) = \frac{1}{2}H_\perp^2(t_0, r_{\rm out})r^3\left[\alpha_0 - \Delta\alpha\left(\frac{1}{2}-\frac{1}{2}\tanh\frac{r-r_0}{2\Delta r}\right)\right], \tag{13}$$

$$k(r) = -H_\perp^2(t_0, r_{\rm out})\left[\beta_0 - \Delta\beta\left(\frac{1}{2}-\frac{1}{2}\tanh\frac{r-r_0}{2\Delta r}\right)\right], \tag{14}$$

where

$$\begin{aligned} t_s(r) = 0,\quad H_\perp(t_0, r_{\rm out}) = 51\ {\rm km/s/Mpc},\quad \alpha_0 = 1,\quad \Delta\alpha = 0.90,\\ r_0 = 1.34\ {\rm Gpc},\quad \Delta r = 0.536\ {\rm Gpc},\quad \beta_0 = 1-\alpha_0 = 0,\quad \Delta\beta = -\Delta\alpha = -0.90,\end{aligned} \tag{15}$$

and $H_\perp \equiv \dot{a_\perp}/a_\perp$. The induced a_{10} is of order 10^{-3} or less observed by Cosmic Background Explorer (COBE) [11], so we find that

$$\delta L \lesssim 15{\rm Mpc}, \tag{16}$$

where δL is the distance from the observer to the center of the void. This is consist with the result of [10].

5 Summary

In the LTB model, we have derived the analytic formulae for the CMB anisotropy dipole (9) and quadrupole (10), which can be used to rigorously compare consequences of this model with observations of the CMB anisotropy. Moreover, we checked the consistency of our formulae with results of the numerical analysis in [10], and constrained the distance from an observer to the center of the void. One

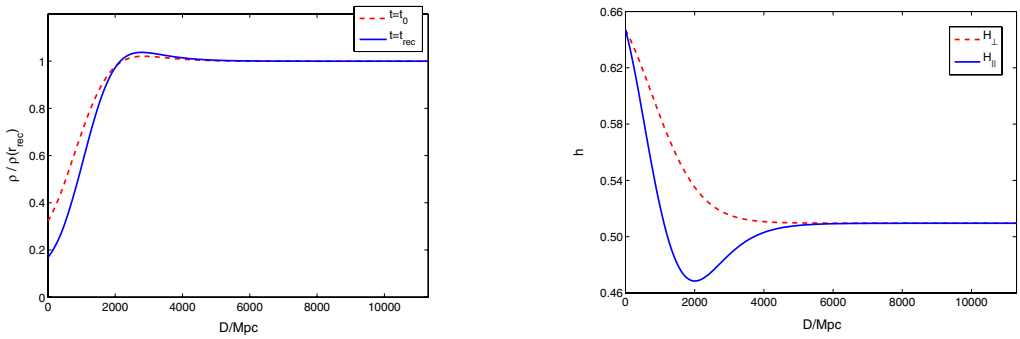

Figure 1: The profile considered in [10]. The subscript *rec* denotes the value at the recombination, and $H_{//}$(or $H_{\perp}$) $= 100h$km/s/Mpc.

of the advantages in obtaining analytic formulae is that we can identify physical origins of the CMB anisotropy in the LTB model. For example, in the CMB dipole formula (9), we can regard the first term as the initial condition at the last scattering surface, and the second term as the Integrated Sachs-Wolfe effect.

References

[1] K. Tomita, Astrophys. J. **529**, 26 (2000).

[2] G. Lemaitre, Ann. Soc. Sci. Brux **53**, 51 (1933).

[3] R. C. Tolman, Proc. Nat. Acad. Sci. USA. **20**, 169 (1934).

[4] H. Bondi, Mon. Not. Roy. Astron. Soc. **107**, 410 (1947).

[5] K. Tomita, Astrophys. J. **529**, 38 (2000).

[6] K. Tomita, MNRAS **326**, 287 (2001).

[7] H. Alnes, M. Amarzguioui, and Ø. Grøn, Phys. Rev. D**73**, 083519 (2006).

[8] M. Kasai, Prog. Theor. Phys. **117**, 1067 (2007).

[9] J. García-Bellido and T. Haugbølle, JCAP 0809: 016 (2008).

[10] H. Alnes and M. Amarzguioui, Phys. Rev. D**74**, 103520 (2006).

[11] C. L. Bennett et al., Astrophys. J. **464**, L1-L4 (1996).

[12] K. Tomita, astro-ph/0906.1325.

Wrapped brane gas as a candidate for Dark Matter

Masakazu Sano[1] and Hisao Suzuki[2]

Department of Physics, Hokkaido University, Sapporo, Hokkaido 060-0810

Abstract

D-branes wrapping over cycles of a six-dimensional torus are discussed to find a possibility of the dark matter candidate. We estimate the mass and charge of the Ramond-Ramond flux and of the scalar interaction in the four-dimensional Einstein frame. For a large volume of the six-dimensional torus and a weak string coupling, we find that there are cases in which the D-brane has a light mass and small charges. It is shown that the mass and charge satisfies the seesaw-like dual relation.

1 Introduction

The origin of the dark matter is one of mysteries of the Universe. The dark matter is not a particle involved in the standard model, because the dark matter is non-relativistic at present and doe not couple with the photon. The dark matter requires a fundamental theory like the string theory to explain the origin. If the string theory which is one of the unified theories correctly describes the Universe, the string theory should the dark matter candidate.

The string theory has two properties, the six extra dimensions and the D-brane in which ends of the open string can move along. If the D-branes wrap over only the small 6-dimensional space, we find the D-branes as particles (or the dust [1]) on the three dimensions. This particle is apparently a nonstandard baryon and a possibility of a dark matter candidate is expected. However, one may consider that the dark matter candidate is difficult. It is well known that the D-brane has interactions through the RR flux and moduli fields which roughly come from the scale of the 6-dimensional space. If the interactions with RR-flux and the moduli fields are strong, the possibility of the dark matter of the wrapped D-branes is difficult. For example, in [2], it has been shown that the density perturbations of string gases give rise to the density evolution different from the cold dark matter by the moduli interactions. We also know that the tension (effective mass) of the wrapped D-brane has a coupling with the inverse of the string coupling. If the string coupling is strong like $g_s = e^{\phi} \sim \mathcal{O}(1)$, the mass of the wrapped D-brane becomes light for $1/\sqrt{\alpha'} \sim$ TeV [3], while the D-brane has a heavy effective mass than the Planck mass for the weak string coupling. Then the observation of the wrapped D-brane is difficult.

In this talk we would like to argue that there are cases where the wrapped D-brane has the light mass and the small charges in terms of the RR-flux and the moduli fields [4]. To do this we consider the brane gas scenario [5] and the homogeneous metric. If we take the string length $\sqrt{\alpha'}$ as $1/\sqrt{\alpha'} \sim m_{\rm Planck}$ in the four-dimensional Einstein frame, it is shown that the Dp-brane ($p < 3$) has the light mass and the small charges for the large volume of the compactified space and the weak string coupling. The reason why the wrapped D-brane has the light mass and the small charges is explained. This consequence opens up the possibility of the dark matter candidate of the wrapped D-branes.

This talk is organized as follows. In Section 2, we show the existence of the light wrapped D-branes. In Section 3, we explain why the wrapped brane becomes light. It will be shown that the seesaw-like dual relation of masses between Dp- and D$(6-p)$-brane is satisfied. In Section 4, we discuss the small charges of the RR-flux and the moduli fields. The Section 5 is devoted to conclusions of our talk.

2 Light particles from wrapped D-branes

In this section we will show that a D-brane has a light mass for a large volume of the compactified space and a weak string coupling. For simplicity, we assume that the NSNS B-field vanishes and wrapped

[1]Email address: sano@particle.sci.hokudai.ac.jp
[2]Email address: hsuzuki@particle.sci.hokudai.ac.jp

branes has no coupling with baryons.

We consider the following homogeneous metric:

$$ds_{10}^2 = G_{AB}dX^A dX^B = -e^{2\lambda_0(t)}dt^2 + e^{2\lambda(t)}d\mathbf{x}^2 + e^{2\lambda'(t)}\sum_{m=4}^{9}(dy^m)^2. \tag{1}$$

G_{AB} (A, $B = 0, 1, \cdots, 9$) indicates the string-frame metric. The line element of the three-dimensional Euclid space is given by $d\mathbf{x}^2$. The coordinates $\{y^m \mid 0 \le y^m \le 2\pi\sqrt{\alpha'}\}$ describe the six-dimensional torus, T^6. The scale factor controls the scaling of the T^6 like $2\pi\sqrt{\alpha'}e^{\lambda'(t)}$ in which $\sqrt{\alpha'}$ is of the order of the Planck scale. Our main interests is to estimate the mass of the wrapped D-brane and then we will tune the scale factor, $e^{\lambda'(t)}$ by hand, although explicit models of the moduli stabilization can be constructed [1].

The Dirac-Born Infeld action of the Dp-brane is given as follows:

$$S_{\mathrm{D}p} = -T_p\int d^{p+1}\xi e^{-\phi(t)}\sqrt{-\gamma}. \tag{2}$$

where $\phi(t)$ is the dilaton which is related to the string coupling like $g_s = e^{\phi}$. The tension, T_p and the induced metric, γ_{ab} are defined by

$$T_p = 2\pi(2\pi\sqrt{\alpha'})^{-(p+1)}, \tag{3}$$

$$\gamma_{ab} = G_{AB}(t)\frac{\partial X^A}{\partial\xi^a}\frac{\partial X^B}{\partial\xi^b}. \tag{4}$$

We consider a static Dp-brane wrapping over only a p-cycle of the T^6 in order to estimate the mass. The configuration is described by $\xi^0 = t$ and $\xi^{m_a} = y^{m_a}$ ($a = 0, 1, \cdots, p$). Substituting (1) for (2), we obtain the effective mass of the wrapped Dp-brane in the string-frame as

$$S_{\mathrm{D}p} = -\int dte^{\lambda_0}\times\left(\frac{1}{\sqrt{\alpha'}}e^{-\phi(t)+p\lambda'(t)}\right) \equiv -\int dte^{\lambda_0}\times m_p^{\mathrm{string}}. \tag{5}$$

In the string frame, the mass, m_p^{string} takes a heavier mass than the Planck mass for $1/\sqrt{\alpha'} \sim m_{\mathrm{Planck}}$, if we consider the large volume of the cycles and the weak string coupling, since the mass is proportional to the volume of the p-cycle and the inverse of the string coupling.

We will, on the other hand, estimate the mass in the four-dimensional Einstein frame. We have to define the four-dimensional Einstein frame which gives moduli-independent gravitational constant for the effective four-dimensional theory. For the string-frame metric the Einstein-Hilbert term is given by

$$\frac{1}{16\pi G_{10}}\int d^{10}X\sqrt{-G}e^{-2\phi}R + \cdots = \int d^4x\sqrt{-g_{string}}\left(\frac{e^{-2\phi}V_6}{16\pi G_{10}}\right)R_{4,\,string} + \cdots \tag{6}$$

where $G_{10} = (2\pi\sqrt{\alpha'})^6(\alpha'/8)$. The four-dimensional Einstein frame is defined by

$$G_{\mu\nu} = e^{2\beta}g_{\mu\nu}, \qquad \beta = \phi - \frac{1}{2}\ln\frac{V_6}{(2\pi\sqrt{\alpha'})^6}. \tag{7}$$

Using (7), we obtain effective Einstein-Hilbert term defined by the four-dimensional Einstein frame:

$$\frac{1}{16\pi G_4}\int d^4x\sqrt{-g}R_4 + \cdots, \qquad G_4 = \frac{\alpha'}{8}. \tag{8}$$

Thus, for this frame, $m_{\mathrm{Planck}} \sim 1/\sqrt{\alpha'} \sim \mathcal{O}(10^{19})$ GeV. By (1) the volume of T^6 is given by $V_6 = (2\pi\sqrt{\alpha'})^6 e^{6\lambda'(t)}$ and then $\beta = \phi - 3\lambda'$. Substituting (7) and the definition of the β for (5), it is found that the mass described by the four-dimensional Einstein frame has the following expression:

$$S_{\mathrm{D}p} = -\int dte^n\times\left(\frac{1}{\sqrt{\alpha'}}e^{(p-3)\lambda'(t)}\right) \equiv -\int dte^n\times m_p. \tag{9}$$

The action of the wrapped D-brane does not depend on the dilaton. We are able to impose a weak string coupling, $e^{\phi} \ll 1$ without changing the mass of the wrapped D-branes. If we take $p < 3$ and $e^{\lambda'} \gg 1$, the mass, m_p is lighter that the Planck mass. For example, we consider $e^{\lambda'} \sim \mathcal{O}(10^5)$ and then the D0-brane mass becomes $m_0 \sim \mathcal{O}(10)$ TeV. From the view point of the Kalza-Klein reduction, we may expect a heavy mass with a scale of $\mathcal{O}(1/(2\pi\sqrt{\alpha'}e^{\lambda'}))$, because the compactification scale is $\mathcal{O}(2\pi\sqrt{\alpha'}e^{\lambda'})$. However the result of (9) implies large hierarchy on the mass of the wrapped D-brane. In the following section we would like to explain the reason of the light mass.

3 Why does the wrapped D-brane have the light mass ?

One may consider the existence of the light wrapped D-brane is peculiar since, in the string-frame, the mass becomes very heavy for a large volume of T^6 and a weak string coupling. In this section we will find that the light mass can be explained by the property of the effective Newton constant and a dual relation among wrapped branes.

We will focus on the strength of the gravitational interaction on the three-dimensional space by assuming constant moduli fields. In the string frame the effective Newton potential is characterized by

$$\tilde{G}_4 m_p^{\text{string}} m_q^{\text{string}} \equiv \frac{G_{10}}{e^{-2\phi}V_6} m_p^{\text{string}} m_q^{\text{string}} = G_4 m_p m_q \tag{10}$$

where $\tilde{G}_4 = e^{2\phi}((2\pi\sqrt{\alpha'})^6/V_6)G_4$. Note the right hand side can be derived by quantities defined in string frame. The right hand side of the above equation is equivalent to one calculated by masses given by the four-dimensional Einstein frame. (10) indicates that, in the four-dimensional Einstein frame, an interaction with the light particles also gives weak interaction in the string frame for heavy particles. This property is understood by the behavior of the effective string-frame Newton constant, $\tilde{G}_4$. If we take a large volume, $V_6 \gg (2\pi\sqrt{\alpha'})^6$ and weak string coupling, $e^{\phi} \ll 1$, we find $\tilde{G}_4 \ll G_4$ in the string frame. Therefore, there are cases in which the weak gravitational interaction is able to appear, although m_p^{string} is heavier than the Planck mass.

Another view point is the existence of a dual relation between a Dp-brane and a D$(6-p)$-brane. By the definition of the mass of the wrapped Dp-brane (9) in the four-dimensional Einstein frame, we can easily obtain the following dual relation:

$$m_p(t)m_{6-p}(t) = \left(\frac{1}{\sqrt{\alpha'}}\right)^2. \tag{11}$$

This relation indicates that if a heavy D$(6-p)$-brane exists, a light Dp-brane necessarily exists. The dual relation (11) support the existence of the light wrapped D-branes.

4 Small charges of the wrapped D-branes

In the previous section we have investigated the masses of various wrapped D-banes. The D-brane has the RR charge and the scalar interactions on moduli fluctuations. If we assume that the baryon does not have interactions with the wrapped D-branes, the self-interaction occurs among the wrapped D-branes. We expect the wrapped D-brane as a candidate for the dark matter, if the wrapped brane has weak interactions. In this section we would like to estimate the various charge in the four-dimensional Einstein frame. As we find below discussions, various charges of the wrapped D-branes do not depend on the dilaton and then we will impose the weak string coupling, $g_s = e^{\phi} \ll 1$.

The action of the RR flux of the Dp-brane is given by

$$S_{\text{RR}} = -\frac{1}{4\kappa_{10}} \int_{M_{10}} d^{10}X\sqrt{-G}|F_{p+2}|^2 + \mu_p \int_{\Sigma_{p+1}} C_{p+1} \tag{12}$$

A Dp-brane wrapping over a p-cycle of the T^6 is interpreted as a point particle and has a role of a source of the RR flux. Then the wrapped D-brane should be coupled with a vector filed for the effective model.

In fact, after the dimensional reduction, we can show that the effective action of the wrapped Dp-brane is explicitly described by

$$S_{\rm RR} \Longrightarrow \int d^4x\sqrt{-g}\frac{-1}{4g_p^2}F_{\mu\nu}F^{\mu\nu} + \int dtC_\mu\frac{dx^\mu}{dt}. \tag{13}$$

where the coupling is defined by $g_p^2 = 2\pi e^{2(p-3)\lambda'}$ which becomes small for $e^{\lambda'} \gg 1$ and $p < 3$. We find that the coupling satisfies the electric-magnetic dual relation, $g_p g_{(6-p)} = 2\pi$, because the D$(6-p)$ -brane is magnetic dual for the Dp-brane.

The wrapped D-brane also has a scalar interaction by fluctuations of the moduli fields. The charge can be derived by expanding the mass of the wrapped D-brane around a constant moduli value like $\lambda' = \lambda'^{(0)} + \sqrt{8\pi G_4}\delta\lambda'$. Then the source term of the scalar interaction is given by

$$\delta S_{{\rm D}p} = -Q_p\int dte^n\delta\lambda' \tag{14}$$

where we have defined the charge as $Q_p \equiv \sqrt{\pi}(p-3)e^{(p-3)\lambda'^{(0)}}$ which satisfies the scale-independent dual relation $Q_pQ_{6-p} = {\rm const.}$. Thus, Q_p also take a small value for the large volume and $p < 3$. For instance, if we consider $e^{\lambda'^{(0)}} \sim \mathcal{O}(10^5)$, the charge becomes quite small, i.e. $Q_p^2 \sim \mathcal{O}(10^{-30})$.

5 Conclusion

We have considered D-branes wrapping over cycles of a T^6 as point particles with self-interactions. In order to extract a possibility on the dark matter candidate of the wrapped D-branes we have estimated the masses and charges in terms of the RR flux and the moduli fluctuations, using the four-dimensional Einstein frame. For a large volume of T^6 and a weak string coupling it has been shown that the wrapped Dp-brane ($p < 3$) has the light mass and the weak couplings. For example, if we consider the compactification scale as $e^{\lambda'} \sim \mathcal{O}(10^5)$, the mass of the D0-brane takes $m_0 \sim \mathcal{O}(10)$ TeV. This is nontrivial, because, in general, one may expect a mass which is of the order of $\mathcal{O}(m_{\rm Planck}e^{-\lambda'})$ for the compactification scale of $\mathcal{O}(2\pi\sqrt{\alpha'}e^{\lambda'})$. The light D-branes have the possibility of the dark matter candidate.

We have to analyze various properties of the wrapped branes to declare the possibility. One of interesting points is the density perturbation of the non-relativistic wrapped branes, since the gravitational, RR, scalar interaction is characterized by

$$\mathcal{O}(G_4m_pm_q) \simeq \mathcal{O}(g_pg_q) \simeq \mathcal{O}(Q_pQ_q). \tag{15}$$

This relation implies that the interactions have a same magnitude and a complicated self-interaction arises among the branes. We cannot ignore the RR and scalar interaction for the perturbation. Then, it is quite nontrivial to re-derive the density perturbation of the ordinary cold dark matter for the non-relativistic wrapped D-branes.

References

[1] M. Sano and H. Suzuki, Phys. Rev. D**78**, 064045 (2008). [arXiv:0804.0176]

[2] S. S. Gubser and P. J. E. Peebles, Phys. Rev. D**70**, 123510 (2004). [hep-th/0402225]

[3] G. Shiu and L. T. Wang, Phys. Rev. D**69**, 126007 (2004). [hep-ph/0311228]

[4] M. Sano and H. Suzuki, Phys. Rev. D**81**, 024042 (2010). [arXiv:0907.2495]

[5] S. Alexander, Robert H. Brandenberger, D. Easson, Phys. Rev. D**62**, 103509 (2000). [hep-th/0005212]

Constraining single-field slow-roll inflation models with Bayesian model selection

Toyokazu Sekiguchi[1](a),(b) and Kawasaki Masahiro[2](b)

(a) *Institute for Cosmic Ray Research, University of Tokyo, Kashiwa, Chiba 277-8582*
(b) *Institute for the Physics and Mathematics of the Universe, University of Tokyo, Kashiwa, Chiba 277-8582*

Abstract

We investigate constraints on power spectra of the primordial curvature and tensor perturbations with priors based on single-field slow-roll inflation models. The Hubble slow-roll parameters are included in cosmological parameters and the primordial power spectra are generated using the inflationary flow equations. Using data from recent observations of CMB and several measurements of geometrical distances in the late Universe, we perform Bayesian parameter estimation and model selection for models that have separate priors on the slow-roll parameters. The same analysis is also performed adopting the standard parameterization of the primordial power spectra. We confirmed that the scale-invariant Harrison-Zel'dovich spectrum is disfavored with more significance than previous studies. While current observations appear to be optimally modeled with some simple models of single-field slow-roll inflation, data is not enough constraining to distinguish these models.

1 Introduction

Inflation is now an essential part of our best description of the Universe. The simplest class of models of inflation is so-called *single-field slow-roll inflation* (simply 'inflation' hereafter) [1, 2]. It predicts generation of gaussian, nearly scale-invariant primordial curvature perturbation, which gives excellent fits to current observational data including the cosmic microwave background (CMB).

As a model of inflation left its vestige in the late Universe in an observable way through generation of the primordial curvature and tensor perturbations, constraints on models have been mainly investigated through constraining power spectra of these primordial perturbations, $\mathcal{P}_\zeta(k)$ and $\mathcal{P}_h(k)$, using various cosmological observations. One of the most familiar ways may be to adopt the standard parameterization, $P_\zeta(k) = A_s(k/k_*)^{n_s-1+\frac{\alpha_s}{2}\ln(k/k_*)+\cdots}$ and $P_h(k) = rA_s(k/k_*)^{n_t+\cdots}$ and derive constraints on them. Assuming a power-law $\mathcal{P}_\zeta(k) \propto A_s k^{n_s-1}$ with $P_h(k) = 0$, WMAP5 [3] recently give $-0.065 < n_s - 1 < -0.009$ (95% C.L.), suggesting a significant deviation from the Harrison-Zel'dovich (HZ) power spectrum (i.e. $r = 0$ and $n_s - 1 = \alpha_s = \cdots = 0$). However, constraints on the primordial power spectra are highly dependent on parameter spaces which we investigate, which consequently affects our final inference on observationally plausible models of inflation.

Since we do not in advance know a parameter space where we should explore a constraint on the power spectrum, we also need to examine whether the parameter space is appropriate. More generally, appropriateness of a model, which possesses its own prior assumption, should also be discussed. A guiding principle in looking for an optimal model is Occam's razor, which penalizes unnecessary assumption in describing observations. Bayesian model selection is Bayesian implementation of Occam's razor, which is now frequently applied in the context of cosmology. In particular, the authors in Ref. [4] have adopted Bayesian model selection to assess optimal orders up to which reconstruction of inflaton potential should be performed. Besides, [5] applied Bayesian model selection in distinguishing some class of inflation models.

Motivated by [4, 5] and other earlier studies, we investigate an optimal constraint on primordial perturbation spectra and make comparison of single-field slow-roll inflation models using recent cosmological

[1]Email address: sekiguti@icrr.u-tokyo.ac.jp
[2]Email address: kawasaki@icrr.u-tokyo.ac.jp

observations. For these purpose we make vigorous use of Bayesian model selection. We compare Bayes evidences for several models which have separate priors on inflationary slow-roll parameters, or parameters of primordial power spectra. Each of these models can be regarded as representing some class of single-field slow-roll inflation models.

2 Hubble slow-roll flow equations

We make use of the *Hubble slow-roll* (HSR) flow equations [6] at leading order. During an epoch of inflation, the slow-rolliing inflaton field ϕ can be regarded as a generalized time coordinate and the Hubble parameters can be given as a function of ϕ. Dynamics in the inflationary universe is described by the HSR flow equations

$$\epsilon_H(\phi) = \frac{1}{4\pi}\left(\frac{H(\phi)'}{H(\phi)}\right)^2 \tag{1}$$

$$\eta_H(\phi) = \frac{1}{4\pi}\frac{H(\phi)''}{H(\phi)}, \tag{2}$$

where $H'(\phi) \equiv dH(\phi)/d\phi$ and $H''(\phi) \equiv d^2H(\phi)/d\phi^2$. Given initial values $\epsilon_* \equiv \epsilon_H(\phi_*)$, $\eta_* \equiv \eta_H(\phi_*)$ at a fiducial ϕ_*, the HSR parameters ϵ, η are solved. Then a wave number that exits the horizon at time ϕ is given by $k = aH(\phi)$.

To leading order in slow-roll approximation, the power spectrum of the primordial curvature and tensor perturbations, $\mathcal{P}_\zeta(k)$ and $\mathcal{P}_h(k)$, respectively, are given by [7]

$$\mathcal{P}_\zeta(k) = \frac{[1-(2C+1)\epsilon(\phi)+C\eta(\phi)]^2}{\pi\epsilon(\phi)}H(\phi)^2\Big|_{\phi=\phi(k)} \tag{3}$$

$$\mathcal{P}_h(k) = \frac{16[1-(C+1)\epsilon(\phi)]^2}{\pi}H(\phi)^2\Big|_{\phi=\phi(k)}. \tag{4}$$

where $C = -2+\ln 2+\gamma \approx -0.729637$ and γ is the Euler constant. In addition, duration of inflation after the horizon exit of a scale k is also computed from the HSR parameters,

$$N(k) = -\int_{\phi_{\rm end}}^{\phi(k)} d\phi \sqrt{\frac{4\pi}{\epsilon_H(\phi)}}, \tag{5}$$

where $\phi_{\rm end}$ is ϕ at the end of inflation, i.e. $\epsilon_H(\phi_{\rm end}) = 1$. If the lowest energy scale of inflation is assumed, $N(k)$ is bounded from below . We impose a prior on the e-folding number, $N > 25$, which means that the energy scale of inflation should be higher than TeV [8].

3 Bayesian model selection

In order to explore an optimal constraint on the primordial power spectra, and compare different models of inflation, we adopt Bayesian model selection. In Bayesian model selection, likelihood of a model is measured by the Bayes evidence. Given data, the Bayesian evidence $E(M)$ of a *model* M with a set of model parameters Θ is given by

$$E(M) \equiv \int d\Theta \mathcal{L}(\Theta)\pi(\Theta|M), \tag{6}$$

where $\mathcal{L}(\Theta) \equiv P(\text{data}|\Theta, M)$ is the likelihood function, and $\pi(\Theta|M)$ is the prior probability distribution function. $E(M)$ assess goodness of a model M, weighing fit to the data and predictability.

The relative likelihood of different models M_i and M_j is assessed by the ratio of their Bayes evidences $B_{ij} \equiv \ln \dfrac{E(M_i)}{E(M_j)}$ which is called Bayes factor. Jeffreys' scale is often adopted to connect numbers and semantics, which states: for $|B_{ij}| < 1$ the evidence is not significant; $1 < |B_{ij}| < 2.5$ significant; $2.5 < |B_{ij}| < 5$ strong; and $5 < |B_{ij}|$ decisive.

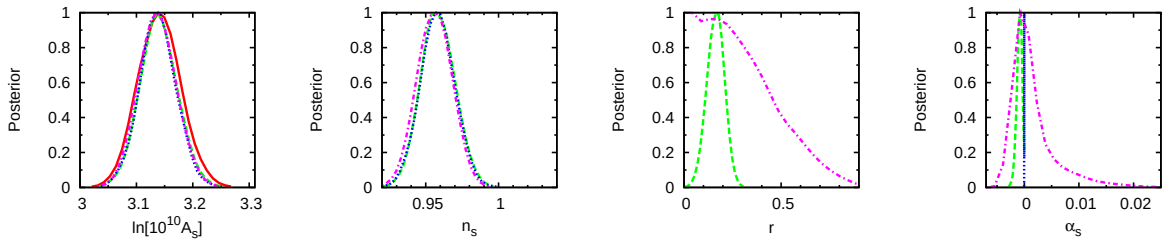

Figure 1: Constraints on *derived* parameters of primordial power spectra. Models shown are M_ϵ (dashed green line), M_η (dotted blue line), $M_{\epsilon\eta}$ (dot-dashed magenta line) and the reference $M_{\rm HZ}$ (solid red line).

4 Analysis with observational data

We adopt CMB data from WMAP5 [9], as well as the observations at small angular scales including ACBAR [10], CBI [11], BOOMERANG [12] and QUAD [13]. In addition, we adopt observational data of geometrical distances of the late Universe, including the Union data set of type Ia supernovae (SN) [14], the measurement of the baryon acoustic oscillation (BAO) scales in galaxy power spectra [15] and the $\rm SH_0ES$ measurement of the Hubble constant $H_0 = 74.2 \pm 3.6$ [16]. We assume a flat ΛCDM universe.

First we adopted the standard parameterization of primordial power spectra. We compared three different models with parameters n_s, r, and/or α_s: M_{n_s}, $M_{n_s r}$ and $M_{n_s \alpha_s}$, where the subscripts represents the parameters allowed to vary in each model. With a model with HZ spectrum $M_{\rm HZ}$ being taken as a reference model, Bayes factors for these models are 4.3, 2.6 and 4.4 for M_{n_s}, $M_{n_s r}$ and $M_{n_s \alpha}$, respectively. We find that HZ spectrum is highly disfavored in modeling of observational data compared with other models M_{n_s}, $M_{n_s r}$ and $M_{n_s \alpha}$. In addition, current data is optimally modeled by M_{n_s}; presence of neither the tensor perturbation nor the running of scalar spectral index is suggested from data. Therefore constraint of M_{n_s} can be regarded as an optimal constraint on primordial power spectra

$$\ln[10^{10} A_s] = 3.137^{+0.028}_{-0.032} \quad (7)$$

$$n_s = 0.957^{+0.010}_{-0.011}, \quad (8)$$

where errors are given at 68% C.L. Regarding the tensor perturbation and the running of the scalar index, we find no evidence at present.

Furthermore, we also investigate comparison of models with HSR parameters. We adopt $M_{\rm HZ}$ and additionally three different models with separate priors on HSR parameters: M_ϵ, M_η, $M_{\epsilon\eta}$, where the subscripts represent the HSR parameters allowed to vary in each model. If these parameters are varied, top-hat priors $0 < \epsilon < 0.1$ and $-0.1 < \eta < 0.1$ are adopted in the analysis. In addition, we also adopt a prior on the e-folding number $N > 25$. With $M_{\rm HZ}$ being continuously taken as the reference model, the Bayes factors are 5.8, 4.7 and 4.2 for M_ϵ, M_η and $M_{\epsilon\eta}$, respectively. Among these models, Bayes factors are very comparable and we observe that current data is not constraining enough to distinguish these models.

The marginal posterior distributions of standard parameters of the primordial power spectra, including A_s, n_s, r and α_s are presented in Figure 1. We note that constraints on A_s and n_s are almost independent on priors and coincide with Eqs. (7-8). This suggests that these parameters are indeed required in modeling the observational data. On the other hand, constraints on r and α_s are very dependent on the priors, which suggests that these parameters or features of the primordial power spectra are not signified in the data.

5 Conclusion

We have investigated constraints on the primordial power spectra and comparison of single-field slow-roll inflation models using data from recent observations of CMB combined with measurements of BAO, SN and H_0. By employing Bayesian model selection, we found that a model with the scale-invariant HZ

spectrum is strongly disfavored from current data, in comparison with several simple models allowing scale-dependence of the power spectra. We have also proposed an optimal constraint (7-8) on the primordial power spectra. Adopting our somewhat artificial division of models for single-field slow-roll inflation, M_ϵ, M_η and $M_{\epsilon\eta}$, with a theoretical prior $N > 25$, we have found the Bayes evidences for these models from current data are almost comparable. Planck [17] and other CMB surveys will probe primordial B-mode down to $r = 0.01$ in the near future and the method we demonstrated here will help us compare different models of inflation and derive an optimal constraint on primordial power spectra.

Acknowledgment

T.S. would like to thank the Japan Society for the Promotion of Science for financial support. This work is supported by Grant-in-Aid for Scientific research from the Ministry of Education, Science, Sports, and Culture (MEXT), Japan, under Contract No. 14102004 (M.K.), and also by World Premier International Research Center Initiative, MEXT, Japan.

6 References

References

[1] A. D. Linde, Phys. Lett. B **108**, 389 (1982).

[2] A. J. Albrecht and P. J. Steinhardt, Phys. Rev. Lett. **48**, 1220 (1982).

[3] E. Komatsu *et al.* [WMAP Collaboration], Astrophys. J. Suppl. **180**, 330 (2009).

[4] J. Lesgourgues and W. Valkenburg, Phys. Rev. D **75**, 123519 (2007).

[5] G. Ballesteros, J. A. Casas, J. R. Espinosa, R. Ruiz de Austri and R. Trotta, JCAP **0803**, 018 (2008).

[6] S. M. Leach, A. R. Liddle, J. Martin and D. J. Schwarz, Phys. Rev. D **66**, 023515 (2002).

[7] E. D. Stewart and D. H. Lyth, Phys. Lett. B **302**, 171 (1993).

[8] H. Peiris and R. Easther, JCAP **0610**, 017 (2006).

[9] J. Dunkley *et al.* [WMAP Collaboration], Astrophys. J. Suppl. **180**, 306 (2009), M. R. Nolta *et al.* [WMAP Collaboration], Astrophys. J. Suppl. **180**, 296 (2009). G. Hinshaw *et al.* [WMAP Collaboration], Astrophys. J. Suppl. **180**, 225 (2009).

[10] C. L. Reichardt *et al.*, arXiv:0801.1491 [astro-ph].

[11] J. L. Sievers *et al.*, Astrophys. J. **660**, 976 (2007).

[12] W. C. Jones *et al.*, Astrophys. J. **647**, 823 (2006), F. Piacentini *et al.*, Astrophys. J. **647**, 833 (2006), T. E. Montroy *et al.*, Astrophys. J. **647**, 813 (2006).

[13] R. B. Friedman *et al.* [QUaD collaboration], arXiv:0901.4334 [astro-ph.CO].

[14] M. Kowalski *et al.* [Supernova Cosmology Project Collaboration], Astrophys. J. **686**, 749 (2008).

[15] W. J. Percival *et al.*, arXiv:0907.1660 [astro-ph.CO].

[16] A. G. Riess *et al.*, arXiv:0905.0695 [astro-ph.CO].

[17] [Planck Collaboration], arXiv:astro-ph/0604069.

Higgs portal heavy neutrino dark matter

Nobuchika Okada[1(a)] and Osamu Seto[2(b)3]

(a) *Department of Physics and Astronomy, University of Alabama, Tuscaloosa, AL 35487, USA*
(b) *Department of Architecture and Building Engineering, Hokkai-Gakuen University, Sapporo 062-8605, Japan*

Abstract

We investigate the right-handed neutrino dark matter in the minimal gauged $U(1)_{B-L}$ model with an additional discrete parity which ensures the stability of dark matter particle. We show that the thermal relic abundance of the right-handed neutrino dark matter with help of Higgs resonances can match the observed dark matter abundance. In addition we estimate the cross section with nuclei and show that the next generation direct dark matter search experiments can explore this model.

1 Introduction

The nonvanishing neutrino masses have been confirmed by various neutrino oscillation phenomena and indicate the evidence of new physics beyond the Standard Model (SM). The most attractive idea to naturally explain the tiny neutrino masses is the seesaw mechanism [1], in which the right-handed (RH) neutrinos singlet under the SM gauge group are introduced. The minimal gauged $U(1)_{B-L}$ model based on the gauge group $SU(3)_C \times SU(2)_L \times U(1)_Y \times U(1)_{B-L}$ [2] is an elegant and simple extension of the SM, in which the RH neutrinos of three generations are necessarily introduced because of the gauge anomaly cancellation, and their masses arise associated with the $U(1)_{B-L}$ gauge symmetry breaking.

Although the scale of the $B-L$ gauge symmetry breaking is basically arbitrary as long as phenomenological constraints are satisfied, one interesting option is to take it to be the TeV scale [3]. In fact, it has been recently pointed out that when the classical conformal invariance is imposed on the minimal $U(1)_{B-L}$ model, the symmetry breaking scale appears to be the TeV scale naturally [4]. For such a case, an additional neutral gauge boson Z', Higgs boson H and the RH neutrinos appear at the TeV scale unless the $U(1)_{B-L}$ gauge coupling is extremely small, and they can be discovered at Large Hadron Collider [5–9]. If these happen, we might understand well the relation between the gauge symmetry breaking and the origin of neutrino mass.

These TeV scale models are interesting and appealing, but one might think that the absence of dark matter (DM) candidate is a shortcoming of models, although sterile neutrino DM is possible [10]. We propose here a very simple idea to posses the DM candidate in the minimal gauged $U(1)_{B-L}$ model [11]. We introduce the Z_2 parity into the model and impose one of three RH neutrinos to be odd, while the other fields even. In this way, the Z_2-odd RH neutrino becomes stable and can be the DM candidate. Note that two RH neutrinos are actually enough to reconcile with the observed neutrino oscillation data with the prediction of one massless left-handed neutrino. Thus, without introducing any additional new dynamical degrees of freedom, the DM particle has been provided in the minimal gauged $U(1)_{B-L}$ model.

2 The minimal gauged $U(1)_{B-L}$ model with Z_2 parity

The model is based on the gauge group $SU(3)_C \times SU(2)_L \times U(1)_Y \times U(1)_{B-L}$. Additional fields besides the SM fields are a gauge field C_μ of the $U(1)_{B-L}$, a SM singlet $B-L$ Higgs boson Ψ with two $U(1)_{B-L}$ charge, and three RH neutrinos N_i which are necessary for the gauge anomaly cancellation. For the two RH neutrinos, N_1 and N_2, we assign Z_2 parity even, while odd for N_3, so that the RH neutrino N_3 is stable and, hence, the DM candidate.

[1] Email address: okadan@ua.edu
[2] Email address: osamu@hgu.jp
[3] speaker

At first, we summarize additional interactions. The covariant derivative is extended so that the additional $U(1)_{B-L}$ gauge interaction with its gauge coupling g_{B-L} is implemented. Yukawa interactions relevant for the neutrino masses are given by

$$\mathcal{L}_{int} = \sum_{\alpha=1}^{3}\sum_{\imath=1}^{2} y_{\alpha i}\bar{L}_\alpha \tilde{\Phi} N_i - \frac{1}{2}\sum_{i=1}^{3}\lambda_{R_i}\bar{N}\Psi P_R N + \text{h.c.}, \tag{1}$$

where $\tilde{\Phi} = -i\tau_2\Phi^*$ for Φ being the SM Higgs doublet. Because of the Z_2 parity, the DM candidate N_3 has no Yukawa coupling with the left-handed lepton doublets. The Higgs fields ϕ and ψ are obtained by expanding Φ and Ψ as

$$\Phi = \begin{pmatrix} 0 \\ \frac{1}{\sqrt{2}}(v+\phi) \end{pmatrix}, \tag{2}$$

$$\Psi = \frac{1}{\sqrt{2}}(v'+\psi), \tag{3}$$

around the vacuum expectation values v and v', and related with the two mass eigenstates h and H through the mixing angle θ.

Associated with the $U(1)_{B-L}$ gauge symmetry breaking, the new massive neutral gauge boson Z' with the mass

$$M_{Z'}^2 = 4g_{B-L}^2 v'^2. \tag{4}$$

arises and the RH neutrinos N_i acquire masses $M_{N_i} = -\lambda_{R_i}\frac{v'}{\sqrt{2}}$. The current lower bound on the Z' boson is obtained to be

$$\frac{M_{Z'}}{g_{B-L}} = 2v' \gtrsim 6\ (7)\ \text{TeV} \tag{5}$$

in Ref. [12] ([13]). Two Z_2 even RH neutrinos N_1 and N_2 are responsible for light neutrino masses via the seesaw mechanism.

3 Right-handed neutrino dark matter

Due to the Z_2 parity, one of RH neutrino N_3 (we denote N hereafter) in our model is the DM candidate. We first estimate its relic abundance and identify the model parameters to be consistent with the current observations. Next we calculate the scattering cross section between the DM particle and nuclei and see the implication on the direct dark matter search experiments.

3.1 Thermal relic density

The dark matter RH neutrino interacts with the SM particles through couplings with $B-L$ gauge and $B-L$ Higgs bosons. Note that neutrino Yukawa interactions are absent because of the Z_2 parity. The most of annihilation modes are s-channel Z', H and h exchange processes. In practice, the dominant contributions come from the Higgs (h and H) exchange diagrams, because the Z' exchange processes are suppressed by the inverse square of the $B-L$ Higgs VEV $v' \gtrsim 3$ TeV. Thus, we obtain effectively a Higgs portal DM of RH neutrino. The relevant annihilation modes are the annihilation into $f\bar{f}$, W^+W^-, ZZ, and $h(H)h(H)$. Since the RH neutrino DM couples to only the $B-L$ Higgs Ψ while a SM particle does to the SM Higgs Φ, the DM annihilation occurs only through the mixing angle θ between these two Higgs bosons which is constrained by the precision electroweak measurements [14].

The thermal relic abundance of DM

$$\Omega_N h^2 = 1.1\times 10^9 \frac{m_N/T_d}{\sqrt{g_*}M_P\langle\sigma v\rangle}\text{GeV}^{-1}, \tag{6}$$

with the Planck mass M_P, the thermal averaged product of the annihilation cross section and the relative velocity $\langle\sigma v\rangle$, the total number of relativistic degrees of freedom in the thermal bath g_*, and the decoupling

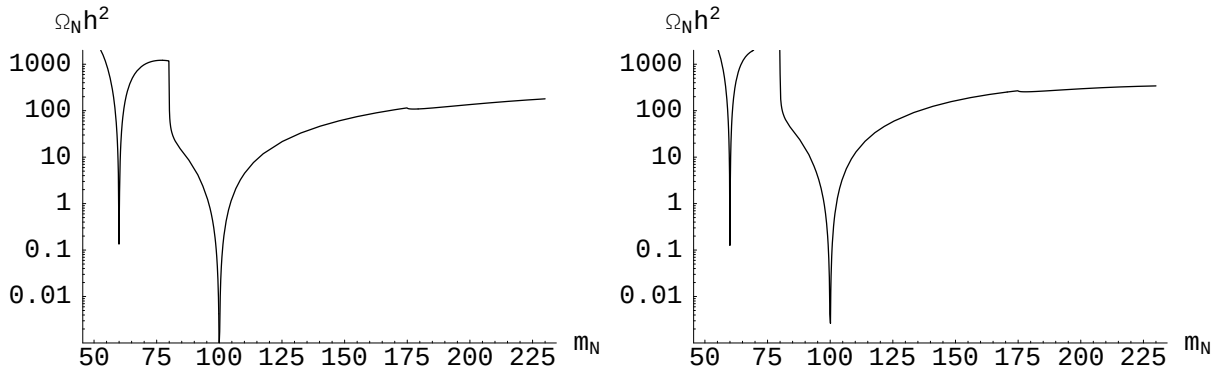

Figure 1: The thermal relic density of RH neutrino dark matter as a function of its mass with $\sin\theta = 0.7$ (0.3) in the left (right) panel for $(v', M_h, M_H, M_{Z'}) = (4\text{ TeV}, 120\text{ GeV}, 200\text{ GeV}, 1\text{ TeV})$.

temperature T_d, is evaluated by solving the Boltzmann equation with the Friedmann equation under the radiation dominated Universe [15]. The figure 1 shows the relic density $\Omega_N h^2$ as a function of the DM mass m_N for $(v', M_h, M_H, M_{Z'}) = (4\text{ TeV}, 120\text{ GeV}, 200\text{ GeV}, 1\text{ TeV})$. The left (right) panel is for $\sin\theta = 0.7$ (0.3). The Willkinson Microwave Anisotropy Probe measured the value of DM abundance as $\Omega_{DM}h^2 \simeq 0.1$ [16]. The figure 1 shows that a desired DM relic abundance can be obtained for only near Higgs resonances, $m_N \approx M_h/2$ or $M_H/2$.

Our model is quite analogous to the so-called gauge singlet scalar DM [17–19]. In the gauge singlet scalar DM model, the thermal abundance and its detection cross section can be controlled by the coupling between the SM Higgs boson and the DM particle. The only Higgs resonance region is available if the scalar DM is lighter than the W-boson, on the other hand, a small coupling is necessary if the scalar DM can annihilate into W-boson pairs. In contrast with this, it is not possible for our RH neutrino DM to obtain the desired DM abundance without the Higgs resonant annihilation, even if the annihilation mode into W-boson pair becomes kinematically available, because the bound on v' given by Eq. (5) is so stringent.

3.2 Cross section for direct searches

Our RH neutrino DM can elastically scatter off with nuclei, unlike another RH neutrino DM model has been proposed by Krauss *et.al.* [20] and studied [21, 22]. The main process is due to Higgs exchange. The figure 2 shows the spin-independent (SI) cross section of RH neutrino with a proton $\sigma_{SI}^{(p)}$.

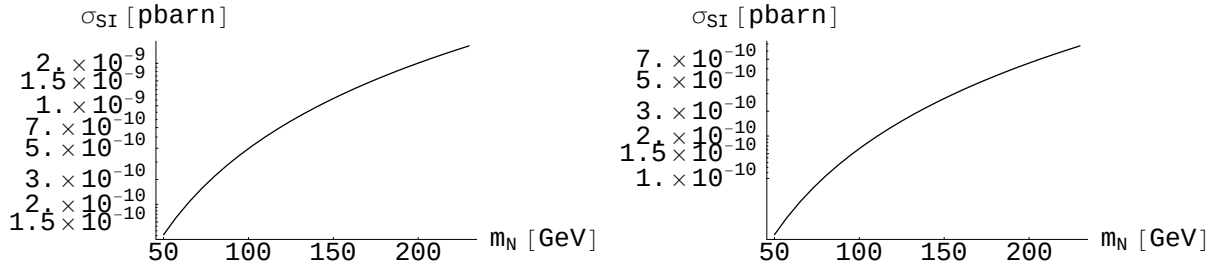

Figure 2: The spin independent scattering cross section with a proton. All parameters are same as these used in the previous subsection. The left(right) figure corresponds to $\sin\theta = 0.7$ (0.3).

4 Summary

We have constructed an effectively Higgs portal RH neutrino DM based on gauged $U(1)_{B-L}$ with an additional discrete Z_2 parity to stabilize the DM candidate. One of RH neutrinos is the available DM candidate, while the rest of two generate nonvanishing neutrino masses with one vanishing mass eigenvalue to explain neutrino oscillation. Due to the stringent bound on the Z' boson by Eq. (5), the canonical value of the relic density is of $\Omega_N h^2 \gg 0.1$ which is too abundant. In other words, cosmological measurements of the DM abundance read the prediction that the DM mass should be about one half of a Higgs mass because the resonance annihilation is required. We have estimated the DM cross section with a proton which is within the reach of near future ton scale direct dark matter search experiments.

References

[1] T. Yanagida, in *Proceedings of Workshop on the Unified Theory and the Baryon Number in the Universe*, Tsukuba, Japan, edited by A. Sawada and A. Sugamoto (KEK, Tsukuba, 1979), p 95; M. Gell-Mann, P. Ramond, and R. Slansky, in *Supergravity*, Proceedings of Workshop, Stony Brook, New York, 1979, edited by P. Van Nieuwenhuizen and D. Z. Freedman (North-Holland, Amsterdam, 1979), p 315; R. N. Mohapatra and G. Senjanovic, Phys. Rev. Lett. **44**, 912 (1980).

[2] R. N. Mohapatra and R. E. Marshak, Phys. Rev. Lett. **44**, 1316 (1980) [Erratum-ibid. **44**, 1643 (1980)]; R. E. Marshak and R. N. Mohapatra, Phys. Lett. B **91**, 222 (1980).

[3] S. Khalil, J. Phys. G **35**, 055001 (2008).

[4] S. Iso, N. Okada and Y. Orikasa, Phys. Lett. B **676**, 81 (2009).

[5] W. Emam and S. Khalil, Eur. Phys. J. C **522**, 625 (2007).

[6] K. Huitu, S. Khalil, H. Okada and S. K. Rai, Phys. Rev. Lett. **101**, 181802 (2008).

[7] L. Basso, A. Belyaev, S. Moretti and C. H. Shepherd-Themistocleous, Phys. Rev. D **80**, 055030 (2009).

[8] P. F. Perez, T. Han and T. Li, Phys. Rev. D **80**, 073015 (2009).

[9] S. Iso, N. Okada and Y. Orikasa, Phys. Rev. D **80**, 115007 (2009).

[10] S. Khalil and O. Seto, JCAP **0810**, 024 (2008).

[11] N. Okada and O. Seto, in preparation.

[12] M. S. Carena, A. Daleo, B. A. Dobrescu and T. M. P. Tait, Phys. Rev. D **70**, 093009 (2004).

[13] G. Cacciapaglia, C. Csaki, G. Marandella and A. Strumia, Phys. Rev. D **74**, 033011 (2006).

[14] S. Dawson and W. Yan, Phys. Rev. D **79**, 095002 (2009).

[15] E. W. Kolb and M. S. Turner, *The Early Universe*, Addison-Wesley (1990).

[16] E. Komatsu *et al.*, arXiv:1001.4538 [astro-ph.CO].

[17] J. McDonald, Phys. Rev. D **50**, 3637 (1994).

[18] C. P. Burgess, M. Pospelov and T. ter Veldhuis, Nucl. Phys. B **619**, 709 (2001).

[19] For a recent study, see e.g., C. E. Yaguna, JCAP **0903**, 003 (2009).

[20] L. M. Krauss, S. Nasri and M. Trodden, Phys. Rev. D **67**, 085002 (2003).

[21] E. A. Baltz and L. Bergstrom, Phys. Rev. D **67**, 043516 (2003).

[22] K. Cheung and O. Seto, Phys. Rev. D **69**, 113009 (2004).

Closed trapped surfaces in higher dimensional Vaidya type solutions

Masahiro Shimano[1] and Tomohiro Harada[2]

Department of Physics, Rikkyo University, Toshima, Tokyo 171-8501

Abstract

In higher dimensional self-similar Vaidya spacetime and five dimensional ring type spacetime which has a self-similar mass function, we have constructed closed trapped surfaces which begin in a flat region, pass through a self-similar Vaidya region, and end in a black hole region, respectively. Moreover, we have shown that in both spacetimes, as long as spacetimes have closed trapped surfaces as above, a naked singularity never occur.

1 Introduction

A black hole is defined by an event horizon which is a boundary of a region in spacetime that cannot be observed from infinity. Therefore, unless we know an entire future evolution of spacetime, we cannot define the black hole. However, Eardley conjectured that the boundary of the region that contains marginally outer trapped surfaces coincide with the event horizon [1]. So, a notion of outer trapped surfaces might be a definition of the black hole. For the four dimensional Vaidya solution, Ben-Dov shown that Eardley's conjecture is true [2]. It should be noted that outer trapped surfaces are difference from trapped surfaces as follows: outer trapped surfaces are closed spacelike $D-2$ surfaces whose outer null expansions is negative, on the other hand, trapped surfaces are closed spacelike $D-2$ surfaces whose both null expansions are negative.

In four dimensional Vaidya spacetime, if we consider trapped surfaces, spacetime has interesting features. Numerical results of Schnetter and Krishnan shown that the outer boundary of trapped surfaces can extend into the flat region of Vaidya spacetime [3], and Bengtsson and Senovilla considered the self-similar Vaidya solution, and they constructed closed trapped surfaces that begin in a flat region, pass through a shell, and end in a Schwarzschild region [4]. Hence, trapped surfaces are able to extend into the flat region. Moreover, Bengtsson and Senovilla shown that if spacetime has closed trapped surfaces as they constructed, a naked singularity never occur in this spacetime.

How are these features in higher dimensional black holes? Can we prove Eardley's conjecture? and Do closed trapped surfaces extend into the flat region? At least, in higher dimensional Vaidya spacetime, if we are able to construct closed trapped surfaces that are similar to Bengtsson and Senovilla's result by using the same manner to Ref. [4], we might be able to consider the definition of black holes as Eardley's conjecture. Therefore, we concern both higher dimensional self-similar Vaidya spacetime and five dimensional ring type spacetime which has a self-similar mass function. Then we will construct closed trapped surfaces as Bengtsson and Senovilla's result in both spacetimes.

In this paper, briefly we only consider higher dimensional self-similar Vaidya spacetime.

2 D dimensional Vaidya spacetime

We consider a D dimensional Vaidya solution [5]

$$ds^2 = -\left(1 - \frac{2m}{(D-3)r^{D-3}}\right) dv^2 + 2dvdr + r^2 \left(d\theta_1^2 + \sin^2\theta_1 d\theta_2^2 + \cdots + \sin^2\theta_1 \cdots \sin^2\theta_n d\theta_{n+1}^2\right), \quad (1)$$

[1]Email address: shimano@rikkyo.ac.jp
[2]Email address: harada@rikkyo.ac.jp

which has a mass function given by

$$m = \begin{cases} 0 & , \quad v \leq 0 \\ \mu v^{D-3} & , \quad 0 \leq v \leq M^{\frac{1}{D-3}}/\mu \\ M & , \quad v \geq M^{\frac{1}{D-3}}/\mu \end{cases}, \tag{2}$$

where $n = D-3$, $D \geq 4$, μ and M are constants, respectively. There is a radial influx of null fluid in an initially empty region of D dimensional Minkowski spacetime. For $0 \leq v \leq M^{1/(D-3)}/\mu$ spacetime is D dimensional Vaidya with the self-similar mass function, and for $v \geq M^{1/(D-3)}/\mu$ we have D dimensional Schwarzschild spacetime. We know that a naked singularity will occur if and only if the mass function satisfies the following condition [6],

$$\mu < \left[\frac{(D-3)}{2(D-2)}\right]^{D-2}. \tag{3}$$

2.1 Two types of trapped surfaces

We consider two types of $D-2$ surfaces as follows:

Table 1: The type of $D-2$ surfaces

Type 1	$\theta_1 = \frac{\pi}{2}, \quad r = R(\rho), \quad v = V(\rho), \quad \theta_2 = \phi_2, \quad \cdots, \quad \theta_{n+1} = \phi_{n+1}.$ $\theta_2 = \frac{\pi}{2}, \quad r = R(\rho), \quad v = V(\rho), \quad \theta_1 = \phi_1, \quad \theta_3 = \phi_3, \quad \cdots, \quad \theta_{n+1} = \phi_{n+1}.$ etc.
Type 2	$\theta_1 = \Theta(\rho), \quad v = V(\rho), \quad r = \text{const}, \quad \theta_2 = \phi_2, \quad \cdots, \quad \theta_{n+1} = \phi_{n+1}.$ $\theta_2 = \Theta(\rho), \quad v = V(\rho), \quad r = \text{const}, \quad \theta_1 = \phi_1, \quad \theta_3 = \phi_3, \quad \cdots, \quad \theta_{n+1} = \phi_{n+1}.$ etc.

In Table.1, Type 1 surfaces follow that r and v are the function of ρ, and the one of angles is constant. On the other hand, Type 2 surfaces obey that the one of angles and v are the function of ρ, and r is constant.

By using these surfaces, we will construct closed trapped surfaces that begin in the flat region, pass through the self-similar Vaidya region, and end in the black hole region.

2.2 Closed trapped surfaces

Closed trapped surfaces are composed of the following parts:

- flat region: we consider type 1 surfaces and a topological disk given by the hyperboloid

$$v = t_0 + r - \sqrt{r^2 + k^2} \tag{4}$$

with constants t_0, k, where $t = v - r$ and $R = \rho$.

- self-similar Vaidya region: we also consider type 1 surfaces and a topological cylinder defined by $\theta = \pi/2$ and

$$\frac{dV}{dR} = \frac{a}{b - X}, \quad \text{where} \quad X = \frac{V}{R}, \quad \text{and} \quad R = \rho. \tag{5}$$

where a, b are constants subject to $a > b^2/4$. Owing to this part, we will connect trapped surfaces in whole region.

- black hole region: we consider type 2 surfaces, and another disk composed of two parts

  - a cylinder with $\theta = \pi/2$; $\gamma M = (D-3)R^{D-3}$ where γ is a positive constant.

- another final capping disk defined by

$$\left(\Theta - \frac{\pi}{2} + \delta\right)^2 + \left(V\left(\frac{D-3}{\gamma M}\right)^{\frac{1}{(D-3)}} - \sigma_0\right)^2 = \delta^2, \quad 0 < \delta \leq \frac{\pi}{2}. \tag{6}$$

with constants σ_0 and δ

In flat and self-similar Vaidya regions, all Type 1 surfaces are closed trapped surfaces, if and only if the mass function satisfies the following condition:

$$\mu > \frac{1}{4}\left(\frac{(D-3)}{\gamma}\right)^{\frac{1}{D-3}}. \tag{7}$$

In black hole region, the condition of trapped surfaces differ from each Type 2 surfaces. the surfaces, where v and θ_1 are the function of ρ, are trapped surfaces, if γ satisfies the following condition:

$$(D-3)\sqrt{\frac{2}{\gamma} - 1}\left(\frac{1}{\gamma} - 1\right) > \frac{1}{\delta}. \tag{8}$$

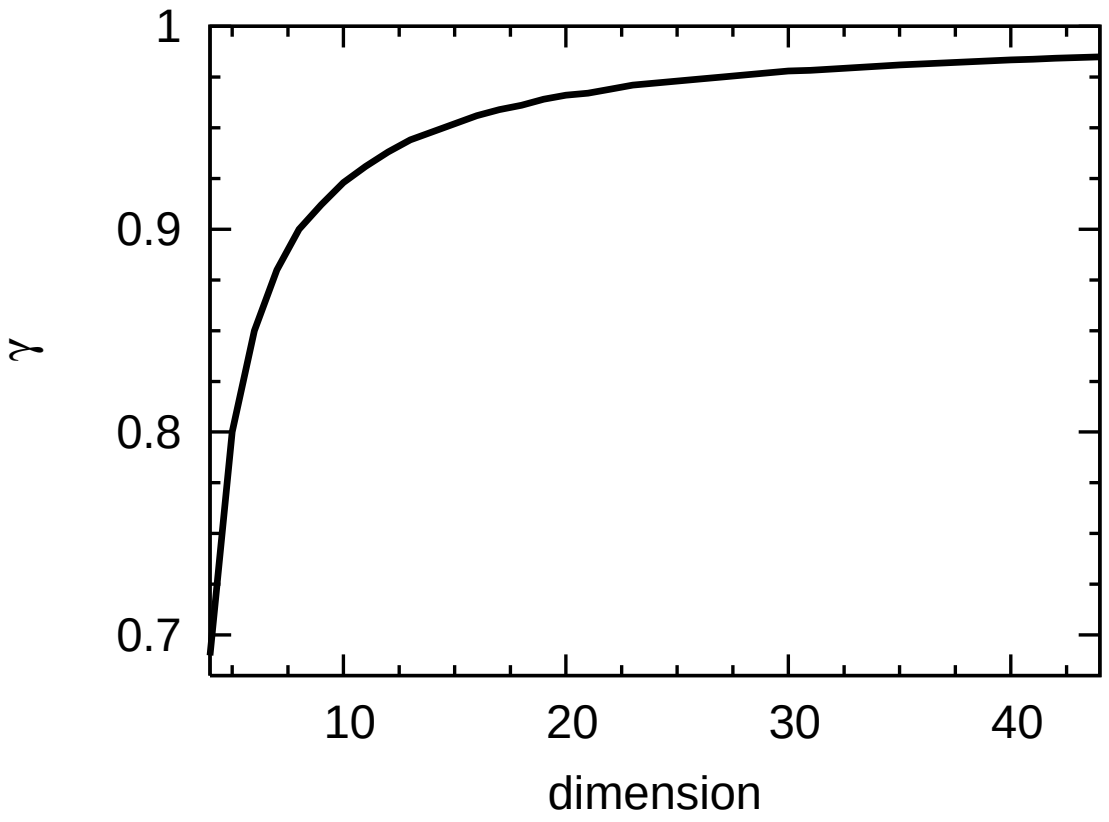

Figure 1: The upper bound of γ in Eq. (8) for dimensions with $\delta = \pi/2$. The solid line is the upper bound of γ. It approaches to one for a infinitely large dimension.

In Figure.1 we plot the upper bound of γ in Eq. (8) for dimensions by taking $\delta = \pi/2$. Since the upper bound of γ approaches to one for a infinitely large dimension, γ is less than one in any dimensions. Therefore, we do have closed trapped surfaces that begin in the higher dimensional Minkowski region and end in the higher dimensional Schwarzschild region.

Similarly, if γ satisfies the condition,

$$(D-3)\sqrt{\frac{2}{\gamma}-1}\left(\frac{1}{\gamma}-1\right) > \frac{1}{\delta}\sin\theta_1, \tag{9}$$

then the surfaces, where v and θ_2 are the function of ρ, are trapped surfaces. It should be noted that in the right hand side of Eq. (9) there is a factor $\sin\theta_1$, however, the right hand side of Eq. (8) does not depend on $\sin\theta_1$. Similarly, when we choose other surfaces and consider the condition of trapped surfaces, the condition also has a factor of the angle dependence as the right hand side of Eq. (9). In Eq. (9), the condition for the upper bound of γ depends on $\sin\theta_1$. If we take $\sin\theta_1 = 1$, then Eq. (9) is the same to Eq. (8). Besides, if $\sin\theta_1$ is negative, then the upper bounds of γ become greater than one. However, since the trapping condition (9) is satisfied for any $\sin\theta_1$ in the region $\gamma < 1$, in this case we also do have closed trapped surfaces. Although the condition of trapped surfaces depends on the choice of the $D-2$ surfaces, all conditions are satisfied in the region $\gamma < 1$. Therefore, we do have obtained the closed trapped surfaces in higher dimensional self-similar Vaidya spacetime.

Here, let us consider about the naked singularity in this spacetime. In Type 2, by substituting Eq. (8) into Eq. (7) we can take the mass function which depends on dimensions. if spacetime satisfies both conditions Eqs. (7) and (3), i.e. if γ satisfies the condition

$$\gamma > (D-3)\left[\frac{1}{4}\left(\frac{2(D-2)}{(D-3)}\right)^{D-2}\right]^{D-3}, \tag{10}$$

then spacetime has the naked singularity. However, Eq (10) does not satisfy $\gamma < 1$. Therefore, in our discussion, if spacetime has closed trapped surfaces given by above discussions, then it never has the naked singularity.

3 Conclusion

We have considered both higher dimensional self-similar Vaidya spacetime and five dimensional ring type spacetime which has the self-similar mass function. In both spacetimes, we have utilized the same manner to Ref. [4] , and then we have shown the following results. First, in both spacetimes, although conditions of the trapped surface depend on the choice of the $D-2$ surfaces, that conditions are satisfied in the region as $\gamma < 1$. Therefore, we do have constructed the closed trapped surfaces, respectively: that begin in the flat region, pass through the self-similar Vaidya region, and end in the black hole region. Second, to notice the constant of the mass function μ we have shown that the naked singularity never occur in both spacetimes with the closed trapped surface given by our discussions.

These results are similar to that in four dimensional self-similar Vaidya spacetime. Hence, we might be able to consider the definition of black holes by using Eardley's conjecture in higher dimensional spacetime.

References

[1] D. M. Eardley, Phys. Rev, D **57**, 2299 (1998).

[2] I. Ben-Dov, Phys. Rev, D **75**, 064007 (2007).

[3] E. Schnetter and B. Krishnan, Phys. Rev, D **73**, 021502(R) (2006).

[4] I. Bengtsson, and J. M. M. Senovilla, Phys. Rev. D **79**, 024027 (2009).

[5] B. R. Iyer and C. V. Vishveshwara, Paramana **32**, 749 (1989).

[6] S. G. Ghosh and N. Dadhich, Phys. Rev, D **64**, 047501 (2001).

Constraints on neutrino masses from WMAP5 and BBN in the lepton asymmetric universe

Maresuke Shiraishi[1](a), Kazuhide Ichikawa(b), Kiyotomo Ichiki(a),
Naoshi Sugiyama(a)(c), and Masahide Yamaguchi(d)

(a) *Department of Physics and Astrophysics, Nagoya University, Aichi 464-8602, Japan*
(b) *Department of Micro Engineering, Kyoto University, Kyoto 606-8501, Japan*
(c) *Institute for the Physics and Mathematics of the Universe (IPMU), The University of Tokyo, Kashiwa, Chiba, 277-8568, Japan*
(d) *Department of Physics and Mathematics, Aoyama Gakuin University, Sagamihara 229-8558, Japan*

Abstract

In this paper, we put constraints on neutrino properties such as mass m_ν and degeneracy parameters ξ_i from WMAP5 data and light element abundances by using a Markov chain Monte Carlo (MCMC) approach. In order to take consistently into account the effects of the degeneracy parameters, we run the Big Bang Nucleosynthesis code for each value of ξ_i and the other cosmological parameters to estimate the Helium abundance, which is then used to calculate CMB anisotropy spectra instead of treating it as a free parameter. We find that the constraint on m_ν is fairly robust and does not vary very much even if the lepton asymmetry is allowed, and is given by $\sum m_\nu < 1.3$ eV (95%C.L.).

1 Introduction

Neutrino masses are the key feature beyond the standard model of particle physics because neutrinos are assumed to be massless in the minimal standard model. However, oscillation experiments recently suggest tiny but non-zero masses of neutrinos. The most stringent constraint on the sum of neutrino masses comes from cosmological observations. The latest WMAP results yield $\sum m_\nu < 1.3$ eV (95% C.L.) for the ΛCDM model [1]. This constraint is shown to be robust over the different cosmological models, even if we abandon the assumption of the spatial flatness of the universe, change the equation of state of dark energy, and include tensor modes.

Another assumption in the standard cosmology that is usually taken is the symmetry in the lepton sector. This is closely related to cosmological neutrinos since neutrinos have all the lepton number of the universe due to its electronic charge neutrality. Several theories, such as [2], propose the possibility of the large lepton asymmetry in the universe. In addition, observational constraint on lepton asymmetry is much weaker than that of baryon asymmetry. Then, one may wonder how robust the constraint on neutrino masses is in the possible presence of large lepton asymmetry. This is the main topic we would like to pursue in this study.

The lepton asymmetry which is usually denoted by the degeneracy parameter ξ is an interesting quantity to be constrained, where ξ is defined as a chemical potential between neutrino and anti-neutrino normalized by the neutrino temperature. We also consider the effects of ξ on CMB through the primordial helium abundance Y_p generated during the process of the Big Bang Nucleosynthesis (BBN) in order to put bound on $\sum m_\nu$ in the lepton asymmetric universe.

In this analysis, we consider three light neutrinos and equal neutrino masses between flavors, such as $m_\nu \equiv m_{\nu_e} = m_{\nu_\mu} = m_{\nu_\tau}$, which yields $\sum m_\nu = 3m_\nu$. It is because the accuracy of the present cosmological observation is not yet up to specify their mass differences. Potentially, the degeneracy parameter ξ can take different values for each flavor of neutrinos by the model of neutrino physics [3]. Therefore, in this study we consider the two cases: one is the case that $\xi_e = \xi_\mu = \xi_\tau$, and the other is that $\xi_\mu = \xi_\tau \equiv \xi_{\mu,\tau} \neq \xi_e$.

[1] Email address: mare@a.phys.nagoya-u.ac.jp

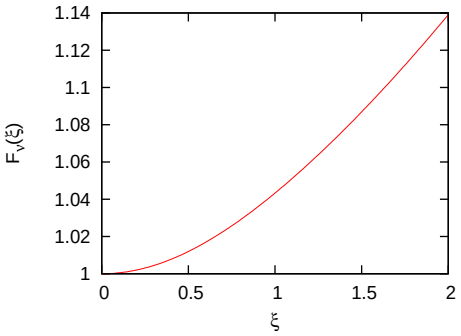

Figure 1: The ratio of the neutrino masses between degenerate and non-degenerate cases for which the neutrinos become non-relativistic at recombination. Here the relation between F_ν and $m_{\nu,c}$ is that $m_{\nu,c}(\xi)/m_{\nu,c}(\xi=0) \simeq P_\nu(\xi)/P_\nu(\xi=0) \simeq F_\nu(\xi)$.

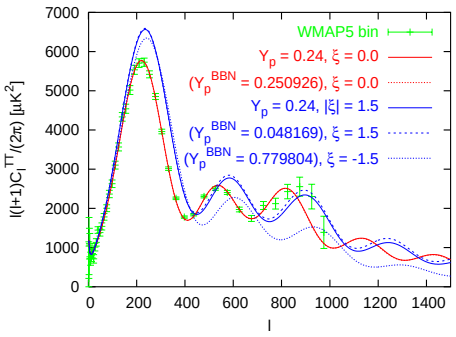

Figure 2: Effects of ξ on C_l^{TT} for the case $\xi_e = \xi_{\mu,\tau}$ with massless neutrinos. Two dotted lines and a dashed line are C_l^{TT}'s affected by Y_p related with ξ at BBN. Solid lines show C_l^{TT}'s affected by Y_p unrelated with ξ. Here we fix $\omega_b + \omega_c$. Other cosmological parameters are taken as the mean value from WMAP5 alone analysis for a power-law flat ΛCDM model [1] i.e. $\Omega_b + \Omega_c + \Omega_\Lambda = 1$.

2 Cosmological effects of ξ_i and m_ν

In this section, we review the effects of the neutrino mass m_ν and the degeneracy parameter ξ_i on the predicted helium abundance Y_p in BBN theory and the predicted CMB power spectrum C_l.

In BBN physics, the lepton asymmetry changes the abundance. The larger $N_{\rm eff}$, which is the effective number of neutrinos and behaves as the increasing function of $|\xi_i|$'s, makes the universe expand faster and more neutrons survive before the nucleosynthesis begins. Therefore the helium abundance becomes larger as $\xi_{\mu,\tau}$ increases. On the other hand, Y_p decreases monotonically as ξ_e increases because the chemical potential of electron type neutrinos suppresses the neutron-proton ratio at the onset of BBN.

On the other hand, the dependence on m_ν can be neglected because m_ν is much smaller than the temperature at the BBN epoch and does not affect the reaction rate.

In CMB physics, the lepton asymmetry changes the CMB spectrum C_l. If $N_{\rm eff}$ increases by increasing $|\xi_i|$, the sound horizon at the last scattering becomes smaller and the epoch of radiation-matter equality delays leading the larger decay of the gravitational potential. These effects shift C_l to the higher l and derive the enhancement of the 1st peak. In addition, through the effects of free streaming of these ultra-relativistic neutrinos, the smaller scale gravitational potentials have been damped just prior to the beginning of the acoustic oscillations of the baryon-photon fluid. This causes the smaller temperature fluctuations.

Next we focus our attention on the dependence of C_l on m_ν. In massive non-degenerate case ($\xi_i = 0$), neutrino mass of O(eV) causes overall horizontal shift and suppression around the first peak (when we fix $\omega_b + \omega_c$ and change ω_ν to keep flatness). The horizontal shift comes from the fact that the larger m_ν (more non-relativistic particles at present epoch) implies that the distance to the last scattering surface is shorter and the peaks move to smaller l. However, this shift is mostly canceled by the downward shift in H_0. Therefore this does not produce a neutrino mass signal. If $m_\nu \gtrsim 0.6\,$eV, massive neutrinos on average become non-relativistic before the epoch of recombination and only in this case, the neutrino mass can significantly imprint a characteristic signal in acoustic peaks (specifically, the matter-radiation equality occurs earlier due to less relativistic degrees of freedom and 1st peak is suppressed by the smaller early-integrated Sachs-Wolfe effect) [4].

In massive degenerate case ($\xi_i \neq 0$), the behavior of C_l can be understood by combining the effects in the massless degenerate case and the massive non-degenerate case. As mentioned above, roughly speaking, neutrino mass constraint from (WMAP-level) CMB observation is determined by a critical mass $3m_{\nu,c}$ which is defined by $z_{rec} \simeq z_{nr}$, where z_{nr} denotes the redshift when neutrinos on average become non-relativistic.

	$\xi \equiv \xi_e = \xi_{\mu,\tau}$		$\xi_e \neq \xi_{\mu,\tau}$	
parameter	$Y_p = 0.24$	$Y_p = Y_p^{\rm BBN}$	$Y_p = 0.24$	$Y_p = Y_p^{\rm BBN}$
$100\omega_b$	2.205 ± 0.070	$2.206^{+0.072}_{-0.074}$	$2.200^{+0.069}_{-0.070}$	2.199 ± 0.075
ω_{dm}	$0.1823^{+0.015}_{-0.043}$	$0.1799^{+0.0079}_{-0.0501}$	$0.2111^{+0.0202}_{-0.0477}$	$0.2158^{+0.0208}_{-0.0575}$
ξ_e	< 2.41	$1.20^{+0.50+1.39}_{-0.40-1.61}$	< 3.47	$1.65^{+0.63+2.00}_{-0.68-1.84}$
$\lvert\xi_{\mu,\tau}\rvert$	-	-	< 2.70	< 2.81
$\sum m_\nu$ (eV)	< 1.2	< 1.3	< 1.2	< 1.3
Y_p	-	< 0.36	-	< 0.32

Table 1: Mean values and 68% C.L. errors of the cosmological parameters obtained from the analysis of WMAP5 alone in the lepton asymmetric universe with massive neutrinos. For the constraints on ξ, 95% C.L. errors are also shown, and the upper bounds on ξ, $\sum m_\nu$, and Y_p are at 95% C.L. The left side of the table is in the case of $\xi_e = \xi_{\mu,\tau}$. The right side is in the case $\xi_e \neq \xi_{\mu,\tau}$. Two parameters at the bottom are the derived parameters from the MCMC sampling.

Numerically we depict $m_{\nu,c}(\xi)/m_{\nu,c}(\xi = 0)$ in Fig. 1. From the figure we found $F_\nu \lesssim 1.14$ for $\xi < 2$. Therefore the critical mass ($3m_{\nu,c}(\xi = 0) = 1.7$ eV for massive non-degenerate case) shifts to, at most, 1.9 eV for massive degenerate case. As m_ν is limited less than $m_{\nu,c}$, we can expect that the upper bound of $\sum m_\nu$ from CMB is almost invariant even in the lepton asymmetric universe, as will be shown later.

Finally, we explain the dependence of the CMB power spectrum on Y_p. The main effect of Y_p on the CMB power spectrum comes from the diffusion damping at small scales. This effect is rather small and not relevant to WMAP5 level observation. However,in our case, since Y_p can take very large or small value with $\xi \sim O(1)$, this may affect constraints. For example, two models with $\xi_e = \xi_{\mu,\tau} = 1.5$ and -1.5 give the same CMB spectra if we fix $Y_p = 0.24$. However, if we consider the effects of ξ at BBN epoch correctly, the two models predict $Y_p = 0.048$ and 0.780. Therefore, the model with negative degeneracy parameter should lead the larger diffusion damping as shown in Fig. 2. The CMB power spectrum can be affected by ξ through such an indirect manner.

3 Likelihood analysis

In what follows we will put constraints on the neutrino degeneracy parameters ξ_i and masses m_ν along with the other standard cosmological parameters.

We first present the result of constraints on cosmological parameters from WMAP5 alone in Table 1. For each panel we separate the results for cases whether we use BBN code to calculate Y_p or we approximately fixed Y_p value to 0.24.

As is found in Table 1, the constraints on ξ from CMB are highly dependent on whether one fixes helium abundance or derives it from BBN theory. First, let us consider the case with fixed helium abundance. In this case, the constraints on ξ from CMB becomes symmetric about $\xi_i = 0$, because positive and negative ξ give identical effects on the CMB spectrum. In reality, however, the positive and negative ξ give different effects on the CMB spectrum through the helium abundance. The CMB can put constraint on Y_p due to the Silk damping, and therefore ξ is further constrained through this effect if one derives helium abundance from BBN theory for the CMB calculations. From the fact that the current upper limit on helium abundance from CMB is found to be $Y_p < 0.44$ and there is no lower bound, negative ξ_e is disfavored, because negative ξ_e leads to large Y_p.

As for the other cosmological parameters, such as ω_b and n_s, are tightly constrained for all cases and the constraints do not change between different models considered here, because the dependence of C_l on these parameters does not degenerate with that on ξ_i and Y_p.

We also find that the upper bound of $\sum m_\nu$ is not changed significantly because this upper bound is lower than the critical mass $3m_{\nu,c}$.

Next, we present the constraints from WMAP5 combined with observations of light element abundances, namely, $Y_p = 0.250 \pm 0.004$ and $D/H = (2.82 \pm 0.27) \times 10^{-5}$. Our constraints on the sum of

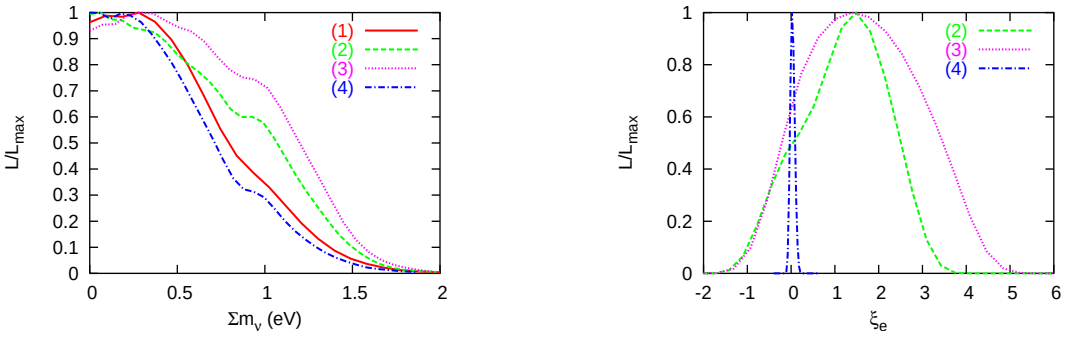

Figure 3: One dimensional posterior distributions of $\sum m_\nu$ (the left panel) and ξ_e (the right one) in the specific 4 cases. Case (1): the WMAP5 alone constraint with $Y_p = 0.24$ and no lepton asymmetry (red solid line), Case (2): the WMAP5 alone constraint with $Y_p = Y_p^{\rm BBN}$ and $\xi_e = \xi_{\mu,\tau}$ (green dashed line), Case (3): WMAP5 alone constraint with $Y_p = Y_p^{\rm BBN}$ and $\xi_e \neq \xi_{\mu,\tau}$ (magenta dotted line), Case (4): the WMAP5+BBN constraint with $Y_p = Y_p^{\rm BBN}$ and $\xi_e \neq \xi_{\mu,\tau}$ (blue dot-dashed line).

neutrino masses are 1.2 eV and 1.1 eV respectively for the cases $\xi_e = \xi_{\mu,\tau}$ and $\xi_e \neq \xi_{\mu,\tau}$. They do not depend on the assumption of $\xi_e = \xi_{\mu,\tau}$ and $\xi_e \neq \xi_{\mu,\tau}$. Again, we have found that neutrino mass constraints do not change much depending on the assumptions on ξ.

As for the constraints on the degeneracy parameters, we obtain $\xi = -0.013^{+0.016}_{-0.017} \pm 0.033$ in the case $\xi_e = \xi_{\mu,\tau}$, and $\xi_e = 0.034^{+0.017+0.075}_{-0.025-0.058}$ and $|\xi_{\mu,\tau}| < 1.60$ in the case $\xi_e \neq \xi_{\mu,\tau}$ from WMAP5 + BBN.

4 Summary

In this paper, we have discussed the effects of neutrino masses and neutrino degeneracies on CMB and BBN, and investigated how the latest observations put constraints on these properties simultaneously. In particular, we have examined how robust the constraint on neutrino masses is in the lepton asymmetric universe. Our constraints on the neutrino masses are $\sum m_\nu < 1.3\,$eV at 95% C.L. from WMAP alone. The constraint does not change very much even if we put the HST prior in the lepton asymmetric universe. We investigate the two types of lepton asymmetry, i.e. the cases with $\xi_e = \xi_{\mu,\tau}$ and $\xi_e \neq \xi_{\mu,\tau}$, and found that the constraints are almost the same for both cases. We also have taken into account the measurements of light element abundances, and found that changes in constraints are very small. These results are summarized in the left panel of Fig. 3.

A part of constraints on the degeneracy parameters are shown in the right panel of Fig. 3. There, we can notice that the posteriors are skewed by the BBN relation for Y_p. In addition, the right panel indicates that ξ_e's prefer the positive value, however, they are still consistent with $\xi_e = 0$. Although these constraints are much weaker than those obtained from Y_p measurements in HII regions and direct use of BBN theory, this would be more useful in future CMB measurements such as Planck to constrain ξ_e.

References

[1] E. Komatsu, J. Dunkley, M. R. Nolta, C. L. Bennett, B. Gold, G. Hinshaw, N. Jarosik, D. Larson, M. Limon, L. Page, *et al.*, ApJS **180**, 330 (Feb. 2009), 0803.0547.

[2] M. Kawasaki, F. Takahashi, and M. Yamaguchi, Phys. Rev. D **66**(4), 043516 (Aug. 2002), arXiv:hep-ph/0205101.

[3] A. D. Dolgov and F. Takahashi, Nuclear Physics B **688**, 189 (Jun. 2004), arXiv:hep-ph/0402066.

[4] K. Ichikawa, M. Fukugita, and M. Kawasaki, Phys. Rev. D **71**(4), 043001 (Feb. 2005), arXiv:astro-ph/0409768.

Constrain on Brans-Dicke Cosmology from view point of Cosmic age

Takayuki Suzuki [1(a)]

[(a)] *Department of Physics, Yamaguchi University, Yamaguchi city, Yamaguchi prefecture 171-8501*

Abstract

Recent observational bounds taken into consideration, I investigated cosmology of Brans-Dicke gravity. Brans-Dicke scalar field at high $\omega_{\rm BD}$ behaves as stiff fluid, And it makes cosmic age short. But, cosmic age is constrained by observation of globular clusters. This paper shows constraint on Brans-Dicke cosmology from view point of cosmic age.

1 introduction

g Is the constants of nature truly constantHh This is one of the radical questions for nature. Especially, varying gravitational constant G is interesting from viewpoint of cosmology, because it decides strength of the gravity which is dominant in macro scale.

2 Brans-Dicke gravity theory

In BD theories, the coupling of a massless scalar field to the Ricci scalar provides a natural framework of realizing the time-variation of the gravitational constant via the dynamics of the scalar field. In the Brans-Dicke theory a constant coupling parameter $\omega_{\rm BD}$ is introduced. In the limit $\omega_{\rm BD}$, the gravitational constant cannot change and Einstein gravity is recovered. The issue that historically influenced the pioneers of the scalar-tensor theory strongly is Mach's principal. It is often said that Brans-Dicke theory, but not general relativity, satisfies Mach's principle.

$$S_{\rm BD} = \int d^4x\sqrt{-g}\left[\frac{c^4}{16\pi G}[\phi R - \omega_{\rm BD}\frac{(\nabla\phi)^2}{\phi}] + \mathcal{L}_{\rm matter}\right] \tag{1}$$

$$G_{\mu\nu} = \frac{8\pi G}{c^4\phi}T^{\rm matter}_{\mu\nu} + T^{(\phi)}_{\mu\nu} \tag{2}$$

$$T^{(\phi)}_{\mu\nu} = \frac{\omega_{\rm BD}}{\phi^2}\left[\phi_{;\mu}\phi_{;\nu} - \frac{1}{2}g_{\mu\nu}\phi_{;\alpha}\phi^{;\alpha}\right] + \frac{1}{\phi}\left[\phi_{;\mu}\phi_{;\nu} - g_{\mu\nu}\Box\phi\right] \tag{3}$$

$$\Box\phi = \frac{8\pi G}{c^4(3+2\omega_{\rm BD})}T^{\mu{\rm matter}}_{\mu} \tag{4}$$

3 Constraint of BD theory

But, idea of varying G and non-Einstein gravity theory are limited by variety of astronomical measurements in recent years . Varing G is constrained by lunar laser ranging experiment. the newest limit is this value: $(\dot{G}/G)|_{\rm now} = (4 \pm 9) \times 10^{-13}$/yr.(William et al.2004)[4]

The value of $\omega_{\rm BD}$ consistent with experiment has risen with time. In 2003 evidence - derived from the Cassini-Huygens experiment- shows that the value of $\omega_{\rm BD}$ must exceed 40000. this value is measured by Shapiro's delay.(Bertotti et al.2003)[5];(Berti et al.2005) [6]

Recent observational bounds taken into consideration, I investigated Brans-Dicke cosmology.

[1]Email address: n003wa@yamaguchi-u.ac.jp

4 Basic Equation of BD cosmology

$$\left(\frac{\dot{a}}{a}\right)^2 = \frac{8\pi G}{3\phi}\,\rho - \frac{kc^2}{a^2} - \frac{\dot{a}}{a}\frac{\dot{\phi}}{\phi} + \frac{\omega_{\mathrm{BD}}}{6}\left(\frac{\dot{\phi}}{\phi}\right)^2 \tag{5}$$

$$\ddot{\phi} = -3\frac{\dot{a}}{a}\dot{\phi} + \frac{-\rho c^2 + 3P}{c^2(3+2\omega_{\mathrm{BD}})} \tag{6}$$

These are Friedman equation of BD theory. Considering equation of state and indeed following parameters.

- present cosmic expantion rate(Hubble constant):$\frac{\dot{a}}{a} = H_0$
- present radiation density:ρ_{r0}
- present dust matter densityρ_{m0}
- present dark energy density:$\rho_{\Lambda 0}$

then rewrite equation,

$$\left(\frac{\dot{a}}{a}\right)^2 = H_0^2\left(\frac{8\pi G}{3H_0^2\phi}\,(\frac{\rho_{r0}}{a^4} + \frac{\rho_{m0}}{a^3} + \rho_{\Lambda 0}) - \frac{kc^2}{H_0^2a^2} + \frac{\omega_{\mathrm{BD}}}{6}(\frac{\dot{\phi}/\phi}{H_0})^2 - \frac{\dot{a}}{a}\frac{\dot{\phi}/\phi}{H_0^2}\right) \tag{7}$$

Defined that:

- present radiation density(normalized):$\frac{8\pi G\rho_{r0}}{3H_0^2} \equiv \Omega_{r0}$
- present dust matter density(normalized)$\frac{8\pi G\rho_{m0}}{3H_0^2} \equiv \Omega_{m0}$
- present dark energy density(normalized):$\frac{8\pi G\rho_{m0}}{3H_0^2} \equiv \Omega_{\Lambda 0}$
- normalized curvuture :$-\frac{kc^2}{H_0^2} \equiv \Omega_{k0}$

then,

$$\left(\frac{\dot{a}}{a}\right)^2 = H_0^2(\frac{\Omega_{r0}}{\phi a^4} + \frac{\Omega_{m0}}{\phi a^3} + \frac{\Omega_{k0}}{a^2} + \frac{\Omega_{\Lambda 0}}{\phi} + \frac{\omega_{\mathrm{BD}}}{6}(\frac{\dot{\phi}/\phi}{H_0})^2 - \frac{\dot{a}}{a}\frac{\dot{\phi}/\phi}{H_0^2} \tag{8}$$

$$\ddot{\phi} = -3\frac{\dot{a}}{a}\dot{\phi} - \frac{H_0}{(3+2\omega_{\mathrm{BD}})}(\frac{\Omega_{m0}}{a^3} + 4\Omega_{\Lambda 0}) \tag{9}$$

These are normalized Friedman equation of BD theory. And,defined $\Omega_{\dot{\phi}}(t)$ conveniently:

$$\Omega_{\dot{\phi}}(t) = \frac{\omega_{\mathrm{BD}}}{6}(\frac{\dot{\phi}/\phi}{H_0})^2 - \frac{\dot{a}}{a}\frac{\dot{\phi}/\phi}{H_0^2} \tag{10}$$

5 BD scalar field behaves as stiff fluid

Brans-Dicke Scalar field at high omega behave as stiff fluid(w=1). This is un-normalized BD Friedman equation.Now,derivate vacuum solution.

$$\left(\frac{\dot{a}}{a}\right)^2 = -\frac{\dot{a}}{a}\frac{\dot{\phi}}{\phi} + \frac{\omega_{\rm BD}}{6}\left(\frac{\dot{\phi}}{\phi}\right)^2 \tag{11}$$

$$\ddot{\phi} = -3\frac{\dot{a}}{a}\dot{\phi} \tag{12}$$

and,following is the solution:

$$\phi \propto t^{\alpha}, a \propto t^{\frac{\alpha+1}{3}} \tag{13}$$

where,$\alpha = \dfrac{1}{1 \pm \sqrt{9+6\omega_{\rm BD}}}$. As compared to relation between equation of state and cosmic expansion solution:$a \propto t^{2/3(1+w)}$ then,we can discribe w parameter of BD scalar field as following.

$$w = \frac{2}{\alpha+1} - 1 \tag{14}$$

If $\omega_{\rm BD} \longrightarrow$ very large,then $\alpha \longrightarrow 0$,$w \longrightarrow 1$.This result is construed the following.

General free(no potential,massless) scalar field's equaiton of states shows that Pressure = Energy density. Parameter of equation state is 1. Such imaginary matter is called stiff fluid. These solutions are known from old days(Mark S.Madsen 1985)[7](Mark S.Madsen 1988)[8]. Expressing BD scalar field and matter eqation again,

$$\Box\phi = \frac{8\pi G}{c^4(3+2\omega_{\rm BD})}T_{\mu}^{\mu\rm matter} \tag{15}$$

If $\omega_{\rm BD}$ is very large, coupling between matter and scalar field decoupled. then BD scalar field behaves as free scalar field.

6 BD cosmology from veiw point of cosmic age

Brans-Dicke scalar field behave as stiff fulid,And it make cosmic age short. But, cosmic age is constrained by observation of globular clusters. Lower limit of cosmic age is surmised thirteen giga years.(Krauss et al.2003)[9] It is desirable that BD scalar field's energy density is small enough. (You may think that if the nature adopt BD gravity, Varying G effect on development of star. But Recent observational bounds taken into consideration,varying of G is very small except only early universe.) I investigated BD cosmic solutions which allowed from recent observational bounds(:$\omega_{\rm BD} > 40000$). This picture show cosmic age of BD Λ CDM@model(Fig. 1).

If there were a little scalar field , cosmic age become short. And it become less than thirteen giga years.

Notice $\Omega_{\dot{\phi}}(0) = 0$ model. That mean $\dot{G}/G|_{\rm now}$ is zero exactly. And composition of universe is equivalent to standard model in GR. But Cosmic age is shorter 0.2 Gyr than standard cosmology. BD cosmology at high $\omega_{\rm BD}$ resemble cosmology with stiff fluid in GR. But The former does not quite correspond to the later.

7 Conclusion

BD scalar field's energy density must be less than 0.001.If $\omega_{\rm BD} > 40000$ then $\dot{G}/G|_{\rm now}$ is less than 10^{-14}. This is more strict limit value at one column than the lunar laser ranging experiment But this limit value suppose that varying G is caused by BD gravity, and this is model-depanding constraint value.

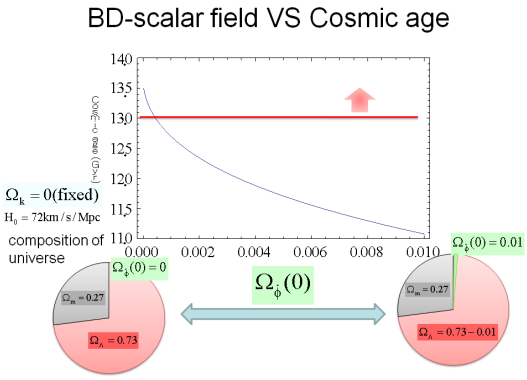

Figure 1: Relation between cosmic age and Scalar field density

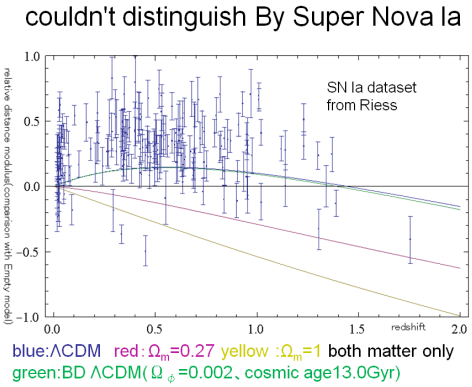

Figure 2: This is magnitude-redshift relation. blue line is ΛCDM model in GR. green line is BD ΛCDM model which is narrowly allowed from view point of cosmic age. we can't distinguish two model at low z region which is observed by type Ia supurnove.

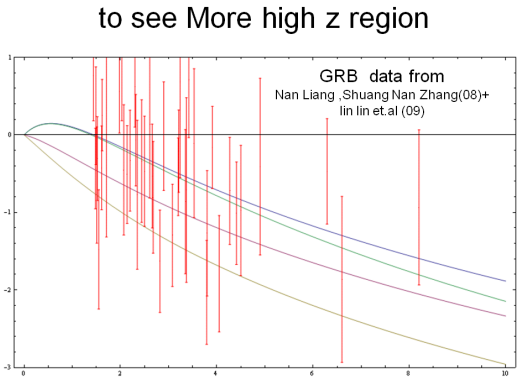

Figure 3: But at more high z region, we can distinguish two model. this sudden drop is peculiarity of BD model. high z region is observed by gammar lay burst. But ,GRB observation is not precise yet. Errer bar is too long to discuss.

8 Supplement

References

[1] Fujii Yasunori and Maeda Kei-Ichi, The Scalar-Tensor Theory of Gravitation, (Cambridge Univ Pr Published, 2003)

[2] C. Brans and R. Dicke, Phys. Rev. **124** (1961), 925.

[3] Valerio Faraoni, Phys.Rev. **D59** (1999), 084021.

[4] James G. Williams. Slava G. Turyshev and Dale H. Boggs, Phys. Rev. Lett. **93** (2004), 261101.

[5] Bertotti, Nature **425** (2003), 374.

[6] Berti Phys. Rev. **124** (2005), 925.

[7] Mark S. Madsen Astrophys. Space Sci. **113** (1985), 205.

[8] Mark S. Madsen Class. Quantum Grav **5** (1988), 627.

[9] Krauss,L.M, and Chaboyer,B. Secience. **299** (2003), 65.

Simulations of Baryon Acoustic Oscillations: Likelihood Analysis of the Matter Power Spectrum

Ryuichi Takahashi[1], Naoki Yoshida[3], Masahiro Takada[3], Takahiko Matsubara[2], Naoshi Sugiyama[2,3], Issha Kayo[3], Takahiro Nishimichi[4], Shun Saito[4], and Atsushi Taruya[3,5]

[1] *Faculty of Science and Technology, Hirosaki University, 3 bunkyo-cho, Hirosaki, Aomori, 036-8561, Japan*
[2] *Department of Physics, Nagoya University, Chikusa, Nagoya 464-8602, Japan*
[3] *Institute for the Physics and Mathematics of the Universe, The University of Tokyo, 5-1-5 Kashiwa-no-ha, Kashiwa, Chiba 277-8568, Japan*
[4] *Department of Physics, School of Science, The University of Tokyo, Tokyo 113-0033, Japan*
[5] *Research Center for the Early Universe, The University of Tokyo, Tokyo 133-0033, Japan*

Abstract

We study the sample variance of the matter power spectrum for the standard Λ Cold Dark Matter universe. We use a total of 5000 cosmological N-body cosmological simulations to study the cosmological parameter estimations using the Fisher matrix analysis with and without including non-Gaussian errors. For the Fisher matrix analysis, we compute the derivatives of the matter power spectrum with respect to cosmological parameters using directly full nonlinear simulations. We show that the non-Gaussian errors increase the unmarginalized errors by up to a factor 5 for $k_{\rm max} = 0.4h$/Mpc if there is only one free parameter (if other parameters are well determined by external information). On the other hand, for multi-parameter fitting, the impact of the non-Gaussian errors is significantly mitigated due to severe parameter degeneracies in the power spectrum.

1 Introduction

The baryon acoustic oscillation (BAO) is imprinted in the distribution of galaxies as is found in the temperature fluctuations in the cosmic microwave background. The acoustic length scale is determined by the sound horizon of the photon-baryon fluid at recombination epoch; it can thus be used as a standard ruler which provides us with a robust method to measure distance scales out to essentially any epoch [1]. Using the observed distance-redshift relation, we can obtain an accurate cosmic expansion history, which in turn gives strong constraints on the nature of dark energy. The large-area galaxy surveys such as two-degree Field Survey (2dF) and Sloan Digital Sky Survey (SDSS) detected the BAO signature in the galaxy distribution [2, 3].

The BAO signature appears as a small wiggle pattern in the galaxy power spectrum. Since the amplitude of BAO wiggle is very small ($\sim$ a few percent), rather accurate theoretical models are needed. Especially, in order to determine the distance within a percent accuracy for the planned or ongoing surveys, we need to be able to predict the acoustic scale with much higher accuracies ($\sim 0.1\%$). However, there are complicated astrophysical processes such as the non-linear gravitational evolution, scale-dependent bias of galaxies, redshift space distortion, and the effect of massive neutrino. Many authors tackled these problems using numerical simulations and analytical perturbation theories.

It is crucial to use not only accurate power spectra but also accurate covariance matrices in order to determine cosmological parameters from the galaxy power spectrum. If the matter density fluctuations obey a Gaussian distribution, the covariance matrix has only diagonal element and the relative error is simply given by the square root of the number of modes in the survey area [4]. However, when the density fluctuations grow to the non-linear regime, the mode coupling between different wavenumbers generates non-zero off-diagonal elements, and the so-called non-Gaussian error is induced [5, 6]. Rimes & Hamilton (2005) first pointed out that there is little information contained in the power spectrum at quasi-nonlinear regime ($k = 0.2 - 0.8h$/Mpc) due to the non-Gaussian error [7].

In our previous paper (Takahashi et al. 2009 [8], hereafter T09), we used 5000 cosmological simulations to obtain the accurate covariance matrix of the matter power spectrum. This is a largest number of realizations ever done for the BAO simulation. We studied the non-Gaussian error contribution to the signal-to-noise ratio for the measurement of the power spectrum, and found that the non-Gaussian error is important at small length-scale $k > 0.2h$/Mpc. In this proceeding, we further investigate the non-Gaussian error contribution to the cosmological parameter estimation. This proceeding is based on our recent manuscript [9].

Throughout the present paper, we adopt the standard ΛCDM model with matter density $\Omega_m = 0.238$, baryon density $\Omega_{\rm b} = 0.041$, dark energy density $\Omega_{\rm w} = 0.762$ with equation of state $w = -1$, spectral index $n_{\rm s} = 0.958$, amplitude of fluctuations $\sigma_8 = 0.76$, and expansion rate at the present time $H_0 = 73.2$km s^{-1} Mpc^{-1}, consistent with the 3-year WMAP results [10].

2 Matter power spectrum and its covariance matrix from numerical simulations

We follow the gravitational evolution of 256^3 collisionless dark matter particles in a volume of $1000h^{-1}$Mpc on a side using the cosmological simulation code Gadget-2 [11]. We generate initial conditions following the standard Zel'dovich approximation at the initial redshift $z = 20$. We use outputs at $z = 3, 1$ and 0. We run 5000 Particle-Mesh simulations to follow the non-linear evolution of the power spectrum and its covariance matrix in detail. We have checked that the power spectra of our simulations agree well with the result of the higher resolution simulation, within 2(10)% for $k < 0.2(0.4)h$/Mpc.

Denoting $\hat{P}_i(k)$ as the power spectrum computed from the i-th realization, the ensemble averaged power spectrum is estimated from the mean of the power spectra between 5000 realizations:

$$\bar{P}(k) = \frac{1}{N_{\rm r}} \sum_{i=1}^{N_{\rm r}} \hat{P}_i(k), \tag{1}$$

where $N_r = 5000$, the number of our realizations. Similarly, the covariance matrix between the spectra of k_1 and k_2 is estimated as

$$\mathrm{cov}(k_1, k_2) = \frac{1}{N_{\rm r} - 1} \sum_{i=1}^{N_{\rm r}} \left[\hat{P}_i(k_1) - \bar{P}(k_1)\right] \left[\hat{P}_i(k_2) - \bar{P}(k_2)\right]. \tag{2}$$

The accuracy of the covariance is analytically estimated for the Gaussian density fluctuations (see Appendix). For example, the relative errors in the diagonal covariance terms are found to scale with the number of realizations as $(2/N_r)^{1/2}$; our 5000 simulations provide a few percent accuracy.

The power spectrum covariance is formally expressed as a sum of the two contributions, the Gaussian and non-Gaussian terms [5, 6]

$$\begin{aligned}\mathrm{cov}(k_1, k_2) &\equiv \left\langle \left(\hat{P}(k_1) - P(k_1)\right) \left(\hat{P}(k_2) - P(k_2)\right) \right\rangle \\ &= \frac{2}{N_{k_1}} P^2(k_1) \delta^K_{k_1,k_2} + \frac{1}{V} \int_{|\mathbf{k}'_1| \in k_1} \int_{|\mathbf{k}'_2| \in k_2} \frac{d^3\mathbf{k}'_1}{V_{k_1}} \frac{d^3\mathbf{k}'_2}{V_{k_2}} \\ &\quad \times T(\mathbf{k}'_1, -\mathbf{k}'_1, \mathbf{k}'_2, -\mathbf{k}'_2).\end{aligned} \tag{3}$$

The first term arises from the Gaussian fluctuations, while the second term is the non-Gaussian error arising from the mode coupling during the non-linear evolution. Here, $P(k) = \langle \hat{P}(k) \rangle$ is the mean power spectrum, T is the trispectrum, the integral is done over the shell of the radius $k_{1,2}$ with the width Δk in Fourier space, and $V_{k_{1,2}}$ is the volume of the shell given by $V_k = 4\pi k^2 \Delta k$. The expression in Eq.(3) depends on the bin width, the first term is proportional to $1/(V\Delta k)$, while the second term is $\propto 1/V$. Hence, for the finer bin width, the impact of the Gaussian term becomes relatively enhanced. Note however that the parameter estimation shown in the following is independent of the bin width. Throughout this proceeding, the bin width is set to $\Delta k = 0.01h$/Mpc.

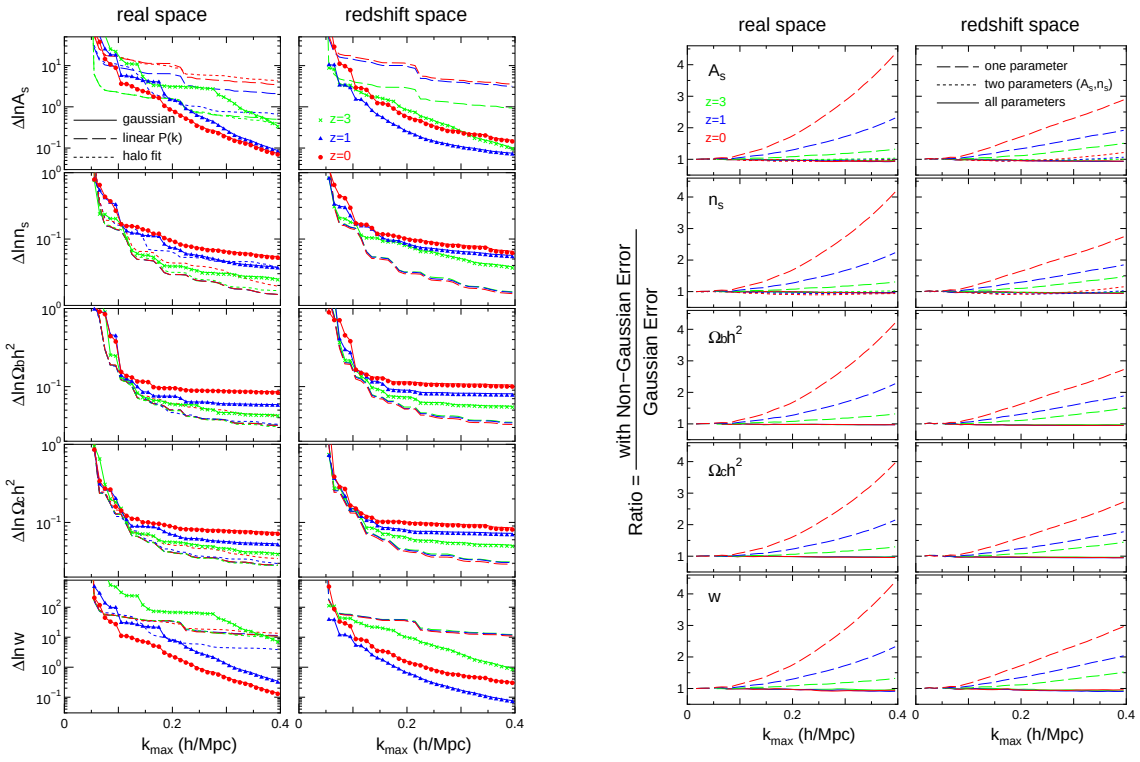

Figure 1: (Left panel) The marginalized errors of each parameter when including the power spectrum information up to the maximum wavenumber $k_{\rm max}$ in the horizontal axis. The left- and right panels show the results for the real- and redshift-space, respectively. The symbols in each panel are as for the previous figures. The cross, triangle and circle symbols show the simulation results at redshifts $z = 3$, 1 and 0, respectively. The solid curves which lie almost on top of the symbols show the results obtained only by including the Gaussian errors in the Fisher analysis. The agreement indicates that the Gaussian error assumption is a good approximation for parameter estimations even at small scales (see text for the details). (Right panel) The ratio of the marginalized errors with and without the non-Gaussian errors, as a function of $k_{\rm max}$. The solid curves show the results for our fiducial set of five cosmological parameters as shown in each panel. For comparison the dashed curves show the results for the unmarginalized errors or equivalently for the case of one parameter fitting in each panel. It is clear that the non-Gaussian errors degrade the unmarginalized errors by up to a factor 5.

3 Parameter estimation for cosmological parameters

In this section, we study the effects of the non-Gaussian errors on the cosmological parameter estimation given the power spectrum measured from a hypothetical survey of $(1h^{-1}{\rm Gpc})^3$ volume. We use the Fisher matrix formalism to estimate the accuracy of parameter estimation [12] :

$$F_{\rm ij} = \sum_{k_{1,2}<k_{\rm max}} {\rm cov}^{-1}(k_1,k_2)\, \frac{\partial P(k_1;\mathbf{x})}{\partial \ln x_{\rm i}}\bigg|_{\rm fid} \frac{\partial P(k_2;\mathbf{x})}{\partial \ln x_{\rm j}}\bigg|_{\rm fid}. \tag{4}$$

where $x_{\rm i}$ denotes cosmological parameters, and the partial derivative such as $\partial P/\partial x_{\rm i}$ is evaluated around the fiducial model. We include 5 parameters (therefore ${\rm i} = 1, 2, \ldots, 5$): the primordial power spectrum parameters, the normalization parameter A_s (not σ_8) and the spectral index $n_{\rm s}$, the baryon density $\Omega_{\rm b}h^2$, the dark matter density $\Omega_{\rm c}h^2$, and the dark energy equation of state parameter w. We assume a flat universe throughout the present paper. In Eq. (4) we use $\ln x_{\rm i}$ (not $x_{\rm i}$) as the variables such that the Fisher matrix gives the relative accuracy of a given parameter estimation: the marginalized error is then given as $\Delta x_{\rm i}/x_{\rm i} = (F^{-1})^{1/2}_{\rm ii}$. From Eqs.(3) and (4), the estimation error $\Delta x_{\rm i}/x_{\rm i}$ is inversely proportional

to the survey volume as $\Delta x_{\rm i}/x_{\rm i} \propto V^{-1/2}$. We need to compute the derivatives of the power spectrum to compute the Fisher matrix in Eq. (4). For each cosmological parameter, we ran simulations with one parameter slightly varied, while fixing other parameters to the fiducial values. We then compute the derivatives by the two-side differences of steps $\Delta x_i/x_i = \pm 0.05$. We use 40 realizations are used for each parameter variation.

The left of Fig.1 shows the marginalized error on each parameter, $\Delta x_{\rm i}/x_{\rm i} = (F^{-1})_{\rm ii}^{1/2}$, as a function of $k_{\rm max}$, where the power spectrum information up to a given $k_{\rm max}$ is included. In each panel the symbols show the simulation results including the full covariance matrix. The simulation results are almost indistinguishable from the solid curves that are computed only by including the Gaussian error covariances, computed from simulations, in Eq. (3). The agreement indicates that the non-Gaussian error assumption actually provides a good approximation for the parameter estimation over scales of interest, even though the non-Gaussian errors have a significant impact on the S/N at $k_{\rm max} > 0.2h/{\rm Mpc}$. A more quantitative interpretation of these results will be given later.

The right panel of Fig.1 shows the relative accuracies of each parameter estimation as a function of $k_{\rm max}$. There, we compare the results derived from the covariances with and without the non-Gaussian error contributions. The solid curves are the results where all the five parameters are included in the Fisher analysis, while the dashed curve shows the unmarginalized error on each parameter, i.e., the error is obtained by considering only one free parameter, $\Delta x_{\rm i}/x_{\rm i} = F_{\rm ii}^{-1/2}$. In other words, the dashed curves correspond to the case where other parameters are well constrained by external data sets. The difference between the solid and dashed curves is caused by the parameter degeneracies; the marginalized error becomes same as the unmarginalized error when the parameters are independent in the measured power spectrum. It is clear that, for the unmarginalized errors, including the non-Gaussian covariances degrades the parameter errors by a factor 4-5 for the redshift $z = 0$, and by a factor 2-3 for $z = 1$, respectively. The level of the degradation is similar to that of the S/N as found in T09. Therefore, the impact of non-Gaussian covariance errors is significantly mitigated by the parameter degeneracies. The degradation of S/N increases the full Fisher ellipsoid volume, and then individual parameters are not tightly constrained due to the parameter degeneracies in such a high-dimension parameter space.

In the upper two panels for A_s and n_s the short dashed curves show the results for the two parameter fitting case (A_s, n_s), which are very similar to the solid curves. In reality, parameters that describe galaxy bias need to be further included. We thus conclude that the impact of the non-Gaussian errors is less important than the parameter degeneracies, and that the Gaussian covariances can provide a good approximation to obtain the statistical uncertainty of given parameters.

References

[1] Eisenstein, D.J., Hu, W. & Tegmark, M., ApJ, 504, L57 (1998).

[2] Eisenstein, D.J. et al., ApJ, 633, 560 (2005).

[3] Percival, W.J., et al., MNRAS, 381, 1053 (2007).

[4] Feldman, H.A., Kaiser, N. & Peacock, J.A., ApJ, 426, 23 (1994).

[5] Meiksin, T. & White, M., MNRAS, 308, 1179 (1999).

[6] Scoccimarro, R., Zaldarriaga, M. & Hui, L., ApJ, 527, 1 (1999).

[7] Rimes, C.D. & Hamilton, A.J.S., MNRAS, 360, L82 (2005).

[8] Takahashi, R. et al., ApJ, 700, 479 (2009).

[9] Takahashi, R. et al., submitted to ApJ, arXiv:0912.1381 (2009).

[10] Spergel, D.N., et al., ApJ, 170, 377 (2007).

[11] Springel, V., MNRAS, 364, 1105 (2005).

[12] Tegmark, M., Taylor, A.N. & Heavens, A.F., ApJ, 480, 22 (1997).

Instability of Small Lovelock Black Holes in Even-dimensions

Tomohiro Takahashi[1] and Jiro Soda[2]

Department of Physics, Kyoto University, Kyoto, 606-8501, Japan

Abstract

We study the stability of static black holes in Lovelock theory which is a natural higher dimensional generalization of Einstein theory. We derive a master equation for tensor perturbations in general Lovelock theory. It turns out that the resultant equation is characterized by one functional which determines the background black hole solutions. Thus, the stability issue of static black holes under tensor perturbations in general dimensions is reduced to an algebraic problem. We show that small Lovelock black holes in even-dimensions are unstable.

1 Introduction

It is well known that string theory can be formulated only in ten dimensions. Hence, it is necessary to reconcile this prediction with our real world by compactifying extra-dimensions or by considering braneworld. Intriguingly, in the context of the braneworld with large extra-dimensions, black holes could be created at the TeV scale [1]. Hence, the stability of higher dimensional black holes becomes important since these black holes could be produced at the LHC if the spacetime has larger than six dimensions.

Examining stability of black holes, it is important to consider more general gravitational theories because black holes are produced at the Planck scale where Einstein theory would be no longer valid. In fact, as is well known, string theory predicts Einstein theory only in the low energy limit [2]. In string theory, there are higher curvature corrections in addition to Einstein-Hilbert term [2]. Thus, it is natural to extend gravitational theory into those with higher power of curvature in higher dimensions. It is Lovelock theory that belongs to such class of theories [3]. In Lovelock theory, it is known that there exist static black hole solutions [4]. Hence, it is natural to suppose black holes produced at the LHC are of this type [5]. Thus, it is important to study the stability of these Lovelock black holes.

2 Lovelock Black Holes

It is Lovelock tensor that is the most general symmetric, divergence free rank (1,1) tensor constructed out of a metric and its first and second derivatives[3]. The concrete expression is

$$\mathcal{G}_\mu^\nu = \Lambda\delta_\mu^\nu - \sum_{m=1}^{k} \frac{1}{2^{(m+1)}} \frac{a_m}{m} \delta^{\nu\lambda_1\sigma_1\cdots\lambda_m\sigma_m}_{\mu\rho_1\kappa_1\cdots\rho_m\kappa_m} R_{\lambda_1\sigma_1}{}^{\rho_1\kappa_1} \cdots R_{\lambda_m\sigma_m}{}^{\rho_m\kappa_m} \ , \tag{1}$$

where $R_{\lambda\sigma}{}^{\rho\kappa}$ is the Riemann tensor in D-dimensions and $\delta^{\lambda_1\sigma_1\cdots\lambda_m\sigma_m}_{\rho_1\kappa_1\cdots\rho_m\kappa_m}$ is the generalized totally antisymmetric Kronecker delta. k means the maximum order which satisfies $k \equiv [(D-1)/2]$ and a_m are arbitrary constants. Hereafter, we set $\Lambda = 0$, $a_1 = 1$ and $a_m > 0$ for simplicity.

As is shown in [4], there exist static exact solutions of vacuum Lovelock equation. Let us consider the following metric

$$ds^2 = -f(r)dt^2 + \frac{dr^2}{f(r)} + r^2\bar{\gamma}_{ij}dx^i dx^j \ , \tag{2}$$

[1]Email address: takahashi@tap.scphys.kyoto-u.ac.jp
[2]Email address: jiro@tap.scphys.kyoto-u.ac.jp

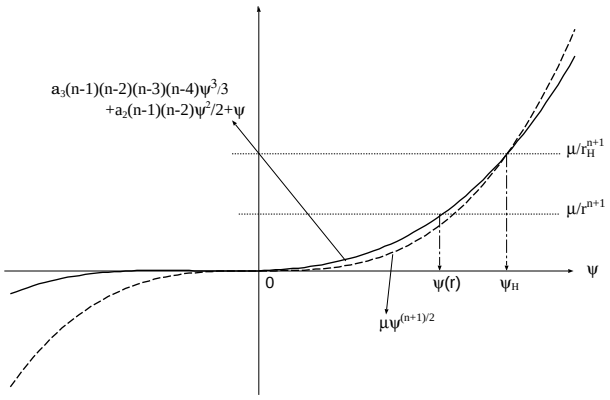

Figure 1: For $n = 5$ case, this figure explains a method for calculating ψ_H or r_H graphically. The positive root of Eq.(4) ψ_H can be obtained from the intersection of the solid and dashed curves. Since the intersection between the horizontal line and the solid curve gives a solution $\psi = \psi(r)$, r_H is determined from the intersection of the horizontal line, the solid and dashed curves.

where $\bar{\gamma}_{ij}$ is the metric of S^n where $n \equiv D-2$. Using this metric ansatz and vacuum Lovelock equation, we can get the Lovelock black hole solutions like following:

$$\begin{cases} f(r) = 1 - r^2\psi(r) \\ W[\psi] \equiv \sum_{m=2}^{k} \left[\frac{a_m}{m} \left\{ \prod_{p=1}^{2m-2} (n-p) \right\} \psi^m \right] + \psi = \frac{\mu}{r^{n+1}} \ . \end{cases} \quad . \tag{3}$$

In this expressions, μ is constant of integral and propoortional to ADM mass, so we assume $\mu > 0$. From (3), ψ has many branches. Under our assummption, however, there is only one asymptotic flat solution, which satisfies $\psi > 0$ and has a horizons. Horizon is defined as $f(r_H) = 0$ or equivalently $\psi_H \equiv \psi(r_H) = 1/r_H^2$. Combining this with (3), It is easily shown that ψ_H satisfies

$$W[\psi_H] = \mu\psi_H^{(n+1)/2} \ . \tag{4}$$

We draw $W[\psi]$ and (4) in Fig1, and we can recgnize from this figure that outside horizon corresponds $0 < \psi \leq \psi_H$ for this branch. Note that, from (4) and fig1, it is obvious ψ_H becomes larger as μ is smaller.

3 Stability Analysis

We consider tensor perturbations around the Lovelock black hole solution

$$\delta g_{ab} = 0 \ , \quad \delta g_{ai} = 0 \ , \quad \delta g_{ij} = r^2\chi(r)e^{-i\omega t}\bar{h}_{ij}(x^i) \ , \tag{5}$$

where $a, b = (t, r)$ and $\chi(r)$ represents the master variable. Here, $\bar{h}_{ij}$ are defined by

$$\bar{\nabla}^k\bar{\nabla}_k\bar{h}_{ij} = (-\ell(\ell+n-1)+2)\bar{h}_{ij} \ , \qquad \bar{\nabla}^i\bar{h}_{ij} = 0 \ , \quad \bar{\gamma}^{ij}\bar{h}_{ij} = 0 \ , \tag{6}$$

and $\bar{\nabla}^i$ denotes a covariant derivative with respect to $\bar{\gamma}_{ij}$ and $\ell = 2, 3, 4 \cdots$.

Perturbing the vacuum Lovelock equation, we can get Schrödinger type equation

$$-\frac{d^2\Psi}{dr^{*2}} + V(r(r^*))\Psi = \omega^2\Psi \equiv E\Psi \tag{7}$$

as the first order perturbation equation [6]. In eq.(7), r^* is tortoise coordinate, Ψ is defined as $\Psi(r) = \chi(r)r\sqrt{h(r)}$ and

$$V(r) = \frac{(\ell(\ell+n-1))f}{(n-2)r}\frac{d\ln h}{dr} + \frac{1}{r\sqrt{h}}f\frac{d}{dr}\left(f\frac{d}{dr}r\sqrt{h}\right) \ , \tag{8}$$

where

$$h(r) = \frac{d}{dr}\left[\frac{r^{n-1}}{n-1}\frac{dW[\psi]}{d\psi}\right] . \tag{9}$$

From eq.(7), black holes are unstable if negative energy states exist. Note that we assume $h(r) > 0$ outside the horizon in deriving this Schrödinger type equation. If this assumption is not fullfilled, there exists singularity. The detail is like following. In asymptotic region $r \to \infty$, $h(r)$ must be positive, so if there is $h(r) < 0$ region, there exists r_0 such that $h(r_0) = 0$. We can show that master variable χ diverges at $r = r_0$ by expanding first order perturbation equation around $r = r_0$.

If this assumption $h(r) > 0$ is fullfilled, we can show that negative energy states exist if and only if dh/dr has negative region[6]. Defining inner product as

$$(\varphi_1, \varphi_2) = \int_{-\infty}^{\infty} \varphi_1^* \varphi_2 dr^* \tag{10}$$

and $\mathcal{H} \equiv -\partial_{r^*}^2 + V(r(r^*))$, we can show that

$$(\varphi, \mathcal{H}\varphi) = \int_{-\infty}^{\infty} \left| \left(\partial_{r^*} - f\frac{d}{dr}\ln\left(r\sqrt{h}\right)\right)\varphi \right|^2 dr^* + (\ell(\ell+n-1)) \int_{r_H}^{\infty} \frac{|\varphi|^2}{(n-2)rh}\frac{dh}{dr}dr \tag{11}$$

for any φ [6–8].

In (11), the first term is always positive. And in second term, all terms other than dh/dr are also positive. Therefore, $(\varphi, \mathcal{H}\varphi) > 0$ for arbitrary φ if $dh/dr > 0$ on $r_h < r < \infty$. We choose, for example, φ as the lowest eigenstate, then we can conclude that the lowest eigenvalue E_0 is positive. Thus, we proved the stability. The other way around, if $dh/dr < 0$ at some point outside the horizon, the solution is unstable. To prove this, the inequality

$$\frac{(\varphi, \mathcal{H}\varphi)}{(\varphi, \varphi)} \geq E_0 \tag{12}$$

is useful. This inequality is correct for arbitrary φ. If $dh/dr < 0$ at some point outside horizon, we can find φ such that

$$\int_{r_H}^{\infty} \frac{|\varphi|^2}{(n-2)rh}\frac{dh}{dr}dr < 0 . \tag{13}$$

In this case, (11) is negative for sufficiently large ℓ. Then, the inequality (12) implies $E_0 < 0$ and the solution has unstable modes. Thus, we can conclude that the solution is stable if and only if $dh/dr > 0$ outside the horizon.

Now, let's check the sign of dh/dr. Using the concrete expression of $W[\psi]$ and $h(r)$,

$$\frac{dh}{dr} = r^{n-3}\frac{L[\psi]}{\left(1 + \sum_{m=2}^{k}\left[a_m\left\{\prod_{p=1}^{2m-2}(n-p)\right\}\psi^m\right]\right)^3} , \tag{14}$$

where

$$\begin{aligned} L(x) &= (n-2) + \cdots \\ &\quad + \frac{a_k^4}{k^2}(n-1)^3\left\{\prod_{p=2}^{2k-2}(n-p)^4\right\}(n-(2k-1))(n-(3k-1))x^{4k-4} . \end{aligned} \tag{15}$$

We note that the highest order $k = [(D-1)/2]$ is related to the dimensions as $n = 2k-1$ in odd-dimensions and $n = 2k$ in even-dimensions. In odd-dimensions, the leading term disappears. Hence, we cannot say anything in general. Hence, we consider only even-dimensions.

Let us examine the sign of $L(x)$ $(x \geq 0)$. If $n = 2k$, the coefficient of the lowest term is positive and that of the leading one of (15) becomes negative. Therefore $L(x) > 0$ near $x = 0$ and $L(x) < 0$ for large

x. This means that there exists roots of $L(x) = 0$ because $L(x)$ is continuity function; we define x_0 as the lowest positive root. If $\psi_H < x_0$, then $L[\psi] > 0$ for $0 \leq \psi \leq \psi_H$, and hence we see $dh/dr > 0$ for $r > r_H$. While, if $\psi_H > x_0$, then there exists a region $L[\psi] < 0$ in $x_0 \leq \psi \leq \psi_H$, and thus there exists an area $dh/dr < 0$ in $r > r_H$. Therefore, black holes are stable if $\psi_H < x_0$ and unstable if $\psi_H > x_0$. Considering the result that ψ_H becomes larger as μ, which is related to ADM mass, becomes smaller, we conclude that there exist critical mass below which black holes become unstable.

Summarizing this section, there is critical mass below which black holes are unstable in $n = 2k$. Thus, we have shown the instability of small Lovelock black holes in even-dimensions.

4 Conclusions

We have studied the stability of static black holes in Lovelock theory which is a natural higher dimensional generalization of Einstein theory. We derived a master equation for tensor perturbations in general Lovelock theory. It turned out that the resultant equation is characterized by one functional $W[\psi]$ which determines the background black hole solutions through Eq.(3). The stability issue of static black holes under tensor perturbations in general dimensions has been reduced to an algebraic problem. We have shown that in even-dimensions there exists the instability of Lovelock black holes with masses which are smaller than critical value. Remarkably, the instability is strong on short distance scales.

It is interesting to investigate the fate of the instability. As the instability is stronger for higher multipole orders ℓ, the resultant geometry would be weird. This issue is very important because black holes lose their mass due to the Hawking radiation and eventually become unstable.

Related to the above, we have to find meaning of the universal function $h(r)$. As was shown in this paper, this function governs the stability of black holes. Therefore, if $h(r)$ has, for example, thermodynamical meaning, the relation between thermodynamical [9] and dynamical instability might be revealed.

References

[1] S. B. Giddings and S. D. Thomas, Phys. Rev. D **65**, 056010 (2002) [arXiv:hep-ph/0106219]; S. B. Giddings and M. L. Mangano, Phys. Rev. D **78**, 035009 (2008) [arXiv:0806.3381 [hep-ph]].

[2] D. G. Boulware and S. Deser, Phys. Rev. Lett. **55**, 2656 (1985).

[3] D. Lovelock, J. Math. Phys. **12** (1971) 498.
C. Charmousis, Lect. Notes Phys. **769**, 299 (2009) [arXiv:0805.0568 [gr-qc]].

[4] J. T. Wheeler, Nucl. Phys. B **273**, 732 (1986).

[5] A. Barrau, J. Grain and S. O. Alexeyev, Phys. Lett. B **584**, 114 (2004) [arXiv:hep-ph/0311238].

[6] T. Takahashi and J. Soda, Phys. Rev. D **80**, 104021 (2009) [arXiv:0907.0556 [gr-qc]].

[7] H. Kodama and A. Ishibashi, Prog. Theor. Phys. **110**, 701 (2003) [arXiv:hep-th/0305147]; A. Ishibashi and H. Kodama, Prog. Theor. Phys. **110**, 901 (2003) [arXiv:hep-th/0305185]; H. Kodama and A. Ishibashi, Prog. Theor. Phys. **111**, 29 (2004) [arXiv:hep-th/0308128].

[8] G. Dotti and R. J. Gleiser, Class. Quant. Grav. **22**, L1 (2005) [arXiv:gr-qc/0409005];
G. Dotti and R. J. Gleiser, Phys. Rev. D **72**, 044018 (2005) [arXiv:gr-qc/0503117].

[9] M. H. Dehghani and M. Shamirzaie, Phys. Rev. D **72**, 124015 (2005) [arXiv:hep-th/0506227]; M. H. Dehghani and R. Pourhasan, Phys. Rev. D **79**, 064015 (2009) [arXiv:0903.4260 [gr-qc]].

On the Meissner-like effect of an extreme black hole

Yousuke Takamori[1(a)] , Ken-ichi Nakao[2(a)] , Hideki Ishihara[3(a)] ,
Masashi Kimura[4(a)], and Chul-Moon Yoo[5(b)]

[(a)] *Department of Physics, Graduate School of Science, Osaka City University, Osaka 558-8585, Japan*
[(b)] *Asia Pacific Center for Theoretical Physics, Pohang University of Science and Technology, Pohang 790-784, Korea*

Abstract

It is known that the Meissner-like effect is seen in the vacuum solutions of black-hole magnetosphere: no non-monopole component of magnetic flux penetrates the event horizon if the black hole is extreme. In this article, in order to see the effects of charge currents, we study the force-free magnetic field on the extreme Reissner-Nordström background. In this case, we should solve one elliptic differential equation called the Grad-Shafranov equation which has singular points called light surfaces. Due to the surfaces, it is difficult to solve the equation in the region from the event horizon to infinity. In order to see the Meissner effect, we consider the region near the event horizon and try to solve the equation by Taylor expansion about the event horizon. Moreover, we assume that the small rotational velocity of the magnetic field, and then, we construct a perturbative method to solve the Grad-Shafranov equation considering the effect of the inner light surface and study the behavior of the magnetic field near the event horizon.

1 Introduction

It is widely believe that there is a super massive black hole in the center of a galaxy. The black holes are expected as engines of active galactic nucleis(AGNs) and gamma ray bursts(GRBs). There are two kinds of energy source. One is the gravitational energy of accreting matter. The other is the rotational energy of an accretion disk or a black hole. In this article, we concentrate on the rotational energy of a black hole and consider the Blandford-Znajek(BZ) mechanism which is one of ways to extract the rotational energy [1]. The BZ mechanism is expected as a mechanism that supports jets in AGNs.

The efficiency of the BZ mechanism is getting larger if the magnetic field lines penetrating the event horizon increase. However, it is known that stationary axisymmetric magnetic fields in a vacuum are expelled from the event horizon of an extremely rotating black hole[2]. This effect is analogous to the Meissner effect in superconductors. The efficiency of the BZ mechanism would decrease by this Meissner effect of the black holes. Since there would be plasma around a rotating black hole in realistic astrophysical cases, it is important to study the effect of charge current for the Meissner effect of the black holes.

The realistic situation is complicated to treat, then we consider a simple toy model in this article; (i)we consider a system of electromagnetic fields and plasma which is stationary, axisymmetric and force-free, (ii)we use a static and spherical black hole spacetime with a degenerate horizon as a background geometry instead of a Kerr spacetime. It is known that a static and spherical symmetric black hole with a degenerate horizon shows the Meissner effect of the black hole[3]. Moreover, we assume that the small rotational velocity of the magnetic field, and then, we study the behavior of the magnetic field near the event horizon by using a pertubative method.

[1]Email address: takamori@sci.osaka-cu.ac.jp
[2]Electronic address:knakao@sci.osaka-cu.ac.jp
[3]Electronic address:ishihara@sci.osaka-cu.ac.jp
[4]Electronic address:mkimura@sci.osaka-cu.ac.jp
[5]Electronic address:c_m_yoo@apctp.org

2 Background geometry

We consider a static and spherical symmetric spacetime with the metric in the form

$$ds^2 = -\frac{\Delta}{r^2}dt^2 + \frac{r^2}{\Delta}dr^2 + r^2(d\theta^2 + \sin^2\theta d\varphi^2), \tag{1}$$

where $\Delta = (r - r_+)(r - r_-)$. The spacetime is known as the Reissner-Nordström(RN) spacetime. The radius of the event horizon is determined by $\Delta = 0$, therefore, there are two event horizons at $r = r_\pm$ in this spacetime. In the case of $r_+ = r_-$, these two horizons coincide, and such a case is called the extreme one.

3 Grad-Shafranov equation

In order to study the effect of charge currents for the Meissner effect of the black hole, we consider stationary and axisymmetric electromagnetic fields on the RN background [6]. Moreover, we ignore the rest mass of plasma, that is, we assume force-free. The formulation of the force-free electrodynamics on a black hole background was constructed by Macdonald and Thorne[4]. Our formulation is based on their work. In this system, we can get one quasi-linear elliptic equation for the magnetic flux, $\Psi(r, \theta)$, so called the Grad-Shafranov(GS) equation,

$$\partial_r^2\Psi + \frac{\sin\theta}{\Delta}\partial_\theta\left(\frac{\partial_\theta\Psi}{\sin\theta}\right) + \frac{U}{D} + \frac{W}{\Delta D} = 0, \tag{2}$$

where

$$U = \left(\partial_r D + \frac{r^2}{2}\sin^2\theta\frac{d\Omega_{\rm F}^2}{d\Psi}\partial_r\Psi\right)\partial_r\Psi, \quad W = \left(\partial_\theta D + \frac{r^2}{2}\sin^2\theta\frac{d\Omega_{\rm F}^2}{d\Psi}\partial_\theta\Psi\right)\partial_\theta\Psi + 8\pi^2 r^2\frac{dI^2}{d\Psi}$$
$$\text{and} \quad D = \frac{\Delta}{r^2} - r^2\Omega_{\rm F}^2\sin^2\theta, \tag{3}$$

$\Omega_{\rm F} = \Omega_{\rm F}(\Psi)$ is the angular velocity of the magnetic field line and $I = I(\Psi)$ is the charge current. In general, the GS equation for the black hole magnetosphere has three regular singular points; one is at the event horizon $\Delta = 0$ and the other two are at the light surfaces determined by $D = 0$. The speed of the magnetic field line becomes the speed of light at the light surfaces.

Due to those singular points, it is difficult to obtain a smooth solution of the GS equation in the global region from the event horizon to the infinity. Our purpose is to see the effect of charge current for the Meissner effect, therefore, we consider a region near the event horizon. Moreover, we assume a small rotating magnetic field. In this case, the inner light surface locates near the event horizon, thus, we can solve the GS equation by Taylor expansion about the event horizon in the region including the inner light surface. The outer light surface is not considered in our approach, but our study would be sufficient to see the Meissner effect of the black hole.

4 Perturbative method

In this section, we focus on the extreme case $r_+ = r_- := r_{\rm H}$ and, for simplicity, assume that the rotational velocity of the magnetic field $\Omega_{\rm F}$ is constant.

4.1 Basic equations

First, we introduce following dimensionless quantities

$$r =: r_{\rm H}y, \quad \Psi =: r_{\rm H}\psi, \quad \varepsilon := r_{\rm H}\Omega_{\rm F},$$
$$I(\Psi) =: \varepsilon\mathcal{I}(\psi) \quad \text{and} \quad 8\pi^2\frac{dI^2}{d\Psi} =: \varepsilon^2 r_{\rm H}^{-1}\mathcal{S}(\psi). \tag{4}$$

[6] Note that we only use the RN spacetime as a background instead of a Kerr spacetime. A RN black hole is a solution of charged black hole in Einstein-Maxwell system, but we treat in the way that the electromagnetic field considered in this article is not related to the Maxwell feild created by the source of the RN black hole. Perturbations of Einstein-Maxwell system without charge currents of the RN black hole was studied by Bičák and Dvořák[3]. They showed that the Meissner effect of the black hole appears in this case.

The regularity conditions for the electromagnetic field at the event horizon lead to

$$\mathcal{I} + \frac{1}{4\pi}\sin\theta\partial_\theta\psi = 0 \quad \text{at} \quad y = 1, \tag{5}$$

$$\frac{d\mathcal{I}}{d\psi}\partial_y\psi + \frac{1}{4\pi}\sin\theta\partial_\theta(\partial_y\psi) = 0 \quad \text{at} \quad y = 1. \tag{6}$$

From these conditions, we can obtain the GS equation at the event horizon as

$$\partial_y^2\psi + \frac{1}{2}L_\theta\psi + 2\partial_y\psi + \frac{1}{2}\partial_y^2\left(\frac{\mathcal{W}}{\mathcal{D}}\right) = 0 \quad \text{at} \quad y = 1, \tag{7}$$

where

$$\mathcal{D} = y\left[(y-1)^2 - \varepsilon^2 y^4\sin^2\theta\right] \quad \text{and} \quad \mathcal{W} = -\varepsilon^2 y^5\left[\sin 2\theta\partial_\theta\psi - \mathcal{S}(\psi)\right]. \tag{8}$$

Moreover, the inner light surface regularity condition can be written as

$$\partial_\theta\psi - \frac{\mathcal{S}}{\sin 2\theta} - \varepsilon y\tan\theta\sin\theta(1 - \varepsilon y^2\sin\theta)\partial_y\psi = 0 \quad \text{at} \quad y = y_{\mathrm{LS}_-}, \tag{9}$$

where y_{LS_-} is the location of the inner light surface.

Here we assume the ψ can be written in the form of Taylor series around $y = 1$ as

$$\psi(y,\theta) = \sum_{n=0}^{\infty}\psi^{(n)}(\theta)(y-1)^n. \tag{10}$$

If we fix the functional form of $\mathcal{I}(\psi)$, the coefficients $\psi^{(n)}$ for $n \leq 2$ are determined by Eqs. (5), (6), (7) and (9). In order to get $\psi^{(n)}$ of $n \geq 3$, we use the derivative of the GS equation with respect to y. The functional form of $\mathcal{I}(\psi)$ must be determined so that the regularity condition (9) at the inner light surface is satisfied [5][6][7][8].

4.2 Perturbative analysis

Hereafter, assuming $0 < \varepsilon << 1$, we construct a perturbative solution for ψ near the event horizon. We assume

$$\psi^{(n)} = \sum_{n=0}^{\infty}\psi_N^{(n)}\varepsilon^N \quad \text{and} \quad \mathcal{I}(\psi) = \sum_{n=0}^{\infty}\mathcal{I}_{N+1}(\psi)\varepsilon^N. \tag{11}$$

Note that $\mathcal{I}_1$ which is the lowest order of $\mathcal{I}$ is the first order of the charge current because we assume $I = \varepsilon\mathcal{I}$. Because of $y_{\mathrm{LS}_-} - 1 = \mathcal{O}(\varepsilon)$, the inner light surface regularity condition can be written in the form of Taylor series around $y = 1$. Thus, we can obtain the regularity conditions in each order of ε and construct a perturbative solution for $\psi^{(n)}$ by solving Eqs. (5), (6), (7) and (9) in each order of ε. In this article, we construct a perturbative solution with corrections up to $\mathcal{O}(\varepsilon^2)$. Since $y_{\mathrm{LS}_-} - 1 = \mathcal{O}(\varepsilon^1)$, the magnetic flux up to $\mathcal{O}(\varepsilon^2)$ behaves near the inner light surface as

$$\psi(y,\theta) = \psi_0^{(0)}(\theta) + \varepsilon^1\psi_1^{(0)}(\theta) + \varepsilon^2\psi_2^{(0)}(\theta) + \left(\psi_0^{(1)}(\theta) + \varepsilon^1\psi_1^{(1)}(\theta)\right)(y-1) + \psi_0^{(2)}(\theta)(y-1)^2 + \mathcal{O}(\varepsilon^3). \tag{12}$$

The results are as follows:

$$\psi_0^{(0)} = C_0^{(0)}(1-\cos\theta), \quad \psi_1^{(0)} = 0, \quad \psi_2^{(0)} = \left[C_2^{(0)}\cos\theta(3\cos^2\theta - 7) + \frac{C'C_0^{(0)}}{4}(\cos^2\theta - 5)\right]\sin^2\theta,$$

$$\psi_0^{(1)} = C'C_0^{(0)}\sin^2\theta, \quad \psi_1^{(1)} = 0 \quad \text{and} \quad \psi_0^{(2)} = \frac{1}{2}\left[3\left(C_0^{(0)}C'^2 - 10C_2^{(0)}\right)\cos\theta + C'C_0^{(0)}\right]\sin^2\theta, \tag{13}$$

where $C_0^{(0)}$, $C_2^{(0)}$ and C' are integration constants. Moreover the small charge current are obtained as

$$\mathcal{I}_1 = -\frac{C_0^{(0)}}{4\pi}\hat{X}\left(2 - \hat{X}\right), \quad \mathcal{I}_2 = 0 \quad \text{and}$$

$$\mathcal{I}_3 = \frac{1}{8\pi^2}\hat{X}^2\left(2 - \hat{X}\right)^2\left[C_0^{(0)}C'\left(1 - \hat{X}\right) + 2C_2^{(0)}\left(2 - 18\hat{X} + 9\hat{X}^2\right)\right], \tag{14}$$

where $\hat{X} = \psi_0^{(0)}/C_0^{(0)}$. The zeroth order of $\psi^{(n)}$ represent a vacuum solution because $\Omega_{\rm F}$ and I become zero in the limit $\varepsilon \to 0$. Therefore, $\psi_0^{(0)}$ represents a monopole solution in the vacuum. It means the Meisnner effect appear in the vacuum case if we accept the fact that there is no magnetic monopole charge in the nature. As a result, our perturbative solutions show magnetic fields with the small corrections to the monopole due to the existence of the charge currents. Here we should note that non-trivial solutions are obtained by our pertubative analysis, only if the configuration of the zeroth order solution $\psi_0^{(0)}$ is monopole, namely, $C_0^{(0)} \neq 0$. If we require $\psi_0^{(0)} = 0$, by integrating Eq. (5) of $\mathcal{O}(\varepsilon^1)$, we can obtain

$$\psi_1^{(0)} = C_1^{(0)} \left[\frac{\sin^2\theta}{(1+\cos\theta)^2} \right]^{-2\pi \frac{d\mathcal{I}_1}{d\psi}(0)}, \tag{15}$$

where $C_1^{(0)}$ is an integration constant. If we impose no-magnetic monopole charge, $\psi(\pi) = 0$, the integration constant should be $C_1^{(0)} = 0$, therefore, we get the trivial solution $\psi_1^{(0)} = 0$. Moreover, we get the same result for all order. Thus, we can obtain the only trivial solution $\psi_N^{(0)} = 0$ in the case $\psi_0^{(0)} = 0$.

5 Summary and Discussion

We constructed an approximate solution of the GS equation considering the inner light surface regularity condition in the region near the event horizon in the case of slow rotating magnetic field by using a perturbative analysis. Non-trivial solutions obtained by our perturbative analysis in the form of deformed monopole fields. However, we can not conclude that the Meissner effect of the black hole appears even if the current exists because our perturbative analysis dose not include all perturbative solutions of vacuum configurations. For example, we know an exact solution of GS equation as

$$\psi = C(1-\cos\theta) \quad \text{with} \quad \mathcal{I} = \frac{\psi}{4\pi}\left(2 - \frac{\psi}{C}\right), \tag{16}$$

where C is an integration constant, and the perturvative solution of (16) can not be obtained by our perturbative analysis with $\psi_0^{(0)} = 0$. Thus, there is a possibility that perturbative solutions with vanishing $\psi_0^{(0)}$. The origin of this possibility may come from the fact that the assumption for the charge current (11) is too strong. Unfortunately, the persent perturbation analysis would be hard to do without this assumption. According to Komissarov and McKinney[9], there was no sign of the Meissner effect in highly conductive magnetoshperes. Our results are not opposed to their results. In order to argue the disappearance of the Meissner effect, we should construct a magnetic configuration with only non-monopole components. This is a future work.

References

[1] R. D. Blandford and R. L. Znajek, Mon. Not. R. Astron. Soc. **179**, 433 (1977).

[2] J. Bičák, V. Kraus and T. Ledvinka, astro-ph/0610841.

[3] J. Bičák and L. Dvořák, Phys. Rev. D **22**, 12 (1980).

[4] D. Macdonald and K. S. Thorne, Mon. Not. R. Astron. Soc. **198**, 345 (1982).

[5] I. Contopoulos, D. Kazanas and C. Fendt, Astrophys. J. **511**, 351 (1999)

[6] J. Ogura and Y. Kojima, Prog. Theor. Phys. **109**, 619 (2003).

[7] D. A, Uzdensky, Astrophys. J. **603**, 652 (2004).

[8] D. A, Uzdensky, Astrophys. J. **620**, 889 (2005).

[9] S. S. Komissarov and J. C. McKinney, Mon. Not. R. Astron. Soc. **377**, 49 (2007).

Stability of gravitating Q-balls via a catastrophe theory

Takashi Tamaki[1(a)] and Nobuyuki Sakai[2(b)]

[(a)] *Department of Physics, General Education, College of Engineering, Nihon University, Tokusada, Tamura, Koriyama, Fukusima 963-8642*
[(b)] *Faculty of Education, Yamagata University, Yamagata 990-8560*

Abstract

We analyze stability of gravitating Q-balls.

1 Introduction and our model

It has been argued that scalar solitons play important roles as dark matter candidates. Boson stars are one of their possibilities. Depending on their potentials and couplings, we can consider various sizes. For example, it has been argued that axidilaton star of $\sim 0.6M_\odot$ accounts for some fraction of the massive compact halo objects [1]. Supermassive boson stars of $10^6 - 10^9 M_\odot$ as an alternative to a black hole in the galaxy center has also been discussed [2]. For these reasons, it is important to argue their stabilities. To tackle this problem, it is instructive to consider their flat limit and examine the method which is useful for stability analysis in this case. In general, boson stars do not have a flat limit. The case having the flat limit is classified as Q-balls [3]. Kusenko showed that Q-balls are stable under the thick-wall approximation for the potential [4]

$$V_3(\phi) = \frac{m^2}{2}\phi^2 - \mu\phi^3 + \lambda\phi^4 \quad \text{with} \quad m^2,\ \mu,\ \lambda > 0\ . \tag{1}$$

The work by Pacceti Correia and Schmidt is very useful which showed that stability of Q-balls is guaranteed if and only if

$$\frac{\omega}{Q}\frac{dQ}{d\omega} < 0\ , \tag{2}$$

where Q and ω are the Q-ball charge and the phase velocity, respectively [5]. Whether or not this criterion can be extended to gravitational Q-balls is one of our interest. We take the action

$$\mathcal{S} = \int d^4x\sqrt{-g}\left(\frac{{m_{\rm Pl}}^2}{16\pi}\mathcal{R} - \frac{1}{2}g^{\mu\nu}\partial_\mu\boldsymbol{\phi}\cdot\partial_\nu\boldsymbol{\phi} - V(\phi)\right), \tag{3}$$

where $\boldsymbol{\phi} = (\phi_1,\ \phi_2)$ is an SO(2)-symmetric scalar field and $\phi \equiv \sqrt{\boldsymbol{\phi}\cdot\boldsymbol{\phi}} = \sqrt{\phi_1^2+\phi_2^2}$. We assume a spherically symmetric and static spacetime, $ds^2 = -\alpha^2(r)dt^2 + A^2(r)dr^2 + r^2(d\theta^2 + \sin^2\theta d\varphi^2)$. We consider spherically symmetric configurations of the field and assume homogeneous phase rotation, $(\phi_1, \phi_2) = \phi(r)(\cos\omega t, \sin\omega t)$. Then the field equations become

$$A' + \frac{A}{2r}(A^2-1) = \frac{4\pi r A^3}{{m_{\rm Pl}}^2}\left(\frac{\phi'^2}{2A^2} + \frac{\omega^2\phi^2}{2\alpha^2} + V\right), \alpha' + \frac{\alpha}{2r}(1-A^2) = \frac{4\pi r\alpha A^2}{{m_{\rm Pl}}^2}\left(\frac{\phi'^2}{2A^2} + \frac{\omega^2\phi^2}{2\alpha^2} - V\right), \tag{4}$$

$$\phi'' + \left(\frac{2}{r} + \frac{\alpha'}{\alpha} - \frac{A'}{A}\right)\phi' + \left(\frac{\omega A}{\alpha}\right)^2\phi = A^2\frac{dV}{d\phi}, \tag{5}$$

where $' \equiv d/dr$. We solve (4)-(5) with boundary conditions,

$$A(0) = A(\infty) = \alpha(\infty) = 1, \quad A'(0) = \alpha'(0) = \phi'(0) = \phi(\infty) = 0. \tag{6}$$

[1]Email address: tamaki@ge.ce.nihon-u.ac.jp
[2]Email address: nsakai@e.yamagata-u.ac.jp

Due to the symmetry there is a conserved charge,

$$Q \equiv \int d^3x\sqrt{-g}g^{\mu\nu}(\phi_1\partial_\nu\phi_2 - \phi_2\partial_\nu\phi_1) = \omega I, \quad \text{where} \quad I \equiv 4\pi\int \frac{Ar^2\phi^2}{\alpha}dr. \tag{7}$$

The Hamiltonian is given by

$$E = \int (\mathcal{H}_{\rm G} + \mathcal{H}_\phi)d^3x = \frac{Q^2}{I} - 4\pi\int r^2\alpha AV dr. \tag{8}$$

We consider (1) which we call V_3 model. For V_3 model, we rescale the quantities as

$$\tilde{t} \equiv \frac{\mu}{\sqrt{\lambda}}t, \quad \tilde{r} \equiv \frac{\mu}{\sqrt{\lambda}}r, \quad \tilde{\phi} \equiv \frac{\lambda}{\mu}\phi, \quad \tilde{V}_3 \equiv \frac{\lambda^3}{\mu^4}V_3, \quad \tilde{m} \equiv \frac{\sqrt{\lambda}}{\mu}m, \quad \tilde{\omega} \equiv \frac{\sqrt{\lambda}}{\mu}\omega, \quad \kappa \equiv \frac{\mu^2}{\lambda {m_{\rm Pl}}^2}, \tag{9}$$

To estimate the parameter regions of $\tilde{\omega}^2$ where solutions exist, we consider the flat case. In this case, the field equation is

$$\frac{d^2\tilde{\phi}}{d\tilde{r}^2} = -\frac{2}{\tilde{r}}\frac{d\tilde{\phi}}{d\tilde{r}} - \tilde{\omega}^2\tilde{\phi} + \frac{d\tilde{V}}{d\tilde{\phi}}\,. \tag{10}$$

This is equivalent to the field equation for a single static scalar field with the potential $V_\omega \equiv \tilde{V} - \tilde{\omega}^2\tilde{\phi}^2/2$. For this case, solutions satisfying boundary conditions (6) exist if $\min(V_\omega) < \tilde{V}(0)$ and $d^2V_\omega/d\tilde{\phi}^2(0) > 0$, which is equivalent to

$$\tilde{\omega}^2_{\rm min} < \tilde{\omega}^2 < \tilde{m}^2 \quad \text{with} \quad \tilde{\omega}^2_{\rm min} \equiv \min\left(\frac{2\tilde{V}}{\tilde{\phi}^2}\right). \tag{11}$$

The two limits $\tilde{\omega}^2 \to \tilde{\omega}^2_{\rm min}$ and $\tilde{\omega}^2 \to \tilde{m}^2$ correspond to the thin-wall limit and the thick-wall limit, respectively. For V_3 potential, we have $\tilde{\omega}^2_{\rm min} = \tilde{m}^2 - \frac{1}{2}$. As we explain below, qualitative features of solutions change at $\tilde{m}^2 = \frac{1}{2}$.

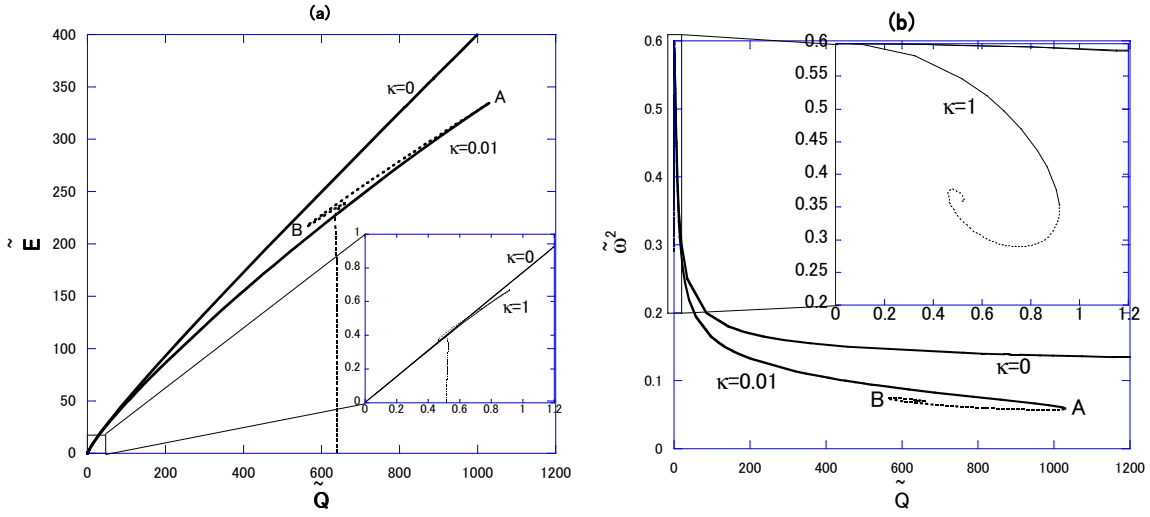

Figure 1: (a) $\tilde{Q}$-$\tilde{E}$ and (b) $\tilde{Q}$-$\tilde{\omega}^2$ for $\tilde{m}^2 = 0.6$.

2 Comparison of gravitating cases with flat cases

2.1 The case for $\tilde{m}^2 > 0.5$

First, we compare $\tilde{Q}$-$\tilde{E}$ and $\tilde{Q}$-$\tilde{\omega}^2$ in the case for $\tilde{m}^2 = 0.6$ with $\kappa = 0$ (i.e., flat case), and with 0.01 and 0.1 in Fig. 1 (a) and (b), respectively. For the flat case, there is an one to one correspondence between

$\tilde{Q}$ and $\tilde{E}$ while there is a cusp structure for the gravitating case as shown in Fig. 1 (a). As a result, we find the $\tilde{Q}$-maximum (the point A) and its local minimum (the point B). It is expected that this property would affect their stability. Actually, if we see Fig. 1 (b), we find that the stability criterion (2) is satisfied for the flat case while it is not necessarily satisfied for the gravitating case. However, since (2) is established by using the explicit form of the perturbative equation for the flat case, it is not evident whether or not it is applicable for the gravitating case.

It is natural to ask what cause these differences. To answer this question, we show the field profiles of the scalar field for $\kappa = 0$ with $\tilde{Q} = 200$ and 800 (dotted lines) and those for $\kappa = 0.01$ with $\tilde{Q} = 200$ and 800 (solid lines) in Fig. 2. If we pay attention to the case $\tilde{Q} = 200$, we notice that the scalar field is a little bit concentrated near the origin if the gravity is taken into account. This tendency becomes clear for the case $\tilde{Q} = 800$ where two solutions exist for $\kappa = 0.01$ (See, Fig. 1). The solution with more condensed configuration around the origin corresponds to that shown by a dotted line in Fig. 1. This implies that the Q-ball having larger charge than that of the point A can not support itself and will collapse or disperse. Limitation of the Q-ball size due to gravity has been pointed out in [6]. This implies that stability changes at the point A. Although we show the example $\tilde{m}^2 = 0.6$ with $\kappa = 0$ and 0.01, qualitative properties for $\tilde{m}^2 > 0.5$ and other κ do not change from these cases. The quantitative properties which are changed by other parameters are sizes of cusp(spiral) structures in these diagrams. If we take large (small) κ and $\tilde{m}^2$, maximum of $\tilde{Q}$ becomes small (large).

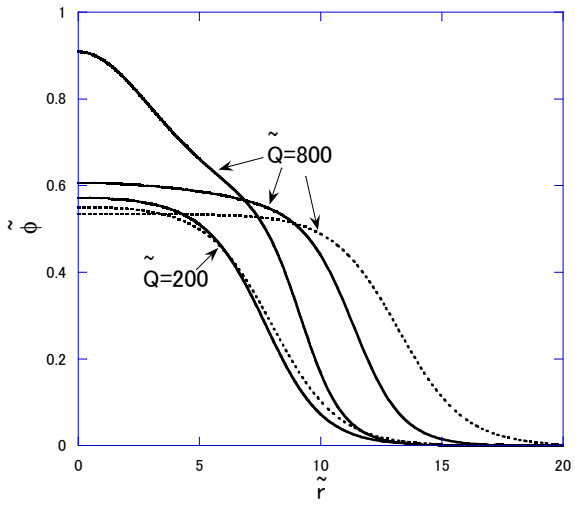

Figure 2: $\tilde{r}$-$\tilde{\phi}$ relation for $\kappa = 0$ with $\tilde{Q} = 200$ and 800 (dotted lines) and for $\kappa = 0.01$ with $\tilde{Q} = 200$ and 800 (solid lines).

2.2 The case for $\tilde{m}^2 < 0.5$

Next, we show (a) $\tilde{Q}$-$\tilde{E}$ and (b) $\tilde{Q}$-$\tilde{\omega}^2$ for $\tilde{m}^2 = 0.2$ in Fig. 3. First, we pay attention to Fig. 3 (a). We should notice that the case $\kappa = 0$ has a cusp structure and has a $\tilde{Q}$-maximum different from that for $\tilde{m}^2 > 0.5$. As a result, we have two solutions for a fixed $\tilde{Q}$ for the flat case. It has been shown that the dotted line is unstable while the solid line stable. We find that the case $\kappa = 1.0$ only show the slight difference from the flat case. Intrinsic differences occur for $\kappa = 1.5$ where two cusp structures appear for each κ (we call each of them lower and higher branch corresponding to their energy, respectively). If one considers the analogy with the flat case where the solid (dotted) line is the stable (unstable), one may suppose that the lower (higher) branch is stable (unstable). However, we should suppose that two cusp structures appear for the same reason for the corresponding one for $\tilde{m}^2 > 0.5$ where gravity makes a $\tilde{Q}$-maximum. Thus, it is natural to guess that the lower branch shown by a solid (dotted) line is stable (unstable).

We also comment on the diagram (b) and the stability criterion (2). The solid (dotted) lines correspond to those in the diagram (a). For the flat case, we can confirm that the solid line satisfies (2) while the

dotted line does not. For the gravitating with $\kappa < 1.4$, we also confirm it while it is not for $\kappa \geq 1.4$. In particular, the solution shown by the solid line and that by the dotted line, both satisfying (2), merge at the cusp for $\kappa = 1.5$. Since the cusp is a typical structure which suggests a stability change via a catastrophe theory, (2) would not be applicable for gravitating Q-balls.

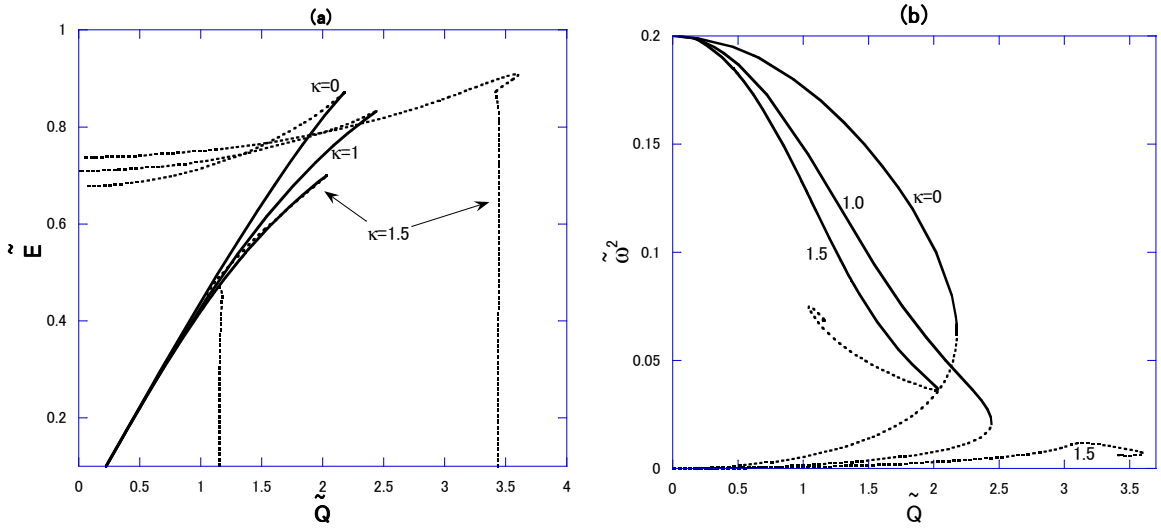

Figure 3: (a) $\tilde{Q}$-$\tilde{E}$ and (b) $\tilde{Q}$-$\tilde{\omega}^2$ for $\tilde{m}^2 = 0.2$.

3 Conclusion

We have analyzed stability of gravitating Q-balls for a V_3 model and revealed their structures.

References

[1] E. W. Mielke and F. E. Schunck, Nucl. Phys. B **564**, 185 (2000); *ibid.,* Gen. Rel. Grav. **33**, 805 (2001).

[2] F. E. Schunck and A. R. Liddle, Phys. Lett. B **404**, 25 (1997); E. W. Mielke and F. E. Schunck, Phys. Rev. D **66**, 023503 (2002).

[3] S. Coleman, Nucl. Phys. **B262**, 263 (1985).

[4] A. Kusenko, Phys. Lett. B **404**, 285 (1997).

[5] F. Paccetti Correia and M. G. Schmidt, Eur. Phys. J. **C21**, 181 (2001).

[6] T. Multamaki and I. Vilja, Phys. Lett. B **542**, 137 (2002).

Asymptotic flatness at null infinity in five dimensions

Kentaro Tanabe, [1](a) Norihiro Tanahashi [2](b) and Tetsuya Shiromizu[3](b)

(a) *Yukawa Institute for Theoretical Physics, Kyoto University, Kyoto 606-8502, Japan*
(b) *Department of Physics, Kyoto University, Kyoto 606-8502, Japan*

Abstract

We discuss the asymptotic structure of null infinity in five dimensional space-time. Since it is known that the conformal infinity is not useful for odd higher dimensions, we shall employ the coordinate based method like the Bondi coordinate firstly introduced in four dimensions. Then we define the null infinity and identify the asymptotic symmetry. We also derive the Bondi mass expression and show its conservation law.

1 Introduction

Inspired by superstring theory, fundamental studies of higher dimensional space-time is important. One of open issue is the asymptotic structure at null infinity. We often introduce the conformal infinity to discuss the asymptotic structure at infinities in four dimensions [1, 2]. Therein the space-time is compactified by conformal transformation and embedded into another space-time. For example, Minkowski space-time is conformally embedded into Einstein static universe. Conformally embedded space-time have two different infinities, i.e., spatial infinity and null infinity. In higher dimensional space-times, the asymptotic structure at spatial infinity can be well-defined. The asymptotic symmetry is identified with Poincare group and conserved quantities associated with the symmetry are constructed [3, 4].

On the other hand, the asymptotic structure at null infinity is not understood completely in higher dimensional space-times [5–7]. Indeed, the definition of null infinity is given only in even dimensions [5, 7]. The difficulty in the definition of null infinity compared with spatial infinity is due to the presence of the gravitational waves at null infinity. At spatial infinity, since there are no gravitational waves, the asymptotic structure is "stationary" and the total mass and total angular momentum are conserved, while the asymptotic structure at null infinity might be disturbed by gravitational waves. Hence, we need a stable definition of null infinity against gravitational waves. We can give such a definition in *even* dimensions if we use conformal embedding method, but cannot in odd dimensional space-times since we cannot show the smoothness of Einstein equations at null infinity. This non-smoothness would be related with the facts that in conformal embedding method we introduce the conformal factor $\Omega \sim 1/r$, and the behavior of gravitational waves near null infinity are order of $\mathcal{O}(\Omega^{(d-2)/2})$ in d dimensional space-times. The problem comes from the half-integer power of Ω.

In this paper, we define null infinity in five dimensional space-time. We do not use conformal embedding method, but the Bondi coordinate to define null infinity, which was introduced firstly by Bondi and Sachs in four dimensions [8–11]. The rest of this paper is organized as follows. In section 2, we introduce the Bondi coordinate in five dimensions. In section 3, we define the asymptotic flatness at null infinity in five dimensions and show the robustness of the definition against gravitational waves by solving Einstein equations. In this section, we define the Bondi mass, and obtain the Bondi mass loss law in five dimensions. In section 4, we discuss the asymptotic symmetry at null infinity associated with the asymptotic flatness defined in section 3. We show that there are no supertranslations in five dimensions unlike in four dimensions. Finally, in section 5, we give a summary.

[1]Email address: tanabe@yukawa.kyoto-u.ac.jp
[2]Email address: tanahashi@tap.scphys.kyoto-u.ac.jp
[3]Email address: shiromizu@@tap.scphys.kyoto-u.ac.jp

2 Bondi coordinate in five dimensions

We consider five dimensional space-time. We introduce the Bondi coordinate to define asymptotic flatness at null infinity. Suppose there is a function $u(x^a)$ which satisfies the equation

$$u_{,a}u_{,b}g^{ab} = 0. \tag{1}$$

Let θ, ϕ, ψ be angular coordinates, which are constant along gradient u. Period of these each coordinates are taken to be π, 2π, 2π, respectively. For convenience, we introduce the notation $(\theta, \phi, \psi) = x^A$, where capital Latin indices run from 2 to 4. Now we define the function r by the equation

$$r^6 \sin^2\theta \cos^2\theta = \det(g_{AB}). \tag{2}$$

Using these coordinates (we call them the Bondi coordinates)

$$x^0 = u\,,\ x^1 = r\,,\ x^2 = \theta\,,\ x^3 = \phi\,,\ x^4 = \psi, \tag{3}$$

we can write down metric such that

$$ds^2 = -(Ve^B/r^2)du^2 - 2e^B dudr + r^2 h_{AB}(dx^A + U^A du)(dx^B + U^B du), \tag{4}$$

where

$$h_{AB} = \begin{pmatrix} e^{C_1} & \sin\theta\sinh D_1 & \cos\theta\sinh D_2 \\ \sin\theta\sinh D_1 & e^{C_2}\sin^2\theta & \sin\theta\cos\theta\sinh D_3 \\ \cos\theta\sinh D_2 & \sin\theta\cos\theta\sinh D_3 & e^{C_3}\cos^2\theta \end{pmatrix}. \tag{5}$$

$V, B, h_{AB}, U^A, C_1, C_2, C_3, D_1, D_2$ and D_3 are function of u, r and x^A. In this coordinate, null infinity is represented by $r \to \infty$.

3 Boundary conditions

The boundary conditions in the Bondi coordinates

$$C_1(u, r, x^A) = \frac{C_{11}(u, x^A)}{r^{3/2}} + O(1/r^2) \tag{6}$$

$$C_2(u, r, x^A) = \frac{C_{21}(u, x^A)}{r^{3/2}} + O(1/r^2) \tag{7}$$

$$C_3(u, r, x^A) = \frac{C_{31}(u, x^A)}{r^{3/2}} + O(1/r^2) \tag{8}$$

$$D_1(u, r, x^A) = \frac{D_{11}(u, x^A)}{r^{3/2}} + O(1/r^2) \tag{9}$$

$$D_2(u, r, x^A) = \frac{D_{21}(u, x^A)}{r^{3/2}} + O(1/r^2) \tag{10}$$

$$D_3(u, r, x^A) = \frac{D_{31}(u, x^A)}{r^{3/2}} + O(1/r^2) \tag{11}$$

$$V = r^2 + V_1(u, x^A)r^{1/2} - M(u, x^A) + O(1/r^{1/2}) \tag{12}$$

$$B = \frac{B_1(u, x^A)}{r^3} + O(1/r^{7/2}) \tag{13}$$

$$U^A = \frac{U_{A1}(u, x^A)}{r^{5/2}} + O(1/r^3) \tag{14}$$

$$\mathbb{C} = \frac{\mathbb{C}_1(u, x^A)}{r^{3/2}} + O(1/r^2) \tag{15}$$

define asymptotic flatness at null infinity. These boundary conditions are determined from Einstein equations $R_{ab} = 0$. We define M in V as Bondi mass and from Einstein equation $R_{uu} = 0$, we get

$\partial_u M(u, x^A)$ as

$$\frac{\partial M}{\partial u} = -\frac{1}{3}\left((C_{11,u})^2 + C_{11,u}C_{21,u} + (C_{21,u})^2 + (D_{11,u})^2 + (D_{21,u})^2 + (D_{31,u})^2\right). \tag{16}$$

Eq. (16) represents mass loss rate by gravitational waves, and total mass always decreases as in four dimension. Then $M(u, x^A)$ describes the mass in $u =$ constant surfaces.

4 Asymptotic symmetry at null infinity

Asymptotic symmetry should be defined as transformations preserving the boundary conditions (12), (13), (14) and (15). By infinitesimal transformation ξ, metric is transformed as

$$\delta g_{ab} = 2\nabla_{(a}\xi_{b)}. \tag{17}$$

To preserve the boundary conditions given in the previous section, the variation of metric, δg_{ab}, should satisfy

$$\delta g_{rr} = 0\,,\ \delta g_{rA} = 0\,,\ g^{AB}\delta g_{AB} = 0, \tag{18}$$

$$\delta g_{uu} = O(r^{-3/2})\,,\ \delta g_{ur} = O(r^{-3})\,,\ \delta g_{uA} = O(r^{-1/2})\,,\ \delta g_{AB} = O(r^{1/2}). \tag{19}$$

From Eq. (18), the components of infinitesimal transformation ξ must take the following forms:

$$\xi_r = f(u, x^A)e^B, \tag{20}$$

$$\xi_B g^{AB} = f^A(u, x^A) - fU^A + \int_r^\infty dr' e^B f_{,B} g^{AB}, \tag{21}$$

$$\xi_u = -\frac{re^B}{3}\left(-\xi_{A,B} + \xi_C\Gamma^C_{AB} + \xi_r\Gamma^r_{AB}\right)g^{AB}, \tag{22}$$

where $\mathcal{D}_A$ is the covariant derivative with respect to the standard metric $h^{(0)}_{AB}$ on 3 sphere. The infinitesimal transformation ξ have four free parameters f, f^A.

Then, the other components of metric variation become

$$\delta g_{uu} = \frac{2r}{3}\mathcal{D}_A f^A{}_{,u} + \frac{2}{3}(3f + \mathcal{D}^2 f)_{,u} + \frac{2}{r^{1/2}}h^{(0)}_{AB}f^A{}_{,u}U_{B1} + O(r^{-3/2}), \tag{23}$$

$$\delta g_{ur} = \frac{1}{3}(\mathcal{D}_A f^A + 3f_{,u}) + \frac{1}{5r^{5/2}}h^{(1)AB}\mathcal{D}_A\mathcal{D}_B f + O(r^{-3}), \tag{24}$$

$$\delta g_{uA} = r^2 h^{(0)}_{AB}f^B{}_{,u} + \frac{r}{3}\mathcal{D}_A(3f_{,u} + \mathcal{D}_B f^B) + r^{1/2}h^{(1)}_{AB}f^B{}_{,u} + \frac{1}{3}\mathcal{D}_A(\mathcal{D}^2 f + 3f) + O(r^{-1/2}), \tag{25}$$

$$\delta g_{AB} = \frac{2r^2}{3}(-\mathcal{D}_C f^C h^{(0)}_{AB} + 3\mathcal{D}_{(A}f_{B)}) + \frac{2r}{3}(-\mathcal{D}^2 f h^{(0)}_{AB} + 3\mathcal{D}_A\mathcal{D}_B f) + T_{AB}(u, x^A)r^{1/2} + O(r^{-1/2}), \tag{26}$$

where $X_{(AB)} := (1/2)(X_{AB} + X_{BA})$ for some tensor X_{AB}, T_{AB} is some traceless tensor with respect to $h^{(0)}_{AB}$ and we expand the metric h_{AB} as

$$h_{AB} = h^{(0)}_{AB} + \frac{1}{r^{3/2}}h^{(1)}_{AB} + O(r^{-2}), \tag{27}$$

and $h^{(1)AB} = h^{(0)AC}h^{(0)BD}h^{(1)}_{CD}$. In the Bondi coordinate, $h^{(0)}_{AB}$ and $h^{(1)}_{AB}$ are

$$h^{(0)}_{AB} = \begin{pmatrix} 1 & 0 & 0 \\ 0 & \sin^2\theta & 0 \\ 0 & 0 & \cos^2\theta \end{pmatrix} \tag{28}$$

and

$$h^{(1)}_{AB} = \begin{pmatrix} C_{11} & D_{11}\sin\theta & D_{21}\cos\theta \\ D_{11}\sin\theta & C_{21}\sin^2\theta & D_{31}\sin\theta\cos\theta \\ D_{21}\cos\theta & D_{31}\sin\theta\cos\theta & -(C_{11}+C_{21})\cos^2\theta \end{pmatrix}. \tag{29}$$

To satisfy the condition (19), we find that f^A and f should satisfy following equations:

$$f^A{}_{,u} = 0, \tag{30}$$

$$\mathcal{D}_A f_B + \mathcal{D}_B f_A = -2\frac{\partial f}{\partial u} h^{(0)}_{AB}, \tag{31}$$

$$\mathcal{D}_A \mathcal{D}_B f = \frac{1}{3}\mathcal{D}^2 f h^{(0)}_{AB}. \tag{32}$$

The part of f not proportional to u generates translation group, and since in general the equation (32) has five solutions, this part have only five degrees of freedom, there is no supertranslation freedom unlike in four dimension. f^A generate Lorentz transformation group, so asymptotic symmetry at null infinity in five dimensional space-time is Poincare group which is semi-direct of five dimensional transformation group and Lorentz group.

5 Summary

In this paper, we define asymptotic flatness at null infinity in five dimensional space-time by using the Bondi coordinates. In conformal embedding method, we cannot show the smoothness of asymptotic structure at null infinity because the gravitational waves behave $\Omega^{3/2}$ near null infinity and in the coordinate using $\Omega \sim 1/r$, the regularity of gravitational fields at null infinity is not guaranteed in general in five dimensions. On the other hand, in the Bondi coordinates, we can show the robustness of the asymptotic structure at null infinity which is defined by boundary conditions of Eqs. (12), (13), (14) and (15). Solving Einstein equations under these boundary conditions, we find that total mass always decreases by gravitational waves as in four dimensions. In addition, we show that the asymptotic symmetry at null infinity would be Poincare group in five dimensions.

References

[1] R. Penrose, Phys. Rev. Lett. **10**, 66 (1963).

[2] R. M. Wald *General Relativity* (Chicago:University of Chicago Press, 1984).

[3] T. Shiromizu and S. Tomizawa, Phys. Rev. D **69**, 104012 (2004) [arXiv:gr-qc/0401006].

[4] K. Tanabe, N. Tanahashi and T. Shiromizu, arXiv:0902.1583 [gr-qc].

[5] S. Hollands and A. Ishibashi, J. Math. Phys. **46**, 022503 (2005) [arXiv:gr-qc/0304054].

[6] S. Hollands and R. M. Wald, Class. Quant. Grav. **21**, 5139 (2004) [arXiv:gr-qc/0407014].

[7] A. Ishibashi, Class. Quant. Grav. **25**, 165004 (2008) [arXiv:0712.4348 [gr-qc]].

[8] H. Bondi, M. G. J. van der Burg and A. W. K. Metzner, Proc. Roy. Soc. A (London) **269**, 21 (1962).

[9] J. Winicour, J. Math. Phys. **7**, 863 (1967).

[10] R. K. Sachs, Proc. Roy. Soc. A (London) **270**, 103 (1962).

[11] R. K. Sachs, Phys. Rev. **128**, 2851 (1962).

[12] R. C. Myers and M. J. Perry, Annals Phys. **172**, 304 (1986).

Toward numerical relativity in RS-II model

Norihiro Tanahashi,[1(a)] Motoyuki Saijo,[2(b),(c)] Masaru Shibata,[3(d)] and Takahiro Tanaka[4(d)]

[(a)] *Department of Physics, Kyoto University, Kyoto 606-8502*
[(b)] *Department of Physics, Rikkyo University, Toshima, Tokyo 171-8501*
[(c)] *Research Center for Measurement in Advanced Science, Rikkyo University, Toshima, Tokyo 171-8501*
[(d)] *Yukawa Institute for Theoretical Physics, Kyoto University, Kyoto 606-8502*

Abstract

To investigate non-trivial connection between gauge theory and higher-dimensional gravity theory, we try to establish a numerical scheme for a higher-dimensional spacetime with negative cosmological constant. The cosmological constant warps the spacetime, and then the asymptotic boundary condition becomes nontrivial. We discuss how such a problem can be circumvented by the modification of the scheme. We illustrate how to subtract the effect of the negative cosmological constant from the metric in the aid of conformal transformation. We also discuss how to take the brane into the scheme to apply this technique to the numerical analysis of the braneworld models.

1 Introduction

The numerical relativity has been developing very rapidly, and now it is possible to simulate highly dynamical stellar object such as coalescing binaries of neutron stars or black holes. Recently, numerical relativity for axisymmetric higher-dimensional flat spacetime was realized [1]. Current scheme of the numerical relativity, however, cannot handle with general spacetimes such as spacetimes with non-zero cosmological constant. Thus the application of this technique is limited to, for example, simulations of simple black objects in asymptotically flat spacetimes. My plan is to improve this code to take the non-zero cosmological constant into account. The goal of my future research is to understand gravitational dynamics in higher-dimensional spacetimes using this numerical technique, and to apply that knowledge to other research field such as AdS/CFT correspondence of the string theory. Since nonlinear dynamics of higher-dimensional spacetimes can be investigated only by numerical techniques, We believe that this study will give a wide contribution to the research of general relativity theory as well as elementary particle theory. For example, this technique enables us to tackle the ambitious projects such as test of bulk/brane correspondence in the Randall-Sundrum II (RS-II) braneworld models [2, 3] or the investigation of the AdS/CFT correspondence of dynamical phenomena.

Basic idea to take the negative cosmological constant into account is to introduce the Poincaré coordinate and subtract its warp factor from the metric to be solved. In Sec. 2, we discuss the warp factor extraction first, and then apply the $(\mathcal{D}-1)+1$ decomposition to the Einstein equations to obtain equations in the ADM formalism in the next section. We also discuss the junction condition and its projection components, which is important when we apply this technique to the dynamical gravity in the braneworld models. These junction conditions give boundary conditions for the dynamical variables as well as the gauge variables. We find that the warp factor subtraction from the original equations are accomplished by adding some terms which comes from the conformal transformation to get rid of the warp factor. In Sec. 3, we summarize this proceedings.

[1]Email address: tanahashi@tap.scphys.kyoto-u.ac.jp
[2]Email address: saijo@rikkyo.ac.jp
[3]Email address: mshibata@yukawa.kyoto-u.ac.jp
[4]Email address: tanaka@yukawa.kyoto-u.ac.jp

2 Warp factor extraction from the Einstein equations

In this section, we discuss the warp factor extraction from the metric for the spacetime with non-zero cosmological constant. We especially focus on the asymptotically AdS spacetime, which is the bulk spacetime of the RS-II model.

Poincaré coordinates of $\mathrm{AdS}_{\mathcal{D}}$ spacetime, which is sometimes called as Fefferman-Graham coordinates or horospherical coordinates, are given by

$$ds^2 = \frac{l^2}{z^2}\left(\eta^{(\mathcal{D}-1)}_{\mu\nu}dx^\mu dx^\nu + dz^2\right) , \tag{1}$$

where $\eta^{(\mathcal{D}-1)}_{\mu\nu}$ is a flat metric in $(\mathcal{D}-1)$-dimensional spacetime. The conformal factor $(l/z)^2$ represents the spacetime curvature due to the negative cosmological constant. This form of the metric suggests us to decompose a general $\mathcal{D}$-dimensional metric as

$$ds^2 = \hat{g}_{\mu\nu}dx^\mu dx^\nu = \frac{l^2}{z^2}g_{\mu\nu}dx^\mu dx^\nu , \tag{2}$$

and to write down the Einstein equations. By this reduction, we can express the Einstein equations for the metric $\hat{g}_{\mu\nu}$ in terms of the metric $g_{\mu\nu}$, which reduces to a flat metric when the spacetime is a pure $\mathrm{AdS}_{\mathcal{D}}$ spacetime. Since the dynamical variable becomes simple by this reduction, we expect that this reduction will help to make the numerical calculations accurate. We also expect that this reduction will simplify the asymptotic boundary conditions at $x, z\tilde{\omega}\infty$ and the junction conditions at the brane.

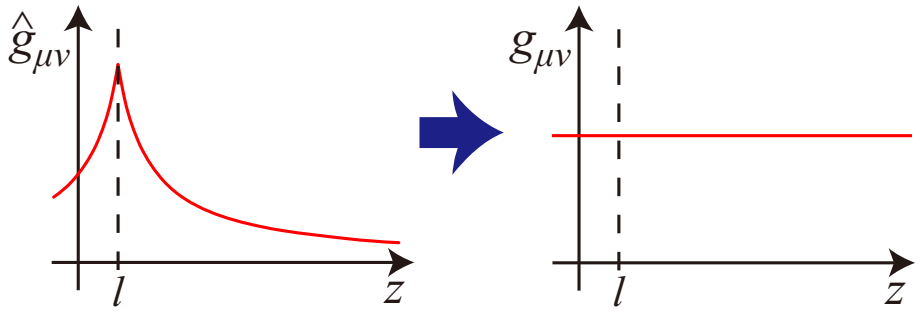

Figure 1: Schematic of the warp factor extraction. With a conformal transformation, we can reduce the background metric into a flat one. Adding to that, the conformally-transformed metric components $g_{\mu\nu}$ becomes smooth at the brane (at $z = l$ in the figure) though those before the transformation, $\hat{g}_{\mu\nu}$, were not. This smoothness will help the numerical computation.

Conformal transformation of Ricci tensor is given by

$$\hat{R}_{\mu\nu} = R_{\mu\nu} + \nabla_\rho C^\rho{}_{\mu\nu} - \nabla_\mu C^\rho{}_{\rho\nu} + C^\rho{}_{\mu\nu}C^\lambda{}_{\lambda\rho} - C^\rho{}_{\mu\lambda}C^\lambda{}_{\rho\nu} , \tag{3}$$

where $\hat{R}_{\mu\nu}$ and $R_{\mu\nu}$ are Ricci tensors for $\hat{g}_{\mu\nu}$ and $g_{\mu\nu}$, respectively. ∇ is covariant derivative with respect to $g_{\mu\nu}$. $C^\rho{}_{\mu\nu}$ is defined as

$$C^\rho{}_{\mu\nu} \equiv \frac{1}{2}\hat{g}^{\rho\lambda}\left(\nabla_\mu\hat{g}_{\lambda\nu} + \nabla_\nu\hat{g}_{\lambda\mu} - \nabla_\lambda\hat{g}_{\mu\nu}\right) = \delta^\rho{}_\mu v_\nu + \delta^\rho{}_\nu v_\mu - g_{\mu\nu}v^\rho , \tag{4}$$

and

$$v_\mu \equiv \nabla_\mu \log(l/z) = -\frac{\delta^z{}_\mu}{z} . \tag{5}$$

Note that the index of v^ρ in the last term of Eq. (4) is raised by $g^{\mu\nu}$, not by $\hat{g}^{\mu\nu}$. By contracting Eq. (4), we obtain $C^\rho{}_{\rho\mu} = \mathcal{D}v_\mu$. Using Eq. (4), we can express $\hat{R}_{\mu\nu}$ in terms of $R_{\mu\nu}$ and v_μ as

$$\hat{R}_{\mu\nu} = R_{\mu\nu} + (D-2)\left(v_\mu v_\nu - \nabla_\mu v_\nu - v^\rho v_\rho g_{\mu\nu}\right) - \left(\nabla_\rho v^\rho\right)g_{\mu\nu} , \tag{6}$$

and the Einstein tensor $\hat{G}_{\mu\nu}$ made from $\hat{g}_{\mu\nu}$ with negative cosmological constant is expressed in terms of $g_{\mu\nu}$ as

$$\hat{G}_{\mu\nu} - \frac{(D-1)(D-2)}{2\ell^2}\tilde{g}_{\mu\nu} = G_{\mu\nu} - \frac{(D-1)(D-2)}{2z^2}g_{\mu\nu} + (D-2)\left\{(v_\mu v_\nu - \nabla_\mu v_\nu) + \left(\nabla_\rho v^\rho + \frac{D-3}{2}v_\rho v^\rho\right)g_{\mu\nu}\right\} . \quad (7)$$

Thus, we can effectively get rid of the conformal factor l^2/z^2 from the "physical" metric $\hat{g}_{\mu\nu}$ by adding some terms made of v_μ to $G_{\mu\nu}$.

The procedure to obtain the equations used in the numerical relativity code is as follows.

1. Apply $(\mathcal{D}-1)+1$ decomposition to the Einstein equations (7).
2. Conformally decompose the spatial metric and the extrinsic curvature as $\gamma_{ij} = \chi^{-1}\tilde{\gamma}_{ij}$ and $K_{ij} = \chi\tilde{A}_{ij} + \chi^{-1}K\tilde{\gamma}_{ij}/(\mathcal{D}-1)$, respectively.
3. Introduce an auxiliary variable $\tilde{\Gamma}^i \equiv -\tilde{\gamma}^{ik}{}_{,k}$.

As a result of this procedure, we obtain the equations of motions in the BSSN formalism [4, 5] as

$$\left(\partial_t - \beta^k\partial_k\right)\chi = \frac{2\chi}{\mathcal{D}-1}\left(\alpha K - \partial_k\beta^k\right) , \quad (8)$$

$$\left(\partial_t - \beta^k\partial_k\right)\tilde{\gamma}_{ij} = -2\alpha\tilde{A}_{ij} + \tilde{\gamma}_{ik}\partial_j\beta^k + \tilde{\gamma}_{jk}\partial_i\beta^k - \frac{2}{\mathcal{D}-1}\tilde{\gamma}_{ij}\partial_k\beta^k , \quad (9)$$

$$\left(\partial_t - \beta^k\partial_k\right)\tilde{A}_{ij} = \chi\left\{-\left(D_kD^k\alpha\right)^{\mathrm{TF}} + \alpha\left(\overset{(\gamma)}{R}{}^{\mathrm{TF}}_{ij} - 8\pi S^{\mathrm{TF}}_{ij}\right)\right\} + \alpha\left(K\tilde{A}_{ij} - 2\tilde{A}_{ik}\tilde{A}^k{}_j\right) - \frac{2}{\mathcal{D}-1}\left(\partial_k\beta^k\right)\tilde{A}_{ij} + \tilde{A}_{ik}\partial_j\beta^k + \tilde{A}_{jk}\partial_i\beta^k \underbrace{-\frac{\mathcal{D}-2}{2}\alpha\chi\left(\overset{(\gamma)}{\Gamma}{}^z_{ij}\right)^{\mathrm{TF}}}_{*} , \quad (10)$$

$$\left(\partial_t - \beta^k\partial_k\right)K = -D_iD^i\alpha + \alpha\left[\tilde{A}_{ij}\tilde{A}^{ij} + \frac{K^2}{\mathcal{D}-1} + \frac{8\pi G_{\mathcal{D}}}{\mathcal{D}-2}\left\{S + (\mathcal{D}-3)\rho\right\}\right] \underbrace{+\frac{\mathcal{D}-1}{z}\left\{\left(\partial_t - \beta^k\partial_k\right)\left(\frac{\beta^z}{\alpha}\right) + \chi\tilde{\gamma}^{zi}\alpha_{,i}\right\} + \frac{\mathcal{D}-3}{z}K\beta^z}_{*} \underbrace{+\alpha\left[\frac{\mathcal{D}-1}{z^2}\left(1-g^{zz}\right) - \frac{\mathcal{D}-3}{2z}\tilde{\gamma}^{zi}\chi_{,i} - \frac{1}{z}\tilde{\Gamma}^z\right]}_{*} , \quad (11)$$

$$\left(\partial_t - \beta^k\partial_k\right)\tilde{\Gamma}^i = -2\tilde{A}^{ij}\partial_j\alpha + \frac{\mathcal{D}-3}{\mathcal{D}-1}\tilde{\gamma}^{ij}\partial_j\partial_k\beta^k + \frac{2}{\mathcal{D}-1}\tilde{\Gamma}^i\partial_j\beta^j - \tilde{\Gamma}^j\partial_j\beta^i + \tilde{\gamma}^{jk}\partial_j\partial_k\beta^i + 2\alpha\left(\overset{(\tilde{\gamma})}{\Gamma}{}^i_{jk}\tilde{A}^{jk} - \frac{\mathcal{D}-2}{\mathcal{D}-1}\tilde{\gamma}^{ij}\partial_jK - \frac{\mathcal{D}-1}{2}\tilde{A}^{ij}\partial_j\log\chi - 8\pi G_{\mathcal{D}}\tilde{\gamma}^{ij}j_j\right) \underbrace{+\frac{2(\mathcal{D}-2)\alpha}{z}\left\{\tilde{\gamma}^{ij}\partial_j\left(\frac{\beta^z}{\alpha}\right) - \tilde{A}^{zi} - \frac{K}{\mathcal{D}-1}\tilde{\gamma}^{zi}\right\}}_{*} , \quad (12)$$

and the constraints as

$$16\pi G_{\mathcal{D}}\rho = \overset{(\gamma)}{R} + \frac{\mathcal{D}-2}{\mathcal{D}-1}K^2 - \tilde{A}_{ij}\tilde{A}^{ij} , \underbrace{+\frac{(\mathcal{D}-1)(\mathcal{D}-2)}{z^2}\left\{1 - \chi\tilde{\gamma}^{zz} + \left(\frac{\beta^z}{\alpha}\right)^2\right\} - \frac{2(\mathcal{D}-2)}{2}\left(\frac{\mathcal{D}-3}{2}\tilde{\gamma}^{zi}\chi_{,i} + \chi\tilde{\Gamma}^z + \frac{\beta^zK}{\alpha}\right)}_{*} , \quad (13)$$

$$8\pi G_{\mathcal{D}}\tilde{\gamma}^{ji}j_i = \partial_i\tilde{A}^{ij} + \overset{(\tilde{\gamma})}{\Gamma}{}^{j}_{ik}\tilde{A}^{ik} - \frac{\mathcal{D}-2}{\mathcal{D}-1}\tilde{\gamma}^{ji}\partial_i K - \frac{\mathcal{D}-1}{2}\tilde{A}^{ji}\partial_i \log\chi \\ \underbrace{+\frac{\mathcal{D}-2}{z}\left\{\tilde{\gamma}^{ji}\partial_i\left(\frac{\beta^z}{\alpha}\right) - \tilde{A}^{zi} - \frac{K}{\mathcal{D}-1}\tilde{\gamma}^{iz}\right\}}_{*} , \tag{14}$$

$$\tilde{\gamma} = 1 , \tag{15}$$

$$\tilde{\gamma}^{ij}\tilde{A}_{ij} = 0 , \tag{16}$$

$$\tilde{\Gamma}^i + \partial_j\tilde{\gamma}^{ji} = 0 . \tag{17}$$

The terms with an asterisk under them ($\underbrace{\cdots\cdots}_{*}$) are the terms added to the original equations. The equations of motions can be solved if we supply good gauge conditions.

The boundary conditions at the positive tension brane in the RS-II model is given by the junction conditions, which is given by

$$\hat{\mathring{K}}_{\mu\nu} = \frac{1}{l}\hat{\mathring{\gamma}}_{\mu\nu} , \tag{18}$$

if the are no additional matter on the brane. $\mathring{\gamma}_{\mu\nu}$ and $\hat{\mathring{K}}_{\mu\nu} \equiv -\hat{\mathring{\gamma}}^{\rho}{}_{\mu}\mathring{\gamma}^{\lambda}{}_{\lambda}\hat{\nabla}_{\rho}\hat{\mathring{s}}_{\lambda}$, where $\hat{\mathring{s}}_{\mu}$ is the unit normal of the brane, are the induced metric and extrinsic curvature of the brane. By extracting the warp factor as $\hat{\mathring{s}}_{\mu} = (z/l)^{-1}\mathring{s}_{\mu}$, we obtain a reduced junction conditions as

$$\mathring{K}_{\mu\nu} = \frac{1-\sqrt{g^{zz}}}{z}\mathring{\gamma}_{\mu\nu} . \tag{19}$$

Since the extrinsic curvature $\mathring{K}_{\mu\nu}$ is equal to $-(1/2)\pounds_{\mathring{s}}\mathring{\gamma}_{\mu\nu} \sim -(1/2)\partial_z\mathring{\gamma}_{\mu\nu}$, this reduced junction conditions is almost given by a Neumann boundary conditions for $\mathring{\gamma}_{\mu\nu}$, which is simple to implement numerically, if g^{zz} is sufficiently close to the unity.

3 Summary

In this proceedings, we showed how to modify the numerical scheme for higher-dimensional asymptotically flat spacetime into that for asymptotically AdS spacetime. We also showed that the boundary conditions at the brane in the RS-II model, which are the junction conditions of the metric at the brane, are reduced to those similar to the Neumann boundary conditions if the metric is sufficiently close to that of the background metric.

The remaining tasks to accomplish a dynamical simulation of strong gravity in asymptotically AdS spacetime is to find a good gauge conditions, to develop the numerical code and to test it in various ways. We would like to establish this simulation method and tackle various problems related to the AdS/CFT correspondence with this technique in the future.

References

[1] H. Yoshino and M. Shibata, Phys. Rev. D **80**, 084025 (2009).

[2] S. S. Gubser, Phys. Rev. D **63**, 084017 (2001).

[3] T. Tanaka, Prog. Theor. Phys. Suppl. **148**, 307 (2003).

[4] T. Nakamura, K. Oohara and Y. Kojima, Prog. Theor. Phys. Suppl. **90**, 1 (1987).

[5] M. Shibata and T. Nakamura, Phys. Rev. D **52**, 5428 (1995).

Robustness of singularity avoidance in loop quantum cosmology

Tomo Tanaka[1(a)], Masahiro Shimano[2(b)], Fumitoshi Amemiya[3(c)] and Tomohiro Harada[4(b)]

[(a)] *Department of Physics, Waseda University, Okubo, Tokyo 169-8555, Japan*
[(b)] *Department of Physics, Rikkyo University, Toshima, Tokyo 171-8501, Japan*
[(c)] *Department of Physics, Keio University, Hiyoshi, Kohoku-ku, Yokohama 223-8522, Japan*

Abstract

We study the flat Friedmann-Robertson-Walker universe with the cosmological constant in the context of loop quantum cosmology. If one considers the original scheme used in Ref. [1], no continuum limit problem arises in the model. We show that the problem is resolved by using the improved scheme introduced in Ref. [2]. It is also shown that the initial singularity is avoided in the improved scheme only when an appropriate operator ordering of the Hamiltonian constraint is chosen.

1 Introduction

Loop quantum cosmology (LQC) [3] is a minisuperspace model quantized by using the methods of loop quantum gravity (LQG) [4, 5]. In LQC, the quantized Hamiltonian constraint equation is written as a difference equation, not the usual Wheeler-DeWitt differential equation. It has been argued that, within the model, the initial singularity is absent in the following two senses. First, there is no curvature singularity because the spectrum of the inverse scale factor operator is bounded from below. Second, the wave function of the Universe can be uniquely determined through the initial singularity from the difference equation [1].

In this paper, we shall study the flat Friedmann-Robertson-Walker (FRW) universe with the cosmological constant in the context of LQC. It is shown that with the model one cannot take the continuum limit of the difference equation in the original scheme used in Ref. [1]. The problem is resolved by using the improved scheme introduced in Ref. [2]. We also discuss the singularity avoidance in the improved scheme. The initial singularity is absent only when an appropriate operator ordering of the Hamiltonian constraint is chosen.

2 Loop quantum cosmology

The Hamiltonian formulation used in LQG is constructed with a SU(2) connection A_a^i where a is a spatial index and i is the Lie algebra index with $a, i = 1, 2, 3$. The conjugate momentum is a densitized triad E_i^a. To quantize the system, the elementary variables are chosen as the holonomies h_e defined by the connection A_a^i along edges e, and the fluxes given by integrating the densitized triad E_i^a over 2-surfaces.

Here we consider the flat FRW spacetime described by the metric

$$ds^2 = -dt^2 + a(t)^2 \left(dx^2 + dy^2 + dz^2\right), \tag{1}$$

where a is the scale factor. There, the gravitational Hamiltonian constraint is written as [6]

$$C_{\rm grav} = \frac{1}{16\pi G\gamma^2} \int_\nu d^3x N \left(\frac{-1}{\sqrt{|\det E_i^a|}} \epsilon_{ijk} F_{ab}^i E^{aj} E^{bk} + 2\gamma^2 \sqrt{|\det E_i^a|}\Lambda \right), \tag{2}$$

where Λ is the cosmological constant, γ is the Barbero-Immirzi parameter, N is the lapse function, G is the gravitational constant, ν denotes an elementary cell introduced to remove the divergence of 3-space

[1]Email address: tomo@gravity.phys.waseda.ac.jp
[2]Email address: shimano@rikkyo.ac.jp
[3]Email address: famemiya@rk.phys.keio.ac.jp
[4]Email address: harada@rikkyo.ac.jp

integral, and F^i_{ab} is the curvature of the connection given by $F^i_{ab} = \partial_a A^i_b - \partial_b A^i_a + \epsilon^i_{jk} A^j_a A^k_b$. In the elementary cell $\mathcal{V}$, one can define a fiducial flat metric ${}^0q_{ab}$, an associated constant orthonormal triad ${}^0e^a_i$ and cotriad ${}^0\omega^i_a$. In the flat FRW case, the variables A^i_a and E^a_i are written as

$$A^i_a = cV_0^{-(1/3)}{}^0\omega^i_a, \quad E^a_i = pV_0^{-(2/3)}\sqrt{{}^0q}\,{}^0e^a_i, \tag{3}$$

where $c = \gamma da/dt$, $|p| = a^2$ and V_0 denotes the volume of the elementary cell $\mathcal{V}$. Now, the holonomy $h^{(\lambda)}_i$ along a line segment $\lambda^0 e^a_i$ is given by

$$h^{(\lambda)}_i = \cos(\lambda c/2)\,\mathbb{1} + 2\sin(\lambda c/2)\,\tau_i, \tag{4}$$

where λ is an arbitrary real number, $\mathbb{1}$ is the identity 2×2 matrix and τ_i is a basis of the Lie algebra SU(2). With these variables, the Hamiltonian constraint (2) is written as

$$C_{\rm grav} = \lim_{\rm Area\to 0}\left[-\frac{4{\rm sgn}(p)}{8\pi\lambda^3 G\gamma}\sum_{ijk}\epsilon^{ijk}{\rm Tr}\left[h^{(\lambda)}_i h^{(\lambda)}_j \left(h^{(\lambda)}_i\right)^{-1}\left(h^{(\lambda)}_j\right)^{-1} h^{(\lambda)}_k \left\{\left(h^{(\lambda)}_k\right)^{-1}, V\right\}\right] + 2\gamma^2 V\Lambda\right]. \tag{5}$$

Following the procedure from LQG the kinematical Hilbert space is defined as $\mathcal{H}^{\rm grav}_{\rm kin} = L^2(\mathbb{R}_{\rm Bohr}, {\rm d}\mu_{\rm Bohr})$, where $\mathbb{R}_{\rm Bohr}$ is the Bohr compactification of the real line. An orthonormal basis for the kinematical Hilbert space is written as $|\mu\rangle$ which satisfies the orthonormality relations $\langle\mu_1|\mu_2\rangle = \delta_{\mu_1,\mu_2}$. The action of the triad operator $\hat{p}$ on the state $|\mu\rangle$ is given by

$$\hat{p}|\mu\rangle = \frac{8\pi\gamma l^2_{Pl}}{6}\mu|\mu\rangle. \tag{6}$$

Thus, the eigenvalues of $\hat{p}$ are labelled by the dimensionless parameter μ. The states $|\mu\rangle$ are also eigenstates on the volume operator: $\hat{V}|\mu\rangle = \widehat{|p|^{3/2}}|\mu\rangle = \left(\frac{8\pi\gamma l^2_{Pl}}{6}|\mu|\right)^{3/2}|\mu\rangle =: V_\mu|\mu\rangle$. Since the operator $\widehat{\exp i\lambda(c/2)}$ acts on $|\mu\rangle$ as $\widehat{\exp i\lambda(c/2)}|\mu\rangle = |\mu+\lambda\rangle$, the holonomy operator has the action

$$\widehat{h^{(\lambda)}_k}|\mu\rangle = \frac{1}{2}(|\mu+\lambda\rangle + |\mu-\lambda\rangle)\mathbb{1} + 1/i(|\mu+\lambda\rangle - |\mu-\lambda\rangle)\tau_k. \tag{7}$$

3 Pre-improved scheme

In the pre-improved scheme, λ is chosen as a constant value. We here choose the operator ordering of the Hamiltonian constraint (5) as

$$\hat{C}_{\rm grav} = \frac{96i\,({\rm sgn}(p))}{8\pi\gamma l^2_{\rm Pl}}\cdot\widehat{\sin}^2\frac{c\lambda}{2}\widehat{\cos}^2\frac{c\lambda}{2}\cdot\left[\widehat{\sin}\frac{c\lambda}{2}\hat{V}\widehat{\cos}\frac{c\lambda}{2} - \widehat{\cos}\frac{c\lambda}{2}\hat{V}\widehat{\sin}\frac{c\lambda}{2}\right] + 2\gamma^2\hat{V}\Lambda. \tag{8}$$

Then the action of the operator on states $\Psi(\mu) = \langle\mu|\Psi\rangle$ leads the difference equation

$$\frac{3}{8\pi\gamma l^2_{\rm Pl}}\Big[(V_{\mu+5\lambda} - V_{\mu+3\lambda})\,\Psi(\mu+4\lambda) - \left\{2\,(V_{\mu+\lambda} - V_{\mu-\lambda}) - \frac{16\pi\gamma^3 l^2_{\rm Pl}}{3}\Lambda V_\mu\right\}\Psi(\mu) + (V_{\mu-3\lambda} - V_{\mu-5\lambda})\,\Psi(\mu-4\lambda)\Big] = 0. \tag{9}$$

If we interpret the triad coefficient p as an internal time, we can regard the difference equation (9) as evolution equation with discrete time. The equation can be uniquely continued through the classical singularity $\mu = 0$. In this sense, it is said that the initial singularity is avoided in the model.

However, in the pre-improved scheme, there is a problem when one considers the model with the cosmological constant. The problem is that, for large μ, one cannot take the continuum limit of the difference equation because the values of the wave function oscillates and its amplitude grows intensively. We refer this problem as the "continuum limit problem".

4 Resolution of continuum limit problem in improved scheme

In this section, we show that the continuum limit problem is resolved by using the improved scheme. The origin of the problem is that the length of holonomies λ is chosen as a constant in the pre-improved scheme. In the improved scheme, one takes λ as a function of p such that $\lambda = \bar{\mu}(p) = (2\sqrt{3}\pi\gamma)^{\frac{1}{2}} l_{\rm Pl} |p|^{-\frac{1}{2}}$. Then the Hamiltonian constraint operator is written as

$$\hat{C}_{\rm grav} = \frac{96i(\mathrm{sgn}p)}{8\pi\gamma l_{\rm Pl}^2} \cdot \widehat{\sin}^2 \frac{c\bar{\mu}}{2} \widehat{\cos}^2 \frac{c\bar{\mu}}{2} \cdot \widehat{\frac{1}{\bar{\mu}^3}} \cdot \left[\widehat{\sin}\left(\frac{\bar{\mu}c}{2}\right) \hat{V} \widehat{\cos}\left(\frac{\bar{\mu}c}{2}\right) - \widehat{\cos}\left(\frac{\bar{\mu}c}{2}\right) \hat{V} \widehat{\sin}\left(\frac{\bar{\mu}c}{2}\right) \right] + 2\gamma^2 \hat{V}\Lambda. \quad (10)$$

It should be noted that in this scheme inverse cube of the holonomy length $1/\bar{\mu}^3$ becomes quantum operator. In this case, it is convenient to use a new label v instead of μ, which is given by $v = K\mathrm{sgn}(\mu)|\mu|^{\frac{3}{2}}$, where $K = 2\sqrt{2}/(3\sqrt{3\sqrt{3}})$. In the v-representation, the action of $\widehat{\exp i(\bar{\mu}c/2)}$ is simple: $\widehat{\exp (i\bar{\mu}c/2)}|v\rangle = |v+1\rangle$, and eigenvalues of the volume operator is given by $\hat{V}|v\rangle =: V_v|v\rangle$. Moreover, we can rewrite $\widehat{1/\bar{\mu}^3}$ in terms of $\hat{V}$ because $\bar{\mu}^2 p = (2\sqrt{3}\pi\gamma) l_{\rm Pl}^2$. Therefore, we obtain the action of the operator (10) on the states $\Psi(v) = \langle v|\Psi\rangle$ as

$$\begin{aligned} &\frac{27K}{16}\sqrt{\frac{8\pi}{6}}\gamma^{1/2} l_{\rm Pl} \big[|v+4|\,||v+3| - |v+5||\,\Psi(v+4) \\ &-\{2|v|\,||v-1| - |v+1|| - \frac{128\pi}{81}\gamma^3 \frac{l_{\rm Pl}^2}{K^2}\Lambda|v|\}\Psi(v) + |v-4|\,||v-5| - |v-3||\,\Psi(v-4)\big] = 0. \end{aligned} \quad (11)$$

In this scheme, for large v, the amplitude of the wave function does not grows intensively, so that we can take the continuum limit of Eq. (11). As a consequence, there is no continuum limit problem in the improved scheme.

5 Singularity avoidance in improved scheme

We here discuss the singularity avoidance in the improved scheme. Although we have not considered the operator ordering of the Hamiltonian constraint operator (10) in Sec. 4, there are actually four types of possible operator orderings in the improved scheme:

Type (a)

$$\hat{C}^{(a)}_{\rm grav} = \frac{96i(\mathrm{sgn}p)}{8\pi\gamma l_{\rm Pl}^2} \cdot \widehat{\sin}^2 \frac{c\bar{\mu}}{2} \widehat{\cos}^2 \frac{c\bar{\mu}}{2} \cdot \widehat{\frac{1}{\bar{\mu}^3}} \cdot \left[\widehat{\sin}\left(\frac{\bar{\mu}c}{2}\right) \hat{V} \widehat{\cos}\left(\frac{\bar{\mu}c}{2}\right) - \widehat{\cos}\left(\frac{\bar{\mu}c}{2}\right) \hat{V} \widehat{\sin}\left(\frac{\bar{\mu}c}{2}\right) \right], \quad (12)$$

Type (b)

$$\hat{C}^{(b)}_{\rm grav} = \frac{96i(\mathrm{sgn}p)}{8\pi\gamma l_{\rm Pl}^2} \cdot \widehat{\frac{1}{\bar{\mu}^3}} \cdot \widehat{\sin}^2 \frac{c\bar{\mu}}{2} \widehat{\cos}^2 \frac{c\bar{\mu}}{2} \cdot \left[\widehat{\sin}\left(\frac{\bar{\mu}c}{2}\right) \hat{V} \widehat{\cos}\left(\frac{\bar{\mu}c}{2}\right) - \widehat{\cos}\left(\frac{\bar{\mu}c}{2}\right) \hat{V} \widehat{\sin}\left(\frac{\bar{\mu}c}{2}\right) \right], \quad (13)$$

Type (c)

$$\hat{C}^{(c)}_{\rm grav} = \frac{96i(\mathrm{sgn}p)}{8\pi\gamma l_{\rm Pl}^2} \cdot \left[\widehat{\sin}\left(\frac{\bar{\mu}c}{2}\right) \hat{V} \widehat{\cos}\left(\frac{\bar{\mu}c}{2}\right) - \widehat{\cos}\left(\frac{\bar{\mu}c}{2}\right) \hat{V} \widehat{\sin}\left(\frac{\bar{\mu}c}{2}\right) \right] \cdot \widehat{\frac{1}{\bar{\mu}^3}} \cdot \widehat{\sin}^2 \frac{c\bar{\mu}}{2} \widehat{\cos}^2 \frac{c\bar{\mu}}{2}, \quad (14)$$

Type (d)

$$\hat{C}^{(d)}_{\rm grav} = \frac{96i(\mathrm{sgn}p)}{8\pi\gamma l_{\rm Pl}^2} \cdot \left[\widehat{\sin}\left(\frac{\bar{\mu}c}{2}\right) \hat{V} \widehat{\cos}\left(\frac{\bar{\mu}c}{2}\right) - \left(\frac{\bar{\mu}c}{2}\right) \hat{V} \widehat{\sin}\left(\frac{\bar{\mu}c}{2}\right) \right] \cdot \widehat{\sin}^2 \frac{c\bar{\mu}}{2} \widehat{\cos}^2 \frac{c\bar{\mu}}{2} \cdot \widehat{\frac{1}{\bar{\mu}^3}}. \quad (15)$$

Whether the initial singularity is absent or not depends on the choice of the operator orderings. It can be shown that the initial singularity is avoided only when one chooses the type (a).

6 Conclusion

In this paper, we have investigated the flat FRW universe with the cosmological constant in the context of LQC. We have pointed out that, whithin the model, the continuum limit problem arises in the pre-improved scheme, and the problem is resolved in the improved scheme. We have also shown that the initial singularity is absent in the improved scheme only when the operator ordering of the Hamiltonian constraint is chosen as the type (a) discussed in Sec.5.

Acknowledgement

MS is supported by Rikkyo University Special Fund for Research, and TH was partly supported by the Grant-in-Aid for Scientific Research Fund of the Ministry of Education, Culture, Sports, Science and Technology, Japan [Young Scientists (B) 18740144 and 21740190].

References

[1] M. Bojowald, Phys. Rev. Lett. **86**, 5227 (2001).

[2] A. Ashtekar, T. Pawlowski, and P. Singh, Phys. Rev. D **74**, 084003 (2006).

[3] M. Bojowald, Living Rev. Relativity **8**, 11 (2005).

[4] C. Rovelli, *Quantum Gravity*, (Cambridge University Press, Cambridge, 2004).

[5] T. Thiemann, *Modern Canonical Quantum General Relativity*, (Cambridge University Press, Cambridge, 2007).

[6] E. Bentivegna, and T. Pawlowski, Phys. Rev. D **77**, 124025 (2008).

Magnitude redshift relation in the Brans-Dicke model constrained from Big-Bang Nucleosynthesis

E.P.B.A.Thushari[1(a)] , R.Nakamura[2(a)] M.Hashimoto[3(a)] K.Arai[4(b)]

[(a)] *Department of Physics, Kyushu University, Fukuoka, Japan*
[(b)] *Department of Physics, Kumamoto University, Kumamoto, Japan*

Abstract

The magnitude redshift relation $(m-z)$ in the Brans-Dicke theory with both a variable and constant cosmological term is investigated. Observations of Type Ia Supernovae (SNIa) are used, in the redshift range of $0.01 < z < 2$. The contribution of the matter and a variable cosmological term (Λ) is examined. As the next approach BDΛ model with a constant cosmological term has been investigated. Later Big Bang Nucleosynthesis has been used to constrain the parameters in BDΛ model for coupling constant $\omega = 10^4$.

Keywords : nucleosynthesis, accelerating universe

1 Introduction

To explain some puzzles in cosmology, new modified theories beyond the standard model are needed. To solve the cosmological constant problem, it can be imagined that the cosmological term decreases from large value at the early epoch to the present value.Therefore various functional forms have been suggested Refs. [1], [2]. Among them the Brans-Dicke(BD) theory is considered with a variable cosmological term Λ as a function of the scalar field Φ. This model has been investigated for the early universe of the Big Bang Nucleosynthesis Refs. [1],[2],[3]. However, an answer is needed to the question "How this model work at the present epoch?" . Therefore to investigate this model, the magnitude-redshift relation of SNIa observation is adopted. Cosmological models with a cosmological term are tightly constrained by the $m - z$ relation derived from SNIa observations. This is because, the cosmological term affects to the cosmic expansion rate of the universe significantly at the low redshifts. SNIa observations imply that the universe is accelerating around the present redshift times Refs. [4],[5], [6]. The magnitude-redshift relation in the Brans-Dicke theory with both a variable and constant cosmological terms for the flat universe are studied in this paper.

2 Brans-Dicke model with a variable cosmological term

The equations of motion in the $BD\Lambda$ model are written as follows Refs. [1]:

$$\left(\frac{\dot{a}}{a}\right)^2 = \frac{8\pi}{3\phi}\left(\rho_m + \rho_\gamma\right) - \frac{k}{a^2} + \frac{\Lambda}{3} + \frac{\omega}{6}\left(\frac{\dot{\phi}}{\phi}\right)^2 + \frac{\dot{a}}{a}\frac{\dot{\phi}}{\phi}, \tag{1}$$

$$\dot{\phi} = \frac{1}{a^3}\left[\frac{8\pi\mu}{2\omega+3}\left(\rho_{m_0} t + \int\left(\rho_e - 3p_e\right)dt\right) + B\right], \tag{2}$$

where $a(t)$, k, ρ, p and ω are the scale factor, the curvature constant, the energy density, the pressure and the coupling constant respectively.
where $\rho_\gamma = \rho_{rad} + \rho_\nu + \rho_{e^\pm}$ at $t \leq 1s$. Subscript m, rad, ν and $e^\pm$ are for matter, photon, nutrino

[1]Email address: berni@phys.kyushu-u.ac.jp
[2]Email address: riou@phys.kyushu-u.ac.jp
[3]Email address: hashimoto@phys.kyushu-u.ac.jp
[4]Email address: arai@sci.kumamoto-u.ac.jp

and electron-positron respectively. Here energy density of matter varies as $\rho_m = \rho_{m0}a^{-3}$. The energy density of radiation is written as $\rho_\gamma = \rho_{\gamma_0}a^{-4}$ except $e^{\pm}$ epoch. Subscript "0" means the values at the present epoch.
Evolution of the cosmological term (Λ) and the Gravitational term in the $BD\Lambda$ model describe as,

$$\Lambda = \frac{2\pi\left(\mu-1\right)}{\phi}\rho_{m_0}a^{-3}, G = \frac{1}{2}\left(3-\frac{2\omega+1}{2\omega+3}\mu\right)\frac{1}{\phi}. \tag{3}$$

where μ is a constant. Original Brans-Dicke theory is deduced for $\mu = 1$. To solve above equations numericaly, physical parameters are used as $\omega = 10^4$ Refs. [8], $G_0 = 6.6726 \times 10^{-8}\ dyn\ cm^2\ g^{-2}$, $H_0 = 71\ km\ s^{-1}\ Mpc^{-1}$ Refs. [9], $-1 \leq \mu \leq 2$ Refs. [3], [2] and $-10 \leq B^* \leq 10$ Refs. [3].

3 $m-z$ relation in the $BD\Lambda$ model

The apparent magnitude m of the source at the redshift z is,

$$m = 5\log_{10}\left(\frac{1+z}{10\text{pc}}r_l\right) + M, \tag{4}$$

where M is absolute magnitude and r_l is the radial distance in the units of parsecs (pc).

For the homogeneous isotropic universe, the relation between the radial distance and the redshift is derived from the Robertson-Walker metric as the followings,

$$\int_0^z \frac{dz}{H} = \begin{cases} k^{-1/2}\sin^{-1}\left(\sqrt{k}r_l\right) & k>0\text{,close universe} \\ r_l & k=0\text{,Flat universe} \\ \mid k \mid^{-1/2}\sinh^{-1}\left(\sqrt{\mid k \mid}r_l\right) & k<0\text{,Open Universe} \end{cases} \tag{5}$$

where $H = \dot{a}/a$ is the equation to describe the expansion of the universe for the modified BD theory is written from the equation(1) as,

$$H = \pm\left[\frac{1}{4}\left(\frac{\dot{\phi}}{\phi}\right)^2 - \left(1+z\right)^2 k - \frac{\Lambda}{3} - \frac{\omega}{6}\left(\frac{\dot{\phi}}{\phi}\right)^{\frac{1}{2}} - \frac{8\pi}{3}\frac{\rho}{\phi}\right]^{\frac{1}{2}} - \frac{1}{2}\frac{\dot{\phi}}{\phi}. \tag{6}$$

If the universe is flat ($k = 0$) at the present, $BD\Lambda$ model is written as,

$$H_0^2 = \frac{1}{3}\left(\frac{8\pi\rho_{m_0}}{\phi_0} + \Lambda_0\right) + \frac{\omega}{6}\left(\frac{\dot{\phi}}{\phi}\right)_0^2 - \left(\frac{\dot{\phi}}{\phi}H\right)_0. \tag{7}$$

Since Last two terms are small compared with the other two terms in the equation (7), energy densities are defined as, $\rho_{m_0} = 4\rho_c^{BD\Lambda}/\mu + 3$ and $\rho_c^{BD\Lambda} = 3\phi_0 H_0^2/8\pi$:
where $\rho_c^{BD\Lambda}$ is the critical density in the $BD\Lambda$ model.
Then the two energy density parameters are written as, $\Omega_{m_0} = \rho_{m_0}/\rho_c^{BD\Lambda}$ and $\Omega_{\Lambda_0} = (\mu-1)\rho_{m_0})/4\rho_{c^{BD\Lambda}}$.

Fig. 1 shows the $m-z$ relation in the $BD\Lambda$ model with SNIa observations. Matter is dominant in this model. Specially in the parameter region $0.7 < \mu < 2$, energy density of the cosmological term is always less than 30%. When we compare with the Friedmann model with the energy density parameters of $(\Omega_m, \Omega_\Lambda) = (1.0, 0.0)$, is merged with this $BD\Lambda$ model with $\chi^2 = 416$. This is inconsistent with present accelerating universe. Therefore as the next approach, $BD\Lambda$ model is modified by adding constant cosmological term Λ_{c_0}.

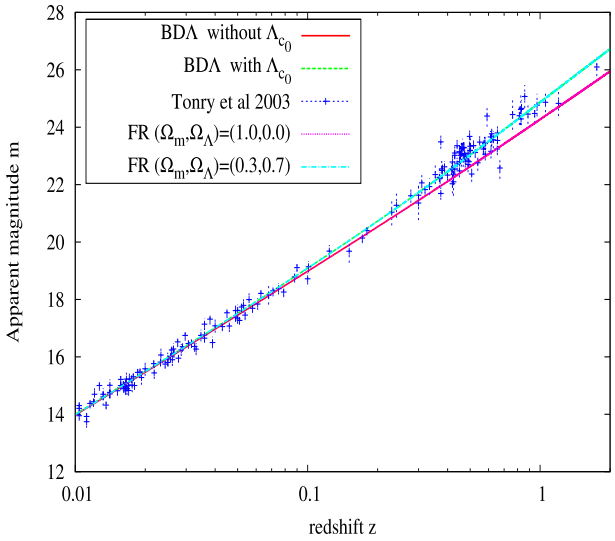

Figure 1: $m-z$ relation for the flat universe in the Friedmann model and $BD\Lambda$ model with and without constant cosmological term for $\mu = 0.7$ and $B^* = -10$, constrain from SNIa observations from Supernova Cosmology Project and High-z Supernovae search team Refs. [10]

4 $m-z$ relation in the $BD\Lambda$ model with a constant cosmological term Λ_{c_0}

Hubble parameter for $BD\Lambda$ model with constant cosmological term (Λ_{c_0}) is written as,

$$H = \left[\frac{1}{4}\left(\frac{\dot{\phi}}{\phi}\right)^2 - (1+z)^2 k - \frac{\Lambda}{3} + \frac{\Lambda_{c_0}}{3} - \frac{\omega}{6}\left(\frac{\dot{\phi}}{\phi}\right)^2 - \frac{8\pi}{3}\frac{\rho}{\phi}\right]^{\frac{1}{2}} - \frac{1}{2}\frac{\dot{\phi}}{\phi}. \tag{8}$$

Here energy density parameter of the constant cosmological term is fixed as 0.7. Fig. 1 shows that this model is consistent with SNIa observations. Total cosmological term is dominant in this model and consistent with present accelerating universe with $\chi^2 = 196$. For $B^* = 10$ and $\mu = 2$, $BD\Lambda$ model with Λ_{c_0} predicts $\Omega_\Lambda = 6.0 \times 10^{-2}$ and $\Omega_m = 0.24$. It is concluded that the $BD\Lambda$ model with Λ_{c_0} has the nearly same energy density parameters as the Friedmann model with $(\Omega_m, \Omega_\Lambda) = (0.3, 0.7)$.
All the parameters which is inherent in the $BD\Lambda$ model become independent as far as $m-z$ relation is concerned at the present epoch. Therefore as the next approach we investigate these parameters for the present values of ω using Big Bang Nucleosynthesis.

5 Parameter constrained from Big Bang Nucleosynthesis

The parameters inherent in the $BD\Lambda$ model have been investigated for $\omega = 500$ Refs. [3]. But these parameters become independent, as far as the $m-z$ relation at the present epoch is concerned. Therefore here we use the Big Bang Nucleosynthesis to investigate these parameter for $\omega = 10000$. We adopt the observed abundances of 4He, D/H and 7Li/H as follows: Yp $= 0.242 \pm 0.002$ Refs. [11], D/H $= (2.82 \pm 0.21)\ 10^{-6}$ Refs. [12], 7Li/H $= (2.19 \pm 0.28)\ \ 10^{-10}$ Refs. [13]. The abundance of 4He, D and 7Li are calculated by considering the value of η=(6.225±0.170) 10^{-10} Refs. [14].
(Fig. 2) shows that the 4He and D are consistent with the value of η for $\omega = 10^4$ in the range of $-0.9 \leq \mu \leq 0.9$ and $-3 \leq B^* \leq 4$.

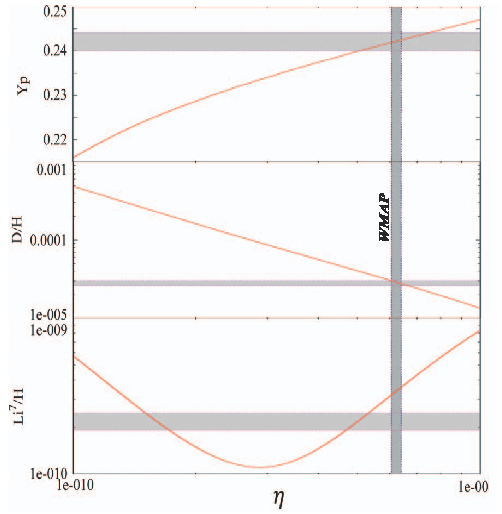

Figure 2: Light elementary abundances of 4He, D and 7Li vs η for $B^* = 1, \mu = 0.8, \omega = 10^4$

6 Concluding Remarks

The models whose parameters are inherent in the $BD\Lambda$ model become independent as far as the $m - z$ relation at the present epoch is concerned. Therefore we can not constrain these parameters around the present epoch using $m - z$ relation. Therefore we limit these parameters for $\omega = 10^4$ by BBN. BBN calculations with the observational abundances and the obtained value of the η from the WMAP restricted the parameters range as $-0.5 \leq \mu \leq 0.8$ and $-10 \leq B^* \leq 10$ Refs. [3] for $\omega = 500$. Comparing with our result, large value of ω is affected to decrease the parameter range of B^*. It is oppositely affected to the parameter μ. Since $BD\Lambda$ model is inconsistent with present accelerating universe, we have done a modification by adding a constant cosmological term. Therefore it is worthwhile to introduce more general functional form to the cosmological term.

References

[1] K. Arai, M. Hashimoto and D . Fukui Astron. Astrophys. **179**, 17 (1987).

[2] T. Etoh, M. Hashimoto, K. Arai and S. Fujimoto, Astron. Astrophys. **325**, 893 (1997).

[3] R. Nakamura, M. Hashimoto, S. Gamow and K. Arai, Astron. Astrophys. **448**, 23 (2006).

[4] S. Perlmutter et al [Supernovae Cosmology Project Collaboration], Astrophys. J. **517**, 565 (1999).

[5] A. G. Riess *et al.*,Astron. J **116**, 1009 (1998).

[6] A. G. Riess *et al.*, Astron. J **117**, 707 (1999).

[7] T. Endo and F. Fukui, Gen. Rel. Grav., 8, 833 (1977).

[8] B. Bertotti, L. Less and P. Tortora, Nature **425**, 374 (2003).

[9] D. N. Spergel *et al.*, Astrophys. J. suppl. **148**, 175 (2003).

[10] J. L. Tonry *et al.*, Astrophys. J. **594**, 38 (2003).

[11] I. Isotov and X. Thuan., Astrophys. J. **602**, 200 (2004).

[12] M. Pettini *et al.*, arXiv:0805.0594v3 [astro-ph] (2008).

[13] P. Bonifacio *et al.*, Astron. Astrophys. **390**, 91 (2002).

[14] J. Dunckley *et al.*, Astrophys. J. suppl. **180**, 306 (2009).

Constraint Propagation of C^2-adjusted Equations — Another Recipe for Robust Evolution Systems —

Takuya Tsuchiya[1(a)] , Gen Yoneda[(a)] and Hisa-aki Shinkai[(b)]

[(a)] *Department of Mathematical Sciences, Waseda University, Okubo, Shinjuku, Tokyo, 169-8555, Japan*
[(b)] *Faculty of Information Science and Technology, Osaka Institute of Technology, 1-79-1 Kitayama, Hirakata, Osaka 573-0196, Japan*

Abstract

We focus the formulation problem in numerical relativity, propose new sets of evolution equations, and demonstrate some numerical tests. The goal is to construct a robust evolution system against numerical instability during long-term numerical integration in strong gravitational field. One key idea is to adjust the evolution equations with constraint terms, as was systematically formulated by Yoneda and Shinkai. We here apply an adjusting method proposed by Fiske (2004) which uses the norm of constraints, C^2, and does not require the background metric for specifying effective Lagrange multipliers. We present sets of evolution equations both in ADM and BSSN formulations and show numerical tests using Gowdy wave propagation. Detail analyses are in progress, but we observe constraint damping effect as expected.

1 Introduction

In numerical relativity, it is essential to perform stable and accurate simulation. The standard way to integrate the Einstein equations is to split spacetime into three-dimensional space and time. Arnowitt-Deser-Misner (ADM) formulation[1] is the fundamental evolution system of spacetime decompositions. However, it is known that this formulation is not appropriate since the constraints are not satisfied during long-term numerical calculation and in strong gravitational field[2]. Several formulations which modified ADM formulation are suggested, Baumgarte-Shapiro-Shibata-Nakamura(BSSN) formulation[3] is widely used among them.

However, there exists more robust systems than the current standard BSSN system (e.g.[4, 5]) depending on problems. Therefore seeking a robust evolution system against the violation of constraints is still an important issue.

Yoneda and Shinkai[5] systematically investigated adjusted systems, which adds constraints to the evolution equations. With this method, we can predict the stability of numerical simulation by analyzing the eigenvalues of the coefficient matrix which is Fourier-transformed constraint propagation equations under assuming a fixed background metric.

Fiske[6] proposed an adjustment which uses the norm of constraints, C^2, and does not require the background metric for specifying effective Lagrange multipliers and applied this method to the Maxwell equations. A good point of his method is what the stability of the numerical simulation can be expected without depending on background metric. We apply his method to the ADM and BSSN formulations, and actually perform the effect of dumping by numerical simulation.

2 C^2-adjusted Systems

For variables u^i and constraint values C^i, evolution equations with constraint equations are generally written as

$$\partial_t u^i = f(u^i, \partial_j u^i, \cdots), \text{ and} \tag{1}$$

$$C^i(u^i, \partial_j u^i . \cdots) \approx 0. \tag{2}$$

[1]Email address: tsuchiya@akane.waseda.jp

Suppose we adjust (1) with $C^2 \equiv C^i C_i$, and evaluate constraint propagation as

$$\partial_t C^2 = \frac{\delta C^2}{\delta u^i}(\partial_t u^i). \tag{3}$$

There exists various combinations of this adjustment. Fiske[6] proposed an adjusted term as

$$\partial_t u^i = [\textbf{Original} \quad \textbf{Terms}] - \kappa^{ij}\frac{\delta C^2}{\delta u^j}, \tag{4}$$

with κ^{ij} of positive definite. The constraint propagation, then, becomes

$$\partial_t C^2 = [\textbf{Original} \quad \textbf{Terms}] - \kappa^{ij}\frac{\delta C^2}{\delta u^i}\frac{\delta C^2}{\delta u^j}, \tag{5}$$

which clearly shows the dumping of constraints. If we set κ^{ij} so that the second term becomes more dominant of (5) than first term in evolution, then C^2 dumps because of $\partial_t C^2 < 0$. Fiske presented an numerical example in the Maxwell system.

3 Applications to the Einstein equations

3.1 For ADM Formulation

Now we apply Fiske's method to the ADM formulation[1], which can be written as

$$\partial_t \gamma_{ij} = -2\alpha K_{ij} + \mathcal{L}_\beta(\gamma_{ij}) - \kappa_{\gamma ijmn}\frac{\delta (C^A)^2}{\delta \gamma_{mn}}, \tag{6}$$

$$\partial_t K_{ij} = \alpha({}^{(3)}R_{ij} + KK_{ij} - 2K_{i\ell}K^{\ell}{}_j) - D_i D_j \alpha + \mathcal{L}_\beta(K_{ij}) - \kappa_{Kijmn}\frac{\delta (C^A)^2}{\delta K_{mn}}, \tag{7}$$

where $(C^A)^2$ is the norm of the constraints,

$$(C^A)^2 \equiv (\mathcal{H}^A)^2 + (\mathcal{M}^A)^i(\mathcal{M}^A)_i, \tag{8}$$

and both of $\kappa_{\gamma ijmn}, \kappa_{Kijmn}$ are positive definite.

For the modified ADM equations, (6)-(7), we confirm this system has better stablility than the standard ADM system by the method proposed by Yoneda and Shinkai[5]. That is, assuming the background metric to Minkowski metric, and setting $\kappa_{\gamma ijmn} = \kappa_{Kijmn} = \delta_{im}\delta_{jn}$, we analyzed the eigenvalues of the constraint propagation matrix . We found that all the real parts of eigenvalues are negative. Therefore the system is expected to dump the violation of constraints.

3.2 For BSSN Formulation

For the BSSN formulation[3, 5], evolution equations with Fiske-type adjustment are:

$$\partial_t \varphi = [\textbf{Original} \quad \textbf{Terms}] - \lambda_\varphi \frac{\delta (C^B)^2}{\delta \varphi}, \tag{9}$$

$$\partial_t K = [\textbf{Original} \quad \textbf{Terms}] - \lambda_K \frac{\delta (C^B)^2}{\delta K}, \tag{10}$$

$$\partial_t \widetilde{\gamma}_{ij} = [\textbf{Original} \quad \textbf{Terms}] - \lambda_{\widetilde{\gamma} ijmn}\frac{\delta (C^B)^2}{\delta \widetilde{\gamma}_{mn}}, \tag{11}$$

$$\partial_t \widetilde{A}_{ij} = [\textbf{Original} \quad \textbf{Terms}] - \lambda_{\widetilde{A} ijmn}\frac{\delta (C^B)^2}{\delta \widetilde{A}_{mn}}, \tag{12}$$

$$\partial_t \widetilde{\Gamma}^i = [\textbf{Original} \quad \textbf{Terms}] - \lambda^{ij}_{\widetilde{\Gamma}}\frac{\delta (C^B)^2}{\delta \widetilde{\Gamma}^j}, \tag{13}$$

where

$$(C^B)^2 \equiv (\mathcal{H}^B)^2 + (\mathcal{M}^B)^i(\mathcal{M}^B)_i + \mathcal{A}^2 + \mathcal{G}^i\mathcal{G}_i + \mathcal{S}^2, \tag{14}$$
$$\mathcal{A} \equiv \widetilde{\gamma}^{ij}\widetilde{A}_{ij}, \quad \mathcal{G}^i \equiv \widetilde{\Gamma}^i - \widetilde{\Gamma}^i{}_{mn}\widetilde{\gamma}^{mn}, \quad \mathcal{S} \equiv -1 + \det(\widetilde{\gamma}_{ij}),$$

and all of $\lambda_\varphi, \lambda_K, \lambda_{\widetilde{\gamma}ijmn}, \lambda_{\widetilde{A}ijmn}$ and $\lambda^{ij}_{\widetilde{\Gamma}}$ are positive definite.

4 Numerical Examples

We demonstrate numerical simulations of above systems with polarized Gowdy wave:

$$ds^2 = t^{-1/2}\mathrm{e}^{\lambda/2}(-dt^2 + dx^2) + t(\mathrm{e}^P dy^2 + \mathrm{e}^{-P}dz^2). \tag{15}$$

which is one of the Apples-with-Apples tests [7], setting all of the numerical parameters to the same.

4.1 Adjusted ADM formulation

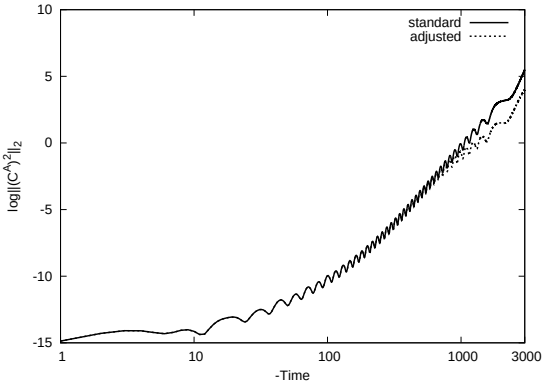

Figure 1: Polarized Gowdy-wave test with the adjusted ADM system. The vertical axis is $\log(||(C^A)^2||_2)$ and the horizontal axis is backward time. The dotted line is the one with (6)-(7) by setting $\kappa_{\gamma ijmn} = 1.0 \times 10^{-4.8}\alpha\gamma_{im}\gamma_{jn}$ and $\kappa_{Kijmn} = 1.0\times10^{-5.4}\alpha\gamma_{im}\gamma_{jn}$. The solid line is calculated with the standard ADM.

We see from Figure 1 that the adjusted ADM system, (6)-(7), has better stability than the standard ADM system. The norm $||(C^A)^2||_2$ of the adjusted ADM is 7.24×10^{-1} times of that of the standard ADM at time $t = -3000$.

4.2 Adjusted BSSN formulation

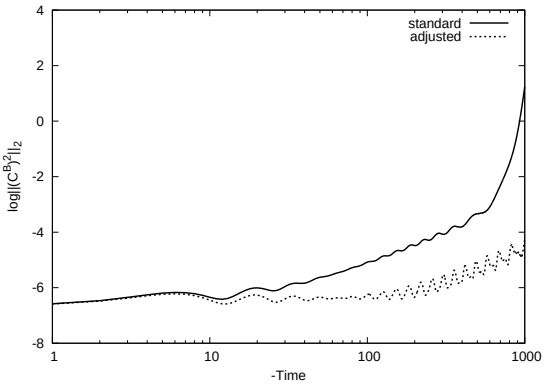

Figure 2: Polarized Gowdy-wave test with the adjusted BSSN system. The vertical axis is $\log(||(C^B)^2||_2)$ and the horizontal axis is backward time. The dotted line is with (9)-(13) by setting $\lambda_\varphi = 1.0 \times 10^{-2.9}\alpha$, $\lambda_K = 1.0 \times 10^{-3.3}\alpha$, $\lambda_{\widetilde{\gamma}ijmn} = 1.0 \times 10^{-3.7}\alpha\widetilde{\gamma}_{im}\widetilde{\gamma}_{jn}$, $\lambda_{\widetilde{A}ijmn} = 1.0 \times 10^{-4.4}\alpha\widetilde{\gamma}_{im}\widetilde{\gamma}_{jn}$, $\lambda^{ij}_{\widetilde{\Gamma}} = 1.0 \times 10^{-0.2}\alpha\widetilde{\gamma}^{ij}$. The solid line is calculated with the standard BSSN.

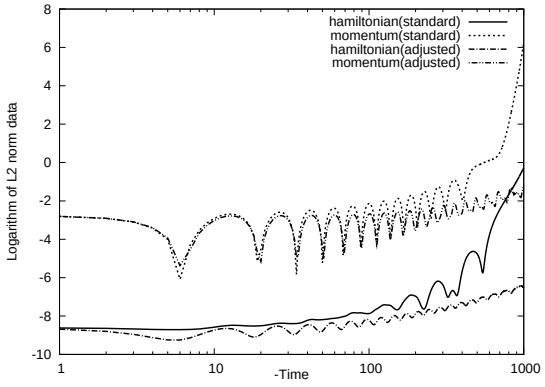

Figure 3: The same with Figure 2, but the result of $\log(||\mathcal{H}^B||_2)$ with the standard BSSN (solid line), $\log(||\mathcal{H}^B||_2)$ with the adjusted BSSN (dot-dashed line), $\log(||\mathcal{M}_i^B||_2)$ with the standard BSSN(dotted line), and $\log(||\mathcal{M}_i^B||_2)$ with the adjusted BSSN(two-dot-dashed line). The vertical axis is logarithm values of L2 norm of $\mathcal{H}^B, \mathcal{M}_i^B$ and the horizontal axis is backward time.

We see from Figure 2 that the adjusted BSSN system has better stability than the standard BSSN system. The norm $||(C^B)^2||_2$ of the adjusted BSSN is 3.95×10^{-3} times of that of the standard BSSN at time $t = -1000$. Kiuchi and Shinkai[4] performed the numerical simulation of polarlized Gowdy wave with other versions of adjusted BSSN systems[5]. We see that our result is better than theirs. Our result of $||\mathcal{H}^B||_2 \leq 2.5 \times 10^{-3}$ at $t = -1000$ but the result[4] of $||\mathcal{H}^B||_2 \geq 1.00 \times 10^{1}$ at $t = -1000$.

We think the stability of the adjusted BSSN formulation is explained by the dumping of $\mathcal{M}_i^B$ at the early time (about $t \leq -20$). As was argued by Kiuchi and Shinkai[4], the key of the stability of the evolution with BSSN system is to dump $\mathcal{M}_i^B$ earlier.

5 Summary

In this report, we applied the adjusting method suggested by Fiske to the ADM and BSSN formulations, and obtained the equations (6)-(7) and (9)-(13). We performed numerical tests with polarized Gowdy wave and showed that the adjusted ADM and BSSN systems have actually better stablility than the standard ADM and BSSN systems.

The advantage of the present systems to the previous adjusted systems [5, 8] is the way of specifying the Lagrange multipliers κ. In the present systems, κs are restricted as "positive definite" from the formulation independent on the background metric, while in the previous systems one needs to specify the signature of κs with eigenvalue analysis which depends on the background metric.

The detail numerical analysis on the range of effective parameters and the comparisons with other systems are underway.

References

[1] R. Arnowitt, S. Deser, and C. W. Misner, in *Gravitation: An Introduction to Current Research*, edited by L. Witten (Wiley, New York, 1962); J. W. York, Jr., in *Sources of Gravitational Radiation*, edited by L. Smarr (Cambridge, University Press, Cambridge, England, 1979); L. Smarr and J.W. York, Jr., Phys. Rev. D **17**, 2529 (1978).

[2] H. Shinkai and G. Yoneda, Class. Quantum. Grav. **17** 4799 (2000)

[3] M. Shibata and T. Nakamura, Phys. Rev. D **52** 5428 (1995); T. W. Baumgarte and S. L. Shapiro, Phys. Rev. D **59** 024007 (1998)

[4] K. Kiuchi and H. Shinkai, Phys. Rev. D **77** 044010 (2008)

[5] G. Yoneda and H. Shinkai, Phys. Rev. D **63** 124019 (2001); G. Yoneda and H. Shinkai, Phys. Rev. D **66** 124003 (2002)

[6] D. R. Fiske, Phys. Rev. D **69** 047501 (2004)

[7] M. Alcubierre *et al*, Class. Quantum. Grav. **21** 589 (2004)

[8] S. Detweiler, Phys. Rev. D **35** 1095 (1987)

Adiabatic regularization of primordial perturbations generated during inflation

Yuko Urakawa[1(a)] and Alexei A. Starobinsky [2(b),(c)]

[(a)] *Department of Physics, Waseda University, Ohkubo 3-4-1, Shinjuku, Tokyo 169-8555, Japan*
[(b)] *Landau Institute for Theoretical Physics, Moscow 119334, Russia*
[(c)] *Research Center for the Early Universe (RESCEU), Graduate School of Science, The University of Tokyo, Tokyo 113-0033, Japan*

Abstract

Recently, L. Parker *et al.* claimed that standard predictions of the slow-roll inflationary scenario of the early Universe regarding primordial spectra of scalar and tensor metric perturbations generated from quantum vacuum fluctuations during inflation should be radically changed because of the necessity of renormalization of the perturbations. Here we prove that, contrary, these basic predictions are robust with respect to any renormalization, if the transition from quantum to effective stochastic classical observables is made consistently. The crucial point is the necessity to follow the behaviour of terms subtracted in the process of the renormalization long after the moment of the first Hubble radius crossing during inflation, up to a period that the Hubble parameter H becomes much less than its value at that moment.

1 Introduction

Unambiguous predictions of the power spectrum and statistics of primordial (post-inflationary) scalar and tensor perturbations play the central role in the whole inflationary scenario of the early universe since only they provide us with a possibility to test and confirm/falsify any concrete inflationary model (the prediction of the approximate spatial flatness of the present Universe follows from a prediction about the amplitude of a monopole, $l = 0$, scalar perturbation on a spatially flat FRW background). Indeed, by comparing these predictions with numerous existing observational data, large amount of inflationary models have been already falsified, while many of them (including the pioneer ones) still remain viable. That is why if consistency of these predictions would be put under question, or it would be shown that they are based on additional and doubtful assumptions, this would have dramatic consequences for the fate of the inflationary scenario as a whole and all its concrete realizations (models). Recently such an attempt was undertaken in the series of papers by L. Parker and his collaborators [1–4]. Their key statement is the following. Since the origin of post-inflationary metric and matter perturbations are quantum fluctuations of the gravitational field and other light scalar fields during inflation, so that this process has quantum and even quantum-gravitational nature, a renormalization is needed, as usually in quantum field theory, to obtain final observable predictions. Applying the standard procedure of the adiabatic (n-wave) regularization [5–9] to the power spectra of both scalar (curvature) perturbations $\mathcal{R}_{\rm c}(x)$ and tensor ones (gravitational waves) $h_{ij}(x)$, they claimed to obtain completely different results for these quantities. In this paper, we revisit this problem and discuss whether any UV renormalization may change the standard inflationary predictions.

2 Quantization and adiabatic regularization of perturbations

First of all, we describe the setup of the problem. As in Ref. [3], we consider slow-roll inflation driven by a single scalar (inflaton) field, whose action is given by

$$S = \frac{1}{2}\int \sqrt{-g}\,[M_{\rm pl}^2 R - g^{\mu\nu}\phi_{,\mu}\phi_{,\nu} - 2V(\phi)]{\rm d}^4x. \tag{1}$$

[1]Email address: yuko@gravity.phys.waseda.ac.jp
[2]Email address: alstar@landau.ac.ru

Assuming that background geometry is described by a spatially flat FRW metric, the background field equations take the form

$$6M_{\rm pl}^2\mathcal{H}^2 = \phi'^{\,2} + 2a^2V(\phi), \qquad \phi'' + 2\mathcal{H}\phi' + a^2V_\phi(\phi) = 0 \ , \tag{2}$$

where $\mathcal{H} := a'/a = aH$ and the dash denotes the derivative with respect to the conformal time η. In the comoving gauge, the spatial part of the metric takes the form

$$g_{ij} = a^2(\eta)[(1 + 2\mathcal{R}_{\rm c}(x))\delta_{ij} + h_{ij}(x)] \ , \tag{3}$$

where $\mathcal{R}_{\rm c}(x)$ and $h_{ij}(x)$ denote a scalar (curvature) curvature perturbation and tensor perturbations (gravitational waves), respectively. Here we neglect vector perturbations which rapidly decays during expansion. Equations for the Fourier mode functions of $\mathcal{R}_{\rm c}$ and h_{ij} have the form

$$\mathcal{R}''_{{\rm c},k}(\eta) + 2\frac{z'}{z}\mathcal{R}'_{{\rm c},k}(\eta) + k^2\mathcal{R}_{{\rm c},k}(\eta) = 0, \quad h''_k(\eta) + 2\frac{a'}{a}h'_k(\eta) + k^2h_k(\eta) = 0 \ , \tag{4}$$

where $z := a\phi'/\mathcal{H}$. Using the positive frequency solutions $\mathcal{R}_{{\rm c},k}(\eta)$ and $h_k(\eta)$ for the initial adiabatic vacuum, two-point functions of the curvature perturbation and the gravitational waves in this vacuum are expressed as

$$\langle\mathcal{R}_{\rm c}(\eta,\boldsymbol{x})\mathcal{R}_{\rm c}(\eta,\boldsymbol{y})\rangle = \int\frac{{\rm d}k}{k}\frac{\sin k|\boldsymbol{x}-\boldsymbol{y}|}{k|\boldsymbol{x}-\boldsymbol{y}|}\Delta^2_{\mathcal{R}_{{\rm c},k}}(\eta), \quad \langle h_{ij}(\eta,\boldsymbol{x})h^{ij}(\eta,\boldsymbol{y})\rangle = \int\frac{{\rm d}k}{k}\frac{\sin k|\boldsymbol{x}-\boldsymbol{y}|}{k|\boldsymbol{x}-\boldsymbol{y}|}\Delta^2_{h,k}(\eta) \ . \tag{5}$$

where dimensional variances are defined as

$$\Delta^2_{\mathcal{R}_{{\rm c},k}}(\eta) := \frac{k^3}{2\pi^2}|\mathcal{R}_{{\rm c},k}(\eta)|^2 \ , \qquad \Delta^2_{h,k}(\eta) := \frac{k^3}{\pi^2}|h_k(\eta)|^2 \ . \tag{6}$$

The adiabatic condition implies that $|\mathcal{R}_{{\rm c},k}(\eta)|^2$ and $|h_k(\eta)|^2$ scale as $1/k$ in the UV limit. Therefore, due to this UV behaviour, the two-point functions diverge in the coincidence limit $\boldsymbol{x}\tilde{\omega}\boldsymbol{y}$.

Next, we briefly review the method of adiabatic (n-wave) regularization which detailed explanation can be found in Refs. [6–9]. Adiabatic regularization is a convenient framework to remove all UV divergences from average values of quantum fields in an expanding universe. In particular, the regularized two-point function for a scalar field ϕ is given by

$$\langle\,\phi(\eta,\boldsymbol{x})\phi(\eta,\boldsymbol{y})\,\rangle_{\rm R} := \langle\,\phi(\eta,\boldsymbol{x})\phi(\eta,\boldsymbol{y})\,\rangle - \langle\,\phi(\eta,\boldsymbol{x})\phi(\eta,\boldsymbol{y})\,\rangle\big|^{(A)}, \tag{7}$$

where $|^{(A)}$ indicates that cross terms from field products which are of an adiabatic order greater than A have to be neglected. It is remarkable that the adiabatic regularization yields the same result as the point-splitting regularization, which is conceived to be an efficient regularization technique in curved space-time. Among advantages of the adiabatic regularization are that subtraction terms thus introduced preserve the conservation property of the average energy-momentum tensor of quantum fields and that the vacuum polarization given by Eq. (7) vanishes in Minkowski limit.

Since the adiabatic expansion coincides with the expansion in powers of $1/k$ (and with the n-wave expansion in terminology of [5]), by using it for the modes ${}^{(A)}\tilde{\mathcal{R}}_{{\rm c},k}(\eta)$ and ${}^{(A)}\tilde{h}_k(\eta)$ where the index (A) denotes the adiabatic order, we can subtract divergent parts of integrals over momentum in Eq. (5). Using Eq. (7), the regularized dimensionless power spectra are obtained as

$$\Delta^{({\rm R})}_{\mathcal{R}_{{\rm c},k}}{}^2(\eta) := \frac{k^3}{2\pi^2}\Big[\,|\mathcal{R}_{{\rm c},k}(\eta)|^2 - |^{(A)}\tilde{\mathcal{R}}_{{\rm c},k}(\eta)|^2\,\big|^{(A)}\,\Big], \tag{8}$$

$$\Delta^{({\rm R})}_{h,k}{}^2(\eta) := \frac{k^3}{\pi^2}\Big[\,|h_k(\eta)|^2 - |^{(A)}\tilde{h}_k(\eta)|^2\,\big|^{(A)}\,\Big], \tag{9}$$

where $|^{(A)}\tilde{\mathcal{R}}_{{\rm c},k}(\eta)|^2\,\big|^{(A)}$ and $|^{(A)}\tilde{h}_k(\eta)|^2\,\big|^{(A)}$ denote subtraction terms for a curvature perturbation and gravitational waves, respectively. In order not to violate the fundamental properties of the adiabatic regularization described above, we have to introduce the subtraction terms not only to the UV modes, but to all modes.

3 Effects of UV regularization

In this section, we discuss whether a UV renormalization can modify power spectra of primordial perturbations. Making use of the WKB expansion of solutions, the subtraction term for $\mathcal{R}_{\rm c}$ is given by

$$|^{(2)}\tilde{\mathcal{R}}_{{\rm c},k}(\eta)|^2\,|^{(2)} = \frac{1}{2z^2k}\Big[\,1+(1+\delta\varepsilon)\Big(\frac{aH}{k}\Big)^2\,\Big]\,, \tag{10}$$

where $\delta\varepsilon$ is expressed in terms of the Hubble (horizon) flow functions ε_i as follows:

$$\delta\varepsilon := -\frac{1}{2}\varepsilon_1+\frac{3}{4}\varepsilon_2+\frac{1}{8}\varepsilon_2^2-\frac{1}{4}\varepsilon_1\varepsilon_2+\frac{1}{4}\varepsilon_2\varepsilon_3\,. \tag{11}$$

Fluctuations from which the present large-scale structure of the Universe has originated cross the Hubble radius during inflation long before inflation ends. In the long wavelength limit $-k\eta \ll 1$, the mode function $\mathcal{R}_{{\rm c},k}$ approaches the constant value

$$\mathcal{R}_{{\rm c},k}(\eta) \simeq e^{i(2\nu+3)\pi/4}\,\frac{2^{\nu-\frac{3}{2}}}{\sqrt{2k}}\frac{\Gamma(\nu)}{\Gamma(\frac{3}{2})}\frac{(1-\varepsilon_1)^{\nu-\frac{1}{2}}}{z(\eta_*)}\,, \tag{12}$$

where η_* is the Hubble radius crossing time. The existence of the constant solution at large scales is assured by the very structure of the Einstein equations and remains valid in the non-linear regime, too. Quantum fluctuations generated deep inside the Hubble radius become indistinguishable from classical stochastic ones at super-Hubble scales after neglecting their decaying mode. Thus, we obtain the average squared value of $\mathcal{R}_{{\rm c},k}$ as

$$|\mathcal{R}_{{\rm c},k}(\eta)|^2 \simeq \frac{1}{4\varepsilon_1(\eta_*)}\frac{1}{k^3}\left(\frac{H(\eta_*)}{M_{\rm pl}}\right)^2(1+\delta\varepsilon_s)\,, \tag{13}$$

in the large scale limit, where $\delta\varepsilon_s := (2\varepsilon_1+\varepsilon_2)(2-\log 2-\gamma)-2\varepsilon_1$. Taking the large scale limit in Eq. (10), the adiabatic subtraction term is approximated as

$$|^{(2)}\tilde{\mathcal{R}}_{{\rm c},k}(\eta)|^2\,|^{(2)} \simeq \frac{1+\delta\varepsilon}{2k^3}\left(\frac{aH}{z}\right)^2 = \frac{1+\delta\varepsilon}{4\varepsilon_1}\frac{1}{k^3}\left(\frac{H}{M_{\rm pl}}\right)^2. \tag{14}$$

Since the Hubble parameter H and the Hubble flow functions are time dependent, the amplitude of the subtraction term changes even after the moment of the Hubble radius crossing. This reflects the fact that, while the adiabatic expansion of the modes $^{(A)}\tilde{\mathcal{R}}_{{\rm c},k}(\eta)$ well approximates the exact solution at sub-Hubble scales, it does not do so at super-Hubble ones. For instance, during the chaotic inflation, the Hubble parameter H decreases and the Hubble flow function ε_1 increases. The amplitude of the subtraction term then becomes smaller and smaller.

Substituting Eqs. (13) and (14) into Eq. (8), we obtain the regularized dimensionless variance of the curvature perturbation as

$$\Delta^{\rm (R)}_{\mathcal{R}_{\rm c},k}{}^2(\eta) = \frac{1}{2M_{\rm pl}^2\varepsilon_1(\eta_*)}\left(\frac{H(\eta_*)}{2\pi}\right)^2\left[1+\delta\varepsilon_s-(1+\delta\varepsilon)\,\frac{\varepsilon_1(\eta_*)}{\varepsilon_1(\eta)}\left(\frac{H(\eta)}{H(\eta_k)}\right)^2\right]. \tag{15}$$

Through the inflationary and the post inflationary evolution, the Hubble parameter H and the Hubble flow function ε_1 scale as $H(N)/H(N_*) = \exp[-\int_{N_*}^{N}{\rm d}N'\varepsilon_1(N')]$ and $\varepsilon_1(N)/\varepsilon_1(N_*) = \exp[\int_{N_*}^{N}{\rm d}N'\varepsilon_2(N')]$. Now it is clear that the subtraction term is suppressed by the factor:

$$\frac{\varepsilon_1(N_*)}{\varepsilon_1(N)}\left(\frac{H(N)}{H(N_*)}\right)^2 = e^{-\int_{N_*}^{N}{\rm d}N'[2\varepsilon_1(N')+\varepsilon_2(N')]}\,. \tag{16}$$

Therefore, for each Fourier mode, terms subtracted in the course of the adiabatic regularization are negligibly small when $H(\eta)$ becomes much less than $H(\eta_*)$ as the Universe evolves. Note that the bare

power spectrum is completely canceled by the adiabatic subtraction terms in the exact de Sitter space-time. However, this does not necessarily mean a problem, because in this case generated fluctuations, stretched beyond the future event horizon, cannot be observed.

The regularized amplitude of gravitational waves can be obtained in a manner similar to curvature perturbations. At large scales, their regularized dimensionless variance is evaluated as

$$\Delta_{h,k}^{(\mathrm{R})\ 2}(\eta) \simeq \frac{8}{M_{\mathrm{pl}}^2}\left(\frac{H(\eta_*)}{2\pi}\right)^2\left[1+\delta\varepsilon_t-\left(1-\frac{\varepsilon_1}{2}\right)\left(\frac{H(\eta)}{H(\eta_*)}\right)^2\right], \tag{17}$$

where $\delta\varepsilon_t = 2\varepsilon_1(1-\log 2-\gamma)$. Now it is clear that the subtraction term is suppressed by $(H(N)/H(N_*))^2 = \exp[-2\int_{N_*}^{N} \mathrm{d}N'\ \varepsilon_1(N')]$. Through the time evolution after the Hubble radius crossing, influence from the adiabatic regularization become negligibly small. This suppression is missed in the computations by L. Parker *et al* where the regime $H \ll H(\eta_*)$ has not been reached. Note that in the case of the exact Sitter space-time, the regularized amplitude for gravitational waves vanishes, too.

4 Summary

We have shown that even if we remove UV divergences in two-point correlation functions of metric perturbations during inflation using the adiabatic regularization, this does not leave any detectable imprints on the final power spectra for both curvature perturbations and gravitational waves after the end of inflation, or even during it but when H becomes much less than $H(\eta_*)$. This happens because any consistent UV renormalization modifies only local quantities (small scale inhomogeneities), ensuring that this regularization may be justified by introducing generally covariant counter terms constituted from local quantities.

Note that subtraction terms have to be introduced at all times, not during inflation only. Here our considerations differ somewhat from the recent paper [10] which otherwise arrives to the same conclusion regarding the papers [1–4]. It is also important that regularization of UV modes should be performed prior to the transition from quantum to classical description of fluctuations. While the bare quantum amplitudes given by the first terms of Eqs. (8) and (9) become indistinguishable from classical stochastic fluctuations after the first Hubble radius crossing, their UV regulators given by the second terms remain quantum up to the present time. This requires us to perform the adiabatic regularization before the consideration of quantum-to-classical transition for metric fluctuations.

In this paper, we have only considered regularization of the UV divergence which appears in the coincidence limit of two-point correlation functions in the one-loop approximation. However, a UV divergence can appear also from higher loop corrections. We leave regularization of these corrections for further study.

References

[1] L. Parker, arXiv:hep-th/0702216.

[2] I. Agullo, J. Navarro-Salas, G. J. Olmo and L. Parker, Phys. Rev. Lett. **101**, 171301 (2008).

[3] I. Agullo, J. Navarro-Salas, G. J. Olmo and L. Parker, Phys. Rev. Lett. **103**, 061301 (2009).

[4] I. Agullo, J. Navarro-Salas, G. J. Olmo and L. Parker, arXiv:0911.0961.

[5] Ya. B. Zeldovich and A. A. Starobinsky, Sov. Phys. - JETP **34**, 1159 (1972).

[6] L. Parker and S. A. Fulling, Phys. Rev. D **9**, 341 (1974).

[7] S. A. Fulling, L. Parker and B. L. Hu, Phys. Rev. D **10**, 3905 (1974).

[8] T. S. Bunch, J. Phys. A **13**, 1297 (1980).

[9] P. R. Anderson and L. Parker, Phys. Rev. D **36**, 2963 (1987).

[10] R. Durrer, G. Marozzi and M. Rinaldi, arXiv:0906.4772.

Supersymmetric Intersecting Branes on the Wave

Kei-ichi Maeda[1a,b], Nobuyoshi Ohta[2c], Makoto Tanabe[3a], and Ryo Wakebe[4a]

[a] *Department of Physics, Waseda University, Shinjuku, Tokyo 169-8555, Japan*
[b] *Waseda Research Institute for Science and Engineering, Shinjuku, Tokyo 169-8555, Japan*
[c] *Department of Physics, Kinki University, Higashi-Osaka, Osaka 577-8502, Japan*

Abstract

The understanding of the fundamental nature and quantum properties of spacetime is one of the most important questions in theoretical physics. String/M theory is one of the most promising theory for research it. And dilaton-gravity plane waves provide a rare example of tractable strongly curved (possibly singular) time-dependent spacetime backgrounds. We construct a general family of supersymmetric solutions in time- and space-dependent wave backgrounds in general supergravity theories describing single and intersecting p-branes embedded into time-dependent dilaton-gravity plane waves of an arbitrary (isotropic) profile, with the brane world-volume aligned parallel to the propagation direction of the wave. We discuss how many degrees of freedom we have in the solutions. We also propose that these solutions can be used to describe higher-dimensional time-dependent "black holes", and discuss their property briefly.

1 Time-dependent brane system in supergravity

The low-energy effective action for the supergravity system coupled to dilaton and n_A- form field strength is given by

$$I = \frac{1}{16\pi G_D}\int d^D x\sqrt{-g}\left[R - \frac{1}{2}(\partial\Phi)^2 - \sum_{A=1}^{m}\frac{1}{2n_A!}e^{a_A\Phi}F_{n_A}^2\right], \tag{1.1}$$

where G_D is the Newton constant in D dimensions and g is the determinant of the metric. The last term includes both RR and NS-NS field strengths, and $a_A = \frac{1}{2}(5-n_A)$ for RR field strength and $a_A = -1$ for NS-NS 3-form. In the eleven-dimensional supergravity, there is a four-form and no dilaton. We put fermions and other background fields to be zero.

We take the following metric:

$$ds_D^2 = e^{2\Xi(u,r)}\left[-2dudv + K(u,r)du^2\right] + \sum_{\alpha=1}^{d-2}e^{2Z_\alpha(u,r)}(dy^\alpha)^2 + e^{2B(u,r)}\left(dr^2 + r^2 d\Omega_{\tilde{d}+1}^2\right), \tag{1.2}$$

where $D = d + \tilde{d} + 2$, the coordinates u, v and $y^\alpha, (\alpha = 1,\dots,d-2)$ parameterize the d-dimensional worldvolume where the branes belong, and the remaining $\tilde{d}+2$ coordinates r and angles are transverse to the brane worldvolume, $d\Omega_{\tilde{d}+1}^2$ is the line element of the $(\tilde{d}+1)$-dimensional sphere. Note that u and v are null coordinates. The metric components Ξ, Z_α, B and the dilaton Φ and K are assumed to be functions of u and r. For the field strength backgrounds, we take

$$F_{n_A} = E_A'(u,r)\, du\wedge dv\wedge dy^{\alpha_1}\wedge\cdots\wedge dy^{\alpha_{q_A-1}}\wedge dr, \tag{1.3}$$

where $n_A = q_A + 2$. Throughout this article, the dot and prime denote derivatives with respect to u and r, respectively. The ansatz (1.3) means that we have an electric background. We could, however, also include magnetic background in the same form as the electric one.

[1]E-mail address: maeda"at"waseda.jp
[2]E-mail address: ohtan"at"phys.kindai.ac.jp
[3]E-mail address:tanabe"at"gravity.phys.waseda.ac.jp
[4]E-mail address:wakebe"at"gravity.phys.waseda.ac.jp

We have shown that the solutions [1] to the field equations are given by

$$\begin{aligned} ds_D^2 &= \prod_B H_B^{\frac{2(q_B+1)}{\Delta_B}} \Bigg[e^{2\xi(u)} \prod_A H_A^{-\frac{2(D-2)}{\Delta_A}} \left(-2dudv + K(u,r)du^2\right) \\ &\quad + \sum_{\alpha=1}^{d-2} \prod_A H_A^{-\frac{2\gamma_A^{(\alpha)}}{\Delta_A}} e^{2\zeta_\alpha(u)} (dy^\alpha)^2 + e^{2\beta(u)} \left(dr^2 + r^2 d\Omega_{\tilde{d}+1}^2\right) \Bigg], \\ E_A &= \sqrt{\frac{2(D-2)}{\Delta_A}} H_A^{-1}, \quad \Phi = \sum_A \frac{\epsilon_A a_A (D-2)}{\Delta_A} \ln H_A + \phi(u), \end{aligned} \tag{1.4}$$

where H_A is a harmonic function

$$H_A = h_A(u) + \frac{Q_A}{r^{\tilde{d}}}, \tag{1.5}$$

with h_A being an arbitrary function of u and Q_A a constant, $\epsilon_A = +1(-1)$ is for electric (magnetic) backgrounds and

$$\gamma_A^{(\alpha)} = \begin{cases} D-2 \\ 0 \end{cases} \quad \text{for} \quad \begin{cases} y^\alpha \text{ belonging to } q_A\text{-brane} \\ \text{otherwise} \end{cases} . \tag{1.6}$$

We have two constraints still to be satisfied:

$$\epsilon_A a_A \phi + 2 \sum_{\alpha \notin q_A} \zeta_\alpha + 2\tilde{d}\beta = 0, \tag{1.7}$$

$$\left(r^{\tilde{d}+1} K'\right)' = -2e^{-2(\xi-\beta)} r^{\tilde{d}+1} \prod_A H_A^{2(D-2)/\Delta_A} \left[W(u,r) + V(u)\right], \tag{1.8}$$

where

$$\begin{aligned} W(u,r) &\equiv \sum_{A,B} \frac{(D-2)^2}{\Delta_A \Delta_B} \Big(\frac{\Delta_A}{D-2} \delta_{AB} + 2 \Big) (\ln H_A)^{\cdot} (\ln H_B)^{\cdot} + 2 \sum_A \frac{D-2}{\Delta_A} (\ln H_A)^{\cdot\cdot} \\ &\quad + 4(D-2)(\dot{\beta} - \dot{\xi}) \sum_A \frac{(\ln H_A)^{\cdot}}{\Delta_A}, \end{aligned} \tag{1.9}$$

$$V(u) \equiv \sum_{\alpha=1}^{d-2} \left(\ddot{\zeta}_\alpha + \dot{\zeta}_\alpha^2\right) + (\tilde{d}+2)\left(\ddot{\beta} + \dot{\beta}^2\right) - 2\dot{\xi} \left[\sum_{\alpha=1}^{d-2} \dot{\zeta}_\alpha + (\tilde{d}+2)\dot{\beta}\right] + \frac{1}{2}(\dot{\phi})^2, \tag{1.10}$$

We regard Eq. (1.8) as the equation for K when other metric functions are given, which is an elliptic type differential equation with respect to r. This approach has recently been taken in Ref. [2] for a single brane. Our solutions here include single and intersecting brane solutions as well as wider solutions including more arbitrary functions than those in [2].

2 Solutions with time-dependent harmonic functions

In this section, we present nontrivial solutions with both r- and u-dependent harmonic functions H_A[3].

Before presenting our solutions, we discuss gauge freedom of null-coordinate transformation. Under the coordinate transformation

$$u = X(\tilde{u}), \quad v = \tilde{v} + Y(\tilde{u}), \tag{2.1}$$

where X and Y are arbitrary functions of u, we recover the same solution (1.4), (1.5), (1.7), and (1.8), by replacing K and ξ with

$$\tilde{K}(\tilde{u},r) = K(X(\tilde{u}),r)\frac{dX}{d\tilde{u}} - 2\frac{dY(\tilde{u})}{d\tilde{u}}, \quad \tilde{\xi}(\tilde{u}) = \xi(X(\tilde{u})) + \frac{1}{2}\ln\left(\frac{dX}{d\tilde{u}}\right), \tag{2.2}$$

respectively. Using X and Y, we can gauge away ξ and a function of u in K in our solutions. We will discuss more details of this procedure in the concrete examples shortly.

2.1 D1-D5 brane system

Let us give a concrete example. The D1-D5-brane is given by

$$\begin{aligned} ds^2 &= H_1^{\frac{1}{4}} H_5^{\frac{3}{4}} \left[H_1^{-1} H_5^{-1} (-2dudv + K(u,r)du^2) + H_5^{-1} \sum_{\alpha=1}^{4} e^{2\zeta_\alpha(u)} dy_\alpha^2 + e^{2\beta(u)} (dr^2 + r^2 d\Omega_3^2) \right], \\ \Phi &= \ln \left(\frac{H_1}{H_5} \right)^{\frac{1}{2}} + \phi(u) \,. \end{aligned} \tag{2.3}$$

And (1.8) yields

$$K = \frac{A_2(u)}{8} r^2 + \frac{1}{2} \left(B_2(u) - \frac{C_2}{r^2} \right) \ln r - \frac{C_2(u) + 2D_2(u)}{4r^2} + E_2(u) \,, \tag{2.4}$$

where

$$\begin{aligned} A_2(u) &= -2e^{-2(\xi-\beta)} \left[\dot{h}_A \dot{h}_B + \ddot{h}_A h_B + \ddot{h}_B h_A + 2(\dot{\beta} - \dot{\xi})(\dot{h}_A h_B + \dot{h}_B h_A) + V h_A h_B \right] , \\ B_2(u) &= -2e^{-2(\xi-\beta)} \left[\ddot{h}_A Q_B + \ddot{h}_B Q_A + 2(\dot{\beta} - \dot{\xi})(\dot{h}_A Q_B + \dot{h}_B Q_A) + V(h_A Q_B + h_B Q_A) \right] , \\ C_2(u) &= -2e^{-2(\xi-\beta)} V Q_A Q_B \,, \end{aligned} \tag{2.5}$$

and $D_2(u)$ and $E_2(u)$ are arbitrary function of u. Considering coordinate transformation (2.1), we can gauge away E_2. It also follows from (1.7) that $\beta(u) = \frac{1}{4}\phi(u) = -\sum_{\alpha=1}^{4} \zeta_\alpha(u)$. Hence this solution has seven arbitrary functions $h_1(u), h_5(u), \zeta_\alpha(u)$, and $D_2(u)$ in K, while A_2, B_2, and C_2 in K are given by (2.5) with $\xi = 0$.

If we assume $V(u) = 0$, (1.7) together with (1.10) yields $\zeta_\alpha = \beta = \phi = 0$. There remain three arbitrary functions of u; $h_1(u), h_5(u)$ and $D_2(u)$.

3 A fluctuating "black hole"

In the static case, one can construct a black hole solution from the intersecting brane system via compactification. Hence we may find a time-dependent black hole solution by compactifying the present time-dependent intersecting brane systems. We give a simple example of this type.

Let us consider the simple case of D1-D5 intersecting brane system with

$$H_A = 1 + \frac{Q_A}{r^2} \ , \text{ and } \quad K = \frac{2Q_{\rm w}(u)}{r^2} \,, \tag{3.1}$$

where $Q_{\rm w}$ is a function of u. This can be obtained for the choice $V(u) = 0$, $h_1 = h_5 = 1$ and $D_2 = -4Q_{\rm w}(u)$. One can check $A_2(u) = B_2(u) = 0$ by (2.5) easily. Introducing new function $H_{\rm w} = 1 + K(u,r)/2$, we find the metric

$$ds_{10}^2 = H_1^{-3/4} H_5^{-1/4} \left[-H_{\rm w}^{-1} dt^2 + H_{\rm w} \left(dz + \frac{(H_{\rm w} - 1)}{H_{\rm w}} dt \right)^2 \right] + H_1^{1/4} H_5^{3/4} \left[H_5^{-1} \sum_{\alpha=1}^{4} dy_\alpha^2 + dr^2 + r^2 d\Omega_3^2 \right], \tag{3.2}$$

where $u = (t - z)/\sqrt{2}$ and $v = (t + z)/\sqrt{2}$.

In order to perform a compactification, we write our metric (3.2) as

$$ds_{10}^2 = \left(H_1^{-\frac{1}{12}} H_5^{\frac{5}{12}} H_{\rm w}^{-\frac{1}{3}} \right) ds_5^2 + H_1^{-3/4} H_5^{-1/4} H_{\rm w} \left(dz + \frac{(H_{\rm w} - 1)}{H_{\rm w}} dt \right)^2 + H_1^{1/4} H_5^{-1/4} \sum_{\alpha=1}^{4} dy_\alpha^2, \tag{3.3}$$

where

$$ds_5^2 = -\Xi_5^2 dt^2 + \Xi_5^{-1} (dr^2 + r^2 d\Omega_3^2), \tag{3.4}$$

and $\Xi_5 = (H_1 H_5 H_{\rm w})^{-1/3}$ gives the five-dimensional metric in the Einstein frame.

All toroidal y_α-coordinates can be compactified, but the compactification of the z-coordinate is not trivial. We have to impose a periodic condition on the metric functions, which explicitly depend on z

through the u-coordinate. Here we assume that the function $H_{\rm w}(u,r)$ is periodic in the u direction. As a concrete example, we choose a periodic function as $Q_{\rm w}(u) = Q_0\left[1+\epsilon\cos\left(\frac{\sqrt{2}u}{R}\right)\right]$, where R is a radius of the z-space and ϵ is a positive constant. If fact, the metric is invariant under the discrete transformation of $z \to z + 2\pi nR$ ($n \in \mathbf{Z}$). The explicit form of the metric function Ξ_5 is given by

$$\Xi_5 = \left[\left(1+\frac{Q_1}{r^2}\right)\left(1+\frac{Q_5}{r^2}\right)\left(1+\frac{Q_0}{r^2}\left[1+\epsilon\cos\left(\frac{t-z}{R}\right)\right]\right)\right]^{-1/3}. \tag{3.5}$$

In order to avoid a closed timelike curve, the z-direction must be spacelike. This condition requires that $\epsilon \le 1$; otherwise $H_{\rm w}$ becomes negative at least in the limit of $r \to 0$, where we expect a horizon. $\epsilon = 1$ must be excluded because the charge $Q_{\rm w}$ vanishes at $u = \pi R/\sqrt{2}$, when a singularity may appear at $r = 0$. Hence we assume that $0 < \epsilon < 1$.

The metric (3.4) with (3.5) gives effectively a five-dimensional time-dependent spacetime although it also depends on the z-coordinate. It describes an explicit example of a spacetime excited by a pyrgon which may appear in Kaluza-Klein compactification. Since it is asymptotically flat, one may define the "mass" of this object as $M = \pi[Q_1 + Q_5 + Q_{\rm w}(u)]/4G_5$, which oscillates in time. The surface of $r = 0$ is a candidate for horizon because it is the case when the spacetime is static ($\epsilon = 0$). Hence one may naively think that this spacetime describes a time-dependent oscillating "black hole". However the "mass" depends not only on time t but also on the inner space coordinate z.

If the compactification radius R is small enough, we may not see z-dependence in a global scale. Taking an average over the internal z-space, we find that the mean mass $\langle M\rangle = \pi(Q_1+Q_5+Q_0)/4G_5$. We may also find that the "mass" M fluctuates around this average value with the amplitude $\sqrt{\langle(\Delta M)^2\rangle}/\langle M\rangle = Q_0\epsilon/\sqrt{2}(Q_1+Q_5+Q_0)$, and the typical frequency $\omega = \sqrt{2}/R$.

The Bekenstein-Hawking black hole entropy, which is proportional to the horizon area, may also fluctuate around the averaged value $\langle S\rangle = \langle\mathcal{A}\rangle/4G_5 = \pi^2\sqrt{Q_1Q_5Q_0}/2G_5$ with the amplitude $\sqrt{\langle(\Delta S)^2\rangle}/\langle S\rangle = \epsilon/\sqrt{2}$.

This spacetime describes a five-dimensional compact object in a global scale, but it shows fluctuations near the "horizon" ($r = 0$). Hence it is not a deterministic five-dimensional spacetime. We can regard it as a fluctuating "black hole", but $r = 0$ may not be a true horizon.

Although this spacetime looks like a fluctuating "black hole" in five dimensions, it is a deterministic spacetime in six dimensions. In fact, when we approach the "horizon", we will see the internal compact z-space as well as the periodic time dependence. Hence the spacetime is essentially six-dimensional, whose metric is given by

$$ds_6^2 = \Xi_6(r)\left[-2dudv + K(u,r)du^2\right] + \Xi_6^{-1}(r)(dr^2 + r^2 d\Omega_3^2), \quad \Xi_6(r) \equiv (H_1H_5)^{-1/2}. \tag{3.6}$$

It is obtained by compactification of all toroidal y_α-coordinates in ten-dimensional spacetime. Although this spacetime is compact in the z-direction as well as in the toroidal y_α-direction, the z-direction is not homogeneous. As a result, the spacetime is time-dependent but it is no longer spherically symmetric, i.e. it depends on z as well as t, r. The inhomogeneity in the z-direction becomes prominent especially in the scale near (or smaller than) the compactification radius R. This spacetime is regular at $r = 0$, which is shown by calculating the curvature invariants.

Hence we conclude that this solution describes a static and spherically symmetric five-dimensional compact object with fluctuations in a large scale, but it becomes a periodically oscillating and non-spherical six-dimensional object in a small scale.

There are several questions with this solution which deserve further consideration. Does this metric really describes a time-dependent black hole or else? Is the horizon, if it exists, time-dependent? How is the mass of the "black hole" defined? When we approach the "horizon", what kind of spacetime structure do we see? Those questions are interesting by themselves and are left for future study.

References

[1] K. Maeda, N. Ohta, M. Tanabe and R. Wakebe, JHEP **0906** (2009) 036 [arXiv:0903.3298 [hep-th]].

[2] B. Craps, F. De Roo, O. Evnin and F. Galli, JHEP **0907** (2009) 058 [arXiv:0905.1843 [hep-th]].

[3] K. Maeda, N. Ohta, M. Tanabe and R. Wakebe, [arXiv:1001.2640 [hep-th]].

Inflationary Universe with Anisotropic Hair

Masaaki Watanabe[1(a)], Sugumi Kanno[2(b)] and Jiro Soda[3(a)]

[(a)] *Department of Physics, Kyoto University, Kyoto, 606-8501, Japan*
[(b)] *Centre for Particle Theory, Department of Mathematical Sciences, Durham University, Science Laboratories, South Road, Durham, DH1 3LE, United Kingdom*

Abstract

We study an inflationary scenario with a vector field coupled with an inflaton field and show that the inflationary universe is endowed with anisotropy for a wide range of coupling functions. This anisotropic inflation is a tracking solution where the energy density of the vector field follows that of the inflaton field irrespective of initial conditions. We find a universal relation between the anisotropy and a slow-roll parameter of inflation. Our finding has observational implications and gives a counter example to the cosmic no-hair conjecture.

1 Introduction

Recent developments of precision cosmology have yielded a slight shift of an inflationary paradigm, and we are now forced to look at fine structures of fluctuations such as spectral tilt, non-gaussianity, parity violation, and so on. Those precise predictions of inflationary scenarios will provide a clue to understand fundamental physics when they are compared with observations.

In this paper, we focus on a role of a vector field in the early universe. Here, there is a prejudice that the vector hair is negligibly small and it is legitimate to ignore the backreaction of magnetic fields to geometry. However, in the context of the precision cosmology, we should not neglect the backreaction if it is around a percent level [3]. Hence, it is important to quantify how small it is. Based on this observation, we study an inflationary scenario where the inflaton is coupled with the kinetic term of a massless vector field. Interestingly, we find a tracking behavior of the energy density of the vector field. As a consequence, we show that there exist sizable vector hair quite generally. That yields a percent level anisotropic inflation.

2 Basic equations

We consider the following action for the gravitational field, the inflaton field ϕ and the vector field A_μ coupled with ϕ:

$$S = \int d^4x\sqrt{-g}\left[\frac{1}{2\kappa^2}R - \frac{1}{2}\left(\partial_\mu\phi\right)\left(\partial^\mu\phi\right) - V(\phi) - \frac{1}{4}f^2(\phi)F_{\mu\nu}F^{\mu\nu}\right], \tag{2.1}$$

where g is the determinant of the metric, R is the Ricci scalar, $V(\phi)$ is the inflaton potential, $f(\phi)$ is the coupling function of the inflaton field to the vector one, respectively. The field strength of the vector field is defined by $F_{\mu\nu} = \partial_\mu A_\nu - \partial_\nu A_\mu$. Thanks to the gauge invariance, we can choose the gauge $A_0 = 0$. Without loss of generality, we can take x-axis in the direction of the vector. Hence, we take the homogeneous fields of the form $A_\mu = (\ 0,\ A_x(t),\ 0,\ 0\ )$ and $\phi = \phi(t)$. Note that we have assumed the direction of the vector field does not change in time, for simplicity. This field configuration holds the plane symmetry in the plane perpendicular to the vector. Then, we take the metric to be

$$ds^2 = -dt^2 + e^{2\alpha(t)}\left[e^{-4\sigma(t)}dx^2 + e^{2\sigma(t)}\left(dy^2 + dz^2\right)\right], \tag{2.2}$$

[1]Email address: mwatanabe@tap.scphys.kyoto-u.ac.jp
[2]Email address: sugumi.kanno@durham.ac.uk
[3]Email address: jiro@tap.scphys.kyoto-u.ac.jp

where the cosmic time t is used. Here, e^{α} is an isotropic scale factor and σ represents a deviation from the isotropy. With above ansatz, one obtains the equation of motion for the vector field which is easily solved as $\dot{A}_x = f^{-2}(\phi)e^{-\alpha-4\sigma}p_A$, where an overdot denotes the derivative with respect to the cosmic time t and p_A denotes a constant of integration. Substituting this into other equations, we obtain basic equations

$$\dot{\alpha}^2 = \dot{\sigma}^2 + \frac{\kappa^2}{3}\left[\frac{1}{2}\dot{\phi}^2 + V(\phi) + \frac{p_A^2}{2}f^{-2}(\phi)e^{-4\alpha-4\sigma}\right] , \tag{2.3}$$

$$\ddot{\alpha} = -3\dot{\alpha}^2 + \kappa^2 V(\phi) + \frac{\kappa^2 p_A^2}{6}f^{-2}(\phi)e^{-4\alpha-4\sigma}, \tag{2.4}$$

$$\ddot{\sigma} = -3\dot{\alpha}\dot{\sigma} + \frac{\kappa^2 p_A^2}{3}f^{-2}(\phi)e^{-4\alpha-4\sigma}, \tag{2.5}$$

$$\ddot{\phi} = -3\dot{\alpha}\dot{\phi} - V'(\phi) + p_A^2 f^{-3}(\phi)f'(\phi)e^{-4\alpha-4\sigma} , \tag{2.6}$$

where a prime denotes the derivative with respect to ϕ.

From Eq.(2.3), we see the effective potential $V_{\rm eff} = V + p_A^2 f^{-2}e^{-4\alpha-4\sigma}/2$ determines the inflaton dynamics. As the second term is coming from the vector contribution, we refer it to the energy density of the vector. Let's check if inflation occurs in this model. Using Eqs.(2.3) and (2.4), equation for acceleration of the universe is given by $\ddot{\alpha} + \dot{\alpha}^2 = -2\dot{\sigma}^2 - \frac{\kappa^2}{3}\dot{\phi}^2 + \frac{\kappa^2}{3}\left[V - \frac{p_A^2}{2}f^{-2}e^{-4\alpha-4\sigma}\right]$. We see that the potential energy of the inflaton needs to be dominant for the inflation to occur. Now, we assume the energy density of the vector can be negligible compared to that of the inflaton for the inflaton dynamics. Then, we examine when the anisotropy is not diluted during inflation. From Eq.(2.5), it is apparent that the fate of anisotropic expansion rate $\Sigma \equiv \dot{\sigma}$ depends on the behavior of coupling function $f(\phi)$. In the critical case $f(\phi) \propto e^{-2\alpha}$, the energy density of the vector field as a source term in Eq.(2.5) remains almost constant during the slow-roll inflation. Using slow-roll equations $\dot{\alpha}^2 = \frac{\kappa^2}{3}V(\phi), \quad 3\dot{\alpha}\dot{\phi} = -V'(\phi)$, we obtain $d\alpha/d\phi = \dot{\alpha}/\dot{\phi} = -\kappa^2 V(\phi)/V'(\phi)$. This can be easily integrated as $\alpha = -\kappa^2 \int V/V' d\phi$. Here, we have absorbed a constant of integration into the definition of α. Thus, we obtain

$$f = e^{-2\alpha} = e^{2\kappa^2 \int \frac{V}{V'}d\phi} . \tag{2.7}$$

For the polynomial potential $V \propto \phi^n$, we have $f = e^{\kappa^2\phi^2/n}$. Given the critical case (2.7), we can parameterize the coupling function as [2]:

$$f = e^{2c\kappa^2 \int \frac{V}{V'}d\phi} , \tag{2.8}$$

where c is a parameter.

Naively, the energy density of the vector field grows during inflation when $c > 1$, which is the case we want to consider. It would not be possible to neglect the vector field in this case. Let us see what happens if the vector field is not negligible.

3 Tracking Anisotropic Inflation

To make the analysis concrete, we consider chaotic inflation with the potential $V(\phi) = m^2\phi^2/2$ $(n = 2)$. For this potential, the coupling function becomes $f(\phi) = e^{c\kappa^2\phi^2/2}$. It is instructive to see what happens by solving Eqs.(2.3)-(2.6) numerically. In Fig. 1, we have shown the phase flow in $\phi - \dot{\phi}$ space where we can see two slow-roll phases, which indicates something different from the conventional inflation occurs. In Fig.2, we have calculated the evolution of the anisotropy $\Sigma/H \equiv \dot{\sigma}/\dot{\alpha}$ for various parameters c under the initial conditions $\sqrt{c}\kappa\phi_i = 17$.

As expected, all of solutions show a rapid growth of anisotropy in the first slow-roll phase. However, the growth of the anisotropy eventually stops at the order of a percent. Notice that this attractor like behavior is not so sensitive to a parameter c.

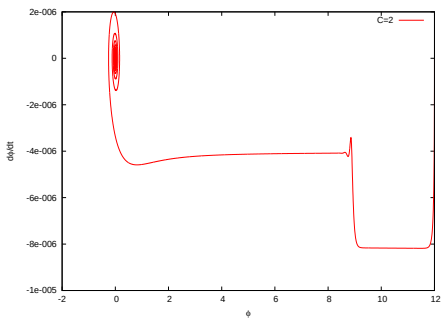

Figure 1: Phase flow for ϕ is depicted.

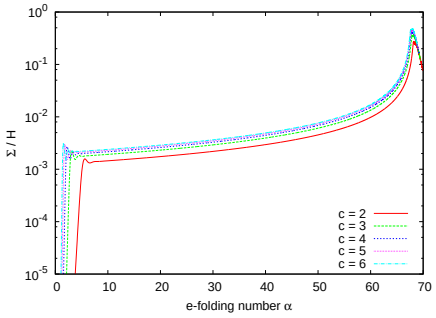

Figure 2: Evolutions of the anisotropy Σ/H for various c are shown.

Now, we will give an analytic explanation of the numerical results and find a quite remarkable relation between the anisotropy and a slow-roll parameter of inflation.

As the energy density of the vector field should be subdominant during inflation, we can ignore σ in Eqs.(2.3), (2.4), and (2.6). However, in Eq.(2.5), all terms would be of the same order. Now, Eqs.(2.3) and (2.6) can be written as

$$\dot{\alpha}^2 = \frac{\kappa^2}{3}\left[\frac{1}{2}\dot{\phi}^2 + \frac{1}{2}m^2\phi^2 + \frac{1}{2}e^{-c\kappa^2\phi^2-4\alpha}p_A^2\right] , \tag{3.1}$$

$$\ddot{\phi} = -3\dot{\alpha}\dot{\phi} - m^2\phi + c\kappa^2\phi e^{-c\kappa^2\phi^2-4\alpha}p_A^2 . \tag{3.2}$$

Let's see how the energy density of the vector field works in these equations. When the effect of the vector field is comparable with that of the inflaton field as source terms in (3.2), we get the relation $c\kappa^2 p_A^2 e^{-c\kappa^2\phi^2-4\alpha} \sim m^2$. If we define the ratio of the energy density of the vector field $\rho_A \equiv p_A^2 e^{-c\kappa^2\phi^2-4\alpha}/2$ to that of the inflaton $\rho_\phi \equiv m^2\phi^2/2$ as

$$\mathcal{R} \equiv \frac{\rho_A}{\rho_\phi} = \frac{p_A^2 e^{-c\kappa^2\phi^2-4\alpha}}{m^2\phi^2} , \tag{3.3}$$

we find the ratio becomes $\mathcal{R} \sim 1/c\kappa^2\phi^2$ when the above relation holds. Since the e-folding number is crudely given by $N \sim \kappa^2\phi^2$

and the scale observed through CMB corresponds to $N \sim \mathcal{O}(100)$, we have typically $\kappa\phi \sim \mathcal{O}(10)$. Hence, the ratio goes $\mathcal{R} \sim 10^{-2}$. Thus we find that the effect of the vector filed in (3.1) is negligible even when it is comparable with that of the scalar field in (3.2).

It turns out that the above situation is not transient one but an attractor. Suppose that ρ_A is initially negligible, $\mathcal{R}_i \ll 10^{-2}$. In the first slow-roll inflationary phase, the relation $e^{-\kappa^2\phi^2} \propto e^{4\alpha}$ holds as was shown in (2.7). Hence, the ratio $\mathcal{R}$ varies as $\mathcal{R} \propto e^{4(c-1)\alpha}$. As we now consider $c > 1$, ρ_A increases rapidly during inflation and eventually reaches $\mathcal{R} \sim 10^{-2}$. Whereas, when $\mathcal{R}$ exceeds 10^{-2}, the inflaton climbs up the potential due to the effect of the vector field in (3.2), hence ρ_A will decrease rapidly and go back to the value $\mathcal{R} \sim 10^{-2}$. Thus irrespective of initial conditions, ρ_A will track ρ_ϕ.

The above arguments tell us that the inflaton dynamics after tracking is governed by the modified slow-roll equations

$$\dot{\alpha}^2 = \frac{\kappa^2}{6}m^2\phi^2 , \tag{3.4}$$

$$3\dot{\alpha}\dot{\phi} = -m^2\phi + c\kappa^2\phi p_A^2 e^{-c\kappa^2\phi^2-4\alpha} . \tag{3.5}$$

We refer to the phase governed by the above equations as the second inflationary phase, compared to the first conventional one. Using above equations, we can deduce

$$\phi\frac{d\phi}{d\alpha} = -\frac{2}{\kappa^2} + \frac{2cp_A^2}{m^2}e^{-c\kappa^2\phi^2-4\alpha} . \tag{3.6}$$

This can be integrated as $e^{-c\kappa^2\phi^2-4\alpha} = m^2(c-1)/c^2\kappa^2 p_A^2 \left[1 + De^{-4(c-1)\alpha}\right]^{-1}$, where D is a constant of integration. This solution rapidly converges to $e^{-c\kappa^2\phi^2-4\alpha} = \dfrac{m^2(c-1)}{c^2\kappa^2 p_A^2}$. Thus, we found ρ_A becomes constant during the second inflationary phase. Substituting this result into the modified slow-roll equation (3.5), we obtain the equation for the second inflationary phase

$$3\dot{\alpha}\dot{\phi} = -\frac{m^2}{c}\phi \ . \tag{3.7}$$

This indicates that $\dot{\phi}$ in the second phase of inflation is about $1/c$ times that in the first phase of inflation. In Fig. 1, we can see the value of $\dot{\phi}$ after the phase transition is about a half of that in the first phase, which agrees with the analytical estimate for $c = 2$.

Now let us consider the anisotropy. In the second slow-roll phase, Eq.(2.5) reads $3\dot{\alpha}\dot{\sigma} = \dfrac{\kappa^2 p_A^2}{3} e^{-c\kappa^2\phi^2-4\alpha}$. where we have assumed $\sigma \ll c\kappa^2\phi^2$, $\ddot{\sigma} \ll \dot{\alpha}\dot{\sigma}$. Using this and Eqs.(3.4), the anisotropy turns out to be determined by the ratio (3.3) as

$$\frac{\Sigma}{H} = \frac{\kappa^2 p_A^2 e^{-c\kappa^2\phi^2-4\alpha}}{9\dot{\alpha}^2} = \frac{2}{3}\mathcal{R}(t) \ . \tag{3.8}$$

In the second inflationary phase, we can calculate the ratio as $\mathcal{R}(t) = \dfrac{c-1}{c^2\kappa^2\phi^2}$. Using this relation, we can relate degrees of anisotropy to the slow-roll parameter as follows. Combining Eqs.(2.3) with (2.4), we obtain $\ddot{\alpha} = -\dfrac{\kappa^2}{2}\dot{\phi}^2 - \dfrac{\kappa^2}{3} e^{-c\kappa^2\phi^2-4\alpha} p_A^2$ where we have used $\dot{\sigma}^2 \ll \kappa^2\dot{\phi}^2$ derived from Eqs.(3.4), (3.7) and (3.8). Thus, the slow-roll parameter is given by

$$\epsilon \equiv -\frac{\ddot{\alpha}}{\dot{\alpha}^2} = \frac{2}{c\kappa^2\phi^2} \ , \tag{3.9}$$

where we used the results (3.4) and (3.7). Thus, combining Eqs.(3.8) and (3.9), we reach a main result

$$\frac{\Sigma}{H} = \frac{1}{3}\frac{c-1}{c}\epsilon \ . \tag{3.10}$$

This remarkable relation shows a quite good agreement with the numerical results for in Fig.2.

4 Conclusion

We have proposed an inflationary scenario with anisotropy. Remarkably, we have find that degrees of anisotropy are universally determined by the slow-roll parameter of inflation. Since the slow-roll parameter is observationally known to be of the order of a percent, the anisotropy during inflation cannot be entirely negligible. Indeed, we can expect rich phenomenology as consequences of the anisotropy during inflation such as the statistical anisotropy of CMB temperature fluctuations [4], and a correlation between curvature and tensor perturbations [1]. These features should be detected through the analysis of temperature-B-mode correlation in CMB. Moreover, because of the anisotropy, there might be linear polarization in primordial gravitational waves. This polarization can be detected either through CMB observations or direct interferometer observations. These predictions can be checked by future observations.

References

[1] S. Kanno, M. Kimura, J. Soda and S. Yokoyama, JCAP **0808**, 034 (2008).

[2] J. Martin and J. Yokoyama, JCAP **0801**, 025 (2008).

[3] A. R. Pullen and M. Kamionkowski, Phys. Rev. D **76**, 103529 (2007).

[4] L. Ackerman, S. M. Carroll and M. B. Wise, Phys. Rev. D **75**, 083502 (2007).

[5] M. a. Watanabe, S. Kanno and J. Soda, Phys. Rev. Lett. **102**, 191302 (2009) [arXiv:0902.2833 [hep-th]].

Constraining alternative theories of gravity with space-borne gravitational wave interferometers

Kent Yagi[1(a)] and Takahiro Tanaka[2(b)]

[(a)] *Department of Physics, Kyoto University, Kyoto, 606-8502*
[(b)] *Yukawa Institute for Theoretical Physics, Kyoto University, Kyoto, 606-8502*

Abstract

We calculate the possible constraints we can put on alternative theories of gravity such as Brans-Dicke and massive gravity theories by gravitational waves from inspiral compact binaries. We take both precession and small eccentricity into account for the first time. We perform Monte Carlo simulations and by using the Fisher analysis, we estimate the determination accuracy of binary parameters including the Brans-Dicke parameter and the graviton Compton wavelength. By using LISA, although the constraint on Brans-Dicke theory is several times weaker than the current strongest one, the constraint on the mass of graviton is four orders of magnitude stronger than the one obtained by the solar system experiment. With DECIGO, the former constraint increases considerably.

1 Introduction

One of the approaches to solve dark energy problem is to modify gravitational theory from general relativity. In this paper, we consider two simple modifications of gravity. One is to add scalar degree of freedom to gravity. This theory is called scalar-tensor theory [1]. This theory also appears in inflation problem and superstring theory. A prototype of scalar-tensor theory is Brans-Dicke theory [2]. This theory is characterised by a parameter $\omega_{\rm BD}$ and by taking the limit $\omega_{\rm BD} \to \infty$, it reduces to general relativity. The current strongest bound on $\omega_{\rm BD}$ is the Cassini bound obtained from the solar system experiment [3]; $\omega_{\rm BD,Cassini} > 40000$.

Another type of modification of gravity introduces a finite mass m_g to a graviton (see [4] for a recent review). This type of theory is called the massive gravity theory. From the solar system experiment, the constraint on graviton Compton wavelength λ_g (which is defined as $\lambda_g \equiv h/m_g c$) has been obtained, by using Kepler's third law, as $\lambda_g > 2.8 \times 10^{17}$cm [5].

The aim of our work is to investigate how strongly we can constrain $\omega_{\rm BD}$ in the strong field regime by detecting gravitational waves from compact object binaries. In Brans-Dicke theory, the additional scalar field contains the dipole radiation [6, 7]. This modifies the binary's orbital evolution from the one in general relativity. The change in the orbital evolution due to this dipole radiation modifies the phasing of the gravitational waveform. In massive gravity theories, the propagation speed of gravitational wave depends on its frequency, which modifies the time of arrival from general relativity. This also affects the phasing of the gravitational waveforms [8]. Recently, Berti *et al.* [9] estimated how accurately one can determine these additinal parameters by using space interferometer LISA. We extend their work by including two important effects, precessions and eccentricities. We also calculate the constraints in the case of using DECIGO.

2 Waveforms

For the waveforms, we use the restricted 2PN waveforms. The Fourier component of binary gravitational waveform in Brans-Dicke theory or massive gravity theory is given by [10]

$$\tilde{h}(f) = \frac{\sqrt{3}}{2}\frac{5}{4}\mathcal{A} f^{-7/6} e^{i\Psi(f)} \left[A^{\rm prec}_{{\rm pol},\alpha}(t(f))\right] e^{-i\left(\varphi^{\rm prec}_{{\rm pol},\alpha}+\varphi_D\right)}, \tag{2.1}$$

[1]Email address: kent@tap.scphys.kyoto-u.ac.jp
[2]Email address: tanaka@yukawa.kyoto-u.ac.jp

where the amplitude $\mathcal{A}$, the polarisation amplitude $A^{\rm prec}_{{\rm pol},\alpha}$, the polarisation phase $\varphi^{\rm prec}_{{\rm pol},\alpha}$ and the Doppler phase φ_D are defined in Ref. [10]. The phase $\Psi(f)$ is given by [10]

$$\begin{aligned}\Psi(f) = 2\pi f t_c - \phi_c - \frac{\pi}{4} + \frac{3}{128}(\pi\mathcal{M}f)^{-5/3}\Bigg[1 - \frac{2355}{1462}I_e f^{-19/9} - \frac{5}{84}\mathcal{S}^2\bar{\omega}x^{-1} \\ - \frac{128}{3}\beta_g\eta^{2/5}x + \left(\frac{3715}{756} + \frac{55}{9}\eta\right)x - 4(4\pi - \beta)x^{3/2} \\ + \left(\frac{15293365}{508032} + \frac{27145}{504}\eta + \frac{3085}{72}\eta^2 - 10\sigma\right)x^2\Bigg].\end{aligned} \tag{2.2}$$

Here, t_c and ϕ_c are the coalescence time and phase, respectively. $\mathcal{M} \equiv \mu^{3/5}M^{2/5}$ is the chirp mass with M being the total mass and μ being the reduced mass, and $\eta \equiv \mu/M$ is the symmetric mass ratio. We defined the squared typical velocity, $x \equiv v^2 = (\pi M f)^{2/3}$. The first term in the square brackets represents the lowest order quadrupole approximation of general relativity. The second term is the contribution from small eccentricity. I_e is the asymptotic eccentricity invariant defined in Ref. [11]. The third term represents the dipole gravitational radiation in Brans-Dicke theory. $\bar{\omega} \equiv \omega_{\rm BD}^{-1}$ is the inverse of the Brans-Dicke parameter. $\mathcal{S} \equiv s_2 - s_1$ with s_i, the so-called *sensitivity*, is defined in Ref. [9, 10]. This roughly equals to the binding energy of the body per unit mass. Binaries with large $\mathcal{S}$ are the ones composed of bodies of different types.

The fourth term is the contribution from the mass of graviton. When graviton is massive, the propagation speed is slower than the speed of light, which modifies the gravitational wave phase from general relativity. β_g is defined as [9, 10] $\beta_g \equiv \pi^2 D\mathcal{M}/\lambda_g^2(1+z)$, where z is the cosmological redshift and the distance D is defined in Ref. [9, 10]. The remaining terms are the usual higher order PN terms in general relativity, where β and σ are spin-orbit coupling and spin-spin coupling, respectively.

Since the polarisation amplitude $A^{\rm prec}_{{\rm pol},\alpha}$ and the polarisation phase $\varphi^{\rm prec}_{{\rm pol},\alpha}$ depend on the direction of the orbital angular momentum $\hat{\mathbf{L}}$, precession affects the waveform through these two quantities. For simplicity, we assume that one of the spins of the binary constituents is negligible. Under this so-called simple precession approximation, the precession equations can be solved analytically [12, 13].

3 Numerical Calculations and Results

We perform the Monte Carlo simulation and estimate the statistical determination accuracies $\Delta\theta^i$ of binary parameters θ^i by using Fisher analysis. $\Delta\theta^i$ can be calculated as $\Delta\theta^i = \sqrt{\Sigma^{ii}}$, where the covariance matrix Σ^{ij} is the inverse of the Fisher matrix $\Gamma_{ij} \equiv (\partial_i h|\partial_j h)$. Here, ∂_i represents the derivative with respect to θ^i and the inner product $(A|B)$ is defined in Ref. [10].

For Brans-Dicke theory, we consider $(1.4{+}10^3)\mathrm{M}_\odot$ NS/BH binaries for LISA and $(1.4{+}10)\mathrm{M}_\odot$ NS/BH binaries for DECIGO. We assume that the signal to noise ratio (SNR) is $\sqrt{200}$ and the difference between NS and BH sensitivities $\mathcal{S}$ is 0.3. For massive gravity case, we think of $(10^7{+}10^6)\mathrm{M}_\odot$ BH/BH binaries for LISA and $(10^6{+}10^5)\mathrm{M}_\odot$ BH/BH binaries for DECIGO. We fix the distances of these binaries to 3 Gpc in this case. We assume that observation starts 1 year before coalescence.

There are 15 parameters in total, which are listed in Ref. [10]. Out of these, we are particularly interested in the determination accuracies of $\bar{\omega}$ and β_g. To perform Monte Carlo simulations, we randomly generate the following 6 quantities: the inner product of the orbital angular momentum and the total spin angular momentum κ; the precession angle α_c (which is defined in Ref. [10]); $(\theta_{\rm S}, \phi_{\rm S})$ for the initial direction of the source; $(\theta_{\rm J}, \phi_{\rm J})$ for the initial direction of the total angular momentum. We calculate the parameter estimation errors for each binary and take the average.

We found that inclusion of eccentricity weakens the constraints. This is because the parameters are strongly correlated and adding parameters dilutes the binary information in the detected gravitational waves. However, when we include the prior information of $\Delta I_e > 0$, we found that the constraint on $\omega_{\rm BD}$ becomes the same as the one without including eccentricity into binary parameters. For massive gravity case, the effect of eccentricity is weaker compared to Brans-Dicke case. This is because the frequency dependence of the eccentricity, Brans-Dicke and massive gravity terms in the phase $\Psi(f)$ (Eq. (2.2)) is $f^{-19/9}$, $f^{-2/3}$ and $f^{2/3}$, respectively, so that eccentricity has more degeneracy with $\omega_{\rm BD}$ than with λ_g.

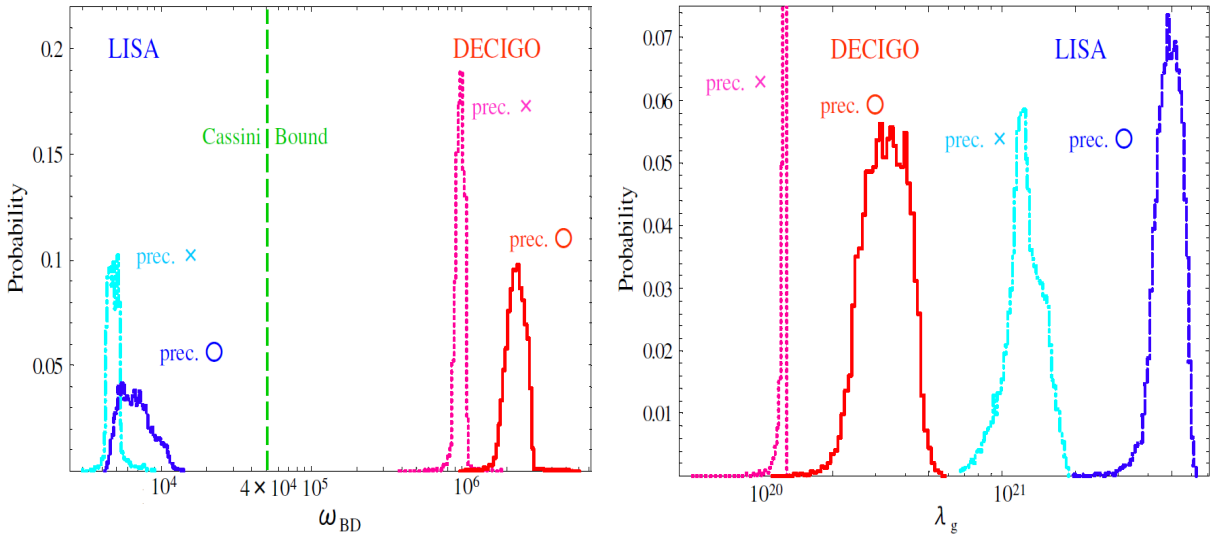

Figure 1: (Left) The histograms showing the probability distribution of the lower bound of $\omega_{\rm BD}$ obtained from our Monte Carlo simulations of 10^4 NS/BH binaries in Brans-Dicke theory. We take the masses of the binaries as $(1.4+10^3)M_\odot$ for LISA and $(1.4+10)M_\odot$ for DECIGO with SNR$=\sqrt{200}$. The (light blue) dotted-dashed histogram shows the constraint without precession and the (blue) dashed one represents the one including precession. The (purple) dotted one represents the estimate without precession and the (red) solid one shows the one including precession using DECIGO. The (green) dashed line at $\omega_{\rm BD}=4\times10^4$ represents the Cassini bound [3]. (Right) The histograms showing the probability distribution of the lower bound of λ_g obtained from our Monte Carlo simulations of 10^4 BH/BH binaries in massive gravity theories. We take the masses of the binaries as $(10^7+10^6)M_\odot$ for LISA and $(10^6+10^5)M_\odot$ for DECIGO at 3Gpc.

In Fig. 1, we show the probability distribution of $\omega_{\rm BD}$ (in the left panel) and λ_g (in the right panel) with and without including precession whilst eccentricity is not included into binary parameters. The (light blue) dotted-dashed histogram shows the constraint without precession and the (blue) dashed one represents the one including precession. The (purple) dotted one represents the estimate without precession and the (red) solid one shows the one including precession using DECIGO. The (green) dashed line at $\omega_{\rm BD}=4\times10^4$ in the left panel represents the Cassini bound [3] From these results it can be seen that the effect of precession makes the constraints stronger. This is due to the fact that precession disentangles the degeneracies between binary parameters. We found that for LISA, the constraint on $\omega_{\rm BD}$ is several times weaker than the Cassini bound, whilst the constraint is 200 times stronger than the Cassini bound when we use DECIGO. This is mainly because the number of gravitational wave cycles is larger for DECIGO and also because the noise levels of DECIGO are lower than that of LISA. For the massive gravity case, the constraint on λ_g is four orders of magnitude stronger than the one from solar sytem experiment when we use LISA. In this case, the constraint obtained by DECIGO is slightly weaker than the one with LISA. This is because the masses of binaries are larger for LISA.

4 Conclusions

We estimated how strongly we can put constraints on $\omega_{\rm BD}$ and λ_g by detecting gravitational waves from inspiralling compact binaries using LISA and DECIGO. We included the effects of eccentricity and precession for the first time. In order to estimate the constraints, we performed following Monte Carlo simulations. We randomly distribute 10^4 binaries all over the sky, evaluate the parameter estimation accuracies for each binary, and take the average. We found that inclusion of eccentricity makes the constraints weaker but the effect of precession enhances the constraints. For the Brans-Dicke case, by

using NS/BH binaries with SNR=$\sqrt{200}$, the constraint by LISA is weaker compared to the Cassini bound whilst DECIGO can put 200 times stronger constraint than the Cassini one. Unlike the case of LISA, these binaries are thought to be the definite sources for DECIGO. The event rate of NS/NS binary mergers is estimated to be 10^5 yr^{-1} [14], and the rate of NS/BH mergers will be about one order of magnitude smaller than that of NS/NS mergers (see Shibata *et al.* [15] and references therein). Therefore it is possible to put even stronger constraint by performing a statistical analysis. In this case, we found that the constraint becomes $\omega_{\rm BD} > 5.74 \times 10^7$. This is three orders of magnitude stronger than the Cassini bound.

For massive gravity case, by using BH/BH binaries at 3 Gpc, LISA can put four orders of magnitude stronger constraint than the one obtained by the solar system experiment. We found that the constraint with DECIGO is slightly weaker than the one with LISA. Please see Refs. [10, 16] for more details.

Acknowledgments

We thank Naoki Seto and Takashi Nakamura for useful discussions and valuable comments. This work is in part supported by the Grant-in-Aid for Scientific Research Nos. 19540285 and 21244033. This work is also supported in part by the Grant-in-Aid for the Global COE Program "The Next Generation of Physics, Spun from Universality and Emergence" from the Ministry of Education, Culture, Sports, Science and Technology (MEXT) of Japan.

References

[1] Y. Fujii and K. Maeda, *The Scalar-Tensor Theory of Gravitation*, Cambridge University Press (2007).

[2] C. Brans and R. H. Dicke, Phys. Rev. **124**, 925 (1961).

[3] B. Bertotti, L. Iess and P. Tortora, Nature **425**, 374 (2003).

[4] V. A. Rubakov and P. G. Tinyakov, Phys. Usp. **51**, 759 (2008).

[5] C. Talmadge, J. P. Berthias, R. W. Hellings and E. M. Standish, Phys. Rev. Lett. **61**, 1159 (1988).

[6] C. M. Will, Astrophys. J. **214**, 826 (1977).

[7] C. M. Will and H. W. Zaglauer, Astrophys. J. **346**, 366 (1989).

[8] C. M. Will, Phys. Rev. **D57**, 2061 (1998).

[9] E. Berti, A. Buonanno and C. M. Will, Phys. Rev. **D71**, 084025 (2005).

[10] K. Yagi and T. Tanaka, arXiv:0906.4269 [gr-qc]

[11] A. Krolak, K. D. Kokkotas and G. Schaefer, Phys. Rev. **D52**, 2089 (1995).

[12] T. A. Apostolatos, C. Cutler, G. J. Sussman, and K. S. Thorne, Phys. Rev. **D49**, 6274 (1994).

[13] A. Vecchio, Phys. Rev. **D70**, 042001(2004).

[14] C. Cutler and J. Harms, Phys. Rev. **D73**, 042001 (2006).

[15] M. Shibata, K. Kyutoku, T. Yamamoto and K. Taniguchi, Phys. Rev. **D79**, 044030 (2009).

[16] K. Yagi and T. Tanaka, arXiv:0908.3283 [gr-qc]

Numerical Study of Ring Objects in Five-dimensional Spacetime[1]

Yuta Yamada[2] and Hisa-aki Shinkai[3]

Faculty of Information Science and Technology, Osaka Institute of Technology, Hirakata, Osaka 573-0196

Abstract

We numerically investigated thin ring in five-dimensional spacetime, both of the sequences of initial data and their initial time evolution. Regarding to the initial data, we modeled the matter in non-rotating homogeneous toroidal configurations under the momentarily static assumption, solved the Hamiltonian constraint equation, and searched the apparent horizon. We discussed when S^3 (black hole) or $S^1 \times S^2$ (black ring) horizons ("black objects") are formed. By monitoring the location of the maximum Kretchmann invariant, an appearance of 'naked singularity' or 'naked ring' under the special situations is suggested. We also discuss the validity of the hyper-hoop conjecture using minimum area around the object.

We also show initial few time evolutions under the maximal time slicing condition, expressing the matter with collisionless particles. We found the dynamical behaviors are different depending on the initial ring radius.

1 Introduction

In higher dimensional general relativity(GR), there are two interesting problems. One is the cosmic censorship hypothesis (CCH) originally proposed in $3+1$ dimensional GR. CCH states collapse driven singularities will always be clothed by event horizon and hence can never be visible from the outside. By contrast, *hyper-hoop* conjecture[1] states that black holes will form when and only when a mass M gets compacted into a region whose $(D-3)$ dimensional area V_{D-3} in every direction is $V_{D-3} \leq G_D M$. There are some semi-analytic studies(e.g. [2]), but the validity and/or generality is unknown.

The other problem is stability of five-dimensional black-hole solutions. The four-dimensional black-holes are known to be S^2 from the topological theorem, while in higher-dimensional spacetime quite rich structures are available including "black ring(s)" [3]. There is, however, no confirmation for stability of such black-ring solutions.

In this report, we show the sequence of the initial data for the toroidal matter configurations. We investigate the validity of hyper-hoop conjecture by searching apparent horizons, and predict dynamics by evaluating the area of horizons[4]. Using the $4+1$ ADM formalism, we next show initial few steps of time evolutions of the initial data under the maximal time slicing condition.

2 Momentarily Static Black Ring Initial Data

2.1 The Hamiltonian constraint equation

We construct the initial data sequences on a four-dimensional space-like hypersurface. A solution of the Einstein equations is obtained by solving the Hamiltonian constraint equation if we assume the moment of time symmetry. We apply the standard conformal approach[5] to obtain the four-metric γ_{ij}. If we assume conformally flat trial metric $\hat{\gamma}_{ij}$, the equations would be simplified with a conformal transformation,

$$\gamma_{ij} = \psi^2 \hat{\gamma}_{ij} = \psi(X,Z)^2 (dX^2 + dZ^2 + X^2 d\vartheta_1 + Z^2 d\vartheta_2), \tag{2.1}$$

[1]The detail report of the content on the initial data is available as [4].

[2]Email address: m1m08a26@info.oit.ac.jp

[3]Email address: shinkai@is.oit.ac.jp

where $X = \sqrt{x^2+y^2}$, $Z = \sqrt{z^2+w^2}$, $\vartheta_1 = \tan^{-1}(y/x)$, and $\vartheta_2 = \tan^{-1}(z/w)$. By assuming ϑ_1 and ϑ_2 are the angle around the axis of symmetry, then the Hamiltonian constraint equation effectively becomes

$$\frac{1}{X}\frac{\partial}{\partial X}\left(X\frac{\partial \psi}{\partial X}\right) + \frac{1}{Z}\frac{\partial}{\partial Z}\left(Z\frac{\partial \psi}{\partial Z}\right) = -4\pi^2 G_5 \rho, \tag{2.2}$$

where ρ is the effective Newtonian mass density, G_5 is the gravitational constant in five-dimensional theory of gravity. We consider the cases with homogeneous toroidal matter configurations, described as

$$\left(\sqrt{x^2+y^2} - R_c\right)^2 + \left(\sqrt{w^2+z^2}\right)^2 \leq R_r^2, \tag{2.3}$$

where R_c is the circle radius of toroidal configuration, and R_r is the ring radius. This case is motivated from the "black ring" solution [3] though not including any rotations of matter nor of the spacetime. From obtained initial data, we also searched the location of an apparent horizon and the maximum value of the Kretchmann invariant $\mathcal{I}_{\max}$.

2.2 Definition of Hyper-Hoop

We also calculate hyper-hoop which is defined by two-dimensional area. We propose to define the hyper-hoop V_2 as a surrounding two-dimensional area which satisfies the local minimum area condition, $\delta V_2 = 0$. When the area of the spacetime outside the matter is expressed by the coordinate r, then $\delta V_2 = 0$ leads to the Euler-Lagrange type equation for $V_2(r, \dot{r})$. The hoop is expressed using $r = r_h(\phi)$ as

$$V_2^{(C)} = 4\pi \int_0^{\pi/2} \psi^2 \sqrt{\dot{r_h}^2 + r_h^2} r_h \cos\phi \, d\phi, \quad \text{or} \quad V_2^{(D)} = 4\pi \int_0^{\pi/2} \psi^2 \sqrt{\dot{r_h}^2 + r_h^2} r_h \sin\phi \, d\phi, \tag{2.4}$$

where $r = \sqrt{X^2+Z^2}$ and $\phi = \tan^{-1}(Z/X)$. $V_2^{(C)}$ expresses the surface area which is obtained by rotating respect to the Z-axis, while $V_2^{(D)}$ is the one with X-axis rotation. We also calculate hyper-hoop with $S^1 \times S^1$ topology for the toroidal cases, $V_2^{(E)}$,

$$V_2^{(E)} = 2\pi \int_0^{\pi} \psi^2 \sqrt{\dot{r_h}^2 + r_h^2} (r_h \cos\xi + R_c) \, d\xi, \tag{2.5}$$

where $r = \sqrt{(X-R_c)^2 + Z^2}$ and $\xi = \tan^{-1}[Z/(X-R_c)]$.

2.3 Horizons and their area

Fig.1 shows two typical shapes of apparent horizons. We set the ring radius as $R_r/r_s = 0.1$ and search the sequence with changing the circle radius R_c. When R_c is less than $0.78 r_s$, we find that only the S^3-apparent horizon ("common horizon" over the ring) exists. On the other hand, when R_c is larger than $R_c = 0.78 r_s$, only the $S^1 \times S^2$ horizon ("ring horizon", hereafter) is observed.

We find that $\mathcal{I}_{\max}$ appears at the outside of matter configuration. Interestingly, $\mathcal{I}_{\max}$ is not hidden by the horizon when R_c is larger [see the case (c) of Fig.1]. Therefore, if the ring matter shrinks itself to the ring, then a "naked ring" (or naked di-ring) might be formed.

We show the surface area of the apparent horizons A_3 left panel in fig.2. In left panel of fig.2, typical two horizons monotonically decrease with R_c/r_c, the largest one is when the matter is in the spheroidal one ($R_c/r_c = 0$). We also observe that the area of the common horizon is always larger than those of the ring horizon and both are smoothly connected in the plot. If we took account the analogy of the thermodynamics of black-holes, this suggest that the black-ring evolves to shrink its circle radius, and the ring horizon will switch to the common horizon at a certein radius.

Right panel in fig.2 shows the hyper-hoop $V_2^{(C)}$, $V_2^{(D)}$, and $V_2^{(E)}$. We plot the points where we found hyper-hoops. We note that $R_c/r_s = 0.78$ is the switching radius from the common horizon to the ring horizon, and that $V_2^{(C)}$ and $V_2^{(D)}$ are sufficiently smaller than unity if there is a common horizon. Therefore, hyper-hoop conjecture is satisfied for the formation of common horizon. On the other hand, for the ring horizon, we should consider the hoop $V_2^{(E)}$. In right panel of fig.2, in the region $R_c/r_s > 0.78$,

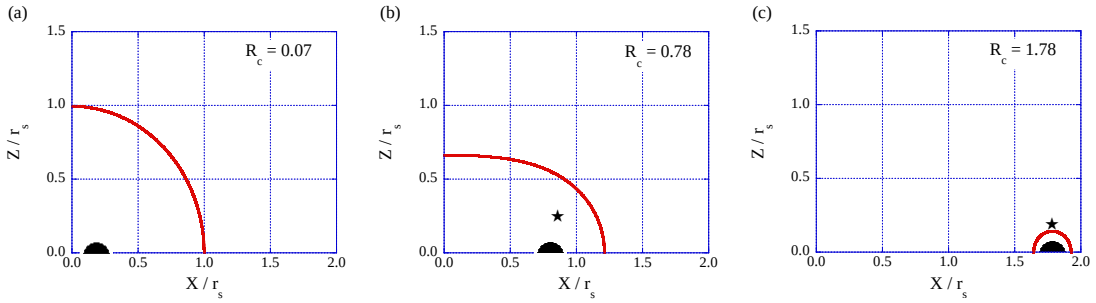

Figure 1: Matter distributions (shaded) and the location of the apparent horizon (line) for toroidal matter configurations. The asterisk indicates the location of the maximum Kretchmann invariant, $\mathcal{I}_{max}$.

$V_2^{(E)}$ exists only a part in this region and becomes larger than unity. Hence, for the ring horizon, the hyper-hoop conjecture is not a proper indicator. We conclude that the hyper-hoop conjecture is only consistent with the formation of common horizon as far as our definition of the hyper-hoop is concerned.

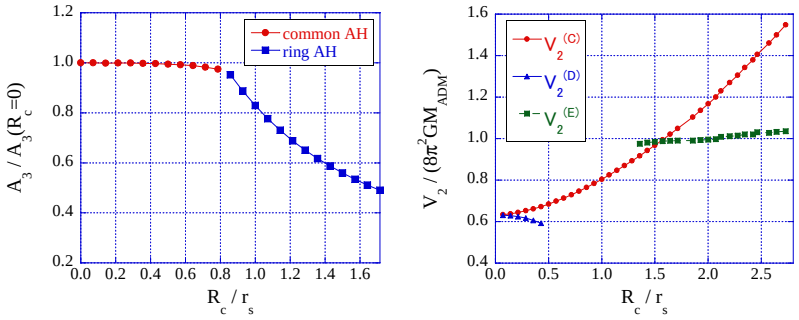

Figure 2: (Left) The area of the apparent horizon A_3. Plots are normalized by the area of spherical case ($R_c = 0$). We see both horizons' area are smoothly connected at $R_c/r_s = 0.78$, and both monotonically decrease with R_c/r_s. (Right) The ratio of the hyper-hoops V_2 to the mass M_{ADM} are shown for the sequence of Fig.1. The ratio less than unity indicates that the validity of the hyper-hoop conjecture.

3 Time Evolution of Toroidal Matter

We developed a numerical code to follow the dynamics of five-dimensinal spacetime. The gravitational field is integrated using the $4+1$ ADM formalism. Evolution equations are written as

$$\frac{\partial \gamma_{ij}}{\partial t} = -2\alpha K_{ij} + D_i\beta_j + D_j\beta_i, \quad \text{and} \tag{3.1}$$

$$\frac{\partial K_{ij}}{\partial t} = \alpha({}^{(4)}R_{ij} + KK_{ij}) - 2\alpha K_{il}K^{lj} - 12\pi^2\alpha(S_{ij} + \frac{1}{3}\gamma_{ij}(\rho - S)) - D_iD_j\alpha + D_i\beta^m K_{mj} + D_j\beta^m K_{mi} + \beta^m D_m K_{ij}, \tag{3.2}$$

where α is the lapse function, β_i the shift vector, and γ_{ij}, K_{ij}, and S_{ij} represent intrinsic metric, extrinsic curvature and stress tensor, respectively.

We express the matter with collisionless particles which move along the geodesic equation. For the lapse condition, we apply the maximal time slicing condition, so as not to hit a singularity in time evolution. We fix the shift vector as $\beta^i = 0$. We wrote our code using the Cartesian coordinate.

Fig.3 shows the lapse function on x-axis($y, z, w = 0$). Left panel shows matter region, ring horizon, and lapse function at $t = 0$. When horizon exists on the initial data, the magnitude of the lapse function

is less than 0.6 inside the horizon. By contrast, center and right panels show the cases of initial data without horizon, for the different initial ring radius. Snapshots of the lapse function imply that the local gravity evolves stronger, and the both lapse becomes less than 0.6 locally. We think that common horizon have possibilities to be formed for center figure because of the magnitude of lapse function less than 0.6. Also, we expect the formation of a ring horizon near $x/r_s = 3.2$ for right case.

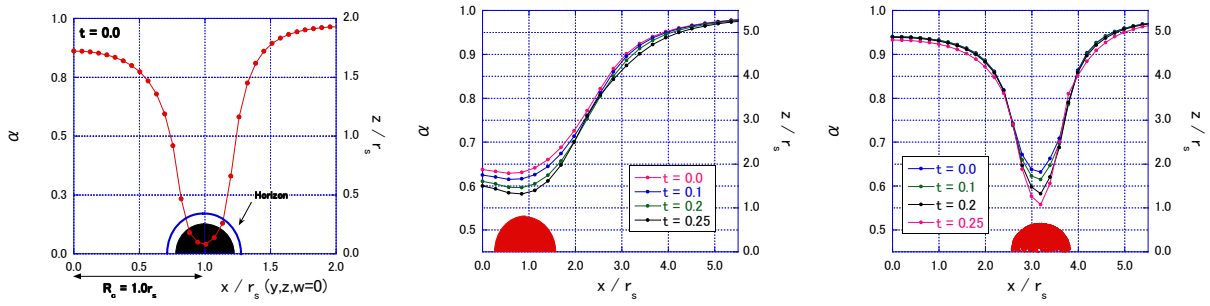

Figure 3: (Left) Matter distributions (shaded), the location of the apparent horizon and lapse function on the initial hypersurface, $t = 0$. (Center, Right) the snapshots of lapse function with the time for the initial data without horizon. Initial matter regions are also drawn.

4 Summary

With a purpose of investigating the stability of black-ring solutions, we constructed initial-data of ring objects in five-dimensional spacetime. By searching apparent horizons and hyper-hoop, we verified the hyper-hoop conjecture and predict the time evolution. We also developed a code to follow the dynamics and showed initial time evolution.

For the analysis of initial data, we found that the shape of the apparent horizon switches from the common horizon to the ring horizon at a certain circle radius, and the former satisfies the hyper-hoop conjecture, while the latter is not. The area of the horizon and the thermo-dynamical analogy of black holes, imply the dynamical feature of the black-ring: a black-ring will naturally switch to a single black-hole. However, if the local gravity is strong, then the ring might begin collapsing to a ring singularity, that might produce also to the formation of 'naked ring' since $\mathcal{I}_{max}$ appears on the outside of the ring for a certain initial configuration.

We also investigate the dynamics of this initial data using collisionless particles under the maximal time slicing condition. We found the dynamical behaviors are different depending on the initial ring radius.

The initial-data sequences we showed here do not include rotations in matter and spacetime, so that those studies are our next subject. In the near future, we plan to report the stability of black-ring solutions.

References

[1] D. Ida and K. Nakao, Phys. Rev. D. **66**, 064026 (2002).

[2] C-M. Yoo, K. Nakao and D. Ida, Phys. Rev. D. **71**, 104014 (2005).

[3] R. Emparan and H. S. Reall, Phys. Rev. Lett. **88**, 101101 (2002).

[4] Y. Yamada and H. Shinkai, Class. Quant. Grav. **27**, 045012 (2010) [arXiv:0907.2570].

[5] N. O Murchadha and J. W. York, Jr., Phys. Rev. D. **10**, 428 (1974).

[6] S. L. Shapiro and S. A. Teukolsky, Phys. Rev. Lett. **66**, 994 (1991).

Skewness in CMB temperature fluctuations from bended cosmic (super-)strings

Daisuke Yamauchi[1](a), Chul-Moon Yoo(b), Keitaro Takahashi(c), Atsushi Naruko(a), Yuuiti Sendouda(a) and Misao Sasaki(a)

(a) *Yukawa Institute for Theoretical Physics, Kyoto University, Kyoto, Japan*
(b) *Asia Pacific Center for Theoretical Physics, Pohang University of Science and Technology, Pohang 790-784, Korea*
(c) *Department of Physics and Astrophysics, Nagoya University, Nagoya 494-8602, Japan*

Abstract

We have computed the one-point pdf of small-angle CMB temperature fluctuations due to cosmic (super-)strings with a simple model of the bended long segments numerically and have showed that it reproduced the feature of the numerical simulation in Fraisse et al. [3], especially skewness in one-point probability distribution function. We found that skewness would appear if we take curvature of segment and its correlation with its velocity into account. If a segment has a curvature, the symmetry of temperature fluctuations between positive and negative value is broken and the amplitude of the asymmetry depends on the angle between the curvature vector and the velocity vector of the segment.

1 Introduction

Cosmic strings are line-like topological defects formed in the early universe through spontaneous symmetry breaking. Their energy per unit length μ is directly related to the energy scale of phase transition. Also cosmic strings have attracted interest of string cosmology community. The brane inflation model motivated by string theory may produce another class of string object,called string superstrings, that could be fundamental- or D-strings [1]. One of the observationally interesting differences is concerning the intercommuting probability P. It can be significantly smaller than unity for cosmic superstrings [2] while $P = 1$ is normally assumed for field-theoretic strings.

Thus, the imprint of cosmic strings on cosmic microwave background (CMB) has been widely studied. Although cosmic strings were excluded as a dominant source of the observed large angular scale anisotropy [4], the signal due to cosmic strings could still be observable at small scale [3, 4] with future arcminutes experiments [6]. The most characteristic signal from cosmic strings is Gott-Kaiser-Stebbins (GKS) effects [10]. When a photon passes through a moving straight string segment, it produces discontinuities of gravitational potential across the string segment.

Also, since the network of the cosmic strings is highly nonlinear object, non-Gaussian feature may help us distinguish cosmic string signals from other secondary effects and hence enhance the observability. Recently Fraisse et al. [3] found that one-point probability distribution function (pdf) of the temperature fluctuations has a non-Gaussian tail and negative skewness at least for $P = 1$. In particular, skewness is a measure of the asymmetry of the probability distribution and the simplest static characterizing the non-Gaussianity [5]. In this case, the skewness is defined by $g_1 \equiv \overline{(\Delta - \bar{\Delta})^3}/\sigma_\Delta^3$ where $\Delta \equiv \Delta T/T$, the bar corresponds to a statistical average over a CMB map and σ_Δ denotes the standard deviation of the probability distribution of the temperature fluctuations.

In [7], we computed analytically the one-point pdf of small-scale temperature fluctuations with a simple model of long straight segments and kinks with intercommuting probability P and study the effect of P. We found that the obtained one-point pdf consists of a Gaussian component due to frequent scatterings by long straight segments and a non-Gaussian tails due to close encounters with kinks. Notice that our one-point pdf is symmetric for positive and negative temperature fluctuation and cannot reproduce the non-zero skewness reported in [3]. This is because we have assumed the long segments to be straight.

[1]Email address: yamauchi@yukawa.kyoto-u.ac.jp

However, the skeness would appear if we take curvature of segment and its correlations with its velocity into account. If a segment has a curvature, the symmetry of temperature fluctuations between positive and negative value is broken and the amplitude of the asymmetry depends on the angle between the curvature vector and the velocity vector of the segment. Therefore, if there is a correlation between velocity and curvature, there would be a skewness of one-point pdf. Furthermore, one can see that the correlation between curvature and velocity of segments requires the breaking of time reversal symmetry, in short cosmic expansion in string network.

In this paper, we compute the one-point pdf of small-angle CMB temperature fluctuations due to cosmic (super-)strings numerically. At small scales where primary fluctuations are damped, only the integrated Sachs-Wolfe (ISW) effect is relevant. We focus on the ISW effect of long segments with the curvature of the segments and its correlations with its velocity taken into account.

2 Analytic model of string network and temperature fluctuations due to string segments

We summarize the equations for the evolution of the string segments by extending a velocity-dependent one-scale model in cosmological background with a intercommuting probability, following [7, 9].

The evolution of the network of segments with the correaltion length ξ and root-mean-square velocity $v_{\rm rms}$ is determined by the cosmic expansion and the energy loss due to loop formation. A loop formation can occur through the intercommutation of two segments or self-intercommutation of a single segment. The characteristic timesscale for loop formation with intercommutation probability P is $\sim \xi/Pv_{\rm rms}$. For a universe with the scale factor $a(t) \propto t^\beta$, the equation of motion for γ and $v_{\rm rms}$ are given by

$$\frac{t}{\gamma}\frac{d\gamma}{dt} = 1-\beta-\frac{1}{2}\beta\tilde{c}Pv_{\rm rms}\gamma-\beta v_{\rm rms}^2\,,\quad \frac{dv_{\rm rms}}{dt} = (1-v_{\rm rms}^2)\left[\frac{k}{\xi}-2Hv_{\rm rms}\right], \tag{2.1}$$

where $\tilde{c}$ is a constant which represents the efficiency of the loop formation. In particular, k denotes the momentum parameter defined by

$$k \equiv \frac{\xi}{a(\eta)v_{\rm rms}(1-v_{\rm rms}^2)}\left\langle \dot{\mathbf{r}}\cdot\frac{1}{\epsilon}\left(\frac{\mathbf{r}'}{\epsilon}\right)'\right\rangle. \tag{2.2}$$

where we have used the averaged symbol given by $\langle\cdots\rangle \equiv \int\cdots\epsilon d\sigma/\int\epsilon d\sigma$ with $\epsilon^2 = \mathbf{r}'^2/(1-\dot{\mathbf{r}}^2)$.

Hereafter, we assume a matter-domination era and set, i.e. $\beta = 2/3$ and identify $R = \xi$ for simplicity. It is known that a string network approaches a so-called scaling regime where the characteristic scale grows with the horizon size. One can see that for small $\tilde{c}P$, Eq. (2.1) can be solved as [7]

$$v_{\rm rms} \approx \sqrt{\frac{1}{2}\left[1-\sqrt{\frac{\pi\tilde{c}P}{3\sqrt{2}}}\right]}\,,\ \gamma \approx \frac{2v_{\rm rms}}{k(v_{\rm rms})} \approx \sqrt{\frac{\pi\sqrt{2}}{3\tilde{c}P}}\,, \tag{2.3}$$

where we have used the approximated form $k = (2\sqrt{2}/\pi)(1-8v_{\rm rms}^6)/(1+8v_{\rm rms}^6)$ [9].

The GKS and kink temperature fluctuations produce the symmetric one-point pdf for positve and negative value as shown in [7]. We should introduce the general formulae for the temperature fluctuations due to cosmic strings. It is known that the temperature fluctuations from a Nambu-Goto action is developed by Stebbins, Veeraraghavan and Hindmarsh [11]. At small scale, Hindmarsh-Stebbins-Veeraraghavan (HSV) formula is

$$\Delta(\mathbf{n}\,,\mathbf{r}_{\rm obs}\,,\eta_{\rm obs}) = -2G\mu\int d\sigma\frac{(1+\mathbf{n}\cdot\dot{\mathbf{r}})\left[(X\mathbf{n}+\mathbf{X})\cdot\mathbf{u}\right]}{(X+\mathbf{n}\cdot\mathbf{X})\,(X-\dot{\mathbf{r}}\cdot\mathbf{X})}\bigg|_{\eta=\eta_{\rm lc}(\sigma)}, \tag{2.4}$$

where $\mathbf{X}(\sigma,\eta) \equiv \mathbf{r}_{\rm obs}-\mathbf{r}(\sigma,\eta)$ is a comoving position of a comoving observer from the string, $\mathbf{u}$ is a vector which represents the stress tensor distortion given by $\mathbf{u} = \dot{\mathbf{r}} - [(\mathbf{n}\cdot\mathbf{r}')/(1+\mathbf{n}\cdot\dot{\mathbf{r}})]\mathbf{r}'$ and we have defined the light-cone time $\eta_{\rm lc}$ as $\eta_{\rm obs}-\eta_{\rm lc}(\sigma) = |\mathbf{X}(\sigma,\eta_{\rm lc}(\sigma))|$. Notice that the temperature fluctuation depends on the matter distribution on the observer's past light cone. Therefore, string trajectory is only required on our past light cone.

2.1 Correlations and Higher-order effects

As we discussed in Sec. 1, skewness would appear if we take curvature of segment and its correlation with its velocity into account. If a segment has a curvature, the symmetry of temperature fluctuations between positive and negative value is broken and the amplitude of the asymmetry depends on the angle between the curvature vector and the velocity vector of the segment. Therefore, if there is a correlation between velocity and curvature, there would be a nonzero expectation value for the asymmetry, i.e. skewness of one-point pdf.

It is clear to see that in scaling regime, we have the correlation:

$$\frac{1}{a}\left\langle \dot{\mathbf{r}} \cdot \frac{1}{\epsilon}\left(\frac{\mathbf{r}'}{\epsilon}\right)' \right\rangle = \frac{k}{\xi} v_{\rm rms}(1-v_{\rm rms}^2) \approx 2Hv_{\rm rms}^2\left(1-v_{\rm rms}^2\right) , \tag{2.5}$$

It is easy to see that the nontrivial correlation requires the nonzero Hubble expansion parameter. Hindmarsh et al. [12] suggested that the generation of a bispectrum by strings simply requires the breaking of time reversal symmetry as a FRW background.

Also, we find that there is an another correlation between the curvature and velocity of the segments, we call light-cone effect hereafter. From HSV formula of the temperature fluctuations Eq. (2.4), one has to integrate the temperature fluctuation along light-cone time $\eta_{\rm lc}(\sigma)$. Since the light-cone time depends only on worldsheet coordinate σ, the position of the segment in small angle limit can be approximated as

$$\mathbf{r}(\sigma,\eta_{\rm lc}(\sigma)) = \mathbf{r}_0 - \left[\mathbf{r}_0' + \left(\frac{d\eta_{\rm lc}}{d\sigma}\right)_0 \dot{\mathbf{r}}_0\right]\sigma - \left[\mathbf{r}_0'' + \left(\frac{d\eta_{\rm lc}}{d\sigma}\right)_0^2 \ddot{\mathbf{r}}_0 + 2\left(\frac{d\eta_{\rm lc}}{d\sigma}\right)_0 \dot{\mathbf{r}}_0' + \left(\frac{d^2\eta_{\rm lc}}{d\sigma^2}\right)_0 \dot{\mathbf{r}}_0\right]\sigma^2 + \tag{2.6}$$

where $d\eta_{\rm lc}/d\sigma$ and $d^2\eta_{\rm lc}/d\sigma^2$ can be estimated as:

$$\left(\frac{d\eta_{\rm lc}}{d\sigma}\right)_0 = -\frac{\mathbf{n}\cdot\mathbf{r}_0'}{1+\mathbf{n}\cdot\dot{\mathbf{r}}_0} , \tag{2.7}$$

$$\left(\frac{d^2\eta_{\rm lc}}{d\sigma^2}\right)_0 = -\frac{1}{1+\mathbf{n}\cdot\dot{\mathbf{r}}_0}\left[\frac{1-\dot{\mathbf{r}}_0^2}{X_0}\left\{\frac{\mathbf{r}_0'^{\,2}}{1-\dot{\mathbf{r}}_0^2} - \left(\frac{d\eta_{\rm lc}}{d\sigma}\right)_0^2\right\} + \mathbf{n}\cdot\left\{\mathbf{r}_0'' + \left(\frac{d\eta_{\rm lc}}{d\sigma}\right)_0^2 \ddot{\mathbf{r}}_0 + 2\left(\frac{d\eta_{\rm lc}}{d\sigma}\right)_0 \dot{\mathbf{r}}_0'\right\}\right] \tag{2.8}$$

where $X_0 \sim d_A/a$ can be approximated as a comoving angular-diameter distance in the small angle limit. It is surprising that string always seems to have a "effective curvature", which means $d^2\mathbf{r}/d\sigma_{\rm lc}^2 \neq 0$, and the effective curvature depends on the velocity of the segment even if string is exactly straight. This is because the intersecting surface between light-cone and string worldsheet always has the curvature. This correlation is also due to breaking of time reversal symmetry since the sign of this effect can determined by the direction of past light-cone. The important observation is that there always exists light cone effects regardless of scaling regime or other kind of evolution of the string network.

This is the mechanism we believe the skewness is induced from. In following section we will show that there really exists skewness in one-point pdf and these correlations play a important role as a generator of skewness.

3 One-point PDF

In order to confirm our prediction in previous section, we compute the one-point pdf of the small-angle CMB temperature fluctuations due to bended string segments included the correlations between the curvature and the velocity of the segments semi-numerically. In VOS model which describes the behavior of cosmic strings, we assume that the scaling behavior is already realized by the recombination time and each scattering of the photon ray with bended segments is assumed to occur at intervals of the mean free path of the photon ray. In addition, the bended segment is assumed to have a larger curvature radius than a length of the segment and we assume that higher derivative terms, i.e. $(\partial_\eta^m \partial_\sigma^n \mathbf{r})$ $(m+n \geq 3)$, are negligible small.

The obtained one-point pdfs are shown in Fig. 1 for $P = 1, 0.5, 0.1$. We found that the one-point pdf with the natural parameter sets has the negative skewness. As we see, the dispersion of the Gaussian part increases as P decreases and the contribution of the curvature of the segments, e.g. the skewness, and the non-Gaussian tail is suppressed.

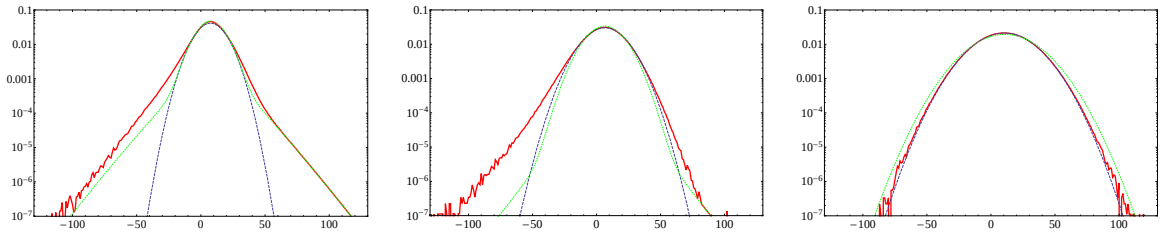

Figure 1: The one-point pdf of the CMB temperature fluctuations induced by bended cosmic strings with the intercommuting probability $P = 1, 0.5, 0.1$. The red line is the obtained one-point pdf numerically. Qualitatively, the standard deviations of the one-point pdf are $\sigma_{\rm sim}(P = 1) \approx 11.2G\mu$, $\sigma_{\rm sim}(P = 0.5) \approx 13.8G\mu$, $\sigma_{\rm sim}(P = 0.1) \approx 18.8G\mu$ the skewnesss are $g_1(P = 1) \approx -0.26$, $g_1(P = 0.5) \approx -0.18$, $g_1(P = 0.1) \approx -3 \times 10^{-5}$. The green dotted line represents the one-point pdf induced by exact straight segments and the kinks with the appropriate phenomenological parameters [7].

References

[1] S. Sarangi and S. H. H. Tye, Phys. Lett. B **536**, 185 (2002) [arXiv:hep-th/0204074]. A. C. Davis and T. W. B. Kibble, Contemp. Phys. **46**, 313 (2005) [arXiv:hep-th/0505050]. M. Majumdar, arXiv:hep-th/0512062.

[2] M. G. Jackson, N. T. Jones and J. Polchinski, JHEP **0510**, 013 (2005) [arXiv:hep-th/0405229].

[3] A. A. Fraisse, C. Ringeval, D. N. Spergel and F. R. Bouchet, Phys. Rev. D **78**, 043535 (2008) [arXiv:0708.1162 [astro-ph]].

[4] L. Pogosian, S. H. Tye, I. Wasserman and M. Wyman, JCAP **0902**, 013 (2009) [arXiv:0804.0810 [astro-ph]]. N. Bevis, M. Hindmarsh, M. Kunz and J. Urrestilla, Phys. Rev. Lett. **100**, 021301 (2008) [arXiv:astro-ph/0702223]. L. Pogosian and T. Vachaspati, Phys. Rev. D **60**, 083504 (1999) [arXiv:astro-ph/9903361]. L. Perivolaropoulos, Nucl. Phys. Proc. Suppl. **148**, 128 (2005) [arXiv:astro-ph/0501590].

[5] E. Komatsu and D. N. Spergel, Phys. Rev. D **63**, 063002 (2001) [arXiv:astro-ph/0005036].

[6] J. E. Ruhl *et al.* [The SPT Collaboration], Proc. SPIE Int. Soc. Opt. Eng. **5498**, 11 (2004) [arXiv:astro-ph/0411122]. A. Kosowsky, New Astron. Rev. **47**, 939 (2003) [arXiv:astro-ph/0402234].

[7] K. Takahashi, A. Naruko, Y. Sendouda, D. Yamauchi, C. M. Yoo and M. Sasaki, JCAP **0910**, 003 (2009) [arXiv:0811.4698 [astro-ph]].

[8] K. Takahashi, A. Naruko, Y. Sendouda, D. Yamauchi, C. M. Yoo and M. Sasaki, in preparation

[9] C. J. A. Martins and E. P. S. Shellard, Phys. Rev. D **65**, 043514 (2002) [arXiv:hep-ph/0003298]. C. J. A. Martins and E. P. S. Shellard, Phys. Rev. D **54**, 2535 (1996) [arXiv:hep-ph/9602271]. A. Avgoustidis and E. P. S. Shellard, Phys. Rev. D **73**, 041301 (2006) [arXiv:astro-ph/0512582].

[10] N. Kaiser and A. Stebbins, Nature **310** (1984) 391. J. R. I. Gott, Astrophys. J. **288**, 422 (1985).

[11] A. Stebbins and S. Veeraraghavan, Phys. Rev. D **51**, 1465 (1995) [arXiv:astro-ph/9406067]. A. Stebbins, Astrophys. J. **327**, 584 (1988). M. Hindmarsh, Astrophys. J. **431**, 534 (1994) [arXiv:astro-ph/9307040].

[12] M. Hindmarsh, C. Ringeval and T. Suyama, arXiv:0908.0432 [astro-ph.CO]. M. Hindmarsh, C. Ringeval and T. Suyama, arXiv:0911.1241 [astro-ph.CO]. D. M. Regan and E. P. S. Shellard, arXiv:0911.2491 [astro-ph.CO].

Density Fluctuations in Thermal Inflation and Non-Gaussianity

Shuichiro Yokoyama[1 (a)], Masahiro Kawasaki[(b),(c)] and Tomo Takahashi[(d)]

[(a)] *Department of Physics and Astrophysics, Nagoya University, Aichi 464-8602, Japan*
[(b)] *Institute for Cosmic Ray Research, University of Tokyo, Kashiwa 277-8582, Japan*
[(c)] *Institute for the Physics and Mathematics of the Universe, University of Tokyo, Kashiwa, Chiba, 277-8568, Japan*
[(d)] *Department of Physics, Saga University, Saga 840-8502, Japan*

Abstract

We present a mechanism of generating the primordial curvature perturbation at the end of thermal inflation utilizing a fluctuating coupling of a flaton field with the fields in thermal bath. We also discuss non-Gaussianity in the mechanism and show that large non-Gaussianity can be generated in this scenario.

1 Introduction

The thermal inflation [1], a mini-inflation which occurs long after the standard inflation, has been discussed, in particular, as a possible solution to the cosmological moduli problem. Here we would like to discuss another aspect of the thermal inflation. When one considers the thermal inflation, primordial fluctuations are usually assumed to be generated from the primordial inflation. However notice that the thermal inflation drives the number of e-folds of about 10 due to the large entropy production. This means that fluctuations corresponding to the present observational scales exit the horizon at later time compared with the case of no thermal inflation. Thus in this respect, the thermal inflation can also affect the predictions of primordial fluctuations. In fact, the primordial fluctuations are not necessarily generated from the inflaton fluctuations. Another light scalar field such as the curvaton, modulus in the modulated reheating scenario and so on are also known to generate (almost) scale-invariant and adiabatic primordial fluctuations consistent with observations. Although by adopting these scenarios, one can alleviate the above mentioned issue, however, here we propose another mechanism which can naturally arise in the framework of the thermal inflation. During the thermal inflation, the effective potential of a flaton, a flat direction in supersymmetric models, is lifted up by a thermal effect due to the coupling between the flaton and particles in thermal bath. The end of the thermal inflation is controlled by the strength of the thermal effect, or the coupling. If the coupling depends on some other scalar field and this scalar field fluctuates, the end of the thermal inflation also differ from place to place in the Universe via the fluctuations of the coupling. If the scalar field is light enough during inflation, almost scale-invariant density fluctuations can be achieved similarly to the case of the modulated reheating[2]. The structure of this paper is as follows. In the next section, we briefly describe the thermal inflation model which we consider here. In Section 3, we present a mechanism of generating the curvature perturbation at the end of thermal inflation and also discuss its non-Gaussianity. In Section 4, we discuss the current observational constraints for the simple chaotic inflation model in our scenario. The final section is devoted to summary of this paper.

2 Basic Picture of thermal inflation

In this section, we briefly review the idea of the thermal inflation [1]. The thermal inflation can be realized by utilizing a flat direction which exists in supersymmetric theory. Let us call such a direction

[1] Email address: shu@a.phys.nagoya-u.ac.jp

[2] In Ref. [2] the author has presented a mechanism of generating large scale curvature perturbation through the inhomogeneous cosmological phase transitions in the early universe. The mechanism proposed here is similar to this kind.

as a flaton field ϕ and assume that the potential of the flaton field is given by

$$V(\phi) = V_0 - \frac{1}{2}m^2\phi^2 + \frac{\lambda}{6}\frac{1}{M_{\rm Pl}^2}\phi^6 \ , \tag{2.1}$$

where the ϕ^2 term comes from soft supersymmetry breaking and we have neglected the higher order nonrenormalizable terms (ϕ^{2n+4}, $n \geq 2$). The VEV of ϕ is given by $\phi_{\rm vev} \equiv v_{\rm flaton} = \lambda^{-1/4} m^{1/2} M_{\rm Pl}^{1/2}$ and $V_0 = m^2 v_{\rm flaton}^2/3$ to have $V(v_{\rm flaton}) = 0$. When the flaton field interacts with some particles in thermal bath, such an interaction gives a thermal contribution to the potential and the total potential of the flaton field is given by

$$V_{\rm eff} = V_0 + \frac{1}{2}\left(gT^2 - m^2\right)\phi^2 + \frac{\lambda}{6}\frac{1}{M_{\rm Pl}^2}\phi^6 \ . \tag{2.2}$$

where g is an effective coupling between the flaton and particles in thermal bath and T is the cosmic temperature. After the standard primordial inflation ends followed by the reheating, the cosmic temperature decreases as the Universe expands. Then, at some temperature when V_0 gets larger than the background radiation energy density, the Universe is dominated by the false vacuum of the flaton's potential, which drives a mini-inflation. When the temperature of the Universe has dropped down to $T = T_c = m/\sqrt{g}$, the flaton starts rolling down to the VEV and then the mini-inflation ends. The total entropy S of the Universe after the thermal inflation increases by a factor $\Delta_S = s(T_r)a_r^3/s(T_c)a_c^3$ where a_r and a_c are the scale factor at the reheating after the thermal inflation and the end of the thermal inflation, respectively. s is the entropy density and T_r is the reheating temperature after the thermal inflation. Δ_S can be estimated as

$$\Delta_S = \frac{4V_0}{3T_r}\frac{45}{2\pi^2 g_* T_c^3} \simeq 0.01\frac{v_{\rm flaton}^2}{mT_r}, \tag{2.3}$$

where $g_*(\simeq 100)$ counts the effective degrees of radiation. Then $\Delta N_{\rm th}$ which describes the e-folds during thermal inflation is estimated as

$$\Delta N_{\rm th} = \frac{1}{3}\ln\Delta_S \simeq 12 - \frac{1}{3}\ln\left(\frac{m}{10^2\ {\rm GeV}}\right) - \frac{1}{3}\ln\left(\frac{T_r}{\rm GeV}\right) + \frac{2}{3}\ln\left(\frac{v_{\rm flaton}}{10^{10}\ {\rm GeV}}\right). \tag{2.4}$$

3 Curvature perturbation generated at the end of thermal inflation

Now we discuss the generation of density fluctuations at the end of the thermal inflation. Based on δN formalism, the curvature perturbation on the uniform energy density hypersurface, ζ, on super-horizon scales is given by the difference of the neighbor background trajectories, which is parametrized by the e-folds. We assume that the coupling g depends on a light scalar field σ, namely, $g = g(\sigma)$. Then the coupling g can fluctuate due to the fluctuation of the light field σ which originates to quantum fluctuations during inflation and hence the fluctuation of the coupling g gives rise to the inhomogeneous end of thermal inflation. In such case, the curvature perturbation from fluctuations of σ at the end of thermal inflation can be given by, up to the second order,

$$\zeta = \delta N = -\frac{\delta T_c}{T_c} + \frac{1}{2}\left(\frac{\delta T_c}{T_c}\right)^2 = \frac{1}{2}\frac{g'}{g}\delta\sigma_* + \frac{1}{4}\left[\frac{g''}{g} - \left(\frac{g'}{g}\right)^2\right]\delta\sigma_*^2 \ , \tag{3.1}$$

where a prime denotes the derivative with respect to σ_*. Here we have used $T_c \propto g^{-1/2}$.

Now the power spectrum is written as

$$\mathcal{P}_\zeta = \frac{1}{4}\left(\frac{g'}{g}\right)^2\left(\frac{H_*}{2\pi}\right)^2 . \tag{3.2}$$

Since σ does not evolve much during inflation, the scale dependence of the power spectrum comes from the time variation of the Hubble parameter during inflation. Then the spectral index is given by

$$n_s - 1 \simeq -2\epsilon \ , \tag{3.3}$$

where ϵ is a slow-roll parameter and defined by $\epsilon = (M_{\rm pl}^2/2)(V_\varphi/V)^2$. Here V is the potential for the inflaton φ and $V_\varphi = dV/d\varphi_*$. Notice that in the standard inflation scenario, the spectral index is given by $n_s - 1 = -6\epsilon + 2\eta$ with $\eta = M_{\rm pl}^2(V_{\varphi\varphi}/V)$ being another slow-roll parameter.

To discuss non-Gaussianity of the curvature perturbation in the mechanism, the non-linearity parameter f_{NL} has been commonly used, which are related to the bispectrum of curvature perturbation. Then, in this model $f_{\rm NL}$ is given by

$$\frac{6}{5} f_{\rm NL} = 2\left[\frac{g''/g}{(g'/g)^2} - 1\right] . \tag{3.4}$$

To investigate observational quantities in more detail, we assume a simple functional form of g as

$$g = g_0\left(1 + \frac{1}{2}\frac{\sigma^2}{M^2}\right) , \tag{3.5}$$

with g_0 and M being a coupling constant and some scale, respectively. When we assume that $(\sigma_*/M)^2 \ll 1$, the non-linearity parameter $f_{\rm NL}$ can be written as

$$f_{\rm NL} \simeq \left(\frac{\sigma_*}{M}\right)^{-2} . \tag{3.6}$$

The constraint on the non-linearity parameter from the WMAP5 [3] is $f_{\rm NL} < \mathcal{O}(100)$, which indicates that $\sigma_*/M \gtrsim \mathcal{O}(10^{-1})$.

4 Primordial fluctuations in scenarios with thermal inflation and models of inflation

When the thermal inflation occurs, $N_{\rm inf}$ which represents the e-folds during standard primordial inflation would be reduced by $\Delta N_{\rm th}$ of Eq. (2.4). Thus, in this case, the number of the e-folds during standard inflation is modified as

$$\begin{aligned} N_{\rm inf} \;\simeq\; & 38 - \ln\left(\frac{k}{a_0 H_0}\right) - \frac{2}{3}\ln\left(\frac{10^{15}{\rm GeV}}{V_{\rm inf}^{1/4}}\right) - \frac{1}{3}\ln\left(\frac{10^6\,{\rm GeV}}{\rho_{\rm reh}^{1/4}}\right) \\ & + \frac{1}{3}\ln\left(\frac{m}{10^2{\rm GeV}}\right) + \frac{1}{3}\ln\left(\frac{T_r}{\rm GeV}\right) - \frac{2}{3}\ln\left(\frac{v_{\rm flaton}}{10^{10}{\rm GeV}}\right) . \end{aligned} \tag{4.1}$$

Since the spectral index and the tensor-to-scalar ratio depend on the number of the e-folds, some models with the reduced $N_{\rm inf}$ due to the thermal inflation may be excluded by current cosmological observations.

Here we focus on the chaotic inflation with quadratic potential and then the spectral index and the tensor-to-scalar ratio in a such model are respectively given by, in terms of $N_{\rm inf}$,

$$n_s - 1 = -\frac{2}{N_{\rm inf}} \;,\; r = \frac{8}{N_{\rm inf}} . \tag{4.2}$$

From the above expressions we can find that as $N_{\rm inf}$ becomes smaller, n_s is more red-tilted and r becomes larger. In Fig. 1, contours are shown for 68 % (green dashed line) and 95 % (red solid line) C.L. allowed region derived from WMAP+BAO+SN. The blue dotted line corresponds to the predictions of quadratic inflation models on the n_s–r plane. The values of n_s and r are also shown with small circles for $N_{\rm inf} = 30, 40, 50$ and 60. When $N_{\rm inf} \lesssim 45$, we find that the quadratic model is excluded at 95 % C.L.. However, if fluctuations come from the inhomogeneous end of thermal inflation, the situation drastically alters. As discussed in the previous section, the spectral index is given by $n_s - 1 = -2\epsilon$ and the tensor-to-scalar ratio would be negligibly small. In Fig. 1, we also plot the predictions of n_s and r from the inhomogeneous end of thermal inflation with small squares. Although the quadratic chaotic inflation model with $N_{\rm inf} \lesssim 45$ are excluded by current observations when the inflaton generates primordial fluctuations, such a model becomes viable in the present mechanism even if $N_{\rm inf}$ is small as 30.

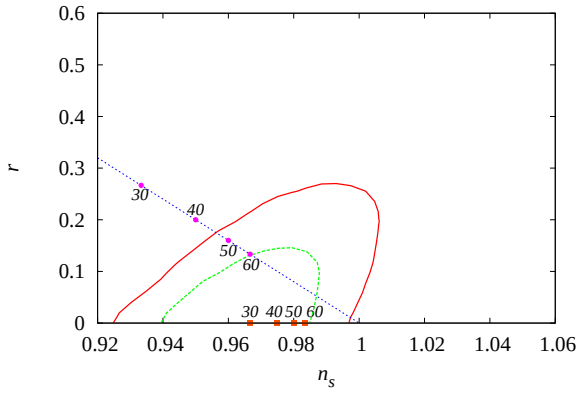

Figure 1: Contours indicate 68 % (green dashed line) and 95 % (red solid line) C.L. allowed regions derived from WMAP+BAO+SN [3]. The blue dotted line corresponds to the predictions for the quadratic chaotic models. The small purple circles and red squares represent the values of n_s and r from the standard inflation and inhomogeneous end of thermal inflation, respectively, for $N_{\rm inf} = 30, 40, 50$ and 60.

5 Summary

In this paper, we have presented a mechanism of generating primordial curvature perturbation at the end of thermal inflation by considering the case where the coupling of a flaton field with the fields in thermal bath can fluctuate. We also show that there is a possibility of generating large non-Gaussianity in this scenario. We have also investigated the constraint on inflation models in the case where the thermal inflation is realized after the primordial inflation. When such a mini-inflation occurs, the time when the fluctuations of the reference scale in the present observations exit the horizon during inflation is shifted toward the end of inflation. This, in most cases, means that the spectral index is more tilted. Thus even if an inflation model is consistent with current observations in the standard case, some models can be excluded when the thermal inflation occurs. We have discussed that this situation can be relaxed by adopting the inhomogeneous end of thermal inflation since fluctuations from the mechanism are generally more scale-invariant as seen from Eq. 3.3. As a final comment, we mention baryogenesis in a scenario with the thermal inflation. Since the thermal inflation dilutes the preexisting baryon asymmetry, one needs to generate the baryon number after thermal inflation. Some authors have discussed Affleck-Dine baryogenesis after thermal inflation [4]. It may also be interesting to investigate observational signature in such model with the inhomogeneous end of thermal inflation scenario, for example, baryon isocurvature fluctuations. This would be a subject of the future study.

References

[1] D. H. Lyth and E. D. Stewart, Phys. Rev. Lett. **75**, 201 (1995) [arXiv:hep-ph/9502417]: D. H. Lyth and E. D. Stewart, Phys. Rev. D **53**, 1784 (1996) [arXiv:hep-ph/9510204]: T. Asaka and M. Kawasaki, Phys. Rev. D **60**, 123509 (1999) [arXiv:hep-ph/9905467].

[2] T. Matsuda, Class. Quant. Grav. **26**, 145011 (2009) [arXiv:0902.4283 [hep-ph]].

[3] E. Komatsu *et al.* [WMAP Collaboration], Astrophys. J. Suppl. **180**, 330 (2009) [arXiv:0803.0547 [astro-ph]].

[4] E. D. Stewart, M. Kawasaki and T. Yanagida, Phys. Rev. D **54**, 6032 (1996) [arXiv:hep-ph/9603324];

Testing the Copernican Principle with the kSZ effect

Chul-Moon Yoo[1 (a)], Tomohiro Kai[(b)], Ken-ichi Nakao[(b)], and Misao Sasaki[(c)]

[(a)] *Asia Pacific Center for Theoretical Physics, Pohang University of Science and Technology, Pohang 790-784, Korea*
[(b)] *Department of Mathematics and Physics, Graduate School of Science, Osaka City University, 3-3-138 Sugimoto, Sumiyoshi, Osaka 558-8585, Japan ,*
[(c)] *Yukawa Institute for Theoretical Physics, Kyoto University Kyoto 606-8502, Japan*

Abstract

The kinematic Sunyaev-Zel'dovich(kSZ) effect in a Lemître-Tolman-Bondi(LTB) universe is discussed. We use the LTB universe model whose distance redshift relation coincides with the concordance ΛCDM model. The physical degrees of freedom on the last scattering surface(LSS) are fixed by using the Gamow's criterion and other additional convenient conditions. We simulate the kSZ effect by solving null geodesic equations numerically. It seems to be difficult to explain observational results with adiabatic inhomogeneities on the LSS. This difficulty would be resolved by introducing the inhomogeneity of the matter to photon ratio on the LSS, which corresponds to the isocurvature perturbation.

1 Introduction

Recently, many authors are discussing the possibility to explain observational results using inhomogeneous universe models without dark energy components. [1–4]. One of the important attempts in this direction is to explain the type Ia supernovae observation using the inhomogeneous universe models. Recently, some of the authors explicitly shown that it is possible to construct the Lemaître-Tolman-Bondi universe model whose distance-redshift relation is equivalent to the concordance ΛCDM model and which is homogeneous at the beginning[5].

One of the most stringent constraints on the inhomogeneous and isotropic universe models is from the observation of the kinematic Sunyaev-Zel'dovich(kSZ) effect. In homogeneous universes, the kSZ effect is the scattering effect on CMB photons due to the cluster with the drift velocity, where the drift velocity is the velocity along the observer's line-of-site relative to the CMB. If the cluster has the finite drift velocity, the CMB thermal spectrum will be distorted by the Compton scattering inside the cluster. On the other hand, due to the Doppler effect of the drift velocity, the CMB temperature distribution on the sky from the observer at the cluster has dipole anisotropy. It means that the dipole anisotropy observed at the cluster can be estimated by observing the spectrum distortion of the CMB photons.

In Ref. [7], Garcia-Bellido and Haugboelle reported that current observations of only nine clusters with large error bars already rule out LTB models with void size greater than $\sim$ 1.5Gpc. They also used asymptotically homogeneous LTB models and the CMB calculation method in the homogeneous and isotropic universe. However, in LTB universe models, it might be possible to introduce radial inhomogeneities around the last scattering surface(LSS) of the CMB photons. In this paper, we analyze the kSZ effect in our LTB universe model whose distance redshift relation is equivalent to the concordance ΛCDM model and investigate the effect of large radial inhomogeneity on the LSS.

2 Last Scattering Surface in the LTB Universe

The metric form of LTB universes is given by

LTB solutions have three arbitrary functions $t_{\rm B}(r)$, $M(r)$ and $k(r)$ of the radial coordinate r. One of them is a gauge degree of freedom and not physical. In this paper, we adopt the gauge given by

[1]Email address: c_m_yoo@apctp.org

$M(r) = \frac{4}{3}\pi\rho_0 r^3$, where ρ_0 is the energy density at the center. ρ_0 is related to the present Hubble parameter H_0 as $H_0^2 + k(0)c^2 = \frac{8}{3}\pi G\rho_0$.

We assume $t_{\rm B}(r) = 0$ as the same in Ref.[5]. Then the fitting function of $\tilde{k}(\tilde{r})$ [2] to the numerical plot in Ref.[5] is given by $\tilde{k}(\tilde{r}) = \frac{0.545745}{0.211472 + \sqrt{0.026176 + \tilde{r}}} - \frac{2.22881}{\left(0.807782 + \sqrt{0.026176 + \tilde{r}}\right)^2}$. It can be easily shown that the distance in our LTB model coincides with that in the ΛCDM model with $(\Omega_{\rm M0}, \Omega_{\Lambda 0}) = (0.3, 0.7)$ in all redshift domain.

Since LTB universes are spherically symmetric and inhomogeneous, the LSS in a LTB universe can be embedded in the spacetime inhomogeneously. In order to consider the LSS in a LTB universe, we adopt the Gamow's criterion given by $H = \Gamma$ on LSS, where H is the Hubble parameter and Γ is the number of interaction per unit time for a photon.

Hereafter, for simplicity, we consider the system composed of dark matter, photons, electrons, protons and hydrogen atoms. The matter density including the dark matter and baryons is given by the density of our LTB model. The baryon number density $n_{\rm b}$ is the total number density of protons and hydrogen atoms. The electron number density $n_{\rm e}$ is equivalent to the proton number density. We also assume that, before the LSS, the universe is in thermal equilibrium and the decoupling between photons and baryons occur instantaneously.

Using the cross section of the Thomson scattering $\sigma_{\rm T}$ and electron number density $n_{\rm e}$, we can write $\Gamma = cn_{\rm e}\sigma_{\rm T}$. In the thermal equilibrium, the ionization rate $X_{\rm e}$ satisfies the Saha's equation. The Saha's equation is approximately given by $X_{\rm e}^2 \sim \frac{\sqrt{\pi}}{4\sqrt{2}\zeta(3)}\frac{1}{\eta}\left(\frac{k_{\rm B}T}{m_{\rm e}c^2}\right)^{-3/2}\exp\left(-\frac{13.59{\rm eV}}{k_{\rm B}T}\right)$. where η, $k_{\rm B}$ and $m_{\rm e}$ are the baryon to photon ratio, the Boltzmann constant and the electron mass, respectively.

Here, we introduce three independent physical quantities which are functions defined on the LSS: the temperature $T_{\rm LSS}(r)$, the baryon to photon ratio $\eta_{\rm LSS}(r)$ and the dark matter to photon ratio $\alpha_{\rm LSS}(r)$. The definition of the $\alpha_{\rm LSS}$ is given by

$$\alpha_{\rm LSS}(r) := \frac{\rho(t_{\rm LSS}(r), r)}{\rho_0}\left(\frac{T_0}{T_{\rm LSS}(r)}\right)^3, \tag{2.1}$$

where T_0 is the present observed CMB temperature $\sim 2.725K$.

Combining the Saha's equation for the ionization rate, we have an equation

$$\eta_{\rm LSS}(r) = \frac{32\sqrt{2\pi}\zeta(3)}{3}\frac{G\rho_0}{(cn_{\gamma 0}\sigma_{\rm T})^2}\left(\frac{k_{\rm B}T_0}{m_{\rm e}c^2}\right)^{3/2}\alpha_{\rm LSS}(r)\left(\frac{T_0}{T_{\rm LSS}(r)}\right)^{3/2}\exp\left(\frac{13.59{\rm eV}}{k_{\rm B}T_{\rm LSS}(r)}\right), \tag{2.2}$$

where $n_{\gamma 0}$ is the present photon number density of the CMB. We note that the functions $T_{\rm LSS}(r)$, $\eta_{\rm LSS}(r)$ and $\alpha_{\rm LSS}(r)$ are defined only on the LSS, and these determine the embedding of LSS in the spacetime as $t = t_{\rm LSS}(r)$ through (2.1).

There are additional conditions for the three functions. One of them is at the intersection of the observer's past light cone and the LSS. The observer's past light cone can be expressed as the past directed radial null geodesics. The past directed radial null geodesics can be parametrized by the redshift z as $t = t_{\rm lc}(z)$, $r = r_{\rm lc}(z)$. Then we have the following relation:

$$\frac{T_{\rm LSS}(r_{\rm lc}(z_{\rm LSS}))}{T_0} = 1 + z_{\rm LSS}, \tag{2.3}$$

Furthermore, observations of the light element abundance ratio around us give a constraint

$$\eta_{\rm LSS}(0) \sim 6 \times 10^{-10}. \tag{2.4}$$

If we consider that the functions $T_{\rm LSS}(r)$, $\eta_{\rm LSS}(r)$ and $\alpha_{\rm LSS}(r)$ are independent functions and $t_{\rm LSS}(r)$ is fixed through (2.1), we have one equation (2.2) and two boundary conditions (2.3) and (2.4) to constrain the three independent functions. To fix the embedding of the LSS, additional conditions are needed as assumptions.

[2] For the notational simplicity, we introduce dimensionless quantities $\tilde{r} = H_0 r/c$ and $\tilde{k}(\tilde{r}) = c^2 k(r) H_0^2$(see Ref.[5] for the definition of $k(r)$).

3 Simplest model

First, we consider the case in which $T_{\rm LSS}$, $\eta_{\rm LSS}$ and $\alpha_{\rm LSS}$ are constants. Then equations (2.2), (2.3) and (2.4) completely fix the values of $T_{\rm LSS}$, $\eta_{\rm LSS}$ and $\alpha_{\rm LSS}$. In this case, all ratios between the photon number density, the dark matter density and the baryon density are fixed. The embedding of the LSS into the spacetime $t_{\rm LSS}(r)$ is given by solving (2.1).

Hereafter, we consider only comoving clusters. Let us consider a cluster at the redshift $z_{\rm cl}$. From this cluster, we can solve the null geodesic equations to all directions(see Fig.1). At the intersection between

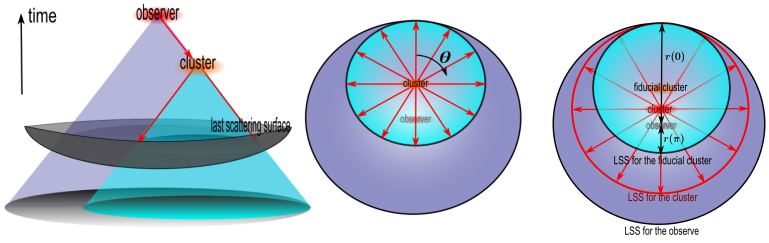

Figure 1: A schematic figure of the spacetime and the last scattering surface.

the past light cone of the cluster and the last scattering surface, we terminate the calculations of the null geodesic equations and read off the redshift $z_*(\theta; z_{\rm cl})$ at that point. Then, the cluster at $z = z_{\rm cl}$ observes temperature anisotropy given by $T_{\rm cl}(\theta; z_{\rm cl}) = T_{\rm LSS}(1+z_{\rm cl})/(1+z_*(\theta; z_{\rm cl}))$ due to the inhomogeneity of the universe. We are interested in only the dipole component given by $T_{\rm dipole} = T_{\rm cl}(0; z_{\rm cl})(c - v_{\rm cl}(z_{\rm cl}))/(c - v_{\rm cl}(z_{\rm cl})\cos\theta)$. By using the least-square method, we obtain the dipole temperature anisotropy due to the inhomogeneity of the universe.

Results are shown in Fig.2. The result in [7](lower line) is also shown in this figure. Obviously, the

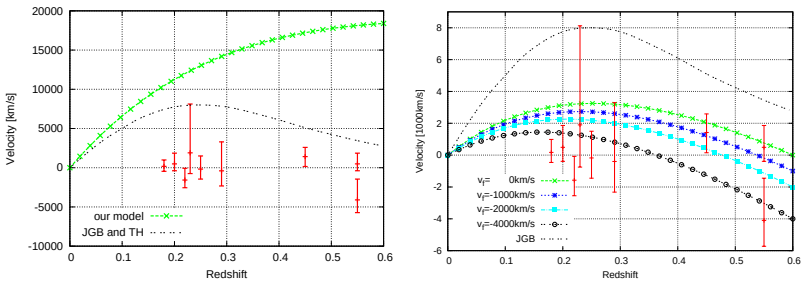

Figure 2: Effective drift velocities for each cluster redshift in the case of the simplest case(left). Effective velocities for each $v_{\rm f}$ are depicted as functions of the cluster redshift $z_{\rm cl}$(right). The redshift of the fiducial cluster is $z_{\rm f} = 0.6$.

result in our model is far from the observational results and worse than the result in [7]. This result means that the fixed ratio between dark matter, baryon and photon densities seems not to be consistent with observational results. In this situation, the inhomogeneities of the all components are adiabatic in terms of cosmological perturbation.

4 Inhomogeneous $T_{\rm LSS}$ and $\alpha_{\rm LSS}$

In this section, we assume $\eta_{\rm LSS}(r) = 6 \times 10^{-10}$, namely the baryon to photon ratio is homogeneous on the LSS. Then, to fix the embedding of the LSS in the spacetime, we need another condition other than the Gamow's criterion. For this purpose, we set the fiducial cluster at the redshift $z_{\rm f} = 0.6$. We assume

that the observer at this fiducial cluster observes completely dipole temperature anisotropy characterized by the effective velocity $v_{\rm f}$ as $T(\theta;z_{\rm f})=\dfrac{1-v_{\rm f}/c}{1-v_{\rm f}/c\cos\theta}T(0;z_{\rm f})=\dfrac{1-v_{\rm f}/c}{1-v_{\rm f}/c\cos\theta}(1+z_{\rm f})T_0$.

The embedding $t_{\rm LSS}$ of the LSS can be found as follows. From the fiducial cluster, we solve null geodesic equations to all directions. At each point on the null geodesic trajectory directed to the angle θ, the temperature can be defined by $T_{\rm geo}(z;z_{\rm f},\theta)=(1+z)T(\theta;z_{\rm f})/(1+z_{\rm f})$, where z is the redshift from the observer at the center. Then, at each point, we can define α as $\alpha_{\rm geo}(z;z_{\rm f},\theta)=\dfrac{\rho(t_{\rm geo}(z;z_{\rm f},\theta),r_{\rm geo}(z;z_{\rm f},\theta))}{\rho_0}\left(\dfrac{T_0}{T_{\rm geo}(z;z_{\rm f},\theta)}\right)^3$, where $t=t_{\rm geo}(z;z_{\rm f},\theta)$ and $r=r_{\rm geo}(z;z_{\rm f},\theta)$ give the trajectory of each null geodesic.

Once $T_{\rm geo}$ and $\alpha_{\rm geo}$ satisfy the Gamow's criterion (2.2), we terminate solving the null geodesic equations. Then, the terminated point $(t,r)=(t_{\rm t}(z_{\rm f},\theta),r_{\rm t}(z_{\rm f},\theta))$ is on the LSS. We also have the value of $T_{\rm LSS}(r_{\rm t}(z_{\rm f},\theta))$ and $\alpha_{\rm LSS}(r_{\rm t}(z_{\rm f},\theta))$. The schematic figure for the trajectory $r=r_{\rm t}(z_{\rm f},\theta)$ is shown in the right of Fig.1. We find that $r_{\rm t}(\pi)\le r_{\rm t}(\theta)\le r_{\rm t}(0)$ for $0\le\theta\le\pi$. The above inequality means that we have the functional form of $T_{\rm LSS}(r)$ and $\alpha_{\rm LSS}(r)$ for only the region $r_{\rm t}(\pi)\le r\le r_{\rm t}(0)$. This information is enough to calculate the temperature anisotropy from another cluster in the redshift $z_{\rm cl}<z_{\rm f}$(see Fig.1).

Using the same procedure as that in the previous section, we can obtain the temperature anisotropy $T(\theta;z_{\rm cl})$ from the cluster at the redshift $z=z_{\rm cl}$. Results are shown in the right of Fig.2. The effective velocities for each $v_{\rm f}$ are depicted as functions of the cluster redshift $z_{\rm cl}$. The effective velocities are evaluated from the dipole temperature anisotropy using the least-square method. It is clear that our results have much better fit to the observational data than the results in [7].

5 Summary and Discussions

In this paper, we have discussed the kSZ effect in a LTB universe. We have used the LTB universe model whose distance-redshift relation is equivalent to the concordance ΛCDM model as the background universe. In our situation, the nature of the LSS is characterized by three independent quantities which are functions of the radial coordinate on the LSS. To fix these functional degrees of freedom, we have used the Gamow's criterion and other two conditions which satisfy the two boundary conditions. We showed that it seems to be difficult to explain the observational results with the pure adiabatic inhomogeneity on the LSS in our LTB universe model.

In order to overcome this difficulty, we introduced temperature inhomogeneity on the LSS. In our procedure, the baryon to photon ratio is constant on the LSS while the matter to photon ratio has radial inhomogeneity. We showed that this degree of freedom can improve the fit to observational data. Actually, we may have much better fit than the result in [7].

acknowledgements

C.M. would like to thank organizers and all participants in the workshop LLTB2009 in KEK Tsukuba, Japan, for helpful comments. The research of C.M. is supported by Asia-Pacific Center for Theoretical Physics under the YST program. This work was supported by Korea Institute for Advanced Study under the KIAS Scholar program in part and the Grant-in-Aid for the Global COE Program "The Next Generation of Physics, Spun from Universality and Emergence" from the Ministry of Education, Culture, Sports, Science and Technology (MEXT) of Japan in part.

References

[1] K. Tomita, Astrophys. J. **529**, 38 (2000) [arXiv:astro-ph/9906027].

[2] K. Tomita, Mon. Not. Roy. Astron. Soc. **326**, 287 (2001) [arXiv:astro-ph/0011484].

[3] K. Tomita, Prog. Theor. Phys. **106**, 929 (2001) [arXiv:astro-ph/0104141].

[4] M. N. Celerier, Astron. Astrophys. **353**, 63 (2000) [arXiv:astro-ph/9907206].

[5] C. M. Yoo, T. Kai and K. i. Nakao, Prog. Theor. Phys. **120**, 937 (2008) [arXiv:0807.0932 [astro-ph]].

[6] M. Tanimoto and Y. Nambu, Class. Quant. Grav. **24**, 3843 (2007) [arXiv:gr-qc/0703012].

[7] J. Garcia-Bellido and T. Haugboelle, JCAP **0809**, 016 (2008) [arXiv:0807.1326 [astro-ph]].